

UNCLASSIFIED

AD NUMBER
AD902099
NEW LIMITATION CHANGE
TO Approved for public release, distribution unlimited
FROM Distribution authorized to U.S. Gov't. agencies only; Test and Evaluation; JUN 1972. Other requests shall be referred to Air Force Aero Propulsion Laboratory, ATTN: POE-2, Wright-Patterson AFB, OH 45433.
AUTHORITY
AFRPL ltr dtd 30 Jun 1975

THIS PAGE IS UNCLASSIFIED

THIS REPORT HAS BEEN DELIMITED  
AND CLEARED FOR PUBLIC RELEASE  
UNDER DOD DIRECTIVE 5200.20 AND  
NO RESTRICTIONS ARE IMPOSED UPON  
ITS USE AND DISCLOSURE.

DISTRIBUTION STATEMENT A

APPROVED FOR PUBLIC RELEASE;  
DISTRIBUTION UNLIMITED.

L  
AD902099

# FLEXIBLE ROLLED-UP SOLAR ARRAY

E. O. Felkel

G. Wolff

Et al.

Hughes Aircraft Company/Space and Communications Group

TECHNICAL REPORT AFAPL-TR-72-61

30 JUNE 1972

"Distribution limited to U.S. Government Agencies only; test and evaluation; June 1972. Other requests for this document must be referred to the Air Force Aero Propulsion Laboratory (POE-2, Wright-Patterson Air Force Base, Ohio 45433)."

Air Force Aero Propulsion Laboratory  
Air Force Systems Command  
Wright-Patterson Air Force Base, Ohio 45433

DDC  
RECEIVED  
AUG 10 1972  
RECEIVED  
B.

## NOTICE

When Government drawings, specifications, or other data are used for any purpose other than in connection with a definitely related Government procurement operation, the United States Government thereby incurs no responsibility nor any obligation whatsoever; and the fact that the government may have formulated, furnished, or in any way supplied the said drawings, specifications, or other data, is not to be regarded by implication or otherwise as in any manner licensing the holder or any other person or corporation, or conveying any rights or permission to manufacture, use, or sell any patented invention that may in any way be related thereto.

Copies of this report should not be returned unless return is required by security considerations, contractual obligations, or notice on a specific document.



# FLEXIBLE ROLLED-UP SOLAR ARRAY

E. O. Felkel

G. Wolff

Et al.

Hughes Aircraft Company/Space and Communications Group

TECHNICAL REPORT AFAPL-TR-72-61

30 JUNE 1972

"Distribution limited to U.S. Government Agencies only: test and evaluation: June 1972. Other requests for this document must be referred to the Air Force Aero Propulsion Laboratory (POE-2, Wright-Patterson Air Force Base, Ohio 45433)."

Air Force Aero Propulsion Laboratory  
Air Force Systems Command  
Wright-Patterson Air Force Base, Ohio 45433

## FOREWORD

This is the final report on the Flexible Rolled-Up Solar Array (FRUSA). The program was conducted for the Air Force Systems Command's Aero Propulsion Laboratory, WPAFB, by the Hughes Aircraft Company, Space and Communications Group, El Segundo, California, under Contract F33615-68-C-1676, Project B/682J.

The program was directed by Mr. L. D. Massie, Solar Power Technical Area (POE-2), Energy Conversion Branch, Aerospace Power Division.

The Space and Communications Group of the Hughes Aircraft Company was assigned the task of designing, developing, manufacturing, and ground and flight testing a self-contained 1.5-kw flexible rolled-up solar array power system. The major objectives of the experiment were to:

- Demonstrate the deployment, extension, and retraction of a 1.5-kw flexible solar array assembly in an orbital environment
- Demonstrate solar array tracking and lockon performance in an orbital environment with changing sun angles
- Demonstrate power generation capability in an orbital environment for a period of up to 1 year
- Verify dynamic behavior of the array system
- Obtain reference measurements from calibrated solar cells, modules, and the main solar cell panels with respect to time

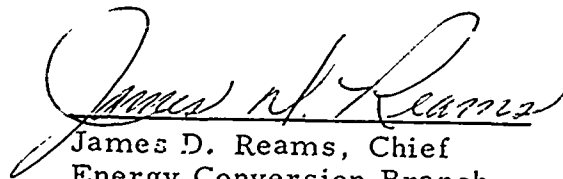
The flight test data were to be used to:

- Develop a flexible solar array system design for a 5-kw operational system
- Conduct parametric studies from 0.5 to 20 kw
- Demonstrate a 5-year capability

Mr. E. O. Felkel was Program Manager, G. Wolff was Associate Program Manager. The major contributors to this report, in addition to the above, were G. Lindenman, M. Olson, D. Plummer, G. Steffen, E. Stofel, W. Turner, and A. Wittmann.

This report was submitted in June 1972 and covers work performed by Hughes Aircraft Company from 1 July 1968 through 31 May 1972. Publication of the report does not constitute Air Force approval of its findings or conclusions. It is published only for the exchange and stimulation of ideas.

This report was reviewed and is approved.

A handwritten signature in cursive script, reading "James D. Reams". The signature is written in dark ink and is positioned above the printed name and title.

James D. Reams, Chief  
Energy Conversion Branch  
Aerospace Power Division  
Air Force Aero Propulsion Laboratory

## ABSTRACT

This report summarizes the design, development, qualification, and flight test of a 1.5-kw flexible rolled-up solar array power system. This system was launched on a thrust augmented Thor/Agena vehicle system into a 400 nm polar orbit on 17 October 1971, has successfully completed a 6 month flight test, and continues to provide spacecraft power.

The criteria, design tradeoffs, and analyses that led to the configuration of the 5.5-by 32-foot solar array, the two axis sun acquisition and tracking orientation mechanism, and the associated power electronics and instrumentation units are described. The results of development, qualification, and flight test are presented, as well as recommendations for design improvements or developments for future similar applications. The recommendations include principal parameters and performance data such as array aspect ratios, weight, and natural frequency for systems ranging from 0.5 to 20 kw.

The flight data illustrate the compatibility of the flexible solar array concept with flight systems. Power output has been excellent with no evidence of mechanical damage from boost, deployment, or operational environments. Peak power degradation has been reflective of the normal reaction of solar cells to the space environment. Spacecraft and array dynamic interactions have been minimal and vehicle integration has proven straightforward and effective.

In conclusion, the report illustrates the viability of the 1.5-kw flexible array design as a flight power system in its own right and also as a module of power systems to the 20-kw level.

## CONTENTS

		<u>Page</u>
I	INTRODUCTION	1
II	SUMMARY	3
	Program Definition	3
	Design Study and Analysis	3
	Manufacturing	5
	Qualification and Flight Acceptance	6
	Flight Test and Data Analysis	6
III	SYSTEM DESCRIPTION	9
	Major System Design Requirements and Goals	9
	System	9
	Solar Array Subsystem Requirements	11
	Solar Panel Assembly	11
	Orientation Subsystem	12
	Power Conditioning and Storage Subsystem	12
	Instrumentation Subsystem	12
	Design Description	13
	Solar Array Subsystem	13
	Orientation Subsystem	13
	Power Conditioning and Storage Subsystem	13
	Instrumentation Subsystem	16
	AGE	16
IV	DESIGN AND DEVELOPMENT	21
	Solar Array Subsystem	21
	Subsystem Requirements and Description	21
	Drum Mechanism	21
	Flexible Solar Arrays	39
	Solar Array Subsystem Conclusions	54
	Orientation Subsystem	54
	Design Requirements	55
	Descriptions	57
	Tradeoffs and Design Changes	83
	Development and Other Tests	96
	Conclusions	105
	Power Conditioning and Storage Subsystem	107
	Subsystem Description	107
	Tradeoff Studies and Analysis	113
	Development Tests	121
	Conclusions	121
	Instrumentation Subsystem	122
	Functional Requirements	122
	Unit Description	122
	Operational and Test Results	130
	Conclusions	130

	System AGE	131
	Conclusions	132
V	SYSTEM TEST	135
	Qualification Tests	135
	Ambient Functional Tests	135
	Vibration Test	138
	Solar-Thermal-Vacuum (STV) Tests	139
	EMI/EMC Tests	141
	Solar Array Deployment Tests	141
	Summary of Test Results	145
	Flight Acceptance Tests	145
	Test Results	149
	Summary of Acceptance Test Results	159
	Integration and Prelaunch Tests	159
	Qualification Model	159
	Flight Model	159
	Prelaunch Tests	160
VI	FLIGHT TEST RESULTS	161
	Mission Summary	161
	Solar Array Panel Temperature Evaluation	163
	Solar Array Power Performance	166
	Solar Cell/Module Experiment Results	169
	Array Dynamic Analysis	174
	Structure Instrumentation	175
	Dynamic Flight Data Evaluation	176
	Finite Element Modeling	193
VII	RELIABILITY/MAINTAINABILITY	197
	In-Flight Anomalies	197
	Recommendations	198
	Maintainability	198
VIII	FIVE-KW DESIGN STUDY	203
	Design Criteria and Requirements	203
	Subsystem Description	206
	Orientation Mechanism	206
	Solar Panel Description	209
	Drum Mechanism	212
	Array Dynamic Characteristic	217
	5-kw Operational FRUSA Reliability	217
	Orientation Subsystem	217
	Solar Array	223
	Instrumentation (Housekeeping)	223
	Power Conditioning and Storage	223
	Experience Factor	223

IX	PARAMETRIC DESIGN STUDY OF 0.5-TO 20-KW SOLAR CELL ARRAY SYSTEMS	225
	Flexible Solar Array Panel Design	225
	Solar Cell	229
	Cover Slide	230
	Interconnections	230
	Electrical Bus	230
	Diodes	231
	Panel Electrical Connect	231
	Solar Panel Support Concepts	231
	Solar Panel Support Boom	236
	Flexible Solar Panel Stowage	239
	Stowage Drum Assembly	239
	Solar Array Support Structure Weight Optimization	246
	Array Support Optimized for Bending Strength	246
	Array Support Optimized for Stiffness	252
	Array Support Optimized for Boom Buckling	253
	Array Orientation Mechanism	256
	Summary Solar Array Configuration Optimization	258
X	CONCLUSIONS AND RECOMMENDATIONS	267
	Conclusions	267
	Recommendations	267
APPENDICES		
A.	Main Solar Array Current-Voltage Performance Data	269
B.	Dynamic Analysis Data	275
C.	5-kw Design Drawings	291
D.	Array Dynamics Analysis	299

## ILLUSTRATIONS

	Page
2-1 Program Schedule	4
3-1 System Functional Block Diagram	10
3-2 FRUSA System Shown on Agena Spacecraft	10
3-3 Solar Array Subsystem	14
3-4 Internal Profile of Orientation Mechanism	15
3-5 Strain Gage and Accelerometer Installation	17
3-6 Location of Reference Cells and Modules	18
3-7 Deployment Test Setup	19
3-8 Flight Model Solar Array on Water Table	19
4-1 Solar Array Subsystem	22
4-2 Drum Mechanism Details	24
4-3 Extendible Boom Actuator	26
4-4 Boom Length Compensator	26
4-5 Drum End Plate and Bearing Installation	28
4-6 Flexible Power Cable Arrangement	30
4-7 Boom Actuator Drive Arrangements	32
4-8 Cushion Take-up Drive Logic Tree	34
4-9 Required Drum Diameter for Several Substrate Materials and 0.6 lb/ft Panel Tension	36
4-10 Weight Comparison of Array Storage Drum Materials	36
4-11 Solar Panel Components	40
4-12 Panel Weight Breakdown	40
4-13 Solar Array Power and Data Buses	42
4-14 Collector Bus Strips Arrangement	43
4-15 Elements of Solar Cell Assembly	44
4-16 Embossed Kapton Film Cushion-Rolled	46
4-17 Solar Array/Cushion Configuration and Storage Drum	46
4-18 Panel Tension Test Setup With Low Temperature Shroud Removed	48
4-19 Thermal Shock and Cycling Test Specimen	51
4-20 Typical Thermal Cycle of Solar Panel Specimen	51
4-21 Cushion Fabrication Equipment	52
4-22 Cushion Forming Die Closeup	52
4-23 Vibration Test Solar Array and Cushion	53
4-24 Panel Segment Vibration Test Setup	53
4-25 Orientation Subsystem Elements	56
4-26 Orientation Subsystem Flight Operations	58
4-27 Orientation Subsystem Block Diagram	59
4-28 Orientation Mechanism	64
4-29 Orientation Mechanism Drum Axis Hardware	65
4-30 Orientation Mechanism Internal Profile	65
4-31 Orientation Mechanism Thermal Finish	66
4-32 Orientation Mechanism Housings and Shafts	68
4-33 Gimbal Bearing	70
4-34 Frameless Pancake dc Tachometer	71
4-35 Orientation Subsystem Drum Axis Data Slip Rings and Brushes	71



4-36	Orientation Subsystem Drum Axis Power and Data Slip Rings	72
4-37	Brush Arrangements	72
4-38	Deployment Mechanism	73
4-39	Sun Sensor Geometry	73
4-40	Sun Sensor Group	74
4-41	Acquisition Sensor	75
4-42	Tracking Sensor	75
4-43	Calibration of Sun Error Sensor	76
4-44	Partial Assembly, Control Electronics Unit	76
4-45	Control Electronics Unit Block Diagram	79
4-46	Orientation Control System Schematic, One Axis	81
4-47	Representative Root Locus of Array Control Loop	82
4-48	Acquisition Performance	84
4-49	Noon Turn Performance	87
4-50	Ideal Array Angles	88
4-51	1.5-kw FRUSA Normalized Momentum Change Per Orbit With and Without Partial Momentum Cancellation	89
4-52	Array Momentum Cancellation	90
4-53	Original Brush Design	93
4-54	Modified Brush Design	93
4-55	Typical Friction and Ring Noise Measurements, Support Axis	98
4-56	Deployment Test Setup	98
4-57	Effect of Temperature Extremes on Deployment Velocity	99
4-58	Deployment Mechanism Static Performance Development Tests, Ambient Temperature	99
4-59	Deployment Mechanism Static Performance, Flight Unit - Ambient Temperature	102
4-60	Orientation Subsystem Solar-Thermal-Vacuum Qualification Test	102
4-61	FRUSA Revolution 10 Sun Acquisition	104
4-62	Power Conditioner and Storage Subsystem Functional Block Diagram	106
4-63	Power Conditioning Unit	108
4-64	Solar Array Overvoltage Switch	108
4-65	$\pm 28$ -Volt Inverter Pulsewidth Modulator	110
4-66	Boost Converter Pulsewidth Modulator	111
4-67	400-Hz Inverter Waveform Generator	112
4-68	Battery/Charge Controller	115
4-69	Battery Charge Control Block Diagram	116
4-70	Load Bank Assembly	117
4-71	Load Bank Load Lines	118
4-72	Location of Reference Cells and Modules	128
4-73	Strain Gage and Accelerometer Installation	128
4-74	Single Line Cable Block Diagram/FRUSA System Tests	132
4-75	Ambient Functional Setup	133
4-76	Flight Model Solar Array Ambient Test Position	133
5-1	Operations Flow Chart	137
5-2	Ambient Functional Setup	137
5-3	Vibration Setup (Orientation Subsystem)	140
5-4	STV Endbell	140

5-5	Screenroom Setup for EMI/EMCTES	146
5-6	Magnetic Moment Measurement Test Position	146
5-7	FRUSA Separation and Deployment Test	148
5-8	Deployment Test Setup (Without Support Springs)	148
5-9	Flight Model Units	151
5-10	Single Line Cable Block Diagram - FRUSA System Tests	154
5-11	Orientation Subsystem on Vibration Table	154
5-12	FRUSA System Setup for Separation and Deployment Testing	155
5-13	FRUSA System Installed on C-4 Chamber Endbell Just Prior to Thermal Vacuum Tests	156
5-14	Random Vibration Test Requirements	157
5-15	Current Versus Voltage for Full Array	160
5-16	Power Performance for Full Array at Worst Case Temperatures	161
6-1	Anomalous (Offset) Tracking	168
6-2	Array Panel Temperatures	168
6-3	FRUSA Array 6 Month Performance Summary	172
6-4	Cell/Module Layout	172
6-5	I-V Data	175
6-6	FRUSA Accelerometer and Strain Gage Instrumentation	182
6-7	Calibration Curve for Boom Root Bending Load Cell	182
6-8	Accelerometer Time History During Array Deployment as Measured by Transducer R304	182
6-9	FRUSA, Revolution 79 Anomalous Sun Acquisition Maneuver	185
6-10	Accelerometer Time Histories for FRUSA Slew Maneuver on Revolution 79	186
6-11	Increase in Array Fundamental Bending Mode Due to Reduced Fixity at Drum as Computed for Simplified Mass Model	189
6-12	Typical Fourier Analysis Frequency Decomposition of Acceleration Time Histories From Revolution 79	191
6-13	Accelerometer Time History	192
6-14	Fourier Analysis Frequency Decomposition of Acceleration Time History	194
6-15	Finite Element Model of FRUSA Flight Configuration	192
6-16	Out-of-Plane Bending and Torsion Modes of FRUSA Finite Element Model	194
7-1	System Reliability Block Diagram	198
8-1	Comparison of Array Configurations for 5-kw Power System Design	204
8-2	FRUSA Orientation Mechanism Cross Section	207
8-3	Solar Array Panel Configuration and Weight Breakdown	210
8-4	Solar Panel Assembly	213
8-5	FRUSA Drum Mechanism	219
8-6	Orientation Subsystem Reliability Block Diagram	221
8-7	Solar Array Reliability Block Diagram	221
8-8	Instrumentation Subsystem Reliability Block Diagram	222
8-9	Power Conditioning and Storage Reliability Block Diagram	222
8-10	FRUSA System Reliability Block Diagram	222

9-1	Weight Efficient Power Ranges for Solar Arrays	227
9-2	Substrate Flexibility Parameter Versus Panel Contact Angle on Rollup Stowage Drum	228
9-3	Power Collector Bus Weight Versus Array Voltage for Varying Power Loss	232
9-4	Center and Edge Panel Support Configurations	234
9-5	Deployer Mechanism Weight For Collapsible Boom Type	235
9-6	Collapsible Boom Concepts	238
9-7	Specific Stiffness of Three Deployable Boom Types Normalized For Diameter-to-Thickness Ratio of 200	240
9-8	Specific Strength of Three Deployable Boom Types Normalized For Diameter-to-Thickness Ratio of 200	240
9-9	Critical Boom Bending Moment For Stainless Steel BI-STEM Booms of Diameter-to-Thickness Ratio of 200	241
9-10	Stainless Steel BI-STEM Boom Stiffness Versus Specific Boom Weight	241
9-11	FRUSA Stowage Drum Cross Section	242
9-12	Drum Assembly Weight Variation With Panel Aspect Ratio	244
9-13	Stainless Steel BI-STEM Boom Weight Versus Boom Diameter, D/t between 168 to 250	248
9-14	Weight of Four Support Booms Versus Panel Aspect Ratio For Variable Quasi-Static Load Factors	248
9-15	Boom Weight Versus Panel Aspect Ratio For Design Condition of 0.1 g Load Factor	249
9-16	Dual Boom Deployer (Two Per Array) Weight Versus Panel Aspect Ratio L/W For 0.1 g Quasi-Static Design Load Factor	250
9-17	Weight of Two Dual Boom Deployer Mechanisms Versus Panel Aspect Ratio For Booms Dimensioned For 0.2 g Quasi-Static Loading	251
9-18	Weight of BI-STEM Steel Booms (Four) Required to Achieve Specified Panel Frequency	254
9-19	Dual Boom Deployer (Two Per Array) Weight Versus Panel Aspect Ratio When Panel Bending Frequency is Design Criteria	255
9-20	Flexible Array System Configuration Optimized For 0.3 Hz	259
9-21	Array Structure Weight Variation With Panel Aspect Ratio When Panel Bending Frequency is Design Criteria	260
9-22	Array Structure Weight (Drum Assembly, Booms, Boom Deployers) of Array Modules Optimized for Bending Frequency	261
9-23	Roll-Up Array System Configurations Optimized for 0.1 g	262
9-24	Array Structure Weight Variation With Panel Aspect Ratio For 0.1 and 0.2 g Load Factors	264
9-25	Array Structure Weight of Array Modules Optimized for Quasi-Static of 0.1 g and 0.2 g	265
10-1	Comparison of Flexible and Rigid Array 5.2 kw Power Subsystems for Near Term Low Earth Orbit Application	268

## TABLES

	Page
1-1 FRUSA Requirements and Goals	2
4-1 Solar Array Subsystem Requirements and Goals	23
4-2 Boom Actuator Drive Tradeoff Summary	31
4-3 Boom Actuator Motor Tradeoff Summary	31
4-4 Comparison of Sliprings and Flexible Cable	35
4-5 Cell Qualification Test Results	45
4-6 Orientation Subsystem Commands	60
4-7 Orientation Mechanism Slipring Assignments	61
4-8 Gimbal Axis Torquer Tradeoff Considerations	91
4-9 Torquer Sizing	92
4-10 Power Conditioning and Storage Subsystem Development Test Summary	120
4-11 Solar Array Commutator A Telemetry	123
4-12 Solar Array Commutator D Telemetry	125
4-13 Orientation Subsystem Commutator B Telemetry Measurements	126
4-14 Power Conditioning and Storage Subsystem Telemetry	127
5-1 Qualification Environments	135
5-2 FRUSA Systems Test Results	136
5-3 Deployment Test Data	143
5-4 FRUSA System Test Results Summary	158
5-5 FRUSA Weight	160
6-1 RTD-806 Mission Operations	162
6-2 Flight Solar Array Temperatures, °F	165
6-3 FRUSA Array Radiative Properties For Baseline Analysis	166
6-4 Predicted (Normalized) Solar Panel Maximum Power Performance Versus Time in Orbit	167
6-5 Measured (Normalized) FRUSA Solar Panel Performance Versus Time in Orbit	169
6-6 FRUSA Test Cell/Module Description Summary	170
6-7 Comparison of In-Orbit Measured FRUSA Modes With Analytical Predictions	175
6-8 Mission Events Summary For Significant Dynamics Data	176
6-9 FRUSA Extension Dynamics	180
6-10 Peak Accelerometer Readings	180
7-1 FRUSA MTTR Estimate	199
7-2 Solar Cell Panel Actual Repair Time Estimates	200
7-3 Overall Solar Cell Panel MTTR Estimate	201
8-1 Weight Summary for FRUSA and 5-kw Array	205
8-2 Solar Panel Design Characteristics for Three Solar Cell Types	211
8-3 Bending Moment Loading of Panel Support Boom (in-lb)	216
8-4 Summary of Minimum Margins of Safety for 1.5-kw FRUSA Array System Design	218
8-5 Orientation Mechanism Reliability	223

9-1	Design Environments and Ground Rules	226
9-2	Array Area Utilization and Weight Penalty	229
9-3	Solar Cell Failure During FRUSA Testing	230
9-4	Solar Panel Support Concepts	233
9-5	FRUSA Stowage Drum Assembly - Weight Breakout	243
9-6	Two-Axis Orientation Drive Mechanism Weight	257

SECTION I  
INTRODUCTION

The Flexible Rolled-Up Solar Array (FRUSA) program addresses the need for a lightweight, low stowage volume, high power satellite power source for the mid-1970's and beyond. The need arises from the continued growth in payload capability and the attendant increases in spacecraft power requirements in the face of the ever-present spacecraft size and weight constraints. As power requirements increase to 1 kw and beyond, economics and launch vehicle constraints dictate the selection and use of deployable planar solar arrays which are actively oriented perpendicular to the incident sunlight. The FRUSA array concept, that of mounting the solar cells on a lightweight, Kapton-fiberglass substrate and stowing this flexible solar panel assembly on a drum in a manner similar to that used for a windowshade, was developed in satisfaction of this need through a progressive series of contracts sponsored by the Air Force Aero Propulsion Laboratory and conducted by Hughes as outlined below.

- An initial feasibility contract awarded in 1965 leading to successful qualification testing of a 500-watt model in 1967 (Flexible Integrated Solar Cell Array Program; FISCA)
- The design and development in 1967 of a two-axis orientation mechanism capable of orienting a 5-kw flexible array to within 10 degrees of the sun line (Orientation Linkage for Solar Cell Array; OLSCA)
- The design, development, qualification, and flight test of the Flexible Rolled-Up Solar Array system (FRUSA), a contract awarded in July 1968 and resulting in the successful flight of the FRUSA aboard a Thorad/Agena, with launch on 17 October 1971.

The FRUSA system, as reported herein, although necessarily detailed for compatibility with the launch vehicle and spacecraft employed in the flight test phase (Thorad/Agena) was designed and configured for the more general application to current and advanced planned Air Force missions. Design criteria, for example, vibration requirements, were shaped to represent worst case combinations of the environments resulting from Atlas, Titan or Thor boosters with Agena or Burner II class spacecraft. The 1.5-kw array configuration was further selected as an incremental building block or module for systems ranging up to the 20-kw power level. The program included, in fact, the generation of specific configurations and performance parameter data on flexible array systems from 0.5 to 20 kw.

This report, the final documentary report for the FRUSA program, encompasses all program activities leading to the successful flight test of the

FRUSA as well as the results of analysis and evaluation of design, qualification, and flight test data leading to specification of dynamic models, weight, stowage volume, and other characterizing parameters of interest to designers of the medium and large high powered spacecraft to which such a power system applies. The major program goals and results are presented in Table 1-1.

TABLE 1-1. FRUSA REQUIREMENTS AND GOALS

Item	Requirement	Goal	Status
Solar array weight*	-	35 lb/kw	46 lb/kw; goal achievable with lightweight cells
Solar array volume	-	2 ft <sup>3</sup> /kw	2.6 ft <sup>3</sup> /kw for 1.5-kw system
Power output	1.5 kw	Same	1.54 kw with full cell complement at BOL (130°F)
Array segment weight*	-	0.15 lb/ft <sup>2</sup>	0.192 lb/ft <sup>2</sup>
Orbital environment	0.1 g	Same	Design meets requirement
Extension/retraction cycles	10 flight	25 ground 10 flight	10 flight and 20 ground cycles completed on flight unit; 380 cycles on mechanism
Life	0.65 probability for 1 year	0.60 probability for 3 years for 5 kw system	Operational after 8 months
Compatibility	Thor, Agena, Titan III, Burner II, Atlas	Same	Verified by qualification and flight tests
Adaptability	From 0.5 to 20 kw	Same	Verified by analysis

\*Goals not achievable with cells which were economically acceptable for a flight test program.

## SECTION II

### SUMMARY

The program for development and test of the 1.5-kw Flexible Rolled-Up Solar Array (FRUSA) system was divided into five major phases:

- Program Definition
- Design Study and Analysis
- Manufacturing
- Qualification and Flight Acceptance
- Flight Test and Data Analysis

As shown in the program schedule, Figure 2-1, all program phases are complete with the exception of the flight test phase, which has been extended to 15 October 1972 to enable another experiment onboard the STP 71-2 spacecraft to provide additional data. The FRUSA, although its flight test was successfully completed on 17 April 1972, is necessary as a power source for the extended STP 71-2 mission and is performing well in this capacity.

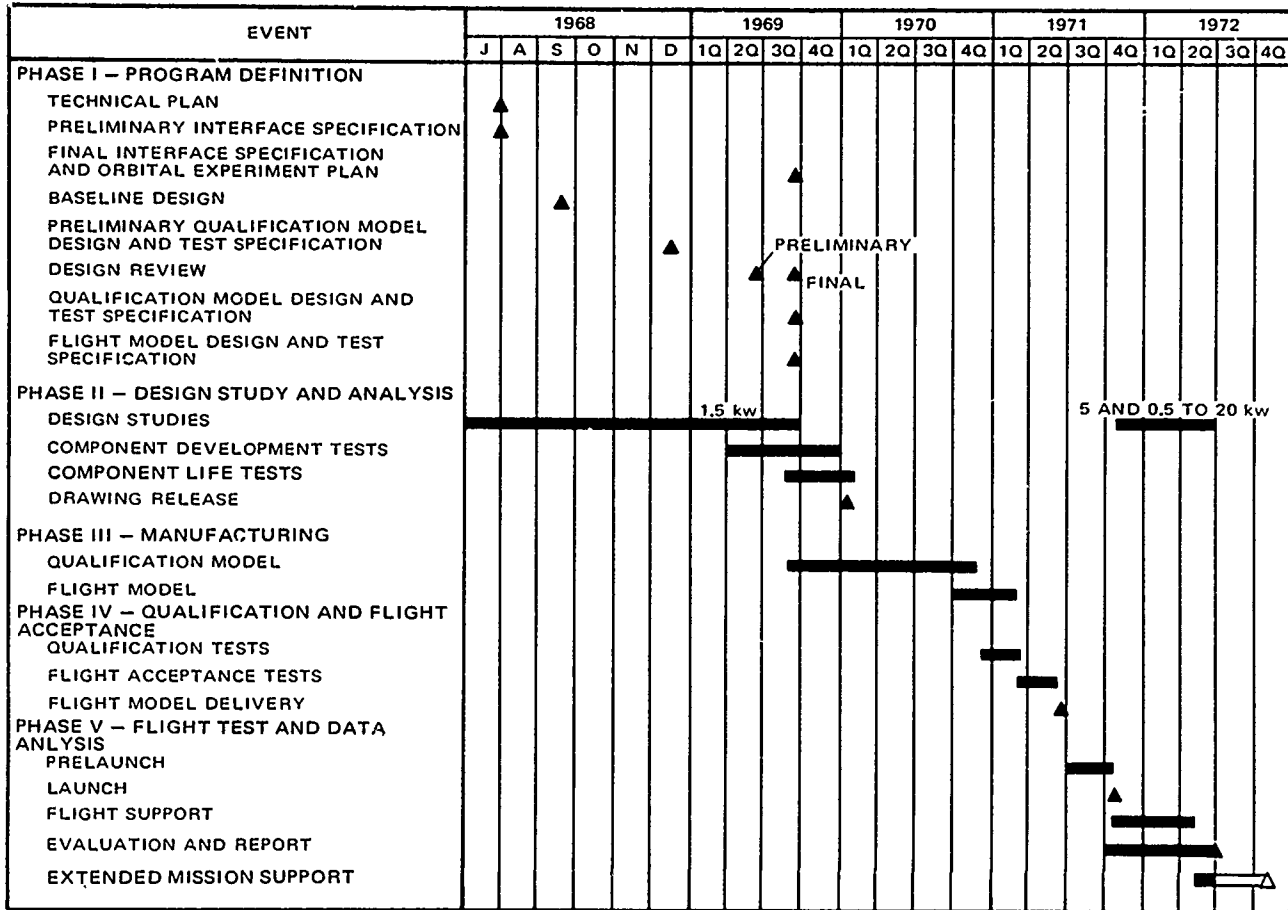
#### PROGRAM DEFINITION

The program definition phase consisted of program planning, preliminary design, and specification development activities necessary to define the baseline system configuration and interface requirements in sufficient detail for development of the individual unit designs and for use by the booster/spacecraft/payload integration contractor (LMSC was selected by the SAMSO STP office for this task). This phase was originally scheduled to last 2 months, but was reprogrammed and actually lasted 12 months, concluding with issuance of qualification model, flight model, and Agena/FRUSA interface specifications in mid-1969. The reprogramming resulted from delays in the selection of the integration contractor and, other than time and cost, had little effect on the evolution of the FRUSA program.

#### DESIGN STUDY AND ANALYSIS

This phase was initiated concurrently with the program definition phase to enable the development of a more comprehensive baseline design and thus to provide a well defined configuration for ease of vehicle integration. As described in detail in Section IV, many component and subassembly tradeoff analyses and tests were run in this phase, allowing full confidence in the baseline design for the actual development. Items included in these





20338-215(U)

Figure 2-1. Program Schedule

evaluations were ac-dc boom actuator drive motors, single-multiple array motors, brush-brushless orientation mechanism drive, component-unit-no redundancy for the control electronics units, flexible cable-sliprings for the solar array to stowage drum interface, solar array cushion configuration, panel aspect ratio, bearing types, orientation mechanism torquer size, battery size and charge rate, and others. The intent was to evaluate all of the building blocks of the final design that could be evaluated without unduly freezing the interface configuration prior to the SAMSO selection of an integration contractor. With selection of the integration contractor, LMSC, in mid-1969, these a priori tradeoffs enabled a rapid and efficient progression into detail design and drafting functions.

A large number of component development and life tests were also conducted at the part or subassembly level. Included in this test phase were tests such as temperature cycling of the drum/Negator <sup>®</sup> /bearing assembly, and of solar cell/substrate coupons and multiple extensions and retractions of the boom actuator unit used to extend and retract the solar array assembly. As a complement to the FRUSA testing, NASA/Lewis conducted 2100 thermal cycles (+189° to -163°F) tests on FRUSA cell modules without degradation. With the confidence built by these tests, it was decided to forego the fabrication and test of a full development model and to proceed directly to the release of drawings for the qualification and flight units, which occurred in January 1970.

Also included in this phase were the conduct of design studies and analyses of flexible array power systems ranging in size from 0.5 to 20 kw. These studies were initiated after the initial flight test activities and are concluding with this report. This timing allowed the assimilation of all development, qualification, and flight test experience into the selection of alternate configurations and into the estimates of weight, power, and other performance characteristics.

## MANUFACTURING

Although there were a number of new processes, handling fixtures, and tooling which had to be developed to fabricate the novel flexible array panels, the fabrication effort proved to be a relatively straightforward activity. Of particular interest with respect to this development were the water table and test fixtures used to deploy the array in an earth gravity field (see SYSTEM TEST SECTION). The solar array assembly, being designed for a 0.1-g environment, could not support the solar panel weight in an earth gravity field. One of the solutions developed was to float the panels on multiple floats in a 2-inch deep water table as the panels were extending. Alternately, booms were decoupled from the panels and drum fixtures were used to roll out the panels for such activities as solar cell assembly and inspection.

## QUALIFICATION AND FLIGHT ACCEPTANCE

Upon completion of the assembly operations, qualification tests, followed by flight acceptance tests, were conducted. During the qualification tests, the principal problems encountered that were unique to the flexible array concept were the occurrence of a control loop instability when the array was on one side of the Agena spacecraft and the susceptibility of the system to EMI/EMC effects. While the EMI and EMC problem was resolved by the addition of appropriate filters and chokes to sensitive or noisy circuits, this kind of problem bears close examination on future large array designs because of the unusual degree of exposure of the bus-bars and the extensive bus-bar lengths on solar array panels of the FRUSA size. The control loop instability problem was eliminated by adding a position resolver and logic to the spacecraft and to the FRUSA, which forced lockon to occur on the side of the spacecraft where the FRUSA was stable.

The qualification tests and, later, the flight acceptance tests were considered to be relatively free from anomalies for units of the size and complexities of the FRUSA units. The water table proved to be an excellent choice for extension and retraction tests of the solar array assembly, introducing little load or drag into the extension/retraction evaluations of panel and boom actuator performance or into the preflight tensioning operation. The vulnerability of the solar assembly to vibration, an early-program concern, proved to be of negligible importance as an issue. A check of the flight unit solar cells just prior to shipment revealed that the cells which had been damaged as a result of all assembly and test operations after the initial assembly of the cells onto the solar panels amounted to less than 0.15 percent of the total, or 52 defects out of 34,500 solar cells. Of the suspect cells, 28 were replaced, although most of the replacements were made because of conservatism rather than need.

With successful completion of flight acceptance testing, the flight model was delivered to LMSC in July, 1971 for vehicle integration.

## FLIGHT TEST AND DATA ANALYSIS

During the system integration and prelaunch testing the only significant event was the retrofit of a new installation for the solar array isolation diodes on the array drum. A late thermal analysis indicated that the diodes would overheat in their original location when the array was supplying its rated output of 1500 watts. As a result of this analysis, the diodes were relocated from the storage drum interior to the outboard end of the drum assembly so that a full view of deep space was provided, thus enabling adequate cooling.

Orbital operations subsequent to the 17 October launch were successful, with full operation of the FRUSA system being attained on orbit 10. In orbit 80, however, it was noted that the support axis was oscillating over a few degrees range and offset about 20 degrees behind the sun. While the

anomalous tracking behavior had little effect on the Agena or FRUSA performance, the automatic tracking mode was disabled and command positioning of the array was substituted pending full investigation of the phenomenon. Fortunately, sufficient power was available to support the spacecraft bus and all functions of the FRUSA experiment. Prior to this incident, power output of the panel was 1460 watts and the vehicle and FRUSA were stable during normal acquisition and tracking modes. There were no significant panel motions when the parent spacecraft was in either active gas or gravity gradient control modes, or during the ten retraction and extension cycles that were conducted late in January 1972.

Subsequent to the control loop anomaly, orbital operations consisted of occasional command positioning of the solar array about the longitudinal axis of the Agena and the acquisition of solar panel and cell module data. In February, the sun tracking mode was initiated and functioned properly. As a result, the normal control electronics modes were used for array positioning for all operations for the rest of the flight. Other flight data also were nominal. Of particular interest was the solar array power performance, which decreased to 1200 watts. Since this reduction was a predictable result of space radiation and increasing panel temperatures, at lower sun/orbit angles, it was concluded that damage from other launch and flight environments or from the ten retraction/extension cycles was negligible.

The flight test phase was concluded on 17 April 1972. Sufficient data were obtained to validate the flexible array concept and to develop models of major parameters for future applications of larger flexible solar arrays. As noted in Figure 2-1, however, the STP 71-2 mission has been extended to 17 October to enable acquisition of additional data on the spacecraft and additional flight test data from another experiment. For full support of these additional data requirements, the FRUSA operation has been sustained and is performing well as a spacecraft power source with about a 1200 watt capacity as of the date of this report.

## SECTION III

### SYSTEM DESCRIPTION

The Flexible Rolled-Up Solar Array (FRUSA) system is a 1.5 kw self-contained power system. It consists of 1) a pair of drum-mounted 16 by 5.5 foot extendable/retractable flexible solar cell arrays to provide primary power, 2) an orientation mechanism and control subsystem to maintain the array in a sun-pointing attitude, 3) a power conditioning and storage subsystem that provides the required regulated ac and dc voltages, controls battery charging and supplies housekeeping power prior to panel deployment and during eclipse periods, and 4) the instrumentation to monitor structural, thermal, and system performance. The system block diagram is shown in Figure 3-1, and an artist's concept of the deployed array on a three-axis stabilized spacecraft is shown in Figure 3-2.

### MAJOR SYSTEM DESIGN REQUIREMENTS AND GOALS

The purpose of the experiment was to prove the feasibility of providing large amounts of power (500 to 20,000 watts) for an extended period of time (greater than 1 year) while maintaining the capability of repeated (more than ten) extensions and retractions of the solar cell array. The flight model was to be capable of providing 1500 watts of electrical power from a roll-up solar array at the beginning of synchronous orbital flight (array temperature 130°F). No electrical power was to be required from the spacecraft, since the FRUSA was to be self-contained, except for the downlink telemetry and command receivers.

In a more specific form, the system and subsystem requirements were as follows:

#### System

- The design was to stress maximum reliability, low weight, low stowed volume, and long life potential.
- The design would be sufficiently general to cover a wide range of orbits and spacecraft
- The flight design would be capable of withstanding 0.1-g loading in the deployed or operational configuration.
- The flight design would be capable of producing 1.5 kw of power at the array/vehicle interface at the beginning of flight for a synchronous orbit
- The experiment would be designed for a mission lifetime of 12 months, with a capability of 3 years as demonstrated by ground testing and analysis.

20338-42(U)

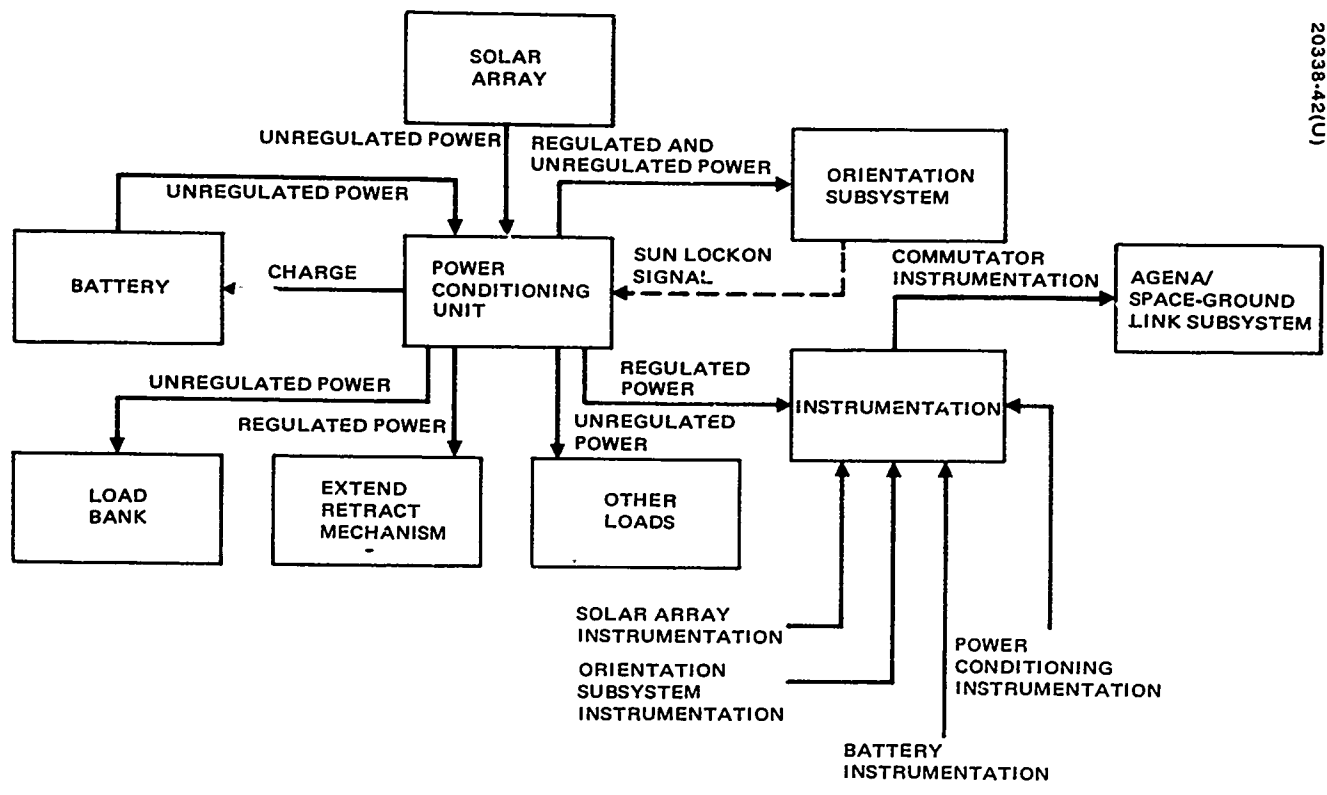
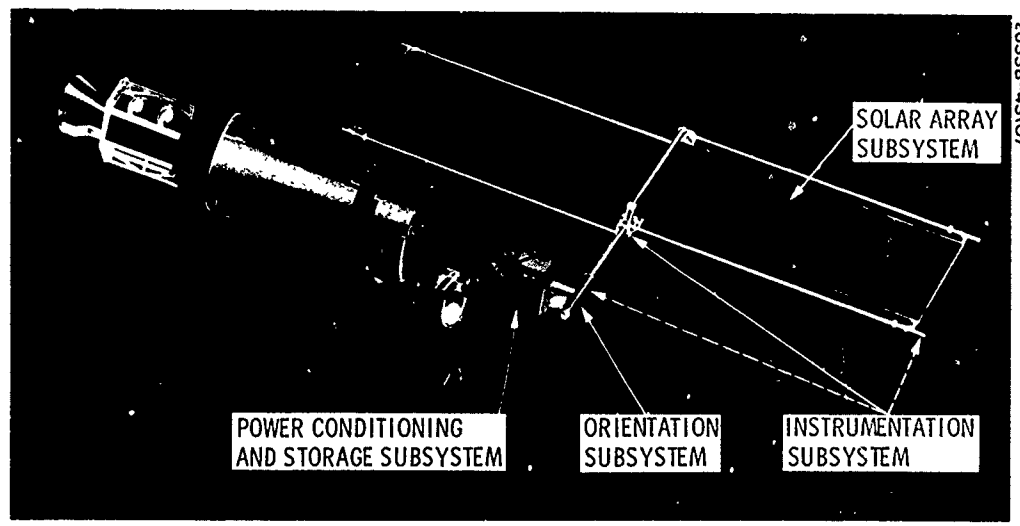


Figure 3-1. System Functional Block Diagram



20338-43(U)

Figure 3-2. FRUSA System Shown on Agena Spacecraft

- The flight experiment would be conducted on a mission vehicle of Agena or Burner II configuration with an Atlas, Thor, or Titan IIC booster (as an environmental specification).
- The experiment had to be self-contained and depend on the vehicle for telemetry and command only.
- The reliability goal for the experiment was to provide data which would illustrate a probability of 0.60 for successfully completing a 3 year mission at synchronous orbit altitude for an end-of-mission power requirement of 5 kw.
- The maintainability goal for the program was to achieve mean and maximum times to repair or replace individual solar cell modules of 4 days and 14 days, respectively.

#### Solar Array Subsystem Requirements

- The solar array assemblies should have a maximum storage volume of 2 ft<sup>3</sup>/kw, not including deployment and mounting hardware (a goal).
- The weight of the qualification test model and the flight model should be 35 lb/kw, not including the orientation subsystem or electrical components associated with experiment monitoring or energy storage (a goal).
- The 1.5-kw flight experiment was to be capable of a minimum of ten deployment/retraction cycles in space.
- An array deployment/retraction capability of a minimum of 35 cycles was to be demonstrated (a goal).

#### Solar Panel Assembly

- The solar panel assembly would be designed to provide a power output of 1.5 kw plus losses in transmission between cell collector buses and mission vehicle interface.
- The panels would have a solar cell area utilization factor of 95 percent (a goal).
- The array segment weight should not exceed 0.15 lb/ft<sup>2</sup> (a goal).
- The models would utilize standard (8-to 16-mil) 2 x 2 cm solar cells with 6-mil coverslides.
- The solar array for the qualification model would be 10 percent covered with live 2 x 2 cm solar cells with 6-mil glass cover slides, sufficient to establish satisfactory electrical behavior.

The remaining area would be covered with simulated solar cell masses.

- The flight models would be completely covered with standard 2 x 2 cm solar cells with 6-mil coverslides.
- Provisions for repair and replacement of array segments would be included in the detail design.

#### Orientation Subsystem

- The orientation concept would be compatible with an earth oriented mission vehicle.
- The design would be sufficiently general to cover a wide range of orbits.
- Two axes of orientation capable of  $\pm 10$  degree pointing accuracy would be provided.
- Rotational capability for each axis would be unlimited.
- Power transfer would be accomplished by using sliprings, flexible cables, or other flight proven means.
- The design would not restrict the attitude of the vehicle in orbit.
- Mutual shadowing of arrays and vehicle would be avoided.

#### Power Conditioning and Storage Subsystem

- All power regulation and control required by the experiment would be supplied as part of the FRUSA system.
- Experiment housekeeping power required for eclipse operation would be provided as part of the FRUSA system.
- A 3-year life potential would be demonstrated through component and functional life testing.

#### Instrumentation Subsystem

- Instrumentation would be provided throughout the system at a sufficient number of points, and of such type, as to enable the determination of system electrical, structural, and thermal operating conditions throughout the life of the mission.
- The only data conditioning and formatting to be provided would be that required by the specific design of the FRUSA system. Conditioning and formatting for compatibility with the launch vehicle were to be mutually worked with the integration contractor.



## DESIGN DESCRIPTION

### Solar Array Subsystem

The solar array subsystem (Figure 3-3) consists of two principal units: drum mechanism and solar arrays. Included in the drum mechanism are the storage drum, extendable boom actuator unit, cushion take-up roller, Negator<sup>®</sup> drum drive mechanism, flexible cable assemblies, and boom length compensator devices with spreader bar. The solar array consists of solar cells, substrate, bus bars, cell interconnects, and array cushion. Also mounted on the subsystem are the orientation sun sensors, accelerometers, strain gage, reference cells, and modules.

### Orientation Subsystem

The orientation subsystem maintains the array in a sun-pointing attitude. It is installed so that the array can maintain two degrees of freedom without shading or colliding with the spacecraft, yet keeping the mechanism simple. Figure 3-4 illustrates the internal profile of the orientation mechanism.

The orientation mechanism comprises a two-axis gimbal system supported in opposed, angular-contact, spring-loaded, dry-lubricated ball bearings. Torquing of each axis is accomplished by a frameless, gearless, magnetically coupled dc torque motor installed with stator and rotor integral with housing and shaft, respectively. Rate sensing and control are accomplished by means of similar units operating as generators rather than motors.

Slip rings transfer the electrical power from the solar array drum to the spacecraft and transfer control and instrumentation signals. They are required because of the continuous (360 degrees) rotation capability of the orientation mechanism in both the drum and support axis. The rings used on the mechanism are cylindrical, polished coin silver, and the brushes are dry, self-lubricated, compacted Ag/MoS<sub>2</sub>/Cu. The control electronics unit (CEU) attached to the orientation mechanism provides the logic and analog computations for the various modes of operation. It derives error signals from commands, sun sensors, and shaft rate sensors, and applies correctional signals to the appropriate torque motor. It limits the torquing rate in the sun search and acquisition mode using the rate sensor signals. Logic control is provided by processing sun sensor data and command inputs.

### Power Conditioning and Storage Subsystem

The power conditioning and storage subsystem conditions the solar array power for the FRUSA system. It also contains two 6-amp-hr batteries which provide power to the experiment during eclipse operation or when the panels are retracted. The subsystem consists of the power conditioning unit (PCU), the load bank assembly, and two battery/charge controller assemblies.

20338-4(U)

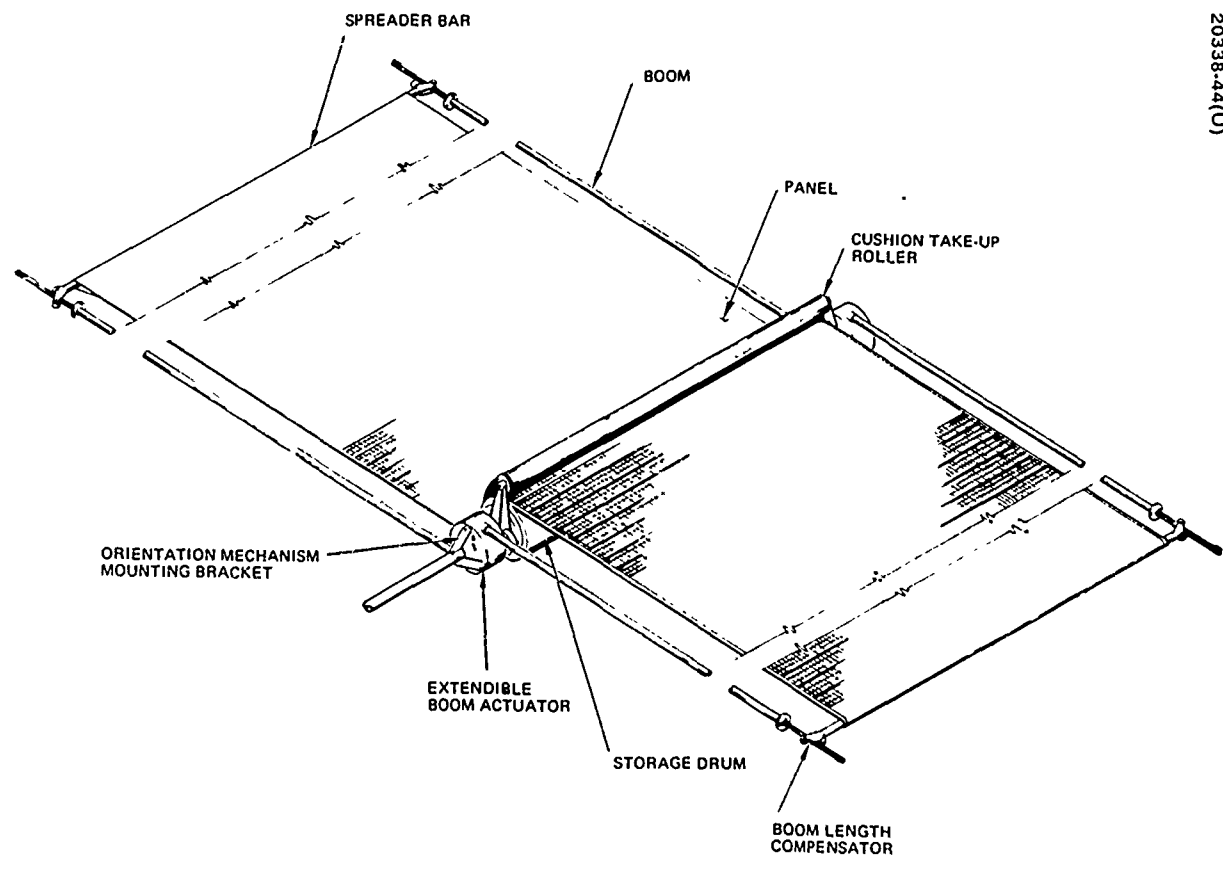


Figure 3-3. Solar Array Subsystem

20338-45(U)

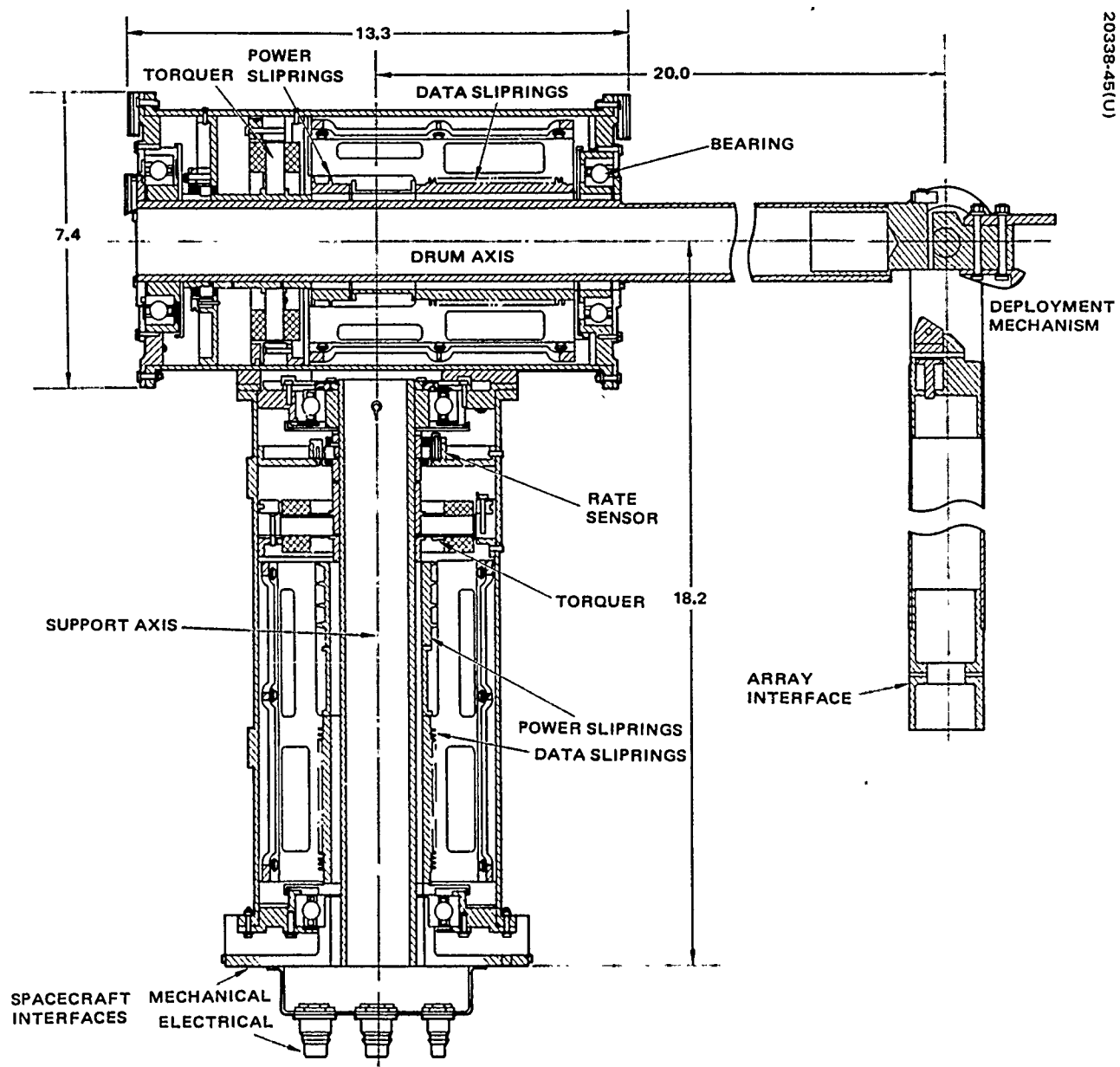


Figure 3-4. Orientation Mechanism Internal Profile

The load bank assembly contains the four resistors necessary to allow measurement of and to dissipate the electrical power generated by the solar array in the process of measuring the solar array capability.

### Instrumentation Subsystem

A PCM compatible instrumentation system was designed for the flexible rolled-up solar array. Current, voltage, temperature, accelerometer, and strain gage measurement sensors were employed.

Periodically during the flight, the main panels are disconnected from the bus and the power is fed directly into the load bank. The load bank of four resistors is switched across the array in sequence so that 16 points on an I-V curve are obtained.

Each panel has a module of 7.2- and 12-mil thick 2 x 2 cm solar cells, as well as two 12-mil cells and two 7.2-mil cells with 6-mil coverslides and two 12-mil cells with 2-mil coverglasses. One of the 7.2-mil cells is pre-irradiated. These cells and modules have four load resistors sequenced across them and 8 points measured so that I-V curves can be constructed that are then compared to the main panel I-V curve.

Accelerometer and strain gage data were taken to analyze the dynamic characteristics of the flexible panels and measure boom deflection. The location of the principal accelerometers, strain gages, and cell groups of the instrumentation subsystem is shown in Figures 3-5 and 3-6.

### AGE

The FRUSA AGE equipment was designed to test the FRUSA system and subsystems with the aid of auxiliary standard equipment such as oscilloscopes, power supplies, and digital voltmeters. All system tests were conducted using telemetry signals to determine basic system performance. The AGE was designed with command and decommutation capability.

The mechanical support AGE consisted of a low friction water table test bed to support the solar array panels during extension and retraction tests. A second test fixture was designed to simulate the mounting of the solar array and orientation mechanism on the spacecraft and verify drum deployment. The water table test position and the deployment test setup are illustrated in Figures 3-7 and 3-8.

20338-46(U)

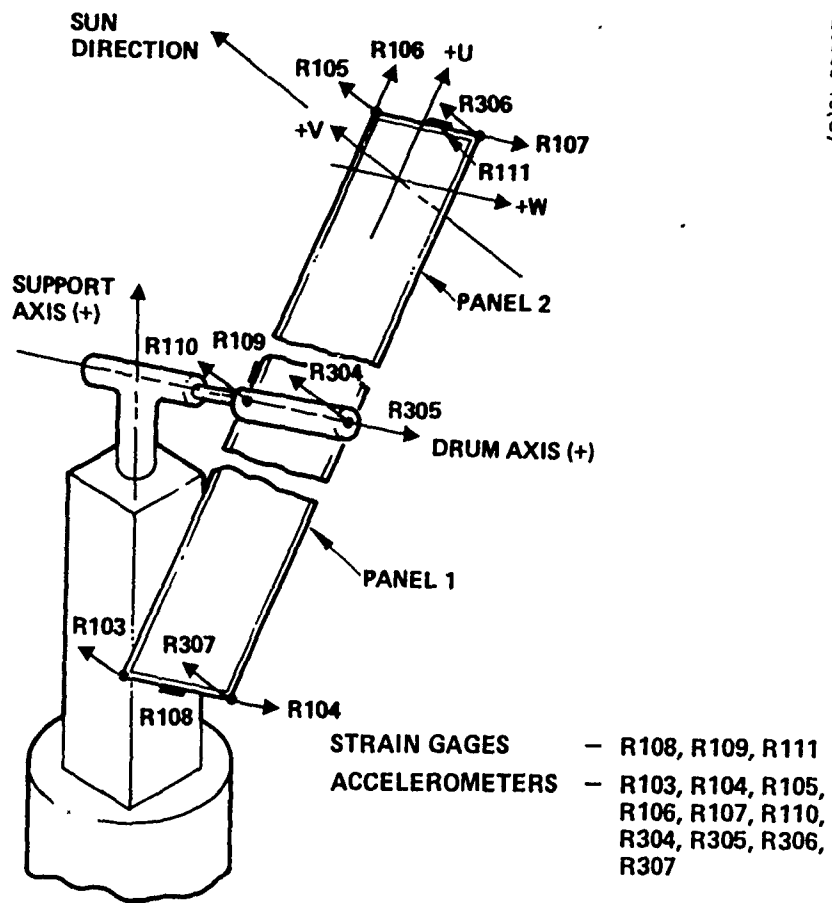


Figure 3-5. Strain Gage and Accelerometer Installation

20338-47(U)

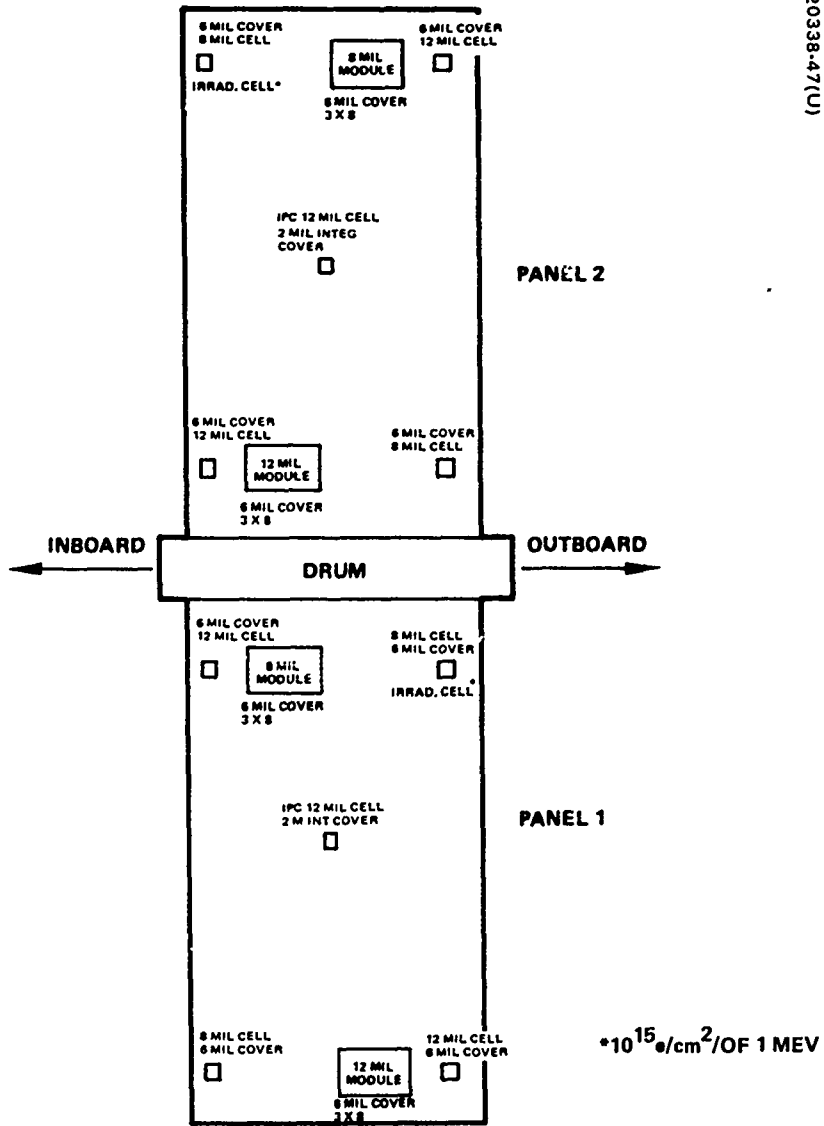


Figure 3-6. Location of Reference Cells and Modules

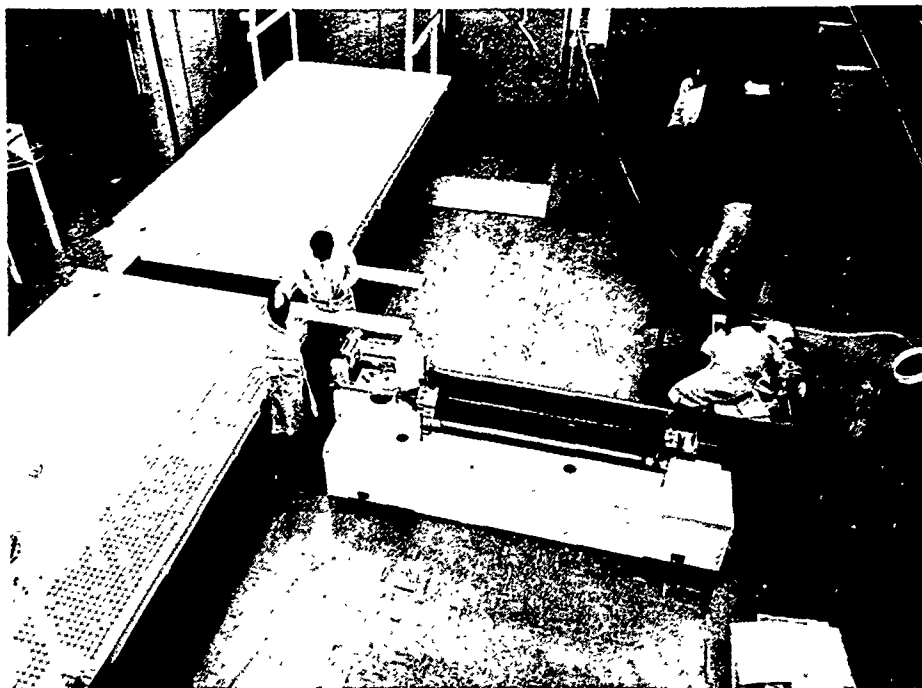


Figure 3-7. Deployment Test Setup (Photo A30381)

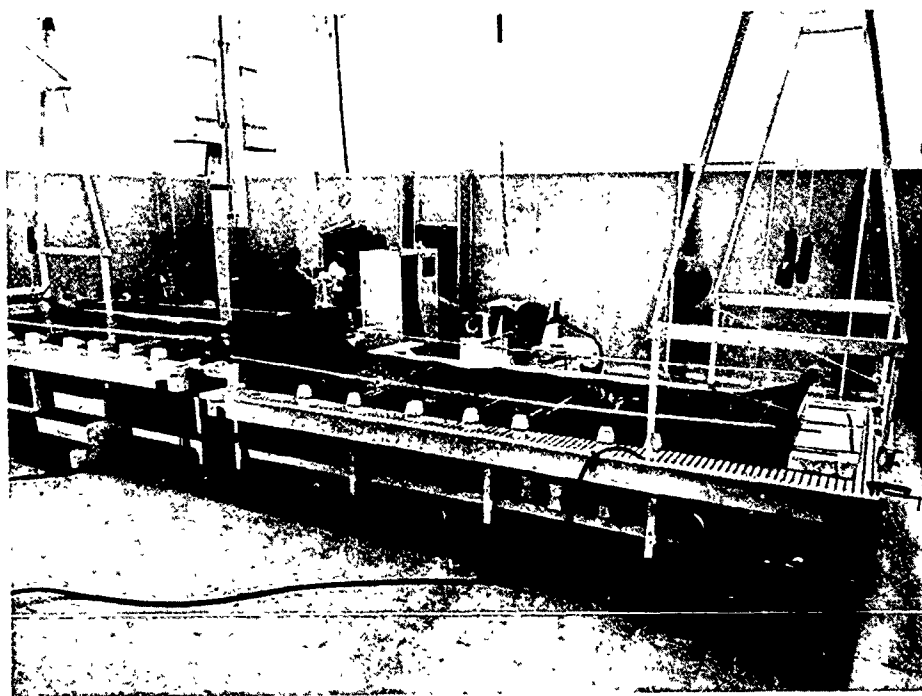


Figure 3-8. Flight Model Solar Array on Water Table (Photo A31412)

SECTION IV  
DESIGN AND DEVELOPMENT

SOLAR ARRAY SUBSYSTEM

Subsystem Requirements and Description

The solar array subsystem consists of a storage drum mechanism with two flexible solar cell arrays (see Figure 4-1). The flexible arrays were wound on the storage drum during the launch environment and deployed after the vehicle attained orbit. Deployment was accomplished by means of boom assemblies mounted on the storage drum structure. Ten retraction and extension cycles were required in orbit with an additional 25 during ground test. Other key requirements of the subsystem are presented in Table 4-1.

Drum Mechanism

Requirements and Description

The drum mechanism was required to perform the following functions:

- Store the solar arrays during the launch phase of the mission and during any retracted mode of operation
- Extend and retract the solar array panels in orbit
- Provide equal tension across the width of the panel during extension/retraction and during fully extended operation
- Transfer electrical power between the solar panels and the spacecraft

The major elements of the drum mechanism (see Figure 4-2) are as follows:

- Extendible boom actuator unit
- Boom length compensator mechanism
- Storage drum assembly
- Panel tension drive
- Panel cushion take-up drive
- Power and data transfer assemblies



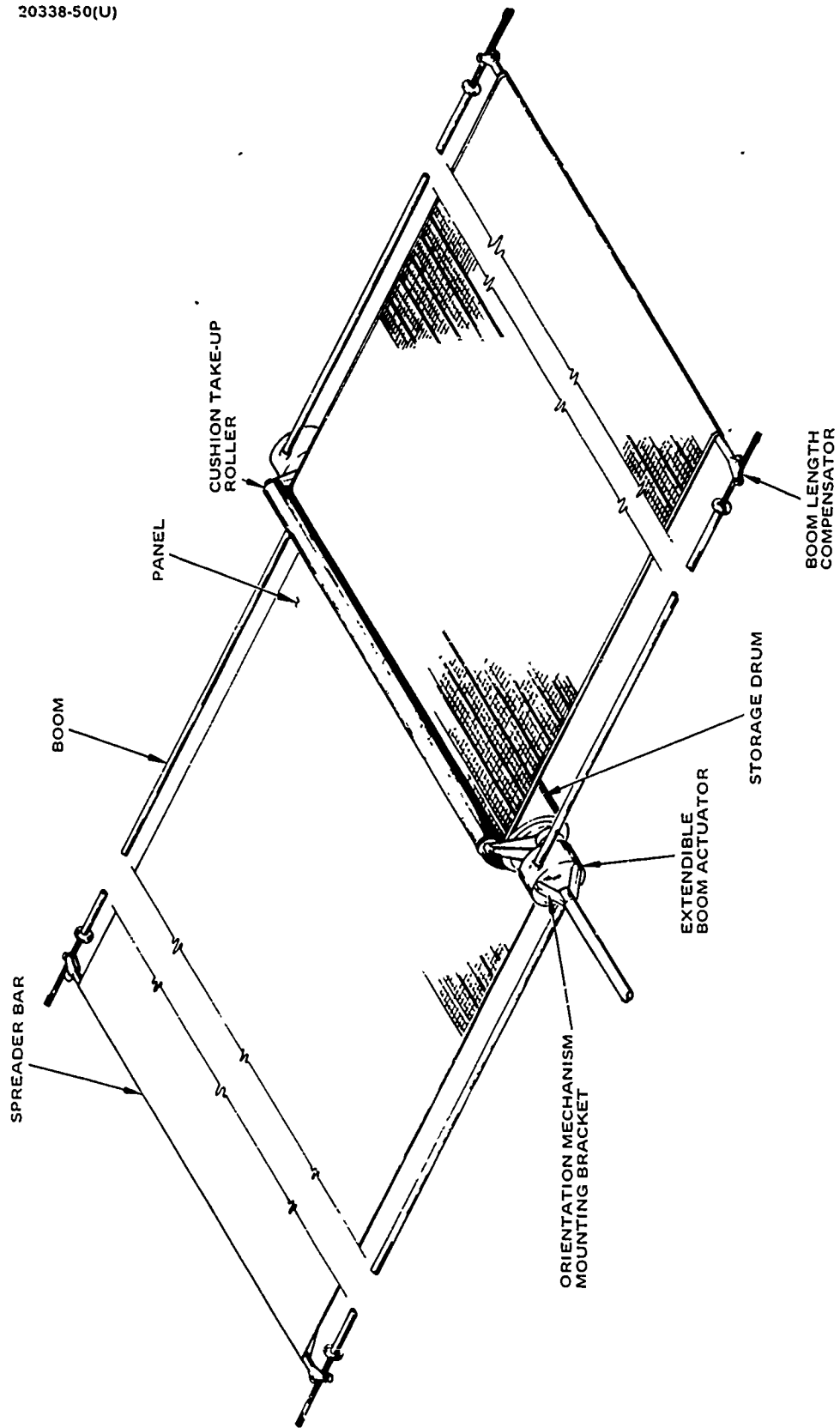


Figure 4-1. Solar Array Subsystem

TABLE 4-1. SOLAR ARRAY SUBSYSTEM REQUIREMENTS AND GOALS

Item	Requirement	Goal	Flight Unit Status
Weight	-	35 lb/kw*	46 lb/kw
Volume	-	2 ft <sup>3</sup> /kw	2.6 ft <sup>3</sup> /kw for 1.5 kw
Power**	1.5 kw	-	1.54 kw with full complement of cells at BOL (130°F)
Cells	8 mils thick, 2 x 2 cm with 6-mil coverslides	-	7.2 mils with 6-mil coverslides
Array segment weight	-	0.15 lb/ft <sup>2</sup> *	0.192 lb/ft <sup>2</sup>
Orbital environment	0.1 g	-	Designed for 0.1-g quasi-static loading
Life	1 year	5 years	Operational after 8 months
Area array utilization factor	-	95 percent	93.5 percent
Extension-retraction cycles	10 flight	25 ground 10 flight	10 in-flight cycles completed

\*Goal not possible for 1.5-kw system with 8-mil cells and 6-mil covers.

\*\*At interface with Agena.

20338-51(U)

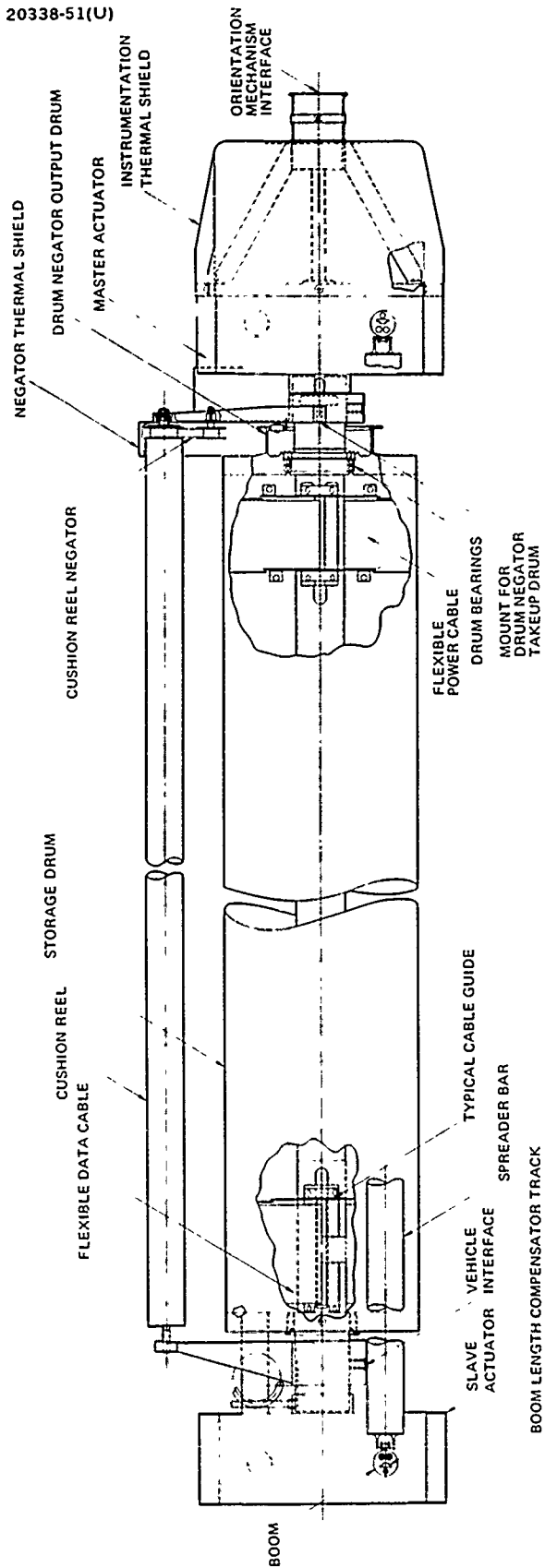


Figure 4-2. Drum Mechanism Details

Extendible Boom Actuator Unit. The boom actuator unit shown in Figure 4-3 with a shortened torque tube was built by SPAR, Toronto, Canada. It is a completely dry lubricated device consisting of the following items:

- 1) Two actuators that store and form the 0.86-inch diameter stainless steel Bi-Stem<sup>®</sup> booms
- 2) A single 115-volt ac, 400-Hz motor/gearhead to extend/retract booms
- 3) An interconnecting torque tube between master and slave units to allow for a single motor drive unit

Each of the four booms is approximately 16 feet long and deploys at a rate of about 1/2 ips. Micro-switches are employed to indicate full extension or retraction. A strain gage installation is built into one of the boom guidance assemblies to measure boom bending.

Boom Length Compensator Mechanism. This mechanism (Figure 4-4) was used to ensure uniform tension on the solar panels in the event of uneven extension/retraction of the individual booms. Such unevenness can develop for the following reasons:

- 1) The extension rates of the individual booms are different because of lost motion and friction within the actuator.
- 2) Each of the two panels extends to a different length because of the dual-panel/single drum design.

Although the latter problem can be partially resolved by using different length booms on each side of the drum, exact compensation is difficult because of the unknown effective thicknesses of the panel and cushion. The lost motion and friction problem within the cassettes could be corrected by sprocket drives, servo systems, etc. Since these approaches all involve complex modifications to existing flight-proven boom designs, the decision was made to compensate for the differences in boom lengths by hardware on the boom tips.

The mechanism design uses dry lubricated ball bearings in pulleys and rollers. A cobalt alloy (Elgiloy or Havar) tape is used between the boom tips. Calibrated strain gages on the tape provide a direct readout of tension in the solar panels.

Storage Drum Assembly. An 8-inch diameter, 70-inch long thin wall magnesium cylinder was used for the storage drum. The end plates (see

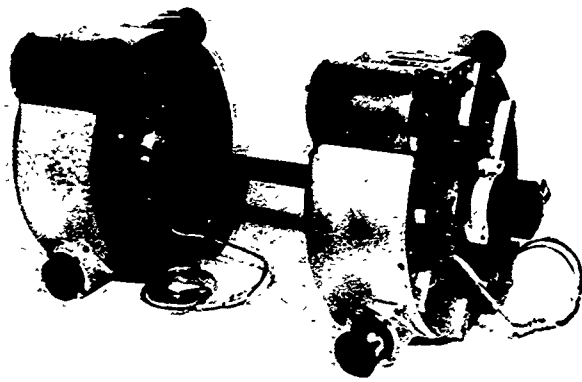
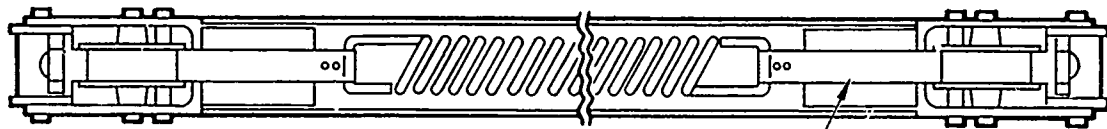


Figure 4-3. Extendible Boom Actuator  
(Photo 20338-52)



20338-53(U)

STAINLESS STEEL TAPE  
(WITH STRAIN GAGES)

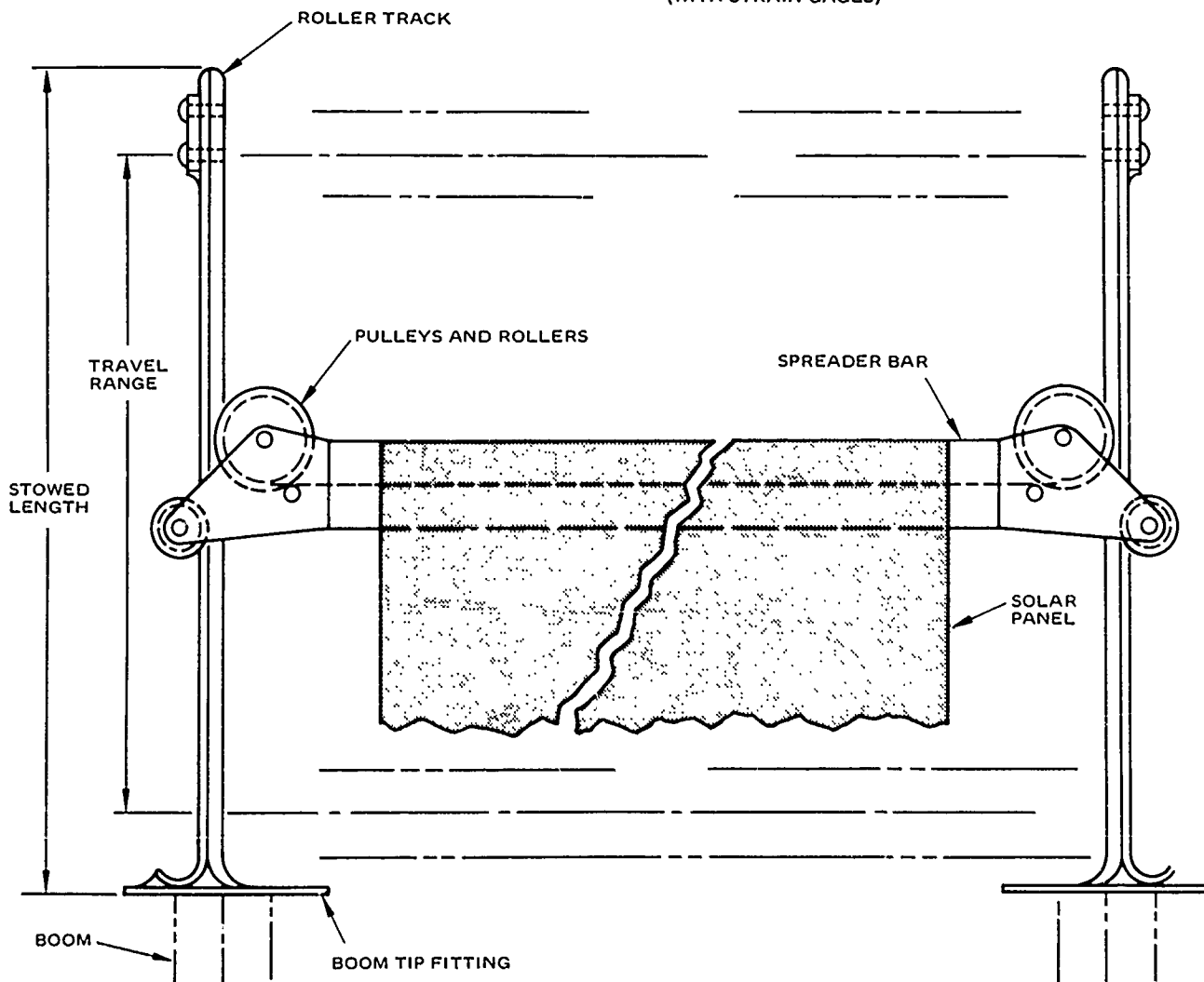


Figure 4-4. Boom Length Compensator

Figure 4-5) are a titanium/aluminum honeycomb structure. The bearings used in the storage drum have the following characteristics:

Type	Angular contact
Material	440C stainless steel
Bore	2.3122/2.3125
Lubrication	Burnished MoS <sub>2</sub> plus Duroid 5813 retainer
Preload	8 to 12 pounds

The installation shown in Figure 4-5 was designed to provide low torque operation over the expected temperature ranges, with temperature differentials between housing/shaft and inboard/outboard bearing pairs. Axial differential expansion is accommodated by allowing one pair of bearings complete axial freedom. In the case of differential temperatures between the inner and outer races of particular pairs, a combination of wavy washer springs and matched materials for housing, shaft, and bearings was used.

Panel Tension Drive. A constant torque Negator <sup>®</sup> spring drive was used to provide tension on the panels during extension and retraction. The Negator <sup>®</sup> spring is a coiled stainless steel band wound on spools to produce a torque essentially constant over the entire travel range. The tape had to be modified by contouring because of the changing radii in the drum and Negator <sup>®</sup> spools. The contouring consisted of varying the tape width with length to produce a slightly negative spring constant. Total two-panel tension provided by this drive arrangement over the entire travel and temperature range was 10 ±2.5 pounds.

Panel Cushion Take-up Drive. The cushion required to protect the solar cells in the stowed condition, particularly during launch, was embossed Kapton. The function of the cushion take-up is to roll up and store the cushion when the panels are deployed and to deploy the cushion between the two panels during the retraction cycle. The cushion tension provided by this drive is between 1 and 2-1/2 pounds.

The system chosen for this task was a Negator <sup>®</sup> motor drive operating directly on the take-up reel, independently of the storage drum. As in the case of the panel tension drive, this motor is a coiled metal band wound on spools to produce a torque essentially constant over the entire travel range.

Power and Data Transfer Assemblies. Transfer of power and data signals within the storage drum is accomplished by means of flexible flat cables. These cables employ copper conductors with 1 mil Kapton insulation. Transition to conventional round wires is made at the hub of the drum to allow use of conventional connectors at the spacecraft interface. For the power cables, a printed circuit board was used as an interface with the panel wiring

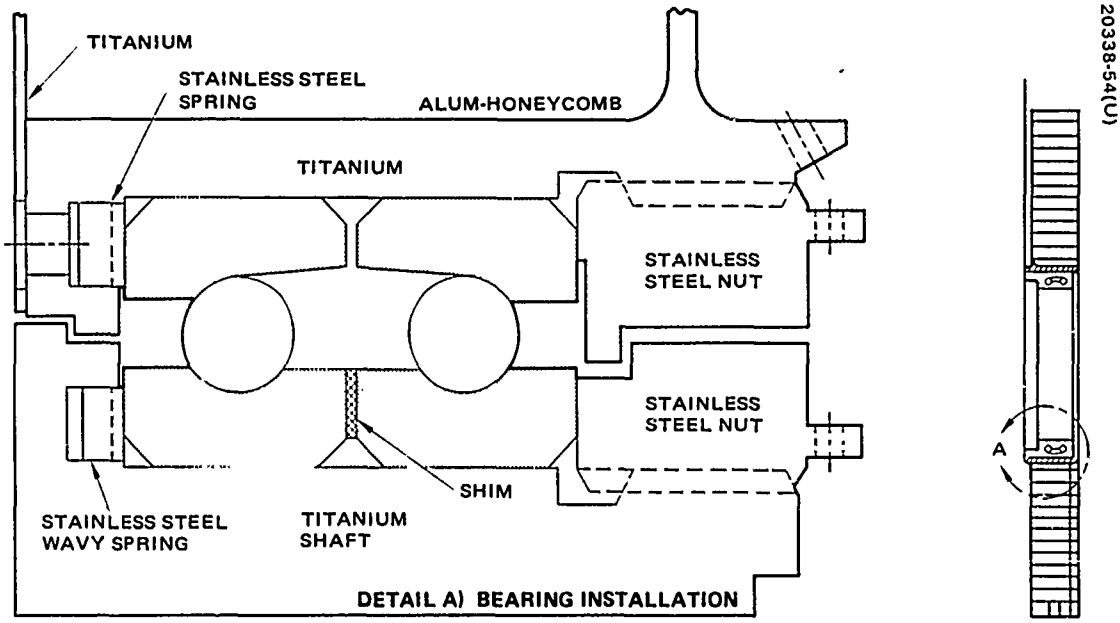


Figure 4-5. Drum End Plate and Bearing Installation

bus (see Figure 4-6). The data cable at the opposite end of the drum was soldered directly to the flat solar panel conductors. The cables are wound up on the center spar of the drum when the panels are fully retracted. As the panels extend, the cables unwind, then rewind in the opposite direction. This feature permits shorter cable lengths and therefore, lower power losses.

#### Drum Mechanism Tradeoff Analyses

The significant tradeoff analyses performed to establish the drum mechanism design involved the following areas:

- Boom diameter
- Single versus dual actuator motor
- AC versus dc actuator drive motor
- Boom length compensator
- Cushion take-up drive
- Slipping versus flexible cables
- Storage drum and end plates

Boom Diameter' Study. The analysis to determine the boom diameter considered the panel mass properties and dimensions as well as the orbital maneuvers of the spacecraft specified to impose a maximum load of 0.1 g. The analysis concluded that two 0.86-inch diameter booms constructed of 5-mil thick stainless steel (instead of 0.75-inch diameter, as originally proposed) were required to support the 16-by 5.6-foot panels. Booms of this type have ample strength and stiffness to satisfy the requirements. In addition, this choice produces the following important design margins and parameters:

- 1) Column buckling load of 9 pounds, which allows 5 pounds panel tension
- 2) Boom tip deflection of approximately 3 feet, under a 0.1-g acceleration normal to the plane of the array
- 3) Boom bending moment of 12 ft-lb at boom root (allowable is 27 ft-lb)
- 4) Fundamental bending frequency of deployed panel of approximately 0.20 cps
- 5) Boom tip deflections of 2.8 and 3.3 inches in response to specified rotational control maneuvers of Agena orbital vehicle and Orientation Mechanism, respectively



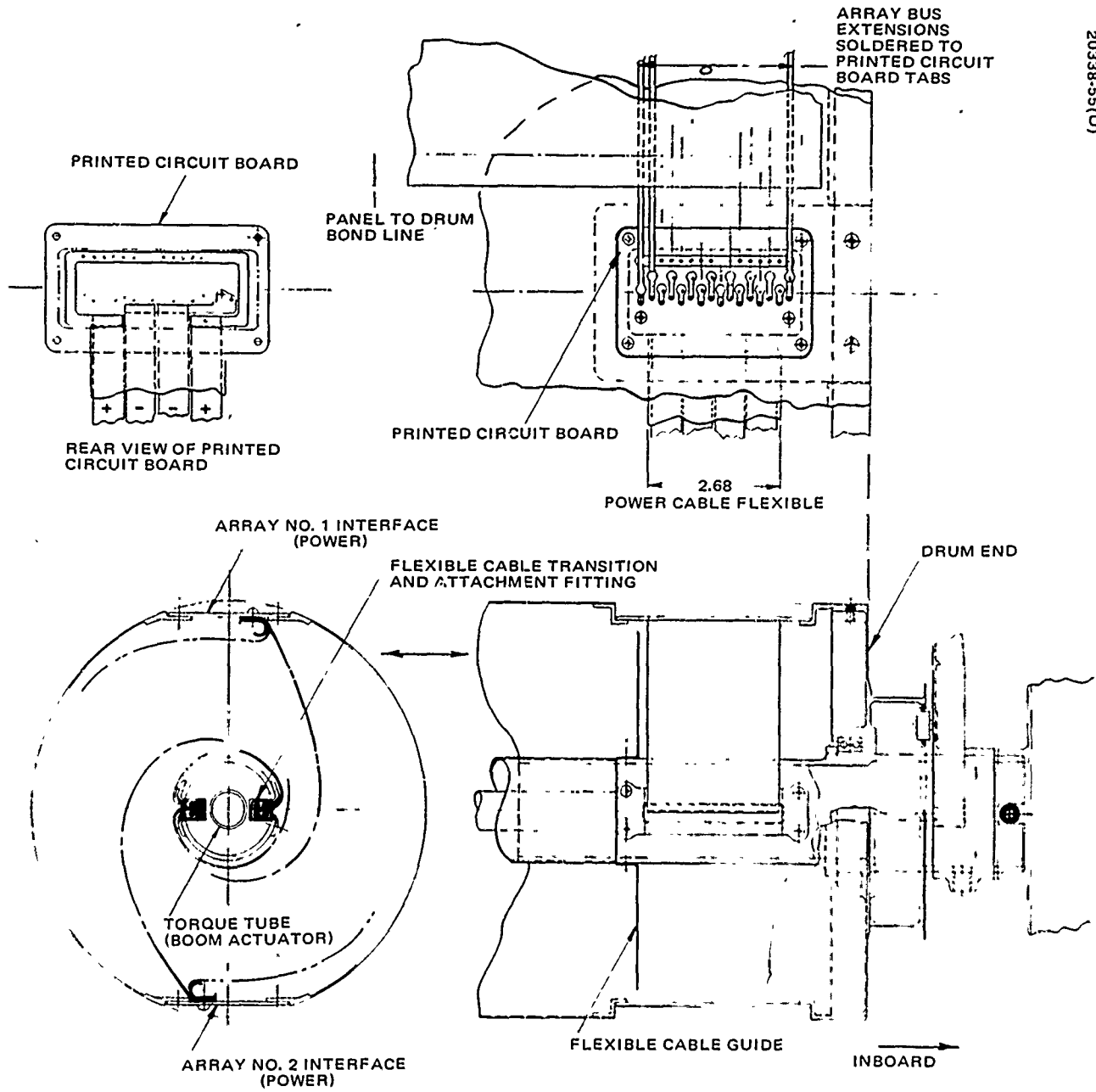


Figure 4-6. Flexible Power Cable Arrangement

Single Versus Dual Actuator Motor Tradeoff. The drive arrangement tradeoff, although considering many drive systems, concentrated on the schemes illustrated in Figure 4-7. Tradeoff criteria were volume, weight, reliability, cost, and growth (see Table 4-2). Based on these factors, the single motor with torque tube coupling was confirmed for the baseline design.

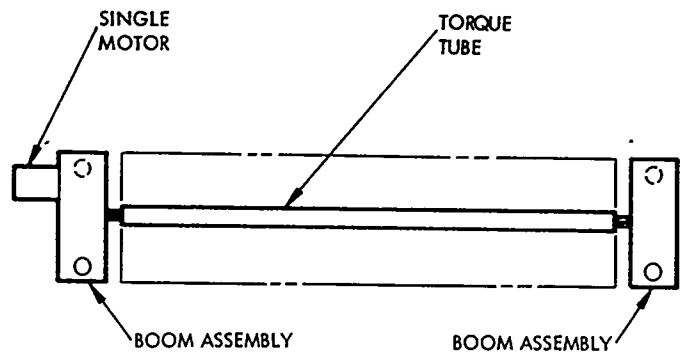
AC Versus DC Actuator Motor Tradeoff. Before the 115-volt, 400-Hz ac servomotor was chosen for driving the actuators, an in-depth analysis of two alternate types was performed. The alternates were the brush dc motor and the brushless dc motor. Although brush wear for the original goal of 500 cycles would be reasonably low (0.005 inch), it was considered significant enough to eliminate the brush type motor for this particular application. The brushless dc motor, while not presenting a brush wear problem was not chosen because of its electronic complexity and its higher development cost. A summary of the motor tradeoff study is given in Table 4-3.

TABLE 4-2. BOOM ACTUATOR DRIVE TRADEOFF SUMMARY

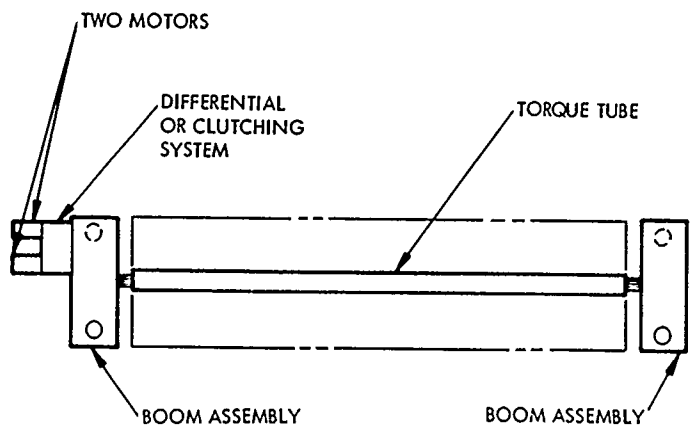
Criterion	Single Motor	Two Motors	Two Motors and Differential	Two Motors and Clutches
Volume	Least	Intermediate	Greatest	Intermediate
Weight	Least	Intermediate	Greatest	Intermediate
Reliability	Equal	Equal	Equal	Equal
Cost	Least	Intermediate	Intermediate	Greatest
Growth	Provides capability	Provides capability	Provides capability	Provides capability

TABLE 4-3. BOOM ACTUATOR MOTOR TRADEOFF SUMMARY

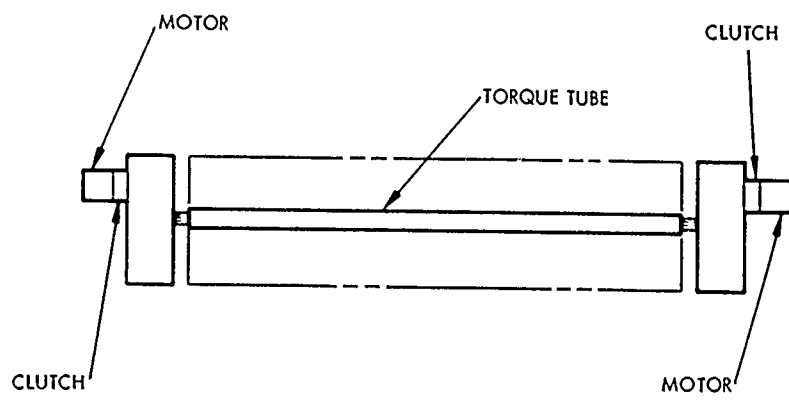
Criterion	AC Motor and Inverter	DC Brushless Motor and Electronics	DC Brush
Volume	Equal	Equal	Equal
Weight	Equal	Equal	Equal
Reliability	Greatest	Intermediate	Least
Cost	Intermediate	Greatest	Intermediate
Growth	Equal	Equal	Equal



a) SINGLE MOTOR DRIVE



b) DUAL MOTOR DRIVE



c) ALTERNATE DUAL MOTOR DRIVE

Figure 4-7. Boom Actuator Drive Arrangements

Boom Length Compensator Design Study. The tradeoff study to determine the most suitable boom length compensator system considered equal tension on both edges of the panel a prime requisite. Equalization of panel tension provides the greatest opportunity for the panels to wind evenly on the storage drum without lateral displacement. Of the many mechanisms considered, the device shown in Figure 4-4 best satisfied this requirement. It also ranks high when compared to other schemes on the basis of weight, volume, reliability, and cost.

Cushion Take-up and Panel Tension Drive Study. The system chosen for both the cushion take-up and the panel tension driver was a Negator <sup>®</sup> spring arrangement. Other devices considered were torsion springs, electric motors, and various pulley/gear mechanisms for the cushion take-up drive. The logic tree for the cushion take-up drive is shown in Figure 4-8.

Flat Flexible Cable Versus Sliprings/Brushes. The 1500-watt FRUSA system employed 8 power conductors and 100 instrumentation conductors between the panels and the drum. On the basis of equal power losses, slip rings would have been lighter for power transfer alone but considerably heavier for the data transfer. By accepting twice the expected slipring/brush system losses, a weight savings was realized with a flexible power cable. The higher power losses are dissipated in the flat cable over a relatively large area and not localized as in the brush/slipring arrangement. Other advantages of the flexible cable are the elimination of slipring noise, lower cost, and decreased complexity of drum design. A summary of the tradeoff for the power transfer task is shown in Table 4-4.

Storage Drum Tradeoff Study. The structural design of the storage drum had to provide sufficient bending strength and stiffness to withstand launch vibrations and quasi-static accelerations, and adequate stability to withstand radial load induced during launch by a breathing mode of vibration of the solar panel layers on the drum. In addition, the minimum drum diameter had to be compatible with the solar panel flexibility, the panel tension required for minimum array frequency, and the panel tension required for the solar cells to survive the launch environment.

The storage drum diameter of 8 inches was established by tradeoff analysis as follows:

- 1) The minimum diameter required to assure proper solar panel wrapping onto a cylinder increases with decreasing panel tension and decreasing panel flexibility (Figure 4-9). The latter depends on the substrate rigidity and the spacing between rows of solar cells. A specified array area utilization of 95 percent translates into an upper gap width of 0.027 inch for 2 x 2 cm solar cells. The panel tension should be as low as the orientation control mechanism allows from an array fundamental frequency point of view. For stowage the panel tension should be as high as necessary for intimate wrapping of the array on the drum without exceeding the compressive strength of the deployment booms.

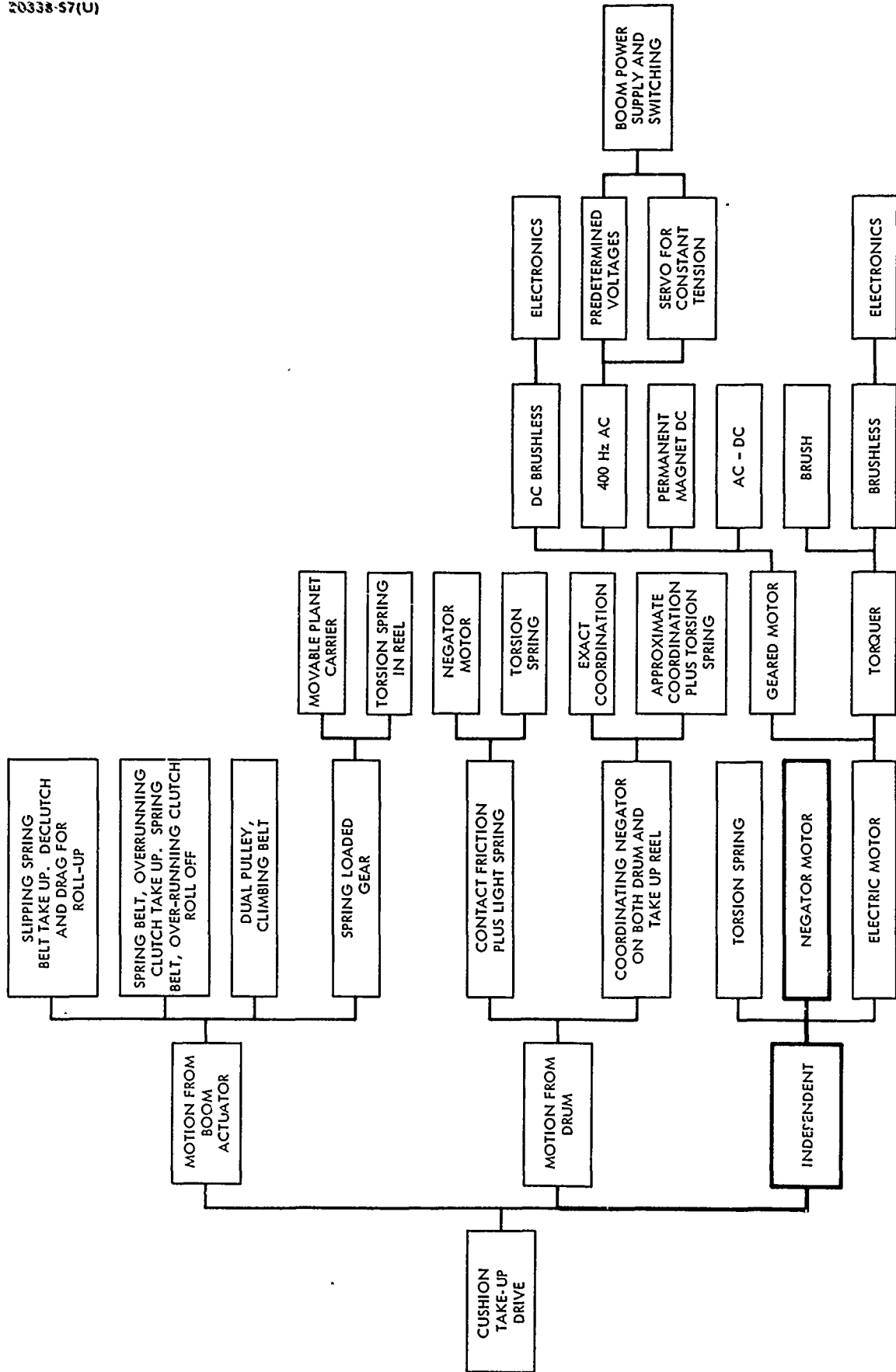


Figure 4-8. Cushion Take-up Drive Logic Tree

TABLE 4-4. COMPARISON OF SLIPRINGS AND FLEXIBLE CABLE

Parameter	Contour Cable	Sliprings	Savings
Weight, pounds 1500 watts (16 ft/panel)	Cable (0.19) + additional panel* (0.15) = 0.34	1.50	1.31** 1.16***
2500 watts (27 ft/panel)	Cable (0.28) + additional panel* (0.41) = 0.69	1.50	1.22 0.81 .
5000 watts (37 ft/panel)	Cable (0.72) + additional panel* (0.81) = 1.53	2.65	1.93 1.12 .
Reliability	Higher	Lower	
Voltage drop, volts			
1500 watts	0.22	0.11	0.11.
2500 watts	0.36	0.18	0.18.
5000 watts	0.36	0.18	0.18.
Power losses, watts			
1500 watts	11.5 (0.77 percent of total)	5.75	5.75.
2500 watts	32.0 (1.28 percent of total)	16.0	16.0.
5000 watts	64.0 (1.28 percent of total)	32.0	32.0 .
Torque about drum axis	Lower	Higher	
Growth factor	Equal	Equal	

\*Cells necessary to make up for larger  $I^2R$ .

\*\*Not including additional cells required to compensate for larger power loss.

\*\*\*Including additional cells required.

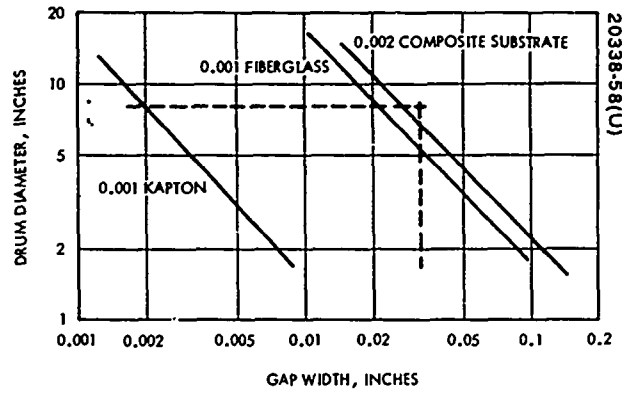


Figure 4-9. Required Drum Diameter for Several Substrate Materials and 0.6 lb/ft Panel Tension

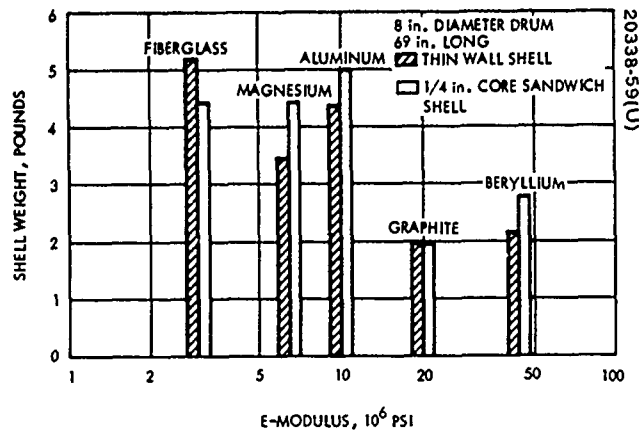


Figure 4-10. Weight Comparison of Array Storage Drum Materials

- 2) The fracture strength of 8-mil thick solar cells with a 6-mil coverglass was predicted and experimentally verified adequate to sustain wrapping tension and vibration loading on a 8-inch diameter storage drum.
- 3) The selected diameter resulted in relatively few wrapped panel layers, which is desirable from the point of view of solar cell dynamic loading, panel evenness in roll-up, and sizing of the Negator <sup>®</sup> tension spring drives.

The choice of the thin wall magnesium cylinder for the FRUSA storage drum was made following a tradeoff study of aluminum, magnesium, beryllium, and the fiber-reinforced epoxy composites of boron, graphite, and fiberglass. The following conclusions were drawn from the structural and weight analysis:

- 1) The choice between a thin wall cylinder and a sandwich cylinder design, when evaluating weight, depends on the material used (Figure 4-10).
- 2) Graphite/epoxy composite is superior to the lightweight conventional alloys of aluminum, magnesium, and beryllium, or the composites of fiberglass and boron/epoxy.
- 3) Use of a magnesium or graphite/epoxy cylinder would effect weight savings of approximately 25 and 60 percent, respectively, over an aluminum cylinder.
- 4) A weight-optimized beryllium storage drum has greatest stiffness and high fundamental frequency — that is, small deflections in response to dynamic excitations. It is an expensive design, however.

A magnesium drum with titanium sandwich end plates was the prime choice when weight and reliability were considered and state-of-the-art technology utilized. The monocoque magnesium cylinder was originally dimensioned for an estimated loading that would require 0.030-inch minimum wall thickness. As the final load analysis indicated lower bending moments however, lightening holes were added to further reduce the weight. This approach was selected in preference to a uniform wall reduction because the thin wall magnesium shell would have been subject to handling damage and excessive local flexibility.

#### Drum Mechanism Development Tests

In addition to the complete subsystem functional tests on the water table, the following components and subassemblies were evaluated:

- Boom actuator units
- Bearing, Negator <sup>®</sup>, and flexible cable installation



- Boom length compensator mechanism

Boom Actuator Units. An engineering model of the boom actuator was subjected to the following series of functional and environmental tests:

- 1) Sinusoidal vibration tests
- 2) Thermal extension/retraction tests
- 3) Boom synchronization, straightness, alignment, and bending evaluation
- 4) Boom bending instrumentation calibration

A single boom breadboard model of the actuator unit was also built and subjected to a life test program. This program consisted of 314 extensions and retractions in an ambient environment with simulated tip loading. The successful demonstration of 314 cycles represents a capability to perform 35 cycles (25 on ground and 10 in orbit) with a 90 percent confidence level.

Bearing, Negator <sup>®</sup>, and Flexible Cable. The development program for the drum bearings, panel tension drive, flexible cable, and cushion reel drive included the following:

- Drum bearings at room temperature, -150°F, and 230°F
- Drum bearings and simulated flexible flat cable at room temperature, -150°F, and 230°F
- Cushion reel drive at room temperature
- Complete system (drum bearings, drum drive, cushion reel drive, and flexible cable) at room temperature, -150°F, and 230°F
- Drum bearings with inner race temperature 5° to 30°F higher than outer races

The test results indicated adequate margins for all components tested when operating in the expected thermal environment. The more significant results and conclusions were as follows.

- Drum bearing torque levels for essentially uniform temperature distribution (no temperature gradients between inner and outer race) were 0.13, 0.22, and 0.27 in.-lb per pair for room temperature, -150°F and 230°F, respectively.
- Drum bearing torque for the expected 5-to 10-degree differential between inner and outer races was approximately 0.20 in.-lb per

pair. For  $\Delta T = 30^\circ\text{F}$ , the torque was 0.35 in.-lb, still within the allowable limit of 1 in.-lb.

- Flexible cable torque levels, based on a simulated cable with representative Kapton/copper, were estimated to be about 2.0 in.-lb maximum. This includes two pairs of data cables and two pairs of power cables at  $-150^\circ\text{F}$ .
- Cushion tension, provided by cushion reel drive, would be between 1.0 and 2.5 pounds. The larger value corresponds to the empty reel condition where the largest tension is required for proper rollup of the cushion.
- Drum negators, when contoured to compensate for changing drum diameters, would provide total panel tension levels (two panels) between about 8 and 12 pounds. Based on panel rollup tests and the allowable boom loads, this range of panel tension was considered acceptable.

A contoured negator was subjected to more than 4450 cycles at room temperature before a bending fatigue failure occurred. This represents a large margin over the 2500 cycle vendor guarantee and the 35 cycle (10 flight plus 25 preflight ground test) life required for the experiment. Measurements made after about 4000 cycles revealed no apparent change in the negator torque characteristics over a typical cycle. These measurements also verified that the contouring operation achieved the features desired.

Boom Length Compensator. The development test program on these devices was performed at room temperature,  $-120^\circ\text{F}$  and  $275^\circ\text{F}$ . Results of the tests indicated the maximum difference between the panel tension from one edge to the other was less than 1 pound. This value was considered well within the difference allowable for satisfactory rollup of the flexible arrays.

### Flexible Solar Arrays

#### Description

The flexible solar arrays consist of the following components, starting at the backside of the panel (see Figure 4-11).

- 1) Etched copper with Kapton insulation for collector bus material
- 2) Bonded Kapton and fiberglass substrate base for supporting cells
- 3) Solar cells connected together by soldered, expanded copper mesh Z-strips

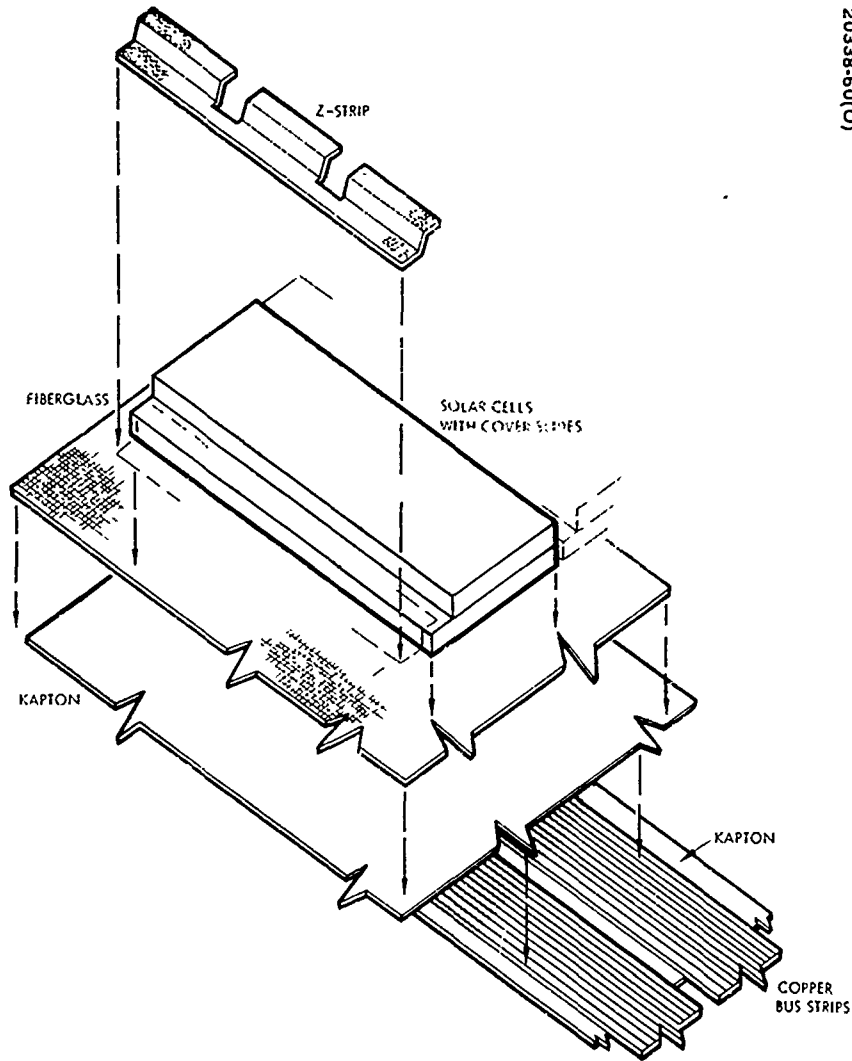


Figure 4-11. Solar Panel Components

	WEIGHT, gm/CELL	PANEL WEIGHT BREAKDOWN, %
0.006 MICROSHEET GLASS COVER ULTRAVIOLET AND ANTIREFLECTIVE COATINGS	0.150	33.04
ADHESIVE DOW R63-489	0.010	2.21
2x2 cm SOLAR CELL 0.008 THICK	0.210	46.35
ADHESIVE AND FIBERGLASS (0.001)	0.014	3.09
SUBSTRATE 0.001 KAPTON	0.0082	1.81
COLLECTORS AND BUS 0.0007 COPPER WITH INTEGRAL KAPTON (0.001) OVERLAY	0.0169	3.73
SOLAR CELL INTERCONNECT 0.002 FISHED COPPER MESH	0.0214	4.72
	0.0224	5.05

20338-61(U)

Figure 4-12. Panel Weight Breakdown

- 4) Glass coverslides for environmental and radiation protection of the solar cells
- 5) Embossed Kapton cushion for protecting cells in rolled-up configuration

The percentage weight breakdown of the solar panel is shown in Figure 4-12.

Panel Bus. The bus systems (see Figure 4-13) for power, as well as for the reference cells/modules, temperature sensors, and spreader bar instrumentation circuits, were fabricated from a copper/Kapton laminate. This laminate was 1/2 ounce (0.0007 inch) copper bonded to 0.001-inch Kapton. In order to provide for constant voltage operation from each sector of the panel, the longest power buses had the widest conductors. Negative and positive power buses were alternated to provide minimum electromagnetic induction. Collector bus strips from the cell strings to the main power buses were folded around the edge of the panel as shown in Figure 4-14.

Panel Substrate. The primary function of the substrate was to provide sufficient mechanical support for the solar cells to maintain a planar configuration and physical alignment within the cell matrix. The substrate had to carry all the required stresses to accomplish this function. Desirable substrate characteristics are 1) high flexibility, 2) electrically insulating surface, 3) resistance to damage from soldering and other manufacturing operations, 4) minimum elongation and high tensile strength, 5) stability in the space environment, particularly with respect to hard vacuum, ultraviolet radiation, and temperature extremes, 6) high transmissibility to infrared wavelengths, thereby permitting radiant heat transfer directly from the solar cell rear surface to space, 7) suitable surface for bonding, 8) high optical transmittance to permit inspection of rear cell contact after array fabrication, and 9) low specific weight. The flexible substrate chosen combined the qualities of two materials, using a 0.001-inch DuPont Kapton H-film bonded to 0.001-inch type 108 fiberglass.

Fiberglass is susceptible to cracking if wrinkled or folded, but it offers more tensile stiffness than film material. Kapton has a tensile strength of 70-lb/mil thickness and will redistribute the load if the substrate is creased. The fiberglass prevents the Kapton from tearing, eliminating the undesirable property of Kapton. The resulting composite therefore takes advantage of the desirable properties of both materials.

Solar Cells. The elements of the solar cell assembly are shown in Figure 4-15. The cell was 2 x 2 cm n/p silicon, 8 mils thick. It had silver-titanium grids and contacts. The grids and N-contact bar were solder-plated on the front side, while the rear surface contact was solder-plated over a small zone. The characteristics of these cells as determined during a qualification program at Heliotek are summarized in Table 4-5.

Each of the panels employed 81 cells across the width of the panel (connected in series) and 222 cells (9 rows were taken up by reference

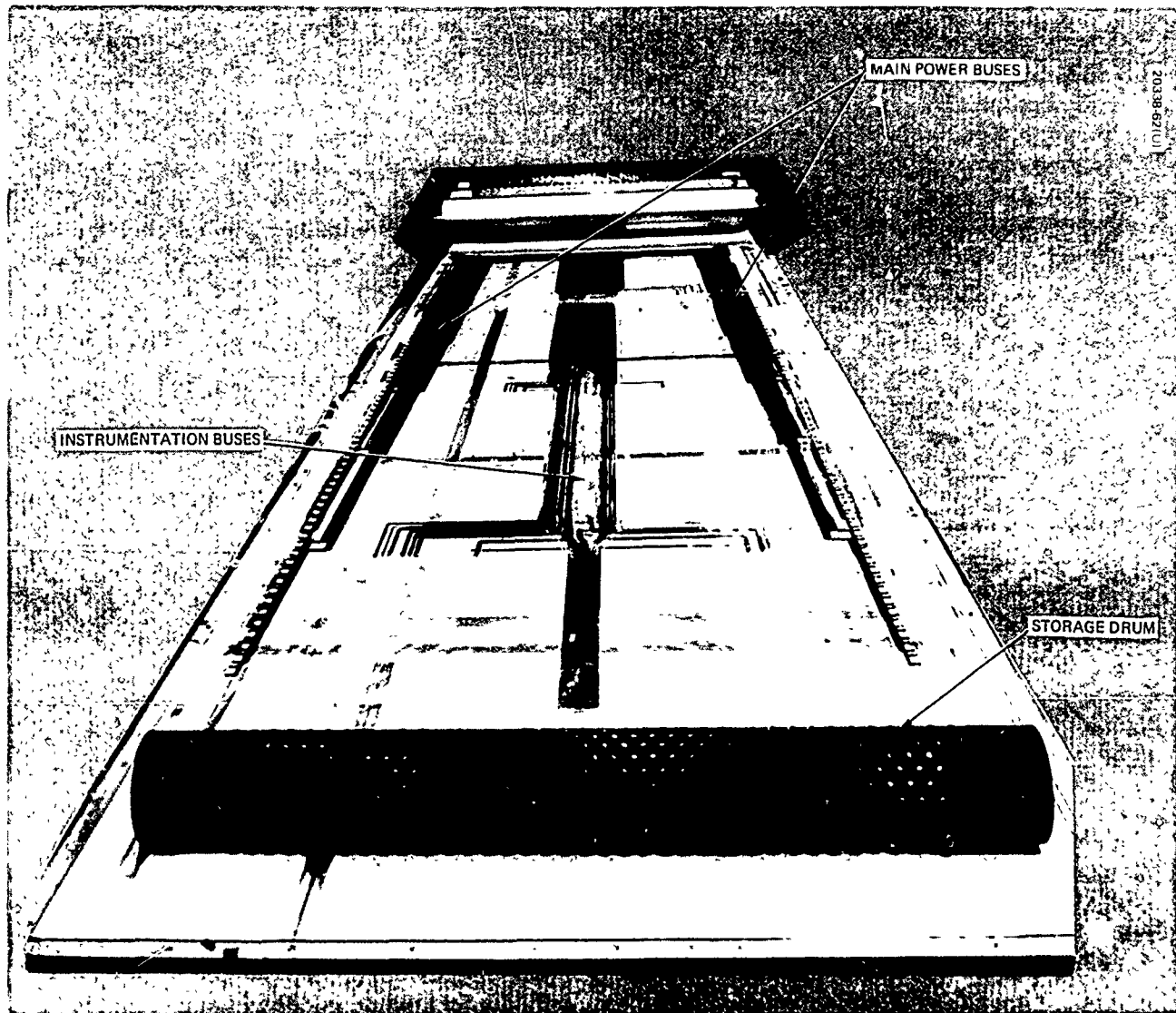


Figure 4-13. Solar Array Power and Data Buses  
(Photo ES28313)

20338-63(U)

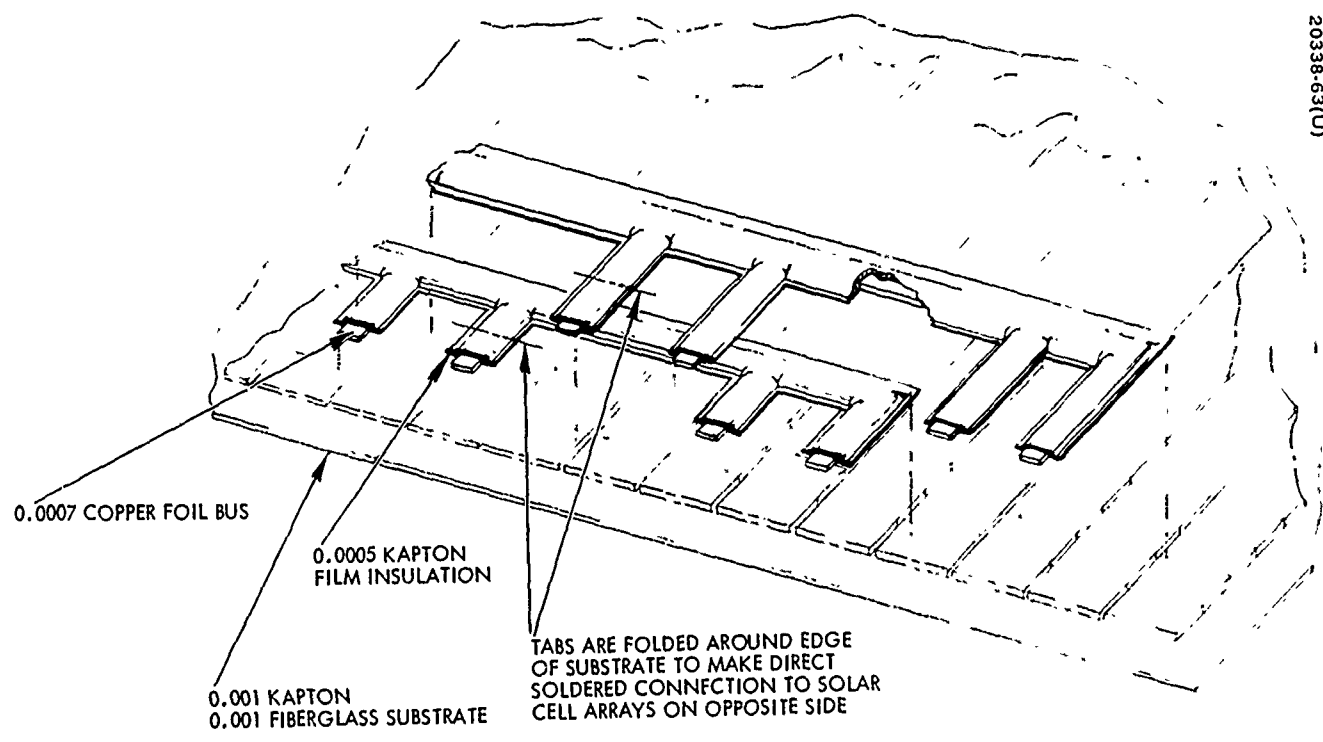
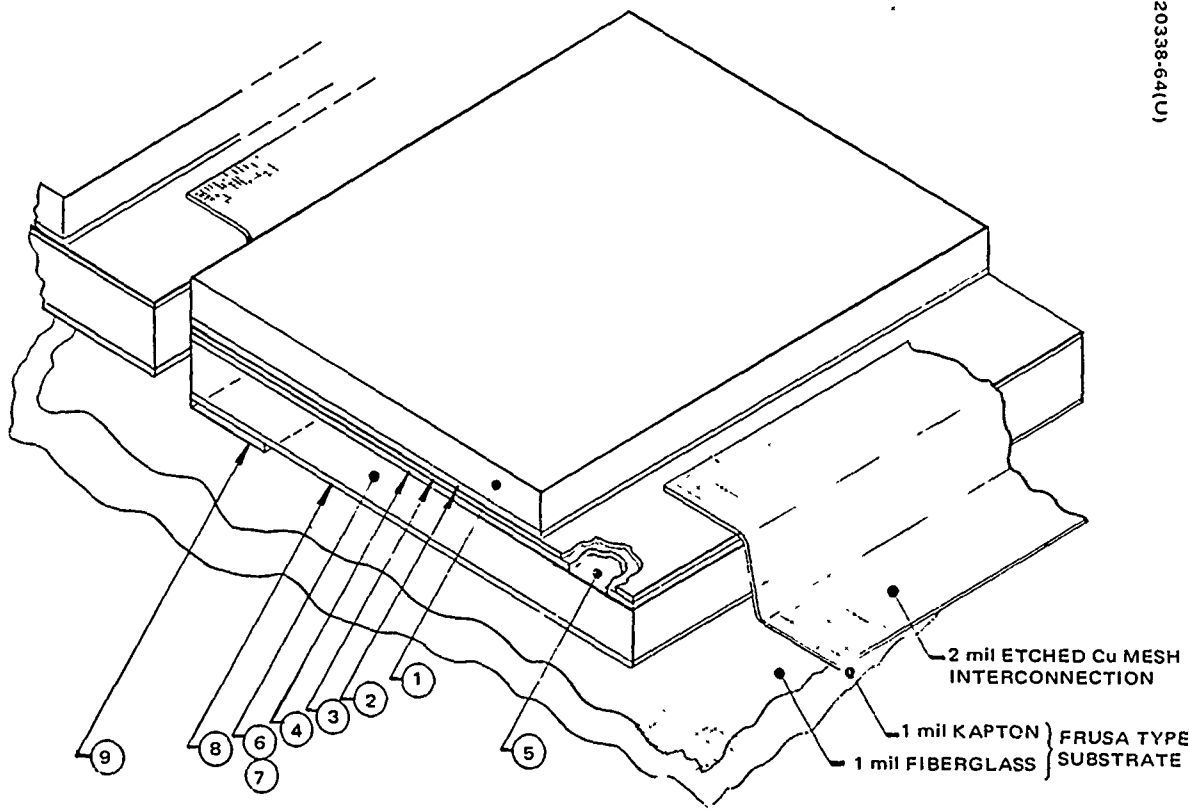


Figure 4-14. Collector Bus Strips Arrangement

20338-64(U)



ITEM	DESCRIPTION	TYPE
1	COVER	6 mil MICROSHEET, Mg F A/R, AND UV FILTER
2	COVER ADHESIVE	RTV 602
3	SOLDER	THIN, CLOSELY CONTROLLED AND PRESSED OVER GRIDS AND BAR
4	'N' CONTACT	Ag - Ti
5	CELL A/R COAT	SiO
6	CELL MAT'L	2Ωcm, CRUCIBLE GROWN, 8 mils
7	EDGE	SMOOTH ETCHED, "PILLOW" FORM
8	'P' CONTACT	Ag - Ti
9	SOLDER	ZONE, THIN, CLOSELY CONTROLLED AND PRESSED

Figure 4-15. Elements of Solar Cell Assembly

TABLE 4-5. CELL QUALIFICATION TEST RESULTS

Measurement	Average Current at 470 mv, ma	Average Output Power, mw
Initial	114.4	53.77
Post temperature-humidity	113.9	53.53
Post thermal shock	114.7	53.91
Final (post temperature-vacuum)	114.8	53.96
Percent change	0.35	0.35

cells/modules on the flight unit) along the length of the panel (connected in parallel).

Glass Coverslides. The solar cells are protected from radiation damage by slides of 0211 microsheet, 6 mils thick. An antireflective coating of magnesium fluoride was applied to the top surface of the cover and a conventional UV rejection filter (Optical Coating Laboratory) was used on the bottom surface. The glass coverslides were bonded to the cells with RTV602.

Solar Array Cushion. The cushion required to protect the solar cells during launch vibration was embossed 2-mil Kapton (see Figure 4-16). It was interleaved between the alternate layers of the dual panel that lie coverslide-to-coverslide when rolled on the storage drum, as shown in Figure 4-17. Its primary function was to provide a means of distributing cell-to-cell stress.

Z Strip. The interconnection between the solar cells was 2-mil etched copper, solder-plated.

Cell-to-Substrate Bonding. The adhesive used to bond the solar cells to the substrate was a Hughes developed modified two-part epoxy.

#### Solar Array Tradeoff Analysis

Most of the tradeoff studies and analyses for the solar array construction and materials were performed prior to the contract award. Other than design studies to determine dimensions, bus routing, conductor sizing, etc., the only significant tradeoff concerned the distribution of active cells to obtain 700 watts from a panel sized for 1500 watts. Since the contract was changed to a flight panel completely covered with active cells, the tradeoff study was invalidated.



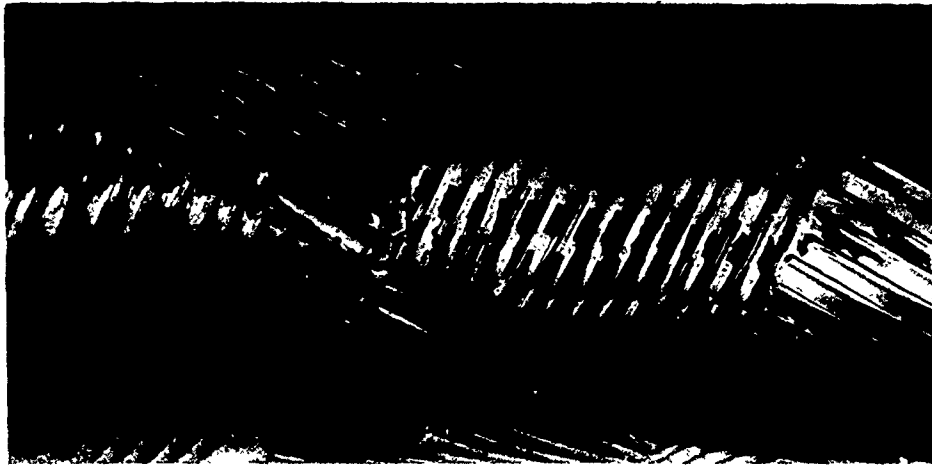


Figure 4-16. Embossed Kapton Film Cushion-Rolled

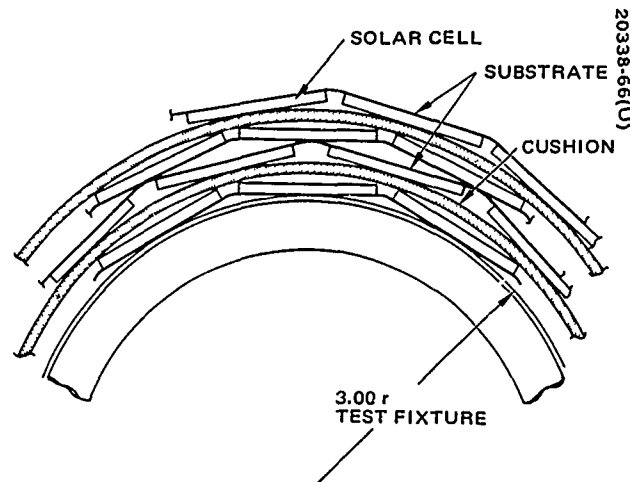


Figure 4-17. Solar Array/Cushion Configuration and Storage Drum (Schematic Representation)

## Solar Array Development Tests

Solar Panel Materials and Processes Tests. The tests on various solar array materials and processes included strength tests of materials and adhesive bonded joints as well as thermal cycling tests of bonded joints. Some observations are as follows:

- The strength of adhesive bonded joints was well above the design requirements.
- The absorption of water by Kapton from a humid environment has no effect on bond quality.
- Minor voids at the bond line have no effect on bonded joint strength when loaded within a thermal-vacuum environment.
- No yielding or peeling of any adhesive joints was observed when loaded beyond the maximum expected loads and subjected to thermal cycling tests.
- Peeling strength of solar cells and bus strip material to substrate exceeded peeling requirements by a high margin.

In addition, the following fabrication processes were developed and evaluated prior to the fabrication of the array:

- 1) Etching of 0.0007-inch copper foil bus strips on 0.5- and 1-mil Kapton base
- 2) Bonding of Kapton lap joints with liquid epoxy adhesive
- 3) Bonding of bus strips to Kapton
- 4) Bonding of fiberglass to Kapton in areas without cells
- 5) Bonding of small solar cell groups to substrate, including areas over bus strips
- 6) Evaluation of thermal stabilization, surface preparation, and humidity effect on bonding operations

Panel Roll-Up Tests. The test specimen for analyzing the panel tension required to wrap the array on an 8-inch diameter drum was 5 inches wide, 25 inches long. It included cell interconnects and bus bars representative of a full-size array with regard to flexure characteristics. Since cell thicknesses have negligible effect on panel tension/roll-up characteristics, rejected 12-mil cells with 12-mil covers were used rather than the flight-quality 8-mil cells with 6-mil covers.

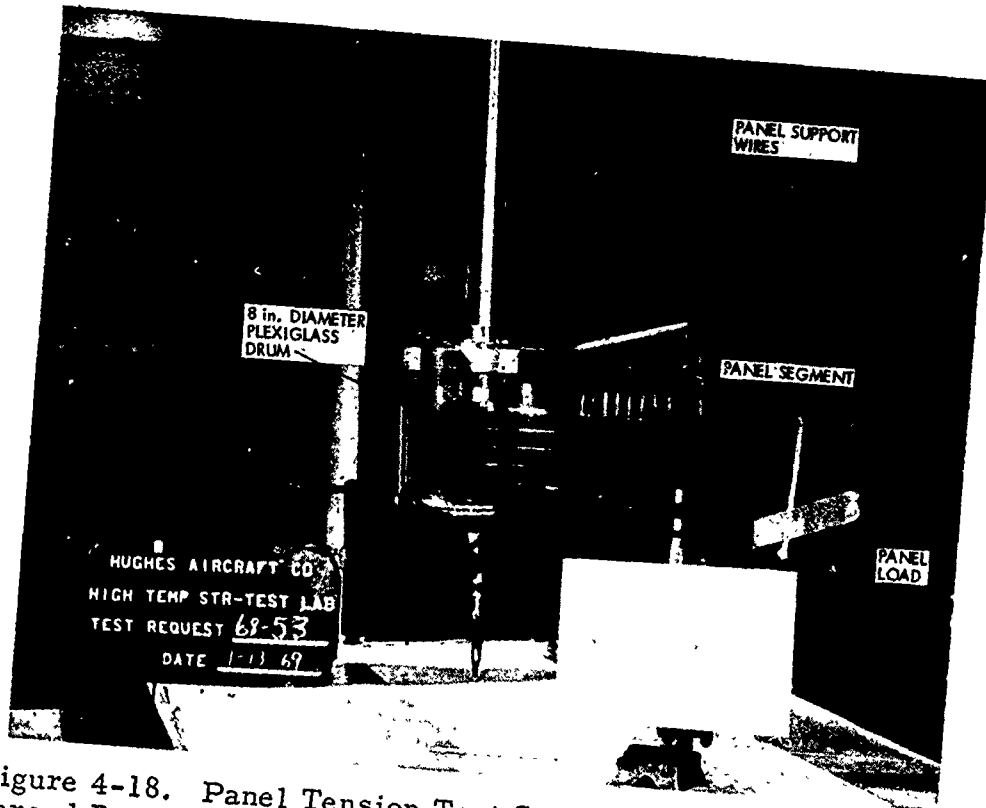


Figure 4-18. Panel Tension Test Setup With Low Temperature Shroud Removed (Photo HT 338-17)

The test program to evaluate the roll-up characteristics of the flexible array with various values of panel tension was performed at room temperature and at -200°F (Figure 4-18). The significant results of these tests are as follows:

- The panel wound up satisfactorily on an 8-inch diameter drum with as little as 0.02-lb/in tension.
- The panel wound on and off the cylinder as well at -200°F as it did at room temperature.

Panel Segment Thermal Cycling Tests. A representative panel segment (see Figure 4-19) was exposed to 100 thermal shock cycles over the temperature range of approximately 200° to -300°F. These tests indicated slight electrical degradation from mechanical damage believed to be the result of excess solder on the contact area of a single cell. After tighter inspection procedures were established, additional samples were fabricated for tests at the NASA Lewis facility. These samples were subjected to 2100 cycles between 189° and -163°F at pressures of about  $1 \times 10^{-7}$  Torr. A typical cycle is 55 minutes at 189°F, followed by cooling to -163°F in 30 minutes (see Figure 4-20). No mechanical or electrical degradation was noted in the test samples. Final test results submitted by NASA Lewis are as follows:

	<u>Test Module TC-1</u>		<u>Control Module TC-2</u>	
	<u>SCC, ma</u>	<u>OCV, volts</u>	<u>SCC, ma</u>	<u>OCV, volts</u>
Pretest	362	1.696	363	1.695
Post-test	364	1.688	367	1.698

All data were corrected to 75°F. The changes in OCV (open circuit voltage) and SCC (short circuit current) were within the measurement accuracy.

Panel Cushion Development. The 2-mil Kapton for the panel cushion was embossed by applying pressure to a heated forming die (see Figure 4-21). A considerable development effort was expended before the proper die dimensions (see Figure 4-22) and correct temperature/pressure combinations were determined. Some of the initial efforts produced too little embossment and/or large tears in the material.

After the production techniques were developed, cushion samples were evaluated. The evaluation included measurement of spring rate and recovery characteristics as a function of time and temperature. Tests were run at room temperature and at 120°, 150°, and 175°F.

Panel Segment Vibration Tests. Reduced width solar panels with live 8-mil and dummy cells were subjected to random vibration levels corresponding to the Titan IIC environment (see Figures 4-23 and 4-24). Amplification

factors were applied to simulate the expected environment at the center of the storage drum. Some slipping of the panels with respect to the cushion was noted during the test exposure. An examination of the live cells following the test revealed about 3 percent of the cells/covers had sustained minor damage, primarily small coverglass cracks. A comprehensive study following the test produced the following conclusions:

- The slipping was not a realistic condition for the full width panel.
- The 1-mil cushion was inadequate for 8 mil cells.
- The 0.53-lb/in. (35 pounds total for full width panel) panel tension was somewhat high for the 8 mil cells.

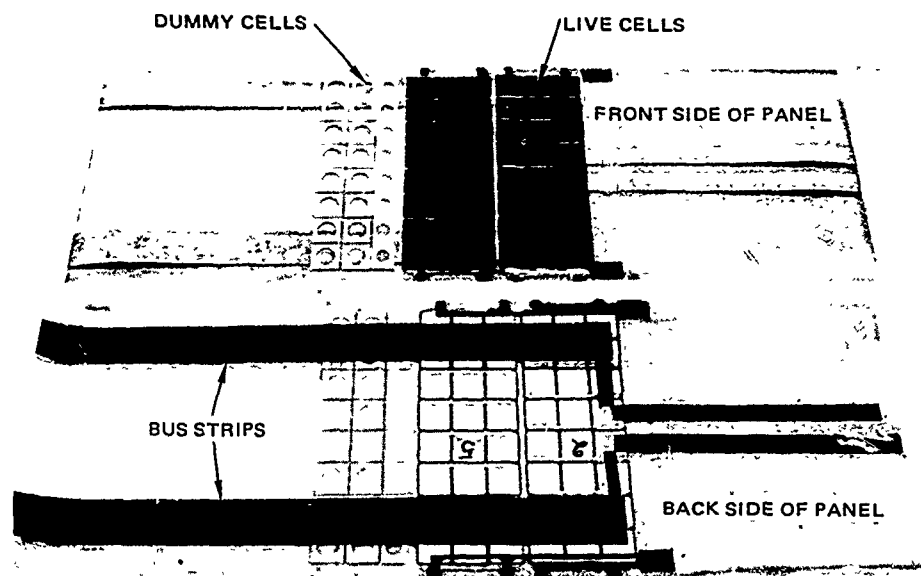
Action taken to correct the problem was as follows:

- The 1-mil cushion with approximately 0.030-inch high embossment was replaced with a 2-mil cushion with 0.040 to 0.045 inch high embossment.
- Windup panel tension was reduced to 25 pounds total for a full width panel.
- Support was provided to prevent unrealistic slippage due to 1-g bias.

A vibration retest of the panels resulted in two coverslide cracks in the 406 live cells. Since the cracks noted were not expected to affect panel performance, the 0.5 percent coverglass breakage under worst conditions was considered acceptable. An electrical check showed no performance degradation. The 0.5 percent was approximately the same as later noted on the full size qualification model panel. Inspection of the flight panel prior to flight indicated that less than 0.1 percent of the cells had failed to an extent requiring replacement after all handling and test operations. Most of the cells replaced, in fact, were replaced more for confidence than for necessity.

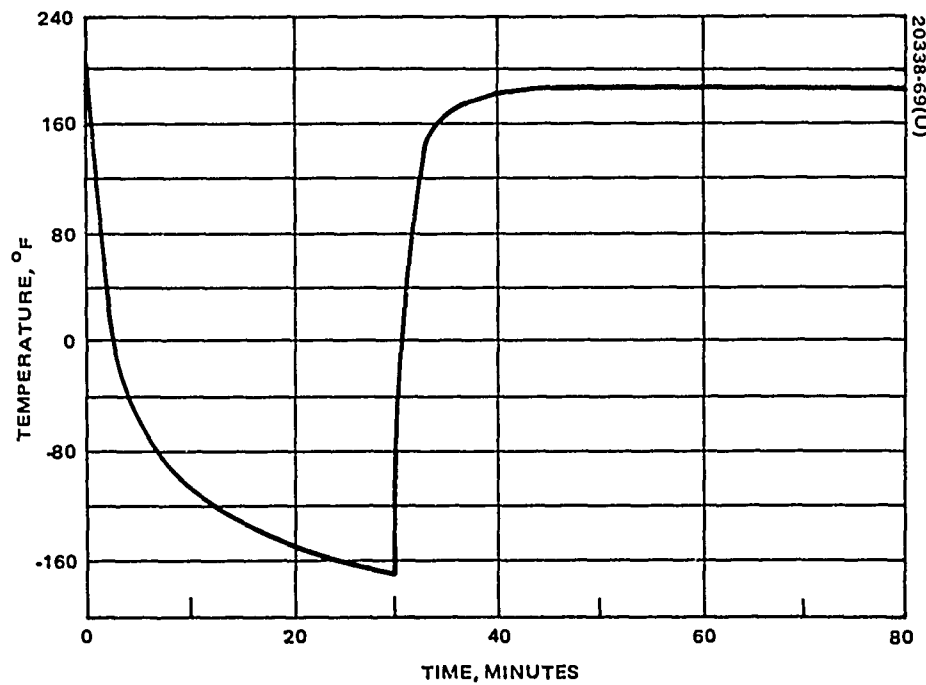
Humidity and Thermal Shock Tests of 8-mil Cells. Three test samples of 8-mil solar cells with 6-mil coverglasses were subjected to temperature, humidity, and thermal shock tests. The configuration of these test samples was as follows:

Group 1 (46 cells)	Fully soldered N contact, P contact, and grids
Group 2 (51 cells)	Fully soldered N contact, zone soldered P contact, and fully soldered grid lines
Group 3 (46 cells)	Fully soldered N contact, zone soldered P contact, and unsoldered grids



20338-68(U)

Figure 4-19. Thermal Shock and Cycling Test Speciman



20338-69(U)

Figure 4-20. Typical Thermal Cycle of Solar Panel Specimen

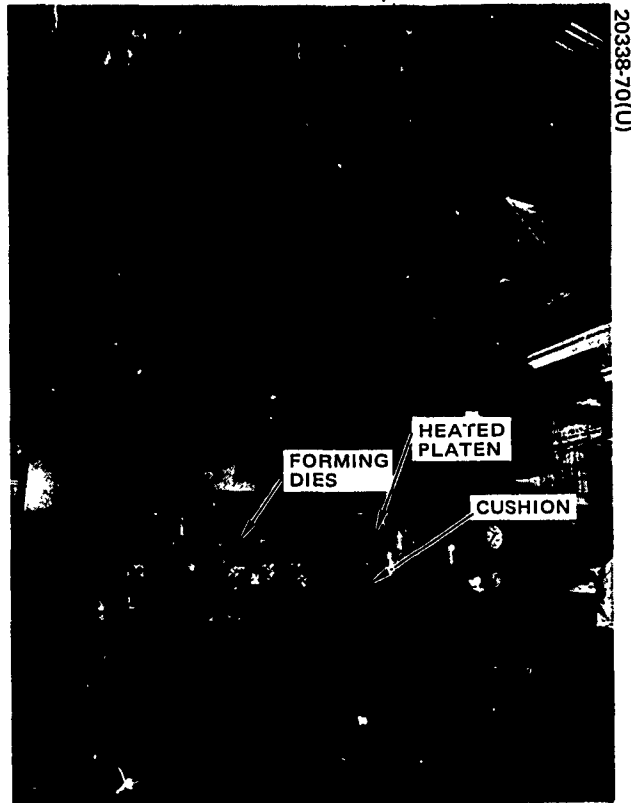


Figure 4-21. Cushion Fabrication Equipment (Photo 4R11804)

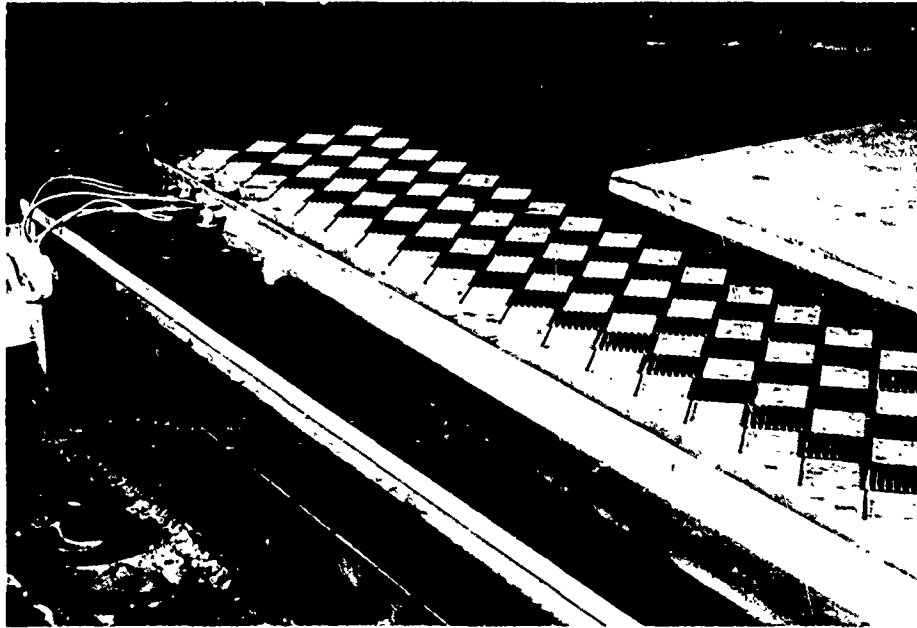


Figure 4-22. Cushion Forming Die Closeup (Photo 4R11803)

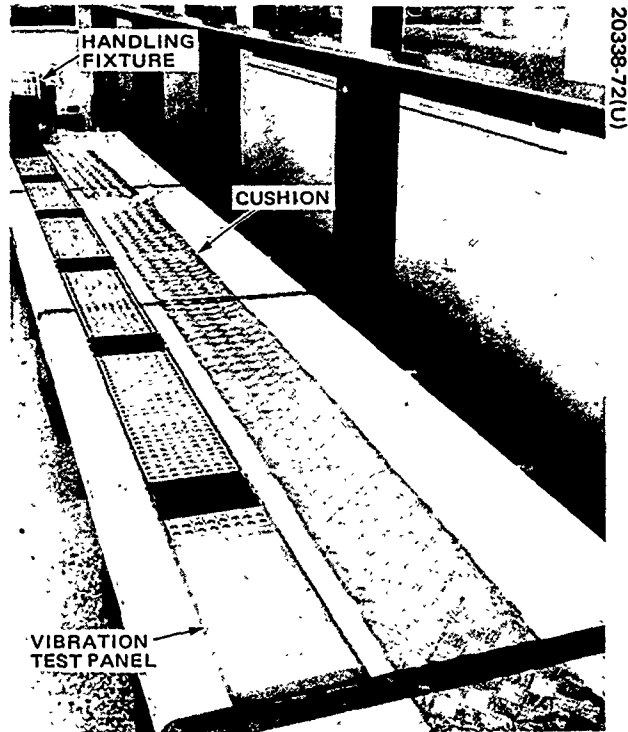


Figure 4-23. Vibration Test Solar Array and Cushion

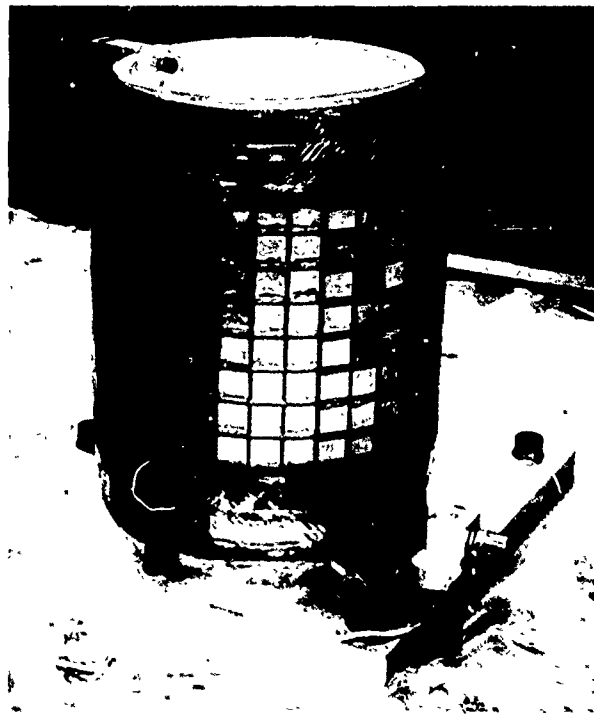


Figure 4-24. Panel Segment Vibration Test Setup (Photo ES24418)



The sequence of inspections and tests was visual inspection, electrical test, temperature and humidity exposure, visual examination, electrical test, thermal shock exposure, electrical test, and visual inspection. In general, the group 2 samples, the flight configuration, appeared to show an insignificant degradation from the environments imposed and were the best of the three groups.

Flight Results and Observations. The complete details of the flight data reduction are included in the flight test section. The flight data show that the design of the solar array subsystem was adequate for the launch environment. In addition, neither the ten full extension and retraction cycles nor the numerous eclipse cycles degraded the solar panel performance. The only recommendation is that, for a system requiring full power output, an oversize coverglass or grouting be used to cover the coverglass voids to prevent low energy proton damage.

#### Solar Array Subsystem Conclusions

The tradeoff studies and development tests on the drum mechanism and solar array components resulted in a subsystem that performed well during the development, qualification, and flight tests. Although satisfying all requirements, the following improvements should be considered for subsequent designs:

- Provide a positive drive system for booms and thereby reduce the size and weight of the boom length compensator mechanisms
- Use panel mounted diodes on each 3 by 81 string to reduce thermal problems due to shadowing

#### ORIENTATION SUBSYSTEM

The orientation subsystem for FRUSA is a direct derivative of the OLSCA (Orientation Linkage for a Solar Cell Array) design, whose background of theory, design, and development was presented in a previous report.\* Modifications were made only as dictated by the special requirements and constraints of the FRUSA program.

---

\*OLSCA, Orientation Linkage for a Solar Cell Array, Technical Report AFAPL-TR-68-76, July 1968.

## Design Requirements

The FRUSA orientation subsystem was required to control automatically a 2-degree-of-freedom drive system so as to align the array panels normal to the sun line of sight on initial sun acquisition and on emerging from an eclipse. This alignment had to be maintained during all periods of sun illumination for all orbital positions. Manual operation, controlled by ground commands, was provided to permit the automatic control functions to be deactivated or overridden in the event of a failure. The manual modes were required to enable either axis to be torqued in either direction but not simultaneously. Backup commands were specified for simulation of the sun lockon signal. The orientation subsystem also had the responsibility for deploying the solar array subsystem from the stowed launch configuration on ground command and for transferring power and signals between the launch vehicle and all subsystems of the FRUSA experiment. To meet these requirements, the orientation subsystem was composed of an orientation mechanism, control electronics unit (CEU), sun sensor group, and a filter unit (see Figure 4-25).

The specific technical criteria or requirements which implement the general requirements for the subsystem are as follows:

- Maintain array pointing within  $\pm 10$  degrees.
- Provide sun acquisition scan rates of 0.5 deg/sec (2 axes).
- Impart minimum reaction forces to mission vehicle.
- Impose minimal maneuvering constraints on vehicle.
- Prevent possibility of collision between the solar array and the spacecraft.
- Avoid array/vehicle mutual shading.
- Be compatible with a circular orbit, of any inclination, of approximately 400 nm altitude.
- Meet specifications for minimum of 1 year, with a goal of 3 years.
- Transfer 1.5 kw of electrical power.
- Provide 30 data and command channels.
- Interface with Titan III-C/Agenda or Thorad/Agenda vehicle.

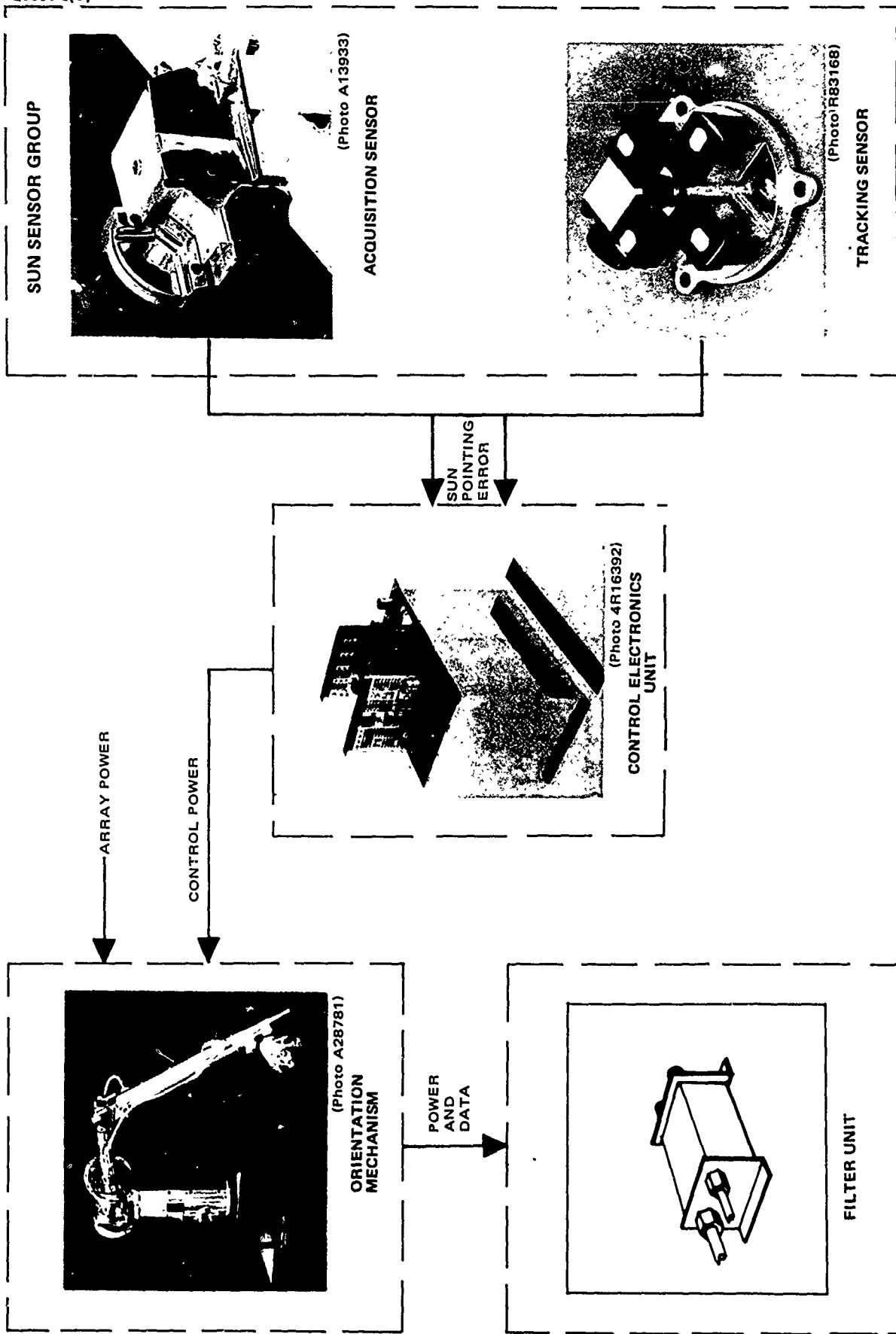


Figure 4-25. Orientation Subsystem Elements

Operations required of the orientation subsystem in orbit are indicated in the functional flow diagram of Figure 4-26. The system must first be deployed from its launch-stowage position; this is accomplished by ground commands which blow pyrotechnic bolts holding the stowed arrays against the payload structure, allowing the subsystem to deploy the solar array assembly into flight position (operation 1.1). System operation is then initiated by ground command to activate control electronics unit power (1.2). Data transfer starts at this time and is continuous thereafter unless the system is deliberately shut down by ground command. When torquers are activated, the system aligns itself to the sun (1.3), the arrays are unfurled (1.4)\*, and power transfer takes place (1.5). Array sun tracking (1.6) is maintained in the face of vehicle earth tracking motions until the earth's shadow is entered (1.7) in some orbits. At this time, the system reverts to the sun acquisition slew mode (1.8) so that, regardless of orbit geometry or eclipse duration, the sun will be automatically reacquired upon emergence without further switching. Since the arrays are already extended, operation 1.4 is by-passed.

## Descriptions

### Subsystem

The orientation subsystem units are illustrated in Figure 4-25. A block diagram, including gross functions within the control electronics unit, is presented in Figure 4-27.

Commands. In the interests of minimizing slipring requirements, both "on" and "off" commands for any given function were designed to be carried on the same path, the command state alternating with each command pulse transmitted. The hindsight provided by flight experience indicated that this "toggle" implementation was undesirable from an operational standpoint because of the susceptibility to out-of-phase states and the accompanying requirement for more careful monitoring. Future designs will, therefore, incorporate discrete channels for "on" and "off" functions despite the slipring penalty.

The subsystem command list is presented in Table 4-6.

Slipring Assignments. Power transfer across the gimbal axis is effected by one power bus ring and one return ring on each axis. In addition, two rings are provided on the support axis to carry unregulated bus power to the CEU for powering the torquer windings.

Thirty signal and command transfer rings are provided on each axis, The lists in Table 4-7 indicate the individual functions serviced and illustrate the complexity of this interface.

\*Alternately, arrays may be extended prior to sun acquisition.

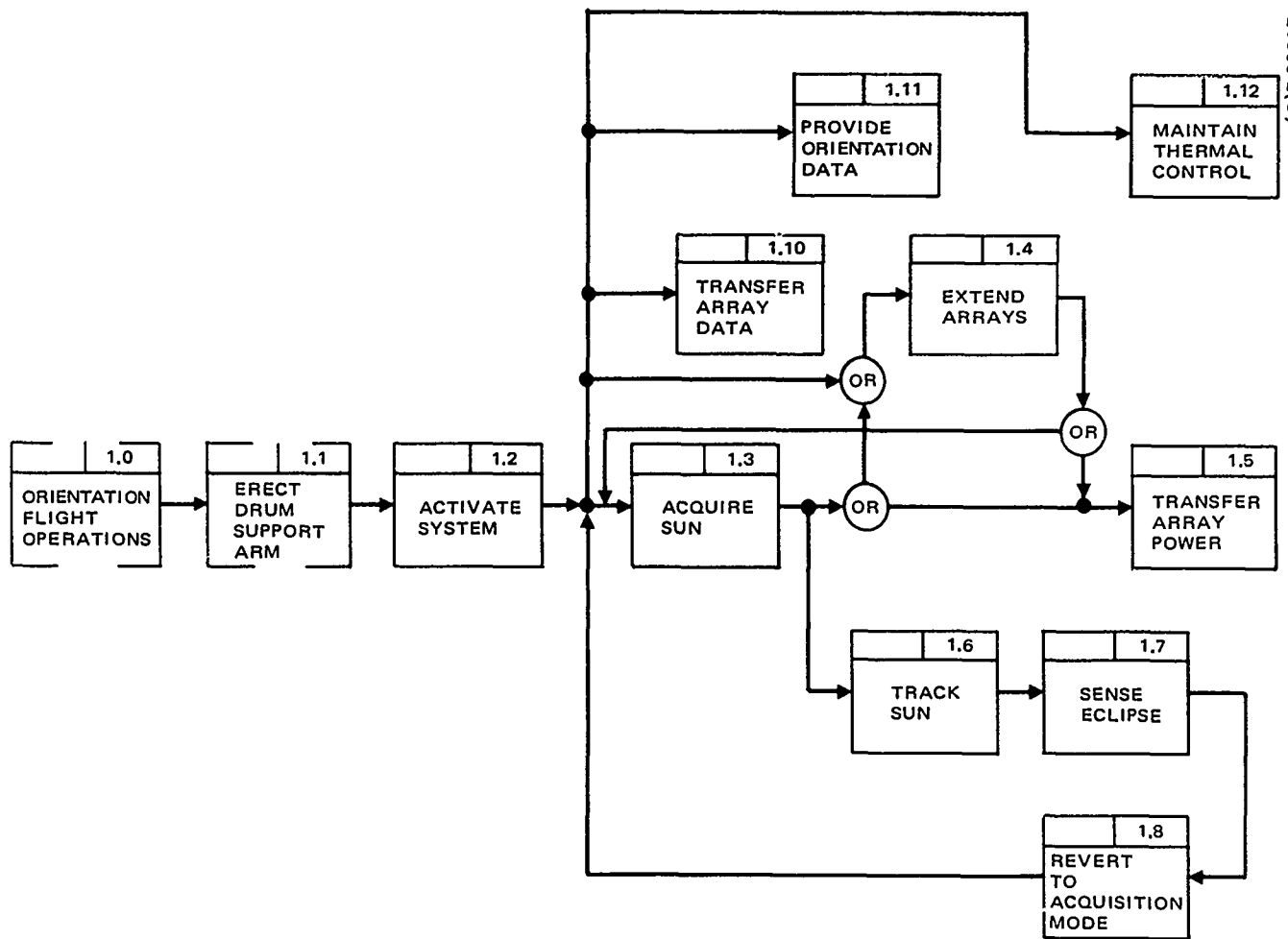


Figure 4-26. Orientation Subsystem Flight Operations

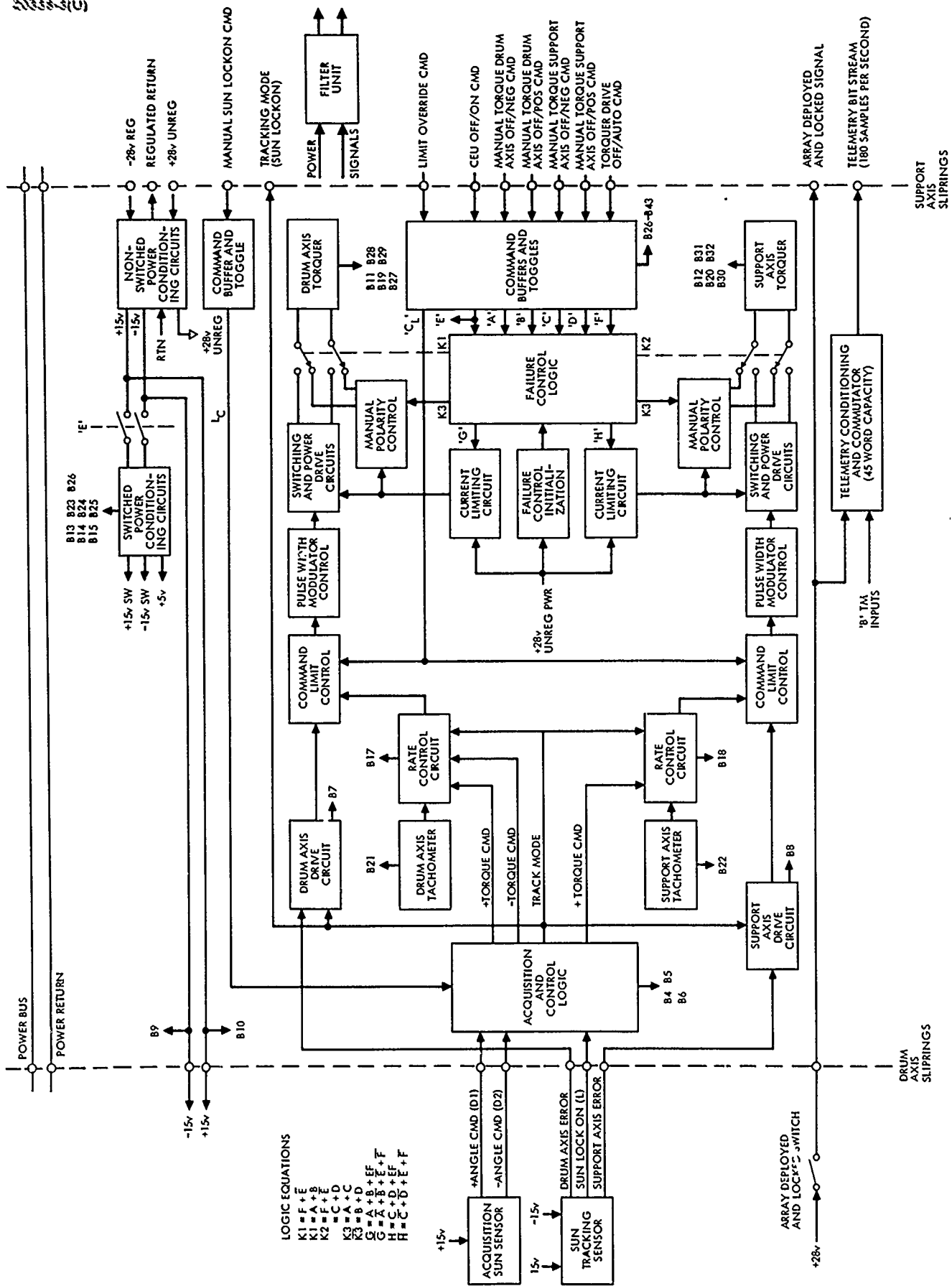


Figure 4-27. Orientation Subsystem Block Diagram

TABLE 4-6. ORIENTATION SUBSYSTEM COMMANDS

Command No.	Command Name*	Command Function
1**	Manual Torque, Support X Axis, OFF/POSITIVE	Apply plus torque to support X axis drive until command off.
2**	Manual Torque, Support X Axis, OFF/NEGATIVE	Apply minus torque to support X axis drive until commanded off.
3**	Manual Torque, Drum W Axis, OFF/POSITIVE	Apply plus torque to drum W axis until commanded off.
4**	Manual Torque, Drum W Axis, OFF/NEGATIVE	Apply minus torque to drum W axis until commanded off.
5	Control Electronics Unit OFF/ON	Receipt of each command alternately turns unit on and off
6	Limit Override OFF/ON	Receipt of each command alternately removes or inserts rate command limit in both channels.
31	Manual Sun Lockon, OFF/ON	Receipt of this command provides control logic with apparent sun lockon signal even though not received from tracking sensor's lockon cell. Subsequent command removes control logic.
33	Torquer Drive, OFF/AUTO	Receipt of each command alternately closes (AUTO) or opens current path to torquers if CEU is on.

\*Command name is structured to denote which logic state is established at initialization.

\*\*Receipt of OFF command leaves the torquer open circuited.

TABLE 4-7. ORIENTATION MECHANISM SLIPRING ASSIGNMENTS

Support Axis	
Ring No.	Function
1	Solar cell electronics unit Off/On command
2	Torquers off/on command
3	Manual sun lockon command
4	Limit O/R off/on command
5	CEU off/on command
6	Manual torque drum command -
7	Manual torque drum command +
8	Manual torque support command -
9	Manual torque support command +
10	Tracking mode
11	2-phase neutral
12	Phase 1
13	Phase 2
14	"A" measurement
15	"D" measurement
16	"B" measurement
17	Deployed and locked
18	Fully extended
19	Fully retracted
20	CEU unregulated bus
21	Structure ground
22	-28 volts dc regulated
23	+28 volts dc regulated
24	Regulated return 1
25	Regulated return 2
26	-z logic signal
27	Commutator index
28	Frame reset
29	Shaft temperature - support axis
30	Motor temperature - support axis



Table 4-7 (continued)

Drum Axis	
Ring No.	Function
1	Solar cell electronics unit off/on command
2	Sun lockon
3	Drum axis error
4	Support axis error
5	Negative acquisition
6	Positive acquisition
7	+15 volts dc
8	-15 volts dc
9	2-phase neutral
10	Phase 1
11	Phase 2
12	"A" measurement
13	"D" measurement
14	Deployment switch, normally open connection
15	Array fully extended
16	Array fully retracted
17	Structure ground
18	Regulator return 1
19	Regulator return 2
20	Regulator return 3
21	+28 volts dc regulated
22	Agena commutator index
23	Frame reset
24	Deployment switch, normally closed connection
25	Spare
26	Motor temperature - drum axis
27	Motor temperature - drum axis
28	Shaft temperature - drum axis
29	Shaft temperature - drum axis
30	Spare

Subsystem Telemetry. To provide sufficient information for evaluation of subsystem status and performance without adding to the slip-ring burden, a 45-word data commutator was incorporated within the CEU. Circuitry was provided to buffer each signal and condition it to a 0-5 volt level at the commutator input. No signals in this subsystem were super-commutated, so all signal sample rates were equal to frame rate, approximately 4 per second. The telemetered signal list is in the Instrumentation Section.

### Orientation Mechanism

The orientation mechanism consists of a basic structure or central gimbal assembly, the torquers and sensors required for orientation drive, and the deployment hinge. Figures 4-28 through 4-30 illustrate various details of the elements and the complete unit.

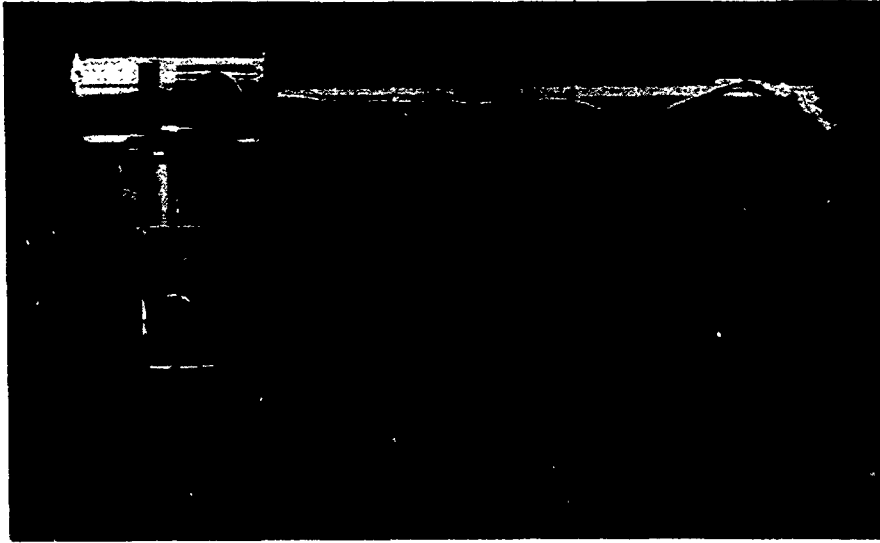
Basic Structure. The basic gimbal structure comprises housings, shafts, and bearings (Figures 4-29, 4-31, and 4-32). Housing shells are machined from magnesium alloy forgings to a 6.45 inch diameter, with wall thickness ranging from 1/10 to 1/8 inch. Cutouts providing access to the brushes are closed with nonstructural sheet aluminum covers. End closures are titanium for a better thermal match with the steel bearings.

Aluminum alloy shafts are machined from tubular stock; final OD is 2.00 inches, with 1/8 inch wall thickness.

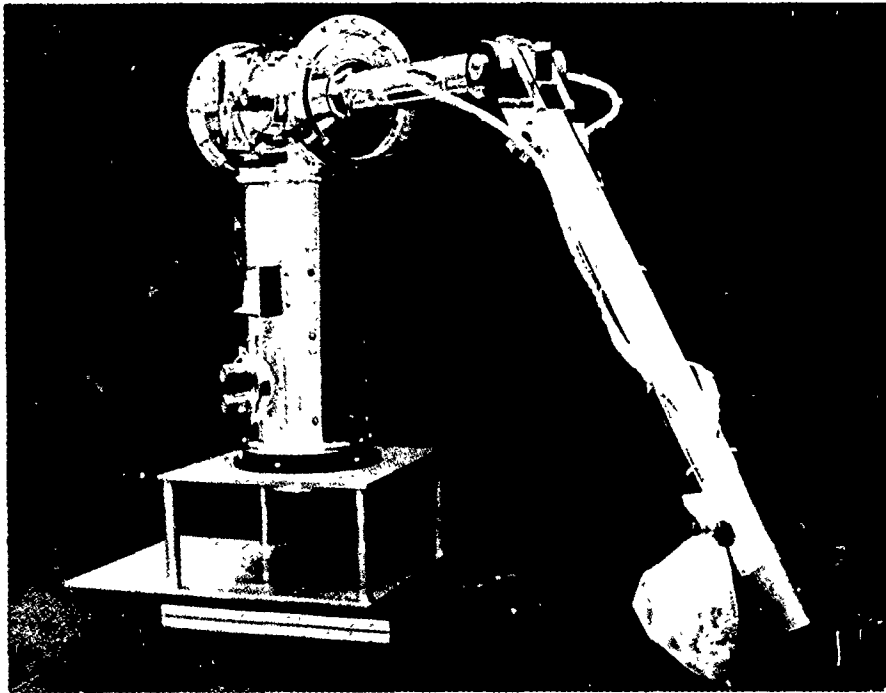
Bearing design is based on an approach successfully employed in several Hughes rotating space mechanisms. A single 25-degree (nominal) contact angle ball bearing is utilized at each end of the housing; one bearing is fixed, the other floats against a wavy washer providing preload on both bearings through the housing (Figure 4-33). This tolerates a -50° to 150° F temperature range, with a radial difference of 25° F across the bearings. Races and balls are burnished with molybdenum disulfide; the ball retainer is Duroid 5813, a Teflon, glass-fiber, MoS<sub>2</sub> composite. The dry lube is adequate for the light loads and low speeds involved, and does not outgas to interfere with optical surfaces.

Static load capability of the bearings is 10,000 pounds axially and 3,650 pounds radially based on a conservative Hertzian stress limit of 285,000 psi. Bending stiffness of the assembly varies with applied load, but is in the range of 0.5 to 1 x 10<sup>6</sup> lb-in./rad.

Rate Sensor. A shaft rate sensor is utilized on each axis in the mechanism as a control feedback element during sun acquisition, as a rate limiting element during sun tracking, and as a telemetry source. The main components are a permanent magnet field, a multipole armature, a commutator, and a brush assembly in a frameless, gearless, pancake configuration (Figure 4-34). No electrical power is required, the rate of rotation generating a proportional electromotive force with a nominal scale factor, in this application of 13 mv/deg/sec. To minimize commutator/brush interface resistance,



a) Deployed in Normal Operating Configuration  
(Photo A28782)



b) Unlatched (Photo A28781)

Figure 4-28. Orientation Mechanism

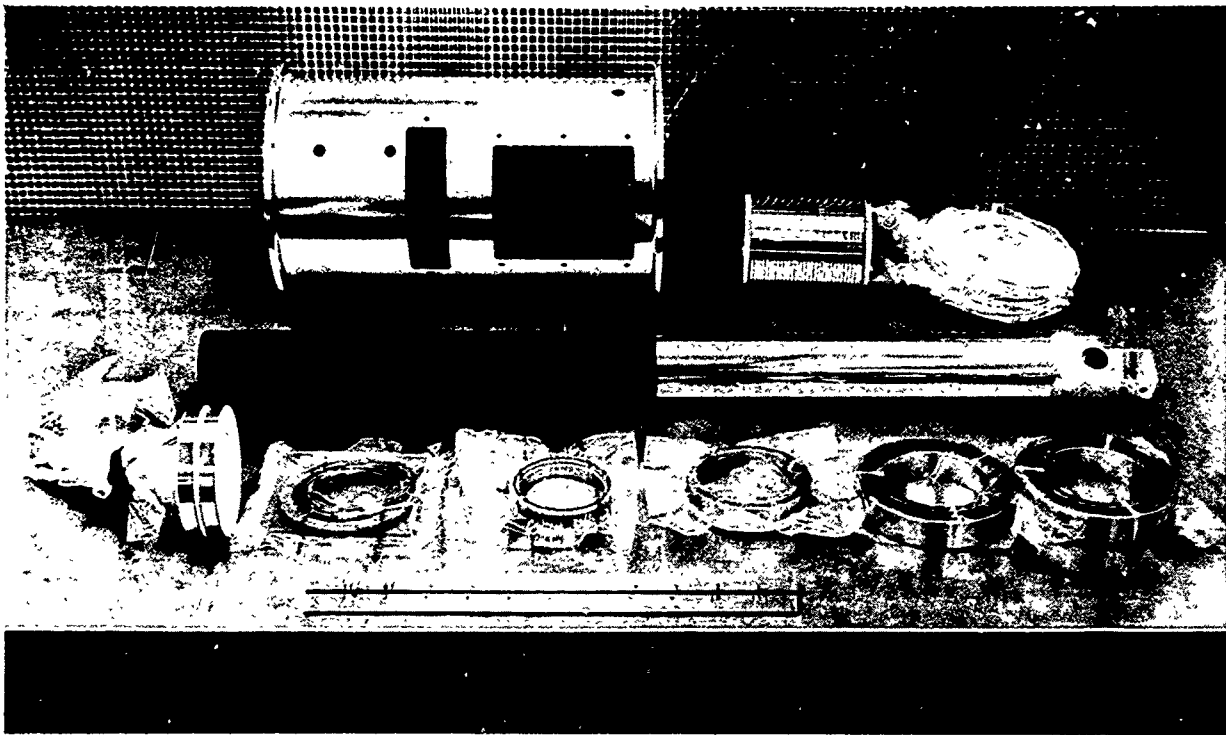
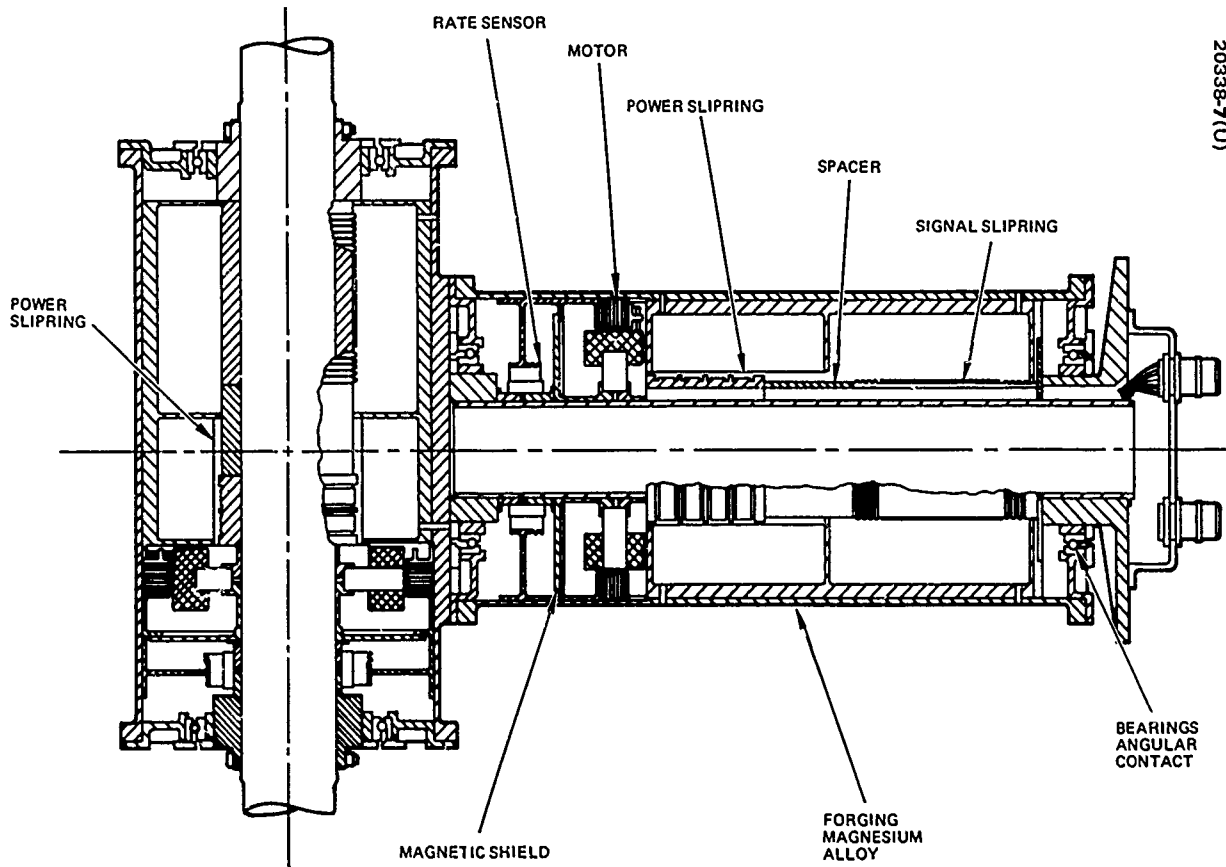


Figure 4-29. Orientation Mechanism Drum Axis Hardware  
(Photo A28317)



20338-7(U)

Figure 4-30. Orientation Mechanism Internal Profile

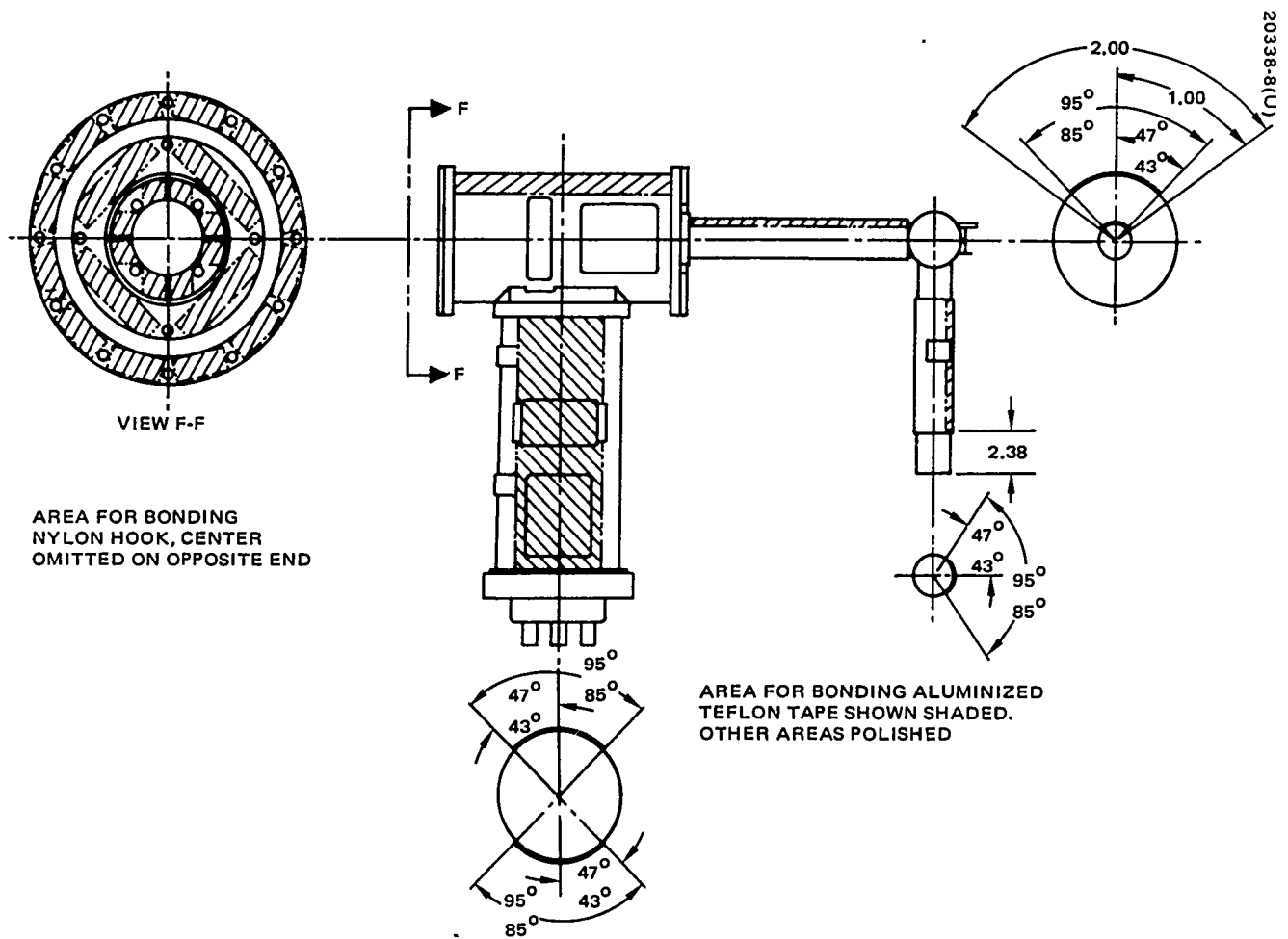


Figure 4-31. Orientation Mechanism Thermal Finish

eight brushes are used (six are redundant). Brush material is the same as that used for other signal and power transfer (see below). Following NASA experience, the basic copper commutator bars are given a nickel strike followed by a thin plating of gold to minimize signal noise.

Torquer. The FRUSA gimbal torquers are frameless, gearless units generically similar to the rate sensors. In the torquer, however, the coil windings are energized to produce torque. Four brushes (two are redundant) utilize a long-wearing, self-lubricating, sintered composite of molybdenum, moly-disulfide, and tantalum, bearing on a bare copper commutator. This combination has been extensively tested by both NASA and Hughes in similar applications. Output, as employed here, is rated at 2.2 lb-ft at 118 watts. Driver design is conservative, however, limiting the torque to 1.8 lb-ft (80 watts) to avoid any possibility of degrading the magnets by overdriving. The motor provides an ample margin over the 0.25 lb-ft of gimbal friction torque specified and experienced in flight application.

Electrical Transfer. Sliprings and brushes are used for the transfer of both power and data across the gimbals. The FRUSA hardware is illustrated in Figures 4-29, 4-35, 4-36, and 4-37. Designs and materials suitable for space use were developed over several years on a number of programs (e.g., OLSCA and several Hughes dual-spin satellites). In the present application, brush travel is so low, even for long duration missions, that wear is not a problem; the primary concern is good seating to minimize interface resistance, and absence of sticktion. FRUSA rings employ coin silver; the brushes are a sintered, self-lubricating composite of silver, moly-disulfide, and copper (Stackpole SM 487), configured to provide a conservative apparent current density through the brush face of 75 amp/in<sup>2</sup> (power circuits). At this value, the brush interfaces contribute less than a tenth of the measured overall (round-trip) subsystem power circuit resistance of 0.023 ohm. Implementation of this design criterion required use of four brushes in parallel on each power circuit ring; nominal brush pressure of 8 psi is supplied by cantilevered springs bearings on the upper brush surface. Slot relief is provided to allow each brush to rock as required to effect a full-face seat.

Data circuit rings carry minimal currents and are configured for fabrication convenience and structural integrity. Each ring is serviced by two brushes in parallel on cantilevered leaf springs.

Satisfactory flight performance of the design was observed at normal tracking rates, in static conditions, and at resumption of tracking operation following prolonged static conditions with full continuous power transfer.

Shaft Position. As an economy measure, shaft position detectors were not incorporated in the FRUSA orientation mechanism design, on the principle that array position could be derived from the known position of a stabilized vehicle in orbit, and the sun-error telemetry. The integration contractor, however, imposed constraints based on view angle and

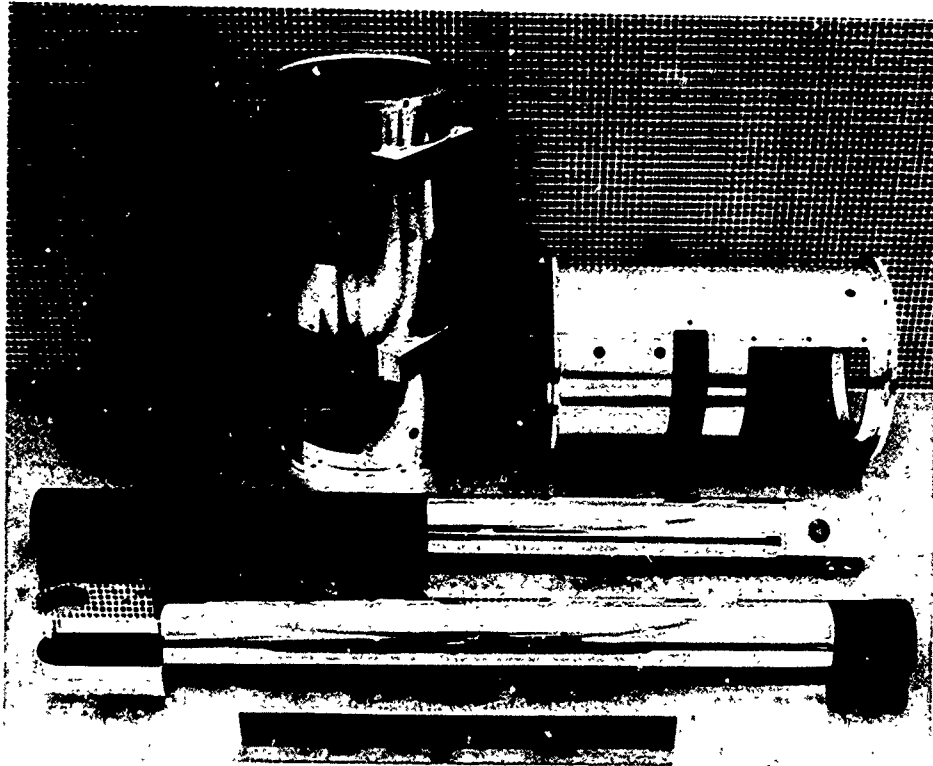


Figure 4-32. Orientation Mechanism Housings and Shafts  
(Photo ES28316)

communication requirements of other experiments and installed, as a minimum operational aid, a magnetic encoder with a 5-degree resolution at the spacecraft/orientation-mechanism interface (support axis). The information so provided proved invaluable during the mission. Because the orientation control was deactivated for long periods, a similar device would have been useful on the drum axis as well. This experience indicates that position pickoffs should be incorporated as a basic feature of future designs.

Deployment Hinge. Simplicity of design and operation was the major goal of the deployment mechanism. The deployment mechanism's function is to swing the array subsystem out from its stowed position and lock it in the flight position (see Figure 4-28a and b) when the pyrotechnic launch lock devices (not part of this subsystem) are fired. The hinge is based on a simple tongue and clevis joint, with ball bearings utilized to ensure low friction (Figure 4-38). Bearing lubrication is by burnished-in moly-disulfide, with additional MoS<sub>2</sub> in the Duroid 5813 ball retainers. Deployment energy is furnished by two symmetrically mounted spiral springs concentric with the hinge pin, wound at assembly to provide a margin adequate to tolerate variations in bearing friction and cable stiffness due to wide ranges in expected temperature at operation. Residual energy at the end of the stroke is absorbed by bending of the drum axis shaft as a consequence of employing a hard stop at the hinge. A door latch type device locks the hinge in the flight position. The mechanism performed flawlessly during unit and system tests and in flight.

#### Sun Sensors

The sun sensor group includes a two-axis tracking sensor and a set of acquisition sensors, all mounted on a bracket at the outer end of the solar array drum mechanism assembly to provide clear, reflection-free fields of view. The general geometry is illustrated in Figure 4-39, an outline drawing of the assembly in Figure 4-40, photographs of the sensors in Figures 4-41 and 4-42, and a calibration of one tracking axis (with  $\pm 15$  v excitation) in Figure 4-43. The slit-type sensors are insensitive to earth shine and are employed during acquisition to avoid false lockon to bright bodies other than the sun.

In operation, the solar array is first slewed about the support axis until the sun appears in the field of view of one of the acquisition sensor sectors. Rotation about that axis is then stopped, and rotation about the drum axis is initiated in a preferred direction. At some point in this rotation, the sun will appear in the lockon cell field of view, whereupon operation is switched to the normal tracking mode, with sun line-of-sight errors detected by bridge circuits which incorporate suitably masked photoresistive cadmium sulfide cell pairs. The sequence is automatic, via logic and switching in the CEU.



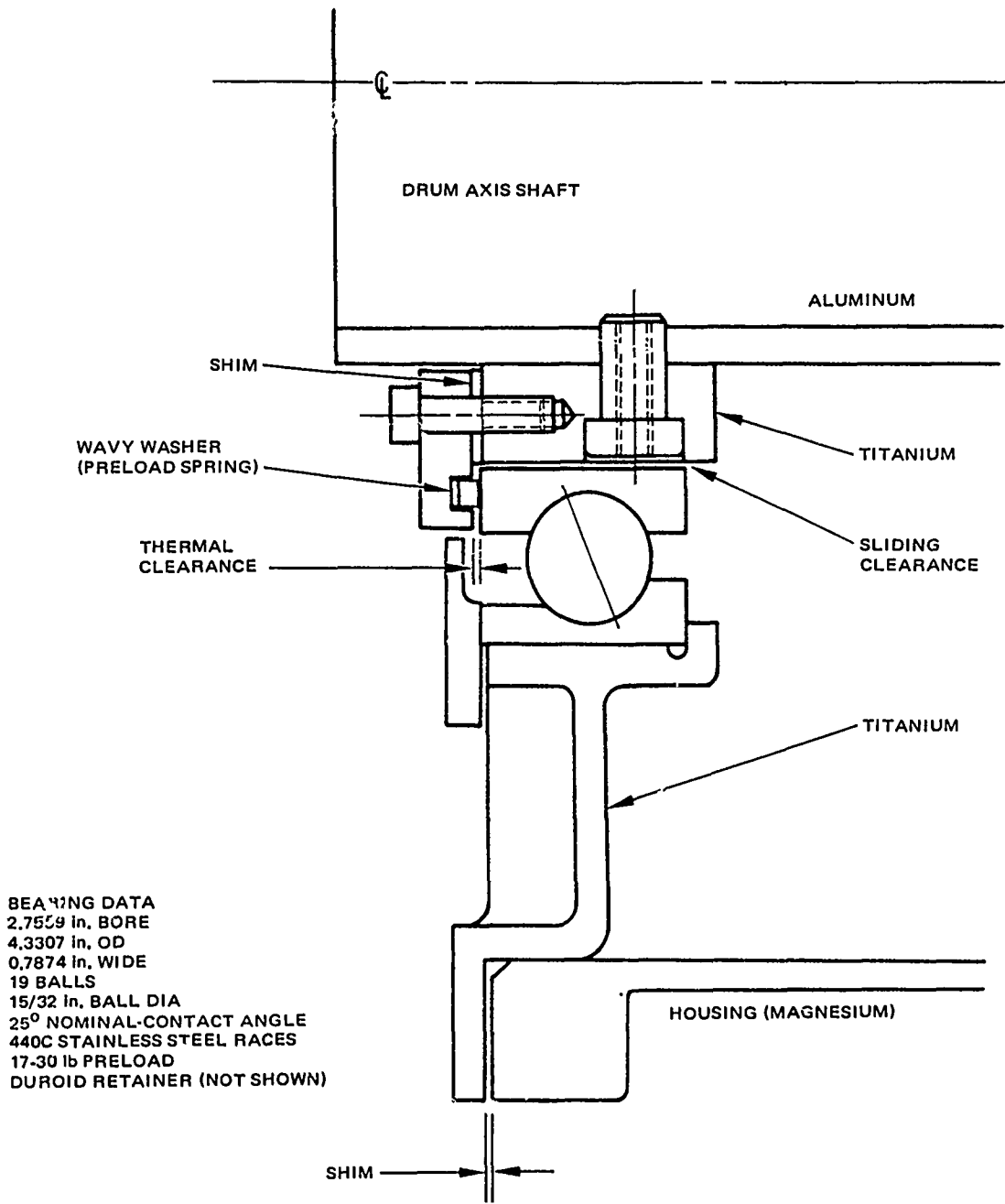


Figure 4-33. Gimbal Bearing



Figure 4-34. Frameless Pancake dc Tachometer

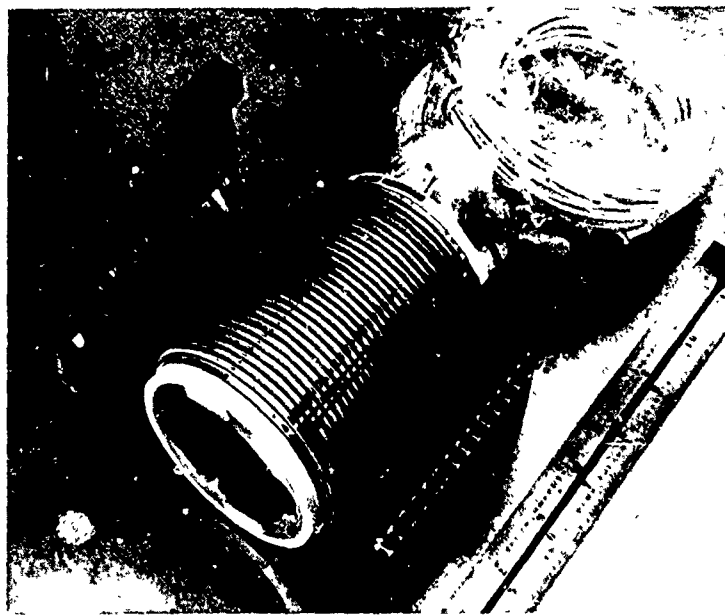


Figure 4-35. Orientation Subsystem Drum Axis Data Slip Rings and Brushes (Photo ES28319)

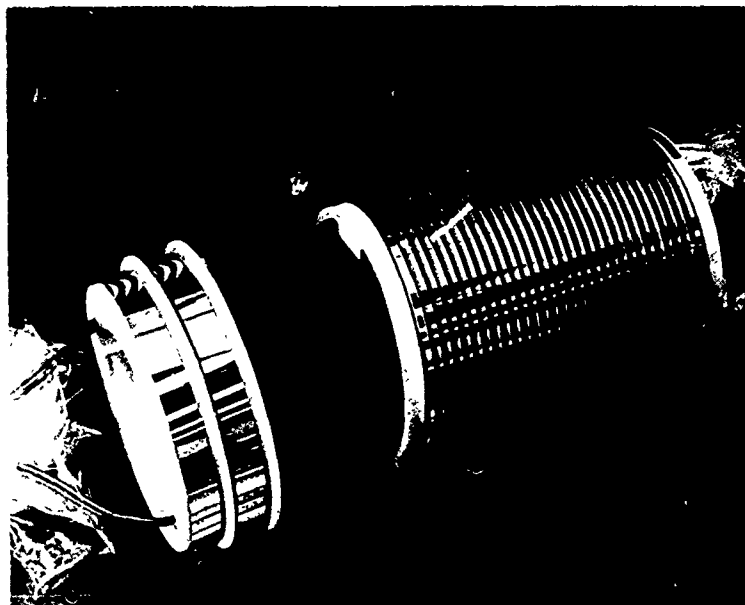
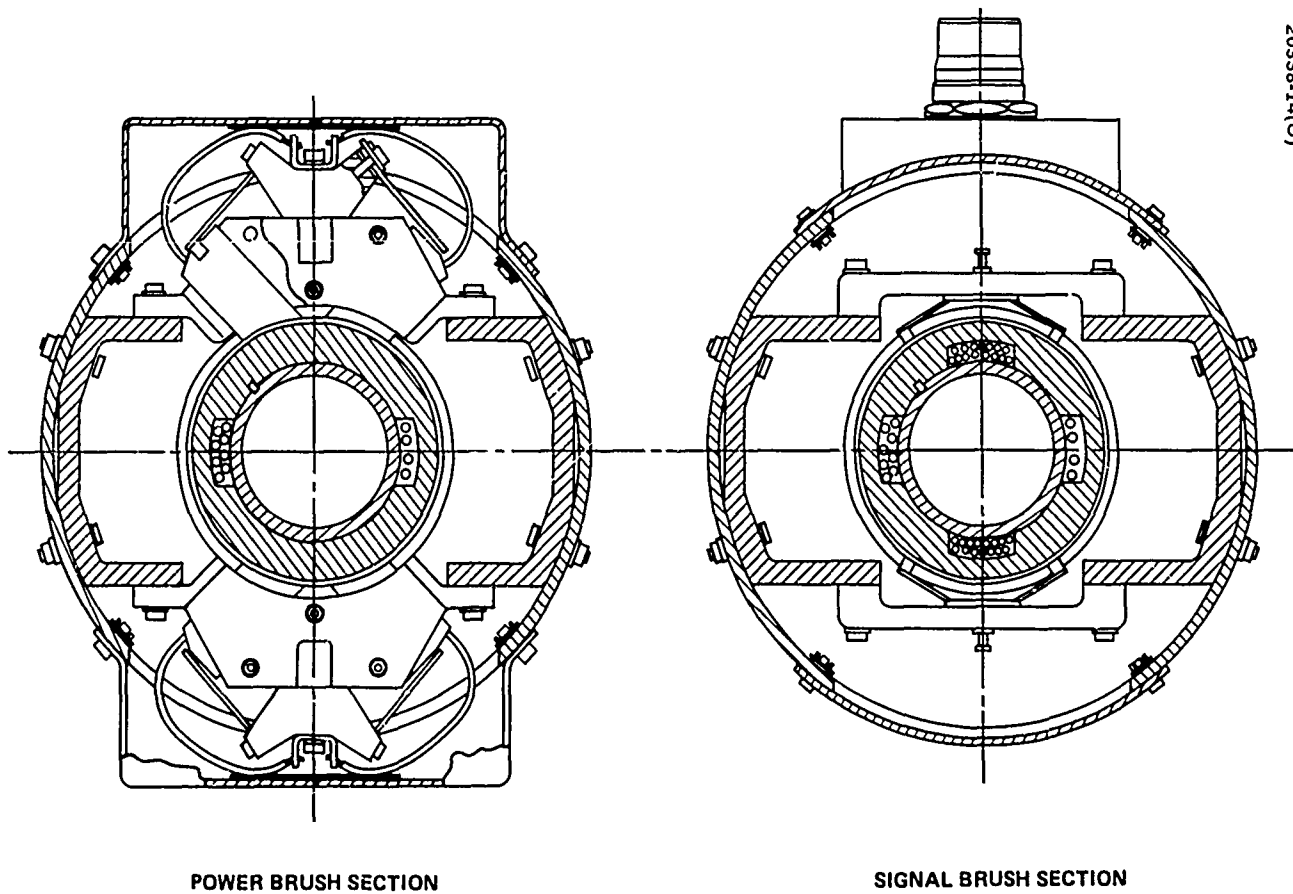


Figure 4-36. Orientation Subsystem Drum Axis Power and Data Slip Rings



20338-14(U)

Figure 4-37. Brush Arrangements

20338-15(U)

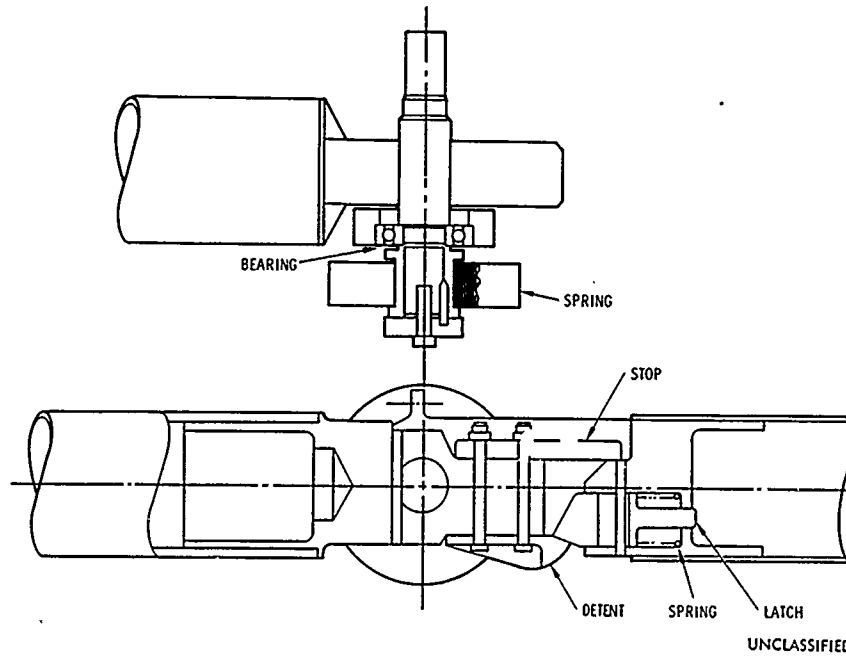


Figure 4-38. Deployment Mechanism

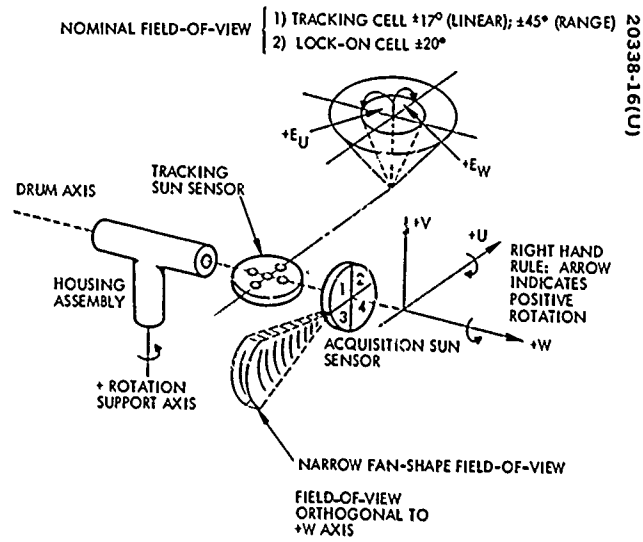
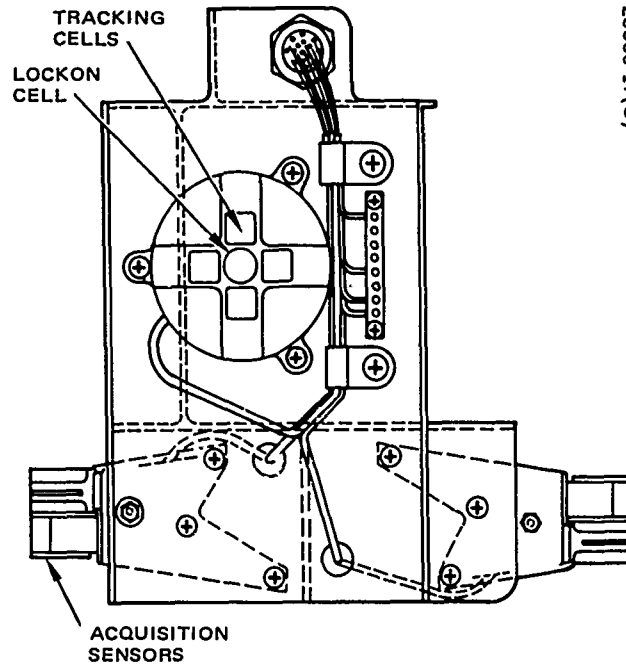


Figure 4-39. Sun Sensor Geometry



20338-17(U)

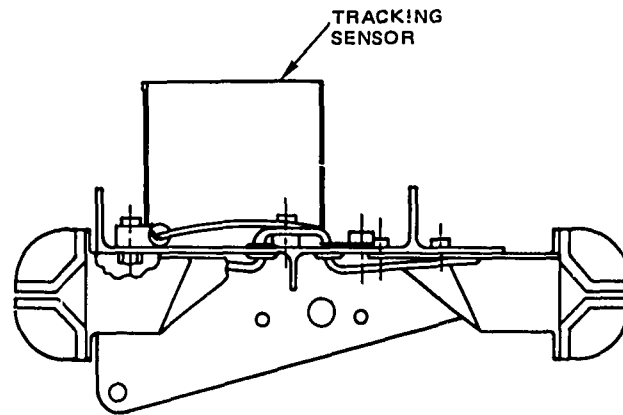


Figure 4-40. Sun Sensor Group

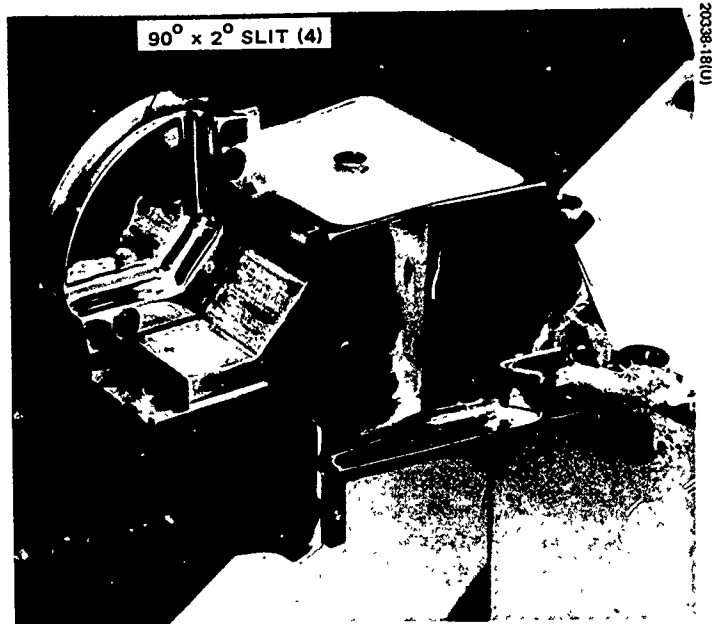


Figure 4-41. Acquisition Sensor  
(Photo A13933)

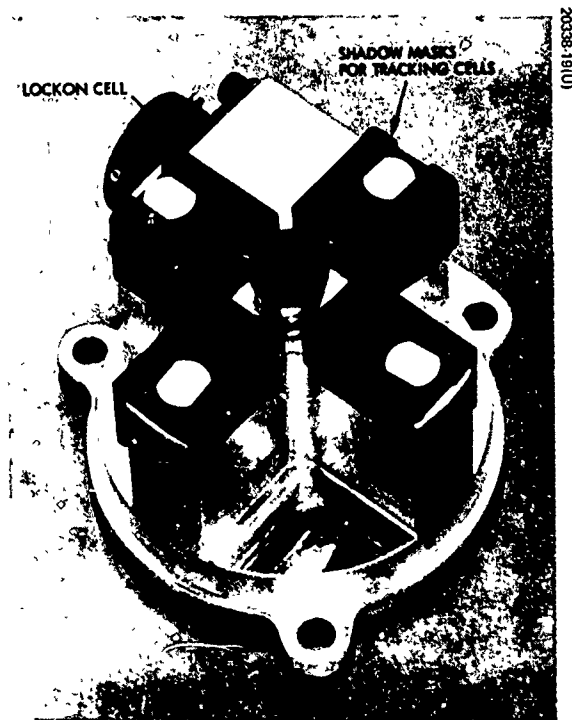


Figure 4-42. Tracking Sensor  
(Photo R83168)

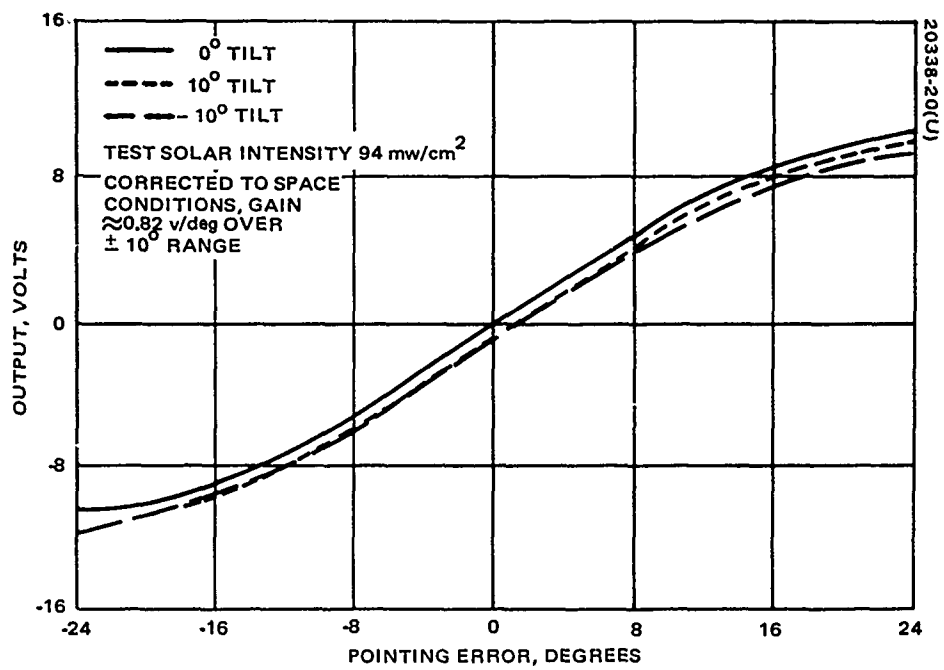


Figure 4-43. Calibration of Sun Error Sensor

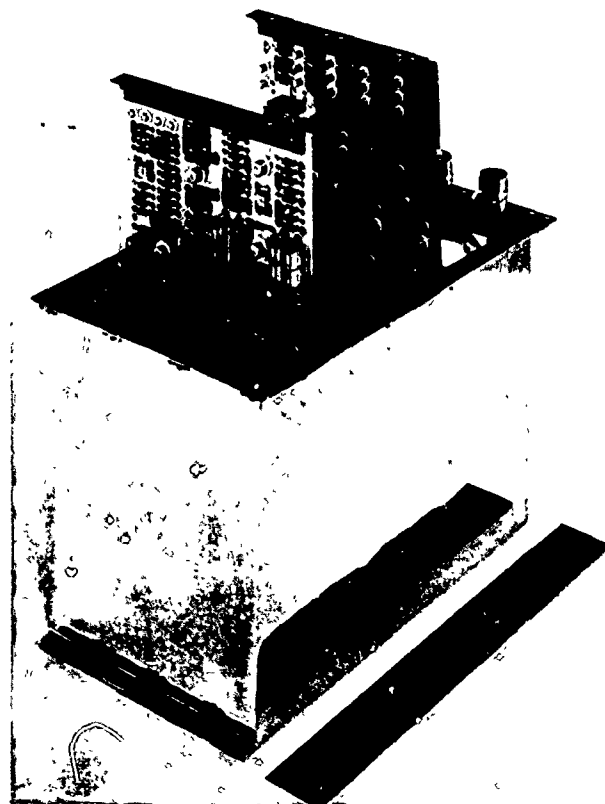


Figure 4-44. Partial Assembly, Control Electronics Unit (Photo 4R16392)

### Control Electronics Unit

The CEU provides the logic and analog computations for the various modes of operation. It derives error signals from commands, sun sensors, and shaft rate sensors, and applies correctional signals to the appropriate torque motor. It limits the torquing rate in the automatic modes by increasing feedback of the rate signals. Logic control is provided by processing sun sensor data and command inputs. Failure mode control torquing is implemented by providing current directly to the torquers, bypassing all the automatic control circuitry. A power conditioning unit develops secondary voltages for use within the subsystem.

The unit weighs 12-1/2 pounds, with overall dimensions of approximately 7 by 7 by 12 inches. Seven circuit boards of five types are enclosed, plus miscellaneous components on separate brackets. Total parts count is about 900. Maximum input power requirements are:

+28 volts dc regulated	8 watts
-28 volts dc regulated	2 watts
Torquer unregulated power (switched) during eclipse/daylight transitions from solar array to internal batteries) at 20 to 44 volts dc	100 watts*
CEU unregulated power (continuous during all operational phases) at 24 to 44 volts dc	2.5 watts

An illustration of the CEU and a mechanization diagram are presented in Figures 4-44 and 4-45.

### Filter Unit

A filter unit was designed and integrated into the subsystem to attenuate noise originating in the 3.3-kHz switching amplifiers driving the torquers. This noise tended to propagate into many of the data channels, degrading the accuracy of the sampled outputs. All power and signal lines except the boom drive power were, therefore, routed through feedthrough filter capacitors in the filter unit, resulting in acceptable levels of noise presented to the spacecraft systems.

This unit is approximately 4 by 5 by 7 inches, and weighs 2-1/2 pounds.

---

\*At torque peaks. Normally about 4 watts steady state.



## Subsystem Functional Control Design

Background theory for the functional design of the FRUSA orientation control loops may be found in the OLSCA final report. The system comprises a linear, closed-loop, sun tracking mechanization. The acquisition mode operates from a fixed rate command, with linear rate followup; no signal shaping is employed in this mode other than a half-second filter to attenuate noise. The tracking mode operates (except for rate limiting) entirely from the optical sensor signals, with lead-lag shaping to provide inherent loop stability, and with a significant added stabilizing contribution from the essentially-Coulomb type axis friction.

Figure 4-46 is a functional block diagram of one of the two identical control channels. Values of inertia for the load block range from 125 slug-ft<sup>2</sup> for the drum axis to 175 to 300 slug-ft<sup>2</sup> for the support axis, depending on array position. Maximum gain of the "geometry" block is unity, which pertains to drum axis tracking normally, and to support axis tracking for certain specific geometries. Normally, support axis gain is somewhat below unity, and in the noon turn reaches zero momentarily; this has not proven to be an operational problem. No dead bands were incorporated, as it is possible to show that minimum changes in array momentum, and therefore minimum disturbances to the vehicle, result from continuous linear control.

At least three design features tend to forestall any unstable coupling between control modes and array structural vibration modes:

- 1) The control system bandpass is configured to cut off well below the array fundamental vibration frequencies.
- 2) The loop does not incorporate an integral control term; as a result, all roots lie in the left half plane (see Figure 4-47).
- 3) The Coulomb friction adds a substantial damping contribution, equivalent to several percent of structural damping.

To substantiate stability of the coupled system, array flexibility was expressed as a dynamic moment of inertia (J as a function of s), taking into account the first three array flexibility modes. For example, with the array parallel to the vehicle and zero structural damping assumed, the equivalent dynamic moment of inertia may be expressed as:

$$J = 175 \times 0.47 \left[ \frac{s^2 + 1.20^2}{s^2 + 1.13^2} \times \frac{s^2 + 1.59^2}{s^2 + 1.20^2} \times \frac{s^2 + 2.81^2}{s^2 + 2.72^2} \right]$$

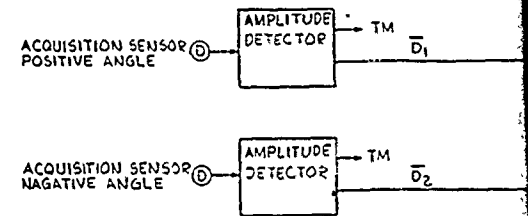
### SWITCH FUNCTIONS AND LOGIC

NO.	AXIS	FUNCTION	POS LOGIC COND TN TO OPEN	POS LOGIC COND TN TO CLOSE
1D	DRUM	STEERING LOOP SHORT	T	$\bar{T}$
2D	DRUM	STEERING LIMIT OVERRIDE	$C_L$	$\bar{C}_L$
3D	DRUM	POS RATE BIAS	$AB_1B_3$	$\bar{A} + \bar{B} + \bar{B}_3$
4D	DRUM	RATE LOOP ACQ	A	$\bar{A}$
5D	DRUM	RATE LOOP TRACK	T	$\bar{T}$
4D	DRUM	NEG RATE BIAS	$AB_2B_3$	$\bar{A} + \bar{B}_2 + \bar{B}_3$
1S	SUPPORT	STEERING LIMIT SHORT	T	$\bar{T}$
2S	SUPPORT	STEERING LIMIT OVERRIDE	$C_L$	$\bar{C}_L$
3S	SUPPORT	POS RATE BIAS	$AB_4$	$\bar{A} + \bar{B}_4$
4S	SUPPORT	RATE LOOP ACQ	A	$\bar{A}$
5S	DRUM	RATE LOOP TRACK	T	$\bar{T}$

NOTE: ALTHOUGH THE SYSTEM IS DEFINED IN POSITIVE LOGIC TERMS, THE ELECTRONIC SWITCHES ACTUALLY REQUIRE THE COMPLEMENT, I.E. SWITCHES OPEN FOR LOGICAL "0" AND CLOSE FOR LOGICAL "1".

### LOGIC DEFINITIONS

- L LOCK-ON CELL ILLUMINATED
- $L_C$  LOCK-ON CELL BACK-UP COMMAND-ON
- T= $L_C$  TRACKING MODE
- A= $\bar{T}$  ACQUISITION MODE
- $D_1$  POSITIVE ANGLE ACQUISITION SENSOR
- $D_2$  NEGATIVE ANGLE ACQUISITION SENSOR
- $B_1$  POSITIVE ANGLE ACQUISITION
- $B_2$  NEGATIVE ANGLE ACQUISITION
- $B_3$  DRUM AXIS ENABLE
- $B_4$  SUPPORT AXIS ENABLE
- $C_L$  COMMAND LIMIT OVERRIDE-ON



### TELEMETRY

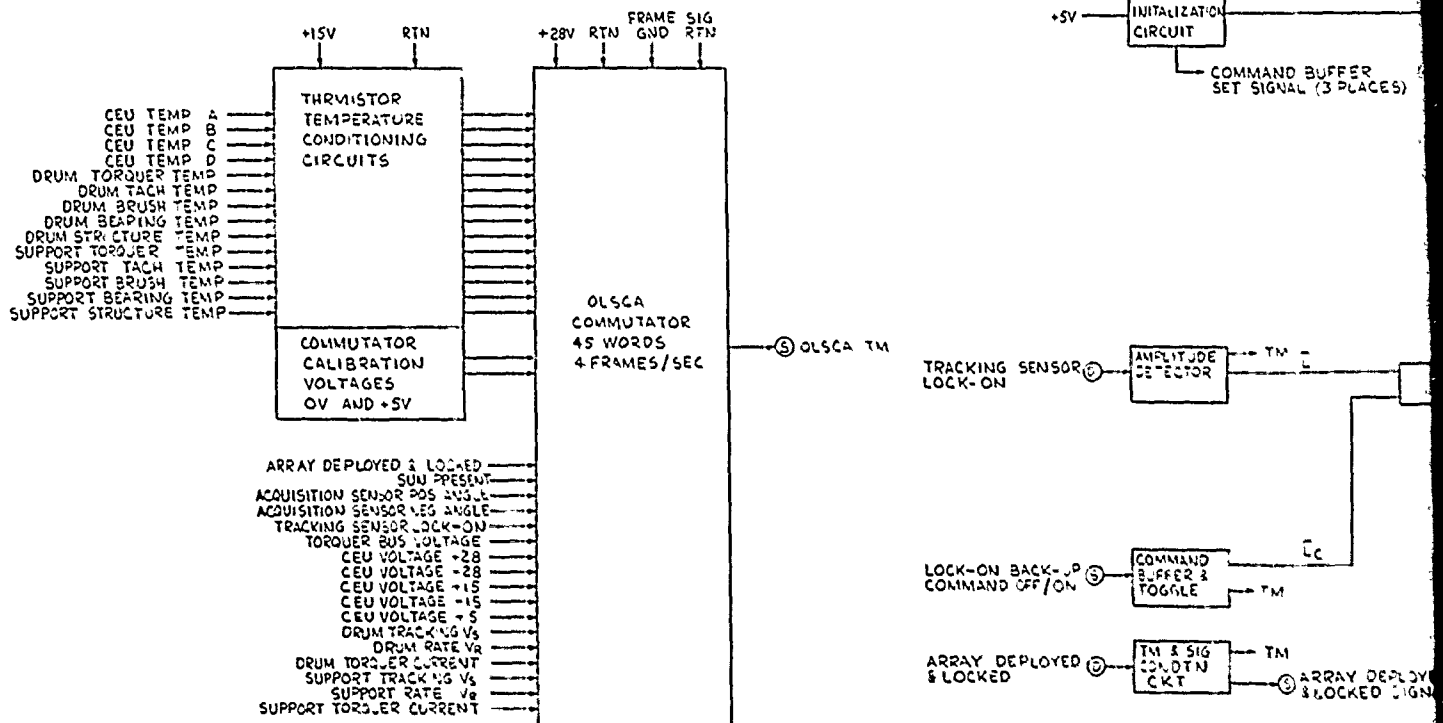
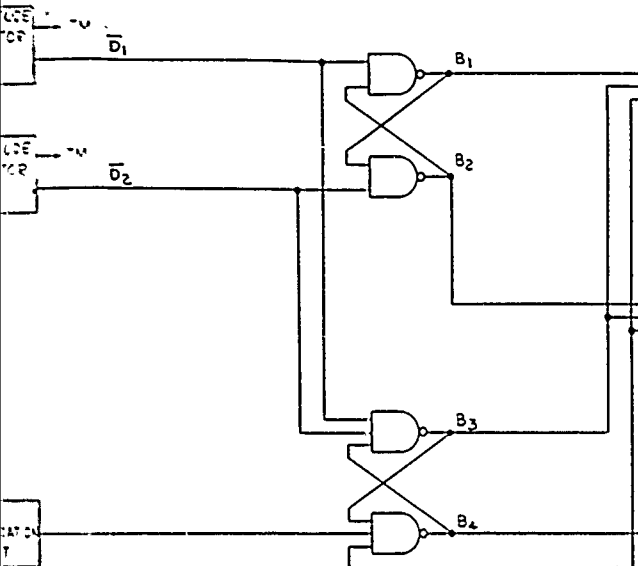


Figure 4-45. Control Electronics Unit Block Diagram

...ILLUMINATED  
 ...COMMAND-ON  
 ...  
 ...LE ACQUISITION SENSOR ILLUMINATED  
 ...LE ACQUISITION SENSOR ILLUMINATED  
 ...LE ACQUISITION  
 ...LE ACQUISITION  
 ...ENABLE  
 ...ENABLE  
 ...MIT OVERRIDE-ON

**ACQUISITION LOGIC**

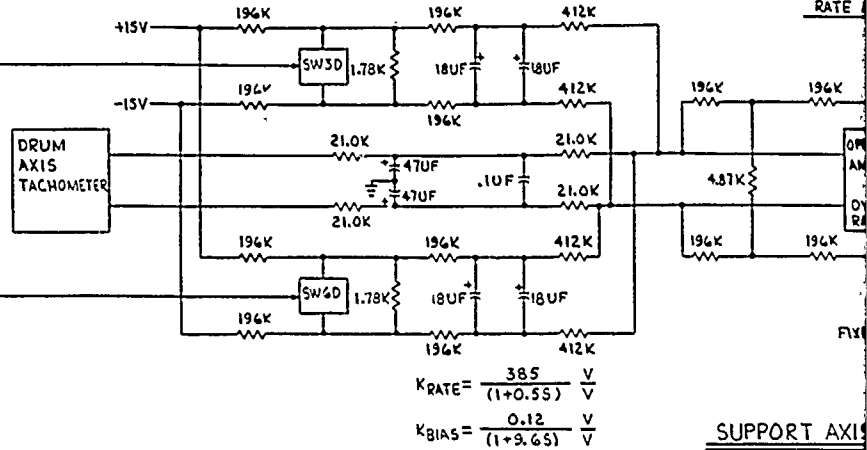
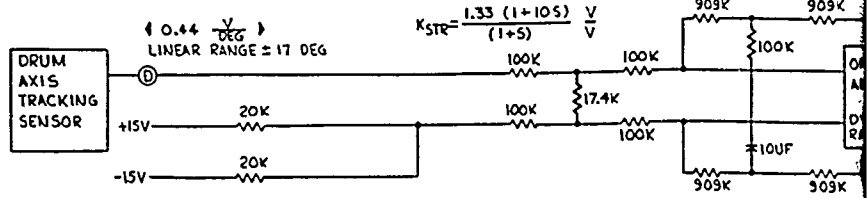


COMMAND BUFFER SET SIGNAL (3 PLACES)

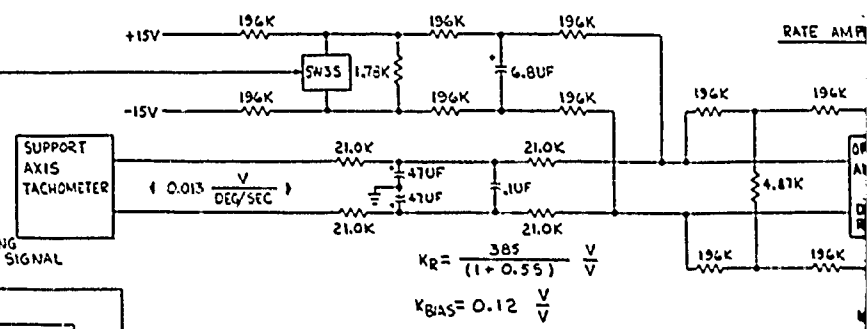
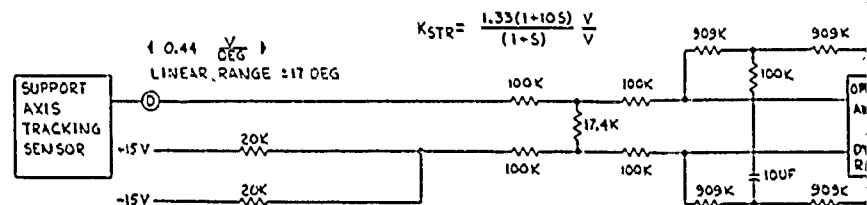
$(L_c \cdot L_d) = T$       $T = A$

ARRAY DEPLOYED  
BLOCKED SIGNAL

**DRUM AXIS**

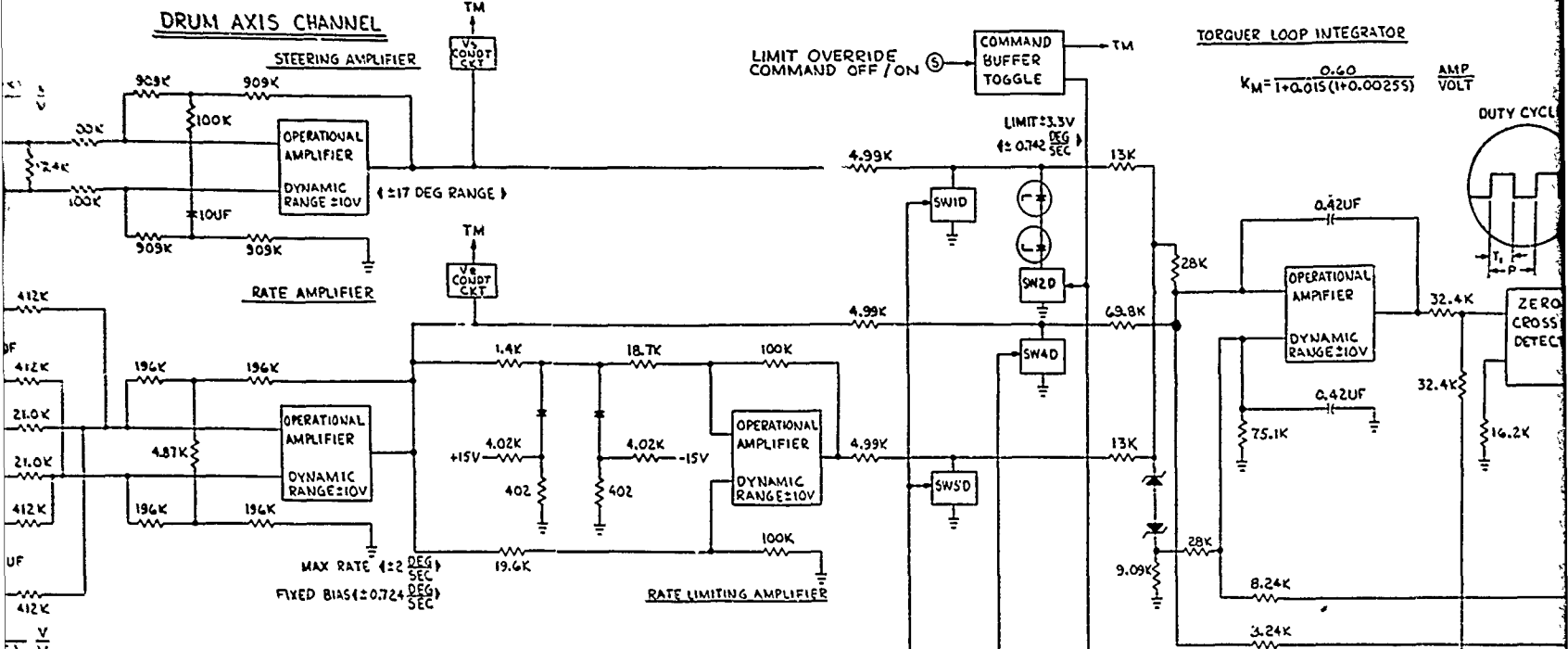


**SUPPORT AXIS**

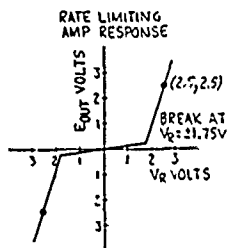
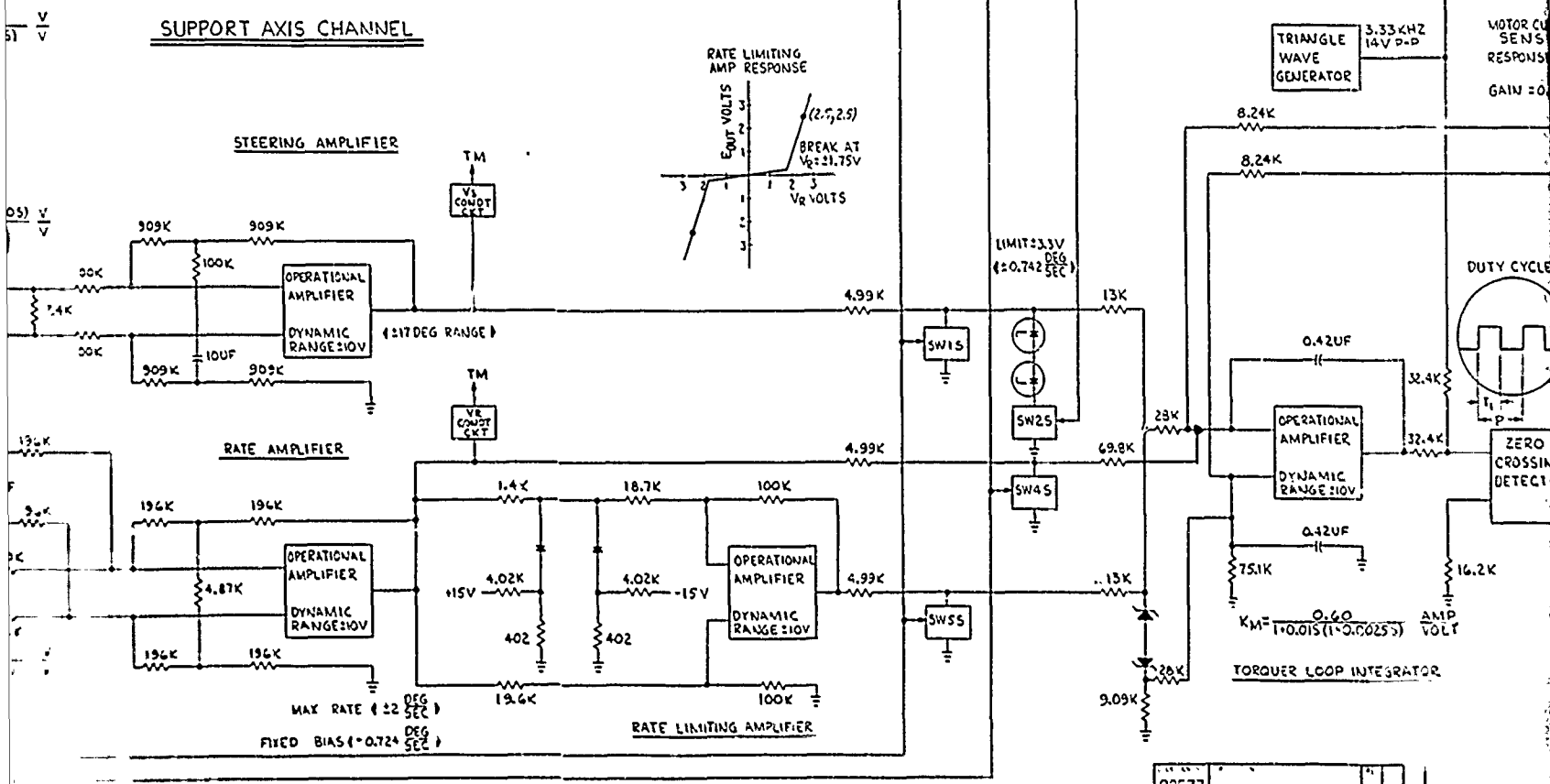


82577

**DRUM AXIS CHANNEL**



**SUPPORT AXIS CHANNEL**

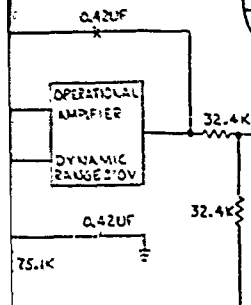


82577

AMP TORQUER

$\frac{0.60}{25.5 \times 0.0255}$  AMP VOLT

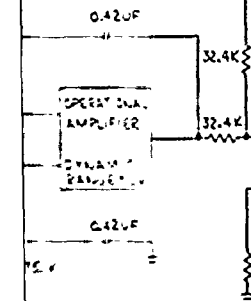
DUTY CYCLE =  $\frac{T_1}{P}$



TRIANGLE WAVE GENERATOR 3.33KHZ 14V P-P

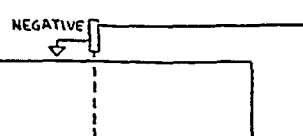
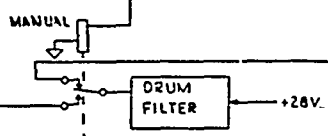
MOTOR CURRENT SENSING RESPONSIVITY =  $0.400 \frac{V}{LB-FT}$   
GAIN =  $0.15 \frac{V}{AMP}$

DUTY CYCLE =  $\frac{T_1}{P}$



AMP TORQUER

$\frac{0.60}{25.5 \times 0.0255}$  AMP VOLT



CURRENT LIMITED SWITCH

DRUM FILTER

MANUAL

NEGATIVE

SWITCHING POWER AMPL

DRUM LINE SWITCH

ZERO CROSSING DETECTOR

AUTO

COMPARATOR

DRUM TORQUER  
 $K_T = .37 \frac{LB-FT}{AMP}$

TEMP COUD CKT  
TM

CURRENT SENSOR AND LIMITER

CURRENT SENSING AND TM CKTS

COMPARATOR

DRUM TORQUER  
 $K_T = .37 \frac{LB-FT}{AMP}$

TEMP COUD CKT  
TM

CURRENT SENSOR AND LIMITER

COMPARATOR

SUPPORT TORQUER  
 $K_T = .37 \frac{LB-FT}{AMP}$

TEMP COUD CKT  
TM

CURRENT SENSOR AND LIMITER

CURRENT SENSING AND TM CKTS

COMPARATOR

SUPPORT TORQUER  
 $K_T = .37 \frac{LB-FT}{AMP}$

TEMP COUD CKT  
TM

CURRENT SENSOR AND LIMITER

SWITCHING POWER AMPL

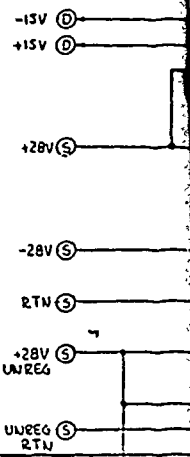
SUPPORT LINE SWITCH

SUPPORT FILTER

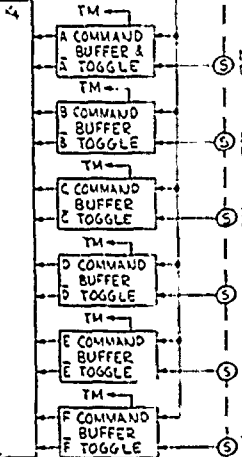
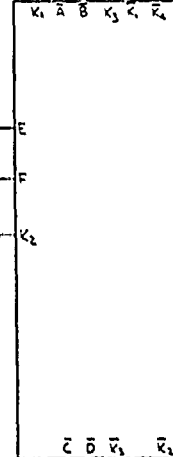
POSITIVE

CURRENT LIMITED SWITCH

MANUAL



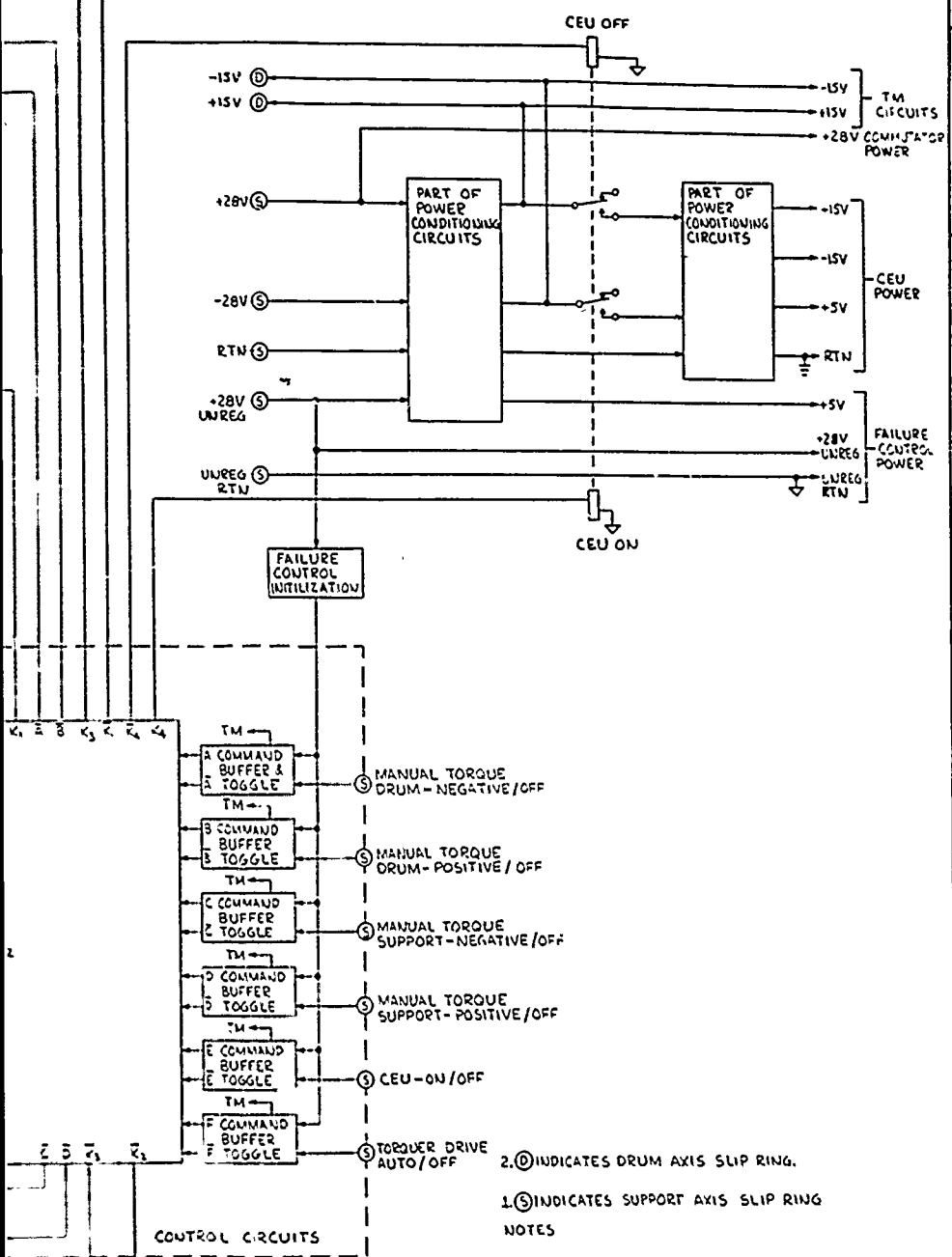
FAILURE CONTROL INITIALIZATION



CONTROL CIRCUITS

C REVISED AND REDRAWN  
 D INCORP .5 DEG/SEC RATE  
 E INCORP SUMMED RATE  
 F LIMIT

30338-22(11)



G  
F  
E  
C  
B  
A

2 ⊙ INDICATES DRUM AXIS SLIP RING.  
 1 ⊙/ INDICATES SUPPORT AXIS SLIP RING  
 NOTES

DESIGN NO.	REV.	DATE	BY	CHKD.
30338-22	11			
MECHANIZATION DIAGRAM CONTROL ELECTRONICS UNIT (ECU)			HUGHES	
J182577			3064220	

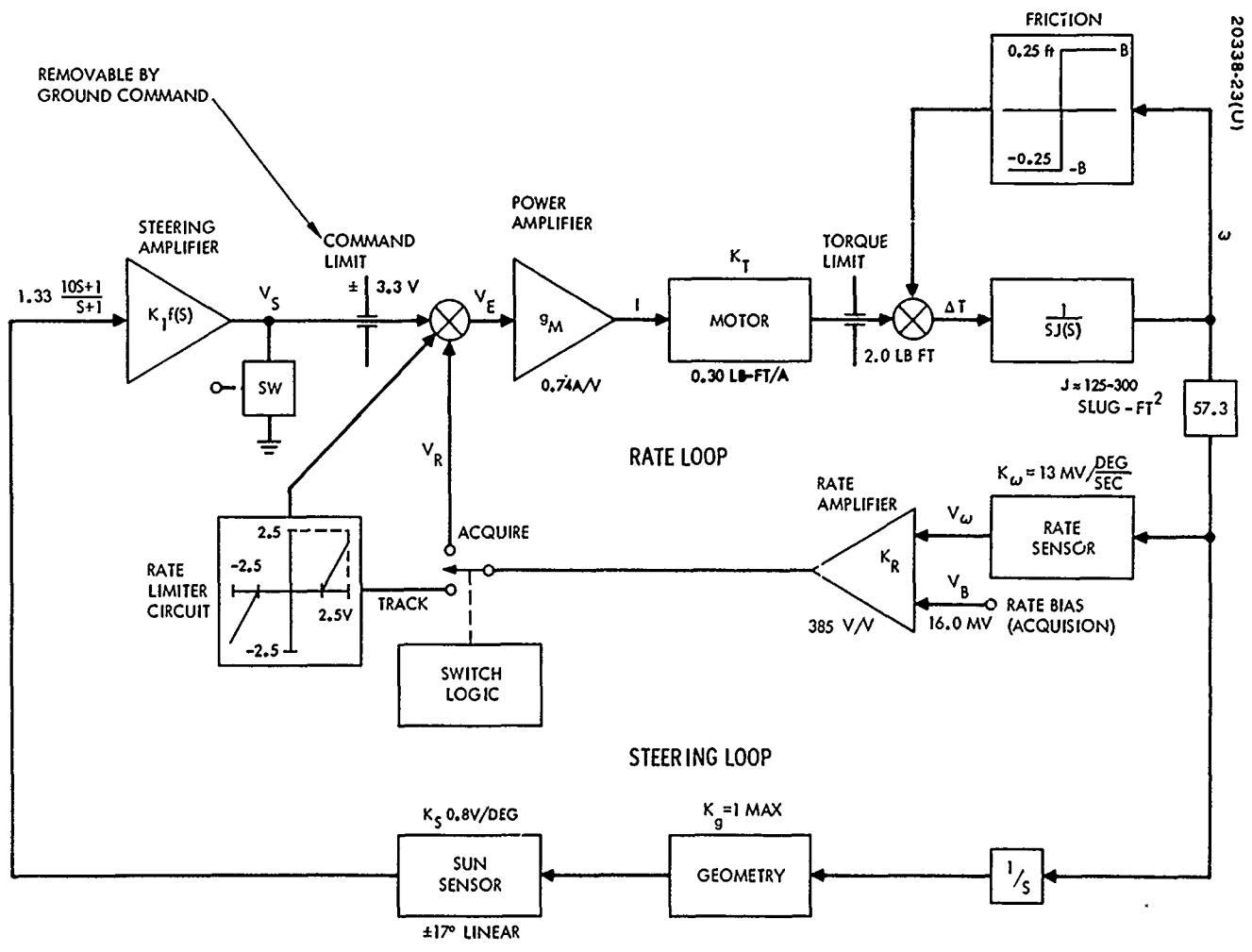


Figure 4-46. Orientation Control System Schematic, One Axis

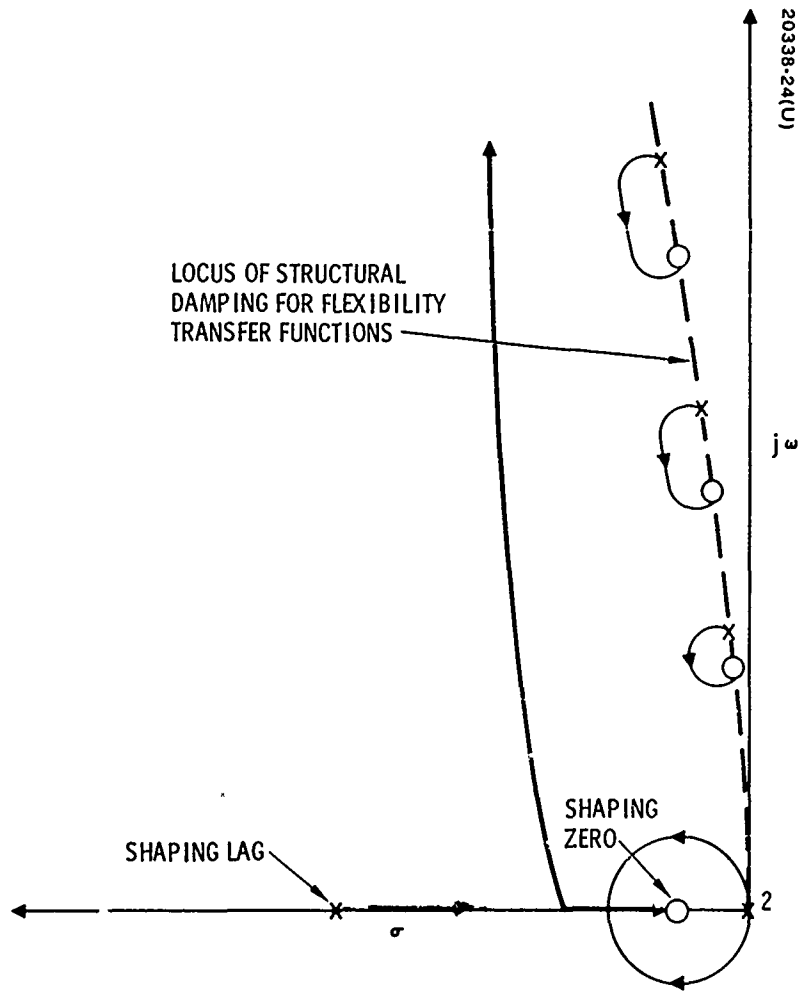


Figure 4-47. Representative Root Locus of Array Control Loop



A root locus plot for the loop so configured is illustrated in Figure 4-47, which demonstrates confinement of the roots in the left half plane.

An analog simulation of the flexible system was set up which included selectable amounts of structural damping and Coulomb friction as well. Comparison of Figures 4-48a and b illustrates the effect of a fivefold increase in structural damping. The even more pronounced effect of Coulomb friction is evident by a comparison of Figures 4-48a and c. The latter figure is reasonably representative of flight performance.

Performance in a noon turn with 1/4 lb-ft of Coulomb friction is illustrated in Figure 4-49. There is some delay in the start of rotation as the sun passes the zenith due to the friction and low geometric gain, but the maneuver is seen to be smooth and without overshoot.

Ideal motions of the arrays relative to the vehicle for any orbit are illustrated in Figure 4-50. When these motions are translated into inertially referenced angular accelerations, it is apparent that, in the general case, the arrays must be gently accelerated and decelerated throughout each orbit. If the vehicle is not to be perturbed, counter-momentum must be applied in some manner, either by operation of the vehicle's controls, or by an independent source such as a controllable reaction flywheel. Magnitude of the momentum change per orbit is illustrated in Figure 4-51. As most of this change occurs about the support axis, a single reaction flywheel aligned to this axis and driven proportionately is highly effective, as noted in the figure. Complete cancellation of the array steering momentum, if not countered by vehicle controls, would require two or three wheels, distributed as in Figure 4-52.

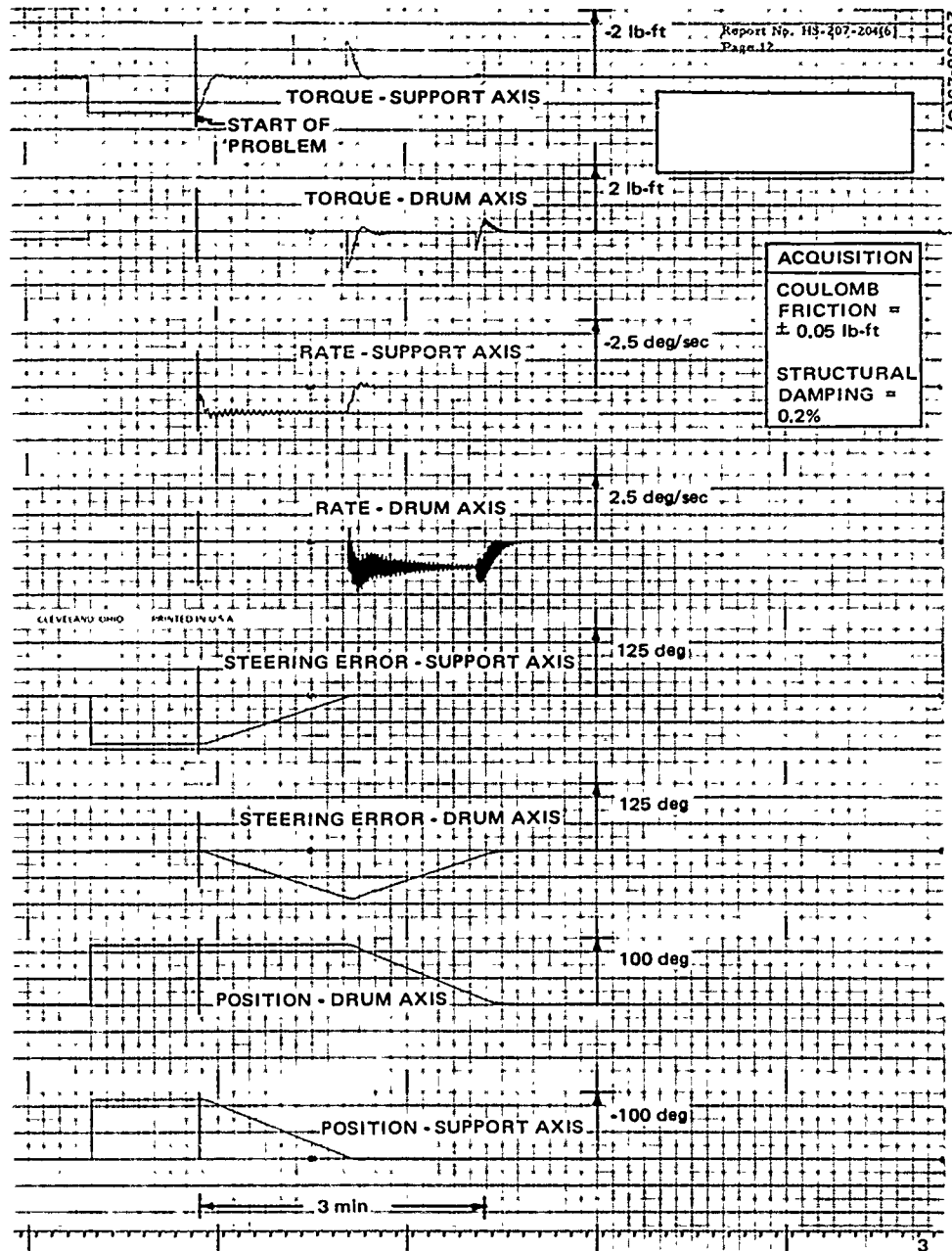
As part of the FRUSA task, a single-axis momentum flywheel cancellation subsystem, including electronic circuits, was designed. Since it was not used on the mission, it is not described here.

#### Tradeoffs and Design Changes

During the course of the program, a number of design changes were made as a result of tradeoff studies or evidence that the original course was no longer suitable. The significant changes are described briefly below.

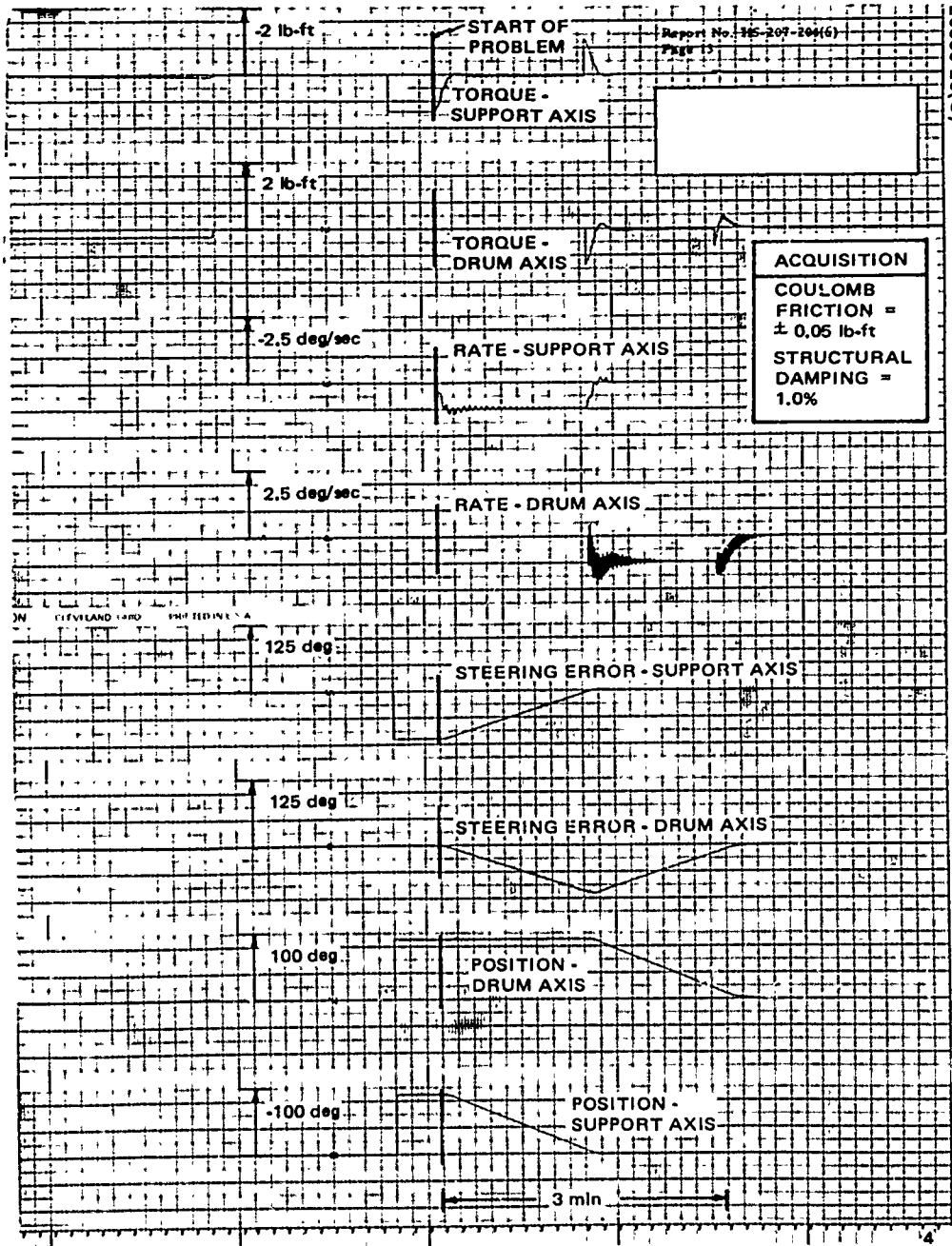
#### Torquers

The design developed during the preceding OLSCA study incorporated brushless dc torquers. During FRUSA development it became evident that torquer brush friction was a negligible portion of total friction and that brush wear would be no problem. As a result, the economy and simplicity of conventional brush-type torquers became attractive. The factors involved in this tradeoff are summarized in Table 4-8. A brush type torquer is clearly the choice.



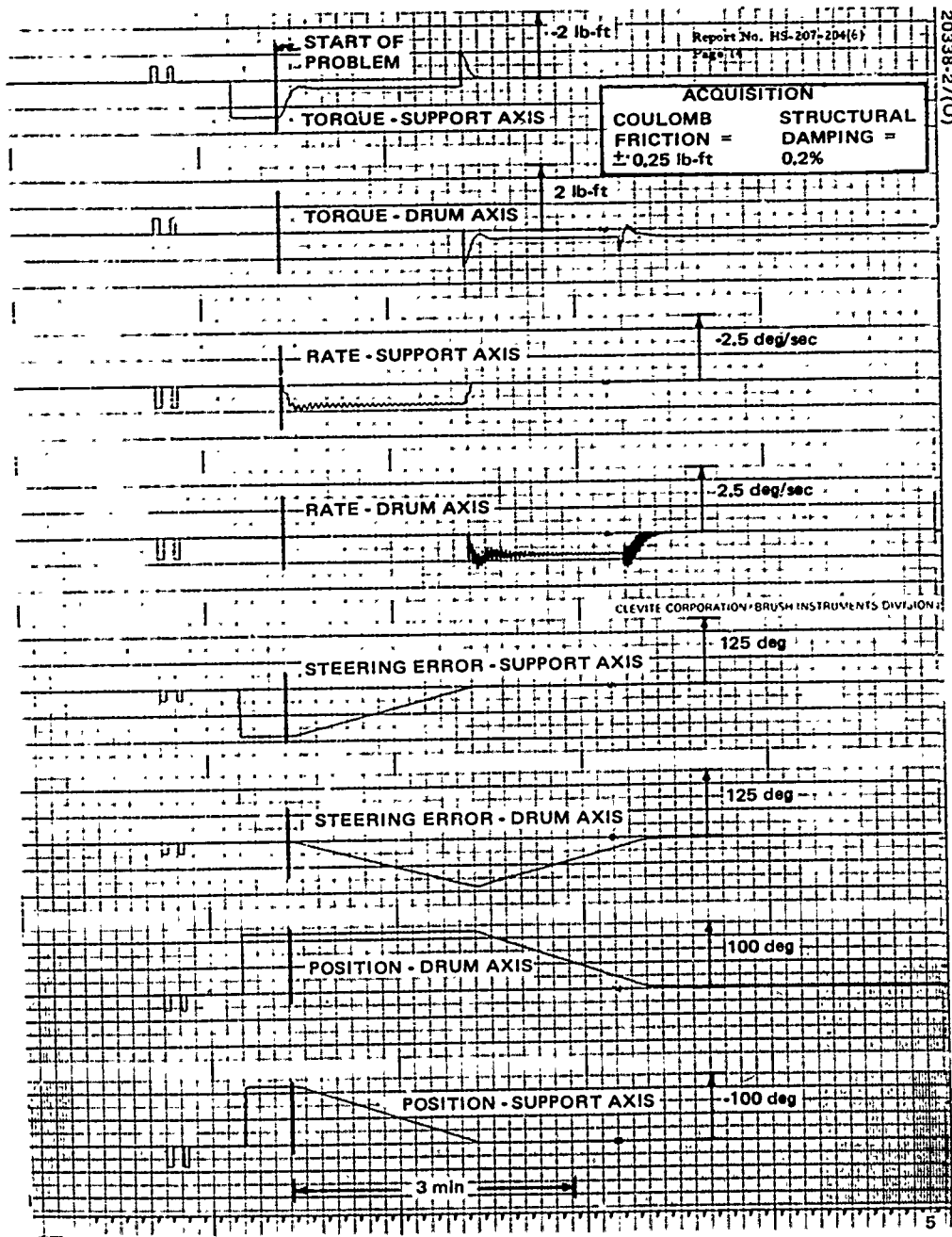
a) Coulomb Friction  $\pm 0.05$  lbf; Structural Damping 0.2 Percent

Figure 4-48. Acquisition Performance



b) Coulomb Friction  $\pm 0.05$  lbf; Structural Damping 1.0 Percent

Figure 4-48 (continued). Acquisition Performance



c) Coulomb Friction  $\pm 0.25$  lbf; Structural Damping 0.2 Percent

Figure 4-48 (concluded). Acquisition Performance

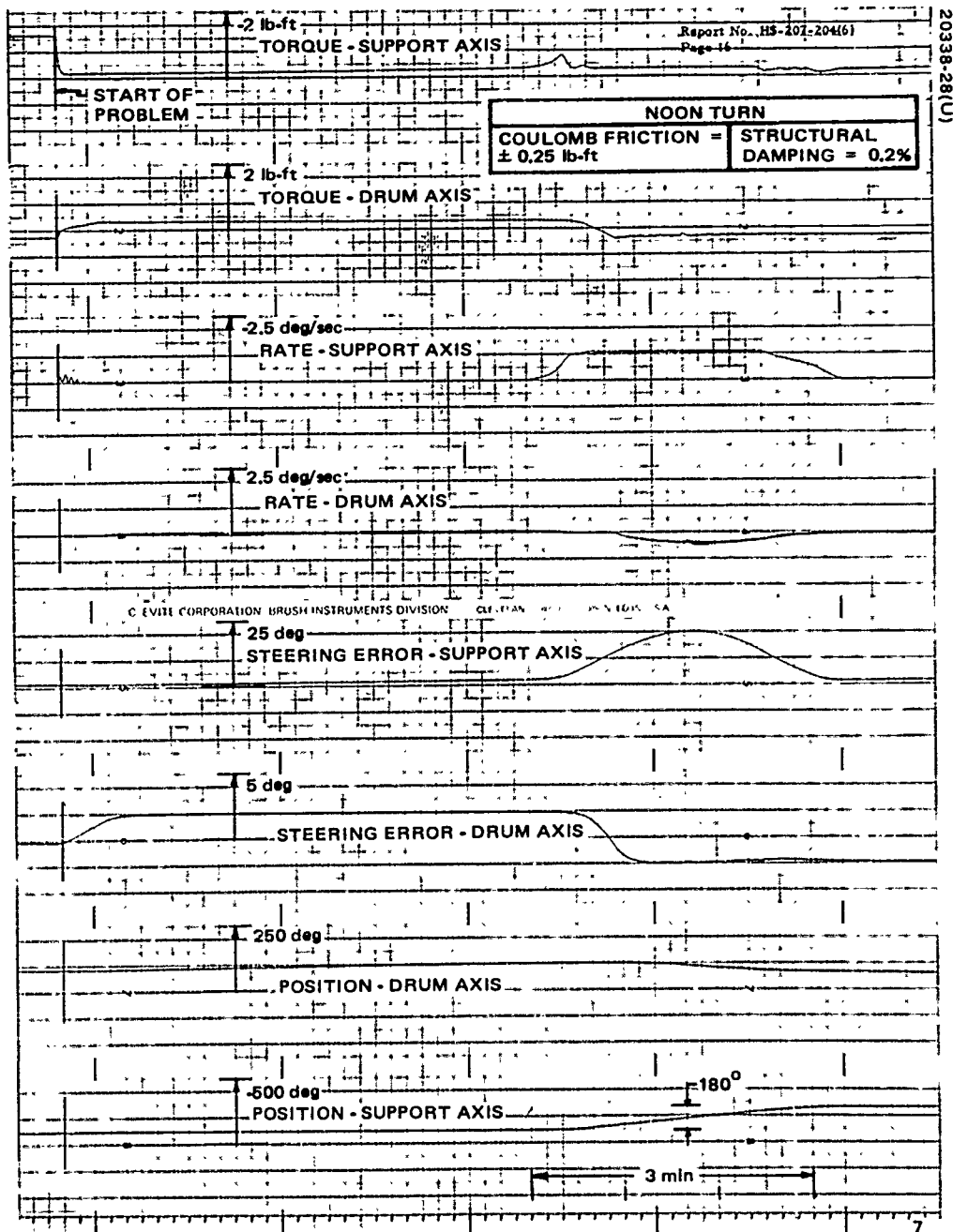


Figure 4-49. Noon Turn Performance

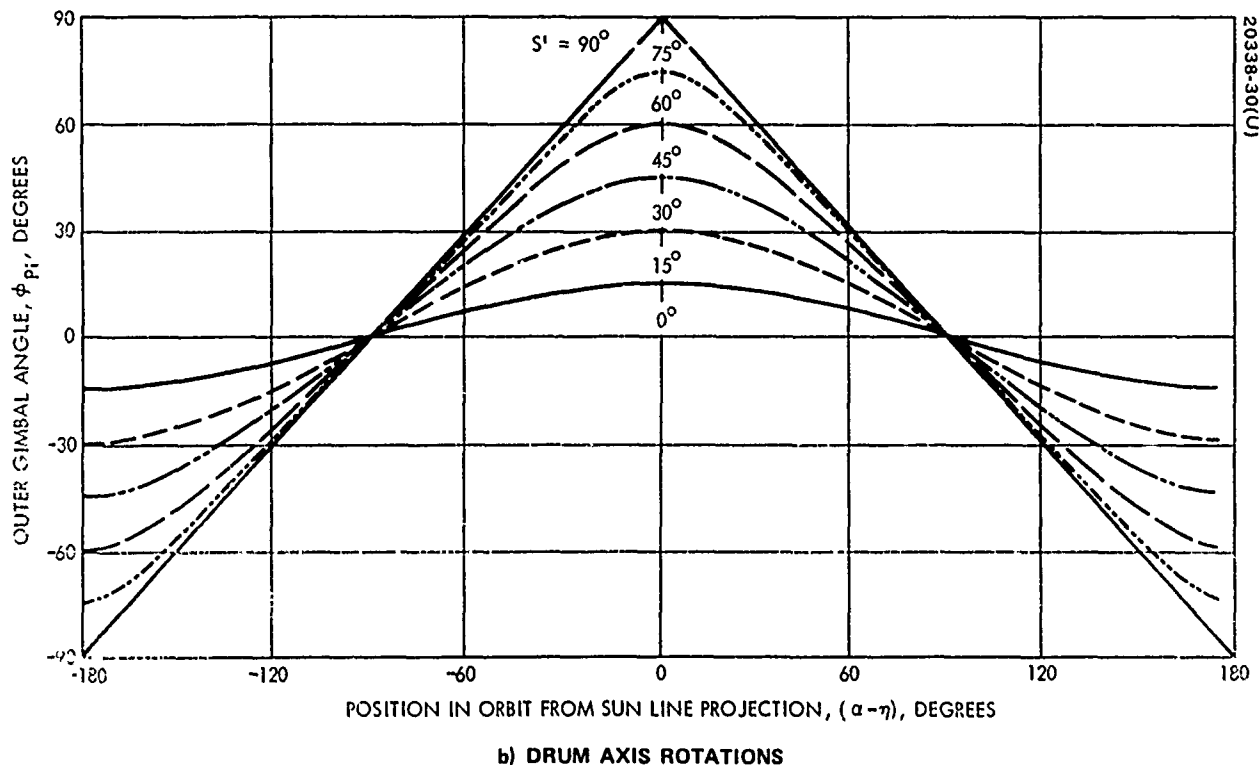
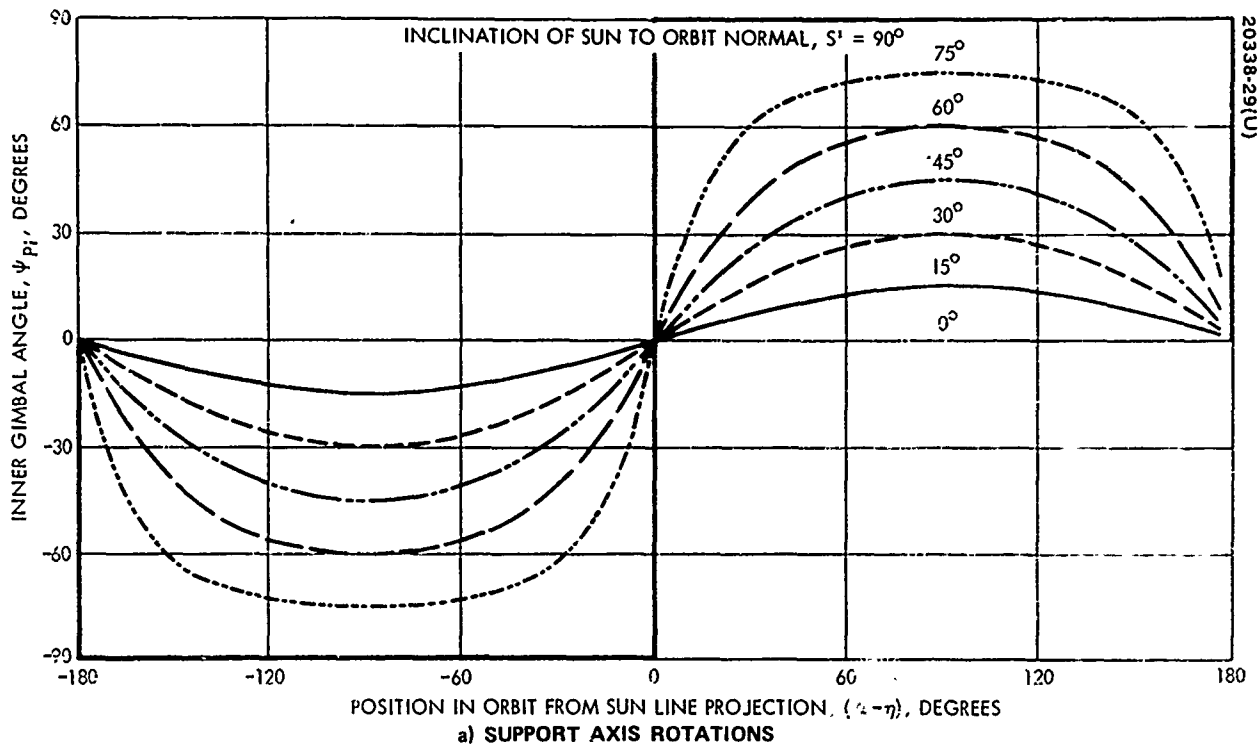


Figure 4-50. Ideal Array Angles

# ARRAY STEERING TORQUE ONLY

20338-31(U)

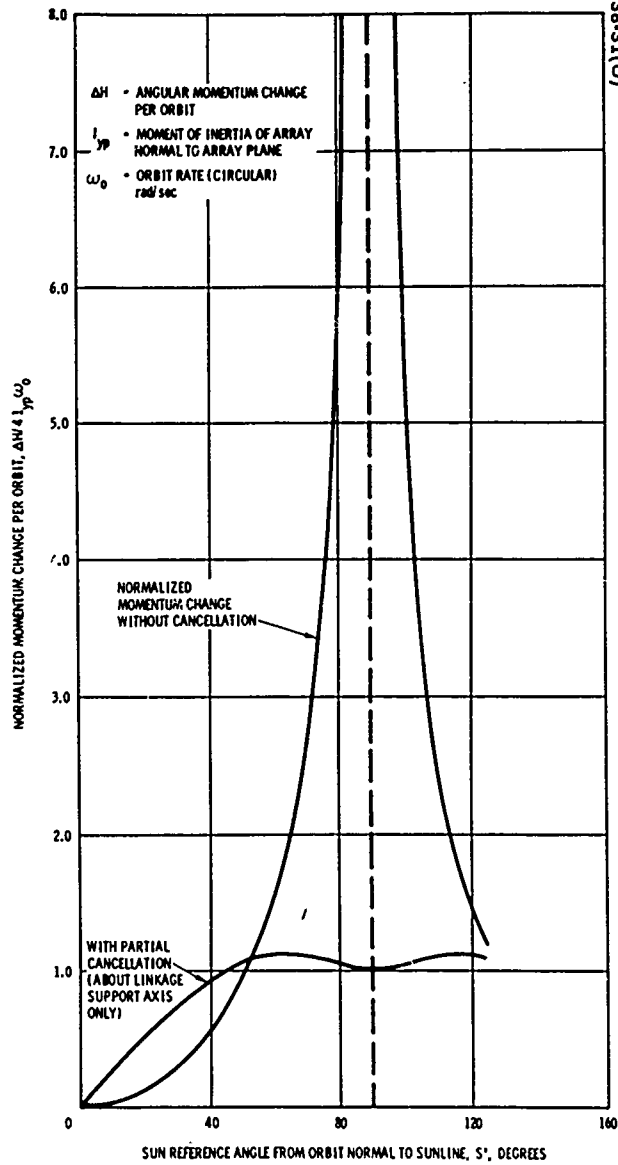


Figure 4-51. 1.5-kw FRUSA Normalized Momentum Change per Orbit With and Without Partial Momentum Cancellation

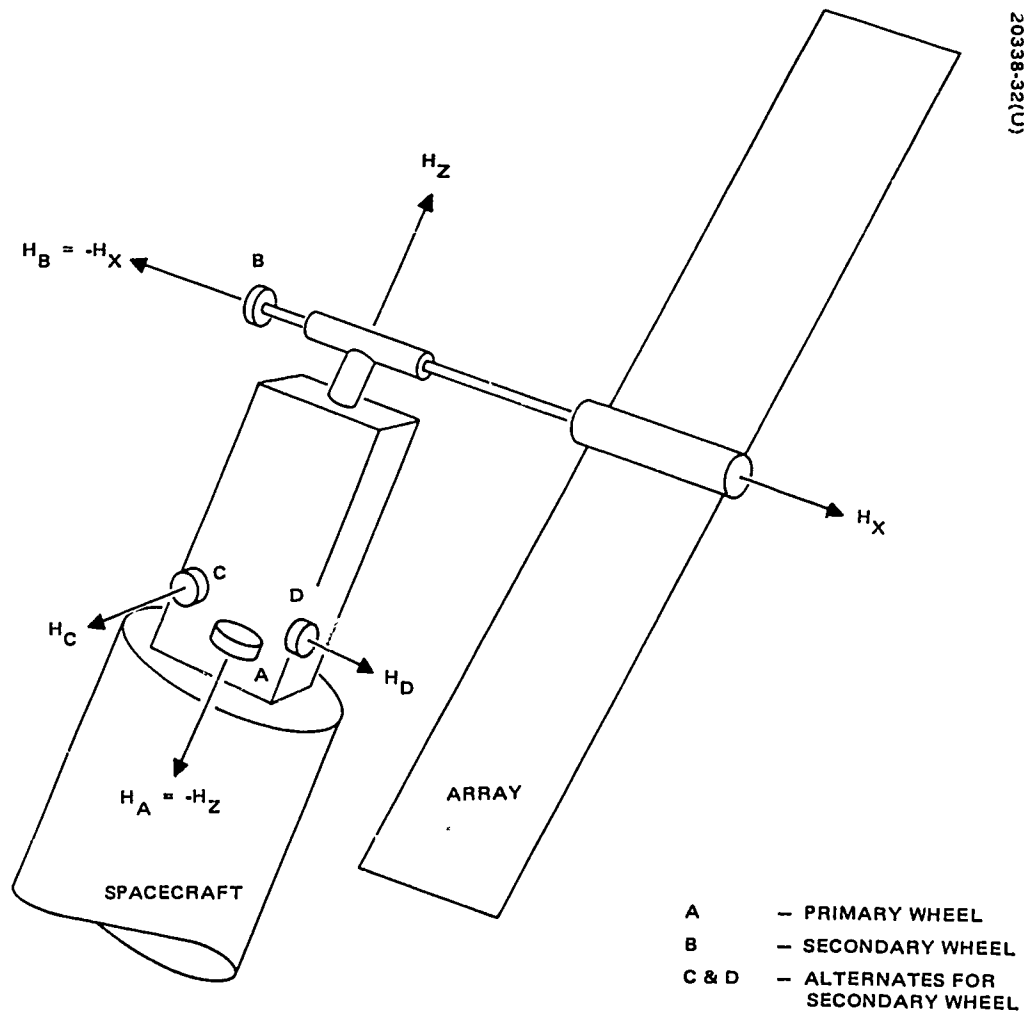


Figure 4-52. Array Momentum Cancellation



TABLE 4-8. GIMBAL AXIS TORQUER TRADEOFF CONSIDERATIONS

Brushless	Brush-Type
Complex drive electronics	Drive has 1/4 to 1/2 number of components of brushless motor
No brushes to wear	Low total travel produces negligible brush wear; less than 0.0003 inch in 5 years
5-year reliability: 0.91	5-year reliability: 0.96
Emergency drive dependent on electronics	Emergency drive direct to motor

Torquer size was also the subject of a trade study. Under worst-case off-design conditions, motor torque available can decrease significantly. While the decrease is normally of no concern, it does represent a lessening of the margin for coping with potential failure mechanisms such as a piece of debris in the bearings. Methods of increasing the margin against such failure include providing more (short-term) power to the motor, or enlarging the motor. In general, a larger motor can produce equivalent torque for less power, resulting in less stress on the electronic components and lower demands on the power supply. Some of the cases studied are summarized in Table 4-9. The larger motor appears desirable. Although heavier, it results in a lighter total system. Case VI was the basis for final selection.

#### Power Brushes

During assembly of the first unit, a problem with the power brushes indicated a need for a design revision in this area. The essence of the problem was that a precise geometric relationship was required between the brush, the brush holder, and the slipring to ensure proper seating of the brush on the rings. It is difficult to achieve this precise relationship initially because of tolerance buildup. Extensive run-in would be required to achieve the desired relationship and would be uneconomical if the tolerance buildup was more than a few thousandths. Even if the assembly could be precise, shifting of components during launch and thermal exposure could possibly cause problems during flight. Therefore, the design was altered to include flexibility for initial tolerance buildup and/or shifting of components during flight. The modified design proved entirely satisfactory. Sketches of the two designs are shown in Figures 4-53 and 4-54.

#### Eclipse Logic

Sun-present sensors were originally incorporated in the orientation subsystem to provide an unambiguous signal that the FRUSA had emerged

TABLE 4-9. TORQUER SIZING

Case	Motor Parameters				Total Power, watts	Weigl. of				Total Weight, pounds	
	Weight, pounds	Torque, lb-ft	Current, Amperes	Power, watts		Slip-rings	CEU	ECU	Battery		
I	Original Current Limited	2.4	1.2*/0.80**	3.3/5.4	74/141	91/157	0.79	6.5	17.5	37.8	67.4
II	Original Specification Winding	2.4	1.5/1.5	8.9/12	112/302	165/351	1.08	6.5	33	37.8	83.2
V	Selected No Current Limiting	4.9	1.3/2.8	6.8/20	36/468	90/586	1.35	7.25	12	37.8	66.4
VI	Selected Current Limited	4.9	1.5/1.5	3.9/5.3	50/137	81/155	1.08	7.25	7	37.8	61.1

\*Nominal.

\*\*Worst-case failure mode.

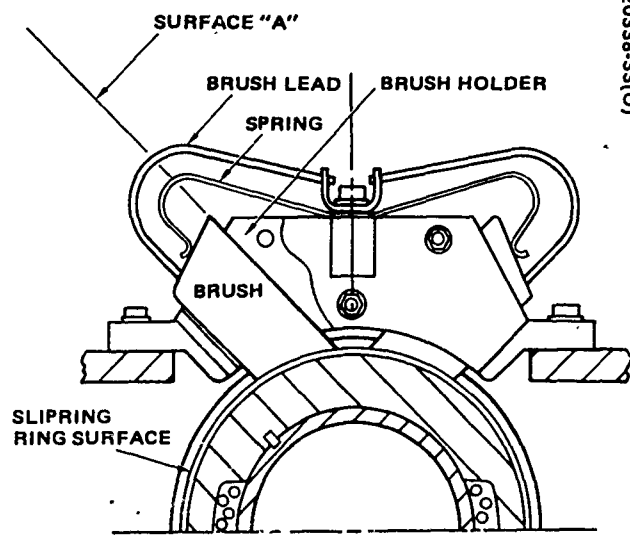


Figure 4-53. Original Brush Design

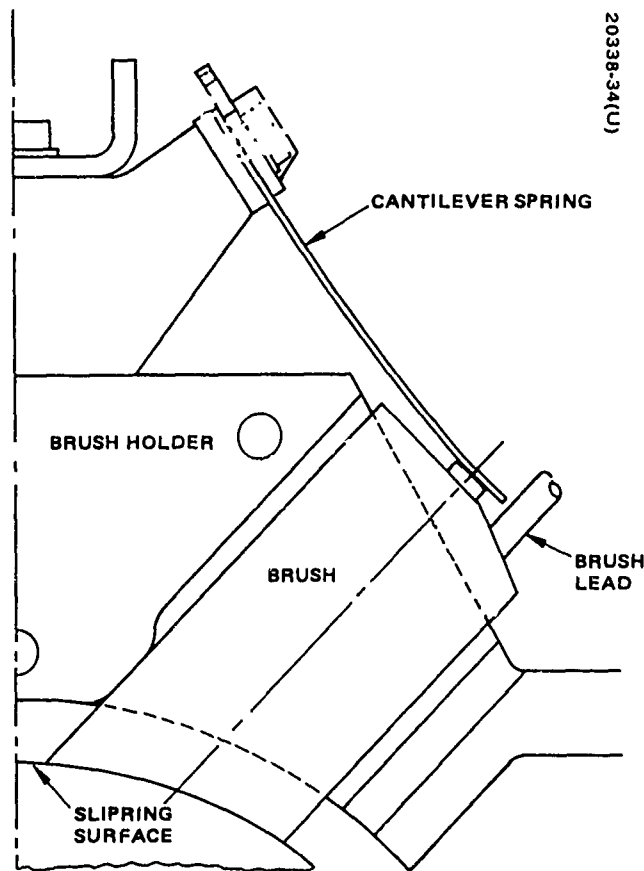


Figure 4-54. Modified Brush Design

from eclipse so that the torquers, which had been dormant, could be immediately reactivated regardless of solar array (and tracking sensor) orientation. In the original design, it had been assumed that it would be necessary to inactivate the torquers during eclipse to conserve battery power. Analysis of system power requirements during eclipse, however, showed this precaution to be unnecessary. The system was therefore simplified by eliminating the sun-present sensors and initiating the support axis search slew whenever the tracking cells went dark.

The portion of the logic used to hold the system in the tracking mode during a noon turn, even if the lockon cell should temporarily go dark, was first retained by deriving a different sun-present signal from the outputs of the tracking error cells. Subsequently, however, a possibility of ambiguity in this derived sun-present signal was noted because of uncertainty in the level of the tracking cell's dark resistance. The actual need for the function itself was therefore reviewed. It became apparent that disappearance of the sun from the lockon cell's cone of view is an event of low probability because 1) the required flight geometry itself is rare and 2) the mechanism must have developed a relatively high friction level. This double probability is exceptionally low.\* If the sun-present function were eliminated from the operational logic, therefore, the worst that could happen would be that the system might undergo a few extra reacquisition maneuvers during noon orbit seasons. This is a minor penalty to pay for the gain in simplicity. The probability of loss of sun lock signal was lowered even further by increasing the apex angle of the lockon cell's field of view another 10 degrees (to 40 degrees). All sun-present logic functions, therefore, were eliminated.

#### Rate-Limit

To minimize array/vehicle momentum interchange, maximum angular rate at which the arrays could be driven was originally set, somewhat arbitrarily, at 1 deg/sec. The integration contractor's studies of the gravity-gradient/cm-g - stabilized mode indicated a preference for a limit of 1/2 deg/sec. Limit-setting components in the CEU circuits were therefore changed, decreasing the proportion of the dynamic range used in some of the amplifiers. In the future, such changes would probably be implemented by altering the gain of the rate sensor amplifiers.

#### Redundancy

The original design plans included use of redundant CEUs to augment subsystem reliability. Because of the relatively short mission lifetime specified, however (6 months to 1 year), and as an economy measure, CEU redundancy was eliminated. A subsequent flight problem, although temporary and not mission-critical, indicated that the redundancy would have been useful to cope with the infant mortality type problems that can crop up in even a short mission.

---

\*Full system simulation by the integration contractor subsequently verified this conclusion.

## Bearings

Although the despin assemblies which experienced in-flight failures on the ATS and Intelsat III spacecraft were not Hughes designs, these anomalies prompted a review of the OLSCA gimbal bearing design in light of what is known or surmised regarding those failures. The Intelsat III problem was attributed in part to the effects of temperature on a thin-race duplex pair (with preload set by race dimensions), similar to that first used at each end of the Hughes orientation mechanism. Adoption of duplexed bearing pairs originally resulted from requirements to reduce both friction and weight to a minimum. Reestimates of the thermal environment, however, indicated temperature ranges and gradients that the design could not be expected to tolerate. The design was revised, therefore, to incorporate larger (more rigid) angular contact bearings used singly, rather than in pairs, and preload was provided through the housing by a spring, which exhibits much less sensitivity to temperature variations. Further tolerance was incorporated by changing the material enclosing the outer races from magnesium to titanium. An added attraction of the new bearings is an approximately doubled load-carrying capability, which reduces the possibility of Brinelling the balls during the launch phase.

The floating end of the new gimbal design is illustrated in Figure 4-33; the other end has both races clamped to the supporting structure. While the total change incurred a 3.3-pound weight penalty, the increased assurance of proper operation under environmental extremes was considered to be ample justification. Test and flight performance confirmed suitability of the final design.

## Drum Axis Shaft

Changes resulting from LMSC's mission feasibility and integration studies included a request to increase the distance from support axis to inner array boom from the original 40 inches to 52 inches in order to provide clearance for items which protrude outside the Agena's basic envelope. This added standoff was incorporated in the drum axis shaft outboard of the deployment hinge. The change produced a minor increase in weight, and noncritical decreases in support axis control gain and resonant frequency of the array support arm.

## Filter Unit

As noted under "Descriptions" above, this unit was a late addition to the subsystem, required to clean up noise propagated into many of the leads from switching transients inherent in the motor drive amplifiers. The filters produced acceptable signal quality as seen by the spacecraft, although some noise was still evident on a number of channels. To avoid the penalty

of the added components and weight of this unit, future designs may adopt one of two alternatives:

- 1) Employ proportional, rather than switching-type amplifiers. Proportional amplifiers are inherently less efficient in this type of operation, however, and may introduce problems with heat dissipation.
- 2) Segregate the motor drive circuits in a separate part of the CEU, thoroughly RF insulated from the other circuits. This appears to be the more feasible approach.

#### Development and Other Tests

A design verification test (DVT) unit was originally included in the program. As an economy measure, however, this unit was eliminated in favor of performing such tests, as required, on the qualification hardware. This approach was successful, although it did result in several crash problem solving efforts late in the program.

#### Unit Level Tests

For testing convenience, the two axes of the mechanism were separated, each being capable of independent operation. A separate mechanism test breadboard was built up and integrated into the test panel. This breadboard provided the capability of driving the unit at selectable rates from zero up to 60 rpm, thus facilitating accelerated run-in, as well as tests at the design maximum of 1/2 deg/sec. Rate control was implemented through a loop containing the unit's own rate sensor. Because dry-lubricated brush friction is substantially lower in a vacuum or a dry inert-gas atmosphere than in normal air, most of the testing was conducted in a chamber continuously purged with dry nitrogen. Due to delayed delivery of the 1500-watt sliprings, the 700-watt electrical and thermal configuration was tested. Qualification of the high powered version was based on 1) the 700-watt test data, 2) analytic extrapolation to the 1500 watt case, and 3) verification of the extrapolation during acceptance tests of the 60-ampere flight unit. Typical friction and ring noise results are illustrated in Figure 4-55.

Seven minor discrepancies were uncovered during the tests:

- 1) Brush force was slightly low on six signal brushes. This is not significant, was not correlated with noise, and was correctable.
- 2) Friction levels in air were high. The specification was intended to apply only to vacuum conditions; the air measurement requirement was deleted.
- 3) A few signal brushes showed occasional (rare) noise spikes in excess of the 5 mv specified. These measurements were made

at a 5-deg/sec rate to reduce test time. It was demonstrated that the noise was in specification at rates approximating the 1/2 or 1 deg/sec maximum flight rates. The specification was changed to call for testing at 1 deg/sec.

- 4) On the drum axis, stall torque measurements were corrupted by attached cables. A better test setup was devised for the second unit.
- 5) Signal circuit resistance was over specification in some channels. This was partly a matter of averaging the specified allocation to each axis, and averaging the correction for test-lead resistance. Specification and technique were refined for tests of the flight unit.
- 6) Two temperature sensors (thermistors) were inoperative. This was subsequently traced to a wiring error, and was corrected.
- 7) Bearing preload was 13 to 14 pounds instead of the 20 (minimum) specified. The actual preload was acceptable from a performance standpoint, and was dispositioned "use as is" for this unit. Following system level qualification tests, it was decided to reduce the specification limit to 17 pounds and use more care in selection of shim thickness during assembly of the flight unit.

Deployment Test. Because of apparent clearance problems resulting from LMSC's placement of their telemetry antennas, an initial series of engineering tests was conducted of deployment arm performance using different geometrical arrangements of the cable loop at the deployment hinge. As the aim was simply to evaluate the effect of differences in cable routing, the latch was removed and no simulated inertia load was provided. A timer was connected to switches operated by the starting and stopping of the outer (deployed) arm. Little effect of loop size or placement was discernible at room temperature, and an arrangement ensuring clearance of the LMSC antennas was adopted.

Verification tests were subsequently conducted with simulated array inertia, and the hinge enclosed in a thermally controlled box (see Figure 4-56). The results may be summarized as follows (see Figures 4-57 and 4-58).

The mechanism, with the two spiral springs adjusted to supply 28 in.-lb of torque with the arm in the stowed position, successfully deployed an inertia equivalent to the arrays in approximately 15 seconds, over a temperature range of 150°F to -50°F. At the extended position, the latch locked the load in the normal operating position (0 degree position) with an impact bending moment at the hinge of approximately 900 in.-lb. These results correspond favorably with analytical predictions.

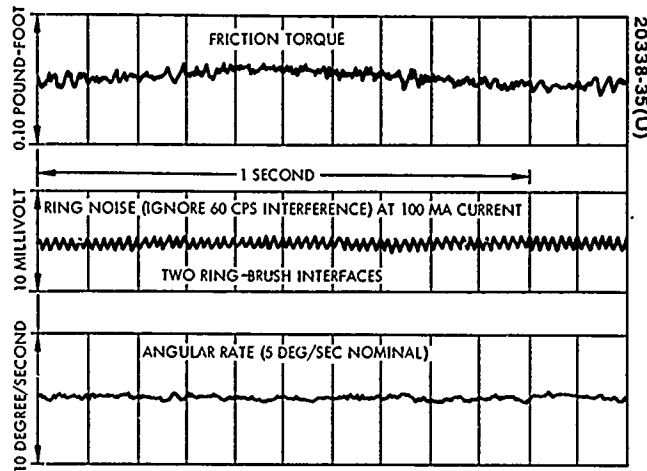


Figure 4-55. Typical Friction and Ring Noise Measurements, Support Axis

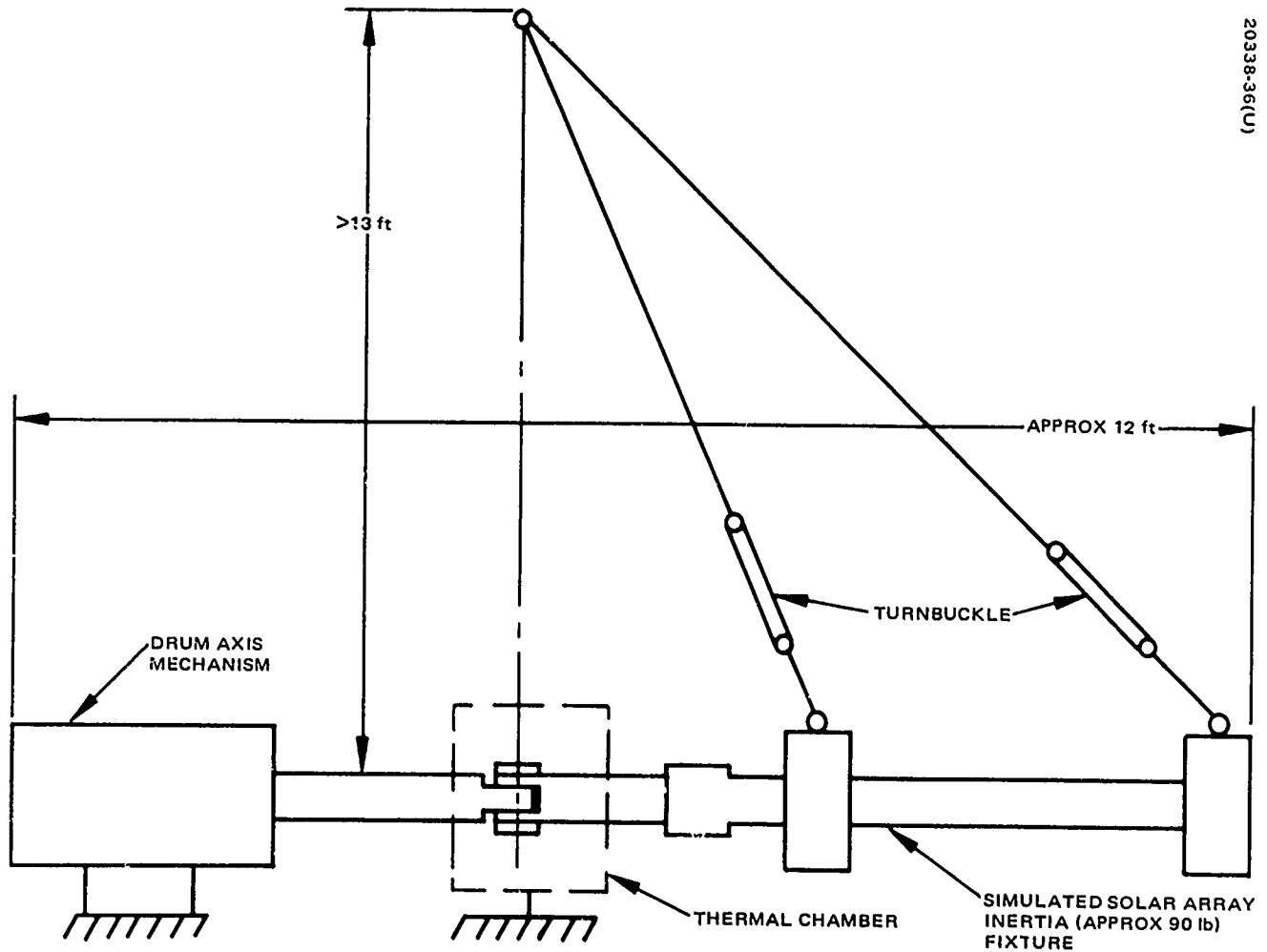


Figure 4-56. Deployment Test Setup



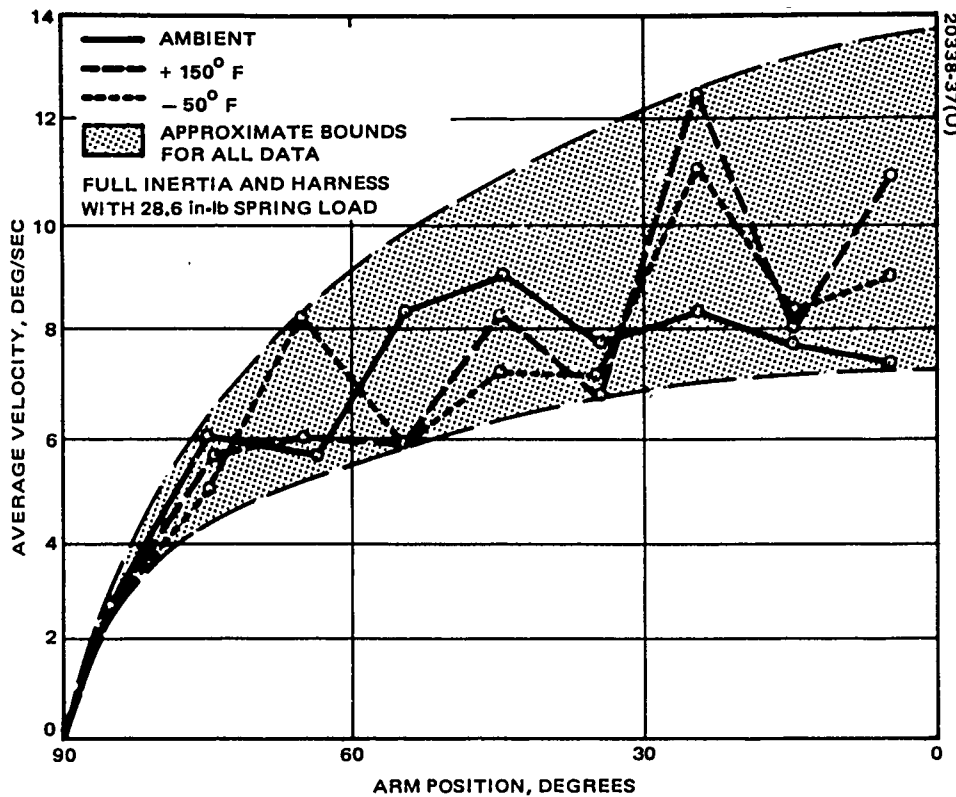


Figure 4-57. Effect of Temperature Extremes on Deployment Velocity

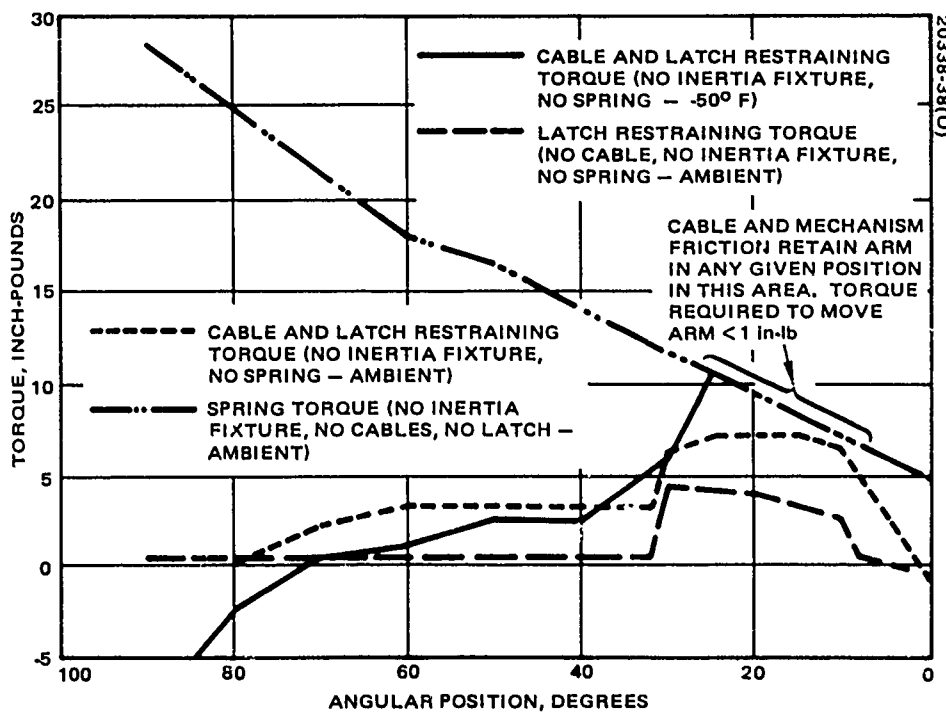


Figure 4-58. Deployment Mechanism Static Performance Development Tests, Ambient Temperature

The latching function was effective. During deployments, no latch bounce was observed and there was no tendency for the latch to cam out even under deliberately applied high torques in both directions. In some cases, there was difficulty in unlatching the mechanism.

The mechanism would supply enough torque to the arm to rotate it from any starting position to the 0-degree position and latch except under cold conditions (-50°F). At cold conditions a small amount of additional torque was required to move the arm to the latched position when the arm was prevented from building up normal kinetic energy.

One of the spiral springs would successfully deploy the array when started from the 90-degree position.

After review of the test data in terms of the design goals, two design changes were found to be desirable and were implemented:

- 1) The two spiral drive springs were adjusted so that a 32 in.-lb torque was available in the 90-degree position rather than 28 in.-lb. This change was desirable so that even under cold conditions the mechanism can move the load to the locked position regardless of the arm position with zero starting velocity. The additional energy results in a bending moment of less than 1600 in.-lb at latch-up.
- 2) The spiral springs were coated with solid film lubricant. When the springs were adjusted, the outer spring coils bears against the adjacent coil on the same spring. (This is the reason that the net spring torque measurement was not linear.) The lubricant reduces the friction between the spring coils and precludes metal-to-metal contact.

With these changes implemented, all design goals were satisfied. (See the flight-unit data, Figure 4-59.)

#### Subsystem Level Tests

A number of problems were encountered during initial checkout and tests of the qualification set of orientation subsystem hardware.

Noise. As also noted elsewhere, a persistent problem in the subsystem involved the corruption of data signals with noise generated by the switching power amplifiers driving the torquers. This type of drive was selected originally because of its much higher efficiency (and therefore lower thermal dissipation) than a comparable proportional dc drive. The 3.3-kHz switching rate, however, produced a ringing at about 1 MHz which was conducted along various paths throughout the system. The noise was ultimately reduced to tolerable levels by a combination of selected filtering and wiring routing changes: a 0.2-microfarad capacitor filter at the CEU commutator

output, a similar filter at the data terminus in the test position, providing a return for the commutator separate from the normal regulated returns, grounding the commutator lead shields, and generalized improvement of grounds in the mechanism. While these changes eliminated the problem at the FRUSA level, the noise source remained a potential problem at the Agena level, ultimately requiring the design and installation of the interface filter unit described previously.

Torquer Dropout. Initial functional tests disclosed an incompatibility between the trip levels of the current limiters in the CEU, which protect the motors from drive levels which could degrade the magnetization, and output capabilities of the rate control circuit amplifiers. Part of this problem resulted from setting too low a current limit in the test power supply; voltage drop under load then caused faulty CEU operation. Another part was the result of operating without an inertia load on the mechanism; resultant limit-cycle oscillations (expected) in the drum axis drive were at too high a frequency for the motor drive to handle, so current increased unidirectionally to the limit value. The oscillations also resulted in momentary adverse combinations of signals, yielding excess current when switching into the tracking mode. Corrections comprised installation of limiting circuitry on the sums of appropriate signals, so that excessive current demands are never possible, adding a small inertia load on the drum axis arm, and providing a caging circuit for the torquer drive amplifiers.

Lockon Anomaly. Initial checkout indicated that the orientation subsystem would not retain lock on the minus Z side of the spacecraft, but would either break lock and reacquire on the opposite or plus Z side, or hang up, in a low-amplitude stable oscillatory mode, at the edge of the lockon cell's field of view. This was found to result from a design omission, in that polarity reversal circuits were not incorporated in the logic associated with certain lockon geometry. For the STP 71-2 flight, the conclusion was that operational adjustment could be made to cope with this deficiency. The problem could have been resolved by mechanically biasing the acquisition sun sensor slits from being normal to the drum axis to pointing approximately 15 degrees outboard from normal. The fix was not mandatory and, in the interests of economy, was not attempted.

Torquer Card Fault. Subsequent to subsystem vibration, a malfunction of the torquer drive electronics was detected which resulted in no torquer current being delivered. The CEU was transported to the electronics laboratory where the malfunction was reproduced. The problem was then traced to the torquer drive shaping card in the CEU. The card was removed and the flight card installed, which resulted in normal operation. The qualification model card was thoroughly cleaned and subjected to a component-by-component detailed checkout. Meanwhile, to maintain delivery schedules the flight model card was utilized to facilitate the solar-thermal-vacuum tests. Detailed checkout of the qualification model card revealed no deficiencies, and the card was reinstalled after STV. The consensus was that the original problem was caused by contamination in the card connector.

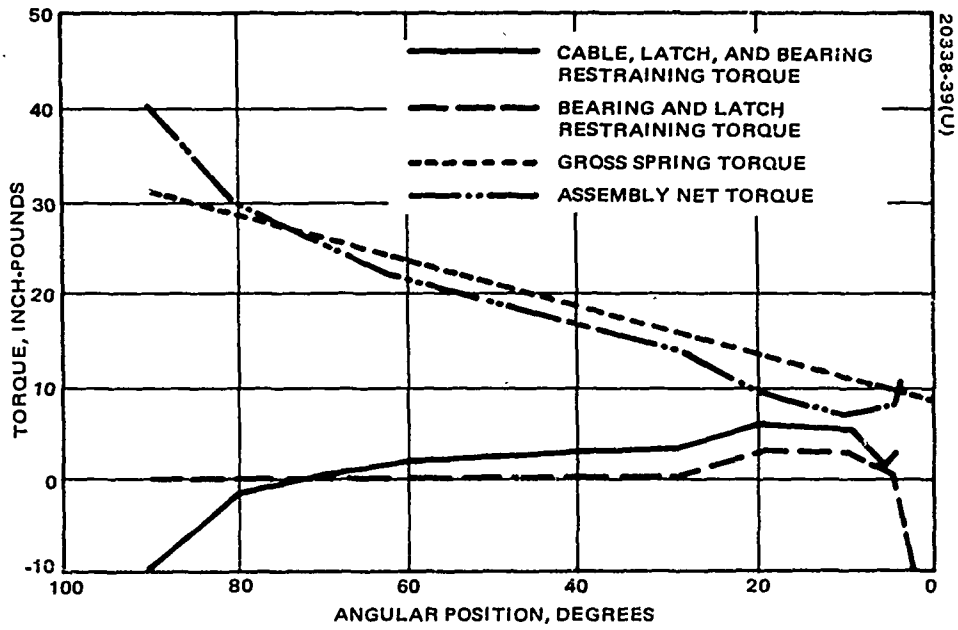


Figure 4-59. Deployment Mechanism Static Performance, Flight Unit - Ambient Temperature

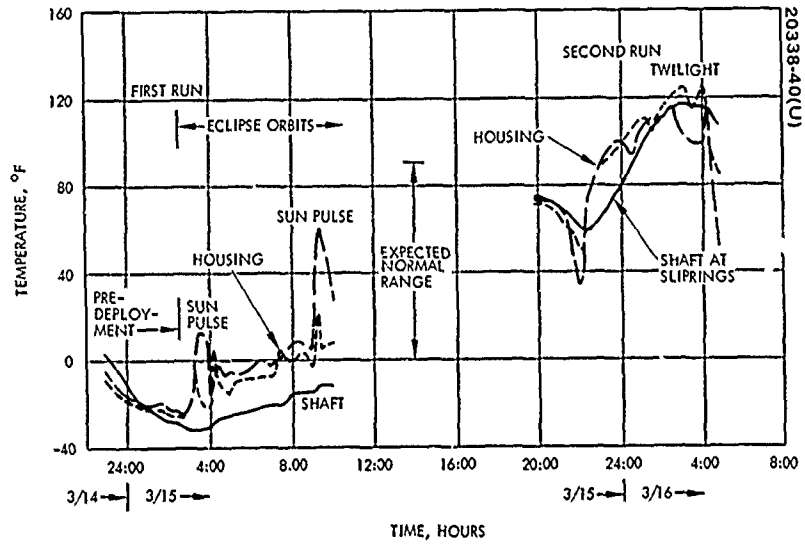


Figure 4-60. Orientation Subsystem Solar-Thermal-Vacuum Qualification Test

Data Commutator. Postvibration checkout showed no output from the telemetry commutator in the orientation subsystem. The commutator was removed and replaced by one of the flight model commutators. The malfunctioning commutator was returned to the vendor for checkout, disassembly, and analysis. The problem was traced to insulation cold flow at a point of contact with an assembly screw. Although the commutator is a potted assembly, the wire was routed across the screw before potting; then during vibration the insulation was agitated sufficiently to cause cold flow. The wire routing within the commutator is not precisely the same for each commutator. It was concluded that this was a random failure, as the vendor attempts to ensure that wires are not routed across screws or sharp corners. The same type of commutators have been used in a large variety of space flight applications without similar failures. The unit was repaired and reinstalled in the CEU.

False Manual Torque Commands. During electromagnetic compatibility tests a problem was encountered with spurious torquer commands when conducted interference was applied to the unregulated bus. Filtering was added to the CEU and proved adequate by subsequent test.

#### Solar-Thermal-Vacuum Tests

The qualification subsystem was subjected to system level solar-thermal-vacuum tests. Selected thermocouple readouts are plotted in Figure 4-60. It is apparent that temperatures were well within the  $-50^{\circ}\text{F}$  to  $150^{\circ}\text{F}$  design range. No anomalies were noted in this phase of testing.

#### Flight Performance

On revolution 10, sun acquisition and tracking were activated. Time histories of selected data channels are shown in Figure 4-61. Performance as designed is apparent in the support axis slew, drum axis slew, lockon, and reduction of tracking error to within 1 degree of null.

Because of a warmer than specified interface, CEU temperatures rose to about  $150^{\circ}\text{F}$  instead of the expected  $120^{\circ}\text{F}$ . At this temperature, sometime around revolution 14-18, support axis control apparently reverted to tracking the edge of the lockon cone, then tripped the torquer shutoff switch on this axis. Because of the twilight orbit which commanded little array motion, the problem was not noticed until revolution 79, when the CEU was shut down, then reactivated for an array retraction-extension experiment. When reactivated, a large initial negative torque transient was observed, culminating in the system's again tracking the edge of the lockon cone in a low amplitude stable switching-oscillation mode. Because the problem was not understood, automatic control was deactivated.

Tests with candidate malfunctions introduced in the qualification unit hardware subsequently indicated that the fault was probably associated with a poor connection to either the negative power supply or the inverting input of the support channel rate limiting amplifier. It was postulated that it was

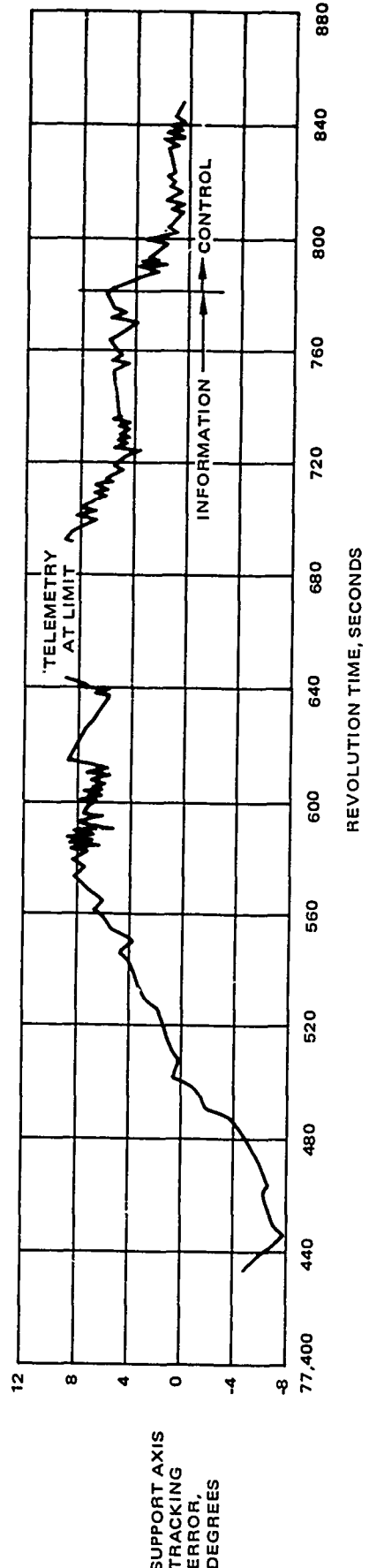
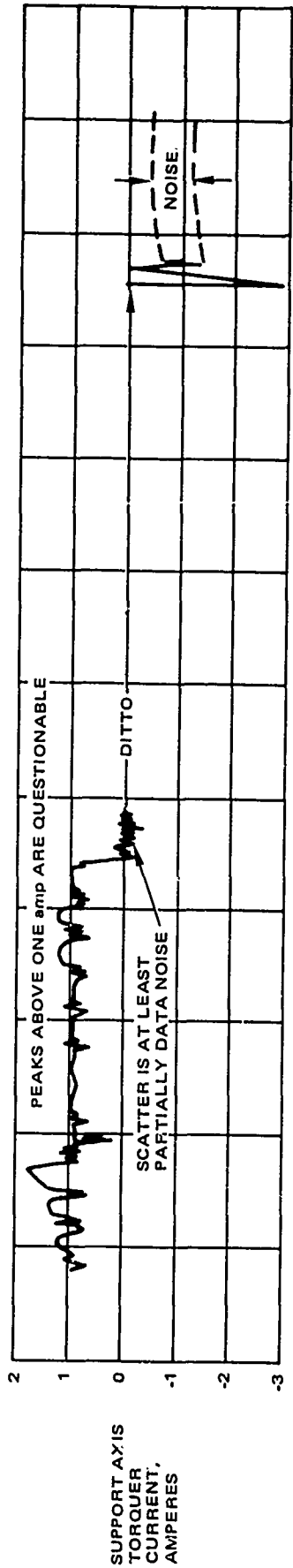
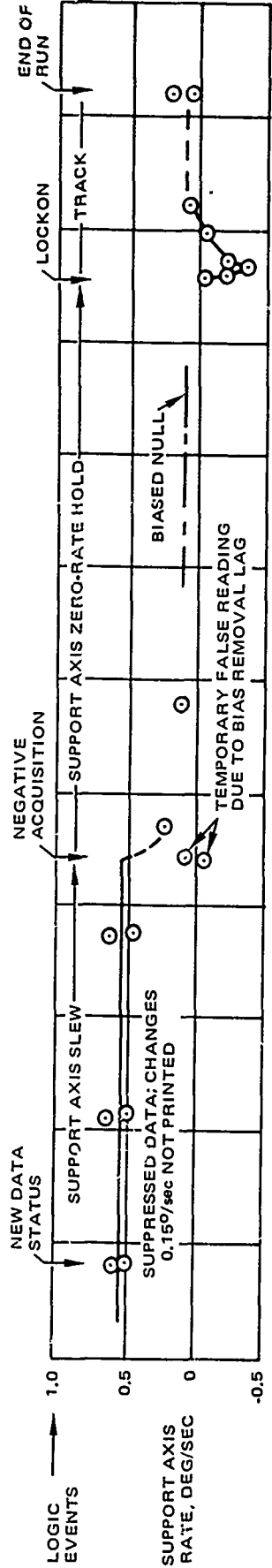


Figure 4-61. FRUSA Revolution 10 Sun Acquisition

associated with the unexpectedly high operating temperature in twilight orbit, and might disappear later in the season when the CEU cooled down.

This proved to be the case. When automatic control was reactivated on 8 February 1972, with the CEU temperature at 18°F, entirely normal performance was observed. Subsequently, many reactivations involving considerable orbit time have been implemented, with consistent and normal results.

It is concluded that the fault was a thermally sensitive connection, not generic, and that subsystem performance was normally as designed.

### Conclusions

It is concluded that the FRUSA orientation subsystem design was sound in concept and implementation, and resulted in a successful demonstration of the technology required to continuously maintain alignment of flexible solar cell arrays normal to the sun and transmit the power so developed into a spacecraft to service both vehicle and experiment loads of large magnitude.

FRUSA experience indicates that the following improvements would be desirable in future subsystems of this type:

- 1) Provide discrete on and off command channels.
- 2) Incorporate rate limited, rather than fixed torque, manual command modes.
- 3) Incorporate shaft position sensors (for telemetry) on both axes.
- 4) Incorporate redundant control electronics.
- 5) Provide for selective reversal of support axis control polarity, so that the sun can be acquired on either side of the vehicle.
- 6) Segregate torquer drivers in an RFI-isolated section of the electronics unit, and ensure that no switching noise is conducted elsewhere. This will allow elimination of the extra filter unit.

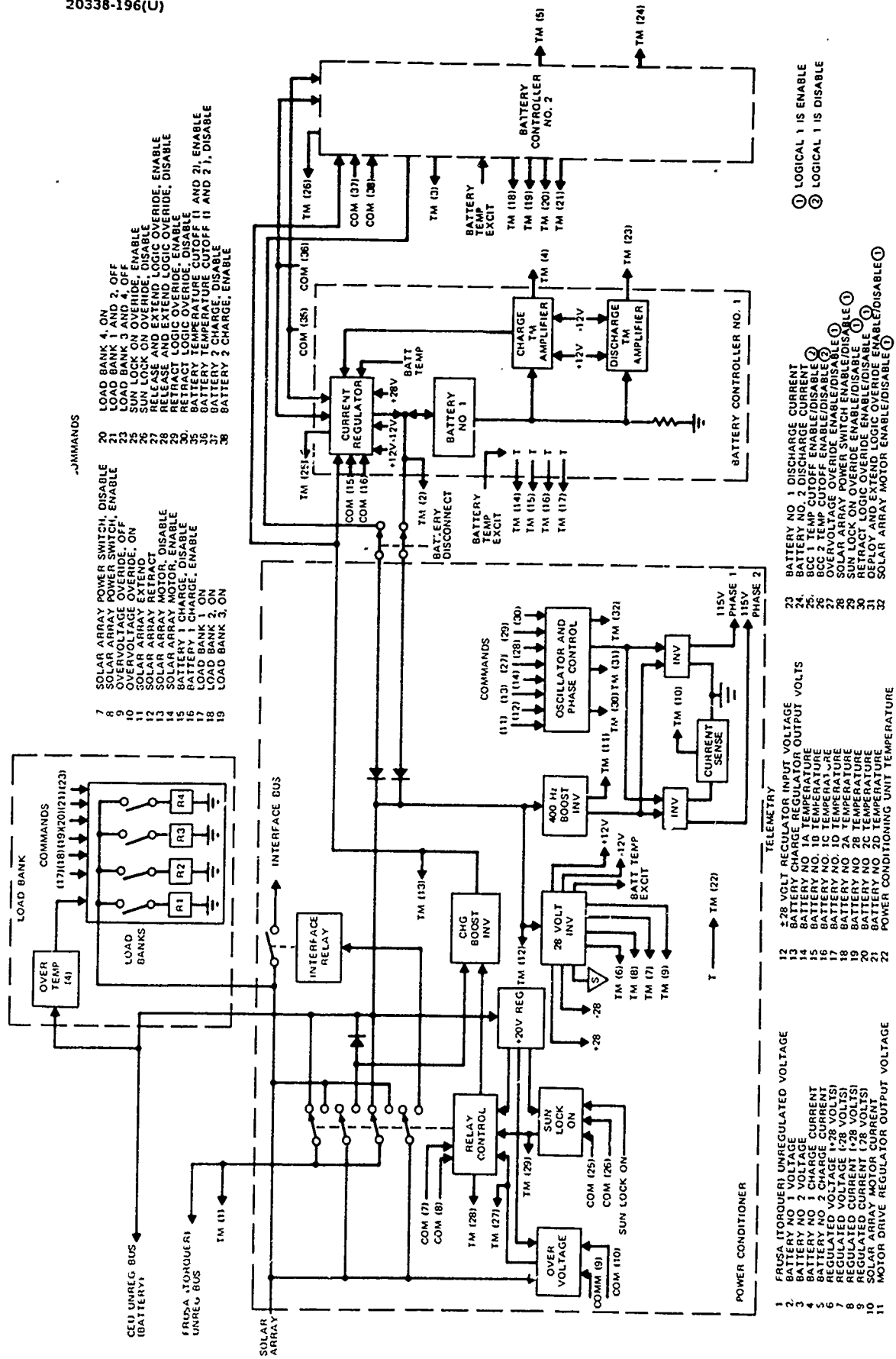


Figure 4-62. Power Conditioner and Storage Subsystem Functional Block Diagram



## POWER CONDITIONING AND STORAGE SUBSYSTEM

### Subsystem Description

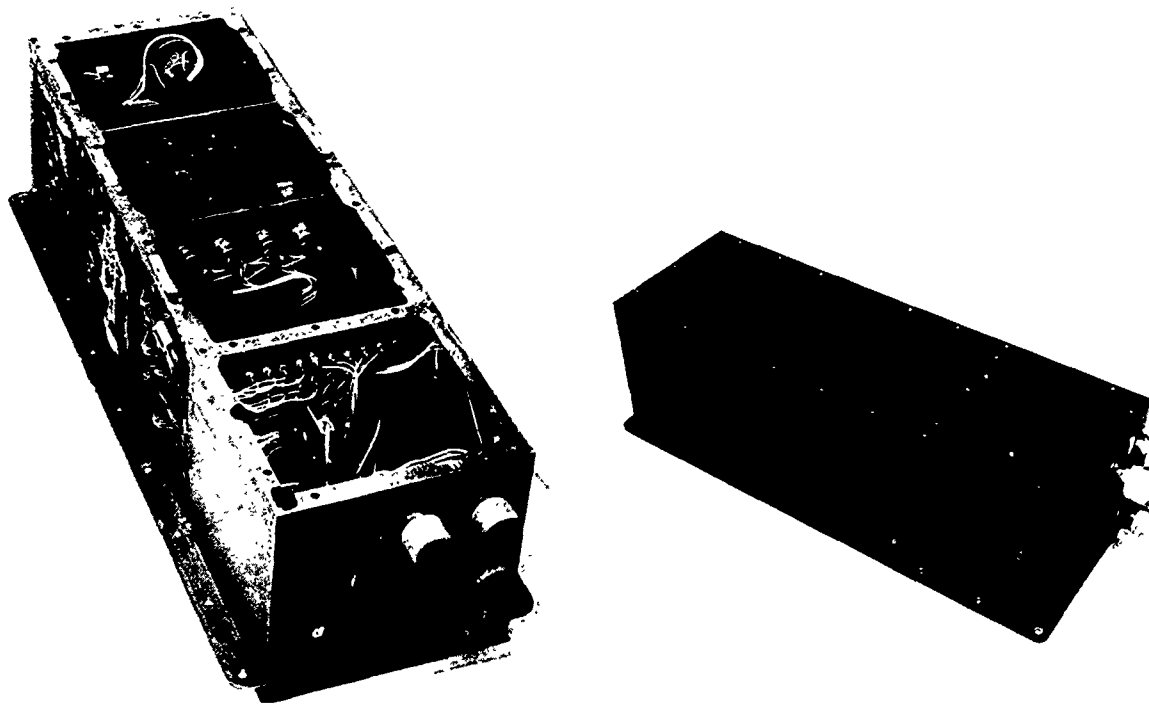
The Power Conditioning and Storage subsystem shown in functional form in Figure 4-62 consists of the power conditioning unit, a pair of battery/charge controller assemblies, and a load bank assembly. In general, this subsystem provided regulated ac and dc voltages, controlled battery charging, and furnished housekeeping power prior to deployment and during eclipses. Specific subsystem requirements were as follows:

- Provide operational power with a solar array power input between 20 and 44 volts dc, and a battery power input between 24 and 36 volts dc.
- Provide unregulated dc power between 24 and 44 volts to remainder of FRUSA units
- Supply regulated dc of  $\pm 28$  volts  $\pm 3$  percent
- Supply regulated 400-Hz, two-phase, 115-volt square wave ac for motor operation
- Enable switching between an external source, battery, and the solar array as dictated by mission operations
- Provide automatic controlled battery charge control
- Provide battery capacity for FRUSA operations and housekeeping functions (12 amp-hr)
- Enable incremental dissipation of the 1.5-kw solar array output for panel performance evaluation.

### Power Conditioning Unit

The Power Conditioning Unit (PCU), (see Figure 4-63) contains the overvoltage sensing circuit, the solar array power switch, the  $\pm 28$ -volt converter/regulator, the 400-Hz motor drive inverter, and a boost converter that provides regulated power for the battery/charge controllers.

Solar Array Overvoltage Switch. The overvoltage switch circuitry is designed to operate from the batteries. The circuit accepts three ground commands and one sun lockon command from the CEU. In the automatic mode, a voltage comparator senses the solar panel voltage, and when the voltage is less than 44 volts the solar array switch is closed. The switch is implemented by using a latching relay.



a) Without Cover  
(Photo ES29814)

b) Covered Configuration  
(Photo ES31342)

Figure 4-63. Power Conditioning Unit

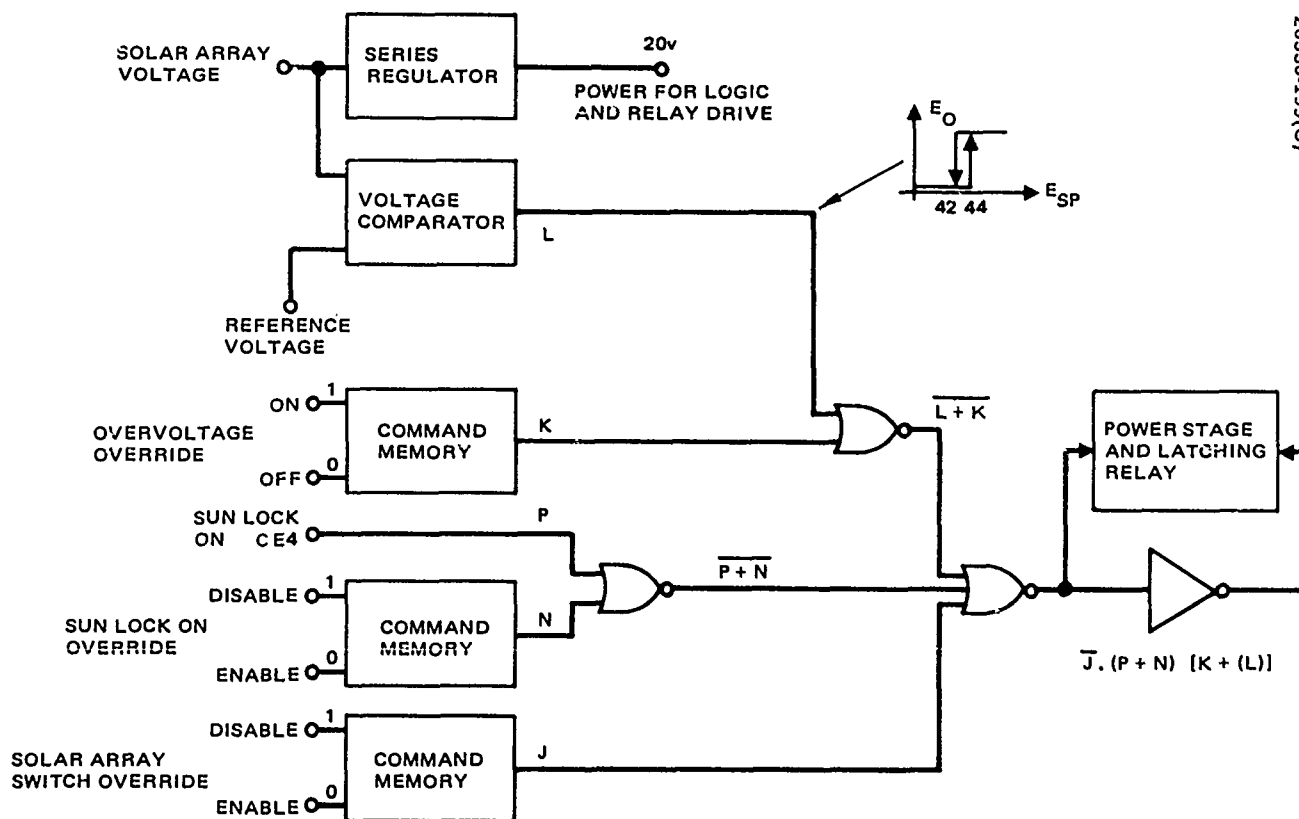


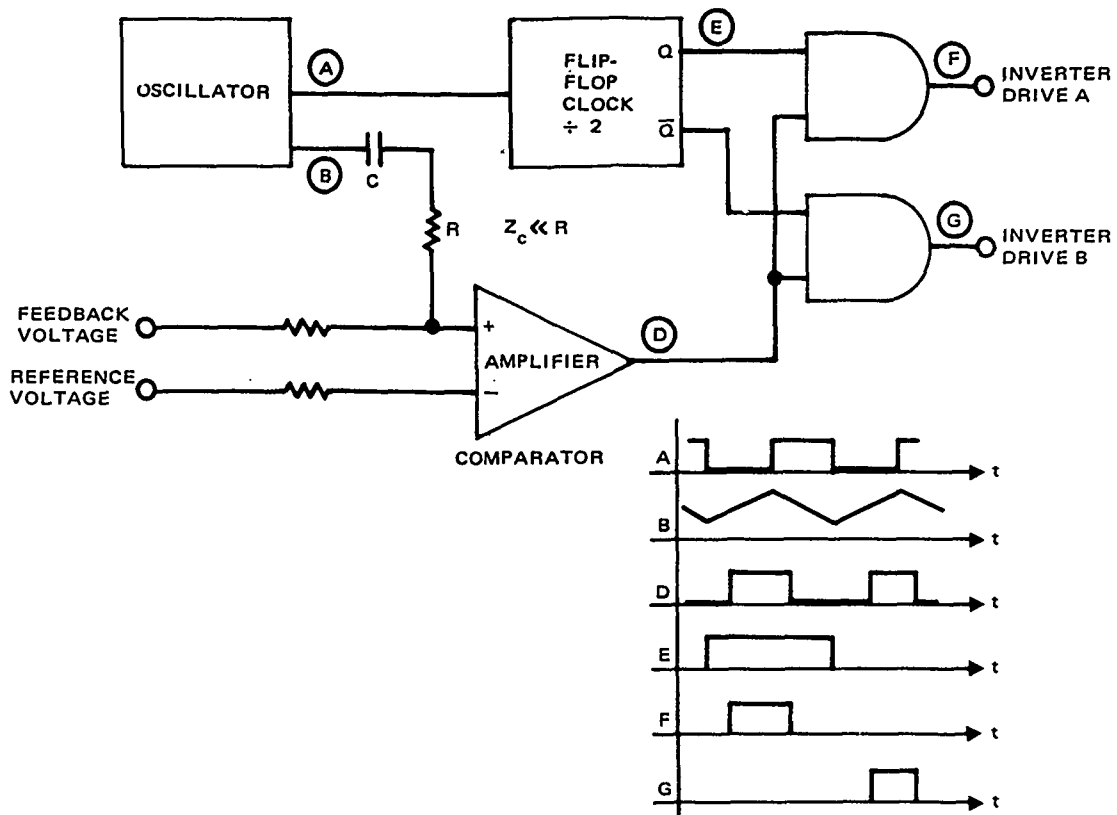
Figure 4-64. Solar Array Overvoltage Switch

The output of the overvoltage comparator along with a sun lockon command and a solar array switch enable command, pulse the latching relay. The comparator output can be overridden by the overvoltage override command. A second command provides a sun lockon override to simulate the sun lockon command coming from the control electronics unit. The solar array switch override command disables the automatic circuitry and resets the latching relay to the battery position. Figure 4-64 shows the Boolean mechanization.

±28-Volt Converter/Regulator. Figure 4-65 shows the pulsewidth modulator used to drive the power stages of the 28-volt converter. The oscillator provides a clock signal and a triangular wave, which is compared with feedback voltage and the reference voltage to create a pulsewidth that is "ANDed" with an output of a flip-flop. The purpose of the flip-flop is to steer the pulsewidth to alternate sides of the output stage. The figures shows the drive and output stage of the converter. The drive transformer is a fly-back transformer that applies base drive to the output transistor when the drive transistor is turned on. The energy stored in the drive transformer causes voltage reversal at the transformer secondary when the drive transistor is turned off, thus removing the stored charge in the base of the power transistor causing it to turn off quickly. The output transistor switching speed and the source for base drive power help to increase converter efficiency.

Boost Converter. The pulsewidth modulator used in the boost converter circuit is shown in Figure 4-66. A sawtooth voltage, generated by the output of the oscillator through an RC network, is compared with the difference between the feedback voltage and the reference voltage to create a pulsewidth that is steered to alternating sides of the power stage by the flip-flop. This converter uses the same form of output stage as does the ±28-volt converter. The output voltage is added to the input voltage to produce a regulated 42 volts output. The power converted by the booster is thus the difference between the input and output voltage times the output current. In this case, any power loss in the converter is compared with the total output power rather than the converted power and, hence, efficiency is relatively high (>90 percent).

400-Hz Inverter. The 400-Hz inverter consists of a pair of driven inverters. The two-phase drive signal is generated by an oscillator and digital phase network. The pair of flip-flops shown in Figure 4-67 generates the necessary two phase drive signal. A phasing diagram shows that the required states are always generated in proper sequence. The figures outside of the circles designate input condition to the flip-flops prior to a clock pulse from the oscillator. From the truth table it can be seen that each successive state of the phasing diagram is generated. To reverse the motor direction, the phase of one inverter is reversed by switching its input to the inverse of the signal used in the normal state. The drive and output stages are similar to the boost and ±28-volt inverter. Since the input voltage to the power stage is regulated, the output voltage is held constant.



20338-200(U)

Figure 4-65.  $\pm 28$ -Volt Inverter Pulsewidth Modulator

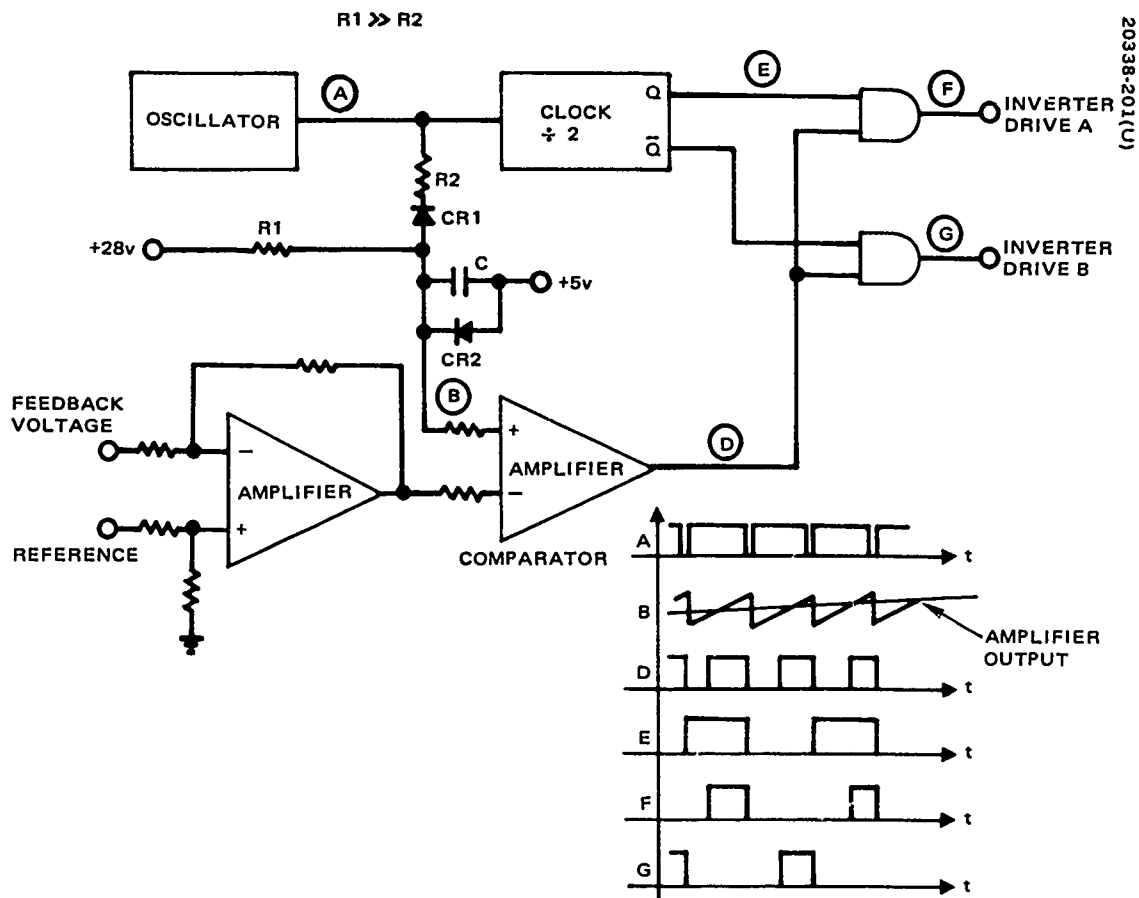
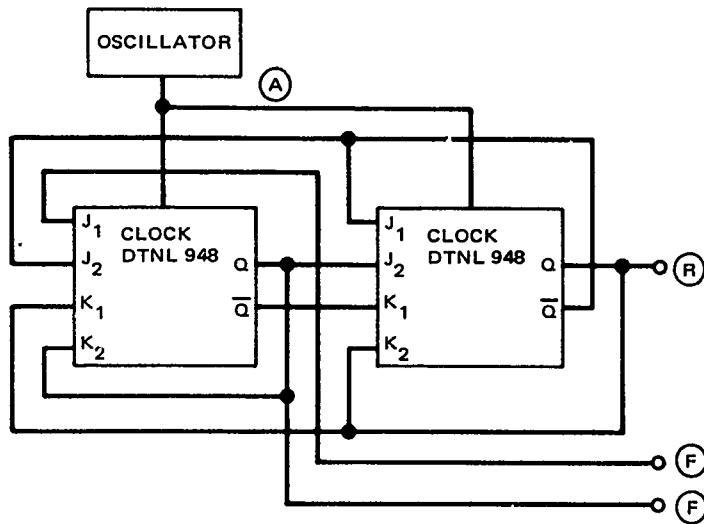


Figure 4-66. Boost Converter Pulsewidth Modulator



20338-202(U)

	$T_n$				$T_{n+1}$
	$J_1$	$J_2$	$K_1$	$K_2$	Q
1	0	X	0	X	$Q_n$
2	X	0	0	X	$Q_n$
3	0	X	X	0	$Q_n$
4	X	0	X	0	$Q_n$
5	1	1	X	0	1
6	1	1	0	X	i
7	0	X	1	1	0
8	X	0	1	1	0
1	1	1	1	1	IND

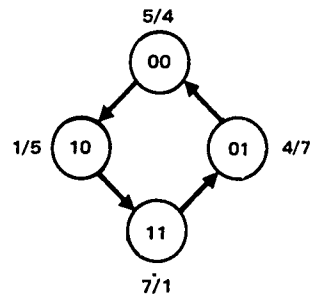
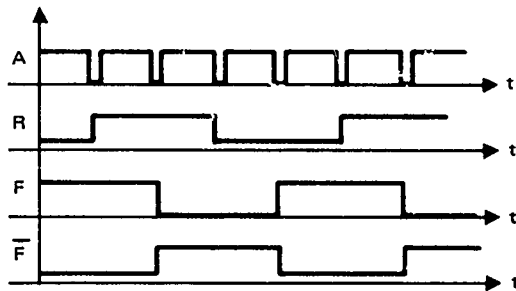


Figure 4-67. 400-Hz Inverter Waveform Generator

## Battery/Charge Controller

Each of the battery/charge controllers (see Figure 4-68) consists of two packs of 12 NiCd battery cells, each integrally mounted on one plate with the charge control electronics. The batteries each have a 6-amp-hr capacity.

Figure 4-69 shows the mechanization of the battery/charge control electronics. The circuit consists of two control loops, one a current control, and the other a cell voltage sensing circuit that provides the reference voltage to the current control loop. The battery charge current is sensed by a resistor, amplified by the charge current amplifier, and compared with a reference voltage from the cell voltage control loop. The differential of these two signals is applied to the constant current power stage to hold the battery charge current at the level selected by the cell voltage circuit. The cell voltage circuit measures a single battery cell and is compared with a reference voltage by a voltage comparator that has built-in hysteresis.

When 1.40 volts per cell is exceeded, the volt comparator drives a relay that switches the voltage reference to the current loop from the 1 ampere position to the 0.6-ampere position and holds it there until the cell voltage drops below 1.28 volts per cell. A battery overtemperature protection circuit is implemented using a thermostat switch. This switch applies a bias to the cell voltage comparator simulating a voltage in excess of 1.40 volts. The reference select relay is driven to the 0.6 ampere position and, at the same time, a second relay is actuated that reduces the reference voltage to the current controls to almost zero, thereby removing battery charge. When the cell voltage decreases to 1.28 volts per cell, the two relays are reset and a 1 ampere charge is initiated. Two command signals provide battery charge shutdown and overtemperature lockout enable or disable.

## Load Bank Assembly

The load bank assembly shown in Figure 4-70 employs four banks of power resistors that can be selected in any of 16 combinations by command. Sufficient data points are obtained through operation of this device to produce I-V characteristics of the panel (see Figure 4-71).

## Tradeoff Studies and Analysis

Among the significant studies performed on the power conditioning and storage subsystem were the following:

- Battery charge rates and depth of discharge analysis including charge termination methods
- Resistive value selections for the load bank assembly
- Power circuits analysis for input or output regulation and power conversion at 10 kHz for all but motor power

- Capacitive phase shift versus a two-phase pulse width modulator tradeoff for 400-Hz inverter
- Temperature rise and thermal cutoff limits analysis for the load bank

### Battery Sizing

The principal consideration in sizing and establishing the depth of discharge of the battery was reliability. Battery life is a sensitive function of discharge depth. For the application, an installed capacity of 12 amp-hr was considered conservative in size and acceptable in weight. In addition, redundancy was provided by configuring the battery as two 24-cell, 6-amp-hr units.

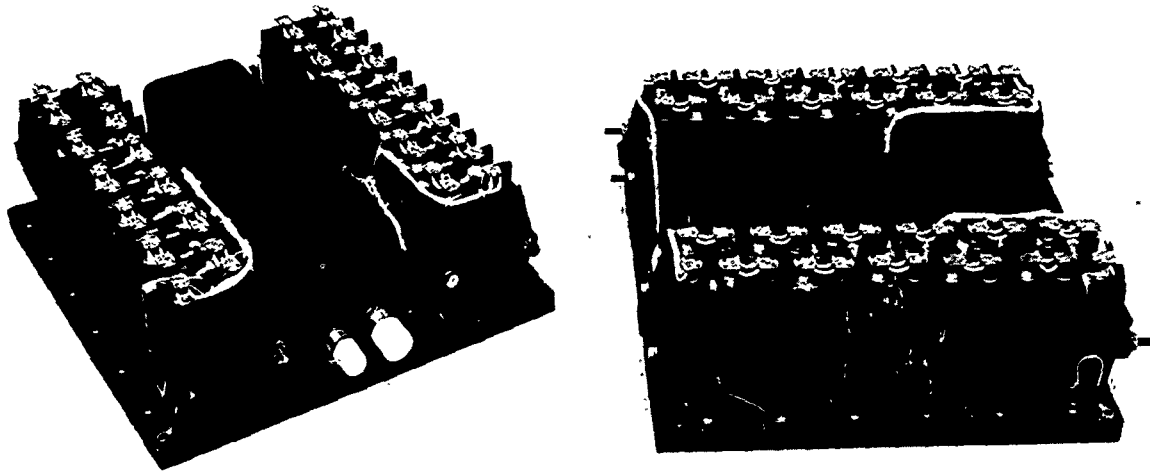
To maintain energy balance in the event of a battery failure, a charge rate of 1.0 ampere is required. This rate, however, was considered to be too high a rate for continuous overcharge of a single 6-amp-hr battery. The highest acceptable continuous charge rate was 0.6 ampere. The charge controller was, therefore, required to initially provide 1.0 ampere to each of the two 6-amp-hr batteries. When the voltage of a cell of either battery increased to a preset value, indicating approach of the full charge, the charge rate of the battery was automatically reduced to 0.6 ampere. Automatic redundancy is provided, because if one battery failed the remaining battery would be discharged deeper, and yet would accept more recharge at the high rate before reaching the switch-back set point. Thermal runaway was prevented by means of an overtemperature sensor which cut off all charging if temperatures exceeded 120°F.

As a further measure of conservatism, the cells specified included a newly developed design feature which permitted continuous overcharge at much higher rates than could be accommodated by previous designs without the development of excessive internal oxygen pressure. Employing the new cell design was considered necessary because of the relatively high charge rates, 1.0 and 0.6 ampere, required to maintain energy balance in the near earth orbit application.

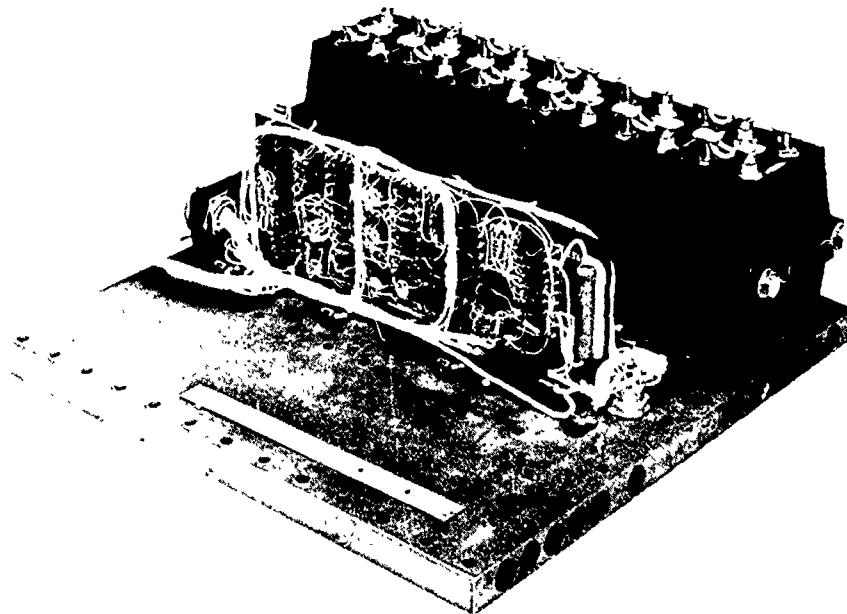
### Load Bank Resistor Selection

The load bank assembly uses fixed resistors that are connected by relays to the solar panel in various combinations to provide a variety of known resistive loads to the panel. Four resistors were found to be adequate to produce 15 different resistive loads, a number sufficient to define the current-voltage operating curve of the panel with good precision. Resistor values were chosen to produce a concentration of load points near the knee of the curve. This region is of most interest because it is the normal operating (maximum power) part of the curve.



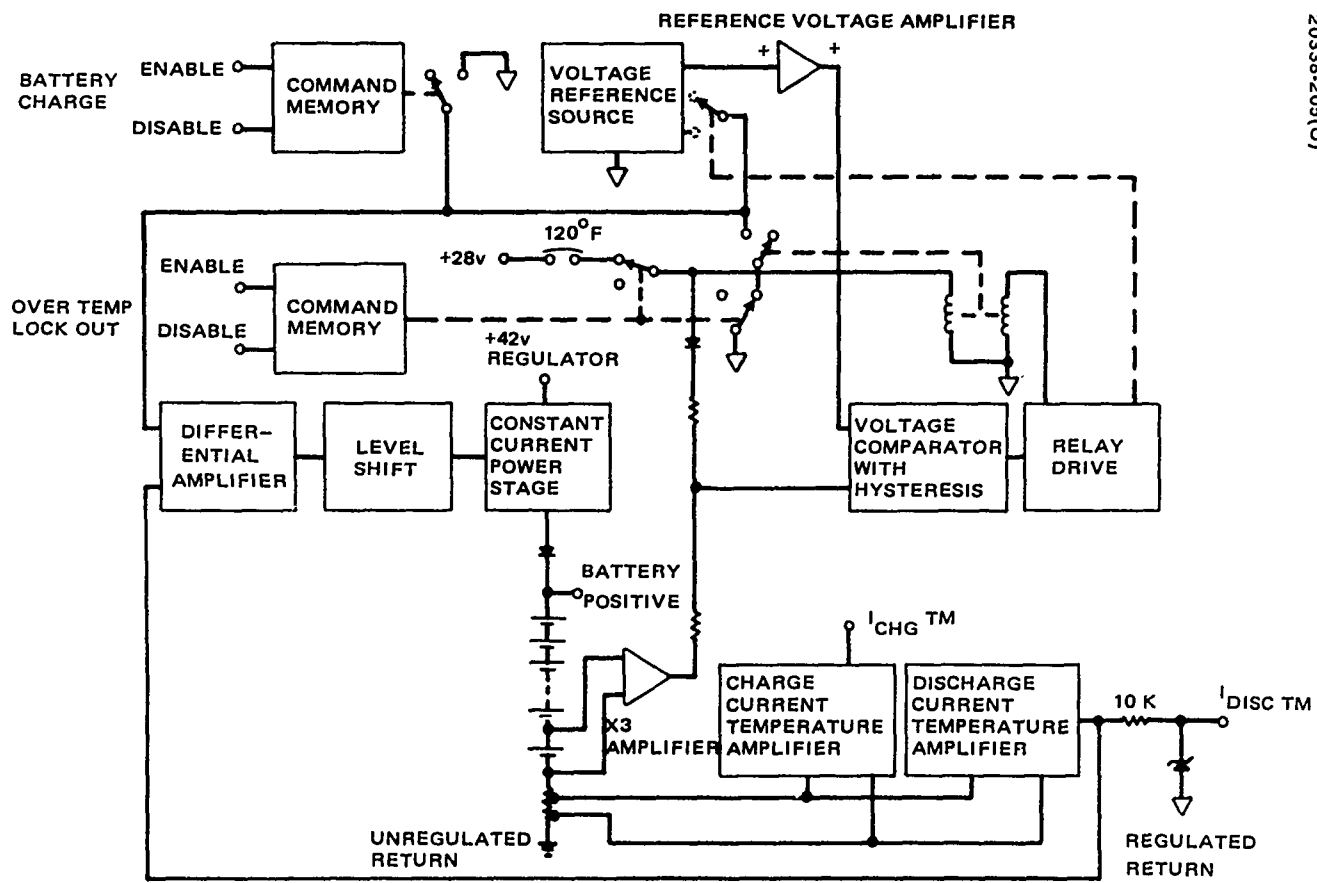


a) Units (Photo ES31340)



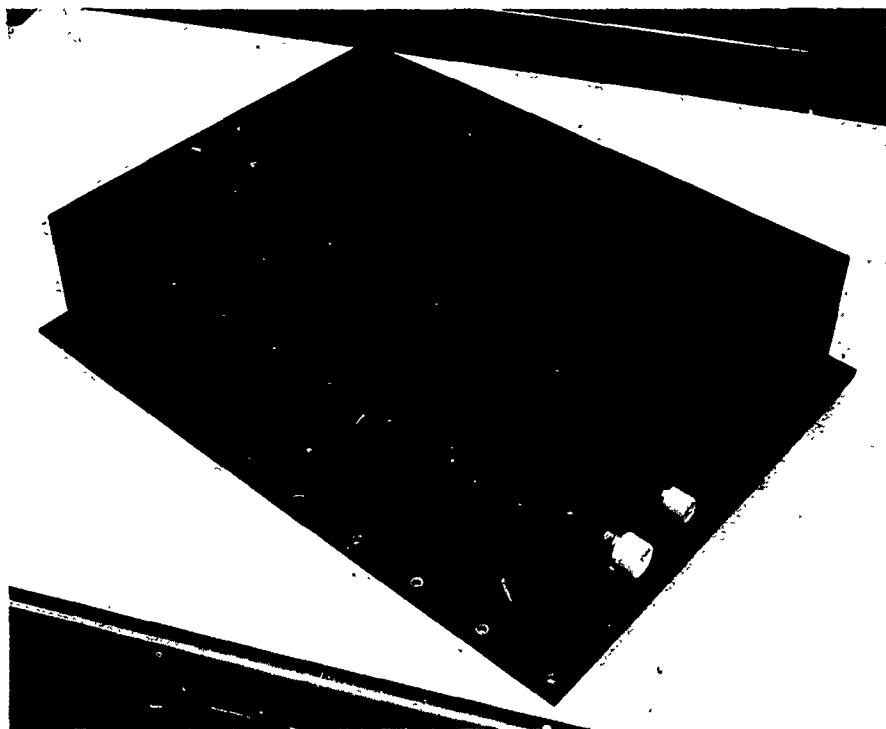
b) Circuitry (Photo ES29816)

Figure 4-68. Battery/Charge Controller

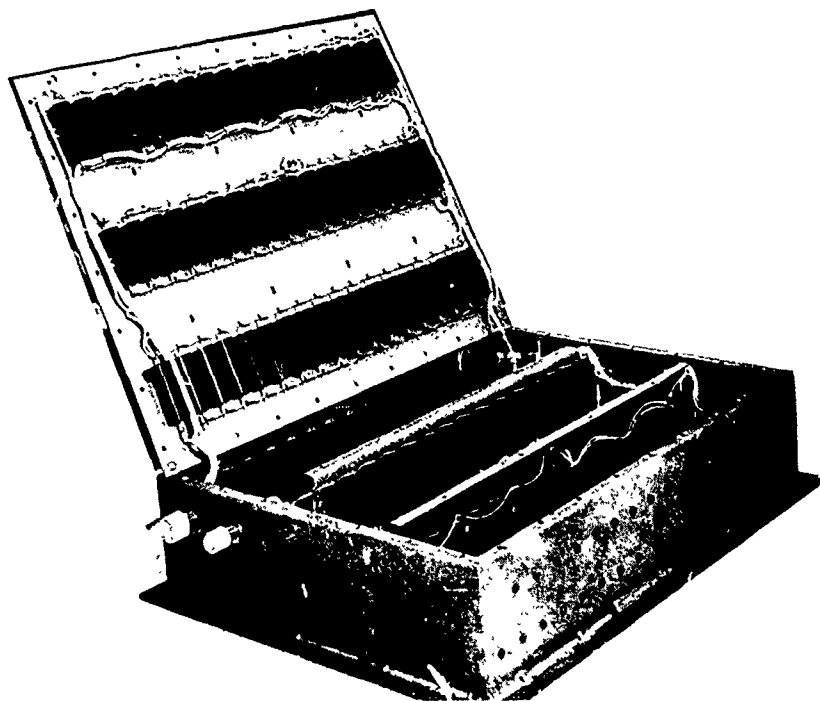


20338-205(U)

Figure 4-69. Battery Charge Control Block Diagram



a) Closed (Photo ES 31341)



b) Open (Photo ES29818)

Figure 4-70. Load Bank Assembly

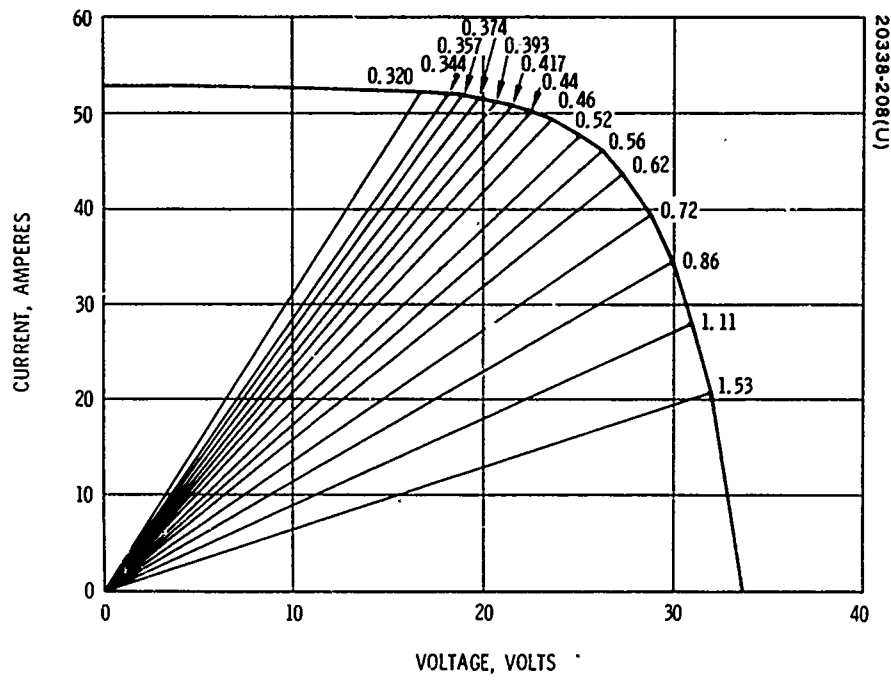


Figure 4-71. Load Bank Load Lines

## Power Conditioning Unit

Two major factors were pertinent in establishing the power circuit configurations and converter frequencies for input or output regulation.

The first consideration was the wide input voltage range for the boost converters and for the  $\pm 28$ -volt regulated converter. The main question was whether a switching preregulator, followed by conventional dc/dc converters would be better than individual pulse width modulated dc/dc regulated converters. The losses of a pulse width modulated dc/dc regulated converter were shown to be lower than a switching preregulator followed by a conventional dc/dc converter for the  $\pm 28$ -volt converter needs, and the boost converters for battery charging and motor power inputs followed the same approach. The battery charge boost circuits fed separate series regulators (one for each battery pack set) which regulated battery charge currents. A preregulated input to these series regulators reduced the range of power dissipation in each of the BCCU's. The regulated input voltage for the motor drive inverters also allowed good square waves to be generated for the array motor drive operation instead of pseudo-square waves which would have had higher EMI content and larger unknowns for motor operation.

The second consideration was to optimize the compromise between decreased filtering requirements for higher frequency converter operation and increased efficiencies in the drivers and power transistors at lower frequencies of converter operation. The 10-kHz frequency was determined as a good frequency to provide reasonably high efficiencies without unreasonably large filtration requirements.

Another power circuit tradeoff was the evaluation of capacitive phase shift in comparison to a two-phase pulse width modulator for the 400-Hz inverter. Our original conceptual approach to generate a two-phase, 400-Hz, 115-volt (rms) square wave output for motor power used a capacitor to change the phase by about 90 degrees from the reference signal. This study showed that the phase shift would have to be obtained before the signal was delivered to the load, that is, not on the main output to the motor itself. This fact was based upon the nonresistive and nonlinear type of impedance presented to the electronics by the motor. Waveform distortions due to variation in motor impedance at idle and at stall was also a problem. The solution was to phase shift earlier in the signal generation chain and provide separate output channels thereafter. A digital approach was then considered to develop the two signals and was found to be superior to the original capacitive phase shift approach. The truth table shown in Figure 4-6<sup>7</sup> illustrates how the digital logic elements were connected to assure proper phasing and synchronization.

Also of significance was a tradeoff to optimize the relationship between load bank temperature rise and thermal cutoff limits. This trade-off was performed to select the best thermostatic switch setting for protection

TABLE 4-10. POWER CONDITIONING AND STORAGE SUBSYSTEM DEVELOPMENT TEST SUMMARY

	Temperature, °F					Δ
	-5	+12	58	74	156	
Battery charger (required operating range 40° to 80°F)	1.456	1.466	0.450	1.450	1.422	+0.016 -0.028
0.6-ampere switching voltage	1.316	1.282	1.305	1.301	1.304	+0.035 -0.000
1.0-ampere switching voltage	0.600	0.610	0.600	0.580	0.580	+0.010 -0.020
0.6-ampere current	1.030	1.025	1.020	1.005	0.980	+0.030 -0.020
1.0-ampere current						
	Temperature, °C					
	-50	-10	+25	+60	+125	
Solar panel switch	43.00	42.86	42.85	42.74	42.47	
High end turn-on	44.29	44.15	44.07	43.89	43.58	
High end turn-off	45		60		100	
Relay pulse time, ms						
400-Hz inverter	115-volt rms no load					112-volt full load
±28-volt inverter	Measured regulation is < ±1 percent. Response is < 0.2 ms					< 0.3 volt
	Efficiency is 80 percent at 34 watts					
	81.5 percent at 14 watts					
	70 percent at 5 watts					

against excessive temperature rise in the load bank. The power resistors were capable of very high temperature operation, and the power relays and other parts also were capable of reasonably high operating temperatures. It was desirable to use a thermostatic switch setting that operated at as high a temperature as could be tolerated so that maximum operational flexibility could be obtained. The expected duration of operation, the thermal time constants, the baseline temperature, and the component capabilities were all considered in the final choice of a 140°C thermostat.

## Development Tests

### Subsystem Circuit Performance Tests

The battery/charge controller was tested within a temperature range of -5° to 156°F, although the normal expected operating range is from 40° to 80°F. The data showed that the nominal values for the current switching periods were not adjusted properly, but the required tolerance was met. The solar array switch circuit was tested from -50° to 125°C and performed well within the specified required levels. The data during the 400-Hz inverter load tests show that, from stall to no load, the motor voltage changes from 112 to 115 volts, which is well within the 5 percent required regulation. The ±28-volt inverter regulated the outputs to within 1 percent and meets the transient response requirements. The inverter efficiency of 80 percent at full load gives a margin of 5 percent over that required. Table 4-10 summarizes the test results.

### Battery Development Tests

To evaluate the performance of the battery cells under simulated orbital operating conditions, the following test parameters were employed:

Charge time	54 minutes
Discharge time	46 minutes
Charge current	1.0 and 0.6 ampere*
Discharge current	0.65 ampere
Expected temperature range	40° to 80°F
Temperature range for tests	30° to 90°F

## Conclusions

Experience with the power conditioning and storage subsystem has been excellent. All power functions related to these units were performed

\*Switched from 1.0 to 0.6 automatically when cell voltage reached 1.45 volts. The breadboard charge controller with two cells from the qualification model lot were used for the tests. A total of 174 simulated orbits were run during the program. The performance of the subsystem was normal at all test temperatures.

to specification without incident in both ground and flight testing operations. Future similar applications could profit by use of the FRUSA power electronics and battery units without change.

## INSTRUMENTATION SUBSYSTEM

### Functional Requirements

The instrumentation subsystem includes sensors, signal conditioning circuits, and data commutators that provide a means of monitoring and evaluating experiment performance with respect to mission objectives. The outputs of the instrumentation subsystem were required to be compatible with the space ground link subsystem (SGLS) in the spacecraft.

Five general classes of data were required:

- 1) Subsystem health and housekeeping information
- 2) Solar array dynamic and strain gage data
- 3) Thermal data
- 4) System configuration status
- 5) Voltage-current data from special experimental cells and modules and from the main solar panels

### Unit Description

#### Solar Array Subsystem

The solar array subsystem instrumentation signals are conditioned by instrumentation amplifiers, the instrumentation conditioning unit (ICU), and solar cell electronics unit (SCEU). The outputs of the conditioning units are multiplexed in PCM-compatible PAM commutators. The commutator outputs are supplied to the spacecraft telemetry system through the drum axis sliprings, the support axis sliprings, and the orbital equipment rack wiring harness. Tables 4-11 and 4-12 list the telemetry.

#### Orientation Subsystem

All orientation subsystem instrumentation signals are conditioned in the control electronics unit (CEU). The conditioned signals from the CEU are multiplexed in a PAM commutator and applied to the spacecraft telemetry system through a support axis slipring and the orbital equipment rack wiring harness. Table 4-13 lists the telemetry.



TABLE 4-11. SOLAR ARRAY COMMUTATOR A TELEMETRY

Data Channel	Function
A-1	Zero calibration
A-2	Full-scale calibration
A-3	Boom tip inboard accelerometer (V-axis) panel 1
A-4	Boom tip outboard accelerometer (W-axis) panel 1
A-5	Boom tip inboard accelerometer (V-axis) panel 2
A-6	Boom tip inboard accelerometer (U-axis) panel 2
A-7	Boom tip outboard accelerometer (W-axis) panel 2
A-8	Boom length compensator strain gage, panel 1
A-9	Boom strain gage
A-10	Drum mechanism inboard accelerometer (V-axis)
A-11	Boom length compensator strain gage, panel 2
A-12	Array position indicator (pulse count)
A-13	Spreader bar 1 temperature
A-14	Solar array fully extended
A-15	Solar array fully retracted
A-16	Spreader bar 2 temperature
A-17	Drum bearing temperature
A-18	Boom tip inboard accelerometer (V-axis) panel 1
A-19	Boom tip outboard accelerometer (W-axis) panel 1
A-20	Boom tip inboard accelerometer (V-axis) panel 2
A-21	Boom tip inboard accelerometer (U-axis) panel 2
A-22	Boom tip outboard accelerometer (W-axis) panel 2
A-23	Boom length compensator strain gage, panel 1
A-24	Boom strain gage
A-25	Drum mechanism inboard accelerometer (V-axis)
A-26	Boom length compensator strain gage, panel 2
A-27	Solar array subassembly released

Table 4-11 (Continued)

Data Channel	Function
A-28	Solar array motor temperature
A-29	Spare
A-30	Solar array voltage
A-31	Solar array return
A-32	Spare
A-33	Boom tip inboard accelerometer (V-axis) panel 1
A-34	Boom tip outboard accelerometer (W-axis) panel 1
A-35	Boom tip inboard accelerometer (V-axis) panel 2
A-36	Boom tip inboard accelerometer (U-axis) panel 2
A-37	Boom tip outboard accelerometer (W-axis) panel 2
A-38	Boom length compensator strain gage, panel 1
A-39	Boom strain gage
A-40	Drum mechanism inboard accelerometer (V-axis)
A-41	Boom length compensator strain gage, panel 2
A-42	Solar array 2 current
A-43	Solar array 1 current
A-44	Synchronization
A-45	Synchronization

#### Power Conditioning and Storage

All power conditioning and storage subsystem instrumentation signals are conditioned to a 0- to 5-volt format. These signals are applied directly to the spacecraft telemetry system via the orbital equipment rack wiring harness. Table 4-14 lists the telemetry.

#### Sensors

The instrumentation sensors are of the following general types:

- Voltage sensors
- Current sensors
- Temperature sensors
- Strain gages
- Accelerometers

TABLE 4-12. SOLAR ARRAY COMMUTATOR D TELEMETRY

Data Channel	Function
D-1	Zero calibration
D-2	Full-scale calibration
D-3	Mid-scale calibration
D-4	Drum mechanism outboard accelerometer (V-axis)
D-5	Drum mechanism outboard accelerometer (W-axis)
D-6	Boom tip outboard accelerometer (V-axis) panel 2
D-7	Boom tip outboard accelerometer (V-axis) panel 1
D-8	Spare
D-9	Spare
D-10	Cell/module selection bit 1
D-11	Cell/module selection bit 2
D-12	Cell/module selection bit 3
D-13	Cell/module selection bit 4
D-14	Array panel 1 temperature, root outboard
D-15	Load condition bit 1
D-16	Load condition bit 2
D-17	Load condition bit 3
D-18	Array panel 1 temperature, midpoint inboard
D-19	Drum mechanism outboard accelerometer (V-axis)
D-20	Drum mechanism outboard accelerometer (W-axis)
D-21	Boom tip outboard accelerometer (V-axis) panel 2
D-22	Boom tip outboard accelerometer (V-axis) panel 1
D-23	Spare
D-24	Spare
D-25	Solar cell electronics unit temperature
D-26	Array panel 1 temperature, root inboard
D-27	Array panel 1 temperature, root outboard
D-28	Array panel 1 temperature, outer sector, outboard
D-29	Array panel 2 temperature, root outboard
D-30	Array panel 2 temperature, midpoint inboard
D-31	Array panel 2 temperature, outer sector, inboard
D-32	Cell/module voltage
D-33	Cell/module current
D-34	Drum mechanism outboard accelerometer (V-axis)
D-35	Drum mechanism outboard accelerometer (W-axis)
D-36	Boom tip outboard accelerometer (V-axis) panel 2
D-37	Boom tip outboard accelerometer (V-axis) panel 1
D-38	Spare
D-39	Spare
D-40	Solar cell electronics unit power
D-41	Array panel 2 temperature, root inboard
D-42	Array panel 2 temperature, midpoint outboard
D-43	Spare
D-44	Synchronization
D-45	Synchronization

TABLE 4-13. ORIENTATION SUBSYSTEM COMMUTATOR B  
TELEMETRY MEASUREMENTS

Data Channel	Function
B-1	Zero calibration
B-2	Full-scale calibration
B-3	Spare
B-4	Acquisition sensor, positive
B-5	Acquisition sensor, negative
B-6	Tracking sensor, lockon cell
B-7	Tracking sensor, drum axis error
B-8	Tracking sensor, support axis error
B-9	Sun sensor excitation, +15 volts dc
B-10	Sun sensor excitation, -15 volts dc
B-11	Drum axis torquer current (high level)
B-12	Support axis torquer current (high level)
B-13	Control electronics unit, +5 volts dc
B-14	Control electronics unit, +28 volts dc
B-15	Control electronics unit, -28 volts dc
B-16	Solar array subassembly deployed and locked
B-17	Drum axis tachometer voltage
B-18	Support axis tachometer voltage
B-19	Drum axis torquer temperature
B-20	Support axis torquer temperature
B-21	Drum axis housing temperature at bearing, 2 o'clock
B-22	Drum axis shaft temperature at bearing
B-23	Control electronics unit temperature A
B-24	Control electronics unit temperature B
B-25	Support axis shaft temperature at bearing
B-26	Support axis housing temperature at bearing, 2 o'clock
B-27	Drum axis housing temperature at bearing, 6 o'clock
B-28	Drum axis brush temperature
B-29	Drum axis housing temperature at bearing, 10 o'clock
B-30	Support axis housing temperature at bearing, 6 o'clock
B-31	Support axis brush temperature
B-32	Support axis housing temperature at bearing, 10 o'clock
B-33	Filtered unregulated bus No. 1
B-34	Drum axis torquer current (low level)
B-35	Support axis torquer current (low level)
B-36	Manual torque drum axis negative
B-37	Manual torque drum axis positive
B-38	Manual torque support axis negative
B-39	Manual torque support axis positive
B-40	Torquer drive command
B-41	Manual sun lockon
B-42	Limit override
B-43	Spare

TABLE 4-14. POWER CONDITIONING AND STORAGE  
SUBSYSTEM TELEMETRY

Data Channel	Function
C-1	Zero calibration
C-2	92 percent calibration
C-3	28 volt regulator input
C-4	+28 volt voltage
C-5	-28 volt voltage
C-6	+28 volt current
C-7	-28 volt current
C-8	Array motor current
C-9	Battery charge regulator output, volts
C-10	PCU internal temperature
C-11	Overvoltage override enable/disable
C-12	Power switch enable/disable
C-13	Sun Lockon override enable/disable
C-14	Retract logic override enable/disable
C-15	Deploy and extend override enable/disable
C-16	SA motor enable/disable
C-17	Battery 1 charge current
C-18	Battery 1 discharge current
C-19	Battery temperature 1A
C-20	Battery temperature 1B
C-21	Battery temperature 1C
C-22	Battery temperature 1D
C-23	Battery 1 voltage
C-24	Battery 1 temperature cutoff enable/disable
C-25	Battery 2 charge current
C-26	Battery 2 discharge current
C-27	Battery temperature 2A
C-28	Battery temperature 2B
C-35	Battery temperature 2C
C-36	Battery temperature 2D
C-31	Battery 2 voltage
C-32	Battery 2 temperature cutoff enable/disable
C-33	FRUSA unregulated voltage
C-34	Motor drive regulator voltage

Precision voltage divider networks or precision shunt type current sensors with conditioning amplification were used for voltage and current sensing. Thermistors, platinum wire, and semiconductor sensors were employed for temperature measurements. All were conditioned to a 0- to 5-volt format.

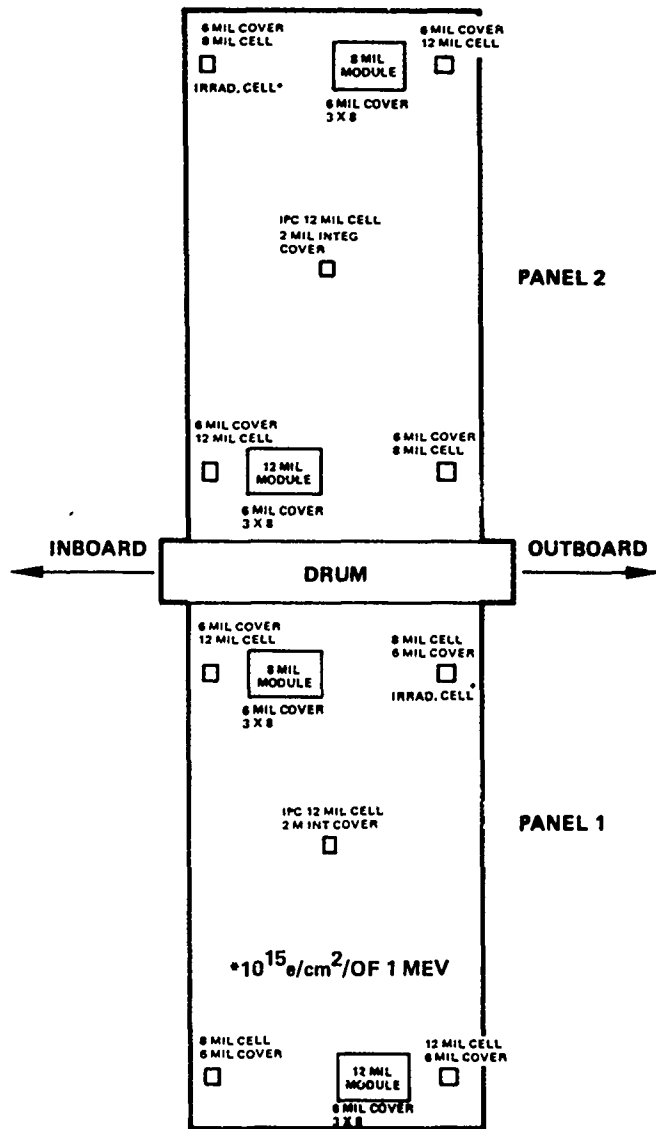
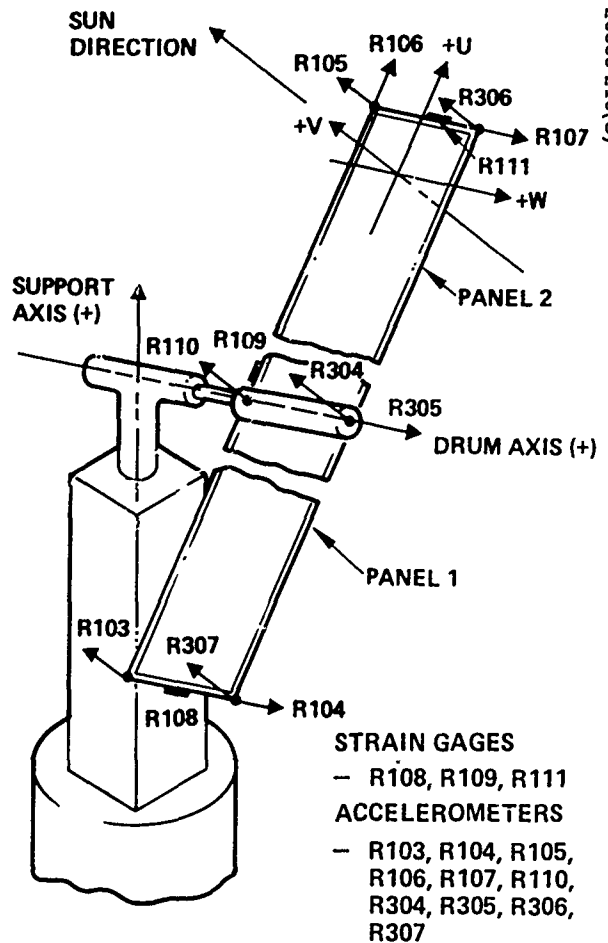


Figure 4-72. Location of Reference Cells and Modules

20338-209(U)



20338-210(U)

Figure 4-73. Strain Gage and Accelerometer Installation

The three solar array subassembly gage measurements consisted of four bridge-connected sensor elements on each boom length compensator tape to measure the array panel tensile force and four bridge-connected sensors to measure the panel bending moment at the root of the panel 1 inboard boom. Three strain gage amplifiers were used to amplify the low level output signal of the strain gage elements to a 0- to 5-volt format. The amplifier also provided a 15-volt excitation source for the strain gage bridge network. The boom compensator strain gage amplifiers were located at the inboard boom tips. The other amplifier, which processed the strain measurement at the inboard boom root of array panel 1, was located on the inboard boom actuator.

Ten force balance  $\pm 0.1$ -g servo accelerometers were required on the FRUSA experiment. Three units were located on solar array panel 1, four on solar array panel 2, and three units on the drum mechanism. The array panel accelerometers measured the dynamic reactions in the U, V, W directions of the inboard and outboard boom tips. The drum mechanism accelerometers measured the dynamic reactions of the inboard (V axis) and outboard (V and W axes) boom actuators. Each accelerometer is an integrated unit, consisting of the sensing element and amplifier in a single case. The accelerometer output was in the 0- to 5-volt range, suitable for commutating, and required no additional signal conditioning. Locations of the principal solar cell and cell models and the accelerometers and strain gages are shown in Figures 4-72 and 4-73.

#### Instrumentation Conditioning

Instrumentation conditioning is performed by the ICU and the SCEU for the solar array and by the CEU for the orientation subsystem. The ICU conditions the following temperature measurements on the solar array subassembly: solar array motor, spreader bar No. 1, spreader bar No. 2, and drum bearing temperatures.

The solar array voltage and current are shaped by a voltage divider network. In addition, the ICU conditions several digital signals originating from microswitches located on the solar array subassembly: array position, array fully extended, array fully retracted, and solar array subassembly released signals.

The SCEU conditions all array temperature sensors (with the exception of the spreader bar temperatures) and the internal SCEU temperature. In addition, the SCEU generates two reference voltages to be used for full-scale and mid-scale calibration of solar array data.

Upon receipt of a dual ground command the unit provides a load cycling for identifying the I-V characteristics of the special solar cells and modules. This function includes: sequentially selecting and loading the ten reference cells and four reference modules located on the two arrays; measuring the voltage and current characteristics of each cell and module

for the selected load condition; and generating a three word identification of the load conditions and a four word identification of the cell or module being measured.

### Operational and Test Results

During the system test phases and initial orbital operations the FRUSA instrumentation was adequate to determine system performance.

During the first 6 months of orbital operation two of the three PAM commutators failed. Both were on the solar array. The principal data lost were solar panel temperatures, accelerometers, strain gages and the test cell and module data. Fortunately, however, enough information was obtained prior to the failures to determine the major performance characteristics of the system in the technical areas affected.

There were some minor instrumentation problems during tests which are mentioned in Section V.

### Conclusions

From an overall point of view, the instrumentation subsystem proved adequate. In future designs, however, consideration should be given to the following:

- 1) Array position indicators should be included for both orientation axis positions and for the amount of array extension. The orientation axis position data would have been quite useful for nonstandard mission operations where the sun tracking system was inoperative or in an eclipse situation (in such cases the array position was indeterminate with the current FRUSA design). The solar panel position indicator (one indication for each drum revolution) was too coarse an indicator for some of the nonstandard panel positions that were necessary on the STP 71-2 mission for Agena bus voltage regulation.
- 2) A more reliable commutation device should be used or the requirement for remote data commutation should be waived in favor of additional sliprings in the orientation mechanism. This tradeoff would change in an operational system where the number of data rings could be quite small compared with an experimental mission of the type flown by FRUSA, where the experimental data requirement was an order of magnitude larger than the operational data requirement.



## SYSTEM AGE

All FRUSA system tests were conducted using the normal system telemetry signals to determine system performance. These signals were calibrated at the subsystem (or unit) level and were not affected by connection into the system. The equipment used for system tests consisted of an AGE panel, power load simulator, solar array simulator, digital voltmeter, oscilloscope, water table test facility, and deployment test fixture.

The AGE panel contained circuits for:

- 1) Selecting one of four PAM commutation outputs to be displayed on an oscilloscope: the SCEU, solar array, CEU, or PCU commutator outputs. The PCU commutator was not part of the system but was provided in the AGE panel itself.
- 2) Generating frame and word synch for PAM commutator synchronization.
- 3) Selecting a desired PCU telemetry point for digital voltmeter reading.
- 4) Generating a selected command for activation of the FRUSA commandable functions.

The power load simulator was used to supply a load for the simulated panel power in order to test the current carrying capabilities of the system wiring, sliprings, relays, etc.

The solar array simulator consisted of regulated dc power supplies connected in parallel, supplying up to 50 amperes to simulate the solar array in testing.

In addition, a digital voltmeter was used to measure the PCU telemetry and a standard laboratory oscilloscope was used to measure the telemetry from the SCEU, solar array, and CEU PAM commutators on a point-by-point basis.

The primary pieces of mechanical AGE were the water table test facility and deployment test fixture. The former was built to enable the extension and retraction functions to be tested without overloading the relatively fragile solar panels and booms. The tables consisted of two 9- by 18-foot tables with shallow water trays on top. The solar array was then supported, as it was extended, by numerous urethane floats riding on 1-1/2 inches of water. Full extension and retraction were performed on this facility in addition to final tensioning for flight.

The deployment test fixture simulated the mounting of the solar array and orientation mechanism on the spacecraft. The array was suspended on

spring-loaded cables and allowed to deploy as it would in space. A block diagram of the AGE hookup is shown in Figure 4-74 and the ambient test positions are illustrated in Figures 4-75 and 4-76.

Conclusions

The telemetry signals were sufficient to test the electrical performance of the FRUSA when used in conjunction with the above test equipment and facilities. In addition, the simple oscilloscope reading of PAM telemetry proved to be a workable scheme.

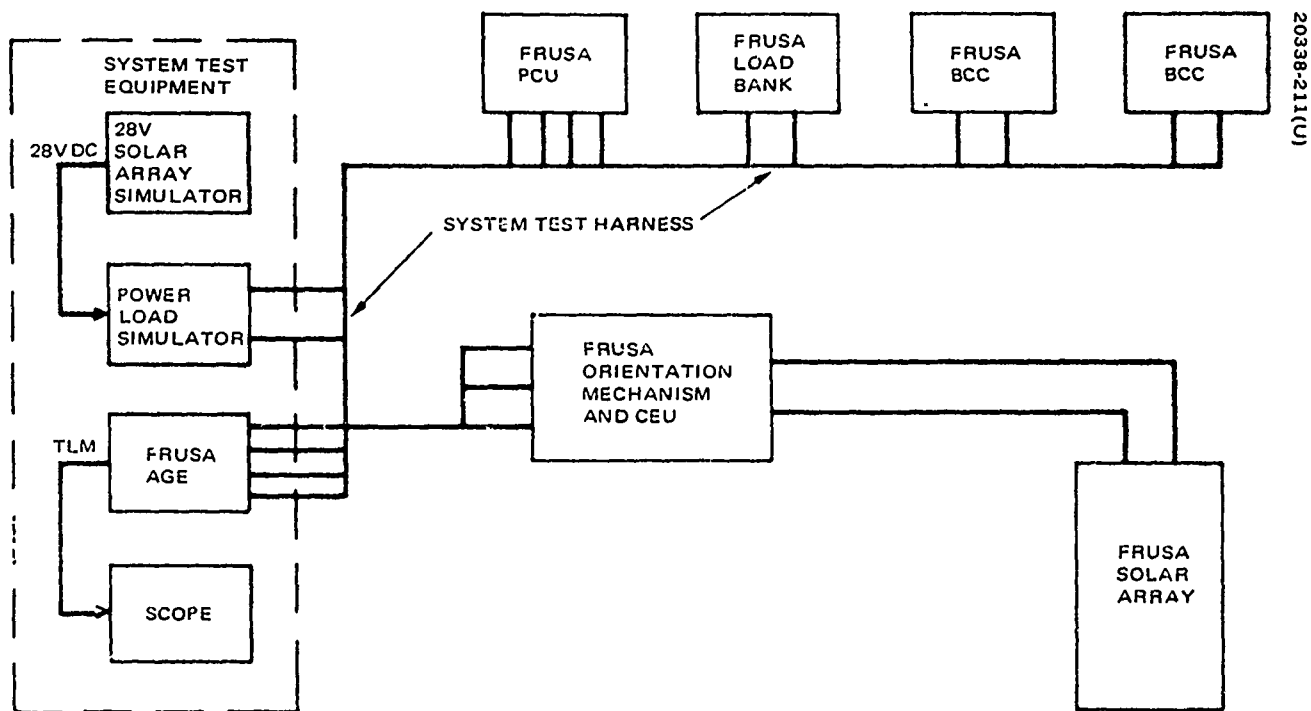


Figure 4-74. Single Line Cable Block Diagram/FRUSA System Tests

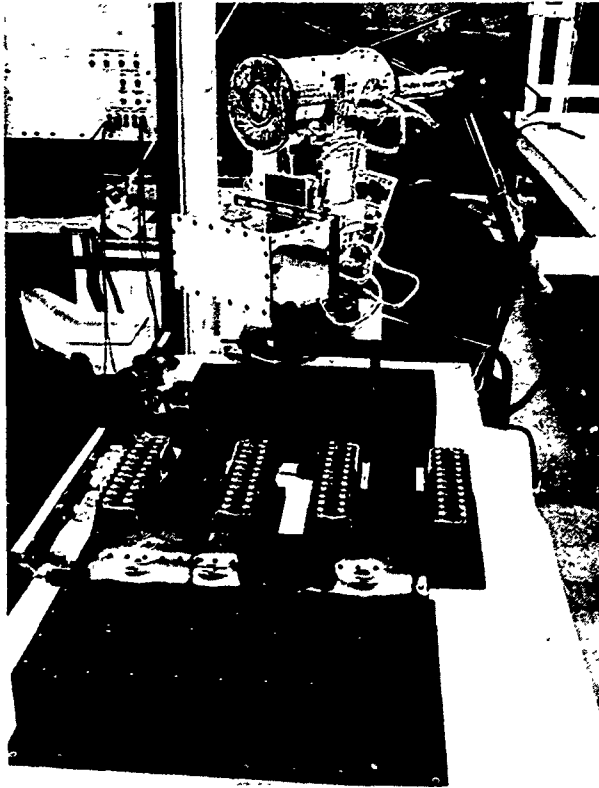


Figure 4-75. Ambient Functional Setup  
(Photo ES31338)

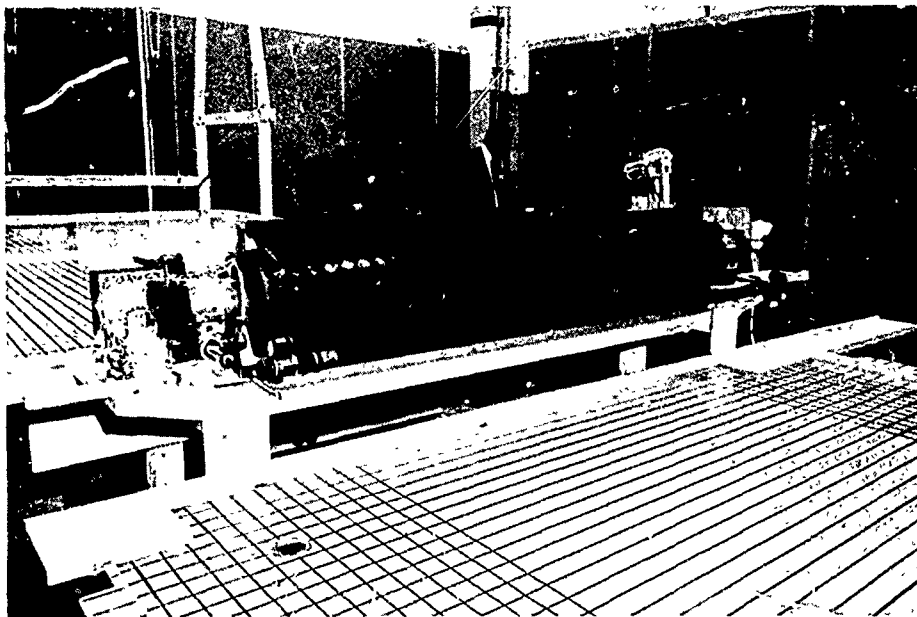


Figure 4-76. Flight Model Solar Array Ambient  
Test Position (Photo A31408)

SECTION V  
SYSTEM TEST

The system tests consisted of the conventional trilogy of tests for aerospace hardware -- qualification, acceptance, and integration. The qualification and acceptance tests were conducted at the Hughes El Segundo facility in February through June of 1971, while the integration tests were conducted in the LMSC facilities at Sunnyvale (for Agena integration) and at Vandenberg AFB (for Thorad integration). Procedures and results from these tests are presented in the following pages.

QUALIFICATION TESTS

The qualification model was subjected to ambient functional, vibration, and solar-thermal-vacuum (STV) tests in accordance with the sequences and levels presented in Table 5-1 and Figure 5-1. A summary of the test results is presented in Table 5-2.

Ambient Functional Tests

During the initial ambient functional tests (Figure 5-2), two problems were encountered with the orientation subsystem, one problem with the solar array subsystem, and one problem with the power subsystem.

TABLE 5-1. QUALIFICATION ENVIRONMENTS

Environment	Requirements		Tests/Analysis Performed	
	Titan	Thorad	Analysis	Test
Quasi-static	12 ±3.8 g	15 ±2.5 g	Yes	No
Acoustic	145 dB	145 dB	No	Covered*
Pyro shock	Squib	Squib	No	Yes
Broadband random	19.5 g rms	13 g rms	Yes	Yes
Sine vibration	None	5-18 cps      0.5 in. double amplitude 18-22 cps      8 g 22-400 cps     5 g 400-2000 cps   7.5 g	Yes	Yes
Deployment	Yes	Yes	Covered	Yes
Electromagnetic compatibility	MIL-STD-461A		Yes	Yes

\*FRUSA was considered qualified by similarity to the prior developmental solar array, the 500-watt FISCA, which was tested to 155 dB.

TABLE 5-2. FRUSA SYSTEMS TEST RESULTS

Test Phase	Orientation Subsystem	Solar Array Subsystem	Power Subsystem	Instrumentation Subsystem	Problems	Solution
Ambient functional qualification	Problems 1 and 2	Problem 3	Problem 4	Successful	<ol style="list-style-type: none"> <li>1. Torquer current trip</li> <li>2. Lockon instability on one side</li> <li>3. Drive motor wiring reversed</li> <li>4. Drive motor 400 Hz noise</li> </ol>	<p>Added limiting to CEU Operational adjustment</p> <p>Corrected wiring</p> <p>Added filtering to PCU</p>
Vibration qualification	Problem 1	Problem 2	Problem 3	Problem 4	<ol style="list-style-type: none"> <li>1. Failure in torquer drive shaping card end</li> <li>2. Panel 2 temperature sensor lead broken</li> <li>3. Load bank could not be commanded on</li> <li>4. Commutator in CEU had no output</li> </ol>	<p>Cleaned card connector</p> <p>Repaired - support added to wiring</p> <p>Broken wire repaired and support added</p> <p>Wire pinched - repaired random failure</p>
Solar-thermal-vacuum qualification	Successful	Successful	Problem 1	Problem 2	<ol style="list-style-type: none"> <li>1. Power conditioning unit voltage failed</li> <li>2. Strain gage amplifier on panel 1 boom length compensator failed</li> </ol>	<p>Partially severed wire repaired. Workmanship.</p> <p>Amplifier subjected to more severe temperature extremes than it experiences in flight.</p> <p>Amplifier not repaired.</p>
Electromagnetic compatibility and interference special tests	Problem 1	Successful	Successful	Successful	<ol style="list-style-type: none"> <li>1. Conducted interference inserted at the unregulated bus; caused extraneous commands to the torquers.</li> </ol>	<p>Filtering added to CEU</p>

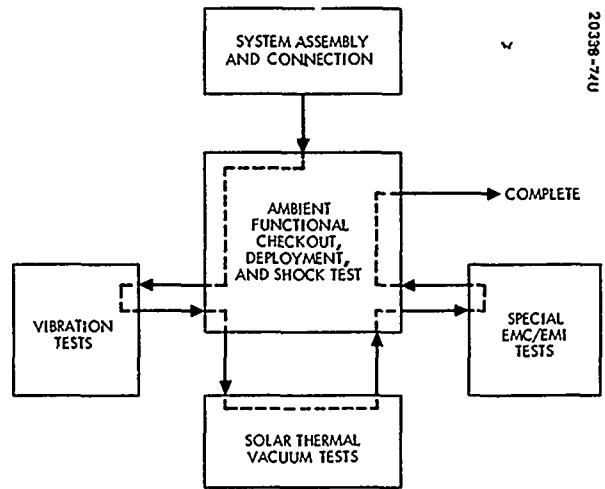


Figure 5-1. Operations Flow Chart

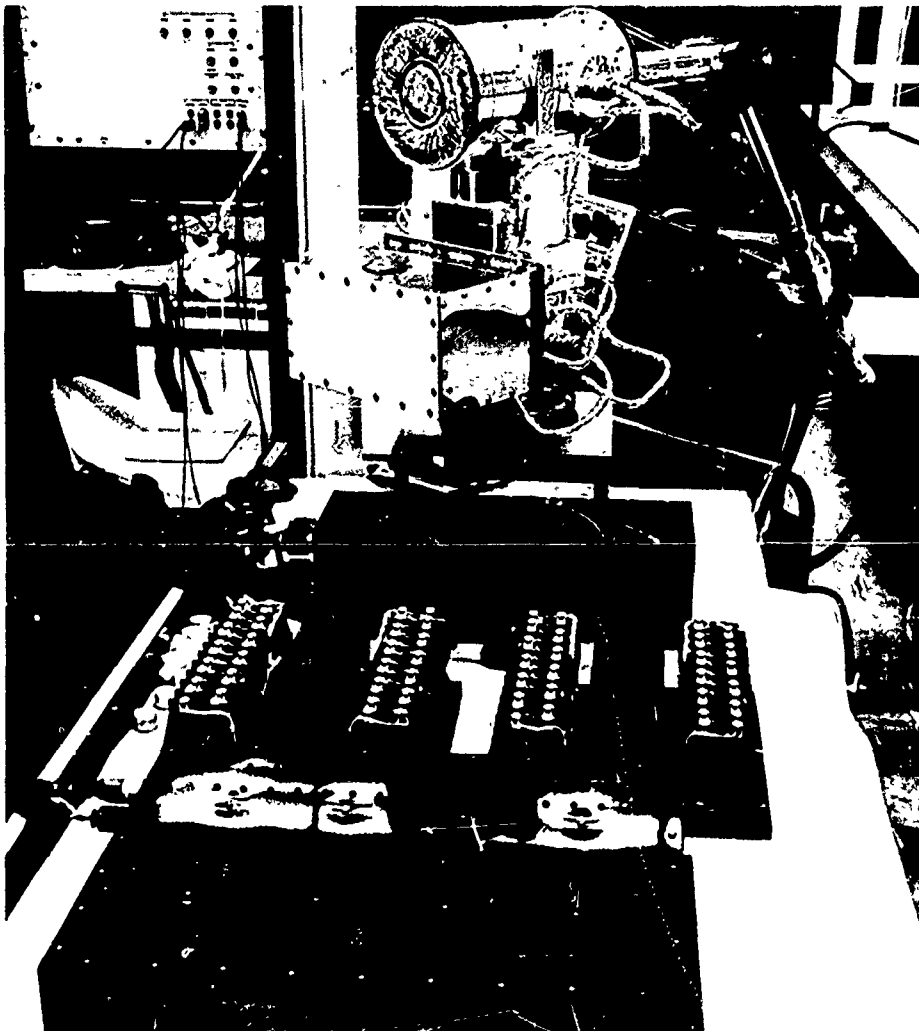


Figure 5-2. Ambient Functional Setup (Photo ES31338)

### Orientation Subsystem

The first problem encountered with the orientation subsystem was a current tripping or dropout during acquisition and/or tracking operation. Although current limiting was included in both the error channel and the feedback channel, under certain conditions these two channel outputs were additive and would therefore exceed the current trip value. A design change was incorporated, which in effect limited not only the individual channels but the summation as well. Subsequent test proved the validity of the modification.

The second problem discovered was that the orientation subsystem would not retain lock on the -Z side of the spacecraft, but would break lock and reacquire on the opposite or +Z side. This was found to be a design deficiency in that polarity reversal circuits were not incorporated in the logic associated with the tracking sensors. For the STP 71-2 flight, a circuit was added to the spacecraft which prohibited locking on the -Z side of the spacecraft. Although a FRUSA design fix was not attempted in the interest of economy, future CEU designs could be modified to preclude this problem (see Orientation Subsystem Section IV).

### Solar Array Subsystem

The solar array drive motor wiring was found to be reversed, so that when an extension command was issued the array actually retracted. This wiring error was corrected on the unit and proven by subsequent test.

### Power Subsystem

The problem encountered with the power subsystem was excessive electromagnetic noise. This noise blanked out the telemetry when the solar array was being extended or retracted. A design modification was made to install filtering in the power conditioning unit. Subsequent test indicated the FRUSA telemetry operated normally during extension/retraction exercises.

### Vibration Test

After the FRUSA system completed ambient functional checkout successfully, each subsystem was in turn subjected to qualification level vibration (Figure 5-3). As each subsystem completed vibration, it was subjected to an ambient checkout to evaluate any malfunction or degraded performance induced by the vibration environment. Each of the subsystems experienced one malfunction as a result of postvibration functional checkout.

### Orientation Subsystem

A malfunction of the torquer drive electronics was detected, which resulted in no current being delivered to the torquer. The CEU was transported to the electronics laboratory where the malfunction was reproduced. The problem was then traced to the torquer drive shaping end card and to

contamination in the card connector. The card was cleaned and returned to the unit after the STV sequence.

#### Solar Array Subsystem

During postvibration functional test, telemetry indicated no output from the panel 2 temperature sensor. The problem was traced to a broken wire at the temperature sensor. A change was made to equivalent flight model installations that provided support for the connecting wires by applying conformal coating material as a support to the wire junction.

#### Load Bank

During postvibration functions checkout, the load bank could not be commanded on. The problem was traced to a broken wire on the control relays. The wire was repaired and engineering generated to provide support for the susceptible wire connections using conformal coating in a manner similar to that employed on the solar array temperature sensor.

#### Instrumentation Subsystem

Postvibration checkout showed no output from the telemetry commutator in the orientation subsystem. The commutator was removed and replaced by one of the flight model commutators. The malfunctioning commutator was returned to the vendor for checkout, disassembly, and analysis. The problem was traced to insulation cold flow at a point of contact with an assembly screw. The unit was repaired and reinstalled in the CEU.

#### Solar-Thermal-Vacuum (STV) Tests

The power and instrumentation subsystems each experienced one malfunction during STV (Figure 5-4).

#### Power Subsystem

The power conditioning unit voltages failed after 16 hours of STV testing. In order to complete the tests, the flight model PCU was installed. The problem was traced to a broken wire resulting from a workmanship error in assembling the unit.

Examination of photographs taken just before potting compound was applied to the PCU showed that the wire was partially severed, apparently the result of trimming performed on an adjacent terminal. Subsequent thermal stresses then broke the remaining strands of wire.



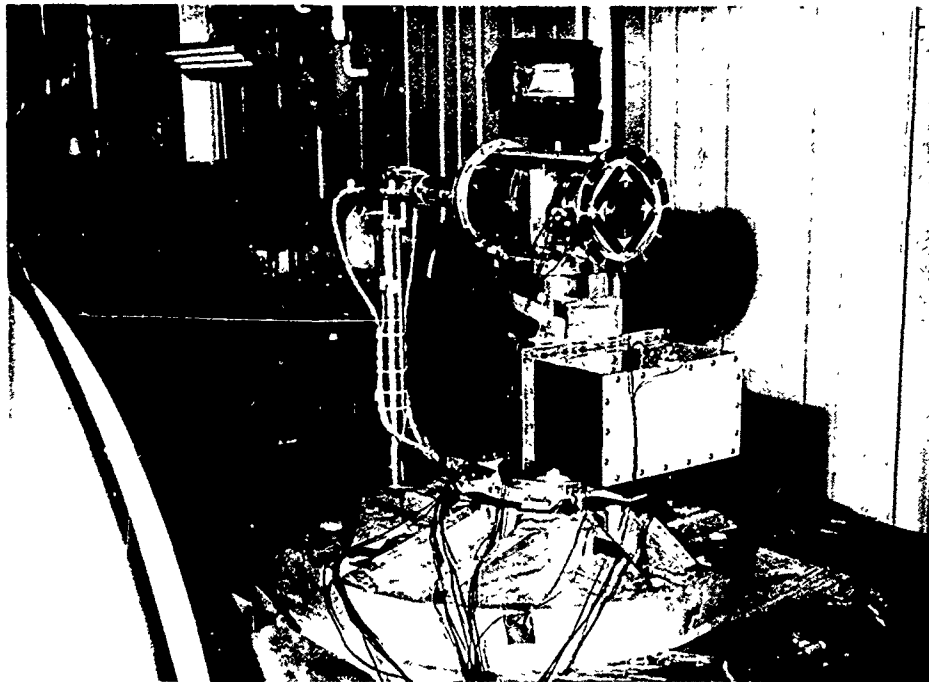


Figure 5-3. Vibration Setup (Orientation Subsystem)(Photo A30631)

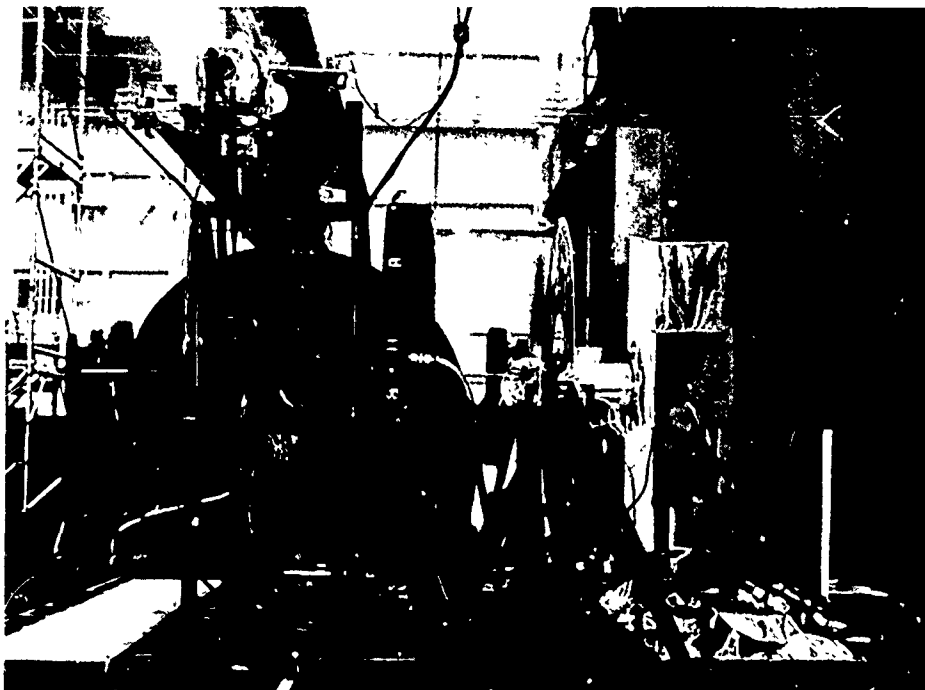


Figure 5-4. STV Endbell (Photo A30737)

## Instrumentation Subsystem

The strain gage amplifier on panel 1 boom length compensator failed during STV testing. In order to chill the orientation subsystem to its lowest qualification temperature, the strain gage amplifiers were subjected to temperatures that far exceeded their specifications. The amplifiers were specified to survive only to  $-65^{\circ}\text{F}$ , but during the chill operation they were subjected to  $-135^{\circ}\text{F}$ . Although the other strain gage amplifiers were unaffected, the failure was attributed to the excessive temperature stress. The coldest temperature that the amplifiers encounter in flight is  $0^{\circ}\text{F}$ .

## EMI/EMC Tests

During electromagnetic compatibility tests (Figure 5-5), a problem was encountered with the orientation subsystem. All other subsystems operated normally in the EMI environment, even though some of the units were radiating more than specified by MIL-STD-461A. The problem with the orientation subsystem was that spurious torquer commands were encountered when conducted interference was applied to the unregulated bus. Filtering was added to the CEU and proven adequate by subsequent test.

During the course of EMC testing, an eighth-scale mockup of the solar array panel was assembled to verify the magnetic moments introduced by the system. This was of particular interest on the STP 71-2 flight because of the "softness" of the gravity gradient/CMG technique used for long-term stability of the parent Agena spacecraft and the sensitivity of the ONR-001 experiment to magnetic fields. The field intensity proved to be less than 0.1 milligauss in a location modeled to simulate the ONR-001 installation, that is, on the other or aft end of the spacecraft. The setup and the instrumentation used are illustrated in Figure 5-6.

## Solar Array Deployment Tests

In addition to the formal qualification tests discussed above, special deployment tests were instituted to evaluate the FRUSA/Agena interface during the deployment phase. The objective of these tests was to provide a quantitative assessment of the capability of the elbow-like deployment mechanism of the orientation subsystem to deploy properly the solar array from the stowed position to the operational attitude. Qualification models of the orientation and solar array subsystems and LMSC installation hardware such as the actual Lockheed flight brackets, studs, and pyro assemblies were used. Of additional interest were the dynamics of separating from the Agena spacecraft and the assurance of freedom from rotational or translational modes which would "snag" the assembly after firing the pyrotechnic separation bolts.

Three manual deployments under panel tensions of 7, 30, and 50 pounds were made. These deployments were conducted on the system test fixture using overhead support cables and soft (Og) springs for support during

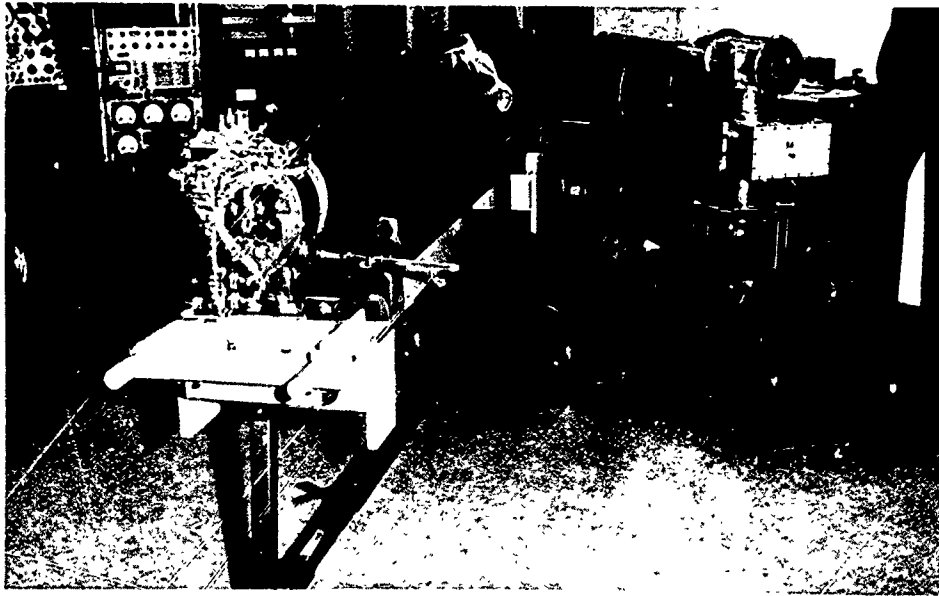


Figure 5-5. Screenroom Setup for EMI/EMCTES (Photo A30740)

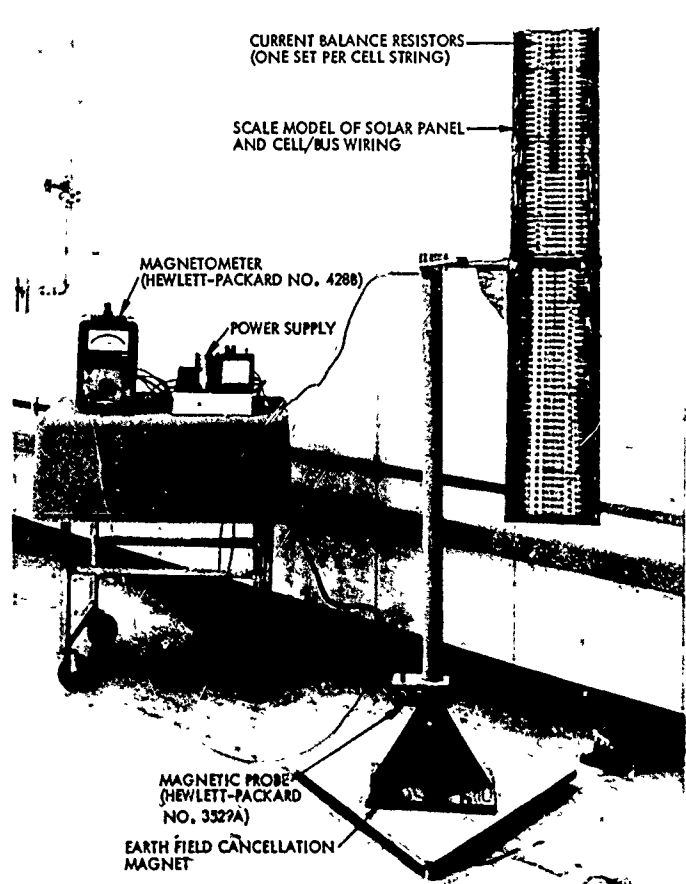


Figure 5-6. Magnetic Moment Measurement Test Position

the 90 degrees of horizontal travel from release to the deployed and locked position. Operation was monitored by appropriate accelerometers, high speed cameras, position potentiometers, and displacement gages as shown schematically in Figure 5-7 and pictorially in Figure 5-8.

One pyro firing was conducted before vibration testing, and five additional firings were conducted after vibration. The support brackets were mounted to a 1 inch thick magnesium plate, which was required to maintain the physical relationship between brackets during transportation, after vibration, to the deployment fixture. Table 5-3 shows the results from each of the manual and pyro deployment/separation tests. Deployment times were all within specification and no solar array hangups or other undesirable array motions were experienced.

TABLE 5-3. DEPLOYMENT TEST DATA

Deployment Type	Panel Tension*, pounds	Time to Deploy, minutes	Comments
Manual 1	14	0.22	
Manual 2	36	0.23	
Manual 2A	3	0.23	
Manual 3	45	0.215	
Pyro 1	51	0.22	Full set of squibs.
Pyro 2	0	0.24	Postvibration, full set of squibs.
Pyro 3	60	0.25	Half set of squibs installed; aft bracket misaligned 1 degree.
Pyro 4	50	0.221	Half set squibs installed. Misalignment 0.11-inch aft bracket toward forward bracket. One pyro had prebroken wire.
Pyro 5	50	0.22	Aft bracket misaligned 1 degree counterclockwise. Mounting raised 0.15 inch.
Pyro 6	60	0.220	Same misalignment as 5 with 1/8-inch additional shim both fore and aft.

\*Nominal launch tension was 50 pounds.

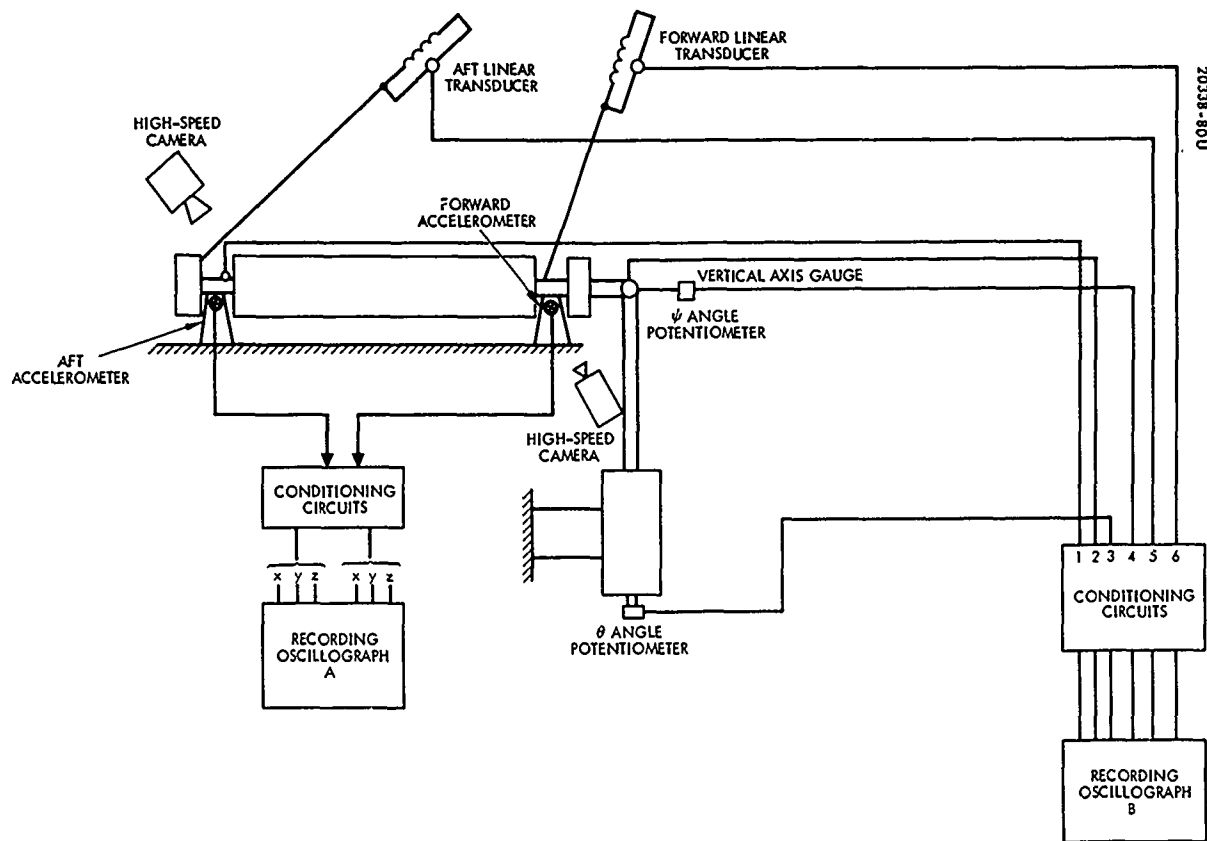


Figure 5-7. FRUSA Separation and Deployment Test

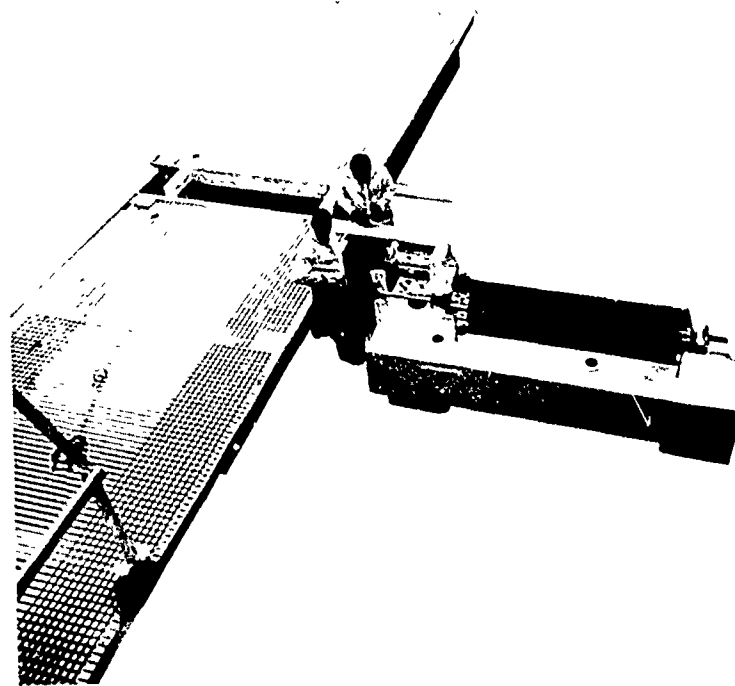


Figure 5-8. Deployment Test Setup (Without Support Springs) (Photo ES30381)

## Summary of Test Results

The system tests on the FRUSA qualification model resulted in the basic system design and fabrication being qualified for space flight. The major problems disclosed in these tests were involved with EMI. Some susceptibility to conducted interference was observed and conducted emission was found. Prior to launch, changes were made to the flight model to lower both the susceptibility and emissions to within acceptable limits. These changes consisted principally of the addition of both internal and external filtering in the PCU and CEU. Details of the test results may be found in the FRUSA Qualification Model System Test Report, dated 7 May 1971.

### FLIGHT ACCEPTANCE TESTS

The flight acceptance test sequence consisted of a complete ambient system functional test including extension/retraction of the solar array and a closed loop sun acquisition and tracking checkout, deployment test, and panel illumination tests. After completion of the ambient functional tests, the system was exposed to vibration, one subsystem at a time, and thermal vacuum tests. After each environmental exposure the system was subjected to an ambient functional test to evaluate the degradation, if any, resulting from the environmental exposure.

Test conditions were designed to demonstrate workmanship and equipment capabilities for orbital flight under environmental stresses predicted for launch and orbital conditions. These conditions were not intended to exceed predicted conditions or to excite unrealistic modes of failure. The units under test are illustrated in Figure 5-9.

Two major deviations were made to the planned sequence:

- Since the total system was not delivered to the systems test laboratory at one time, subsystems were checked out as they became available.
- Due to problems with the solar array booms, the solar array subsystem vibration test was delayed until completion of the thermal vacuum tests.

The test equipment and system configuration block diagram are shown in Figure 5-10 and several of the test positions are illustrated in Figures 5-11, 5-12, and 5-13. The major test equipment used for electrical functional testing consisted of the following:

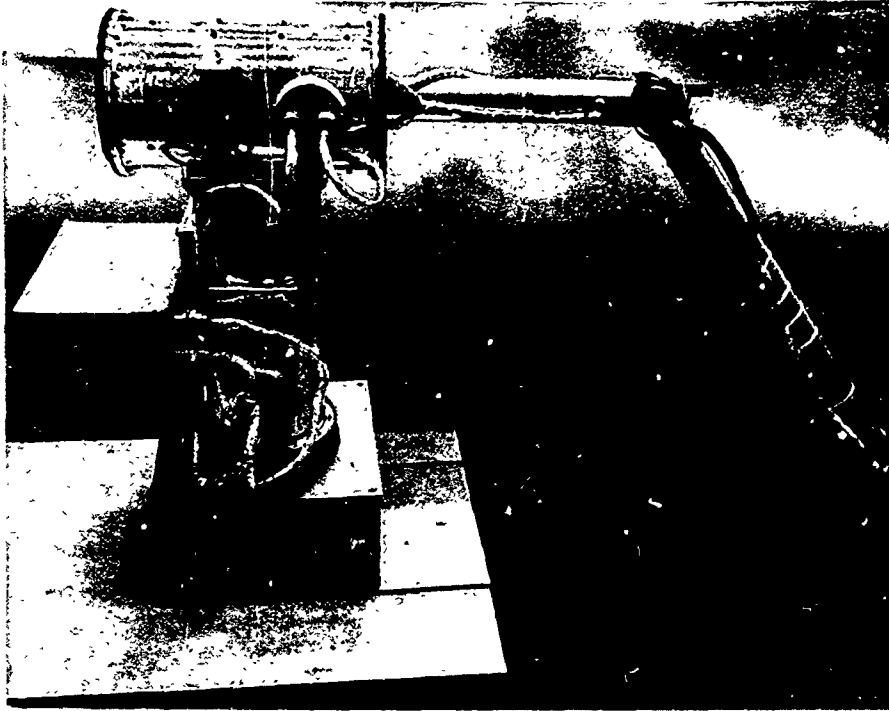
- 1) FRUSA AGE panel. This panel contained circuitry to send commands and provide telemetry signal switching, as well as special circuits for test cell/module calibration and telemetry point calibration. A test telemetry commutator and a switchable DVM were included in order to read out the telemetry data which

were not commutated in the FRUSA system but were normally sent to the Agena telemetry system directly.

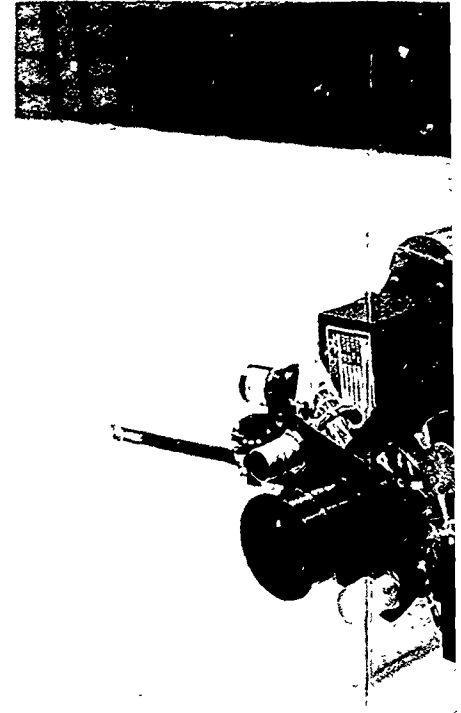
- 2) Power load simulator. Switchable resistive loads to simulate external FRUSA loads were provided in the power load simulator (PLS). In addition, switches for actuating battery power and the Agena interface relay were contained in this panel.
- 3) Solar array simulator. The test equipment included a 28-volt (adjustable 0 to 45 volts), regulated 50-ampere power supply to simulate the solar array or the launch stand umbilical power supply.

The above equipment was used to conduct the following tests before and after each environmental exposure:

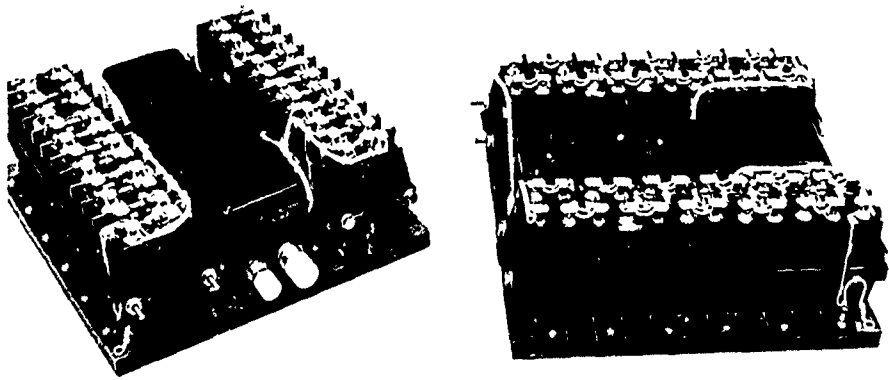
- 1) Orientation subsystem
  - Manual torque
  - Sun acquisition mode
  - Sun tracking mode using sun sensor group and "sun gun"
  - Commanding and verification
  - Complete telemetry assessment
- 2) Power subsystem
  - Battery mode
  - Battery charge through umbilical
  - Battery charge through orientation mechanism cable
  - Regulator operation at maximum and minimum voltages
  - Overvoltage circuits and override
  - Minimum voltage battery takeover
  - Load bank test
  - External load test running full power through orientation mechanism cables and slip rings
  - Complete command repertoire
  - Complete telemetry assessment



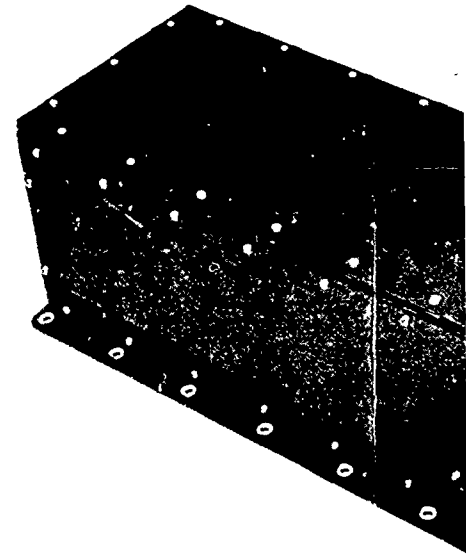
Orientation Mechanism and Control Electronics Unit  
(Photo ES 31287)



Solar Array - Inboard



Battery Charge Controller Units (Photo ES 31340)

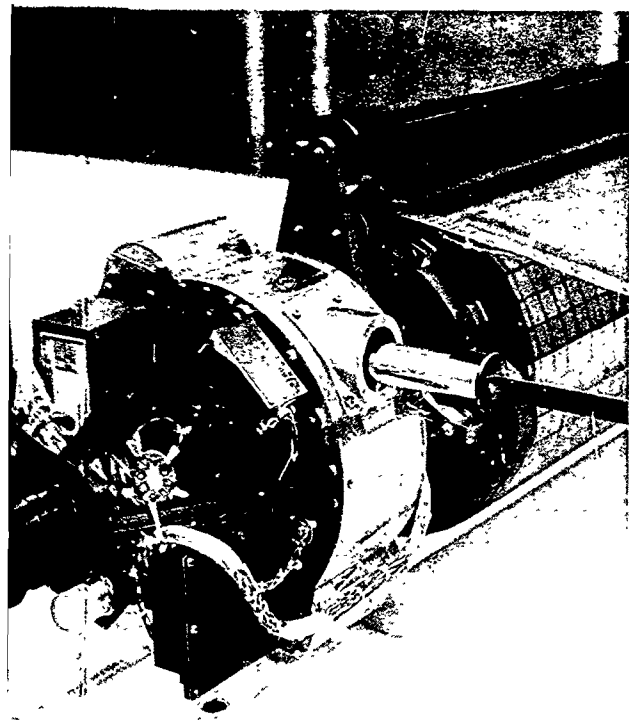


Power Conditioning Unit

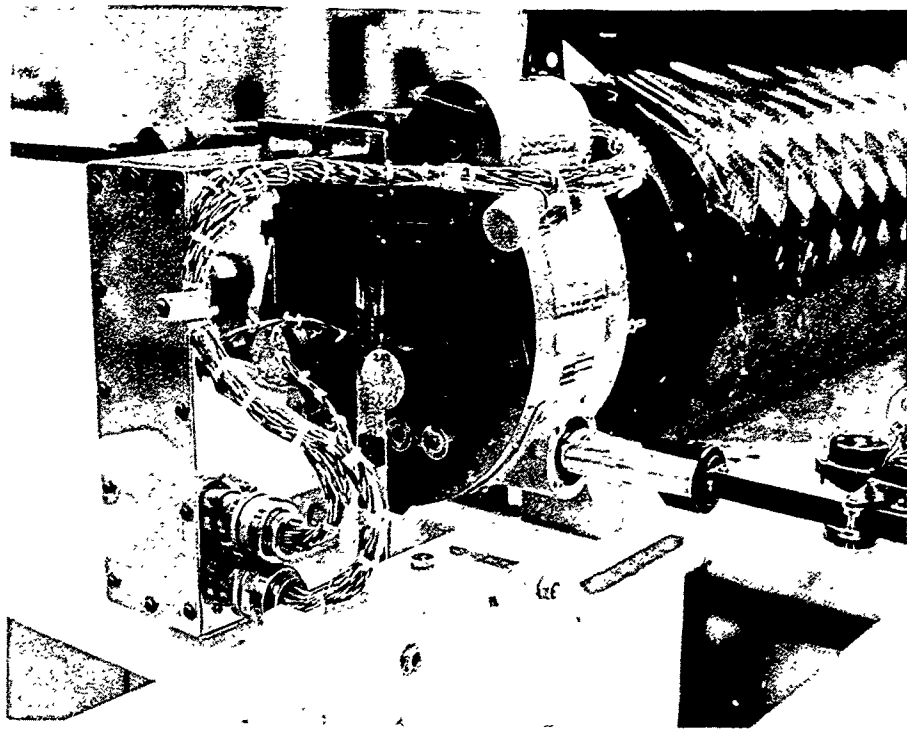
Figure 5-9. Flight Model Units



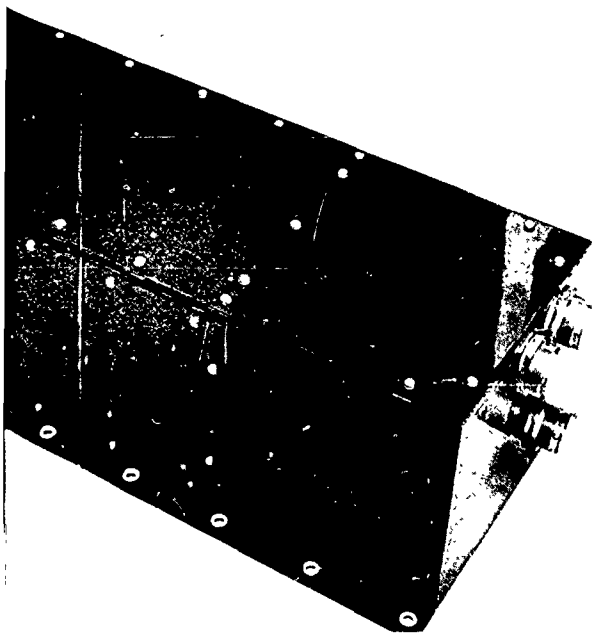




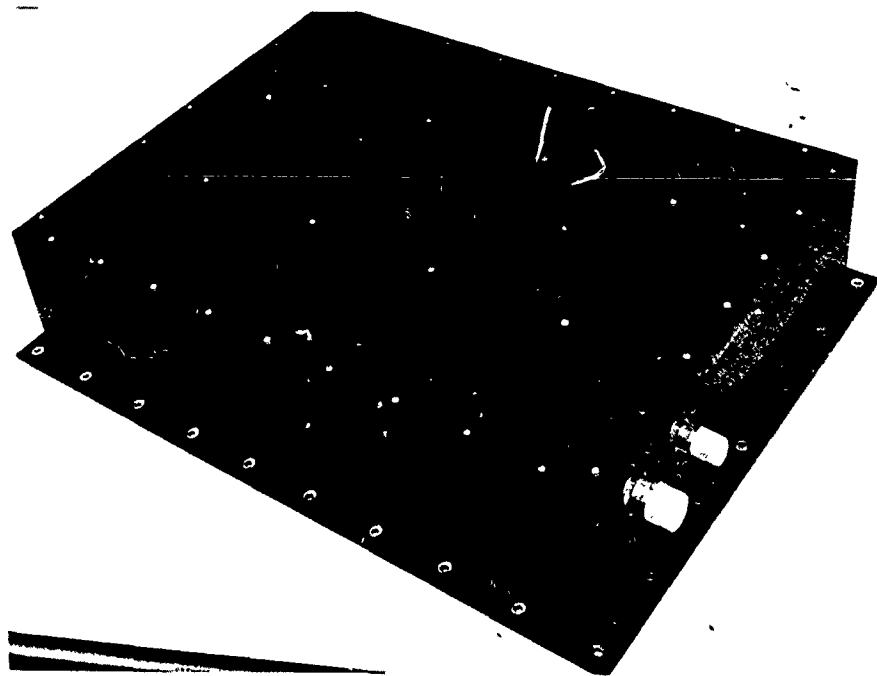
...y - Inboard End (Photo A31120)



Solar Array - Outboard End With Solar Cell Electronics Unit  
Photo A31118)



Conditioning Unit (Photo ES 31342)



Load Bank (Photo ES 31341)

- 3) Solar array subsystem
  - Full extension and retraction of array
  - Strain gage calibration
  - Cell/module check and telemetry calibration
  - Accelerometer identification
  - Complete command check
  - Complete telemetry assessment
- 4) Telemetry subsystem - complete telemetry assessments

### Test Results

#### Vibration Tests

Each of the three major subsystems was subjected to 10-g rms broadband random vibration along each principal axis in accord with the spectrum presented in Figure 5-14. The units were in a nonoperating condition during vibration, since the system is not operated during the boost phase, which is the main source of the dynamic environment.

Postvibration functional tests were made, consisting of the appropriate parts of the overall system tests outlined above. These checks disclosed no failures due to vibration.

During the first tensioning operation prior to vibration of the solar array, however, the booms of panel 1 were damaged. The damage was severe enough to require replacement of both booms. Analysis of the failure indicated that the problem resulted from excessive side loads produced by uneven winding of the array on the drum at the high tension levels required for boost phase vibration survival. Consequently, a new procedure for tensioning was devised. In this procedure the array is physically disconnected from the booms, and is extended and rewound on the water table with the tensioning force applied by a hand-operated winch.

Subsequent to vibration, the array was mounted on the water table, the drum tension was released, and the array extended and retracted in a normal manner (orbital panel tension) without incident.

Inspection of the solar cells of the FRUSA panels following environmental test exposures indicated 52 defects (of 34,500 cells), none of which would affect solar panel performance. Twenty-eight of the solar cells were replaced, however, since their defects might progress to the point where further damage would occur during the prelaunch tensioning and boost

vibration. The defects found included 43 cover cracks and chips, 8 cover adhesive delaminations, and 1 solar cell crack. Distribution of the defects by panel is as follows:

	<u>Panel 1</u>	<u>Panel 2</u>	<u>Total</u>	<u>Percent of Full Array</u>
Defective cells	24	28	52	0.153
Replacement cells	12	16	28	0.081

As this inspection was the first full panel mechanical inspection after initial assembly of the panels on the array drum and thus included many handling and extension/retraction cycles as well as the vibration exposure, the low level of defective cells was considered exceptionally good for the flexible array and suggested that in-flight degradation due to the roll-up configuration would be minimal.

#### Deployment Tests

The special set of test fixtures used on the qualification model to demonstrate solar array separation from the Agena and deployment of the drum mechanism was used to test deployment of the flight model (Figure 5-12). The solar array was mounted on a 1-inch thick magnesium plate using the LMSC engineering model mounting brackets. The orientation mechanism was mounted horizontally on the fixture in a position simulating its relationship to the array on the Agena. The array was coupled to the orientation mechanism deployment arm and supported by two spring-loaded cables from the ceiling of the test area to simulate as far as possible the 0-g environment. The support cables were pivoted at the top so that when released from the brackets, the solar array was free to swing out from the mounting as it would in orbit.

Manual separation was utilized and the motion of the array during deployment was observed and timed. Deployment was normal, with full deployment occurring in  $12.7 \pm 0.3$  seconds.

#### Thermal Vacuum Tests

The entire system was subjected to a simulated space environment in the Hughes thermal vacuum chamber (see Figure 5-13). A temperature controlled mounting plate was provided for the battery charge control (BCC) units to maintain a temperature between 40° and 80°F at the mounting interface per the requirements of the Agena interface specification. The test was scheduled as a 20-hour test, including chamber conditioning time. Chamber walls and floor were maintained at approximately 0°F for 6 hours after conditioning and then reconditioned to 100°F and held for 6 hours to produce the unit temperatures anticipated during eclipse and illuminated orbits. Ambient pressure during this test was about  $10^{-5}$  Torr or less.

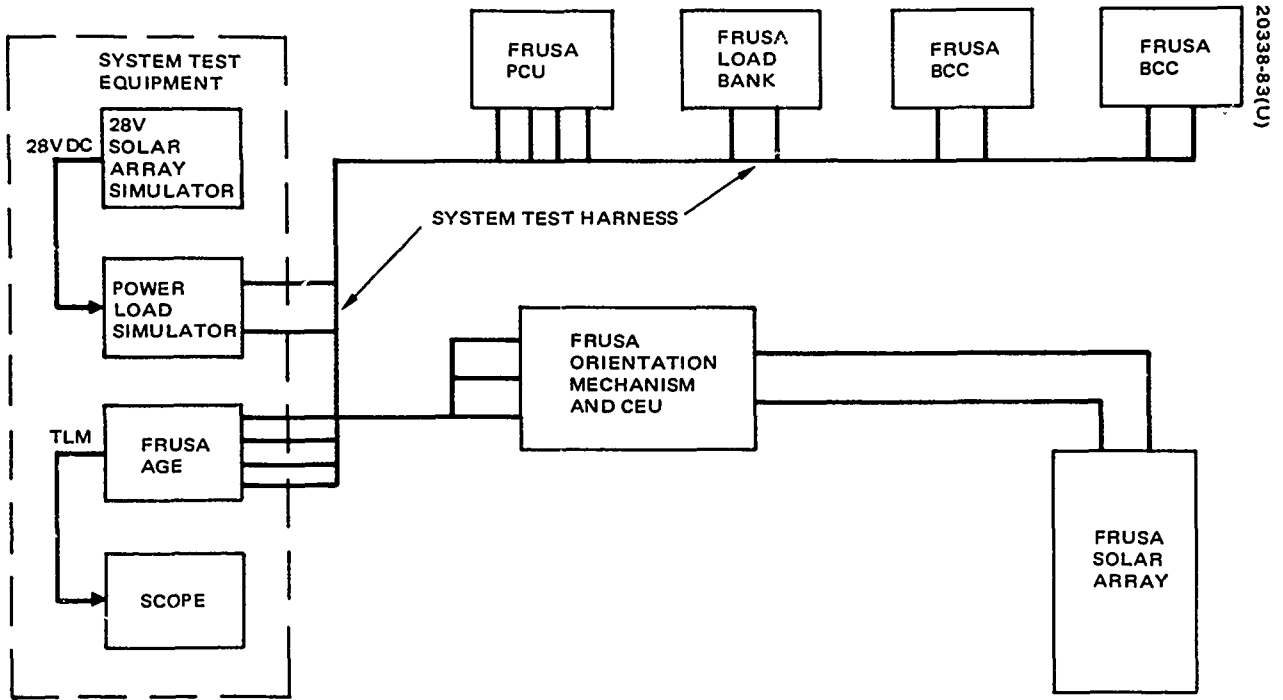


Figure 5-10. Single Line Cable Block Diagram - FRUSA System Tests

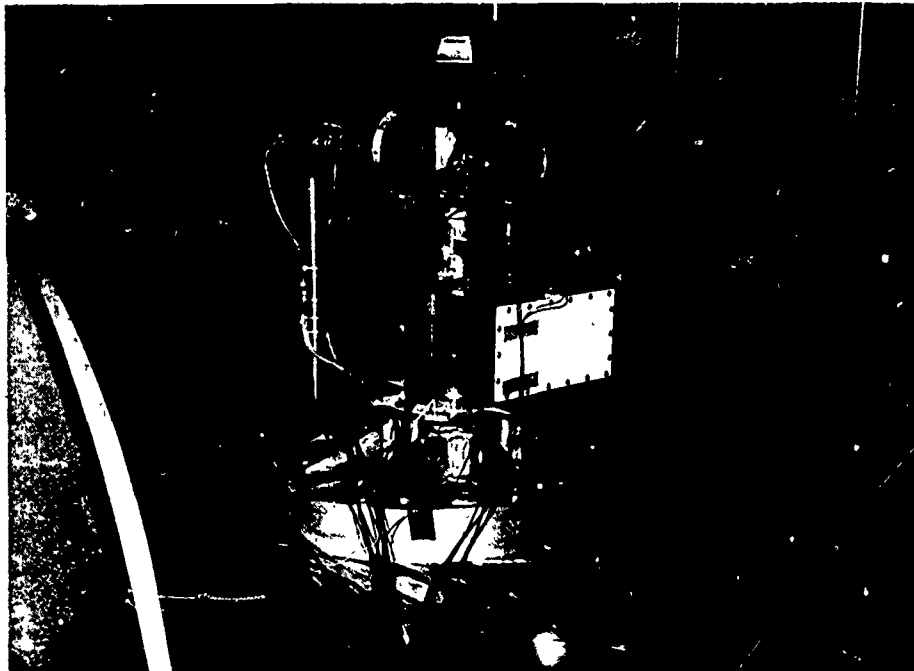


Figure 5-11. Orientation Subsystem on Vibration Table (Photo A30631)

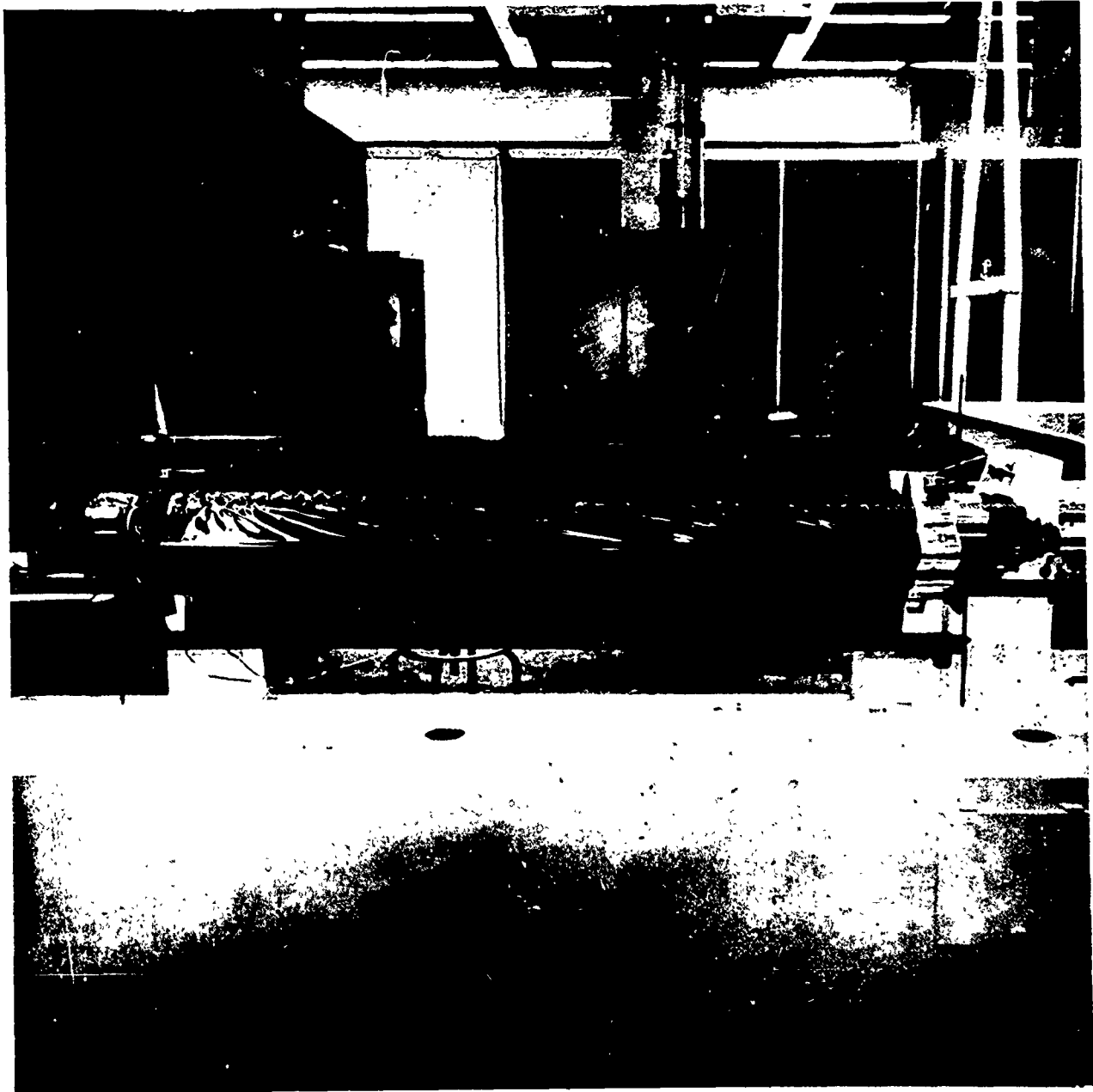


Figure 5-12. FRUSA System Setup for Separation and Deployment Testing (Photo 20338-85)



Figure 5-13. FRUSA System Installed on C-4 Chamber Endbell Just Prior to Thermal Vacuum Tests (Photo 20338-86)

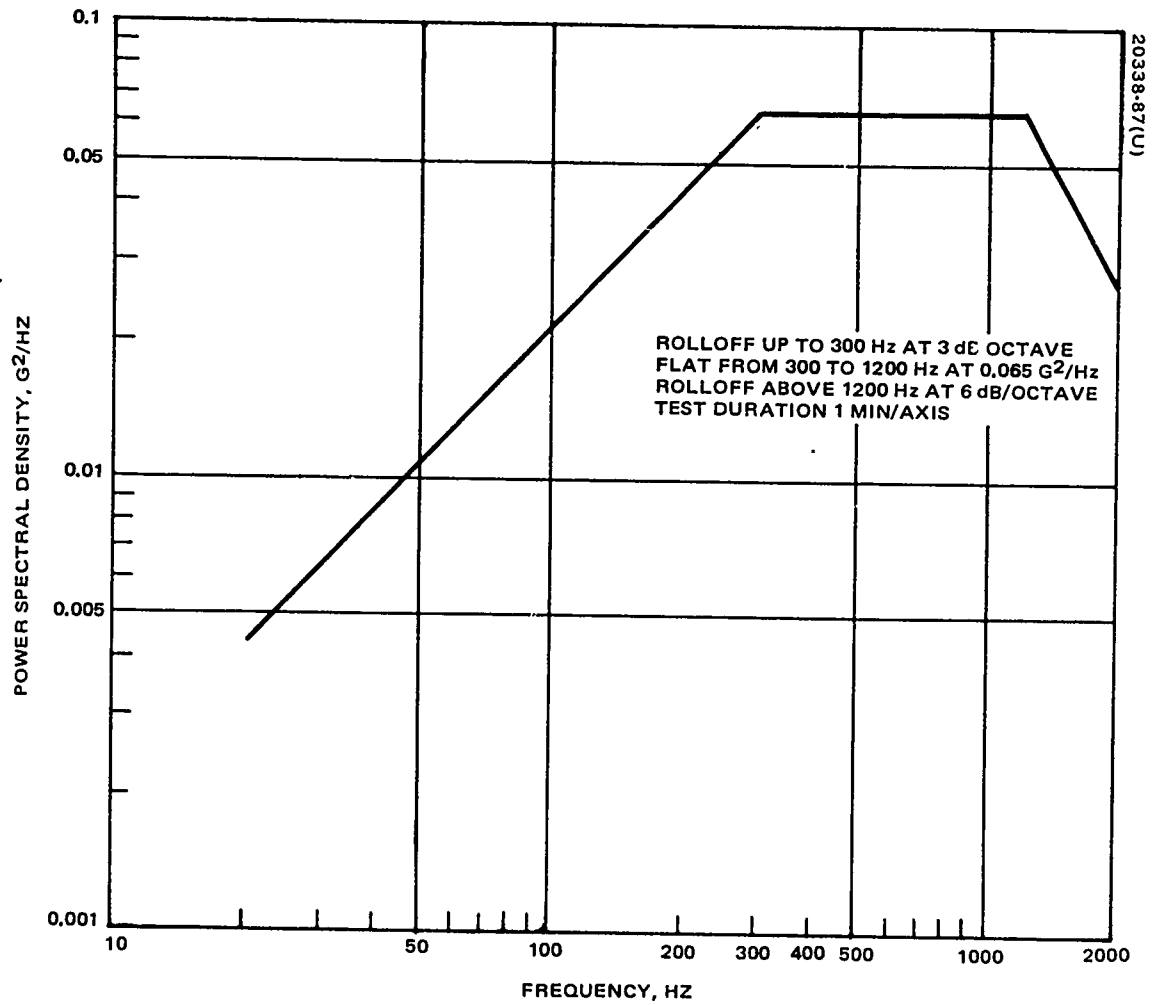


Figure 5-14. Random Vibration Test Requirements

Functional tests were performed on the system after mounting on the chamber endbell at ambient conditions. Functional tests were also performed on the system while in the chamber and at space environment conditions. These tests included a partial array extension and retraction. Performance was nominal with one exception. During the 0°F portion of the test, BCC S/N 003 could not be commanded into the charge condition, while BCC S/N 002 functioned normally. Checks were made at the chamber endbell penetration plate and the command was functioning up to this point. The test was continued and at 100°F, BCC S/N 003 functioned normally. After the test, the cables and connections were carefully examined for intermittence, but no abnormality was detected. Subsequent to the thermal vacuum system test, BCC S/N 003 was subjected to a number of environmental cycles and the trouble could not be duplicated.

During subsequent final system functional test, just prior to shipment, a similar commanding difficulty was experienced with the BCC in the test position designated "BCC 2." In this case the trouble was traced to the AGE. Further detailed examination of the AGE and the cable designated "BCC 2" disclosed identifiable faults, so that both the final system test problem and the thermal vacuum problem were attributed to the AGE test equipment and not to the flight hardware.

#### Panel Illumination Tests

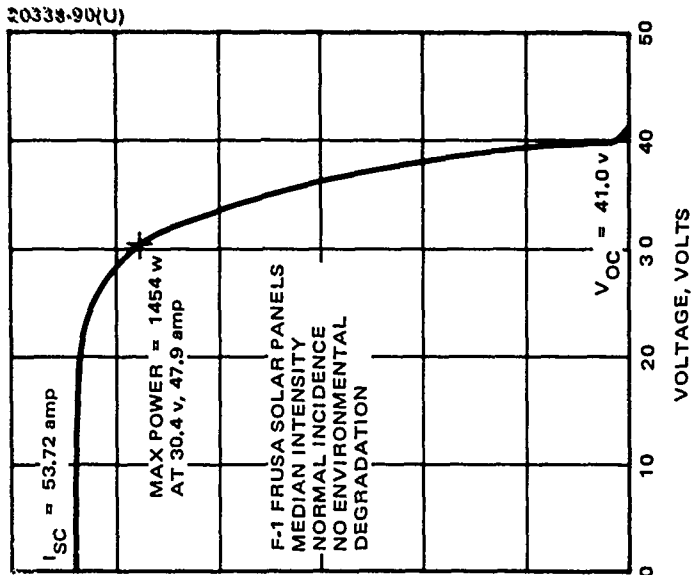
In addition to the tests called out in the formal procedure, a solar panel illumination test was run. For the power cells, the panel was illuminated in sectors by a calibrated pulsed xenon light source, and voltage and current data were taken. For the test cells and modules, a constant amplitude calibrated light source was used and data of the voltage-current characteristics were taken via the end-to-end telemetry data from the solar cell electronics unit (SCEU).

Panel power performance on the basis of these tests at the base of the orientation mechanism (i. e., the Agena interface) for median solar intensity and without environmental degradation is illustrated by Figures 5-15 and 5-16. Using the worst-case temperature situation (high sun, noon orbit for temperature, and low sun for power output) as illustrated by Figures 5-15 and 5-16, and assuming 192 watts of FRUSA housekeeping loads, reduces the worst-case estimate of power to the Agena interface to 1040 watts (worst-case requirement is 940 watts). Under more favorable orbital conditions such as full load on the panel and with low earth albedo such as for the initially planned twilight orbits, the gross output would be nearer the performance of Figures 5-15b or 5-15c, and the system power output would, accordingly, be 200 or 300 watts higher.

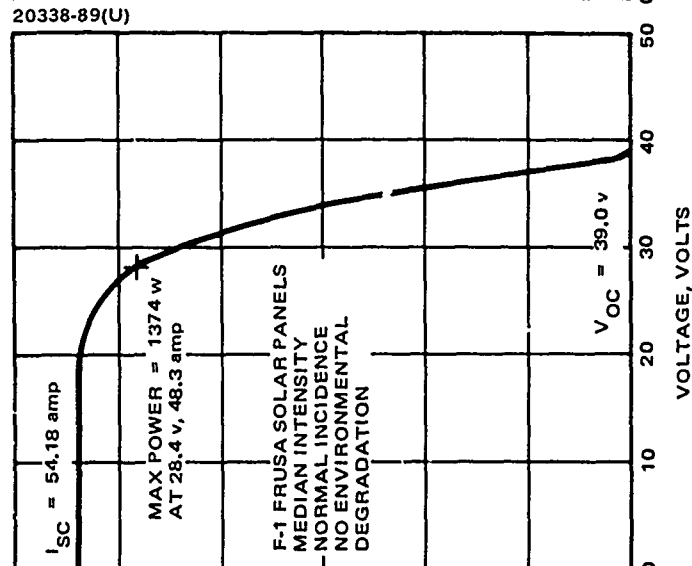
#### Special EMI Tests

Because of schedule constraints, it was necessary to conduct EMI tests with qualification hardware and an external filter unit which was provided to correct some of the conducted emissions observed during qualification testing. These tests were conducted in the Hughes El Segundo screen room.

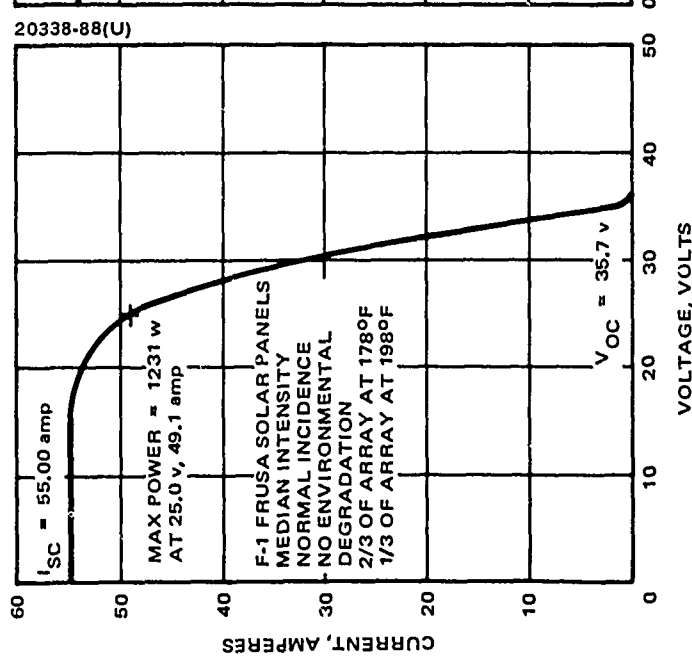




c) At 130° F



b) At 150° F



a) Worst Case Temperatures

\* VOLTAGE AT OLSCA/AGENA INTERFACE VOLTS  
\* NOT DIRECTLY COMPARABLE TO TELEMETRY VOLTAGE

Figure 5-15. Current Versus Voltage for Full Array

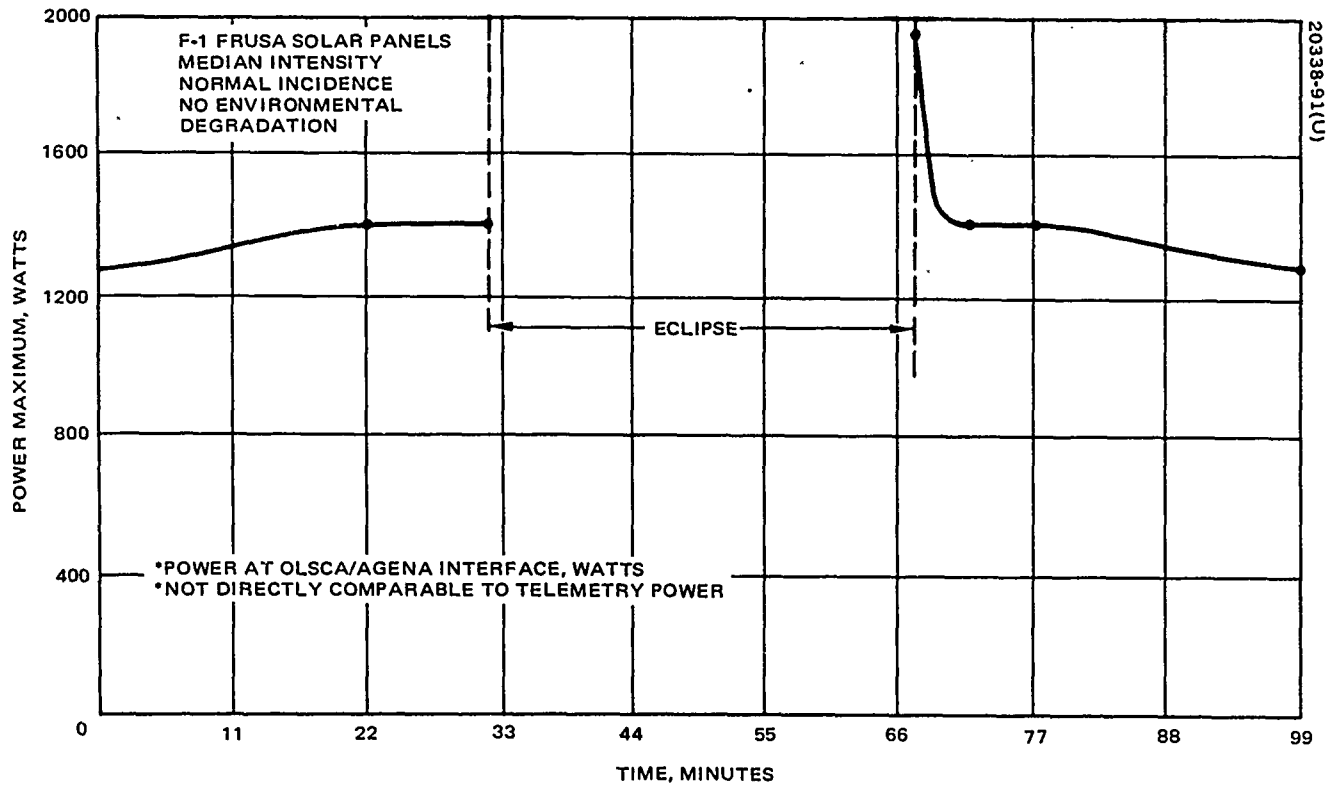


Figure 5-16. Power Performance for Full Array at Worst Case Temperatures (See Figure 5-15a)

TABLE 5-4. FRUSA SYSTEM TEST RESULTS SUMMARY

Test Phase	Orientation Mechanism	Solar Array	Power Subsystem	Instrumentation Subsystem	Problem	Solution
Ambient functional	Problems 5 and 7	Problems 2 and 4	Successful	Problems 1, 3, and 6	<ol style="list-style-type: none"> <li>1. Boom strain gage polarity reversed</li> <li>2. Boom extension not even and boom damage</li> <li>3. Commutator "A" intermittent</li> <li>4. Root inboard test module panel inoperative</li> <li>5. Deployed and locked switch wired incorrectly</li> <li>6. Wire reversal at 2P2</li> <li>7. No commutator "A" output</li> </ol>	<ol style="list-style-type: none"> <li>1. Installed new strain gage and rewired</li> <li>2. Vendor installed new booms</li> <li>3. Cleaned and reinstalled connector</li> <li>4. Resoldered connection at drum</li> <li>5. Rewired</li> <li>6. Rewired</li> <li>7. Wiring reversed; rewired, rechecked</li> </ol>
Vibration	Problem 2	Problem 1	Successful	Successful	<ol style="list-style-type: none"> <li>1. Panel 2 root inboard cell inoperative</li> <li>2. Screw at base of orientation mechanism fell out during vibration</li> </ol>	<ol style="list-style-type: none"> <li>1. Checked OK, test readout error</li> <li>2. Reinstalled and lockwired</li> </ol>
Thermal vacuum	Successful	Successful	Problem 1	Successful	<ol style="list-style-type: none"> <li>1. BCC S/N 3 could not be commanded to charge mode at low temperature</li> </ol>	<ol style="list-style-type: none"> <li>2. Problem definitely identified to intermittent AGE connector</li> </ol>
Deployment	Successful	Successful	NA	NA	None	None
Prelaunch tensioning	NA	Problem 1	Successful	Successful	<ol style="list-style-type: none"> <li>1. Booms on panel 1 damaged during tensioning</li> </ol>	<ol style="list-style-type: none"> <li>1. Replaced booms; changed tensioning procedure</li> </ol>
Final system test	Successful	Problem 1	Problem 2	Successful	<ol style="list-style-type: none"> <li>1. Acquisition sensors 2 and 4 would not function</li> <li>2. Failure to command properly in BCC 2 position</li> </ol>	<ol style="list-style-type: none"> <li>1. Handling damage; repaired, recalibrated and tested.</li> <li>2. AGE and test cable problem not flight hardware; fixed AGE</li> </ol>

All of the EMI correction filters were added to the qualification units to make them identical to the flight units and a flight model external CEU filter unit was added to the system.

The tests indicated that the EMI was within acceptable limits and the unit was sent to LMSC to be installed with the flight model on the Agena.

#### Summary of Acceptance Test Results

Results from the flight model acceptance tests are summarized in Table 5-4, which also illustrates the anomalies or problems that developed during the test sequence. Many of the problems noted have not been discussed in the preceding text because of their minor importance or the self-explanatory nature of the solutions.

As a result of the tests the flight model was accepted by the Air Force at Hughes, El Segundo on 19 June 1971. The units were subsequently delivered to LMSC and integrated with the Agena for flight as reported in the following subsection. Weights of the flight units as shipped are summarized in Table 5-5.

### INTEGRATION AND PRELAUNCH TESTS

#### Qualification Model

After completion of the tests on the qualification model at Hughes the system was shipped to LMSC, Sunnyvale, for preliminary integration with the Agena spacecraft. Just prior to installation a complete "bench" system test was performed. After installation the integration tests consisted of a quick functional test and the FRUSA portion of an overall STP-71-2 test sequence. This series of tests confirmed the mechanical and electrical interface of the FRUSA with the Agena subsystems.

Subsequent to the removal of the qualification model from the spacecraft a special EMI test was conducted at LMSC to determine if the FRUSA would be affected by the RF radiation of the ONR experiment on the STP-71-2 spacecraft. There was no evidence of any problems and the qualification model was returned to Hughes for EMI tests with the new PCU and CEU modifications and the CEU filter unit.

#### Flight Model

The flight model was "bench" tested at LMSC prior to integration with the spacecraft. During initial FRUSA turn-on with the EMI filter unit installed with the system on the Agena the solar array motor drive filters in the filter unit shorted, causing severe damage to the PCU. Both the filter unit and PCU were returned to Hughes for trouble analysis and repair. It was decided that the qualification model PCU would be upgraded to flight status. This was accomplished, along with a design change in the filter unit and both units were returned to LMSC for the successful completion of integration tests.

TABLE 5-5. FRUSA WEIGHT

<u>Unit</u>	<u>Actual Weight, pounds</u>
Battery charge controller (2)	42.46
Power conditioning unit	18.31
Load bank	27.13
Orientation mechanism and control electronics unit	74.17
Solar array	82.20
Filter unit	<u>3.50</u>
Total weight	247.77

#### Prelaunch Tests

Tests at VAFB consisted of the FRUSA portions of overall STP-71-2 tests both in the Agena assembly area and on the launch stand. During the stand tests a thermal problem was discovered on the solar array. This was found as a result of thermal analysis of a similar design on another program and not as a result of VAFB stand tests. It was necessary to remove the solar array from the Agena and return it to Hughes for modification. This was accomplished without delay to the launch schedule. All subsequent prelaunch tests at VAFB indicated normal FRUSA operation.

## SECTION VI

### FLIGHT TEST RESULTS

#### MISSION SUMMARY

Early orbital operations after the October 17 launch of the system were nominal in all respects except timing (see Table 6-1 for an operations summary). As the result of a thermal runaway of one of the spacecraft primary batteries, a decision was made to pitch down the spacecraft in orbit 8 rather than orbit 16 in order to deploy the FRUSA so that the spacecraft could be supported by the FRUSA power, thus enabling the spacecraft primary cells to cool and providing for the safety of the spacecraft in the event of total failure of the primaries. By orbit 10, extension and acquisition had been achieved with totally nominal performance of the FRUSA. Power output was approximately 1460 watts at the peak power point, which compares well with acceptance test data for a panel temperature of about 130°F. The panels were dynamically quiet with no significant response noted by the accelerometers.

After several days of operation and to facilitate charge regulation of one of the spacecraft buses, it was decided to retract the array about 1/6 or 1/3. A trial retraction was accomplished during the Vandenberg station pass in order to calibrate the retraction rate and to develop a retraction signature. Precision retraction was a necessity, since array temperatures could reach 350°F (solder melting temperatures) in the rolled-up sectors of the panel if power were being supplied in that configuration. If any particular panel sector was fully shadowed, such damaging temperatures could be obviated. The trial retraction (40 percent) was successful and the panel was later retracted 1/6 using the time of shading a solar cell module as a signature. This retraction modulated the power output sufficiently to enable efficient power management of the SAMSO-002 bus. Power output in this condition is about 1200 watts at the peak power point.

Subsequent to the trial retraction on orbit 79, however, an oscillatory motion of the panel was observed on orbit 80. This oscillation results from a loss of bias to an amplifier in the support axis rate limiting circuit. The effect of this loss is to change the rate circuit performance such that when the system is in a sun acquisition motion about the support axis (0.5 deg/sec) and when the field of view (FOV) of the sun lockon signal is entered, a negative current of large magnitude is generated that causes the FRUSA to be rejected from the field of view. As soon as this rejection occurs, the system switches back to an acquisition mode. This cycle repeats at about a one-half cycle per second rate without significant effect on the FRUSA or the spacecraft. The panel "wiggles" about  $\pm 10$  to 15 milli-g at the tips, and the interface relay opens and shuts because of its dependency on the sun lockon signal. The latter effect was overcome by sending a manual sun lockon command. While such a limit cycle oscillation was benign as far as system and FRUSA effects, it was decided to disable the control electronics unit (CEU), and thus to leave the array in its last fixed position, 327 degrees, or about 20 degrees off the nominal sun tracking null position (see Figure 6-1). This approach was taken

TABLE 6-1. RTD-806 MISSION OPERATIONS

<u>Operation</u>	<u>Orbit</u>
First status check	2
Pitchdown and FRUSA deployment	8
Extension of solar array panels	9
Sun acquisition	10
Application of FRUSA power to spacecraft bus	10
Thirty-six loadbank and SCEU tests	Various (11 through 2639)
Retraction of FRUSA panels 1/3 and re-extension	79
Retraction of FRUSA panels 1/6 to reduce spacecraft power	171
Failure of commutator A	197
Re-extension of panels	621
Repositioning of support axis to 047 degree position	835
Repositioning of support axis to 297 degree position	838
Retraction and extension of FRUSA panels	936 947 948 949 950 1136 1137
	Panel } 1138 in } 1143 eclipse } 1144
Failure of commutator D	1478

## SECTION VI

### FLIGHT TEST RESULTS

#### MISSION SUMMARY

Early orbital operations after the October 17 launch of the system were nominal in all respects except timing (see Table 6-1 for an operations summary). As the result of a thermal runaway of one of the spacecraft primary batteries, a decision was made to pitch down the spacecraft in orbit 8 rather than orbit 16 in order to deploy the FRUSA so that the spacecraft could be supported by the FRUSA power, thus enabling the spacecraft primary cells to cool and providing for the safety of the spacecraft in the event of total failure of the primaries. By orbit 10, extension and acquisition had been achieved with totally nominal performance of the FRUSA. Power output was approximately 1460 watts at the peak power point, which compares well with acceptance test data for a panel temperature of about 130°F. The panels were dynamically quiet with no significant response noted by the accelerometers.

After several days of operation and to facilitate charge regulation of one of the spacecraft buses, it was decided to retract the array about 1/6 or 1/3. A trial retraction was accomplished during the Vandenberg station pass in order to calibrate the retraction rate and to develop a retraction signature. Precision retraction was a necessity, since array temperatures could reach 350°F (solder melting temperatures) in the rolled-up sectors of the panel if power were being supplied in that configuration. If any particular panel sector was fully shadowed, such damaging temperatures could be obviated. The trial retraction (40 percent) was successful and the panel was later retracted 1/6 using the time of shading a solar cell module as a signature. This retraction modulated the power output sufficiently to enable efficient power management of the SAMSO-002 bus. Power output in this condition is about 1200 watts at the peak power point.

Subsequent to the trial retraction on orbit 79, however, an oscillatory motion of the panel was observed on orbit 80. This oscillation results from a loss of bias to an amplifier in the support axis rate limiting circuit. The effect of this loss is to change the rate circuit performance such that when the system is in a sun acquisition motion about the support axis (0.5 deg/sec) and when the field of view (FOV) of the sun lockon signal is entered, a negative current of large magnitude is generated that causes the FRUSA to be rejected from the field of view. As soon as this rejection occurs, the system switches back to an acquisition mode. This cycle repeats at about a one-half cycle per second rate without significant effect on the FRUSA or the spacecraft. The panel "wiggles" about  $\pm 10$  to 15 milli-g at the tips, and the interface relay opens and shuts because of its dependency on the sun lockon signal. The latter effect was overcome by sending a manual sun lockon command. While such a limit cycle oscillation was benign as far as system and FRUSA effects, it was decided to disable the control electronics unit (CEU), and thus to leave the array in its last fixed position, 327 degrees, or about 20 degrees off the nominal sun tracking null position (see Figure 6-1). This approach was taken



TABLE 6-1. RTD-806 MISSION OPERATIONS

<u>Operation</u>	<u>Orbit</u>
First status check	2
Pitchdown and FRUSA deployment	8
Extension of solar array panels	9
Sun acquisition	10
Application of FRUSA power to spacecraft bus	10
Thirty-six loadbank and SCEU tests	Various (11 through 2639)
Retraction of FRUSA panels 1/3 and re-extension	79
Retraction of FRUSA panels 1/6 to reduce spacecraft power	171
Failure of commutator A	197
Re-extension of panels	621
Repositioning of support axis to 047 degree position	835
Repositioning of support axis to 297 degree position	838
Retraction and extension of FRUSA panels	936 947 948 949 950 1136 1137 Panel in eclipse } 1138 1143 1144
Failure of commutator D	1478

because enough power could be made available to the spacecraft without autotracking, and the reluctance to depend on the stability of a failed component in the CEU. Further slewing of this axis to maintain a sufficient average power level was accomplished by locking the control electronics in an acquisition mode, which generates a 0.5 deg/sec excursion of the support axis. As desired positions are attained, the CEU is commanded off and the slew stops.

While the support axis tracking anomaly and the later intermittency of commutator A (revolution 197) and failure of commutator D (revolution 1478) were annoying in the sense that nonstandard and time consuming operations such as command positioning of the solar array became necessary, the basic test objectives of establishing the principal structural, thermal, and power characteristics of a flexible array are continuing as discussed in the following performance evaluation analysis sections of this report.

To this point in the mission (eighth month), it appears that degradation of the overall solar cells and modules is consistent with the effects of space radiation (indicating little mechanical damage), that solar array thermal performance is about 7°F cooler than anticipated, and that dynamic response of the panel system is small to the point of being insignificant during deployment, tracking, or the ten retraction extension operations which were performed late in the third month of the mission. The panel stability is so exceptional that it became necessary to plan a special test for late in the mission to stimulate dynamic modes. This test would consist of applying torque pulses about each control axis such that the panel modes would be stimulated to the point of rising above the noise level.

#### SOLAR ARRAY PANEL TEMPERATURE EVALUATION

A comparison of flight solar array panel temperature data with pre-flight predictions (Figure 6-2) shows the array panels to be operating up to 7°F cooler than anticipated for the applicable twilight orbit and electrical output conditions.

The flight data that have been used for comparison are given in Table 6-2. These data indicate that panel 2 is consistently warmer than panel 1, apparently resulting from the Agena albedo, since panel 2 is parallel to and alongside the Agena. As such effects were not included in the analytic model, only panel 1 data were used in evaluation of the analytic models. Since all data correspond to twilight environmental conditions ( $\beta \approx 80$  degrees), the variations of the mean panel 1 temperatures between orbits is almost certainly due to the sun line being other than normal to the panel surface. Comparing revolution 12 data with that from revolutions 18 and 76, and with the knowledge from other data that the panel was normal to the sun line for revolution 12, it can be shown from the temperatures that the panel normal was the order of 25 degrees off the sun line for revolutions 18 and 76. This compares reasonably well with the analysis of the support axis tracking anomaly discussed earlier which indicated that the panel was about 20 degrees off the sun for these orbits.

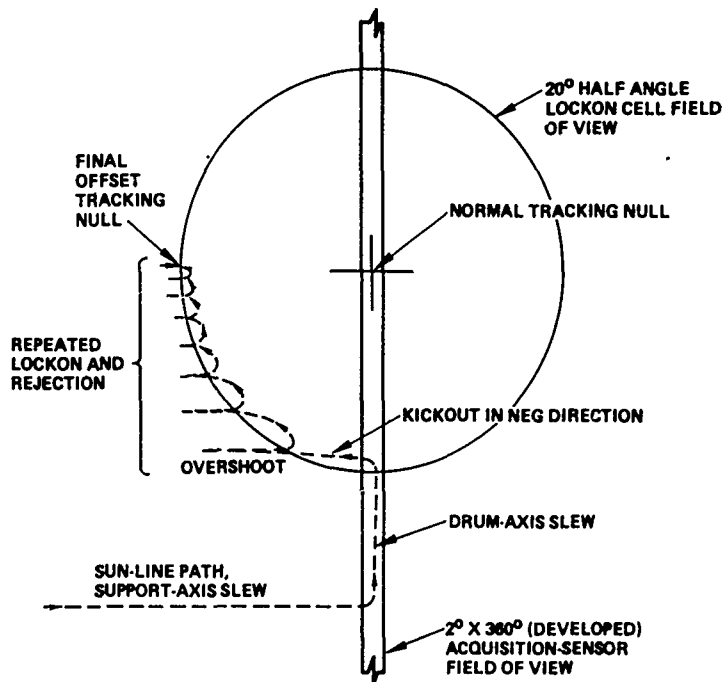


Figure 6-1. Anomalous (Offset) Tracking

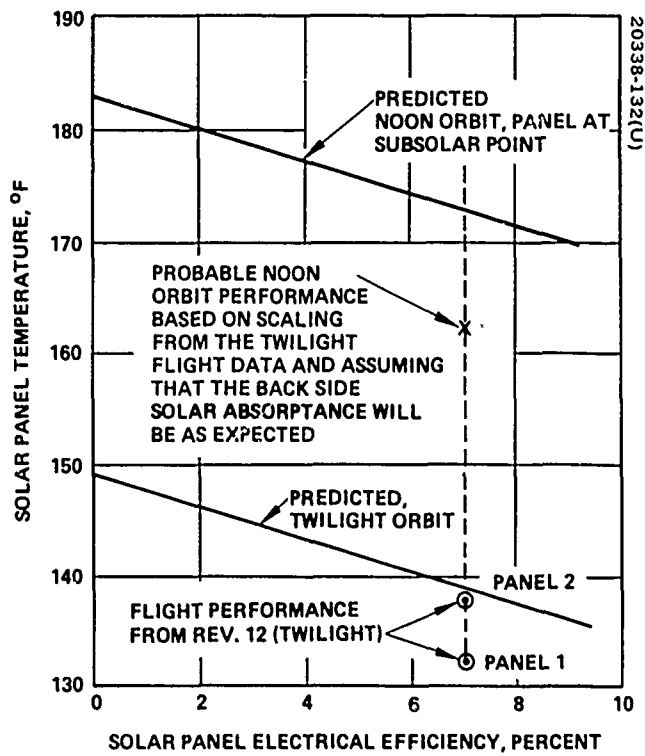


Figure 6-2. Array Panel Temperatures

TABLE 6-2. FLIGHT SOLAR ARRAY TEMPERATURES, °F

Location	Revolution		
	12	18	76
Panel 1			
Middle inboard	131	125	125
Middle outboard	131	123	125
Root inboard	137	128	124
Root outboard	127	124	124
Average	131.5	125	124.5
Panel 2			
Middle inboard	141	137	135
Root outboard	136	135	133
Average	138.5	136	134

Using the revolution 12 panel 1 data as most representative of twilight orbit flight performance and a preflight analysis based on the properties of Table 6-3 results in the comparison shown in Figure 6-2. The noon orbit case was extrapolated from the twilight orbit data by assuming that the 10°F difference in performance is due to either the effective emittances and/or the front side solar absorptance being different from those used in the analysis. However, other factors affecting the flight data, such as the ±2-degree measurement uncertainty in panel sun angles, or temperature and efficiency uncertainties could also account for the difference. Uncertainties in backside solar absorptance, which do not enter into the twilight case, also can affect the noon orbit flight performance. In any case, it is reasonable to assume from these data that the nominal prediction for noon orbit temperature will not be exceeded in flight and that the temperature may be up to 8° to 10°F lower as indicated by this analysis. Unfortunately, data acquisition problems have not allowed the foregoing conclusions concerning the noon orbit maximum temperature to be verified. Commutator D was lost on Orbit 1478, approximately 17 days before the noon turn occurred. This commutator carried the panel temperature and its loss terminated data retrieval from these sensors. In addition to this difficulty, all available flight data prior to Orbit 1478 were for vehicle orbital positions close to the earth's terminator. In this condition no significant panel albedo loads existed. The panel temperature results for all these cases were similar to those presented in Table 6-2 for the twilight orbit case.

TABLE 6-3. FRUSA ARRAY RADIATIVE PROPERTIES FOR  
BASELINE ANALYSIS

(Specific heat at 70°F = 0.19 Btu/lb°F).

Location	Effective Solar Absorptance, $\alpha$	Total Hemispherical Emittance
Solar cell side	0.81 (no electrical load)	0.83
	0.75 (full electrical load)	
Back side	0.52	0.81

#### SOLAR ARRAY POWER PERFORMANCE

The electrical performance of the main solar array has been monitored periodically since the eleventh revolution of the mission. This performance provides an important means of checking on the condition of the array. Flight data for the first 6 months of operation (reduced to standard conditions of Air Mass Zero illumination, normal sun incidence, and panel temperature of 130°F) are summarized in Figure 6-3. Early postlaunch performance (revolution 11) matches prelaunch performance within the precision normally obtained between ground measurement and early space performance on other spacecraft. Performance after 6 months of operation (revolution 2639) was somewhat less; power had degraded about 10 percent, a magnitude consistent with the degradation predicted to be caused by particulate radiation. This result gives overall confidence that the array is functioning as expected. No evidence of mechanically induced damage was observed for either launch or roll-out/roll-in maneuvers.

Data from the first 173 revolutions were obtained with good precision using the instrumentation intended for this purpose. The failure of commutator A on revolution 197 precluded direct measurements of panel voltage and current on subsequent revolutions. Acceptable data for these latter cases were obtained by measuring the load voltage and then using the values of the various load resistors to deduce the panel current. Corrections were made to allow for voltage drops in the orientation mechanism and leads as well as for the current used by the load switching relays and for battery charging. Corrections were also made for seasonal changes in the sun/earth distance. Data were corrected for panel orientation angle and earth albedo effects through revolution 1147 using LMSC supplied data.

For subsequent revolutions, where LMSC data were not available, reasonable assumptions were made for these effects. For the special case of revolution 173, when one-sixth of the panel was kept retracted (i. e. five-

sixths of the panel was illuminated, corrections were made to show panel power as if the panel had been fully deployed. Thus, for all revolutions, the data were reduced to the standard conditions of a fully deployed pair of panels operating at 130°F and oriented normally to sunlight with no earthshine additions to the power. When thus normalized, any differences observed in performance from one revolution to another could be attributed directly to panel degradation. Comparison of Table 6-4 and Table 6-5 shows that measured degradations are consistent with predicted radiation effects. Therefore, these data support the conclusion that the launch conditions, initial full deployment, subsequent partial retraction/extension and the ten full retraction/extension operations as well as the many sunlight/earth shadow induced

TABLE 6-4. PREDICTED (NORMALIZED) SOLAR PANEL <sup>(1)</sup>  
 MAXIMUM POWER PERFORMANCE <sup>(2)</sup>  
 VERSUS TIME IN ORBIT

Months in Orbit	Penetrating Damage P <sup>+</sup> and e- P <sub>t</sub> /P <sub>o</sub>	Penetrating Damage Plus Low Energy Protons P <sub>t</sub> /P <sub>o</sub>	Penetrating Damage, Low Energy Protons and 0211 Coverslide Darkening P <sub>t</sub> /P <sub>o</sub>
1	0.994	0.974	0.955
2	0.982	0.953	0.934
3	0.970	0.931	0.912
4	0.960	0.913	0.895
5	0.950	0.898	0.880
6	0.940	0.884	0.866
12	0.900	0.833	0.816

(1) Utilizing 2 by 2 cm 2 ohm-cm 8-mil n/p solar cells with 6-mil microsheet cover slides.

(2) 400-nm , 90-degree inclining orbit, NASA SP-3024 radiation environment.

(3) Cover glass and adhesive degradation assumed to occur very early in life.

20338-134(U)

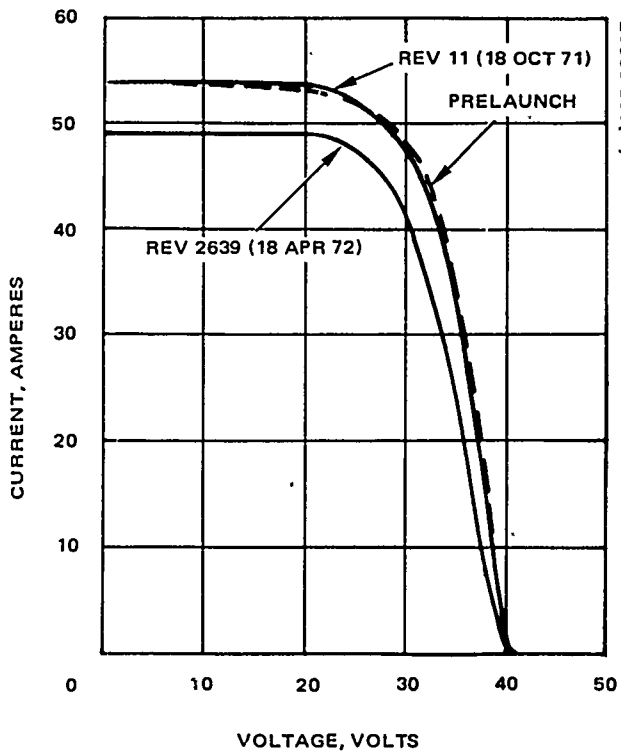


Figure 6-3. FRUSA Array 6 Month Performance Summary

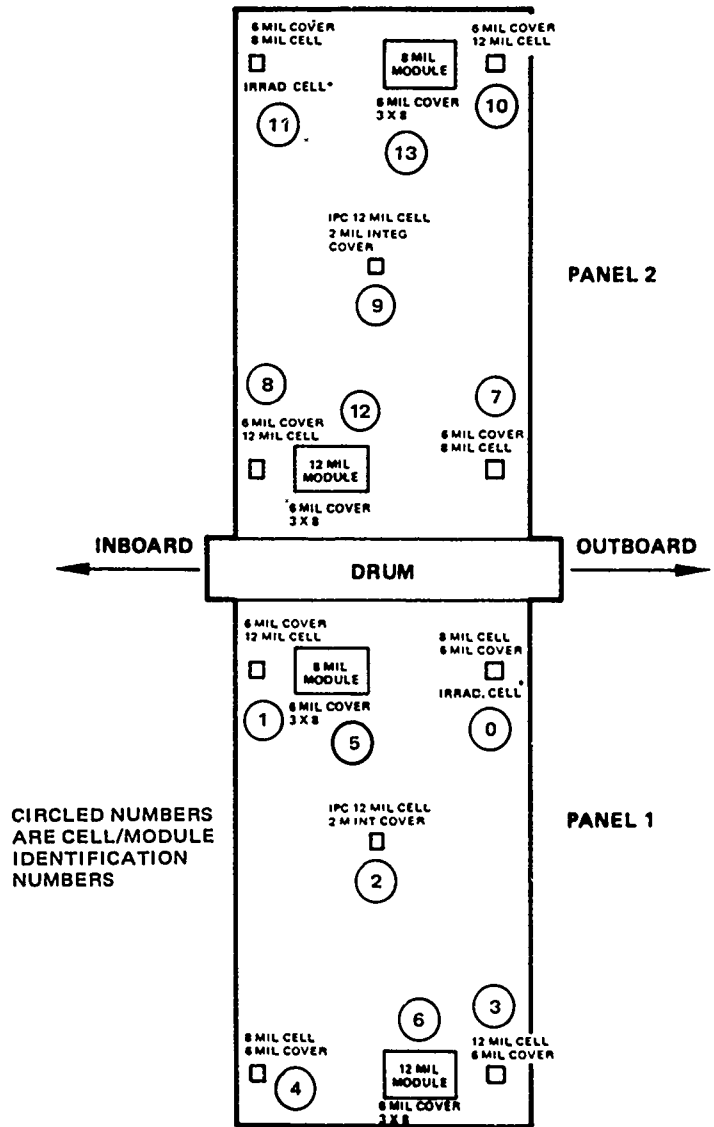


Figure 6-4. Cell/Module Layout

TABLE 6-5. MEASURED (NORMALIZED) FRUSA SOLAR PANEL PERFORMANCE VERSUS TIME IN ORBIT

Months in Orbit	Rev. No.	$I_{SC}$ , ampères	$I_{SC}/I_{SCO}$	$V_{OC}$ , volt	$V_{OC}/V_{OCO}$	$I @ 28V$ , amperes	$I_{28}/I_{28_0}$
0	Prelaunch	53.7	1.0	40.9	1.0	50.5	1.0
0	11	54.0	1.006	41.0	1.002	49.9	0.988
0.16	76	53.5	0.996	40.5	0.990	49.8	0.986
0.4	173	52.0	0.968	41.0	1.002	49.4	0.978
1.7	735*	51.0	0.950	39.5	0.966	48.4	0.958
2.6	1147*	54.1	1.007	40.0	0.978	48.8	0.966
4.0	1762	49.8	0.927	40.0	0.978	45.9	0.909
5.4	2365	50.6	0.942	38.0	0.929	44.8	0.887
6.0	2639	49.0	0.912	40.0	0.978	44.5	0.881

\*Severe data scatter.

temperature cycles did not produce any measurable degradation of the electrical power capability of the FRUSA. The ten retraction/extension cycles, performed between revolutions 735 and 1147, are particularly noteworthy in that some of these occurred while the panels were cold in eclipse conditions. The current-voltage curves for representative revolutions, as well as the data points used to generate these curves, are shown in Appendix A.

#### SOLAR CELL/MODULE EXPERIMENT RESULTS

The 14 test cells and modules on the FRUSA were monitored individually for electrical performance. The types of cells and covers included in these test samples are listed in Table 6-6; the positions of the samples on the panels are indicated in Figure 6-4. Cells and module performances were monitored periodically from revolutions 13 through 1348. Beyond this, the data became too erratic to be of any use. By revolution 1478, the data commutator failed completely.



TABLE 6-6. FRUSA TEST CELL/MODULE DESCRIPTION SUMMARY

Cell Number	Cell Type	Cover Type
2, 9	Ion Physics, 10 ohm-cm n/p, 2 x 2 cm	2-mil integral
7, 4	Heliotek, 2 ohm-cm n/p, 2 x 2 cm, 8-mil thick	0211 microsheet 6-mil thick
8, 1, 3 10	Heliotek, 10 ohm-cm n/p, 2 x 2 cm, 12-mil thick	0211, 6-mil thick
11, 0	Heliotek, 2 ohm-cm n/p, 2 x 2 cm, 8-mil thick, irradiated with 1-mev electrons before launch	0211, 6-mil thick
12, 6	Heliotek, 10 ohm-cm n/p, 3 x 8 cell module, 12-mil thick cells	0211, 6-mil thick
5, 13	Heliotek, 2 ohm-cm n/p, 3 x 8 cell module, 8-mil thick cells	0211, 6-mil thick

Early performance (through revolution 173) of these cells was as expected, showing no significant degradation during this short period. Data from subsequent revolutions also showed little or no degradation. However, the noise in these latter data precluded the precision required to resolve small differences in performance that may have existed by revolution 1348 (3 months after launch). The performance of typical cells and modules is shown in Figure 6-5 (the remaining cell and module data are shown in Appendix A). All data in this figure have been reduced to standard conditions of Air Mass Zero illumination, normal sun incidence, and panel temperature of 130°F.

The cause of data noise is not known but is suspected of being incipient trouble with the data commutator. Panel temperature data, monitored by this same commutator, also were erratic. Since these temperature measurements were used as a basis for correcting all cell and module current-voltage data to the standard 130°F condition, the erratic nature of the temperature data is reflected in the values of the normalized cell and module data. This effect is most pronounced with voltage data and is believed to be the cause of some cells and modules showing an increase with time of open circuit voltage.

The only two modules showing significant deviation from full power output were modules 5 and 12 during revolution 173. These two modules were

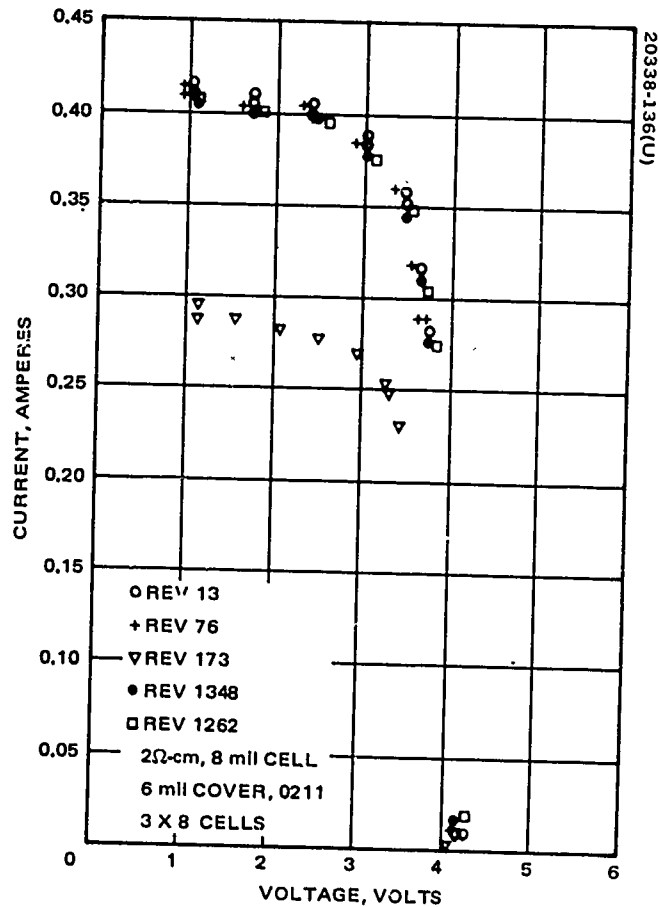
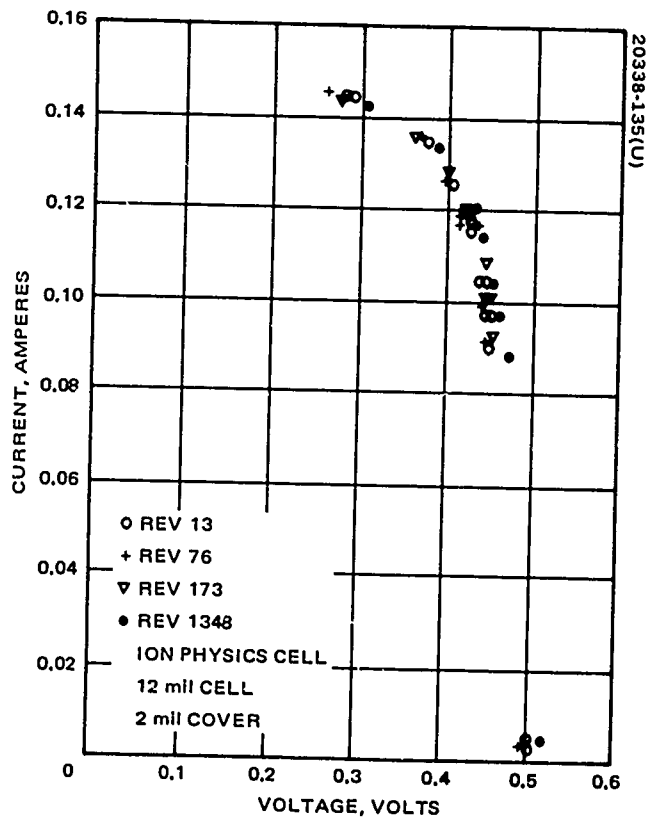
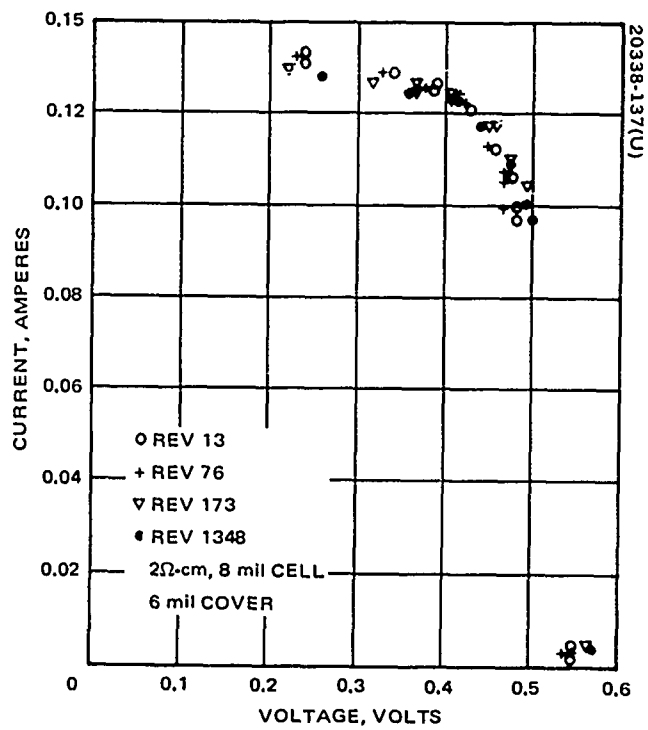
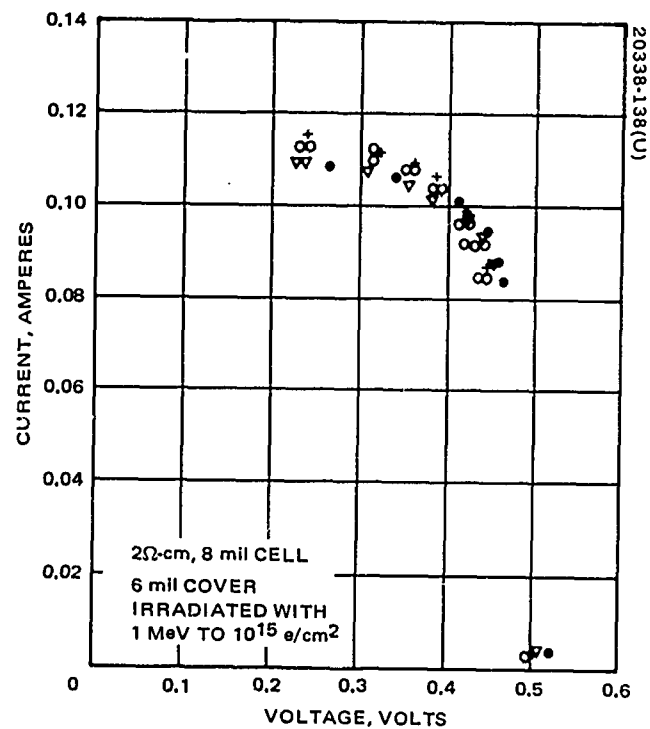


Figure 6-5. I-V Data

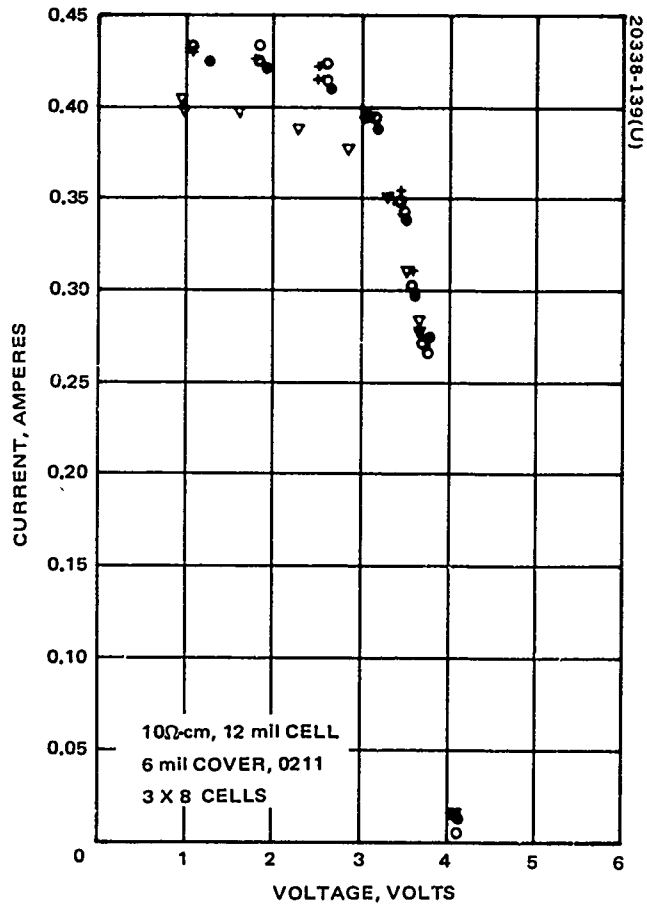


c) CELL 7



d) CELL 11

Figure 6-5 (continued). I-V Data



e) MODULE 12

Figure 6-5 (concluded). I-V Data

partially shadowed at this time by the cushion takeup roller and by the drum, respectively, due to the condition of 1/6 panel retraction maintained between revolution 171 and 621.

## ARRAY DYNAMIC ANALYSIS

In support of the dynamic analysis phase of the flight experiment complete analytic models of the flexible array were developed. These models included the effects of compression loading in the supporting booms and finite tip deflections in the determination of vibration frequencies and modes. In this analysis, the support booms are treated as cantilevered beams of uniform mass and stiffness with the flexible panel suspended as a wide string of uniform mass tensioned between the storage drum and the tip of the booms. The two support booms deflect in the same direction in bending modes, and in opposite directions in torsional modes (differential bending). The equations of motion for this analytical model were derived and solved in closed form.

To the extent of completeness dictated by consideration of small strains but not necessarily small deflections, the above treatment includes all significant features that are germane to the basic dynamic representation of the FRUSA type structure. Further analysis effort was expended for investigating the array panel behavior under combined substrate bending and membrane loading conditions as well as alternate boom mounting constraints and nonuniform boom stiffness. A finite element modeling technique is employed for this latter analysis.

Verification of the analytical modeling by ground testing of the flexible roll-up array is difficult at best. The FRUSA flight experiment was therefore instrumented with the accelerometers and three strain gages for measurement of array dynamic characteristics in orbital flight. The primary objective for this flight instrumentation is to validate and to improve the analytical modeling of the array structure system for use in future array applications.

FRUSA accelerometer data indicate that the array is exceptionally stable with no significant dynamic interaction with the Agena space vehicle control system. A comparison of predicted array modes and frequencies with those derived by Fourier analysis of flight data shows excellent agreement (see Table 6-7). The first three array modes are identified for the fully extended panel and partial panel extension. Close spacing of bending and torsional vibration and coupling between both frequencies makes it difficult to separate clearly the modes in the flight data. The frequency of the predicted fundamental cantilever beam mode as shown is expected to be lower than the measured first mode frequency because the drum was not constrained from motion as assumed in the analysis. The damping of the fundamental vibration mode was determined from flight data to be about 2 percent.

In conclusion, the model representation of the flexible array for dynamic analysis as a cantilevered beam with a tensioned string proved to be excellent for fundamental vibration modes. For analyzing lateral panel bending modes (chordwise deflections), a finite element computer routine was developed.

TABLE 6-7. COMPARISON OF IN-ORBIT MEASURED FRUSA MODES WITH ANALYTICAL PREDICTIONS

Order	Mode	Fully Extended Array Frequency, ~ Hz		5/6 Extended Array Frequency, ~ Hz		2/3 Extended Array Frequency, ~ Hz	
		Analysis*	Flight	Analysis	Flight	Analysis	Flight
1	Boom-cantilever	B 0.209	0.25	B 0.291	0.3 to 0.4	B 0.424	0.5 to 0.6
		T 0.235		T 0.34		T 0.49	
2	Panel	B 0.545	0.55	B 0.663	0.6 to 0.73	B 0.853	0.8 to 0.86
		T 0.56		T 0.702		T 0.946	
3	Panel	B 0.909	1 to 1.18	B 1.087	0.8 to 1.1	B 1.35	1 to 1.3
		T 0.917		T 1.11		T 1.4	

\*The bending (B) and torsion (T) mode frequencies are predicted to be close. Mutual coupling makes it difficult to separate both modes in the flight data.

#### Structure Instrumentation

The location of all structural instrumentation on the FRUSA panels is illustrated in Figure 6-6. The sensitive axis of each accelerometer is indicated by an arrow. The number assignment is stated as used by the STP 71-2 data recording code. The accelerometer and strain gage signal flow employs two commutators. R1XX instrumentation channels are routed through the FRUSA inboard commutator A, and R3XX channels utilize the commutator B which is mounted to the FRUSA outboard actuator housing. All measurements are conditioned to a 0 to 5 volt format by amplifiers, commutated, and supplied to the Agena telemetry subsystem for processing into SGLS PCM formats. The data sampling rate is 11 23/32 per second.

The Systron-Donner Model 4311 accelerometer was used on the flight experiment. This model has a measurement range of  $\pm 0.1g$ , an excellent frequency response up to 10 Hz, and provides a signal accuracy of about 2 percent of full-scale. Since the transducer signal output is digitized by an 8-bit system, a minimum acceleration measurement increment of  $\pm 0.00087 g$  is possible.

Strain gage load cells are used for measuring the boom No. 1 bending moment at the actuator housing, and the tension in both array panels. The root bending load cell employs a temperature compensating circuit bridge arrangement. Figure 6-7 shows the calibration curve for the boom bending load cell. The nonlinear shape of this curve is caused by the changing cross section of the boom as the bending moment changes direction. However, because of a slight offset between the boom axis and the vector of the panel tension, the load cell is generally being utilized in its linear portion of greater sensitivity.

The tension for both array panels is generated by a single constant torque spring motor which is placed between the array mechanism spar and the roll-up drum. As knowledge of the panel tension is essential for predicting the array dynamic behavior, provision has been made for measuring panel tension. This measurement is effected by a tension strain gage mounted to the steel tape of each boom length compensator mechanism. The FRUSA panel tension measured in orbit is 5.8 pounds.

#### Dynamic Flight Data Evaluation

Data from flight events with expected structural array dynamic content have been investigated. Table 6-8 summarizes these mission events which are discussed in the following paragraphs. Fully as well as partially extended panel configurations have been studied.

TABLE 6-8. MISSION EVENTS SUMMARY FOR SIGNIFICANT DYNAMICS DATA

Event	Actual Time (revolution)	Comments
Deployment	8	Deployed and locked in 12.2 seconds
Extension	9	Extension time, 5 minutes
Sun acquisition	10	Sun acquisition normal
Roll in array 1/3 and re-extend	79	Retraction/extension normal
Reacquisition	79	Tracking at edge of lock on cone
Roll in array 1/6	171	Retraction successful
Fully extend array	621	Extension successful

## Array Deployment

The rolled-up solar array was separated from the Agena equipment module after activation of two pyro bolts and was deployed into a position normal to the Agena axis by two torsion springs mounted at the hinge on the drum axis shaft; all operations were performed in a nominal manner. The initiation of the deployment was clearly indicated by all accelerometers on the array. Levels of about 0.1-g peak were monitored at separation, and the oscillatory motion damped quickly, as can be seen in Figure 6-8 for accelerometer R304.

The panel pretension is reacted by an off-center antirotation lock that stays with the space vehicle as the array moves away into the flight position. The offset between the drum axis and the reaction force on the lock introduces a rotation of the entire array assembly. This rotation was monitored by accelerometer R106 with sensitive axis normal to transducer R304. Presence of array rotation proves that the panel pretension was maintained during launch and, therefore, solar cell damage should be as negligible on the flight array as it was found to be in array qualification and acceptance vibration testing. The period for the 90-degree deployment motion between separation release and hinge latchup impacts is 12.2 seconds, as indicated by accelerometer response (see Figure 6-8). This deployment time of 12.2 seconds correlates well with 12.5 seconds as measured during flight acceptance testing.

A bending frequency of 2/3 Hz is indicated in Figure 6-8 for the array on its structural support arm. This frequency is slightly lower than predicted due to orientation mechanism structure flexibility which was not accounted for in the analysis. There is, however, sufficient frequency separation between the array and its support structure to ensure low dynamic coupling. The damping of the impact motion was approximately 3 to 4 percent as determined by the amplitude decay of array vibration when it had been damped to below accelerometer saturation. The peak acceleration at latching impact was computed to be  $\pm 0.25$  g, and the bending moment on the support arm is then predicted to be less than the expected maximum value of 1600 in.-lb for this extrapolated g-factor.

The good correlation of analytical predictions, ground test results, and in-flight data provides confidence in future array deployment mechanism design.

## Panel Extension

The array extension on the ground was performed with the aid of a water table and closely spaced floats. The sag of the panel and the booms in between the support floats and the associated structural deformations caused the accelerometer axes to slope sufficiently so that 10 percent of the 1-g field saturated the transducers. The FRUSA roll-out in revolution 9 and the recorded accelerometer data, provided the first real demonstration of the functional performance and the dynamic characteristics of the roll-up array concept. The start of the panel extension saturated the accelerometers with



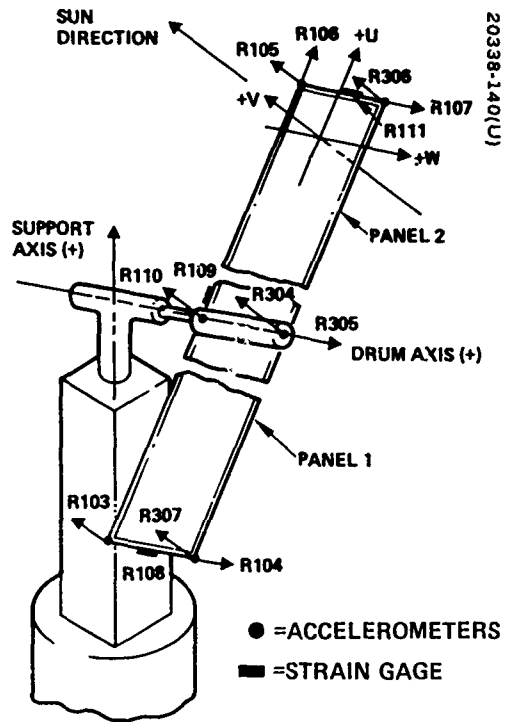


Figure 6-6. FRUSA Accelerometer and Strain Gage Instrumentation

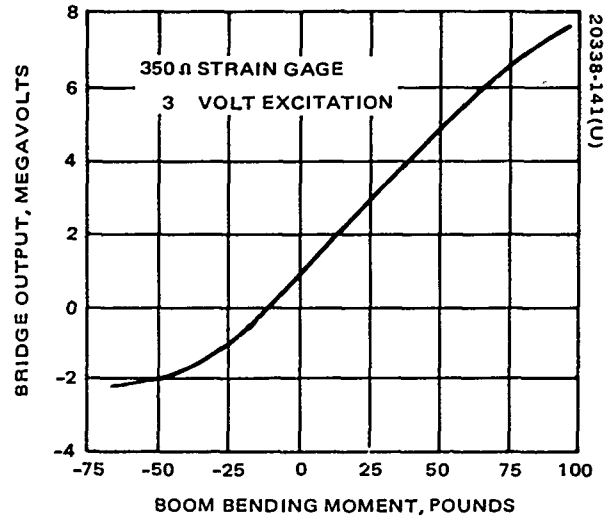


Figure 6-7. Calibration Curve for Boom Root Bending Load Cell

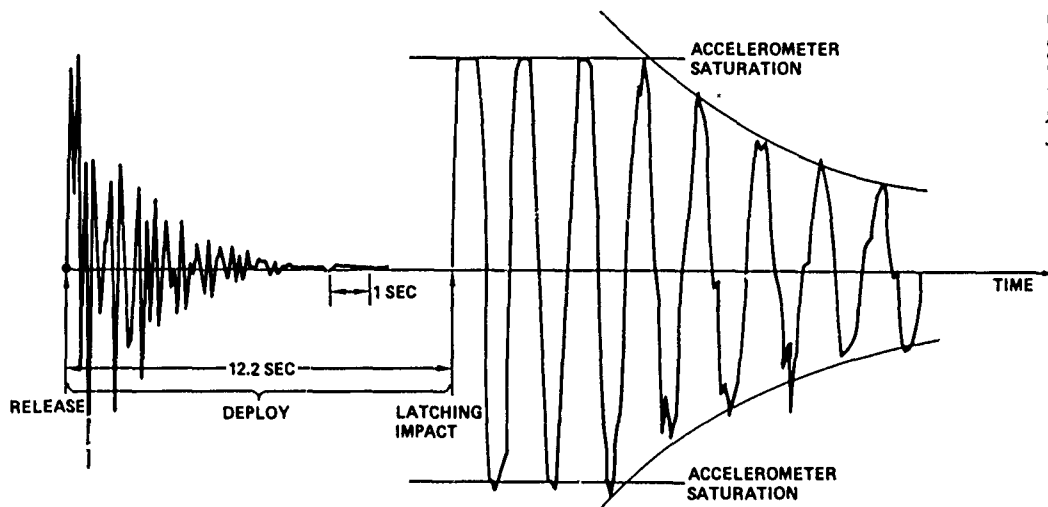


Figure 6-8. Accelerometer Time History During Array Deployment as Measured by Transducer R304

sensitive axis (u, w) in the plane of the panel. Acceleration normal to the solar panel peaked at about 70 milli-g. During roll-out to the fully extended panel length of 16 feet, the accelerations averaged about 15-to 30-milli-g-peak. Termination of the roll-out did not generate any noticeable dynamic excitation, as shown by low acceleration values in Table 6-9.

#### Fully Extended Array Response

In its orbital flight, the fully extended FRUSA has experienced periods of complete quiescence (no control maneuvers conducted by the array and Agena space vehicle), maneuvers of sun acquisition and sun tracking, as well as oscillatory excitations caused by malfunctioning of the support axis control electronic system of the orientation mechanism. Table 6-10 lists peak accelerometer readings for the nominal events. Panel 1 tension was measured as 5.8 pounds, which agrees with a nominal setting of the panel tension as defined by ground testing. The boom bending moment (gage R 109) of 26 in-lb is also nominal. The amplitudes of structural dynamic response during these sustained events proved too low for extraction of array modal configurations and damping factors with a sufficient degree of confidence. Start up of the support axis oscillations in revolution 79 produced dynamic data which is used to verify the array dynamic modeling.

#### Support Axis Acquisition Slew in Revolution 79

At the beginning of revolution 79, the fully extended array was positioned with its panels parallel to the Agena space vehicle axis and the array plane about 40 degrees off the sun line normal with respect to the support axis. In order to achieve sun pointing, the mechanism control system for sun acquisition was, therefore, initiated. The support axis torquer responded with a peak torque of 1.8 ft-lb, a level maintained for 13.5 seconds due to a malfunction in the control electronics. The sustained acceleration imposed by the 1.8 ft-lb of motor torque (reduced by a friction torque of about 0.2 ft-lb) on the array is predicted and exhibited by the accelerometer data to be approximately 2.5 milli-g. After 13.5 seconds, the torquer current was switched in polarity when the array passed the sun normal position as defined by a sun lock-on sensor cell. This torque reversal provided again a step impact to the array. About 10 seconds later, the array movement about the support axis had been reversed and the lock-on sensor once more triggered the torquer current switch as the sun normal array position was transversed. During this array slewing, the space vehicle rotated in an opposite direction to the array in accordance with the law of conservation of momentum. This array cycling repeated itself with ever shorter periods and, finally, oscillatory motion at 0.5-Hz frequency remained about the sun normal axis. Figure 6-9 illustrates the anomalous array maneuver.

A summary of nine accelerometer transients is provided in Figure 6-10 for the initial 23.5 seconds; that is, the two initial slew torque steps of sustained array acceleration. The transients for accelerometer R106 (sensitive axis along panel axis) and the strain gage transducers are not shown because of their low reading during the maneuver. The panel tension was essentially

TABLE 6-9. FRUSA EXTENSION DYNAMICS

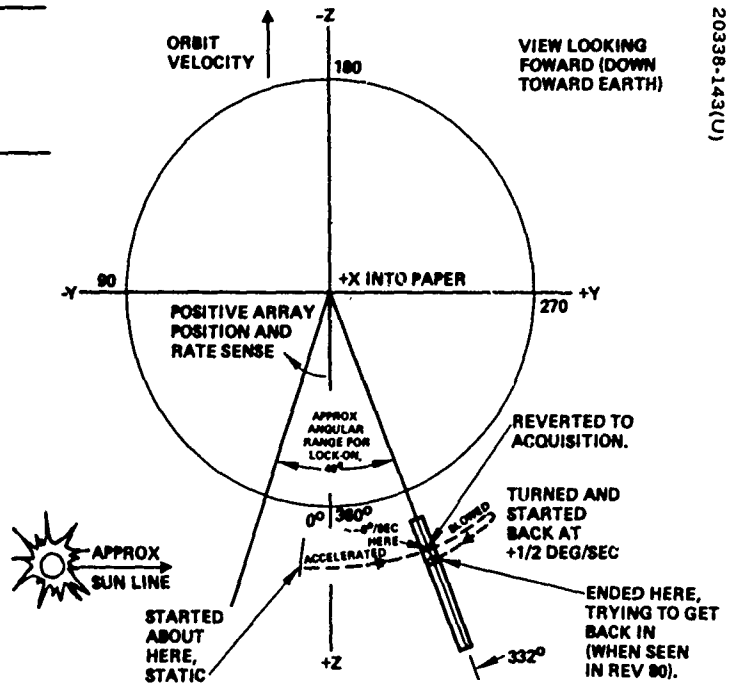
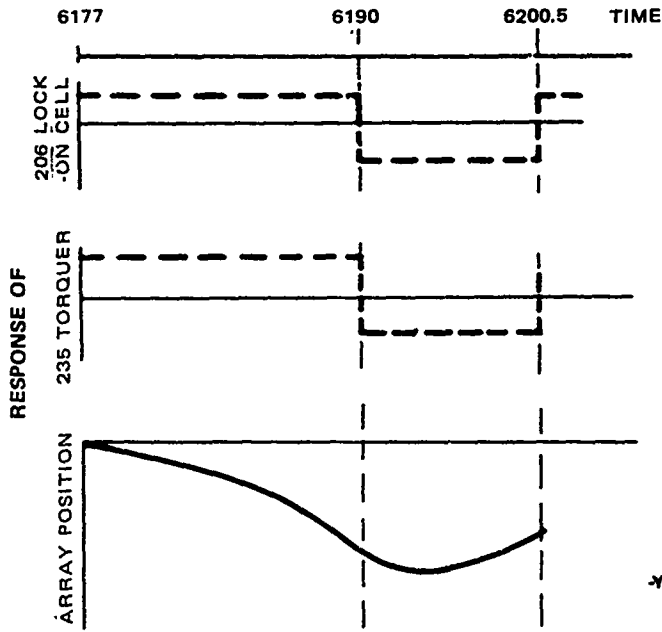
Direction of Acceleration	Peak Accelerations		
	Start of Extension	During Extension	End Extension
U direction	(Saturated)	59.1	18.3
V direction	70.4	32.2	23.5
W direction	(Saturated)	27.0	13.9

TABLE 6-10. PEAK ACCELEROMETER READINGS

	Quiescent (Revolution 9)	Tracking Mode (Revolution 10)	Oscillatory Malfunction (Revolution 80)
Peak accelerations, milli-g			
U	10.3	12.0	6.8
V	8.5	12.9	21.0
W	9.4	10.3	4.2
Panel tension, pounds	5.9	5.9	5.9

constant at a nominal value of 5.8 pounds. The boom root strain gage did not indicate any load variation during torque step one. After torque reversal, step two, four variations bending moment readings were recorded which exceeded the data printout aperture. Since these values occurred at time intervals of approximately 2 seconds and since a change in the boom moment reading can be correlated with a vibration mode, the 2-second spacing indicates a vibration mode at 0.25 Hz.

The dynamic array response to the relatively violent slew maneuver was low as measured by the accelerometers. As mentioned above, the steady state acceleration associated with the motor torque is predicted to be 2.5 milli-g. The measured maximum dynamic V-axis responses at the drum (R110, R304) and the panel tips (R103, R105, R306, R307) were about 3 and 15 milli-g, respectively.



20338-143(U)

Figure 6-9. FRUSA, Revolution 79  
Anomalous Sun Acquisition Maneuver

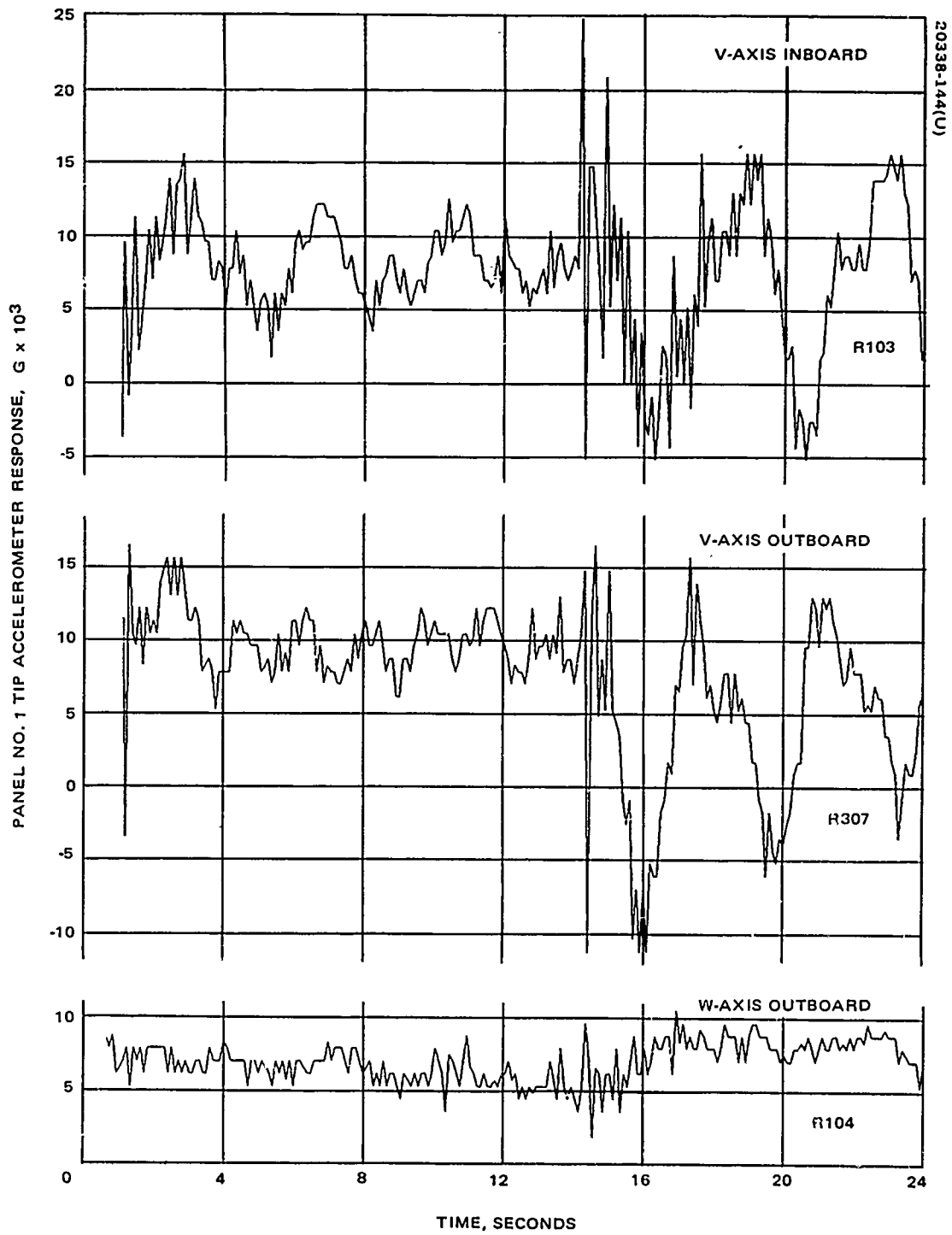


Figure 6-10. Accelerometer Time Histories for FRUSA Slew Maneuver on Revolution 79

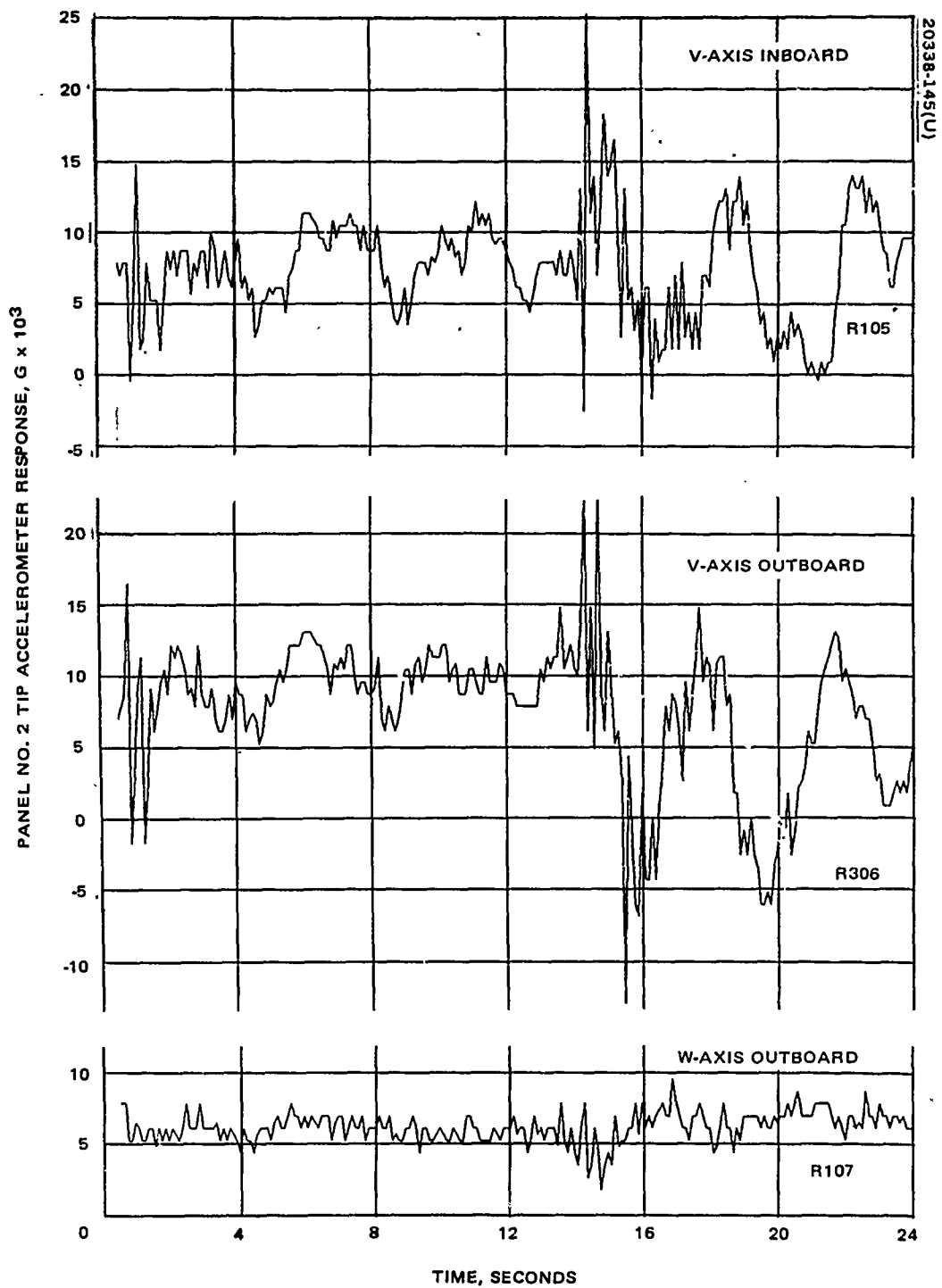


Figure 6-10 (continued). Accelerometer Time Histories for FRUŠA Slew Maneuver on Revolution 79

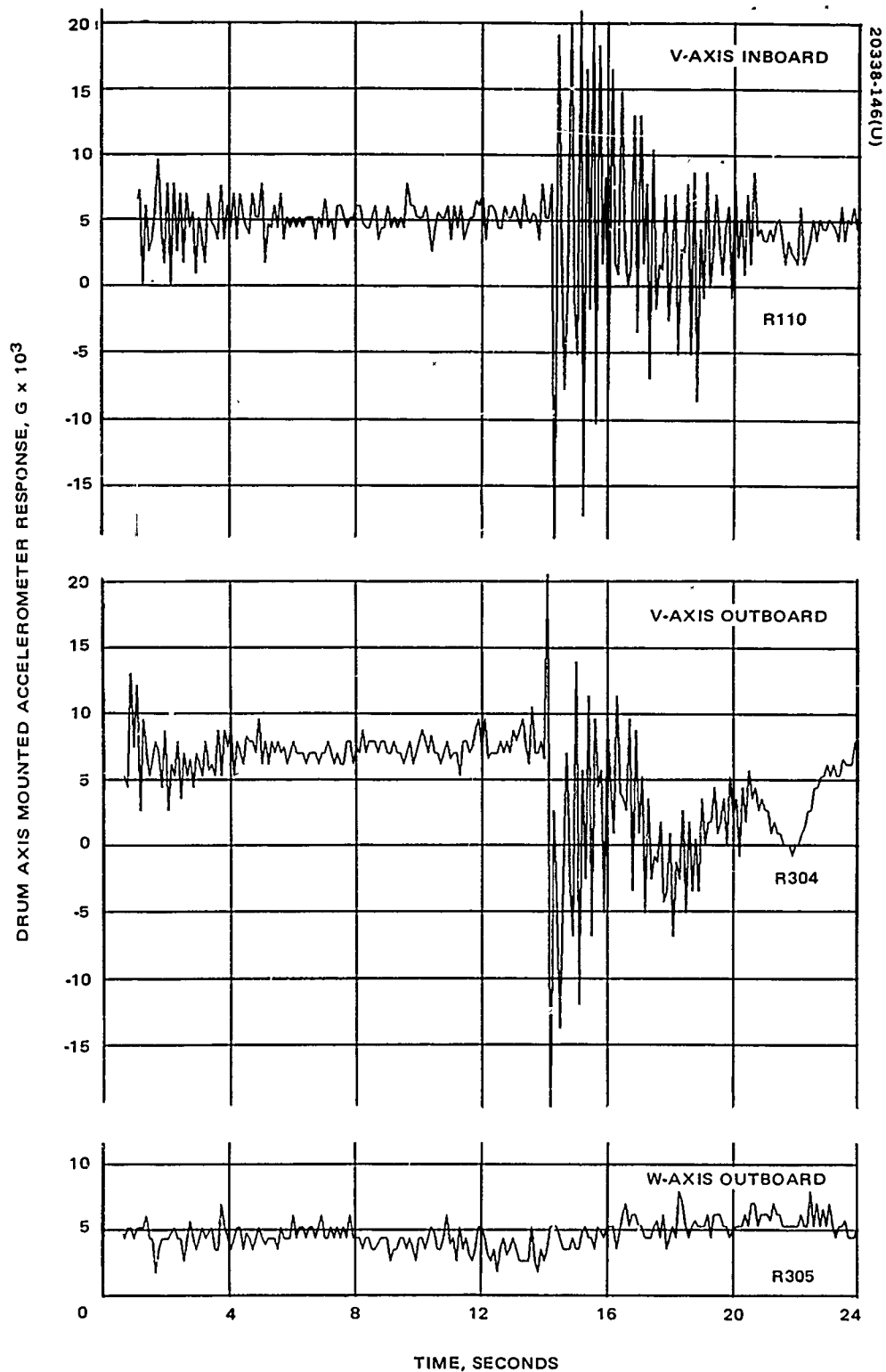


Figure 6-10 (concluded). Accelerometer Time Histories for FRUSA Slew Maneuver on Revolution 79

A 4- to 5-Hz structural frequency was monitored by all transducers upon torque step applications. The amplitude of this high frequency vibration was most dominant at the drum inboard accelerometer, and was reduced in level at the outboard drum accelerometer. The panel tip transducers show considerably lower response in this 5-Hz vibration. It is assumed that the drum and support shaft bearing assemblies were the source for this vibration, since considerable damping was indicated in the decay of this vibratory mode. This high frequency vibration seems to be superimposed on a fundamental array mode of about 0.25 Hz, as exhibited by the transient time histories of Figure 6-10.

This measured frequency compares with a predicted first panel bending frequency of 0.21 Hz for a support boom of  $EI = 60,000 \text{ in}^2\text{-lb}$  stiffness. The prediction, however, was based on a rigid panel support at the drum. As can be seen by superposition of the transients from the transducers R103, R110, and R105, as well as from R307, R304, and R306, the drum is moving out of phase with respect to the panel tips (first flopping mode). Analysis of a simplified three-mass model which assumes the array completely freed from the space vehicle does show that the first bending frequency increases when the panel constraint is reduced, as exhibited by reducing the dynamic inertia of the drum mass  $M$  (Figure 6-11).

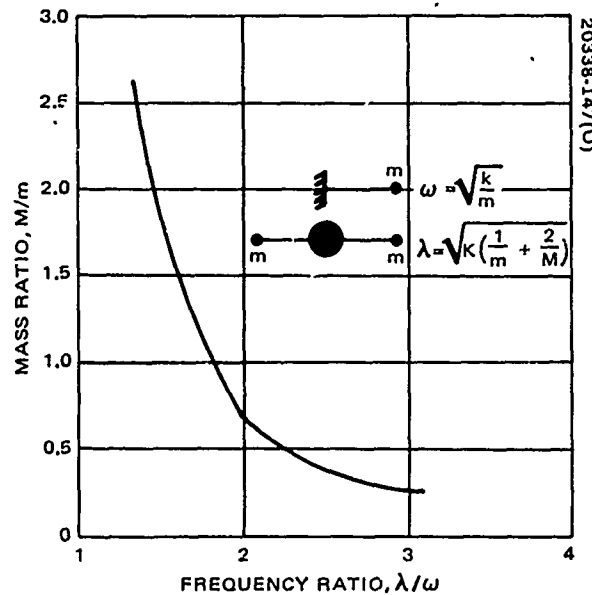


Figure 6-11. Increase in Array Fundamental Bending Mode Due to Reduced Fixity at Drum as Computed for Simplified Mass Model



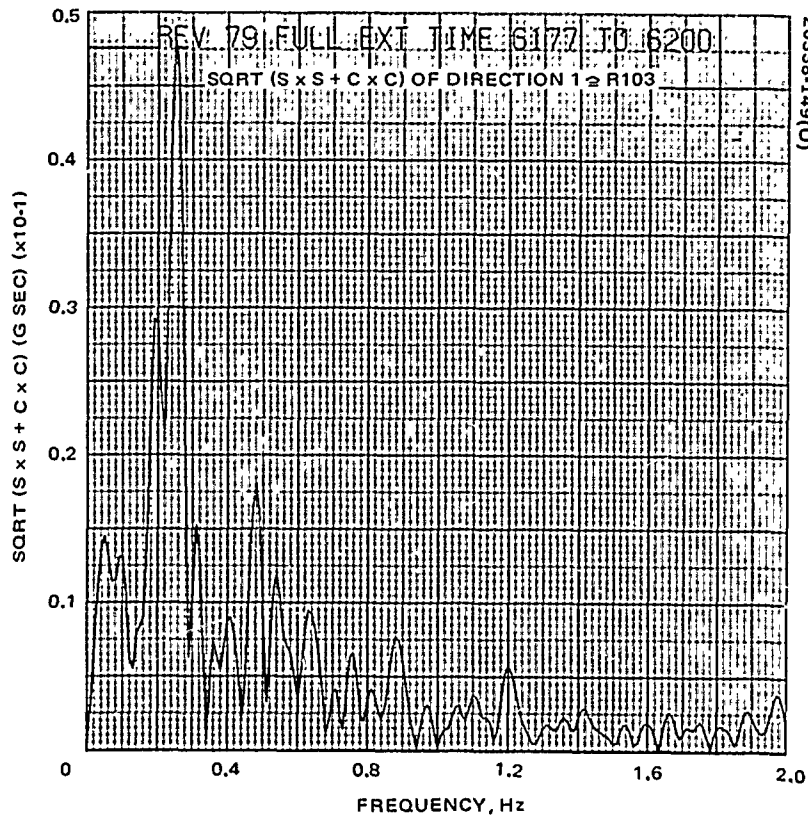
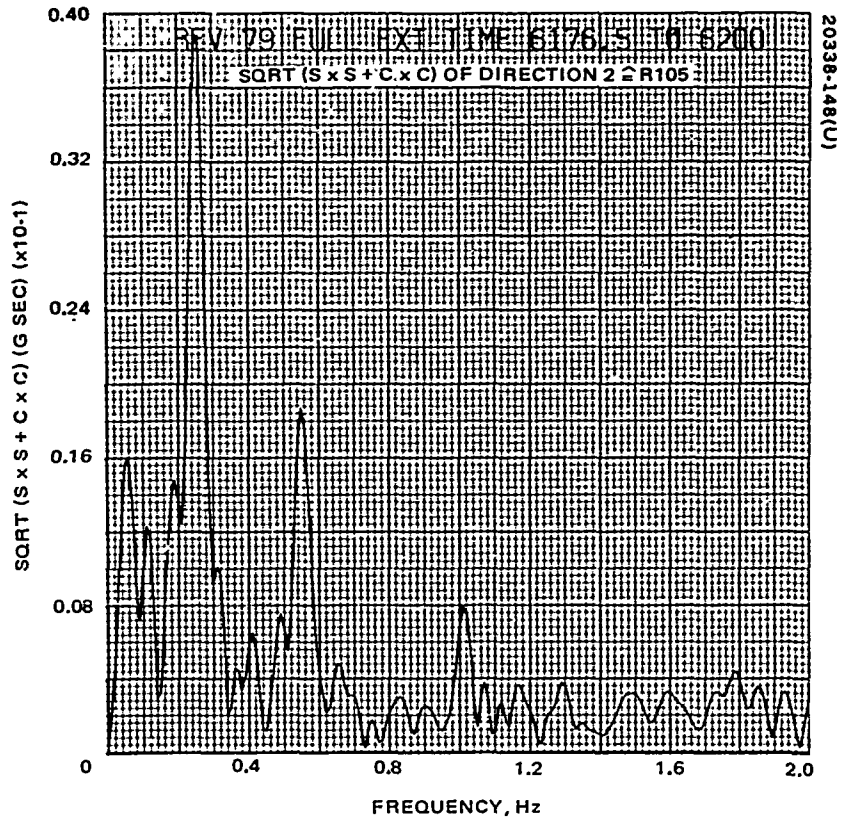


Figure 6-12. Typical Fourier Analysis Frequency Decomposition of Acceleration Time Histories From Revolution 79

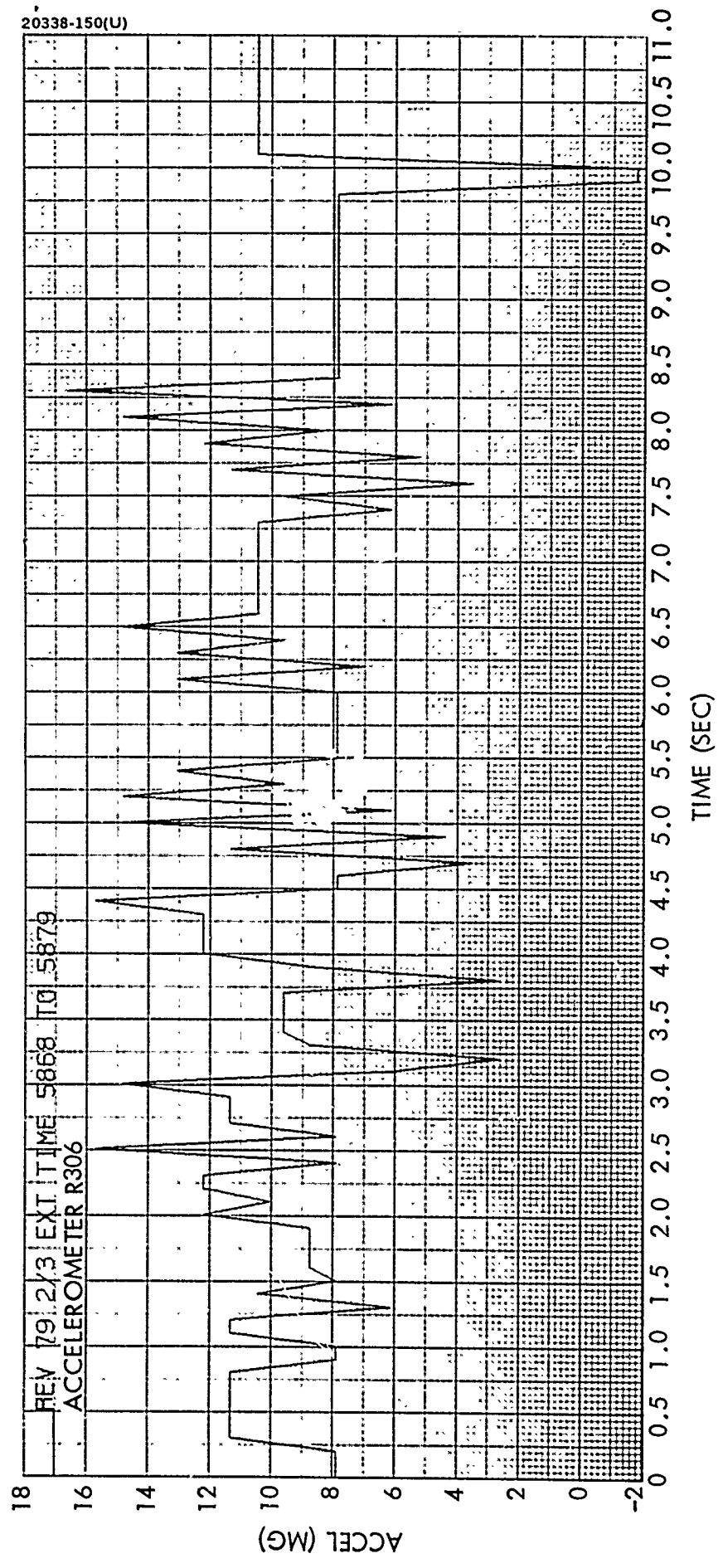
The amplitude of array dynamic tip response to a step excitation of 2.5 milli-g applied at the drum end was predicted to be about 4 inches. The measured tip deflection as computed by using the boom tip accelerometer dynamic response is considerably less because of the greater fundamental frequency of 0.25 Hz. This low dynamic deflection response is further borne out by the boom root bending load cell, which showed only once during the array slew in revolution 79, a bending moment change of 2 in. -lb.

The damping of the 0.25-Hz frequency mode is computed to be about 2 percent on the basis of the 23 seconds of transient traces. This level of damping is about an order of magnitude greater than was expected by accounting for boom damping only. The relatively high level of damping reduced the dynamic response of the array considerably.

The array instrumentation is mainly arranged to allow monitoring of the fundamental array modes (bending and torsion). It appears, however, from the Fourier frequency decomposition analysis (see Figure 6-12 and Appendix B) that the accelerometer transducers show a significant response at about 0.55 Hz, which is predicted to be the frequency of the second symmetric bending mode. This mode is principally a panel mode (booms essentially rigid). The third vibration mode is predicted to fall at 0.91 Hz. This mode is also indicated in the flight data reduction, however, with a considerably lower amplitude (Figure 6-12).

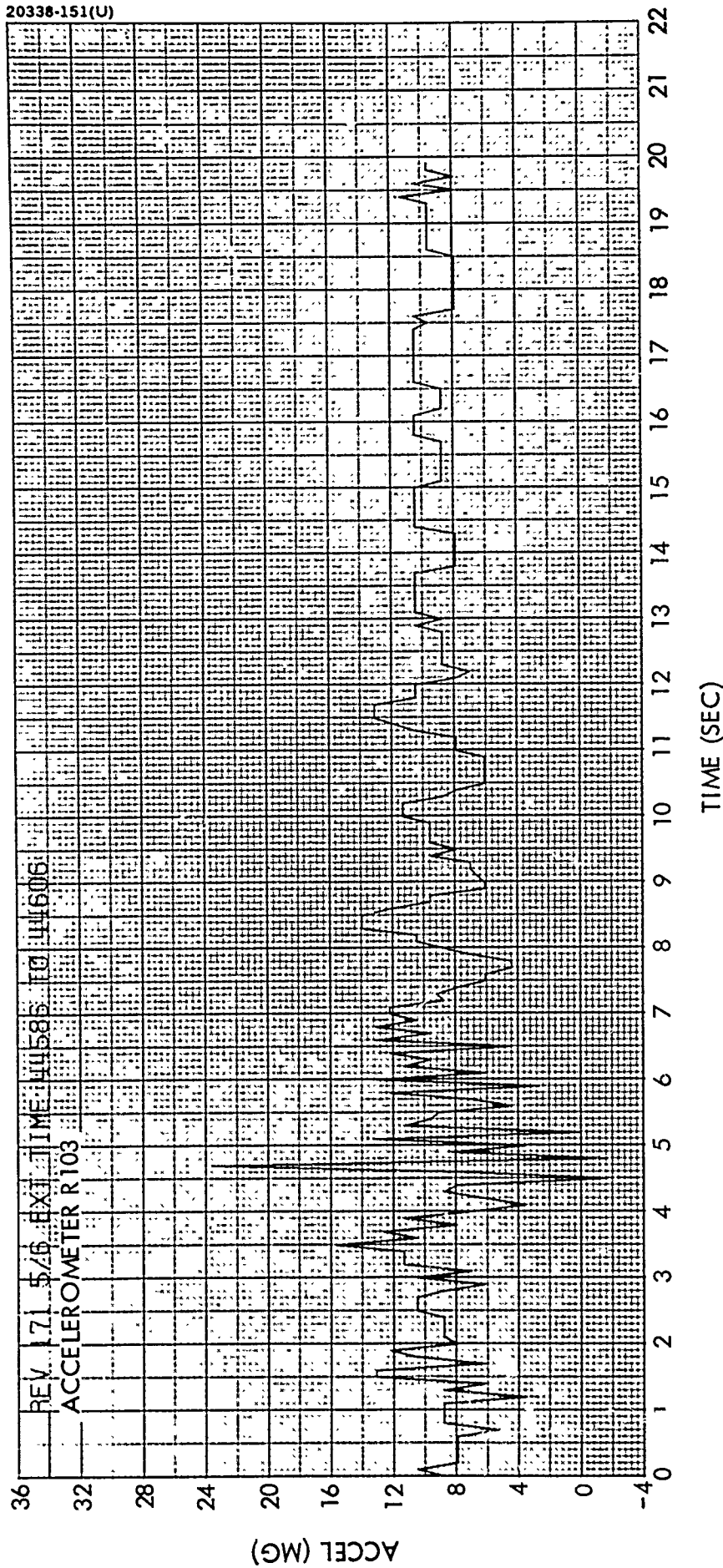
#### Partially Extended Array Response

Changes in the power demand required reduction of the flexible arrays to 5/6 and 2/3 of their full panel length during the FRUSA mission life. The array dynamic responses for the reduced panel sizes were monitored; however, there were no specific control maneuvers, nor active sun tracking while the array was partially extended. In the search for periods of some array dynamic motion, transducer time histories immediately at termination of retraction were chosen for analysis. These time histories (acceleration versus time for the out-of-plane, tip accelerometers) are illustrated in Figure 6-13 and the Fourier decomposition is shown in Figure 6-14. Although the transducer response is extremely low and the duration of indicated array vibration is only about 15 seconds, modal analysis has yielded useful results. The frequencies identified by Fourier analysis for the first three array vibration modes agree well with predictions (Table 6-7).



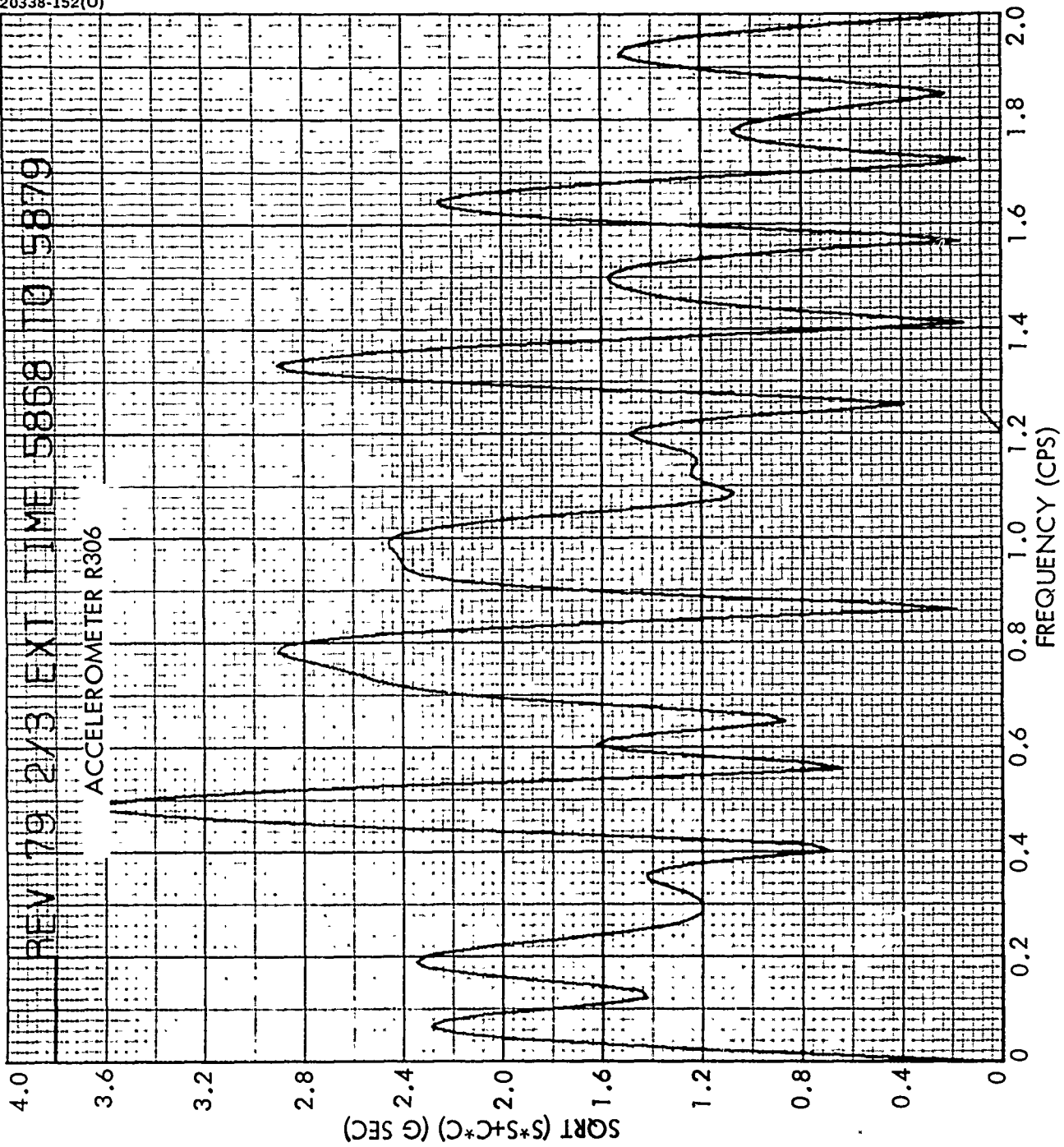
a) For 2/3 Extended Array (Revolution 79)

Figure 6-13. Accelerometer Time History



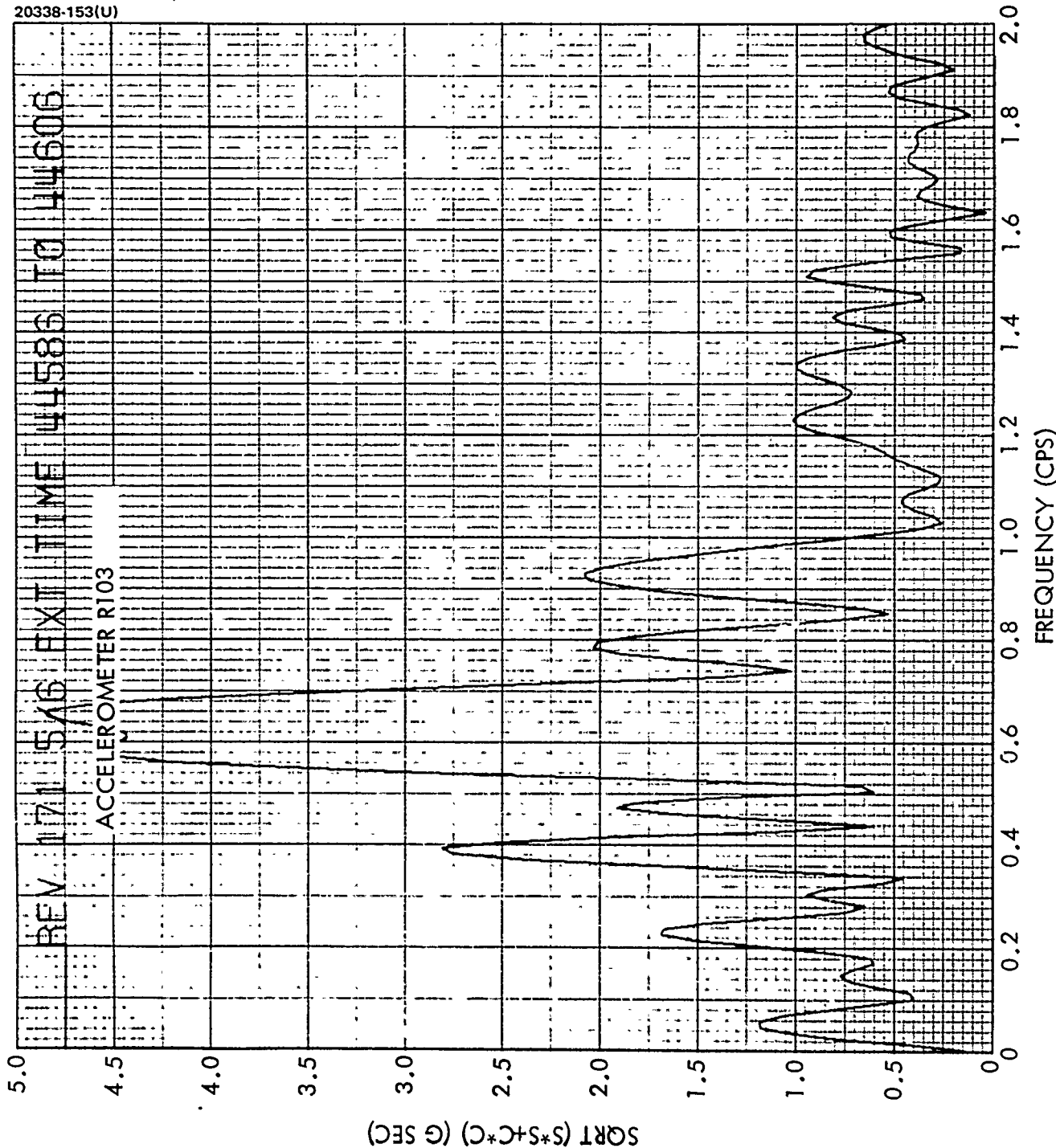
b) For 5/6 Extended Array (Revolution 171)

Figure 6-13 (concluded). Accelerometer Time History



a) For 2/3 Extended Case

Figure 6-14. Fourier Analysis Frequency Decomposition of Acceleration Time History



b) For 5/6 Extended Case

Figure 6-14 (concluded). Fourier Analysis Frequency Decomposition of Acceleration Time History

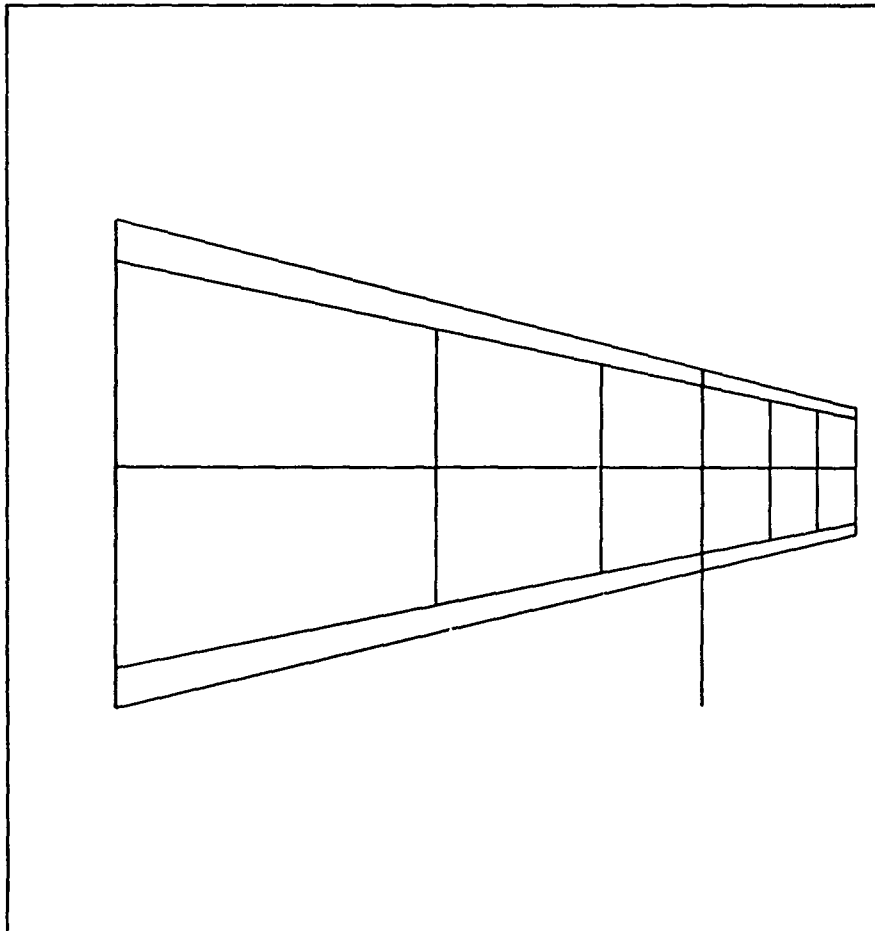


Figure 6-15. Finite Element Model of FRUSA Flight Configuration

## Finite Element Modeling

The continuum mechanics method of predicting vibrational frequencies of the unfurled FRUSA has proved its worth, as shown by the comparisons of predictions with observed in-orbit data (Table 6-7). However, it was felt that, in order to adequately investigate some aspects of flexible solar array designs, a finite element approach to FRUSA dynamics would be worthwhile. This would permit study of the effects of unequal boom stiffnesses, panel bending stiffness, and flexible supporting structure on the vibrational behavior of flexible arrays.

An existing Hughes program, the MARS (Matrix Analysis Routine for Structures) finite element computer program, was modified to accommodate flexible array structures. The modifications consisted of adding incremental stiffness matrix routines to the program; these routines add new terms to the element stiffness matrices to account for the stiffening or weakening effect of preloads in a structure\*. These preload effects have a strong influence on the dynamic behavior of FRUSA structures.

The finite element model of the FRUSA flight configuration generated for these investigations is shown in Figure 6-15 (this figure is taken from a CRT Computer Graphics Terminal display). The model consists of 36 mass points, connected by 25 beams and 12 plate elements. The initial investigations incorporated the flexibility of the OLSCA support structure, but the freedom of motion afforded by the bearing/motor combinations was neglected. These first runs assumed fully extended solar panels.

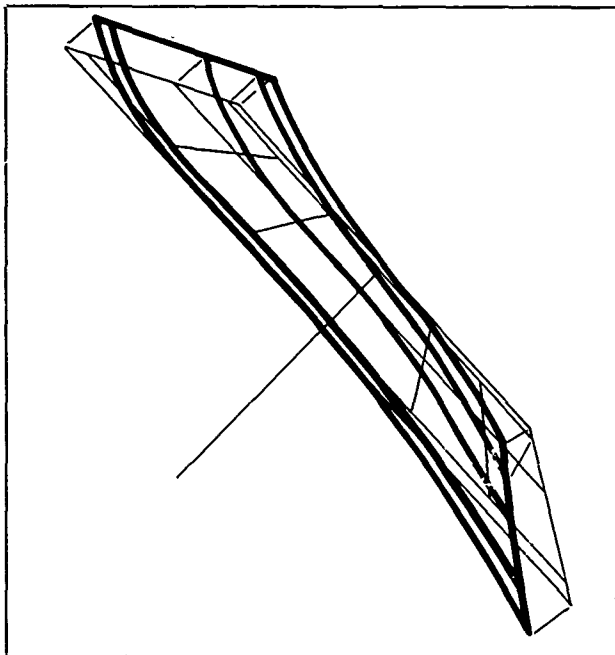
The results obtained from computer runs using this model yield, first, a group of four close frequencies representing out-of-plane bending and torsion modes of the FRUSA. The mode shapes for these four modes are shown in Figure 6-16. The numerical values of the lowest bending modes are quite close to those obtained from the continuum mechanics analysis. Further, study of the Fourier decompositions of flight data did indeed reveal the presence of several frequencies near the frequency range for the four lowest modes predicted by the present analysis.

As for higher order modes, the finite element analysis predicted frequencies of 0.42 and 0.57 cps for the second and third out-of-plane bending frequencies, as compared to the continuum mechanics predictions (partially verified by the flight data) of 0.55 and 0.9 cps, respectively (Table 6-7). These large errors are due to the relative crudity of the finite element model. These higher modes involve, principally, large scale ripples of the tensioned panel; and these modes are inadequately approximated by the small number of nodes on each panel in the model. Hence, a more accurate representation of the higher order bending modes of the FRUSA will require a more detailed finite element model of the structure, using perhaps twice as many nodal points.

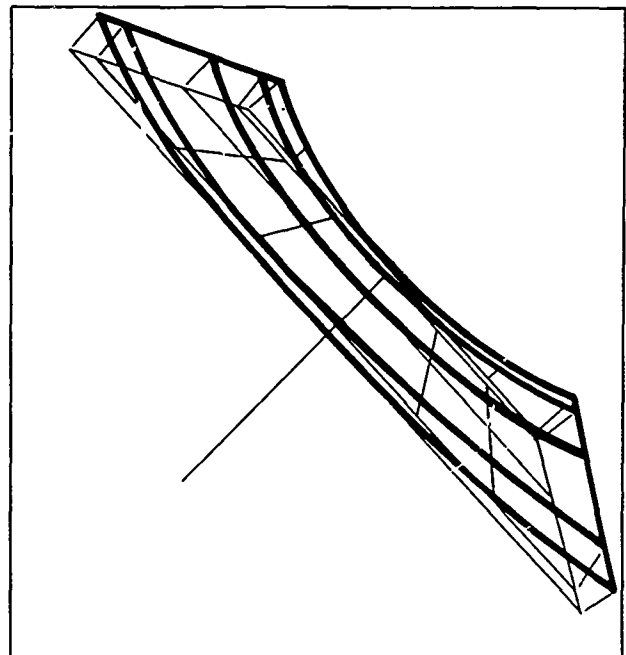
---

\*Przemieniecki, J. S., Theory of Matrix Structural Analysis, McGraw-Hill (1968), pp. 383-407.

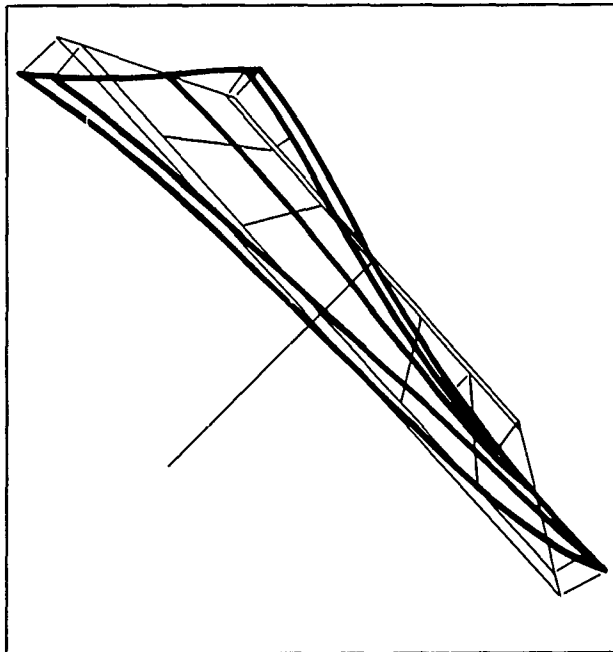




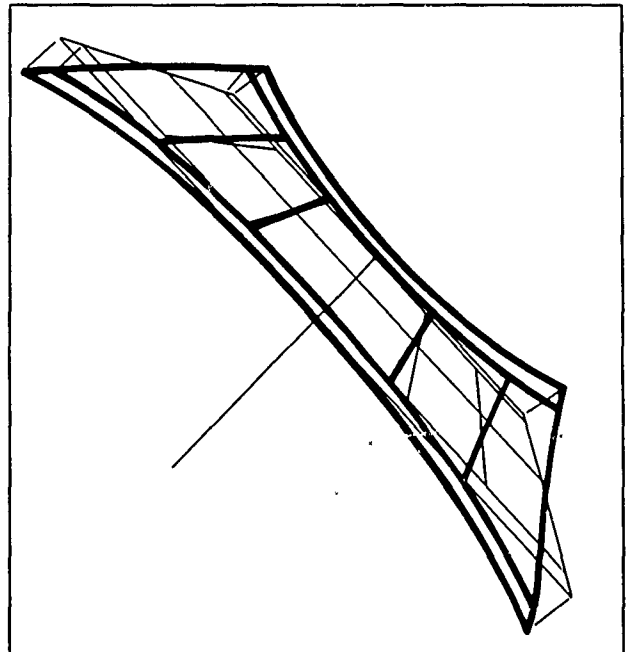
20338-217(U)



20338-218(U)



20338-219(U)



20338-220(U)

Figure 6-16. Out-of-Plane Bending and Torsion Modes of FRUSA Finite Element Model

Thus, although the finite element method shows great promise for use in investigating effects, such as support structure flexibility and degrees of freedom, which cannot be easily treated by continuum mechanics methods, much more detail must be employed in the finite element modeling than has been used in these initial studies. These studies also indicate that the continuum mechanics approach is adequate and, indeed, is more efficient for preliminary design studies of conceptual FRUSA systems. However, for more advanced design stages, such as control system syntheses, for which flexible solar array structural transfer functions are required, the finite element approach promises to provide much more accurate numerical values of these parameters than does the continuum mechanics method.

## SECTION VII

### RELIABILITY/MAINTAINABILITY

The reliability goal for the FRUSA program was 0.65 for 1 year. The reliability estimate for each subsystem is shown in Figure 7-1. The total system reliability is shown to be 0.695 for a 1-year mission life. Re-estimated for an operational system, without the instrumentation subsystem, the reliability estimate for the present FRUSA is 0.742 for a 1-year mission life.

The anomalies observed on the FRUSA flight do not invalidate the above estimate because of their nature, as discussed in section VIII of this report.

#### IN-FLIGHT ANOMALIES

Three equipment anomalies were observed during the FRUSA flight. Commutator A, which was located on the solar array inboard actuator housing, and Commutator D, located on the outboard actuator, failed. These commutators, while not required for overall system performance, provided dynamic, thermal, and electrical performance data of the solar array subsystem.

Except for a vendor modification to permit external clock pulse synchronization to enable compatibility with the spacecraft PCM system, the commutators were standard 45-word PAM that had been flown on numerous space vehicles. The failures of these units have been attributed to a breakdown of the silicon oxide coating in the MEM R-S-T flip flop circuit added to accept external clock pulses. Failure of this circuit would prevent proper reset of the commutator clock. Possible causes of the breakdown are poor quality control procedures at manufacture, excessive heat load of the device, or high EMI pulses due to insufficient filtering of system noise (in particular, that resulting from another spacecraft experiment, the ONR-001).

The third anomaly involved the control electronics unit (CEU) which was mounted to the orientation mechanism. This unit showed anomalous behavior when subjected to excessive heat loading. Although operated at 35°F above qualification temperature (120°F), the unit would be expected to operate in a normal manner. The problem appears to be a poor connection to or inside a microcircuit that is heat sensitive, as demonstrated by later flight experience wherein the CEU has operated normally on every sun acquisition or tracking operation when the unit is operated within the qualification temperature range.

These failures do not invalidate the previous reliability analysis, since the CEU was subjected to excessive heat loading. In addition, although the commutators are not required for operational mission success, quality

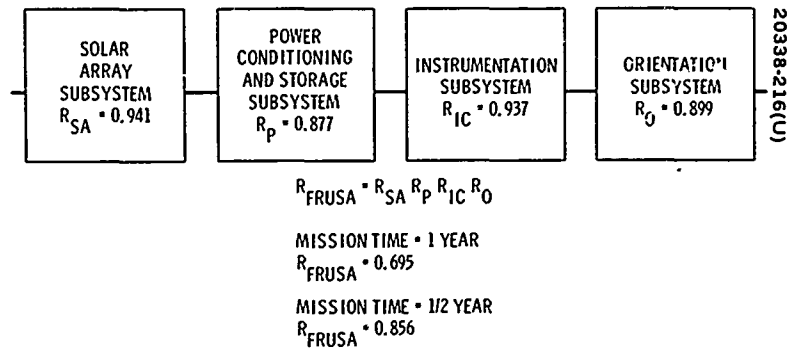


Figure 7-1. System Reliability Block Diagram

assurance of the MEM device can be improved and confidence tests run, now that the failure mode is understood.

#### RECOMMENDATIONS

On future systems, stringent quality control requirements would be imposed on the commutator vendor in addition to requiring unit redundancy for critical data.

Although the CEU operated normally within its qualification specification environment, future systems would have redundant CEUs qualified at a higher temperature.

#### MAINTAINABILITY

A final estimate has been made of the mean time to repair. The analysis is in accordance with the requirements of MIL Handbook 472, Procedure IV (Maintainability Prediction). For the purpose of this analysis, MTTR is defined as the average corrective maintenance time to isolate a failure, remove the failed item, install an interchangeable item or repair the failed item, and retest to assure that the equipment has been restored to the same status that existed prior to the failure.

The MTTR estimate, Table 7-1, shows that the design goal of 4 days will easily be met. Table 7-2 lists, for the various modes of failure of a solar cell panel, estimates of the minimum, mean, and maximum times to repair. The overall solar cell panel MTTR estimate was calculated as shown in Table 7-3.

TABLE 7-1. FRUSA MTTR ESTIMATE

FRUSA Subsystem Unit	Number of Units	MTTR <sub>i</sub> , hours	λ <sub>i</sub> (per 10 <sup>5</sup> hours)
<b>Solar Array Subsystem</b>			
Drum mechanism	1	56	1.8
Array panel	2	6.0	0.001
<b>Power Conditioning and Storage Subsystem</b>			
Battery assembly	2	4.5	0.910
Power conditioning unit	1	40	0.604
Charge controller	2	4.5	0.223
<b>Instrumentation Subsystem</b>			
Accelerometer	1	3.5	0.0625
Instrumentation conditioning unit	1	20	0.033
Commutator	2	20	0.255
<b>Orientation Linkage System</b>			
Orientation mechanism	1	56	1.2
Control electronics unit	1	40	2.2
Sun sensor	1	3.0	0.0045

$$\text{MTTR} = \frac{\sum_{i=1}^{15} \lambda_i \text{MTTR}_i}{\sum_{i=1}^{15} \lambda_i} = \frac{300.1 \times 10^{-5}}{8.87 \times 10^{-5}} = 33.83 \text{ hours}$$

TABLE 7-2. SOLAR CELL PANEL ACTUAL REPAIR TIME ESTIMATES

Case	Failed Item	Fault	How Discovered	Minimum, hours	MTTR, hours	Maximum, hours	Failure Rate
1	Cells	Cracked, cover broken, plating off back	Electrical test	4.33	5.75	7.58	$\lambda$
2	Cells	Cracked, cover broken, plating off back	Visual inspection	4.33	5.25	6.58	$\lambda$
3	Cells	Peeled from substrate	Visual inspection	3.75	4.25	5.17	1/10 $\lambda$
4	Bus contacts	Broken off	Electrical test	1.17	2.25	3.33	1/20 $\lambda$
5	Bus contacts	Broken off	Visual inspection	1.00	2.00	3.00	1/10 $\lambda$
6	Bus	Broken through	Electrical test	4.83	7.00	10.67	1/100 $\lambda$
7	Bus	Broken through	Visual inspection	4.58	6.00	7.67	1/100 $\lambda$
8	Substrate	Torn	Visual inspection	4.08	5.50	7.50	1/100 $\lambda$

TABLE 7-3. OVERALL SOLAR CELL PANEL MTTR ESTIMATE

Case	MTTR <sub>i</sub> (hr.)	λ <sub>i</sub> (per 10 <sup>5</sup> hr)	MTTR <sub>i</sub> λ <sub>i</sub> (per 10 <sup>5</sup> hr)
1	5.75	1.0λ	5.75λ
2	5.25	1.5 λ	5.25λ
3	4.25	0.1λ	0.425λ
4	2.25	0.05λ	0.112λ
5	2.00	0.1λ	0.200λ
6	7.00	0.01λ	0.070λ
7	6.00	0.01λ	0.060λ
8	5.50	<u>0.01λ</u>	<u>0.055λ</u>
		2.28λ	11.922λ

$$MTTR' = \frac{\sum_{i=1}^8 MTTR_i \lambda_i}{\sum_{i=1}^8 \lambda_i} = \frac{11.922\lambda \times 10^{-5}}{2.28\lambda \times 10^{-5}} = 5.2 \text{ hr (not including administrative and logistic downtimes)}$$

$$MTTR = 5.2 + 0.8 = 6.0 \text{ hr. (including administrative and logistic downtimes)}$$

The FRUSA mean time to repair was calculated from:

$$MTTR = \frac{\sum_{i=1}^n \lambda_i MTTR_i}{\sum_{i=1}^n \lambda_i}$$

where

$MTTR_i$  = subsystem unit mean time to repair

$\lambda_i$  = subsystem unit failure rate

$n$  = number of subsystem units of the FRUSA



## SECTION VIII

### FIVE KW DESIGN STUDY

The configuration selected for the 5-kw array system and the qualitative tradeoffs that led to the selection are illustrated in Figure 8-1. The system employs a central orientation mechanism and an array on each side. Each array consists of two 5.5- by 25-foot panels. The panels are wound onto two 8 inch diameter drums, which in turn are nested alongside the space vehicle during launch. These drums are sequentially released in orbit from their space vehicle support brackets by activating explosive tie-down bolts. When both drums are positioned and locked normal to the orientation mechanism support axis, the array panels are unrolled by four 25-foot long extendible booms on each array assembly.

The orientation and drum mechanisms of this 5-kw array system are essentially identical to those of the flight-qualified FRUSA design. In order to accomplish the 5-kw power output, the number of array panels has been doubled and the panel length increased from 16 to 25 feet. The current FRUSA panel width is maintained because of the assumed design requirement for an identical array voltage. A weight breakdown and summary are provided in Table 8-1 for the 5-kw array system. These weights are realistic since they are based on flight-qualified hardware without relying on lightweight cells. On the general figure of merit scale, as expressed by watts of power per pound of weight, the 5-kw array achieves 26.2 and 18.5 w/lb for the solar array exclusive and inclusive of the orientation mechanism, respectively. The array stowage volume figure of merit is 1.75 ft<sup>3</sup>/kw, which compares with the requirement of 2 ft<sup>3</sup>/kw.

The design goal of 30 w/lb for roll-up solar arrays can be achieved merely by using lightweight solar cells. Further improvement of the figure of merit is possible by using lightweight materials in the drum and boom actuator structure assemblies.

#### DESIGN CRITERIA AND REQUIREMENTS

The general criteria and requirements for the 5-kw array system were assumed to be identical to those for the FRUSA system. In particular, the panel voltage and electrical design, the retraction capability, and the two-axis sun acquisition and tracking features are retained. The orientation subsystem provides for continuous, 360-degree sun-normal tracking of the solar array panels. A complement of sliprings for power transfer between the array and the space vehicle and for control system signal transfer across the axes of rotation is provided.

The array and its support structure must be capable of sustaining 0.1-g quasi-static acceleration loading in orbit. The structural design requirements for the array during launch and ascent are those specified for

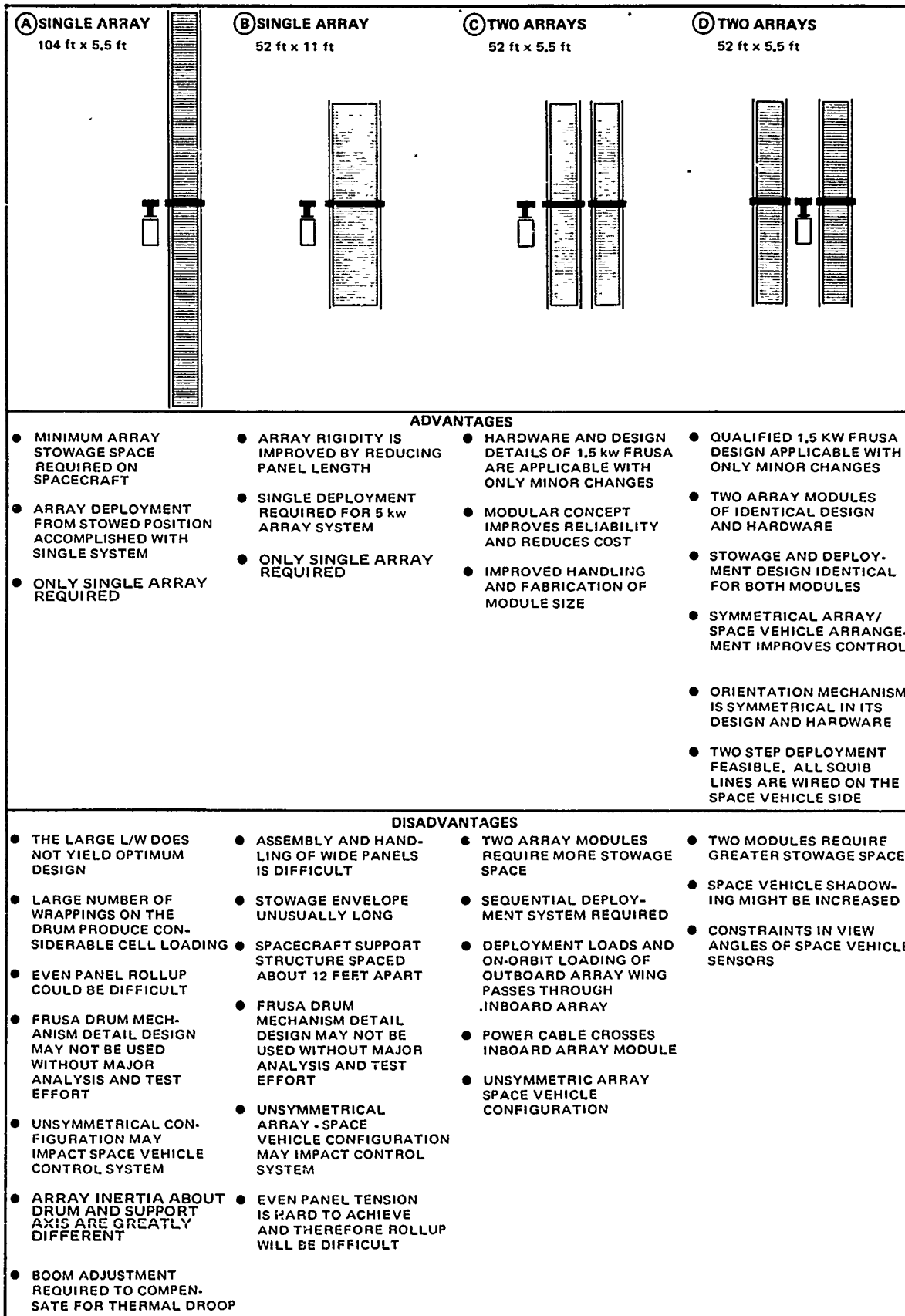


Figure 8-1. Comparison of Array Configurations for 5 kw Power System Design

TABLE 8-1. WEIGHT SUMMARY FOR FRUSA AND 5-KW ARRAY

	FRUSA	5-kw Array	Remarks
<u>Orientation Subsystem</u>			
Housings	4.3	4.3	
Shafts	3.6	5.2	
Deployment mechanism	3.2	6.4	
Bearings	5.8	5.8	
Motors	10.4	10.4	
Tachometers	3.2	3.2	
Slipring assemblies	11.0	13.0	
Sun sensors	1.0	1.0	
Miscellaneous hardware and cabling	13.8	16.0	
Electronics	<u>15.0</u>	<u>15.0</u>	
	71.3	80.3	
<u>Solar Array Subsystem</u>			
Solar panels	30.1	97.5	2 x 2 cm, 8-mil cell and 6-mil cover.
Composite substrate	4.3	13.8	Includes cell bonding adhesive.
Cushion	1.5	4.8	
Storage drum	3.4	8.4	
Bearings and housings	2.8	5.6	
Spar	1.5	3.0	
Torque springs	1.3	4.6	
Power cable	0.7	1.4	
Boom actuator assembly	17.4	39.2	Includes booms
Cushion reel and supports	1.0	1.9	
Cushion reel drive	0.5	1.5	
Spreader bars	1.9	3.0	
Boom length compensator	0.6	1.2	
Miscellaneous hardware	2.2	3.6	
Arm, orientation mechanism	<u>0.4</u>	<u>0.7</u>	
	70.1	190.2	
<u>Total</u>	141.4	270.5	

component design for Titan IIIC payloads. In brief form, the random vibration requirement is 19.5 g rms; the quasi-static acceleration levels are  $\pm 10$  g in the longitudinal and  $\pm 2.5$  g in the lateral direction relative to the boost vehicle axes. (These quasi-static load levels were augmented to  $\pm 13.5$  and  $\pm 3.8$  g in the FRUSA design in order to cover the STP 71-2 Thorad/Agema specific loading conditions.)

Stowage volume requirements are 2 ft<sup>3</sup>/kw and the figure of merit weight objective is 30 w/lb for the solar array assembly (excluding orientation components).

## SUBSYSTEM DESCRIPTION

A complete array power system consists of the solar panels, the drum stowage and panel support structure, an array orientation mechanism, and battery/power conditioning subsystems. The battery/power conditioning subsystem is excluded from this design effort because its design is more dependent on space vehicle payload requirements than on array size or configuration. The individual subsystems and the tradeoffs which influenced their configuration and sizing are described in the following paragraphs.

### Orientation Mechanism

The two-axis orientation mechanism employed by the 1.5-kw FRUSA flight experiment was designed for a 5-kw array size. In its present configuration (see Figure 8-2), it is adaptable for a two-wing array system by merely extending the drum-axis shaft to both sides of the support axis shaft. A duplicate for the array deployment linkage is needed. Bearings and other structural elements have been dimensioned for stiffness rather than strength and therefore are adequate for the larger array size.

Sun sensors are functional units unaffected by system power. The unit developed for the 1.5-kw FRUSA is employed for a 5-kw system without change.

Control electronics for the 5-kw system are similarly identical to the 1.5-kw unit. Because of the large number of components, this is the least reliable unit in the orientation subsystem; for mission lifetimes in excess of 1 year, provision of a redundant unit is indicated. This can be accommodated by an additional pair of support pads on the opposite side of the support-axis housing, with appropriate intercabling and command switching.

Structural details of the mechanism, aside from the obvious two-way extension of the drum axis shaft, change little from the 1.5-kw design. The primary change required is to open up the passages in the component spacers to accommodate an increase in the number and total cross-sectional area of the power conductors.

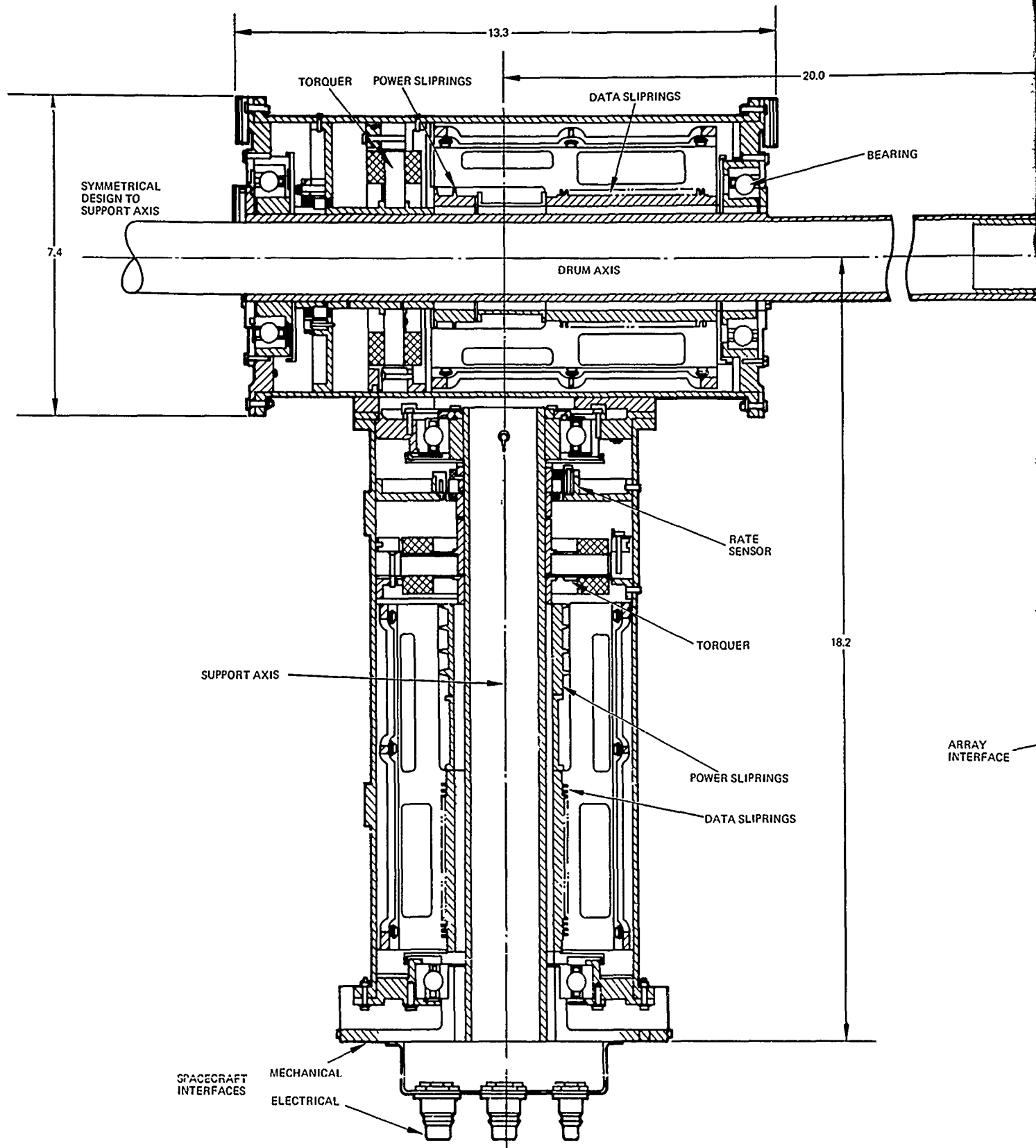
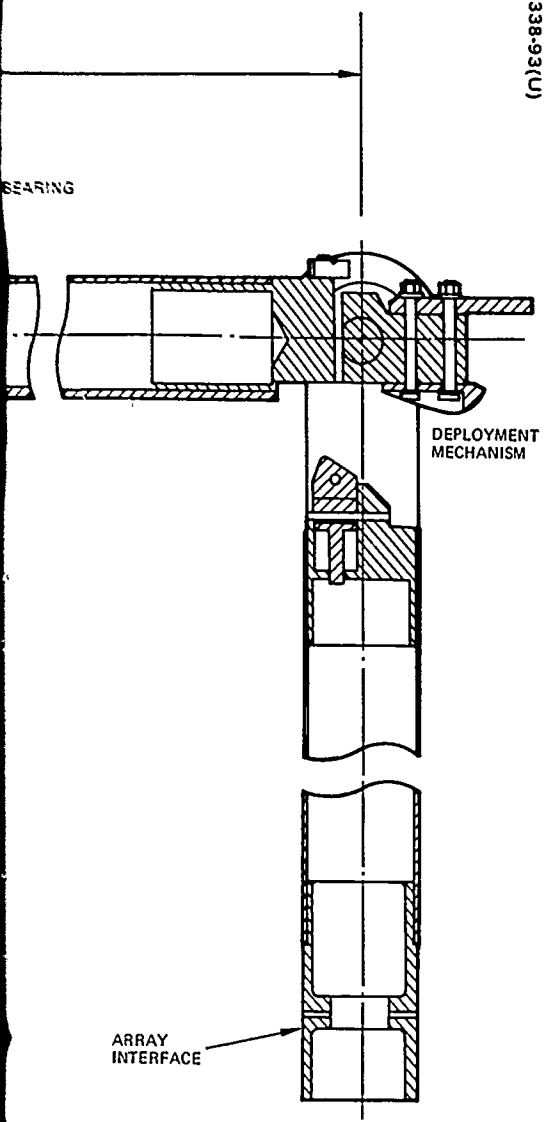


Figure 8-2. FRUSA Orientation Mechanism Cross Section



2038-93(U)



Longer booms present no problem to the orientation controls per se. However, it will be necessary to maintain the frequency separation between fundamental boom vibration modes and upper end of the control-loop band-pass. Adjustment of control parameters is implemented by selection of relative sizes of a few components, such as resistors and capacitors, rather than by any fundamental design changes.

Torquer size, for the restricted range from 1.5- to 5-kw mechanisms, is primarily a function of axis friction and the torque margin desired over worst case conditions. Friction is contributed by the gimbal bearings and the power and signal transfer brushes. Secondarily, the time to accelerate to slew speed is a function of motor torque, but this time is so short for the 1.5-kw FRUSA (on the order of 1 second) that a moderate increase due to greater 5 kw array inertia is of little consequence to performance.

Bearings and bearing friction will be identical for both 1.5 and 5 kw designs. Approximately the same number of signal rings would be used, with a similar contribution to friction. Additional power-transfer rings and brushes will tend to increase axis friction if the same brush pressure is maintained. The 1.5-kw system was conservative in this respect; brush pressure and friction could be reduced by a factor of two, thus compensating approximately for the added number of brushes. In short, 5-kw system friction should not significantly exceed that of the 1.5-kw system, allowing use of the same 2-lb-ft torquer. The FRUSA system, however, is also designed to accept the next model number torquer rated at 4 lb-ft. This unit will certainly cover any contingencies.

Adequate slipping space for a 5-kw system power transfer requirement exists in the 1.5-kw unit housing provided the arrays are not subdivided into too many independent sections, or require many independent circuits for automatic power regulation. Two independent circuits for each of the two arrays, for a total of four circuits (eight sliprings) will be accommodated with the present size housing and conventional power ring designs.

#### Solar Panel Description

The 1.5-kw FRUSA system employs two solar cell panels, each 66 inches wide and 182 inches long. The width of the panels is essentially defined by the number of cells required in series to achieve the array design voltage of 28 volts. Since the 5-kw array system is to be configured for the same average voltage level, the width of its panels will also be about 5.5 feet. Multiples of 1.5 or 2 of this basic width might be considered for possible weight savings, but at the expense of the more complicated electric collector bus layout. Minor adjustments in panel width result from the particular choice of solar cells. The FRUSA flight experiment used 2 x 2 cm cells of

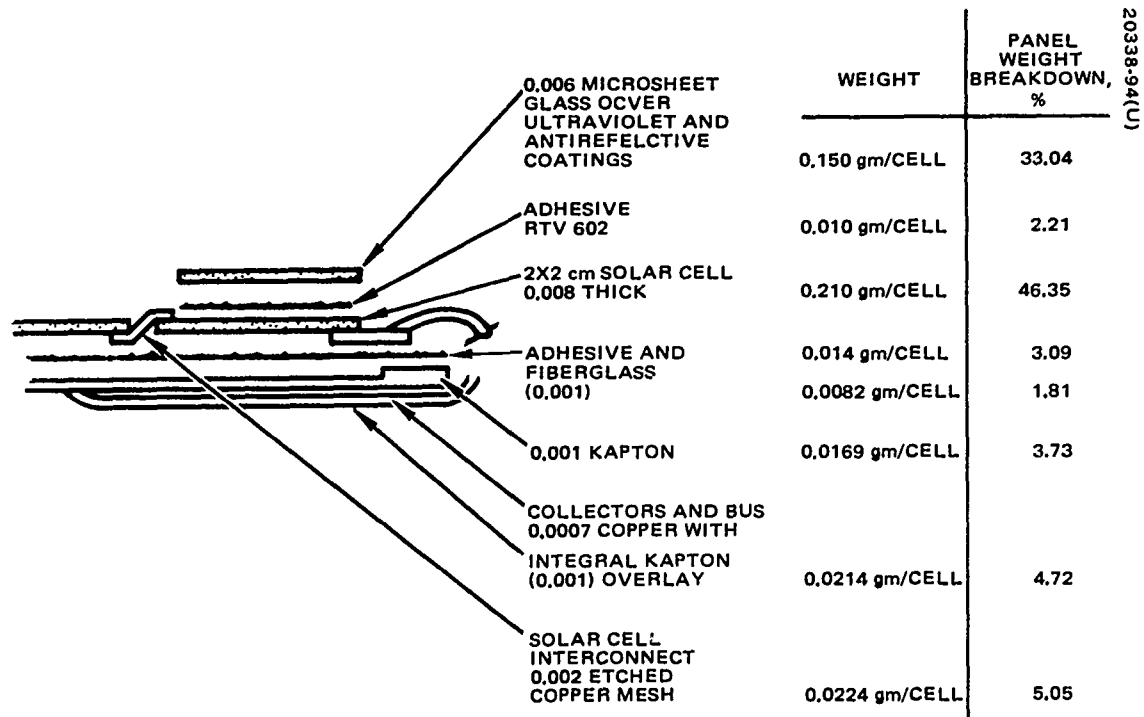


Figure 8-3. Solar Array Panel Configuration and Weight Breakdown



nominal 8-mil thickness. Presently, array designs such as proposed by Hughes for forthcoming Air Force satellite programs are being configured to use 2 x 6 cm solar cells of 8- or 12-mil thickness. Advanced array systems of extremely lightweight design will use 4 mil thick cells with integral cover sheets. The panel width and other pertinent panel design data for these three types of solar cells are listed in Table 8-2. All cell performance data are shown for synchronous orbit conditions (130°F cell temperature) and at the beginning of life (BOL). Details of the panel/substrate configuration are shown in Figure 8-3. This configuration is identical to the FRUSA design.

TABLE 8-2. SOLAR PANEL DESIGN CHARACTERISTICS FOR THREE SOLAR CELL TYPES

	FRUSA	Large Size Cell	Lightweight Cells	Remarks	
Cell size	2 x 2	2 x 6	2 x 2	Thin cell not currently available in production quantities	
Thickness cell/cover, mils	8/6	8/6	4/2		
Number of cells in series	81	31	82		
BOL power output, w/ft <sup>2</sup> *	10	10.2	9.0		
Panel width, inches	66	66	67		
Specific weight, lb/ft <sup>2</sup>	0.19	0.19	0.13		Includes substrate and interconnects
BOL power, w/lb	52	53	70		

\*Cell resistivity is 2 ohm-centimeters.

The cells are interconnected in groups of three in parallel by 81 in series. Instead of installing the blocking diodes that electrically isolate the sectors at the drum end of the panel as was done on FRUSA, flat solar cell-like diodes will be installed on the front of the panel at the positive terminal of each group.

Along the 25-foot panel length, 124 groups are placed with the series direction running along the panel width. The groups will be aligned so that adjacent groups have reversed electrical polarity; the resulting opposite flows of current tend to cancel induced magnetic moments, thus minimizing the net magnetic moments. As with FRUSA, groups will terminate along each edge of the panel. The positive and negative group terminals are then connected to the back side of the panel by 0.0007-inch thick copper ribbon buses; these termination buses wrap around the substrate edge and are soldered to the main conductor buses.

Placing the electric buses on the back side of the panel permits the solar cells to cover completely the front side of the panel. There will be buses running to ten sectors, i. e., each sector will pick up the parallel outputs from 12 or 13 groups. Each sector has four main buses, two negative and two positive. Dividing the panel into ten individual sectors provides redundancy in the main bus systems. The power collector bus is dimensioned such that panel power loss is limited to 5 watts or 1.25 percent loss of the total array power.

On FRUSA, the area covered by the bus material increased toward the root end of the panel. Approximately 35 percent of the 5.5-foot wide panel was covered with the bus material. The panel will be about 65 percent covered with electrical conductor at the root end.

The details of the solar panel are shown in Figure 8-4.

#### Drum Mechanism

The design concept proposed for the 5-kw array system uses two drum mechanisms of the FRUSA flight-qualified design. This configuration is superior to alternate concepts illustrated in Figure 8-1a through 8-1c. The Figure 8-1a concept is in its flight configuration identical to the 1.5-kw FRUSA experiment with the solar panels extended to an overall length of 53 feet for added cell area. The drum mechanism weight for this concept, however, increases considerably due to the boom size required for sustaining a five-fold increase in bending loading at 0.1-g gravity. The boom bending loading is somewhat improved for the alternate single drum concept shown in Figure 8-1b which uses about an 11-foot wide panel of 26 feet length. This array layout, however, requires complete redesign, analysis and testing for all components of the drum mechanism. Additionally, a cylindrical stowage volume and structural support for a relatively long drum are not readily available on space vehicles.

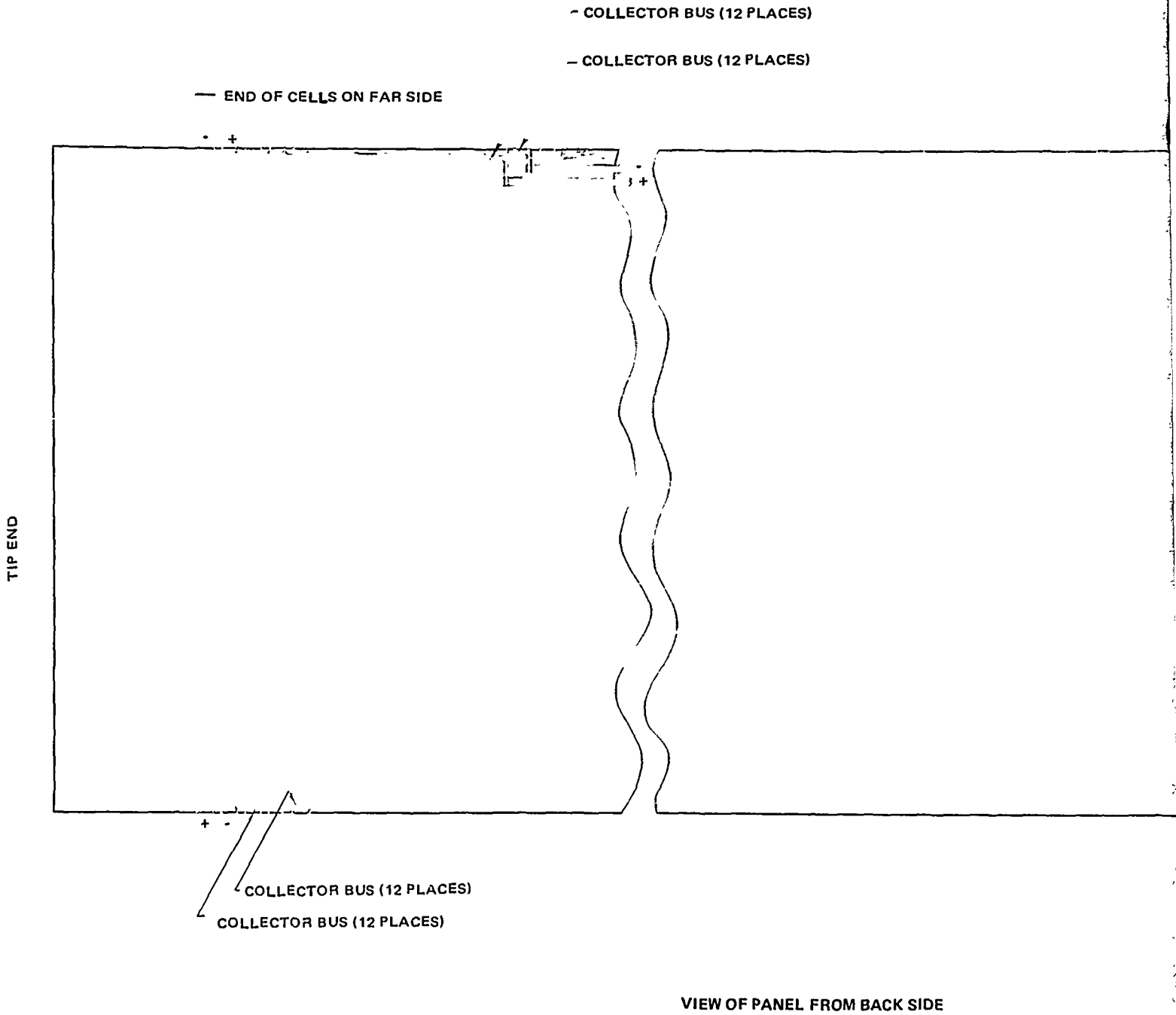
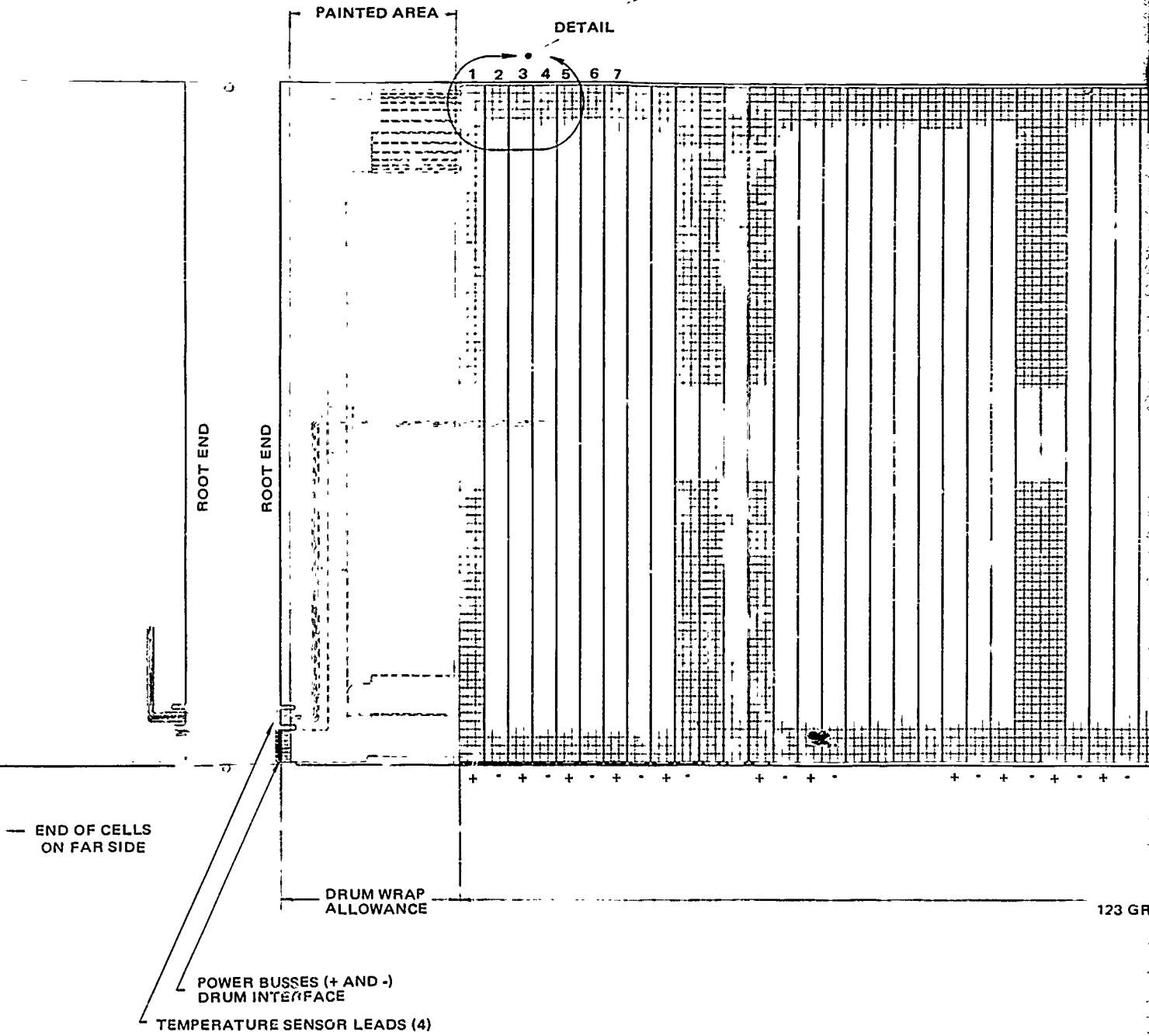
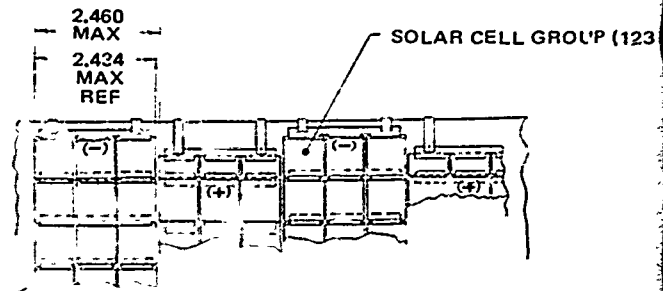
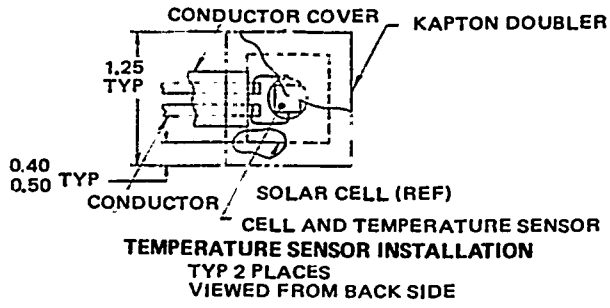


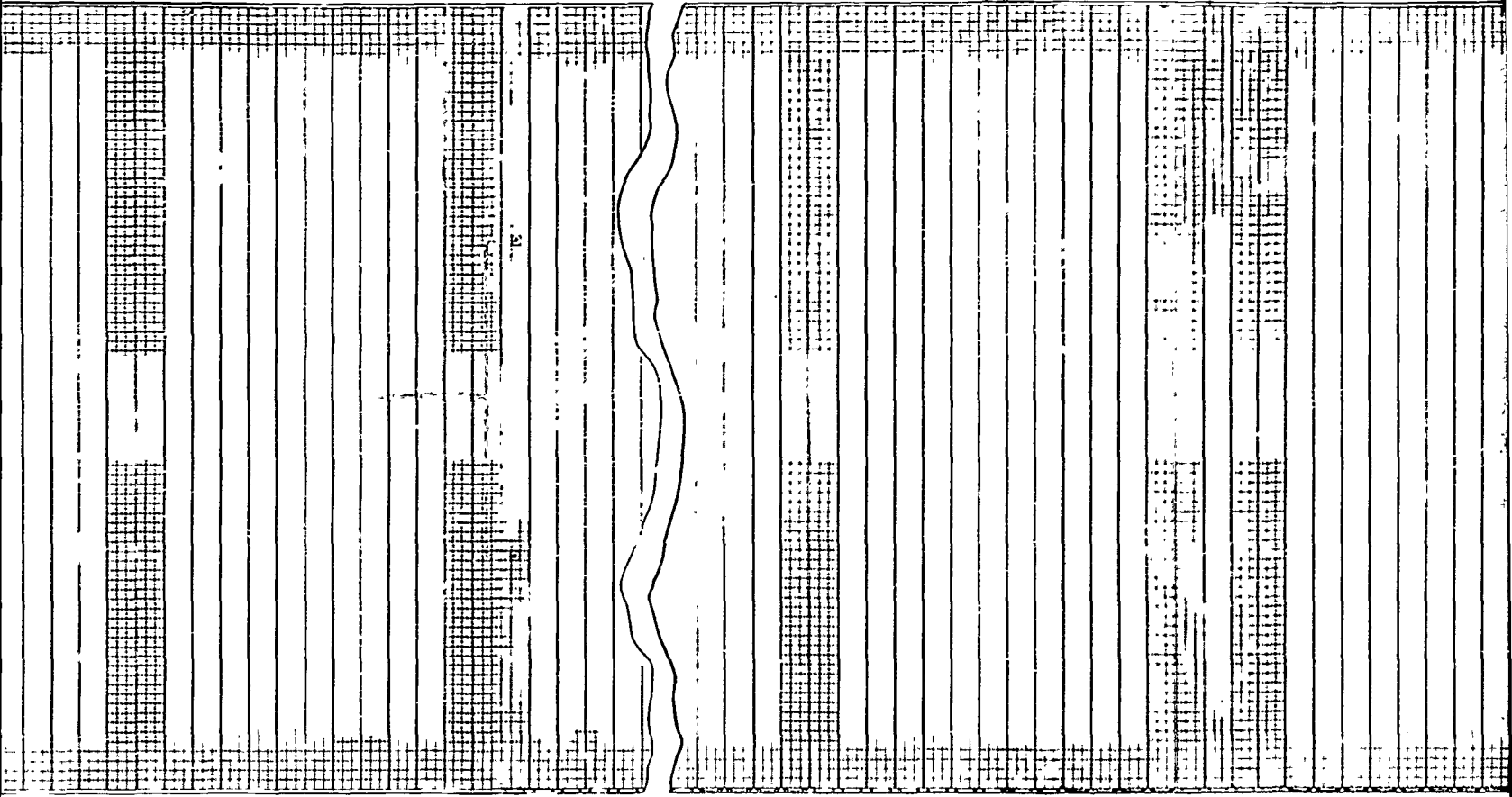
Figure 8-4. Solar Panel Assembly





PLAN CELL GROUP (123 PLACES)

120 12  
119 121



302.58  
123 GROUPS AT 2.460 MAX PITCH

3

20338-95(U)

120 122  
119 121 123

TIP END

67.00  
SUBSTRATE

IMIL FIBERGLASS  
FABRIC STYLE 104,  
VOLAN "A"

IMIL KAPTON FILM  
MIL-P-46112, TYPE I

SPREADER BAR  
WRAP  
ALLOWANCE

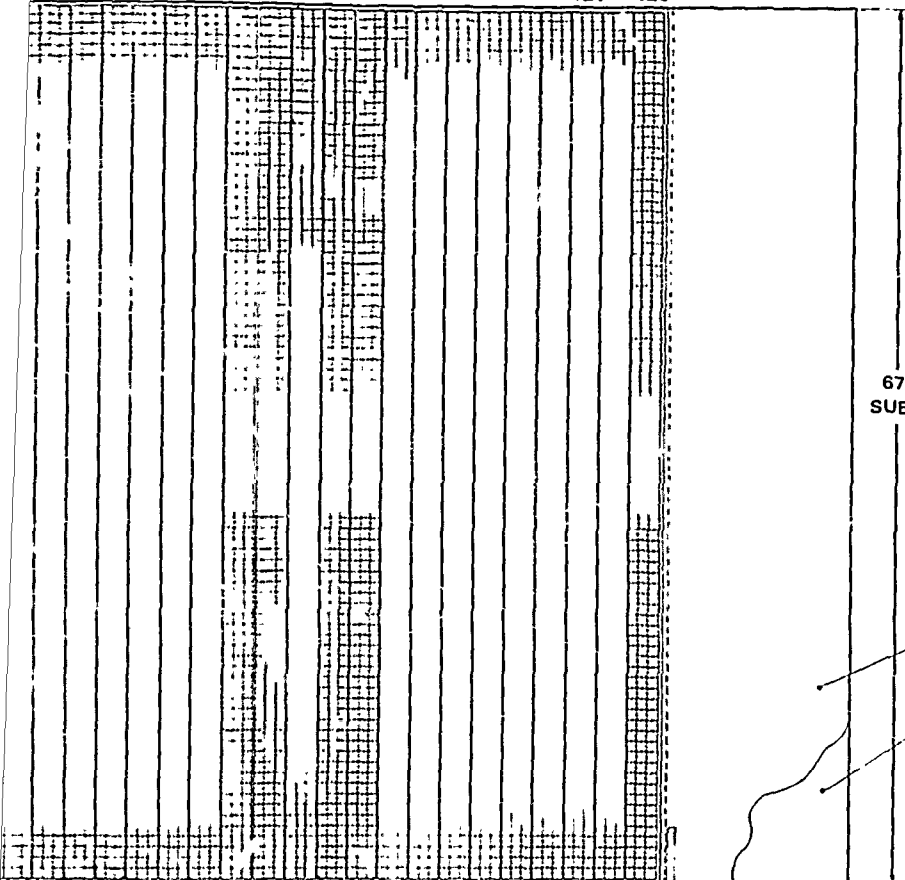


Figure 8-1c illustrates a tandem drum assembly for the 5-kw array system which attaches to one side of the orientation mechanism drive. Disadvantages apparent for this arrangement as compared to the preferred configuration 8-1d are that the:

- Inboard drum mechanism structure has to support the outboard unit (added strength and stiffness required)
- Electrical power has to be conducted across a drum mechanism
- Wiring for deployment locks is not tied to the space vehicle
- Direct coupling of the arrays is not favored from a dynamic point of view

The most compelling reason for the selection of a dual drum arrangement with the orientation drive in the center is the symmetry inherent to this configuration for a 5-kw array system. This symmetry provides a great saving in design, analysis, fabrication, and qualification testing of the array. Also, interchangeability of hardware increases design reliability and reduces cost.

Because the drum mechanism for the 5 kw array is very similar to that of the 1.5 kw FRUSA flight system and because the design requirements are identical, the 5-kw structural analysis was minimal. The principal elements examined were the boom and actuator assembly and the stowage drum. Loads on these element were higher due to the increased panel weight and boom length. The analysis shows that when using 8-mil thick solar cells on the 5-kw array, the boom strength capability will be marginal with respect to the applied bending moment at the specified 0.1-g gravity (see Table 8-3). The applied loading margins are considerably improved by selecting a lightweight 4-mil thick solar cell with 2-mil integral cover or by a reduction in the requirement. Recent flight experience on the STP 71-2 mission indicates that a 0.05-g flight requirement would be sufficient.

In addition to quasi-static bending loading, the extended booms are loaded in compression under nominal on-orbit conditions. The solar cell panels are tensioned between their stowage drum and spreader bar. This tension load is in the FRUSA drum mechanism design generated by a set of constant torque springs (negator springs) which are dimensioned for a minimum panel tension of 4 pounds. Friction, uneven boom extension, and panel winding established an upper limit of approximately 7 pounds panel tension. This same maximum level of panel tension would exceed the buckling strength for the boom when it is extended to 25 feet. The present design approach can be maintained by specifying the maximum panel tension for the fully deployed panels to be about 3 pounds. This tension level is adequate for contouring the flexible solar cell panels to the stowage drum, and it will not exceed the buckling potential of the 0.86-inch diameter stainless steel boom. As the panel is being rolled up, the tension increases, but so does the buckling allowable. It is therefore possible to utilize the dual boom actuator mechanism developed and flight-qualified by the FRUSA 1.5-kw array.

TABLE 8-3. BENDING MOMENT LOADING OF PANEL  
SUPPORT BOOM (in-lb)

	1.5 kw FRUSA	2.5 kw FRUSA	2.5 kw Lightweight	Remarks
Bending Moment Contributor				
Panel	88	204	130	FRUSA array uses 2 x 2 cm 8-mil cells and 6-mil cover sheets
Boom	12	33	33	For 0.86 inch diameter boom (0.087 lb/ft)
Spreader bar and boom length compensator	11	16	16	
Instrumentation	<u>20</u>	<u>--</u>	<u>--</u>	Accelerometers attached to FRUSA boom tip
Total	131	252	179	247 in.-lb allowable
Boom Compressive Loading, lb	2.0 to 3.5	max. 2.2	max. 2.2	7.3 and 3.2 pounds maximum allowable for 16- and 25-foot boom length

The weight of the boom actuator assemblies is 19.6 pounds, which includes two dual boom actuators, a drive motor, and the connecting torque shaft between master and slave unit, and the weight for a total of 106 feet of boom element.\*

The larger panel area for a 2.5-kw wing of the 5-kw array system produces a 60 percent increase in drum loading in accordance with the panel wing weight ratio of 55 pounds versus 34 pounds for the FRUSA flight experiment. Since the FRUSA magnesium drum is dimensioned for buckling strength, it is necessary to increase its wall thickness by the square root of the load ratio, that is, by 27 percent, or to consider materials of greater E modulus such as beryllium or fiber composites. At this point, it seems most attractive to maintain the magnesium drum design and utilize the developed fabrication technique by increasing the drum thickness at a weight

\*The present actuator cassette will stow 23 feet of boom. The redesign effort for housing about 30 feet of boom should be minor.



increase of 0.8 pound per array wing. Detail trade studies, however, have been performed which indicate potential weight savings by use of beryllium or high modulus fiber composites. In case of extremely weight-critical applications, these sources might be called upon. Table 8-4 summarizes structural margins of the 1.5 kw FRUSA array and shows adequate growth potential for all other elements of the drum mechanism subsystem. Detail FRUSA drawings (see Figure 8-5 and Appendix C) and weights generated are therefore applicable with only minor adjustment for the 5-kw drum mechanism design.

#### Array Dynamic Characteristic

The dynamic characteristic of individual solar panels of the 5-kw array system has been determined by the analysis technique successfully employed in the FRUSA flight experiment. A listing of three bending and torsion modes and frequencies, as well as appropriate sets of coupling coefficients is provided in the Appendix for use in control system design and spacecraft stability analysis. The first array bending frequency is 0.082 Hz for the 5-kw array panel size and compares with 0.2 Hz computed for the 1.5-kw FRUSA array.

#### 5 KW OPERATIONAL FRUSA RELIABILITY

The operational FRUSA design is similar to that of the existing FRUSA. The differences, aside from the larger power capacity, are chiefly in the reduction of sensors and commutators for telemetry, and the doubling up of the orientation control electronics, commutator, and power conditioning to provide redundant operation. The reliability of a 5-kw FRUSA has been estimated to be 0.849 for a 3-year mission. Although this figure for 3 years operation might be considered unnecessarily high, the risk in making the control electronics nonredundant is considered unwise. A reliability estimate of each subsystem is shown in Figures 8-6 through 8-9; Figure 8-10 is the reliability model and block diagram of the complete system.

The subsystems have been modified in the following ways to make them suitable for a 3-year mission.

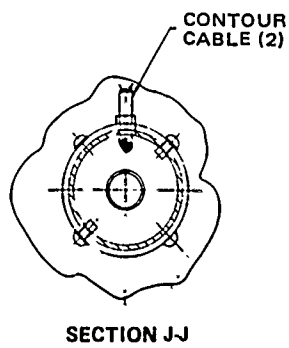
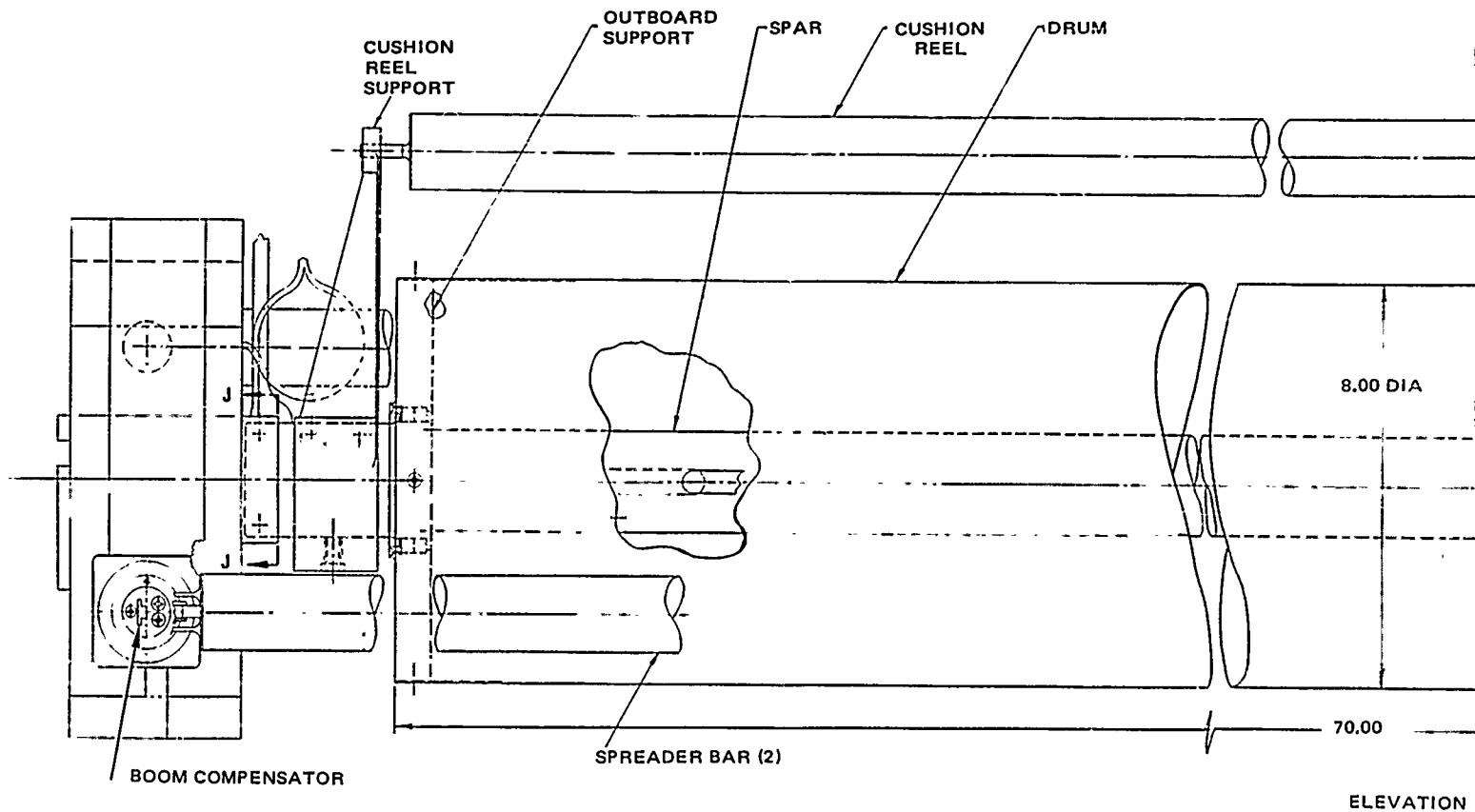
#### Orientation Subsystem

The control electronics is duplicated so that one unit is redundant to the other. This will greatly increase the reliability over the 3-year period. The sun sensor will remain the same. The reliability of the orientation mechanism has been recalculated (see Table 8-5). Hughes' experience in testing sliprings and the use of sliprings on satellites in space over the past year have shown a greatly reduced failure rate; hence, the failure rate of the orientation mechanism has been reduced correspondingly.

TABLE 8-4. SUMMARY OF MINIMUM MARGINS OF SAFETY FOR 1.5 KW FRUSA  
ARRAY SYSTEM DESIGN

Part Number	Part Name	Critical Condition	Type of Loading	Margins of Safety	
				M.S. y	M.S. u
3169901	SPAR	3 $\sigma$ - random vibration	Combined shearing and shear	High	+0.49
3169901	SPAR	Deployment	Bearing	High	+1.04
3169901	SPAR	Deployment	Bending		+0.71
3169901	SPAR-end fittings	Deployment	Tensile	High	+4.15
3169902	Support, bearing inboard	3 $\sigma$ - random vibration X-excitation	Core shear		+0.17*
3169003	Support, bearing outboard	Thermal	Differential expansion	+1.02	+2.1
3169005	Support, inboard cushion reel	3 $\sigma$ - random vibration X-excitation	Bending	High	+0.05
3169006	Support, outboard cushion reel	Deployment	Bending	High	High
3169007	Cushion reel	Preloading bearings	Combined shearing and bending	+1.20	+1.56
3169007	Cushion reel	Preloading bearings	Bond shear		+4.50
3169004	Drum	3 $\sigma$ random vibration X-excitation	Bearing		+1.13
3169004	Drum	3 $\sigma$ random vibration Y-excitation	Buckling		+0.50
3169005	Support, inboard cushion reel	3 $\sigma$ random vibration X-excitation	Bearing (screw)	High	+0.65
3169046	Support, drum mechanism	Deployment	Bending	1.06	+0.7

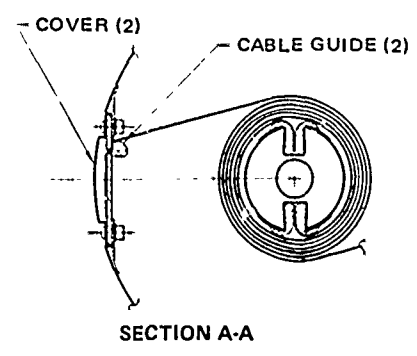
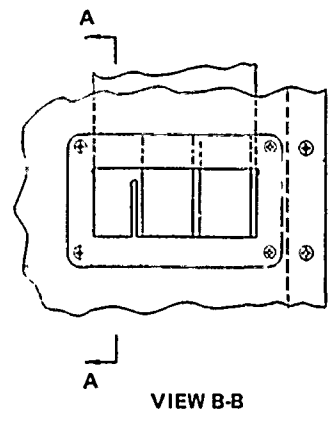
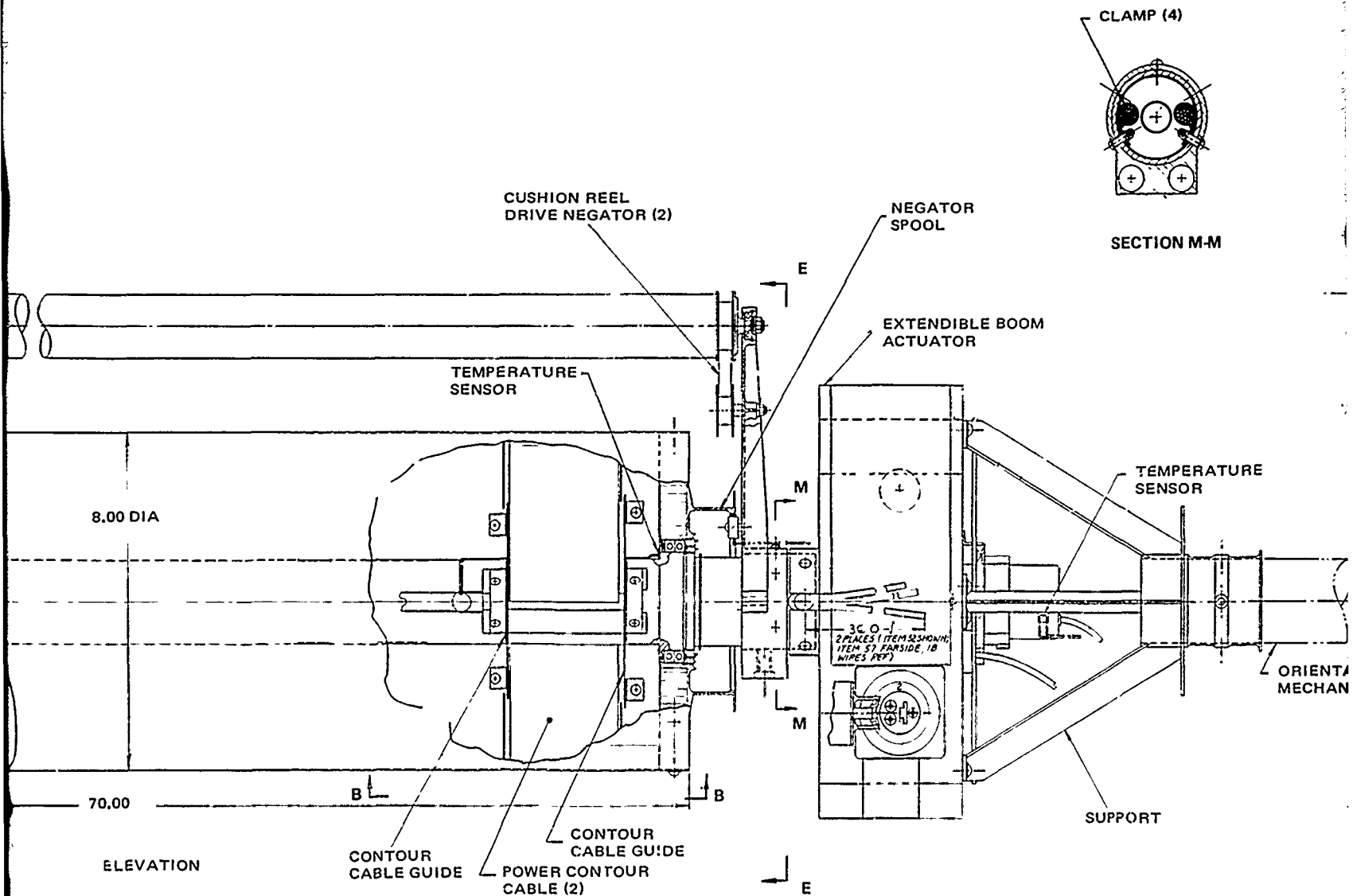
\*Design loads were predicted for 3 percent structural damping. Qualification testing indicated considerably greater damping.



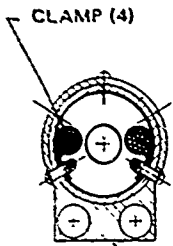
DIMENSIONS IN INCHES

Figure 8-5. FRUSA Drum Mechanism

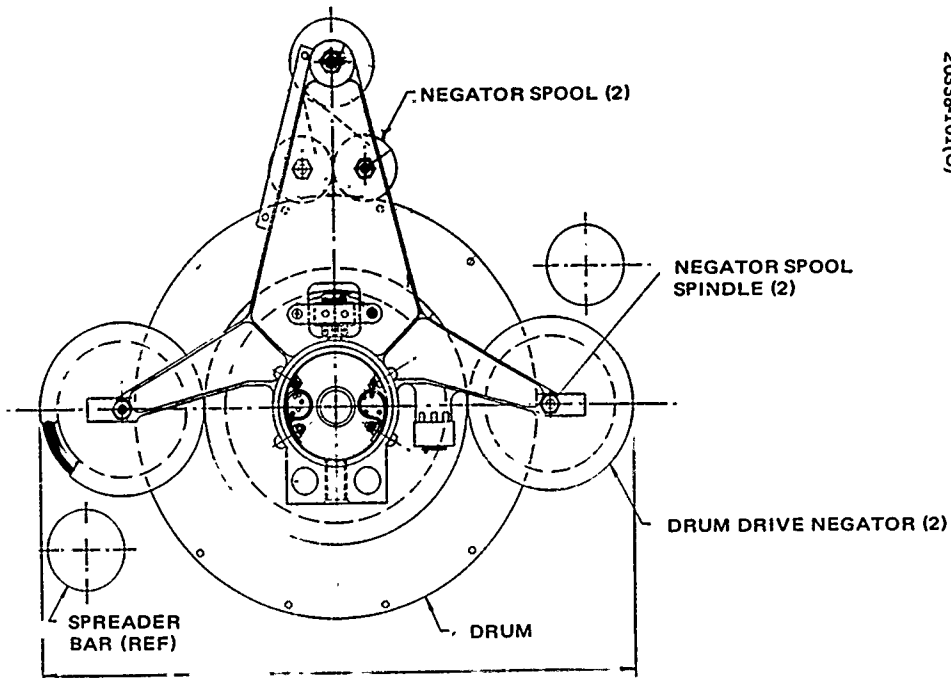




20388-101(U)



SECTION M-M



SECTION E-E

OM

TEMPERATURE  
SENSOR

SPREADER  
BAR (REF)

DRUM

DRUM DRIVE NEGATOR (2)

ORIENTATION  
MECHANISM

SUPPORT

GUIDE (2)



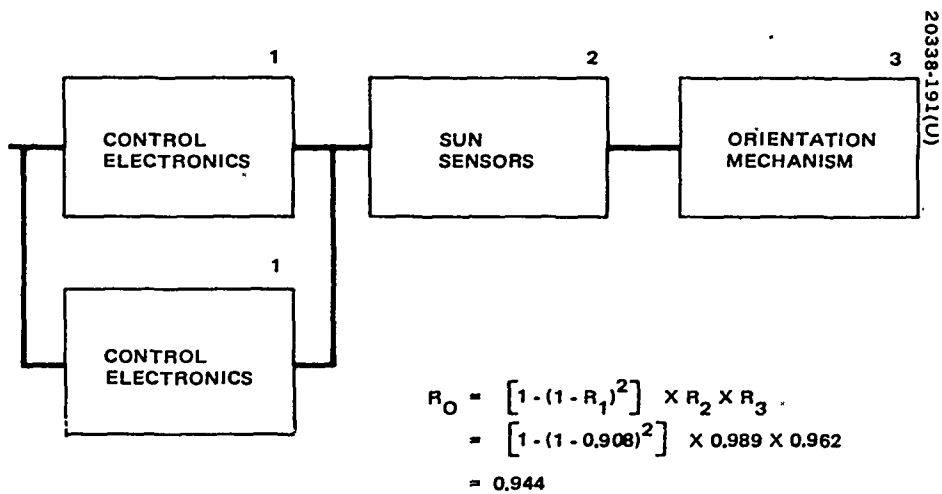


Figure 8-6. Orientation Subsystem Reliability Block Diagram

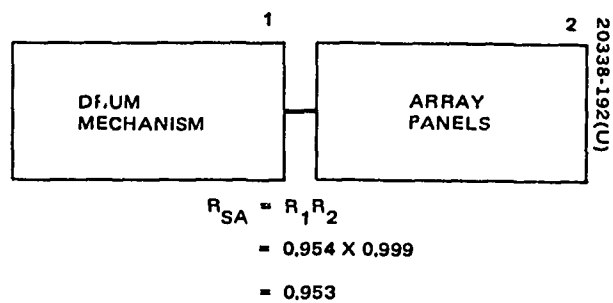


Figure 8-7. Solar Array Reliability Block Diagram

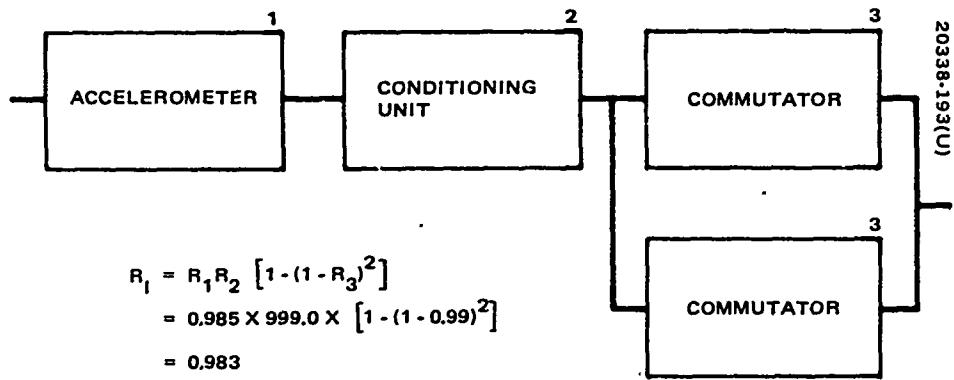


Figure 8-8. Instrumentation Subsystem Reliability Block Diagram

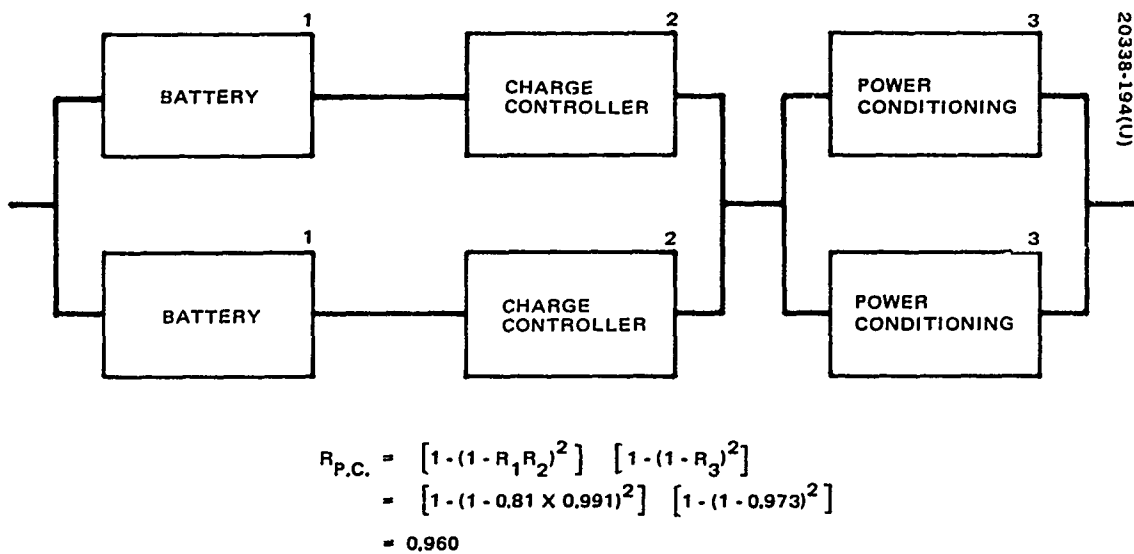


Figure 8-9. Power Conditioning and Storage Reliability Block Diagram

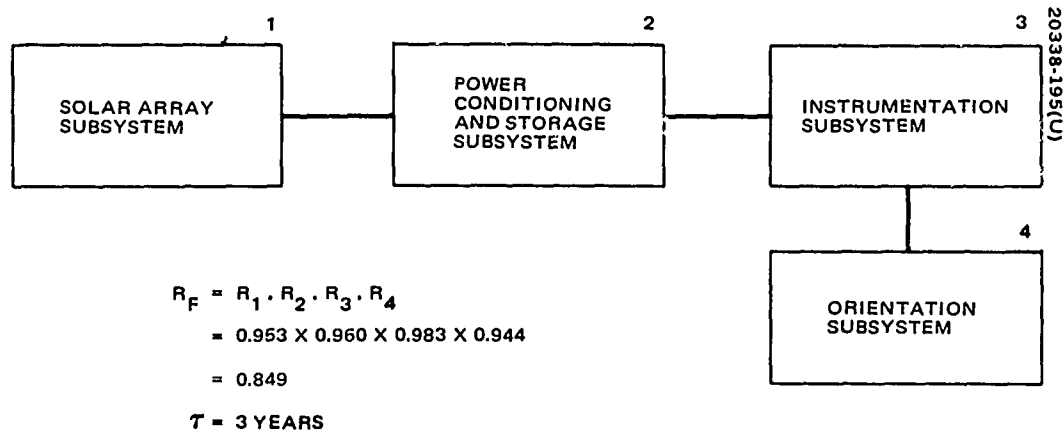


Figure 8-10. FRUSA System Reliability Block Diagram

## Solar Array

The failure rate of the mechanical parts remains the same. The drum mechanism reliability is the same for the 3-year mission as it was on the previous FRUSA estimate since the number of times it will operate is still ten. The array panel will have additional cells attached to it to compensate for radiation degradation. The additional cells will be more than enough to maintain the reliability of 0.999.

TABLE 8-5. ORIENTATION MECHANISM RELIABILITY

Spring	0.999
Bearing	0.974
Tachometers (two)	0.995
Torquers (two)	0.999
Power sliprings* (six)	0.999
Signal slipring assembly* (two)	0.999
Connectors	<u>0.997</u>
	0.962

\*Laboratory experiments have shown that the failure rate of sliprings is  $2.3 \times 10^{-12}$ .

## Instrumentation (Housekeeping)

One accelerometer will be used instead of six as previously. The conditioning unit is identical to that used before, but the commutators are of a new design. The commutators are made redundant which brings the reliability up to 0.99.

## Power Conditioning and Storage

Fifty-two battery cells are required at beginning of life, based on an end of life requirement of 48 cells. This assumes a failure rate of  $420 \times 10^{-9}$  for cells, slightly higher than that used previously. The charge controller and power conditioning units are identical in design to those used previously. However, the power conditioning unit is made redundant.

## Experience Factor

The reliability of electronic units has decreased slightly due to a change in the experience factor "E", a factor which is calculated from experience of electronic parts operating in space on synchronous satellites having increased from 0.475 to 0.53.)



## SECTION IX

### PARAMETRIC DESIGN STUDY OF 0.5 TO 20 KW SOLAR CELL ARRAY SYSTEMS

The purpose of this parametric design analysis is to provide guidelines and preliminary design criteria for solar array system designs from 0.5-to 20-kw power output. These objectives are approached by identifying the relationships between pertinent design parameters and by establishing combinations which yield optimal performance characteristics. Experience and knowledge gained from the 1.5-kw FRUSA flight experiment are being utilized extensively and they provide the primary point of reference. FRUSA design requirements are shown in Table 9-1.

The use of the flexible array concept for large solar power requirements has been demonstrated by the flight of FRUSA. Based on weight studies performed at Hughes, it appears that the FRUSA type solar array becomes competitive at the 0.5-kw power level with cylindrical body mounted and rigid substrate paddle-type solar arrays (Figure 9-1).

The major subassemblies of a flexible roll-up solar array system are the 1) solar panels, 2) drum mechanism, 3) support booms and their deployer, 4) array orientation mechanism, and 5) interconnecting structure between array drum and orientation drive. These subassemblies and their parametric design factors are analyzed in the following sections.

The study is limited to the solar array and orientation elements since other conventional components of a power subsystem (battery charge controls, batteries, power conditioning electronics) are dependent on spacecraft and payload power requirements rather than on array type.

#### FLEXIBLE SOLAR ARRAY PANEL DESIGN

A solar array panel consists typically of a flexible substrate, the electrically interconnected cell stack and a power bus.

The substrate material developed for the 1.5-kw FRUSA system is a composite of 0.001 inch of kapton-H film and 0.001-inch fiberglass cloth of great flexibility. Panel flexibility is of concern in the packaging of the solar panels for launch and it is most important if array roll-up is required on orbit. The less flexible a solar panel is, the greater will be the panel tension and cell loading in the roll-up array. Increased panel tension reflects on the support boom and stowage drum sizing which ultimately means greater weight for structural elements. Since flexing of the solar panels essentially occurs in the gaps between strings of solar cells, a tradeoff exists between greater panel tension or drum diameter and increase of flexibility by enlarging the gap width. The relationship between these tradeoff parameters - panel

TABLE 9-1. DESIGN ENVIROMENTS AND GROUND RULES

Mechanical

- Launch loads as specified for Titan IIC payload components:
  - Static  $\pm 10$  g axial,  $\pm 2.5$  g lateral
  - Vibration: 19.5 g rms random
  - 0.25  $g^2$ /Hz from 300 to 1200 Hz
  - +3 dB roll-up from 20 to 300 Hz
  - 6 dB roll-off from 1200 to 2000 Hz
- Array control maneuver loads are generated by the orientation mechanism only.
- Orbital perturbation loads are assumed not to exceed 0.1 g quasi-static acceleration.
- Maximum array tip deflection due to thermal and dynamic loads,  $\delta$ , for any boom length, L, shall be such that  $\delta/L \leq 0.1$
- Array structural stiffness is considered a design parameter.
- Design factors on ultimate strength and buckling is 1.5.
- The array must be a structurally self-sufficient component with minimal interfaces to space vehicle structure.
- Modularized design concepts are preferable.
- Array specific stowage volume is  $< 2 \text{ ft}^3/\text{kw}$ .
- Controlled array extension in orbit.
- Partial extension should be possible.
- Retraction capability is required  $\sim 500$  cycles.
- State-of-the-art fabrication and material techniques will be employed.

Electrical

- A maximum "watts per pound" figure of merit is the goal.
- Design life is 5 years (any orbit).
- Silicon solar cells of 2 cm maximum width should be used.
- Thin solar cell (4 mils) must be acceptable.
- Array area utilization goal is 95 percent.

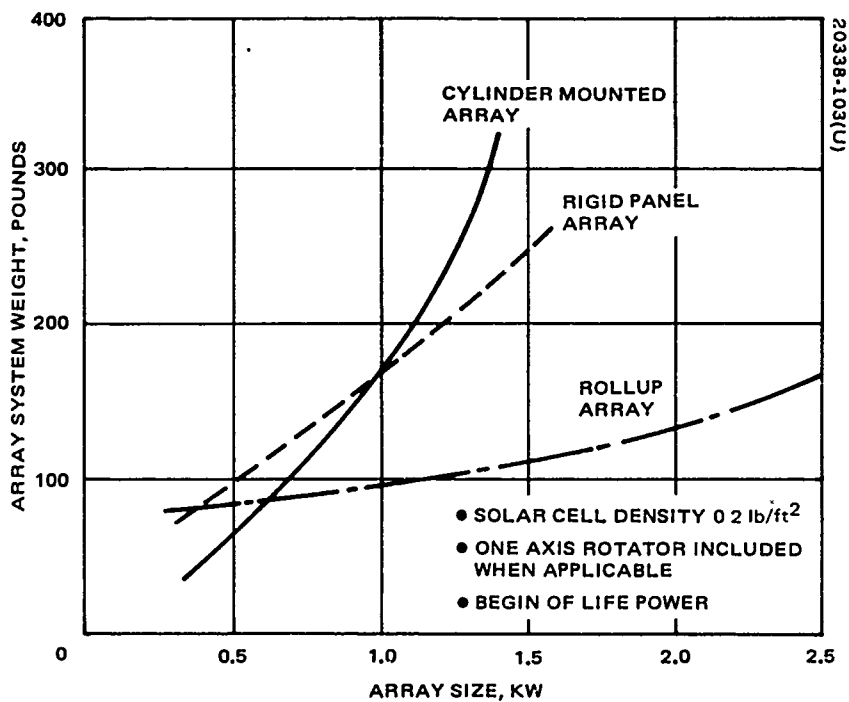


Figure 9-1. Weight Efficient Power Ranges for Solar Arrays

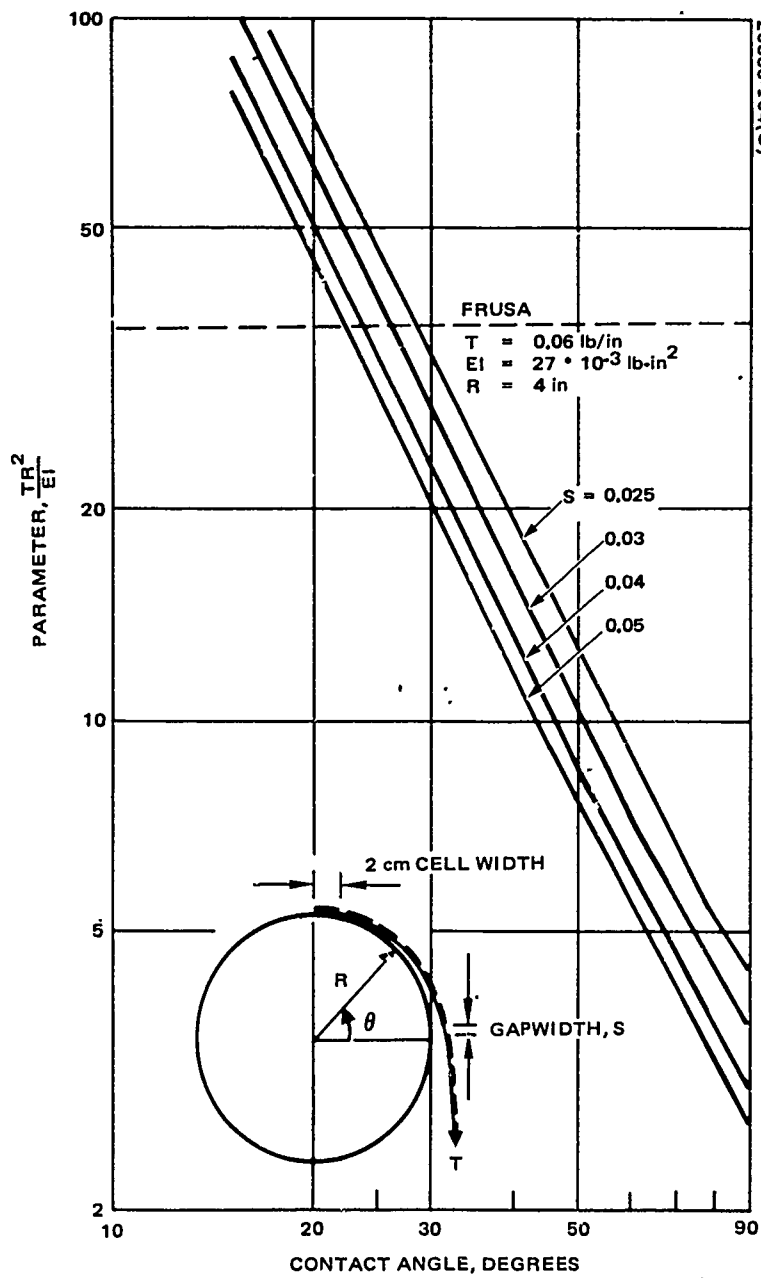


Figure 9-2. Substrate Flexibility Parameter Versus Panel Contact Angle on Rollup Stowage Drum

tension  $T$ , drum diameter  $2R$ , panel rigidity  $EI$ , and gap width  $S$  — is illustrated in Figure 9-2. The drum rotation  $\theta$ , which is required before the panel will contact the drum, is used in this figure as a design variable.

The  $\theta$  angle employed in the FRUSA design was selected to be 30 degrees. An upper physical limit for contouring a solar panel to the stowage drum is 180 degrees. Realistically,  $\theta$  should always be kept below 90 degrees to ensure proper panel roll-up. When the gap width is varied in order to accomplish panel contouring to the drum, the area utilization of the array will decrease and the array weight will proportionally increase. A sample calculation of the weight penalty is summarized in Table 9-2 for the 5-kw array system design. It shows that doubling of the nominal design gap width of 25 mils will produce an array weight increase of about 4 pounds. The area utilization factor will decrease by 2 percent. The alternate approach is to vary  $TR^2/EI$  from a value of 2 to 3.2 as delineated in Figure 9-2. If it is assumed that this change is accommodated by increasing the panel tension, the thickness of the support boom must increase accordingly, and a weight penalty of 10 pounds is predicted. If the stowage drum diameter were increased by 27 percent, the more rigid panel can be handled at the cost of adding 1.5 pounds drum weight. The latter approach, however, results in an increased stowage volume.

#### Solar Cell

The solar cell selection in spacecraft design is generally based on a tradeoff between cost, weight, and area specific power output at beginning and end of mission life. Since the flexible array concept eliminates mounting area

TABLE 9-2. ARRAY AREA UTILIZATION AND WEIGHT PENALTY

Area Utilization, percent	Gap Width Between Strings, inches	Weight Penalty for 5-kw Array System, pounds
95.5*	0	-
93.6	0.025	Design point (ref)
93.0	0.030	1.2
92.5	0.040	2.1
91.5	0.050	4.0

\*A minimum gap of 0.022 inch between 2 by 2 cm cells in series and a 0.050-inch minimum assembly gap between groups of three cells in parallel is used.

as an essential design constraint, lightweight solar cells of a slightly lower power efficiency become attractive. The 1.5-kw FRUSA flight experiment utilizes 7.2-mil thick, 2 by 2 cm cells. The failure rate of this cell in handling and mounting to the substrate was not different from that of the 12-mil standard cell. Additionally the breakage rate in mechanical (Table 9-3) and thermal qualification testing was extremely low. In an earlier development program, 30-cm long dendritic cells were used without any inherent difficulty. It is expected that even thinner cells of 4-mil thickness may be utilized for further weight savings. The cell width should be kept at about 2 cm.

### Cover Slide

The cover slide selection is of lesser importance in a flexible array application than it is for a rigid array. A thick cover glass will provide more front protection against low energy electrons and protons. The cell backside is protected only by the flexible substrate.

### Interconnections

Solar cell interconnections on the FRUSA panel are of 2-mil thick, etched copper ribbon which is soldered to the cell contacts for connecting three parallel cells into a series string. Interconnect flexibility and its resistance to temperature cycling between +250° and -300°F are of primary concern in flexible array applications. Welding as well as soldering is successfully utilized for attachment. The cell interconnections for flexible solar arrays appear to present no more problems than for rigid substrate cell mounting.

### Electrical Bus

The electrical bus routing and sizing depends largely on the array voltage and the panel sector layouts. The bus is bonded to the backside of the flexible substrate and the strings of cells are connected at the panel edges to the bus. In the 1.5-kw FRUSA experiment a 0.0007-inch thick copperclad

TABLE 9-3. SOLAR CELL FAILURE DURING FRUSA TESTING

	Number of Cells	Failure	Percent Failure
Qualification vibration	3,400	21	0.6
Qualification deployment	3,400	4	0.12
Acceptance vibration*	34,400	52	0.15

\*The defect was severe enough only in 28 cells to warrant replacement.

sheet mounted on 1-mil thick kapton was used. The cross section (width) of the bus depends on the panel voltage, array size and the power loss considered acceptable from a design point of view. A parametric relationship is shown in Figure 9-3 which correlates electric bus weight and array voltage for various panel sizes.

### Diodes

Diodes are required to protect the solar cells strings against reverse current type failures which can be caused by short circuits and shadowing. On the FRUSA design, each group of strings had a separate bus and the protective diode was installed on the drum. This arrangement required a multiplicity of buses and flex-cables in the drum. Future development in the diode technology will allow the utilization of panel mounted diodes. These essentially will be similar to solar cells in size and appearance. Their area will be 1 by 2 cm and they will have the same thickness as the solar cells. Plans are to place single or multiple parallel diodes in series with each of three parallel cell strings, depending on reliability requirements. With this diode arrangement, a minimum number of buses will be needed on the panel.

### Panel Electrical Connect

The roll-up array stowage concept requires sliprings or flexible cables for power transfer from the solar panels to the drum support structure. In the 1.5-kw FRUSA system, flexible flat cables of copper ribbon embedded in 1 mil kapton insulation are used for the power transfer as well as panel instrumentation signal transfer. The flexible cable was found by tradeoff analysis to be weight-effective and it has greater reliability. The results of this trade study are summarized in Table 4-4 for array modules up to 5 kw.

## SOLAR PANEL SUPPORT CONCEPTS

Three basic considerations require evaluation in selecting the panel support concept which is most suitable for a particular array size and application. These considerations concern the joining of the flexible solar panel to its support structure, the approach being taken in achieving torsional rigidity of the array/support structure system, and the location from which the in-orbit deployed array panel is supported. The essential alternates available for selection are listed in Table 9-4. The advantages and disadvantages of the competing concepts have been thoroughly weighed in arriving at the FRUSA design.

In the FRUSA flight experiment configuration, the panel substrate ties to a pair of extendible support booms only at their tip via a rigid leading edge member, the spreader bar. The flexible substrate is tensioned between this spreader bar and the stowage drum to maintain panel flatness, provide for even panel roll-up and deployment on orbit, and to achieve control of the array dynamic characteristics.

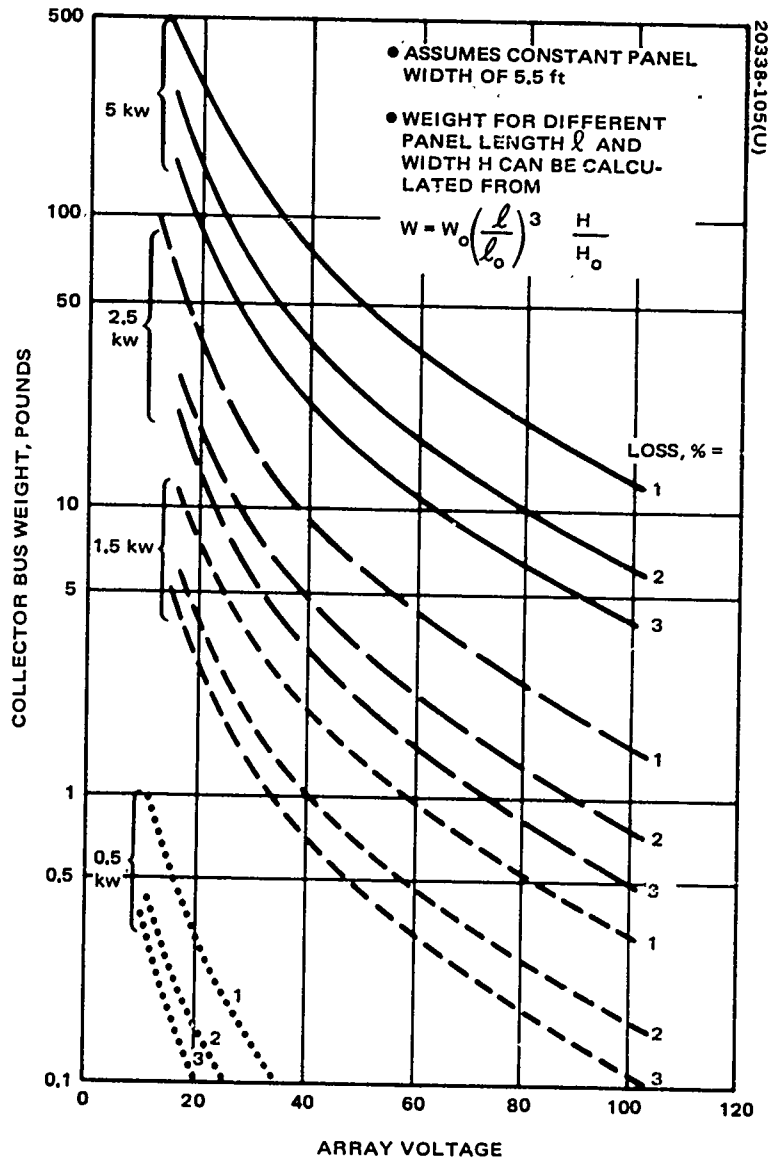


Figure 9-3. Power Collector Bus Weight Versus Array Voltage For Varying Power Loss



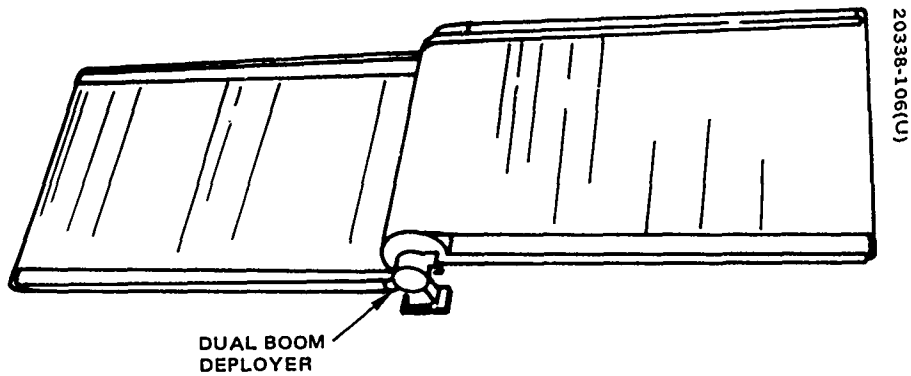
TABLE 9-4. SOLAR PANEL SUPPORT CONCEPTS

	FRUSA Concept	Alternate
Panel/support interface	Panel ties to tip of support structure	Panel ties uniformly to support structure
Torsional rigidity	Support structure provides torsional rigidity	Torsional rigidity derived through panel tensioning
Stowage (support) mechanism location	Center of panel	End of panel

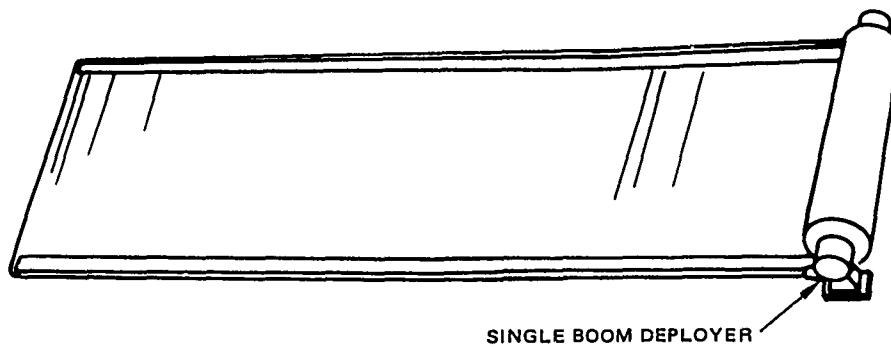
A basic consideration in designing array systems of up to 20-kw power output must concern the location of the array support in orbit. The tradeoff is between a single-sided panel mount and the center drum two-panel support concept. These concepts are illustrated in Figure 9-4, for a roll-up array configuration. In the single-sided panel concept, the flexible solar panel cantilevers to one side of the stowage drum. In the FRUSA configuration the stowage drum mechanism is placed in the middle of the array from which two shorter panels extend.

The prime tradeoff between these array concepts is the panel support structure. The length of booms for a center panel support is half of the overall array length and each boom will have to carry half of the array panel. The reduced boom length as compared with that of the single-sided array concept results in less weight and greater efficiency. The actuator mechanism for a dual boom mechanism, however, is heavier than a single boom actuator as shown in Figure 9-5. A parametric companion of the weight for the extendible booms and actuator system has been developed for the 5-kw array design with respect to strength and stiffness design criteria.

An extendible boom of this design is  $d_0 = 0.86$  inch in diameter, and weighs  $w_0 = 8.7$  pounds, and is approximately 100 feet long. The two dual unit actuators weigh 10.9 pounds for a total of 19.6 pounds for the system. The bending load in an equivalent single-sided supported array system of 50 feet panel length will be four times as great. Since the bending strength of a boom is proportional to the third power of its diameter, the diameter of the longer boom is  $d = d_0 (4)^{1/3} = 1.38$  inches. The specific weight of this boom is proportional to the square of the diameter ratio. The total weight predicted for the larger booms and their deployer is 32.4 pounds, which compares with 19.6 pounds computed for the center array support configuration.



CENTER PANEL SUPPORT CONCEPT



SINGLE-SIDED PANEL SUPPORT CONCEPT

Figure 9-4. Center and Edge Panel Support Configurations

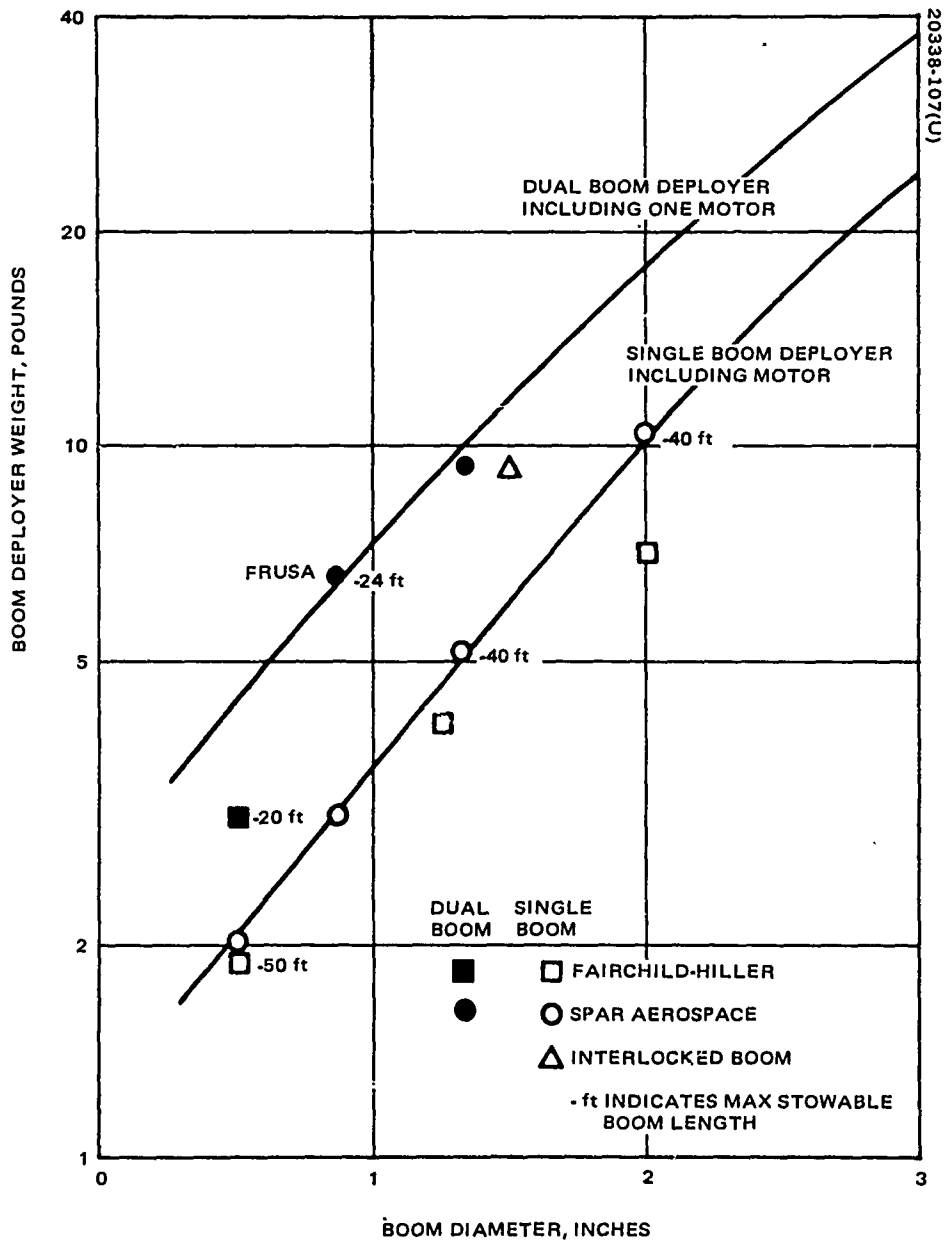


Figure 9-5. Deployer Mechanism Weight For Collapsible Boom Type

A different parametric relationship applies for the support boom system if the boom is designed for column buckling. The boom buckling strength is inversely proportional to the square of boom length (that is, a factor of 4 exists in favor of the center drum arrangement). This factor might be cancelled by increasing the boom moment of inertia and enlarging the boom diameter. Since the section moment of inertia of a thin wall, deployable boom is proportional to its diameter to the fourth power, a four times greater boom stiffness requires a diameter increase of about 40 percent. The total weight for the larger booms and their two actuator mechanisms is predicted to be 26.1 pounds. Therefore, if column buckling is the critical design criterion, the center support concept has a weight advantage of 6.5 pounds.

The weight comparison is most dramatic for an array design of equal array bending frequency. In a first approximation, the fundamental bending frequency  $f$  is expressed by

$$f^2 \approx \frac{EI}{l^3 M} \quad (1)$$

where

$EI$  = boom bending stiffness ( $\sim d^4$ )

$l$  = support boom length

$M$  = array panel weight

The alternate support concepts differ by a factor of 2 both in their boom length and panel weight. The  $l^3 M$  term is therefore 16 times greater for the single-sided support configuration. To maintain the same bending frequency by the single-sided boom, diameter must be doubled. The resulting weight comparison for the 5-kw case is 49.8 pounds versus 19.6 pounds in favor of the center mounting method.

In conclusion, the weight tradeoff shows the center mounting far superior from a support structure point of view and it should be preferred in array design.

#### SOLAR PANEL SUPPORT BOOM

In general, the loading imposed on the panel support structure in orbital flight is relatively small and the primary criteria for selection are structural stiffness, compact stowage, and dependable extension and retraction capability. Cylindrical booms are available which satisfy these requirements effectively. The Bi-STEM boom employed in the 1.5-kw FRUSA flight experiment is one of the deployable cylindrical boom family. The Bi-STEM

boom (shown in Figure 9-6a) is formed by nesting two or more overlapping circular shells which are typically stowed as flat ribbons on two separate reels. An alternate design is the STEM unit which accomplishes the same circular tube cross section with a single metallic sheet, as shown in Figure 9-6b. Advantages of the Bi-STEM system derive from the narrower ribbon which reduces the packaging dimensions and allows a shorter distance for transition from flat to cylindrical configuration.

The STEM and Bi-STEM are of open cross section and are therefore essentially without torsional strength. Tubular extendible models have been made which have mechanically interlocking or hinging ribbon edges for enhanced torsional boom rigidity. The prototype for a torsion rigid, closed section boom is the NASA collapsible boom (Ref. NASA TM-8-1137). Figure 9-6c illustrates the typical configuration of this boom. Two quasi biconvex metallic ribbons are welded along their edges to form a closed section.

The high yield strength of beryllium-copper, high strength steel, and titanium, the materials from which collapsible booms are made, allows elastic flattening and coiling of booms with low diameter (D) to ribbon thickness (t) ratio. (The minimum value for D/t is typically 200.) This ratio  $D/t = \lambda$  appears in the boom weight (W), strength (M)\*, and bending stiffness (EI) equations as expressed by

$$W = k_1 \rho D t = k_1 \rho D^2 \frac{1}{\lambda} \quad (2)$$

$$M = k_2 \frac{E t}{D} \frac{I}{D} = k_2 E D^3 \frac{1}{\lambda^2} \quad (3)$$

$$EI = k_3 E D^4 \frac{1}{\lambda} \quad (4)$$

where  $k_1$ ,  $k_2$ , and  $k_3$  account for geometrical and empirical shape factors peculiar to the cylindrical tubes; E is the modulus of elasticity; and  $\rho$  is the material density. The specific bending strength and stiffness formulates from these equations to be

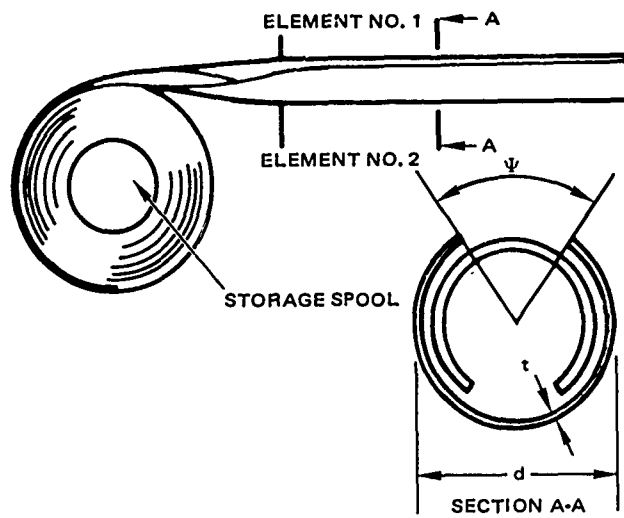
$$\frac{M}{W} = k_4 \frac{E}{\rho} \frac{1}{\lambda} \quad (5)$$

$$\frac{EI}{W} = k_5 \frac{E}{\rho} D^2 \quad (6)$$

The ratio  $E/\rho$  is about the same for most conventional metal alloys. Factors  $k_4$  and  $k_5$  are ratios of  $k_2/k_1$  and  $k_3/k_1$ , and they express boom configuration

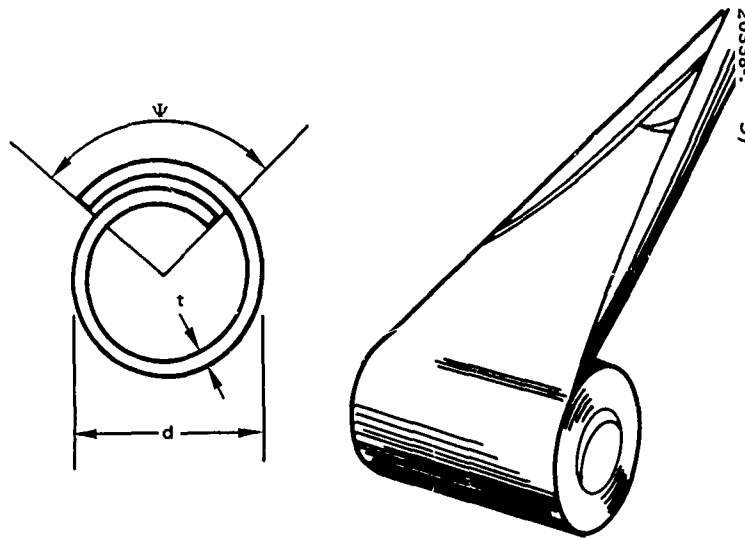
---

\*The strength of a thin wall tube is limited by the thin shell buckling rather than material strength.

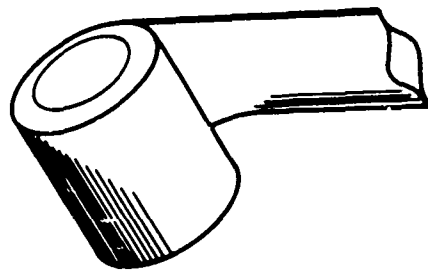


20338-108(U)

a) BI-STEM BOOM CONCEPT



b) OVERLAP BOOM CONCEPT



20338-110(U)

c) TORSION RIGID COLLAPSIBLE BOOM

Figure 9-6. Collapsible Boom Concepts

related characteristics. These characteristics are evaluated in Figures 9-7 through 9-10. As shown in Figure 9-7, the Bi-STEM concept ranks superior in bending stiffness to the overlap stem and the torsion rigid NASA boom. On the basis of specific bending strength, the overlap stem boom becomes preferable to the Bi-STEM as shown in Figure 9-8. The closed section boom design is inferior to the STEM and Bi-STEM for both figures of merit.

To approximate the weight and size of deployer mechanisms for the 0.5-to 20-kw power system configuration tradeoffs, typical dimensions for deployer mechanisms have been scaled from existing designs. The resulting empirical relationships for single and dual boom deployer mechanism weights as a function of boom diameter are shown in Figure 9-5. Data presented in this figure represent actual hardware produced by various manufacturers.

### FLEXIBLE SOLAR PANEL STOWAGE

The flexible solar array substrate does not have sufficient structural strength or stiffness to protect the solar cells in ground handling and during space vehicle launch. A separate support structure is therefore needed. In the 1.5-kw FRUSA experiment, this support structure is a thin wall magnesium cylinder 8 inches in diameter.

The primary reasons for using a drum are 1) controlled panel motion in roll-up and deployment, and 2) simple panel packaging. Drum rotation during panel extension and retraction can readily be controlled, which assures minimum disturbance on the space vehicle control system. Additionally, partial array deployment provides an attractive feature in system design for regulating power output, conducting crucial space vehicle maneuvers, and balancing drag or solar pressure.

### STOWAGE DRUM ASSEMBLY

The parametric analysis conducted for the drum uses the 1.5-kw FRUSA design configuration as a baseline for extrapolations over the 0.5-to 20-kw power range. Elements of the stowage drum assembly are shown in Figure 9-11 and their actual weights for the FRUSA flight hardware are listed in Table 9-5. The scaling of these individual drum assembly elements for larger array sizes and for panel length-to-width ratios from  $L/W = 1$  to  $L/W = 8$  was conducted by computer analysis which employed geometric, section property, and weight factors.

The primary structural design criteria for the stowage drum assembly derive from boost accelerations, staging transients, vibration during transonic flight, and from ground handling environments. The FRUSA

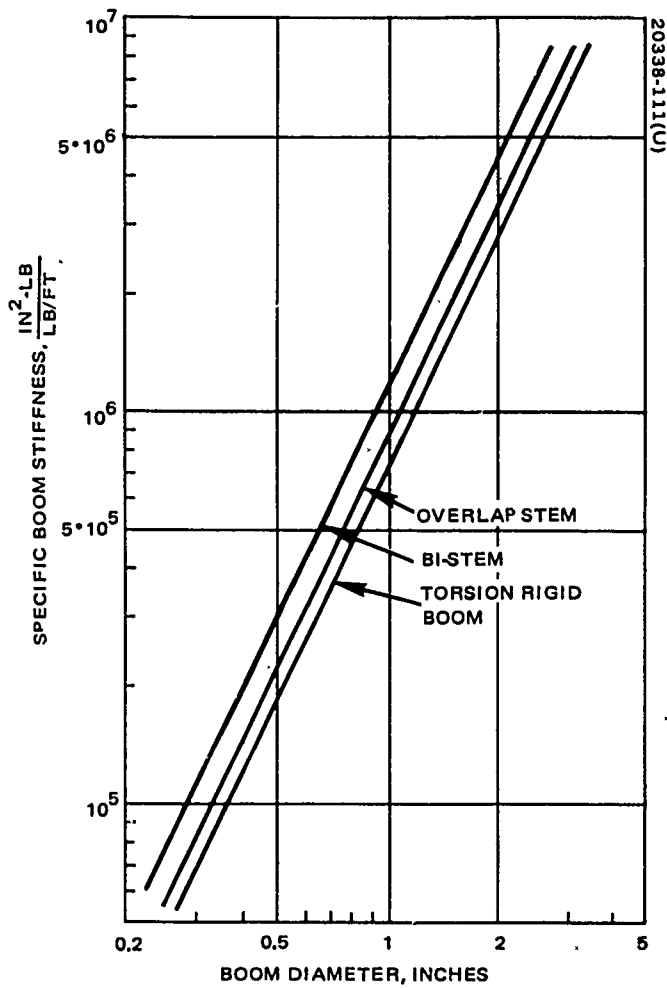


Figure 9-7. Specific Stiffness of Three Deployable Boom Types Normalized For Diameter-to-Thickness Ratio of 200

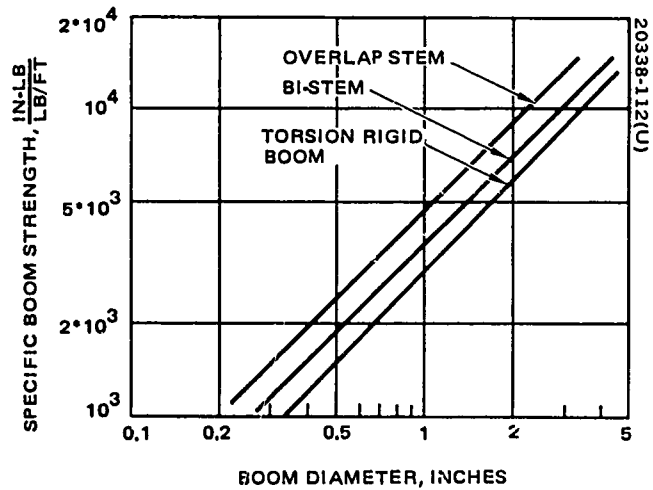


Figure 9-8. Specific Strength of Three Deployable Boom Types Normalized For Diameter-to-Thickness Ratio of 200



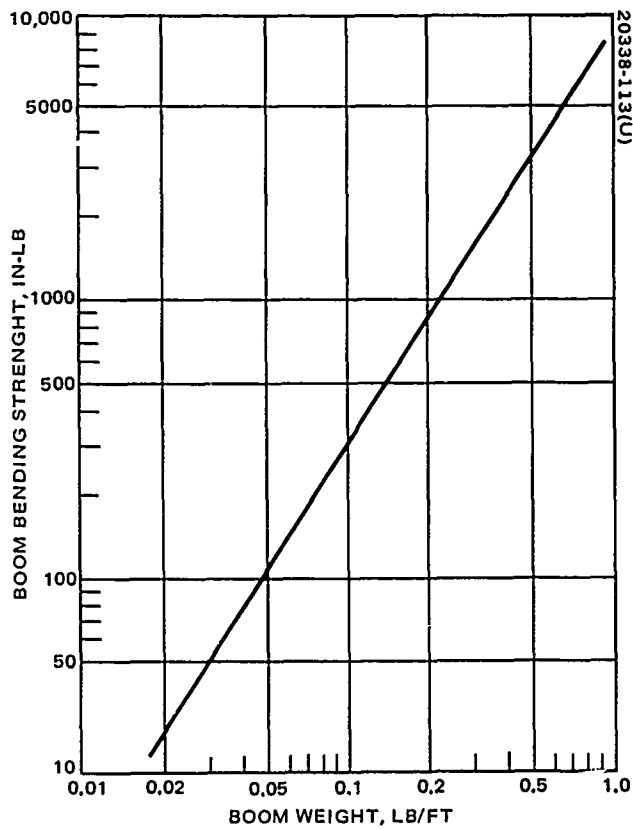


Figure 9-9. Critical Boom Bending Moment For Stainless Steel BI-STEM Booms of Diameter-to-Thickness Ratio of 200

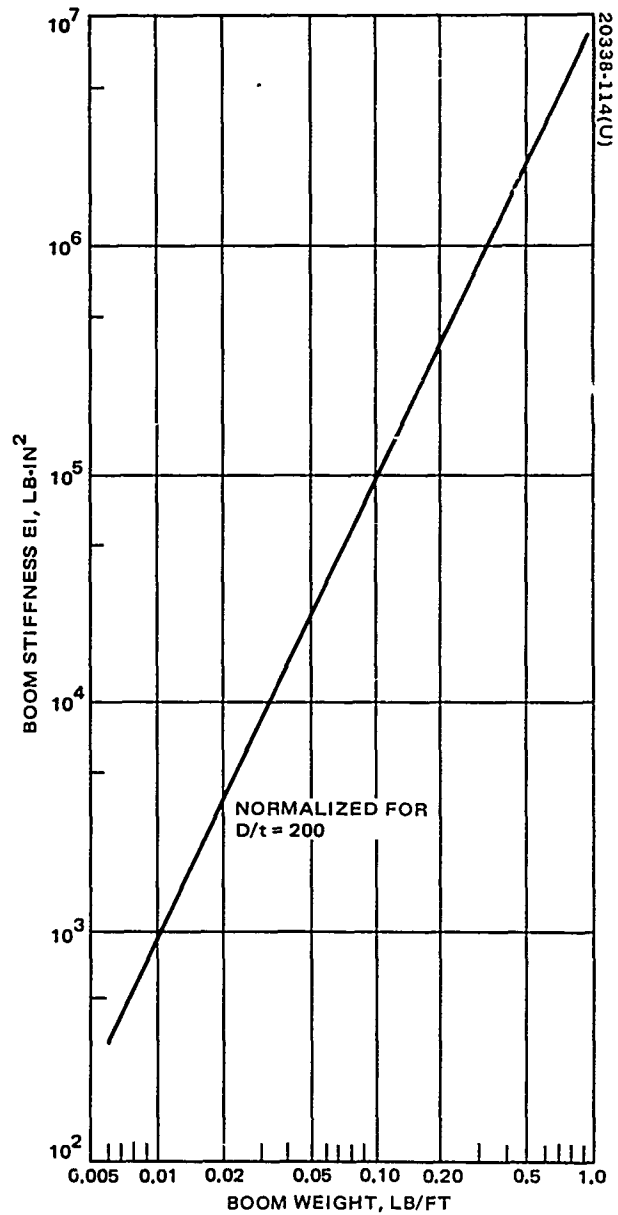


Figure 9-10. Stainless Steel BI-STEM Boom Stiffness Versus Specific Boom Weight

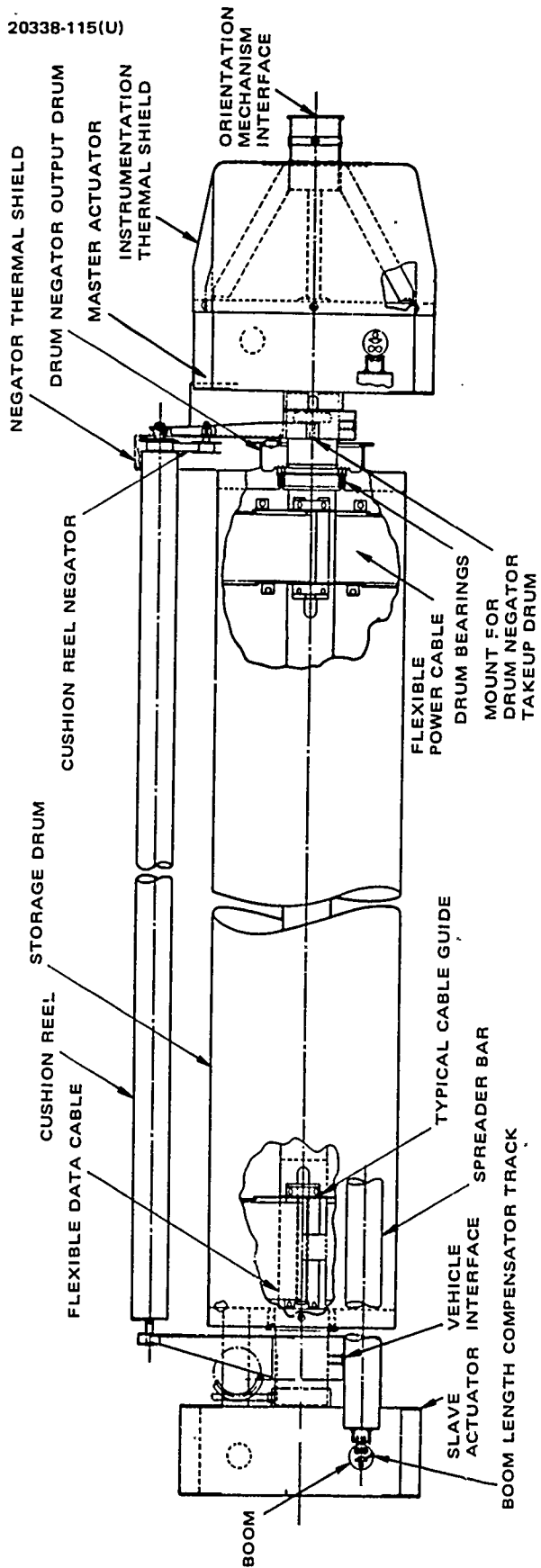


Figure 9-11. FRUSA Stowage Drum Cross Section

TABLE 9-5. FRUSA STOWAGE DRUM ASSEMBLY - WEIGHT BREAKOUT

Item	Description	Weight, pounds
Drum	8-inch diameter, 0.030-inch thick, 70-inch long, magnesium cylinder	3.46
Drum end plates	3/4-inch honeycomb disks, titanium facesheets (includes reel for torque spring motor)	2.22
Spar	2-inch diameter, 75-inch long, aluminum	1.57
Cushion reel and support	Reel 1.5-inch diameter, 0.020-inch wall, aluminum. Support, magnesium	0.98
Torque shaft	0.75-inch diameter, t = 0.050-inch wall, aluminum; connects drive and slave.	0.74
Spreader bars	1.5-inch diameter, 0.018-inch wall, aluminum (2 required per drum in dual panel system)	1.50
Torque spring motors	Constant torque springs. Negator; <sup>®</sup> for panel tensioning and cushion reel drive	1.7
Miscellaneous hardware	Includes flex cable, electrical fittings, thermal cover, boom length compensator (0.6 pound) bearings and miscellaneous structural hardware	3.87
Drum assembly	Total	16.08

design requirements for those environments are summarized in Table 9-1. A stowage drum diameter must be chosen which ensures that the solar cells will not break when bent around the cylinder and that flexible solar cell panels will wind properly under low panel tension. A small drum diameter is desired to achieve minimum array stowage volume. The drum diameter of 8 inches was found suitable for roll-up of 2 by 2 cm, 8-mil thick solar cells, as was exhibited by extremely low failure rates (see Table 9-3) during FRUSA testing. This drum diameter is therefore maintained. The cylinder wall thickness is then determined by analysis to provide 1) sufficient overall buckling

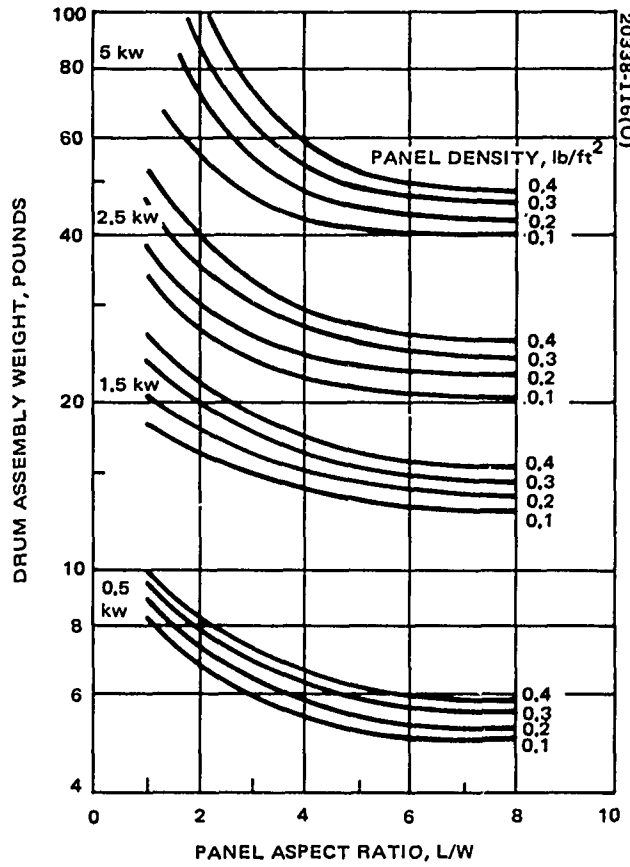


Figure 9-12. Drum Assembly Weight Variation With Panel Aspect Ratio

strength, bending strength, and drum bending stiffness and 2) adequate stability for sustaining radial load connected with a breathing vibration mode of the panel layers on the drum during launch.

The parametric computer analysis routine initiates the drum optimization by finding the minimum wall thickness for a magnesium drum and a trapezoidal lateral load distribution of 5 g at the drum ends and 50 g in the drum center. This simplified load pattern was also used in the FRUSA preliminary design phase. Next, the peak bending stress and the drum bending frequency are calculated. If the bending stress exceeds the magnesium yield limit, or the drum assembly bending frequency is lower than the design goal of 30 Hz, then the cylinder thickness will be increased. In a parallel computation, properties of beryllium are substituted ( $41 \times 10^6$  psi E-modulus as compared to  $6.5 \times 10^6$  psi for magnesium) to bound the minimum weight achievable for the 8 inch diameter drum when drum stiffness is critical in design.

The honeycomb drum end closures are dimensioned for an acceleration of 30 g in the direction of the drum axis applied to the drum and solar panel mass. The drum weight is then computed for parameter combinations of array sizes of 0.5, 1.5, 2.5, and 5-kw power output, area specific panel densities of 0.1, 0.2, 0.3, and 0.4 lb/ft<sup>2</sup>, and panel length-to-width ratios up to  $L/W = 8$ .

Similar weight scaling was performed for the remaining elements of the stowage drum assembly which are listed in Table 9-5. With the exception of the torque spring motors (negator) and miscellaneous hardware, the weight of all items depends on the array size, area density, and the array length-to-width ratio  $L/W$ . The spring motor weight is a function of the array size only because the panel tension is maintained constant per unit panel width and the negator spring torque is essentially independent from the number of spring turns. The miscellaneous hardware items were assumed to vary with array size only.

Results of the weight analysis for the storage drum assembly are summarized in Figure 9-12. This figure shows the drum structure assembly weight for four array sizes and panel densities versus the panel length-to-width ratio  $L/W$ . It is apparent that the  $L/W$  ratio is of minor importance for array sizes of up to about 2-kw power. For larger array sizes, the stowage structural elements get to be relatively long for small  $L/W$  values. Their weight increases considerably in order to maintain adequate structural stiffness. When array panels of great width are used and minimum weight is desirable, the design effort should concentrate on providing enlarged stowage volume or use of advanced structural materials becomes mandatory.

The drum assembly weights shown in Figure 9-12 will be used in the following as part of the array system weight toward finding the optimized array system.

## SOLAR ARRAY SUPPORT STRUCTURE WEIGHT OPTIMIZATION

The major objective of this parametric optimization analysis is to determine the lightest weight support structure for factors of most concern in preliminary array design.

- Support structure bending strength
- Minimum deployed panel frequency
- Support structure buckling due to panel tensioning

The weight optimization was conducted for these design parameters as a function of the panel length to width ratio (L/W). The largest array module employed in this weight optimization is that of 5-kw power output. Array sizes up to 20 kw are achieved by assembling array modules of optimized size into an array system.

The solar cell panel density is maintained as a design parameter because solar cell and cover slide thickness is usually optimized for mission specific requirements. Similarly, the collector bus and cell layout on the flexible substrate is mission-related. The weight of the cushion material is about 1 to 2 percent of the panel weight and is assumed to be included in the panel weight.

### Array Support Optimized for Bending Strength

In the FRUSA flight experiment design, a quasi-static load factor of 0.1 g was employed to account for all steady state and dynamic acceleration peaks anticipated in orbital flight. This design factor proved to be conservative in nominal flight as demonstrated by flight data (see Section VI). During malfunctioning of the space vehicle, however, accelerations greater than 0.1 g were experienced.

Omnidirectional quasi-static acceleration may impose tension, compression, and bending loading on the support structure. The bending loading caused by uniform acceleration is considered here for parametric analysis. The peak bending moment in the support boom occurs at its deployer exit (boom root). For a dual panel array, this moment M is defined by

$$M = g \left( \frac{1}{8} W_P \ell + \frac{1}{2} W_B \ell + \frac{1}{2} W_S \ell \right) \quad (7)$$

where

$g$  = load factor in g

$\ell$  = panel length in inches

$W_P$  = total array panel weight (includes two panels)

$W_B$  = Bi-STEM boom weight in pounds ( $w * \ell$ )

$W_S$  = spreader bar weight in pounds

Stainless steel Bi-STEM booms are assumed here for parametric evaluation. Their bending strength  $M_B$  is determined from Figures 9-8 and 9-13 as well as the following equations.

$$M_B = C_1 (w)^{3/2} \quad (8)$$

$$\frac{M_B}{w} = C_2 D \quad (9)$$

The constants  $C_1$  and  $C_2$  depend on the boom material (density, E-modulus), the diameter to thickness ratio  $D/t$ , and the ribbon overlap factor. The Bi-STEM boom property data employed in the analysis are those provided by SPAR Aerospace normalized for a  $D/t$  ratio of 200 and reduced by 25 percent for added conservatism. Their values for  $C_1$  and  $C_2$  are 9500 and 3000 when  $M_B$  is measured in in.-lb,  $w$  in lb/ft, and  $D$  in inches.

By combining Equations 7 and 8, and expressing panel weight, spreader bar weight, and panel length in terms of array power  $P$ , panel density  $\rho$ , and aspect ratio  $L/W = R$ , an equation is found for computing the weight  $w$  per linear foot of boom;

$$C_1 w^{3/2} = 60 g \left[ 25\rho P \sqrt{\frac{1}{2} PR} + 5 PRw + P \right] \quad (10)$$

The weight  $W$  for a complete set of four booms is then

$$W = 40 w \sqrt{\frac{1}{2} PR} \quad (\text{pounds}) \quad (11)$$

and the associated boom diameter is determined from

$$D = 3.17 \sqrt{w} \quad (\text{inches}) \quad (12)$$

Equations 10 through 12 were solved by computer analysis. The results of this analysis are illustrated in Figures 9-14 through 9-17 which show the boom weight and diameter respectively for the design parameters of panel size, panel density, and load factors versus the panel aspect ratio  $L/W$ . By knowing the boom diameter, the deployer mechanism weight is found from Figure 9-5. The total weight of an array designed for quasi-static loading is gained by adding drum assembly weight (Figure 9-12) and the solar cell panel weight. This summing will be performed later in the system configuration analysis.

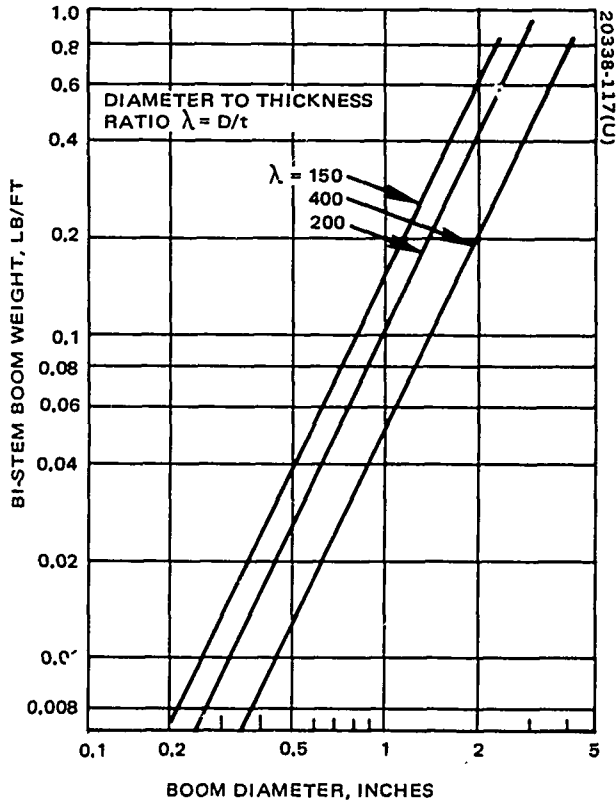


Figure 9-13. Stainless Steel BI-STEM Boom Weight Versus Boom Diameter.  $D/t$  between 168 to 250

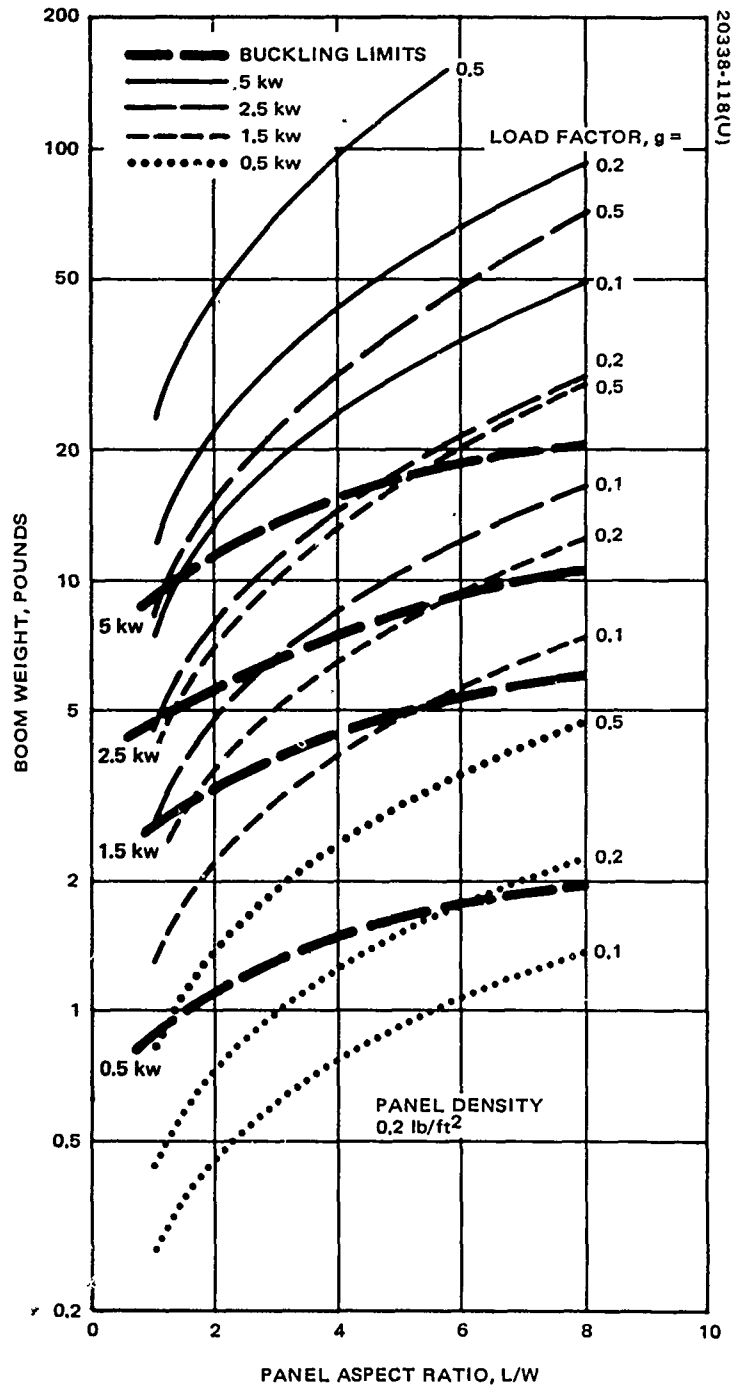


Figure 9-14. Weight of Four Support Booms Versus Panel Aspect Ratio For Variable Quasi-Static Load Factors



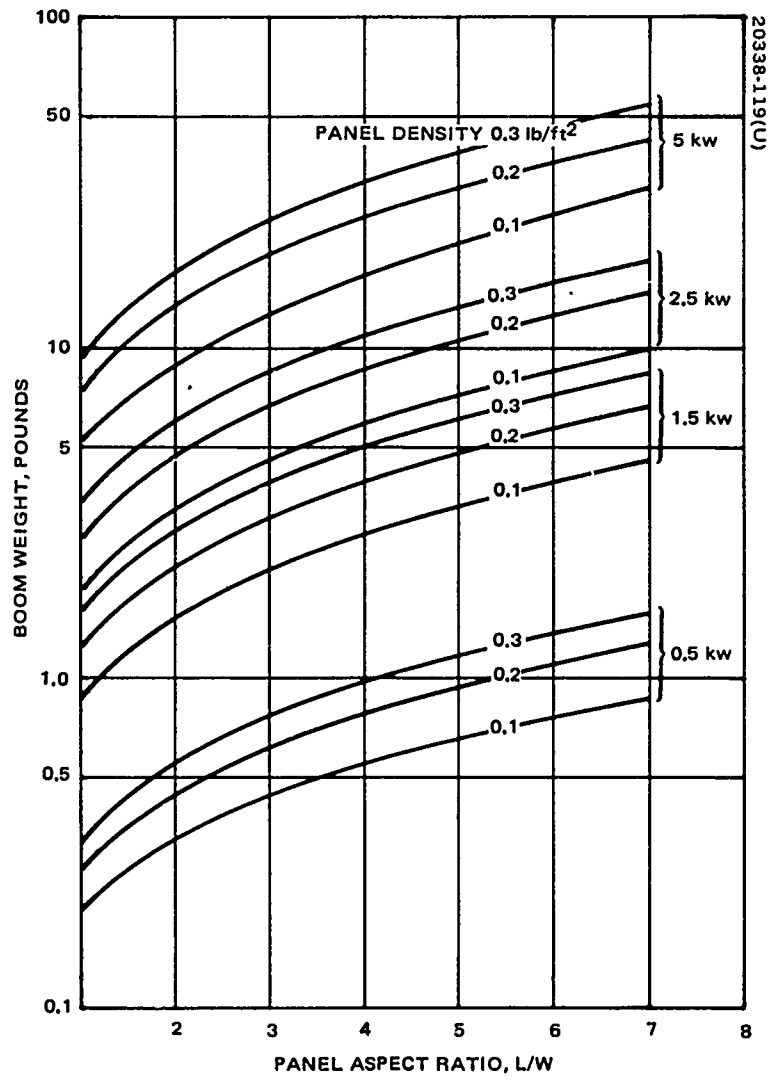


Figure 9-15. Boom Weight Versus Panel Aspect Ratio For Design Condition of 0.1 g Load Factor

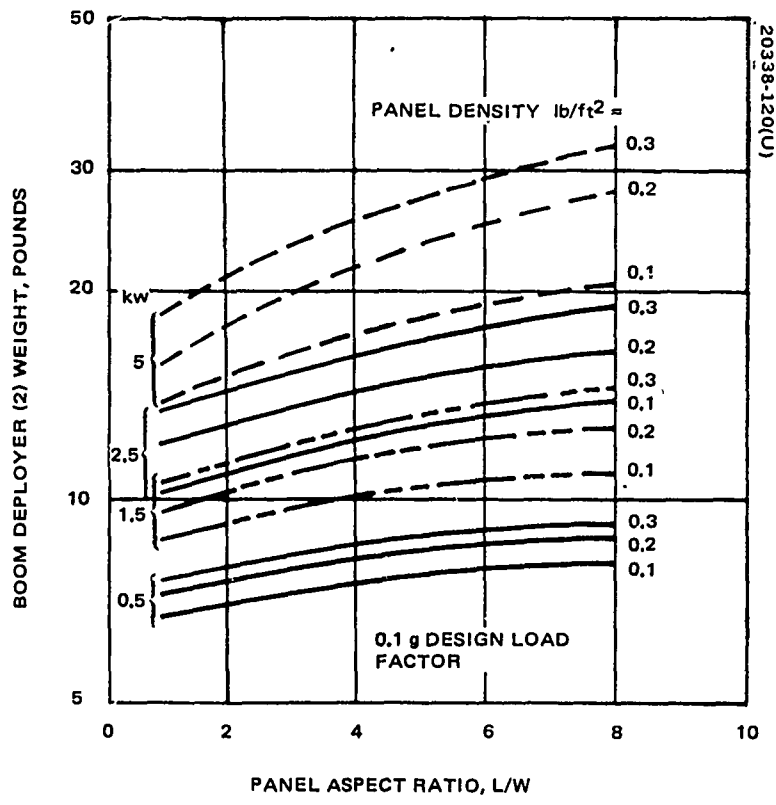


Figure 9-16. Dual Boom Deployer (Two Per Array) Weight Versus Panel Aspect Ratio L/W For 0.1 g Quasi-Static Design Load Factor

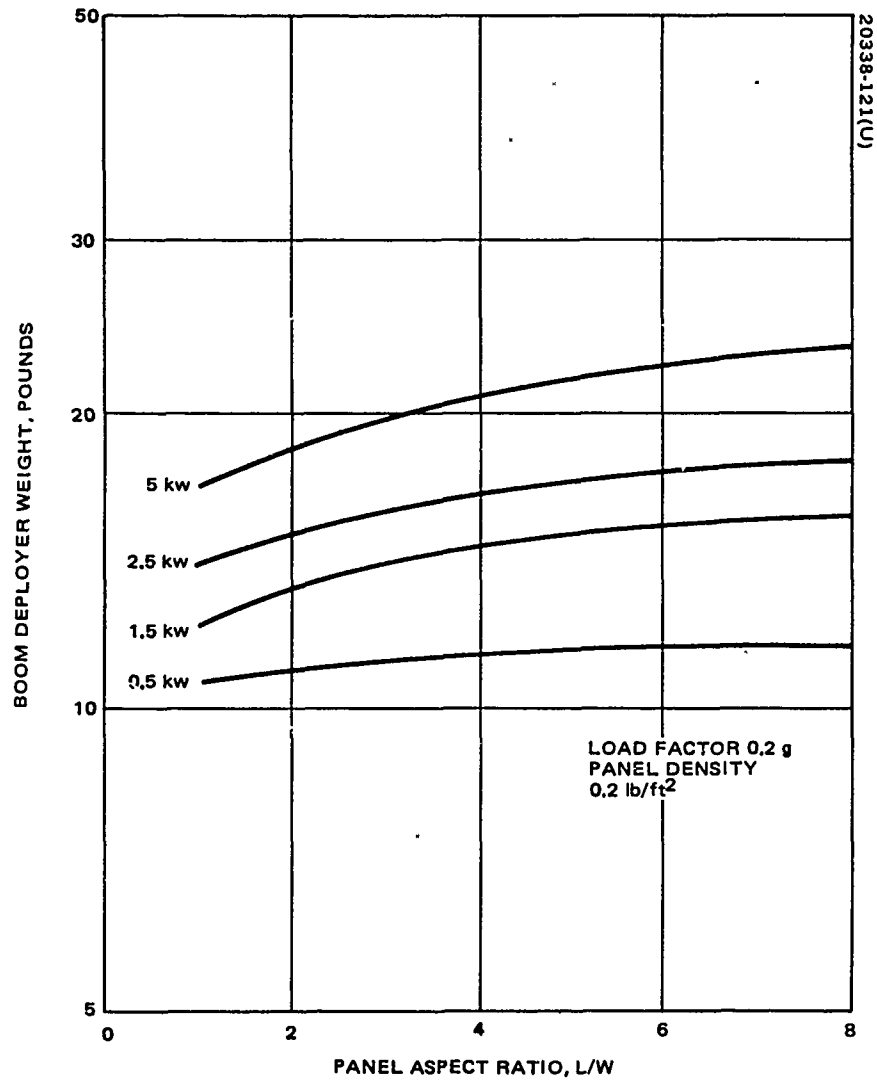


Figure 9-17. Weight of Two Dual Boom Deployer Mechanisms Versus Panel Aspect Ratio For Booms Dimensioned For 0.2 g Quasi-Static Loading

### Array Support Optimized for Stiffness

A computer routine has been developed for analyzing torsional and bending frequencies of a tensioned flexible solar cell panel which is tied at one end to cantilevered support booms of uniform bending stiffness and which is anchored to the roll-up drum at the opposing end. This program has been successfully used for predicting the 1.5-kw FRUSA flight characteristics (see Section VI, Flight Test Results). A simplifying assumption was made that the fundamental panel bending frequency is defined for a cantilevered boom of uniform mass and stiffness with a tip mass representative of the panel loading. The fundamental bending frequency predicted by this approach compares reasonably with results obtained by the above computer technique provided the panel tension is not too low. The bending frequency  $f$  of this simplified model is given by

$$f = \frac{1}{2\pi} \left( \frac{1158 EI}{l^3 \left( \frac{1}{8} W_P + \frac{1}{2} W_S + 0.23 W_B \right)} \right)^{1/2} \quad (13)$$

By substituting the equations for boom stiffness, boom weight, panel weight, and panel size as expressed by

$$EI = C_3 D^2 w$$

$$w = C_4 \frac{D^2}{\lambda}$$

$$W_B = w L$$

$$W_P = 100 \rho P$$

$$W_S = \sqrt{\frac{2P}{R}}$$

$$L = \sqrt{50 PR}$$

Nomenclature is the same as above;  $C_3 = 1.16 \times 10^6$ ;  $C_4 = 20$  (see Figures 9-11 and 9-13); a parametric relationship is developed between the boom diameter and array bending frequency:

$$\frac{4450}{\lambda f^2 (PR)^{3/2}} D^4 - \frac{141.5}{\lambda} (PR)^{1/2} D^2 - \left( 50 \rho P + \sqrt{8 \frac{P}{R}} \right) = 0 \quad (14)$$

Knowing the required boom size for a specified frequency the weight for four support booms of an array is then predicted from

$$W = \frac{400 D^2}{\lambda} \sqrt{2 PR} \quad (15)$$

and the boom deployer weight is found as discussed above. The boom stiffness employed in the analysis was reduced to 80 percent of the reference data. Results of the parametric computations are illustrated in Figures 9-18 and 9-19. These results can be used for any parameter combination for array system weight optimization. A sample calculation will be shown later in the Summary Solar Array Configuration Optimization section.

#### Array Support Optimized for Boom Buckling

The roll-up flexible array concept employed as baseline design in this parametric study requires panel tension for maintaining the array planar, contouring the panel to the stowage drum in roll-up, and for control of the array dynamic characteristics. This panel tension produces compressive loading onto the support booms which must have sufficient strength to resist column buckling. Since the compression force vector will always be aligned from the boom tip to the boom root (bow-string model), the critical Euler buckling load is expressed by

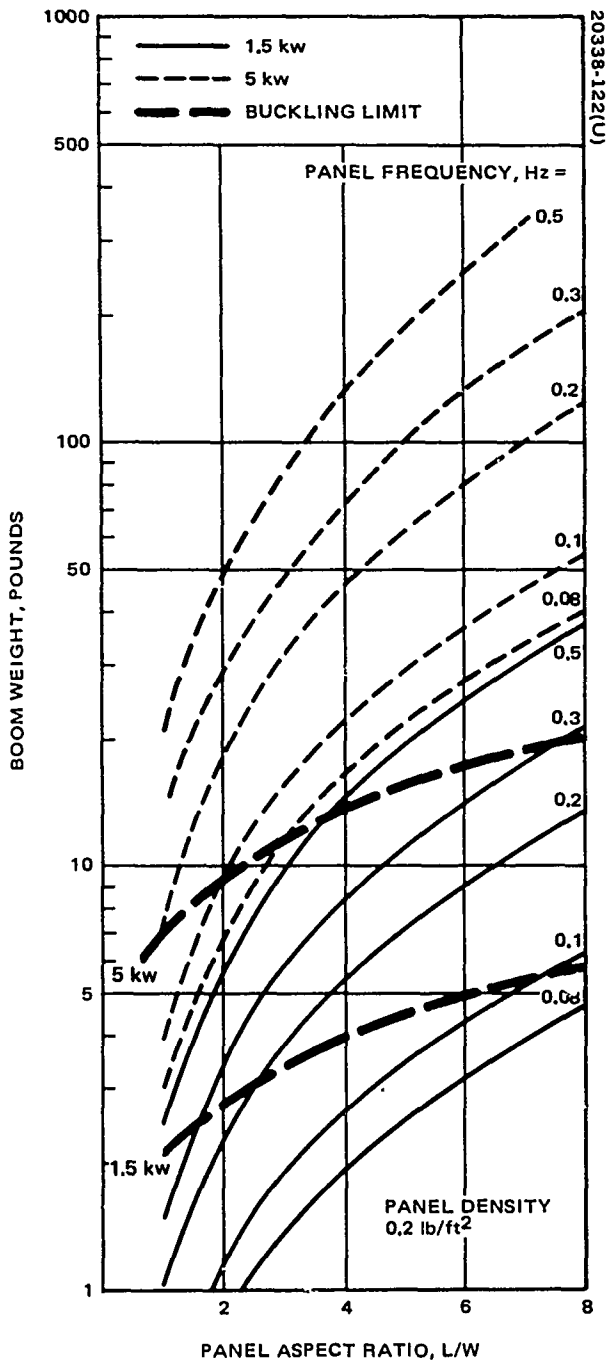
$$F = \frac{\pi^2 EI}{\ell^2} \quad (16)$$

This buckling load may be reduced by a minor offset between boom root and panel termination, as well as by lateral boom loading. To account for such conditions, a reduction factor of 2 is introduced in Equation 16.

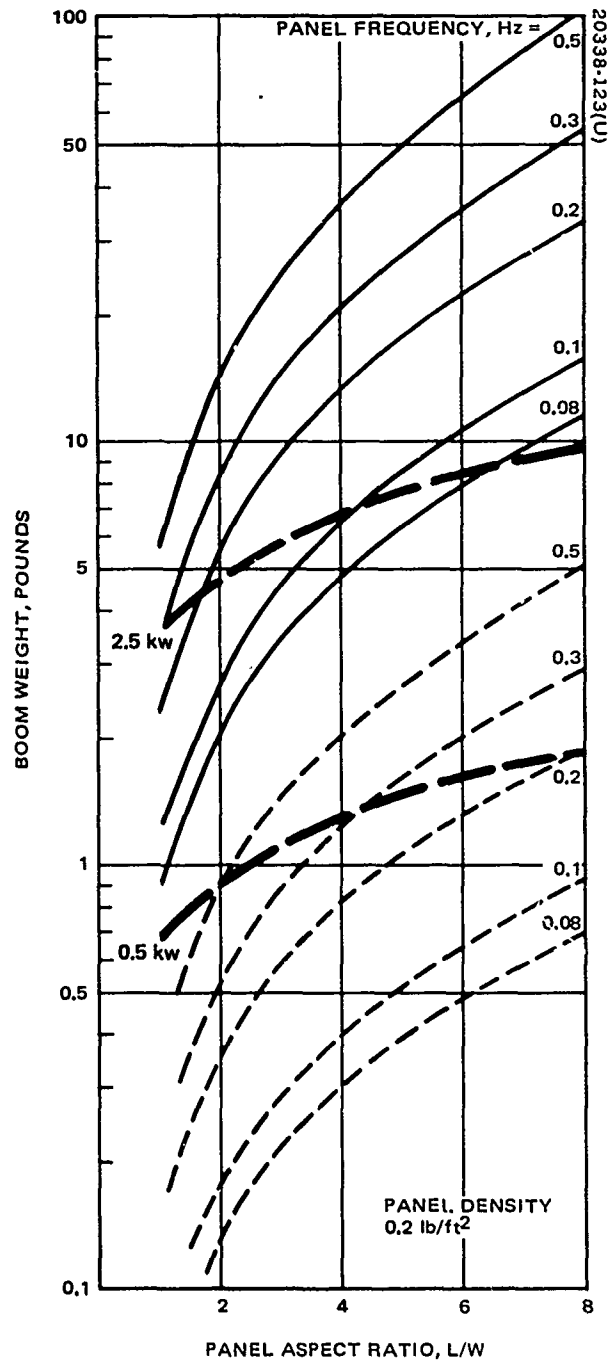
Optimization of the boom dimensions and weight for buckling follows essentially the same procedure used for strength and stiffness optimization. By parameter substitution for  $EI$  and  $\ell$  in Equation 16, formulas are derived for the required specific boom weight  $w$  and the total weight  $W$  of four support booms:

$$w = (0.025 \frac{PRF}{\lambda})^{1/2} \quad (17)$$

$$W = 28.3 w \sqrt{PR} \quad (18)$$



a) 1.5 AND 5 kW



b) 0.5 AND 2.5 kW

Figure 9-18. Weight of BI-STEM Steel Booms (Four) Required to Achieve Specified Panel Frequency

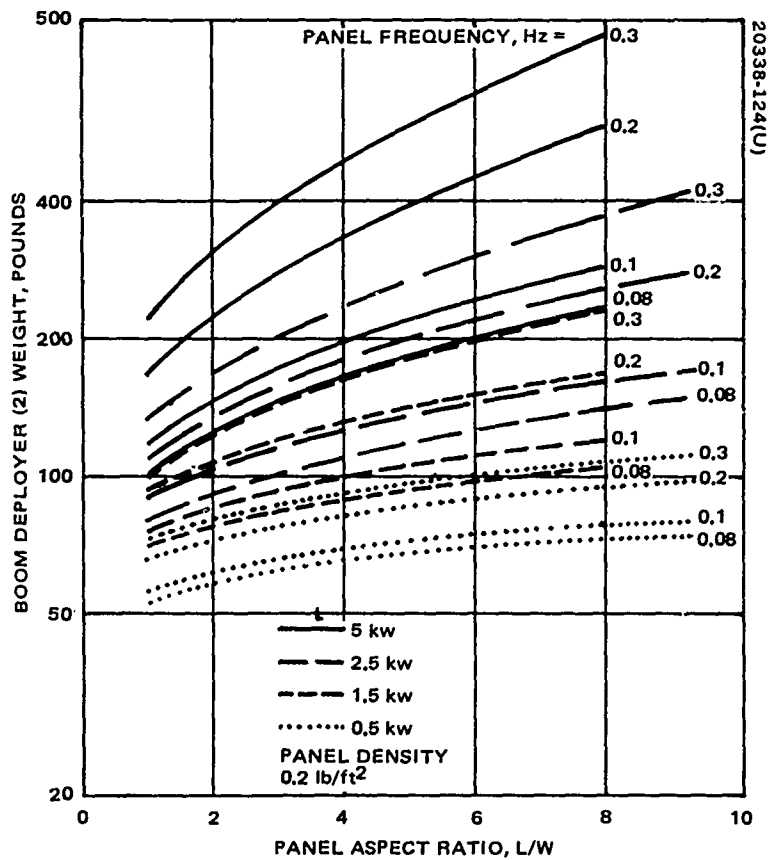


Figure 9-19. Dual Boom Deployer (Two per Array) Weight Versus Panel Aspect Ratio When Panel Bending Frequency is Design Criteria

If the tension force is assumed to be proportional to the panel width the parametric boom design might be extended as shown:

$$F = \frac{q H}{2} = \frac{q}{2} \sqrt{\frac{50 P}{R}} \quad (19)$$

where H is the panel width and q is the panel tension per linear foot. With 19 in 17, a parametric relationship is obtained for boom weight and specific panel tension

$$w = (0.885 q \sqrt{\frac{P^3 R}{\lambda^2}})^{1/2} \quad (20)$$

If the minimum value of q is assumed to be 0.5 lb/ft as required for proper winding of the FRUSA type panel, then the weight for buckling-limited booms can be computed from Equation 18. Results of such calculations were entered in Figures 9-14 and 9-18. By comparing buckling boom weight with that required to accomplish either a specified panel frequency and/or to comply with a design load factor, the critical design criteria are found. When boom buckling is the critical design condition, the panel aspect ratio is defined by the intersection of buckling and frequency or strength parameter lines.

#### ARRAY ORIENTATION MECHANISM

The final link in this parametric analysis of array sizes from 0.5 to 20 kw is the orientation control drive for sun pointing of the array in orbital flight. The two-axis drive employed by the 1.5-kw FRUSA experiment was developed for array sizes up to 5-kw and it presents an excellent reference point for system studies when primarily size and weight are of interest. The scaling in any specific application, however, must be exercised with care since many factors bearing on the problem could lead to unrealistic results. Questions arise such as:

- 1) Shall the space vehicle grow proportionally to the array moment of inertia (upon which motor size depends)?
- 2) Is a massive 20 kw array required to acquire the sun in the same time as a 0.5 kw array?

The simplest approach, and one which is entirely practical if design criteria are allowed to vary over reasonable limits as size varies, is to employ the nominal 5-kw design for all applications between 0.5 and 20 kw. The 5-kw design thus becomes a universal design. For application to the



smaller arrays, if they are structure-limited to a fixed value of applied acceleration, it is a simple matter to limit the motor-driving current accordingly. In the larger sizes, the primary concessions that must be made are to allow slower acquisition and slew maneuvers and to allow the brush current density to increase. Without adding brushes, the nominal design would then pass 150 amp/in.<sup>2</sup> at 10 kw, and 300 amp/in.<sup>2</sup> at 20 kw. It should be noted that the brush materials used have been found to operate satisfactorily at this level in tests and in space (on the Nimbus satellite). The thermal-control design would also be affected in the larger sizes, with possible requirements for added radiating area and/or application of heat-pipe thermal transfer techniques.

Should the design approach preclude adaptation of the 5-kw design, the approximate size variation with power may be estimated if assumptions are made that: 1) the array size will vary, but not the diameter of the vehicle which the panels must clear, 2) motor size will depend primarily on drive function in the smaller sizes, and on maintaining a fixed torque-to-inertia ratio in the larger sizes, and 3) the number of power brushes will be varied to keep the current density at 75 amp/in.<sup>2</sup>. With these ground rules, motor weights vary significantly and estimated mechanism weights are as follows (Table 9-6):

TABLE 9-6. TWO-AXIS ORIENTATION DRIVE  
MECHANISM WEIGHT

System Power, kw	Weight, pounds
1	52
2	55
5	69
10	100
20	176

The weights quoted may appear heavy for the application, but it must be remembered that the design has the capability for unlimited motion on two axes, and sufficient redundancy to ensure a high probability of a 3-to 5-year lifetime. Elimination of mechanical redundancy would cut the weight by about 1/8th, with an associated low risk of reducing lifetime, and elimination of electronic redundancy would save 7 to 8 pounds, with about an 8 percent reduction in probability of meeting a 3-year requirement. For shorter lifetimes, elimination of both redundancies is a logical step.

A single-axis drive mechanism should weigh approximately half of the tabulated weight since the mechanism components are quite similar for both axis drives. Since the control electronics is relatively independent of the system power, the weight of the FRUSA control electronics, 15 pounds, may be used for parametric studies.

## SUMMARY SOLAR ARRAY CONFIGURATION OPTIMIZATION


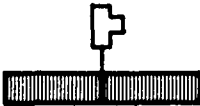
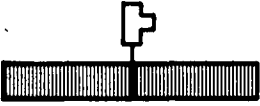
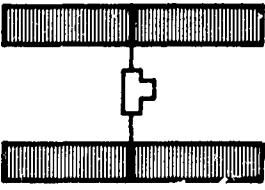
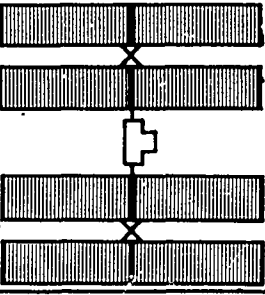
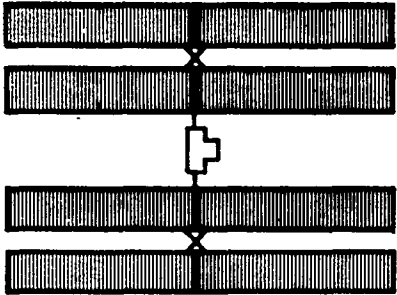
The array optimization analysis and its results have been presented for the individual subassemblies of the drum mechanism, the solar panel support structure and its deployment mechanism, and a two-axis array positioner mechanism in order to:

- 1) Assess the relationships which exist between array performance characteristics and design parameters
- 2) Provide the designer with parametric data which allow him to determine an optimum roll-up array configuration for a wide range of design requirements and array sizes between 0.5 and 20 kw.

The application of these parametric data is illustrated in the following by determining array dimensions, weight, and configuration concepts for array sizes of 0.5, 2.5, 5, 10, and 20 kw. The optimization is illustrated for a 0.3-Hz minimum panel frequency and a 0.1-g in-orbit loading requirement. A panel density of 0.2 lb/ft<sup>2</sup> is used which is representative of 8-mil solar cells and 6-mil cover glasses as employed by the FRUSA flight experiment.

Figure 9-20 summarizes the essential results of this sizing optimization for 0.3 Hz minimum frequency. The weight optimal array configurations were determined from Figure 9-21 and 9-22, which summarize the parametric weight computations performed for the stowage drum, boom deployer, and the panel support booms. Figure 9-21 depicts the solar array weight for discrete array sizes and design frequencies as a function of the panel aspect ratio. As shown, the aspect ratio for optimized array weight varies widely with the frequency parameter, but it is relatively independent of the array size. By cross-plotting the weight minima versus array size, Figure 9-22 is obtained. The important result to be gleaned from this figure is the optimum array module size for any specific power level and array stiffness requirement, e. g. , a 3-kw array system dimensioned for 0.3 Hz bending frequency will weigh the same when configured as a single or double module system. For smaller array sizes, the single module approach is weight-effective, and conversely larger array systems of minimum weight should use multiple array units on the basis of array panel weight optimization. In the system evaluation, however, the weight for the orientation mechanism as well as the array deployment hardware and fittings for joining modules must also be considered. The weight for various sizes of orientation mechanisms was tabulated above. Estimates for array module support arm and fittings joining the orientation mechanism as well as individual arrays in their deployed position are shown in Figure 9-20.

The system performance as rated by the specific power output varies between 6 and 16.8 watts per pound for the depicted array configuration. It is noted that the 20-kw array system does not utilize the optimized panel size

KW	0.5	1.5	2.5	5	10	20
						
PANEL DIMENSIONS, FT	8.4 X 3	11 X 6.9	14.2 X 8.9	14.2 X 8.9	14.2 X 8.9	22.4 X 11.2
L/W	2.8	1.6	1.6	1.8	1.8	2.0
WEIGHT, LB	27	65	104	208	416	932
ARRAY	53	64	87	80	110	194
ORIENTATION**	3	4	8	12	70	102
SUPPORT	83	133	179	300	596	1228
WATT/LB	18.5	23	24	24	24	21.4*
ARRAY SYSTEM	6.0	11.3	14	16.6	16.8	16.2*
ALLOWABLE LOAD FACTOR "g"	0.12	0.2	0.2	0.2	0.2	0.25

\*ARRAY PANEL NOT OPTIMAL

\*\*2 AXIS DRIVE

Figure 9-20. Flexible Array System Configuration Optimized For 0.3 Hz

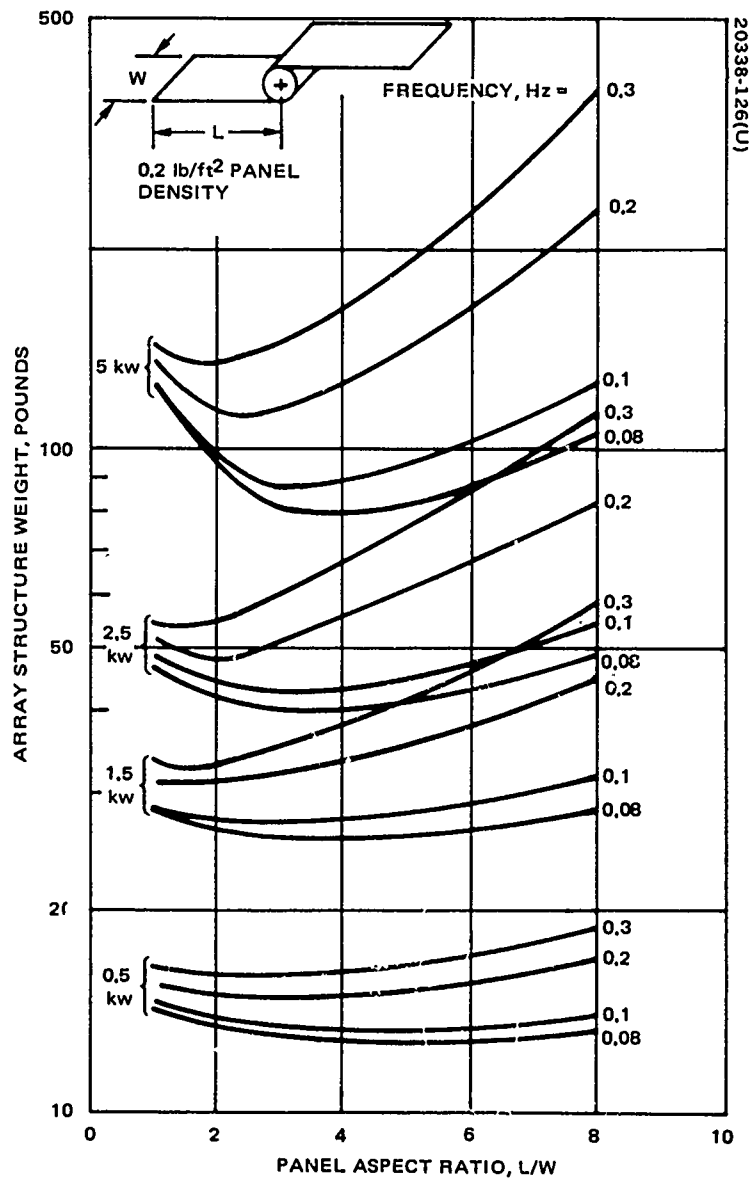


Figure 9-21. Array Structure Weight Variation With Panel Aspect Ratio When Panel Bending Frequency is Design Criteria

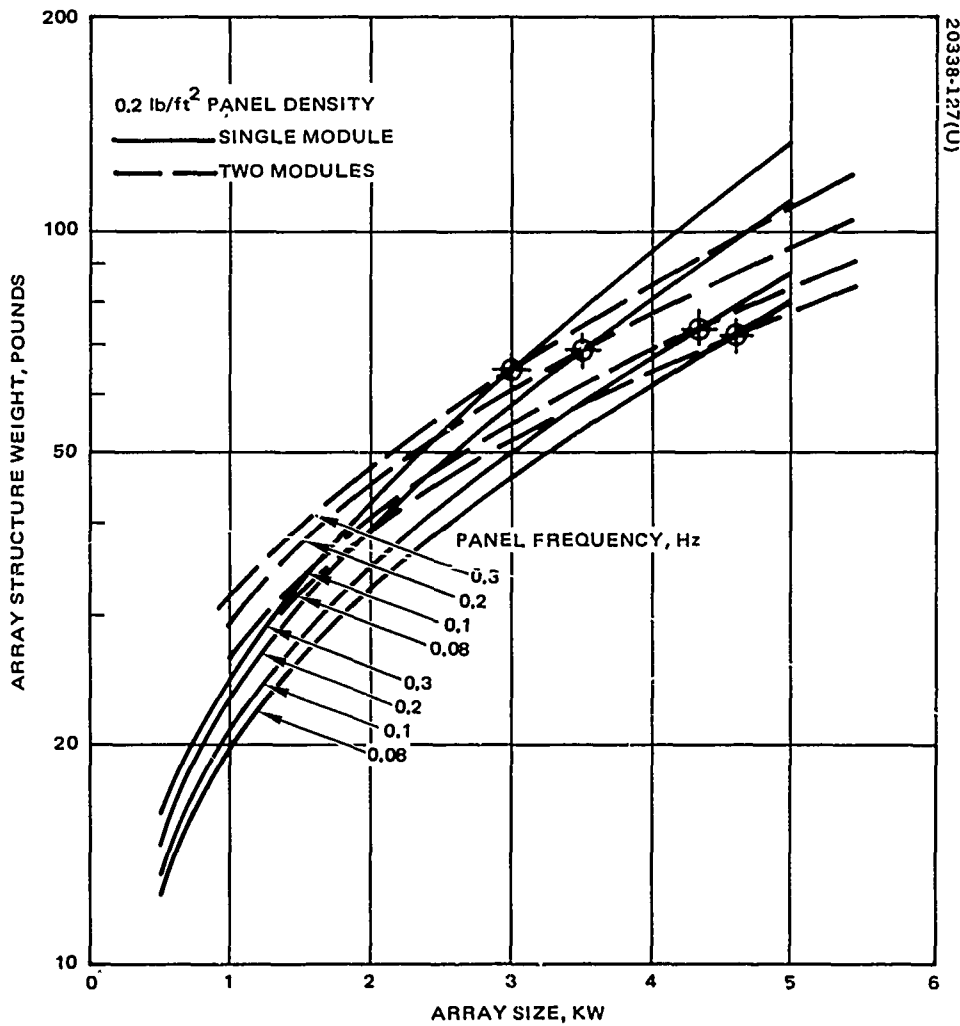


Figure 9-22. Array Structure Weight (Drum Assembly, Booms, Boom Deployers) of Array Modules Optimized for Bending Frequency

KW	0.5	1.5	2.5	5	10	20
PANEL DIMENSIONS, FT	9.5 X 2.7	15 X 5	18.7 X 6.7	18.7 X 6.7	30 X 8.4	30 X 8.4
L/W	3.5	3	2.8	2.8	3.6	3.6
WEIGHT, LB	25	60	95	190	386	772
ARRAY	53	64	67	80	120	190
ORIENTATION	3	4	8	16	30	95
SUPPORT	31	128	170	286	536	1057
WATT/LB	20	25	26.3	26.3	26	26
ARRAY SYSTEM	6.2	11.7	14.7	17.5	19	18.7
PANEL FREQUENCY Hz	0.24	0.18	0.12	0.12	0.11	0.11

Figure 9-23. Roll-Up Array System Configurations Optimized for 0.1 g

which would reduce the array weight by about 100 pounds. This indicated array weight saving all but disappears on a system basis for added module fittings and array module support hardware. When the 5-kw array module is substituted in the 10-kw system, a weight increase of 32 pounds on a system basis is predicted. This weight penalty might look favorable when array stowage space and deployment complexity are considered.

Array configurations optimized for the design criteria of 0.1-g quasi-static acceleration loading are summarized in Figure 9-23. The method of optimization followed the above approach (Figures 9-20 and 9-24). The strength optimal array module size is that of 4.5-kw as shown in Figure 9-25. This module is used in systems above 5-kw output. Specific power output of about 26 and 19 watts per pound weight are predicted for the array and the complete power system respectively. These figures of merit are based on a 0.2-lb/ft<sup>2</sup> panel density which can be improved by using thinner solar cells and cover glasses. To achieve array systems of extremely light weight, less stringent design criteria must be acceptable in array design.

The packaging figure of merit, cubic feet of array stowage volume per kilowatt power, will for array sizes above 2.5 kw be equal or better than the design goal of 2 ft<sup>3</sup>/kw on the basis of the 2.5-kw module size which has been shown in section (5-kw array design) to accomplish 1.75 ft<sup>3</sup>/kw. The packaging volume for the 5-kw module will approach 1 ft<sup>3</sup>/kw. When the stowage volume is of primary importance in the array application, a minor weight penalty is incurred associated with a module size, which is not optimized for weight.

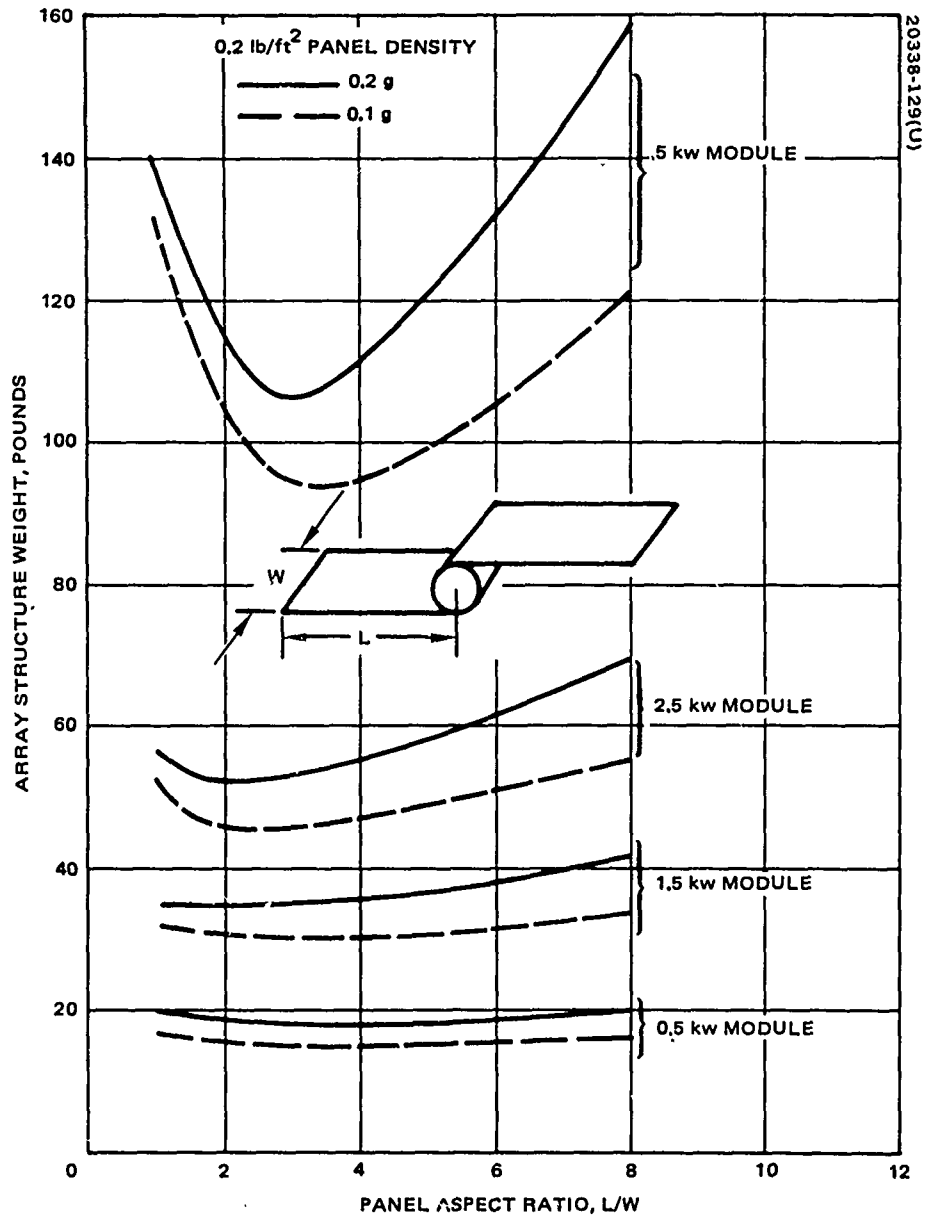


Figure 9-24. Array Structure Weight Variation With Panel Aspect Ratio For 0.1 and 0.2 g Load Factors



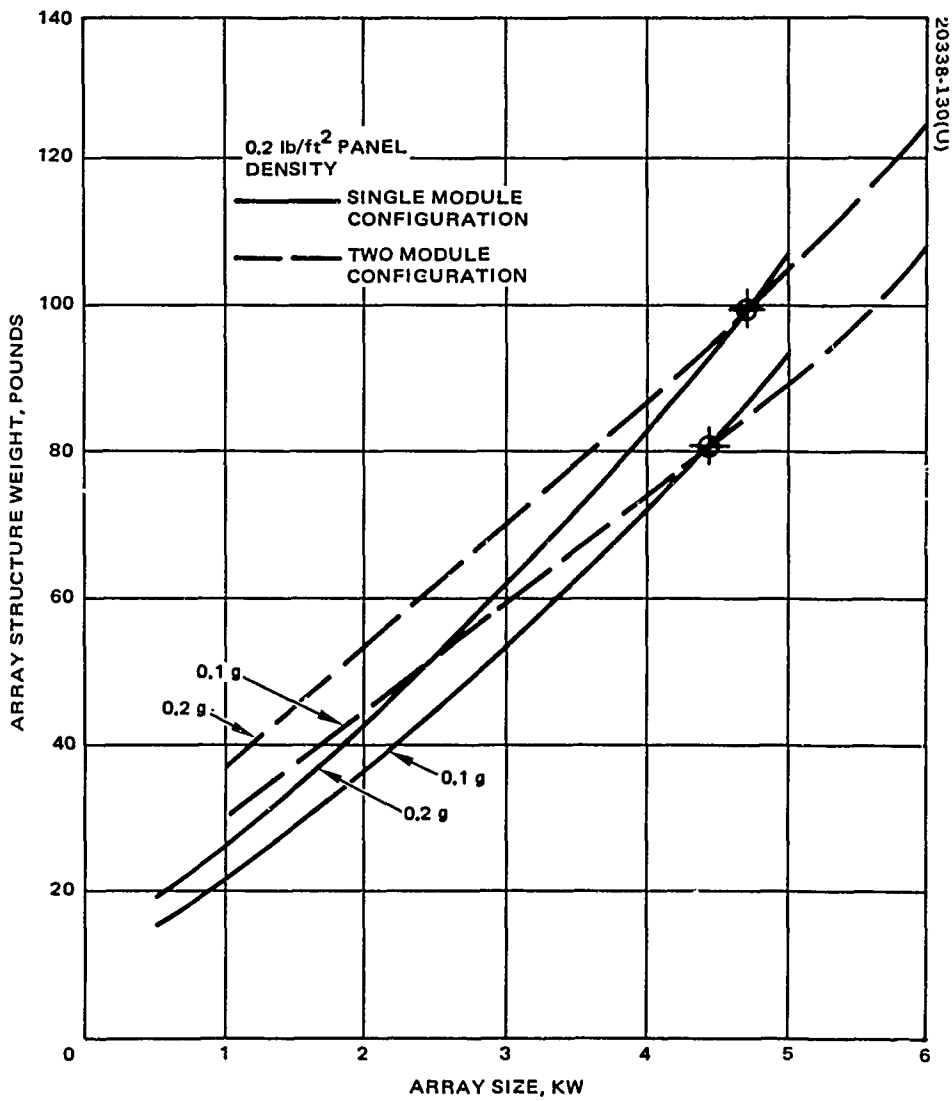


Figure 9-25. Array Structure Weight of Array Modules Optimized for Quasi-Static Loads of 0.1g and 0.2g

## SECTION X

### CONCLUSIONS AND RECOMMENDATIONS

#### CONCLUSIONS

A 1.5-kw oriented flexible rolled-up solar array system was designed, developed, fabricated, qualified for flight, and successfully flown on Space Test Program Vehicle 71-2.

Integration of the system with the spacecraft has proved simple and the analytical techniques and dynamic model used in the design have proved valid. During cyclic retraction/extension operations, and eclipse operation, as well as periods of sun acquisition and tracking, the array has been dynamically stable and has not adversely interacted with either the pneumatic or the control moment gyro/gravity gradient attitude control system of the parent three-axis stabilized Agena vehicle.

The flight proven FRUSA concept offers substantial weight and volume savings over oriented rigid array concepts for meeting a wide range of power requirements from 0.5 to 20 kw and beyond. Figure 10-1 illustrates a weight comparison of a 5.2 kw (EOL) flexible versus rigid array power system.

#### RECOMMENDATIONS

Although the flight of the FRUSA was an unqualified success, certain improvements, as discussed in detail in the subsystem area of this report (Section IV), would be incorporated in a follow-on system. While most of these improvements are simple, a few (listed below) would require advanced development so that they may be available for use in a timely manner.

- 1) On-panel-diode - to prevent panel failure when panel strings are shaded and preclude the need for large radiators
- 2) Positive-drive boom deployment - to eliminate the need for boom length compensators yet allow equal panel extension/retraction
- 3) Extension only boom actuator mechanism - to reduce complexity, cost, and weight for systems which do not require panel retraction capability
- 4) Slew rate programmer - to minimize vehicle perturbations for large area array systems by preventing the need for reacquisition after each eclipse period

In addition to the above hardware development, studies should be conducted to evaluate:

- Control system interaction for various size and type arrays, control systems, and spacecraft. Subsystem/vehicle integration should be included in these studies so that the data would be usable in preliminary spacecraft designs.
- Weight, size, reliability, and cost tradeoffs of single versus numerous deployment type systems. This study would include other than flexible roll-up systems.

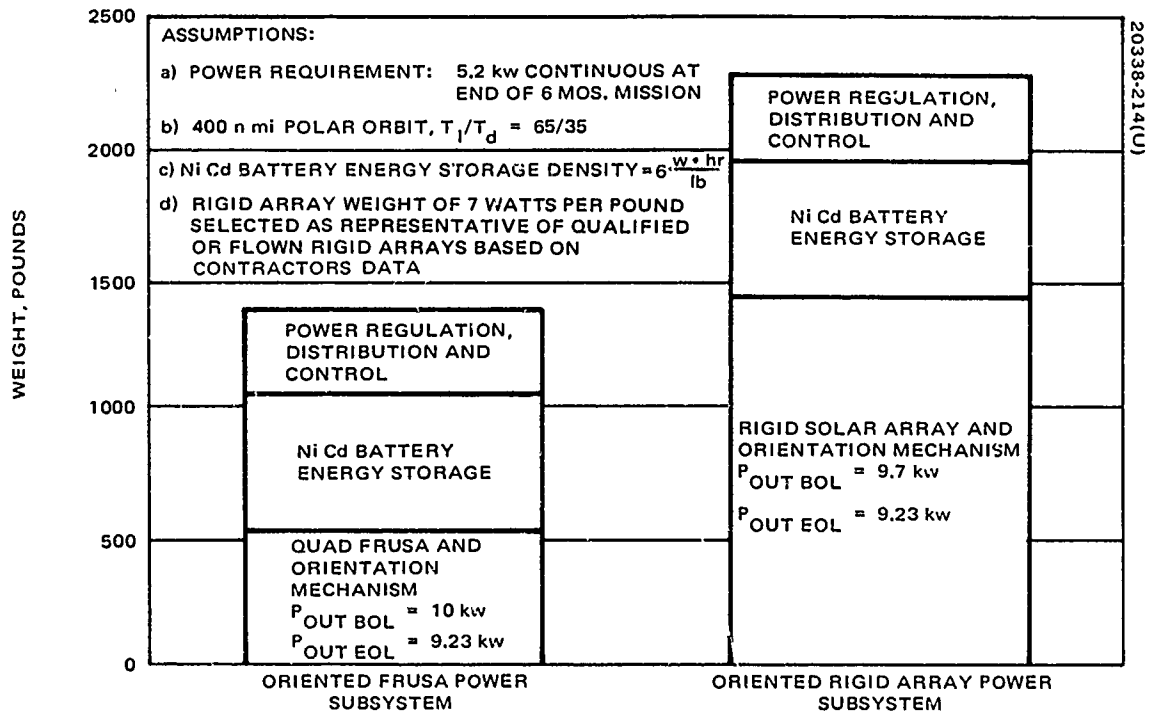


Figure 10-1. Comparison of Flexible and Rigid Array 5.2 kw Power Subsystems for Near Term Low Earth Orbit Application

APPENDIX A. MAIN SOLAR ARRAY CURRENT-VOLTAGE  
PERFORMANCE DATA

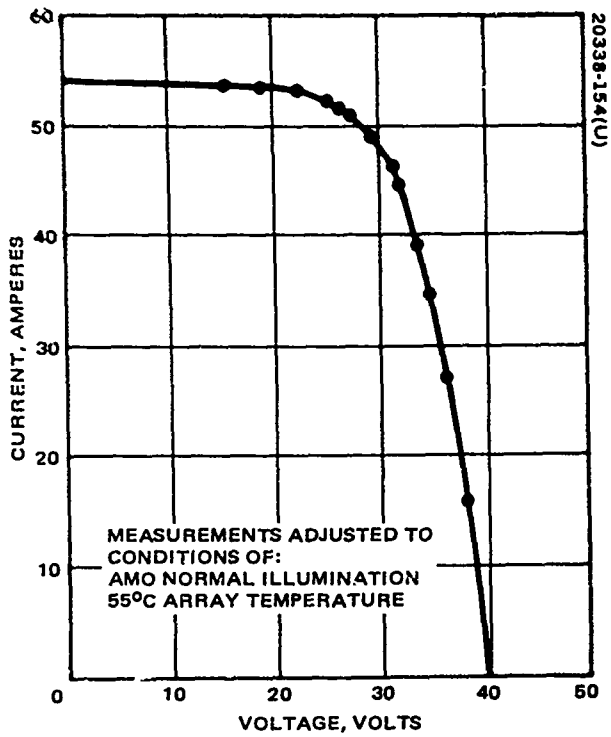


Figure A-1. Main Array Prelaunch I-V Data

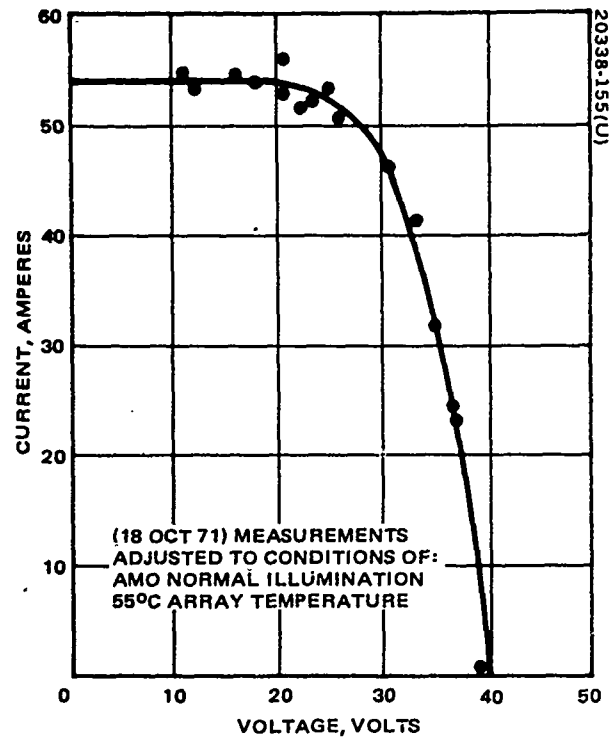


Figure A-2. Main Array Revolution 11 I-V Data

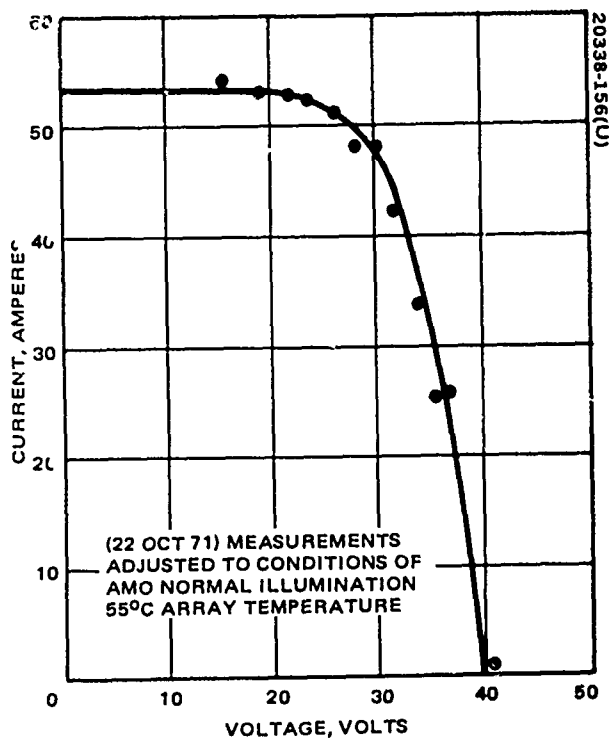


Figure A-3. Main Array Revolution 76 I-V Data

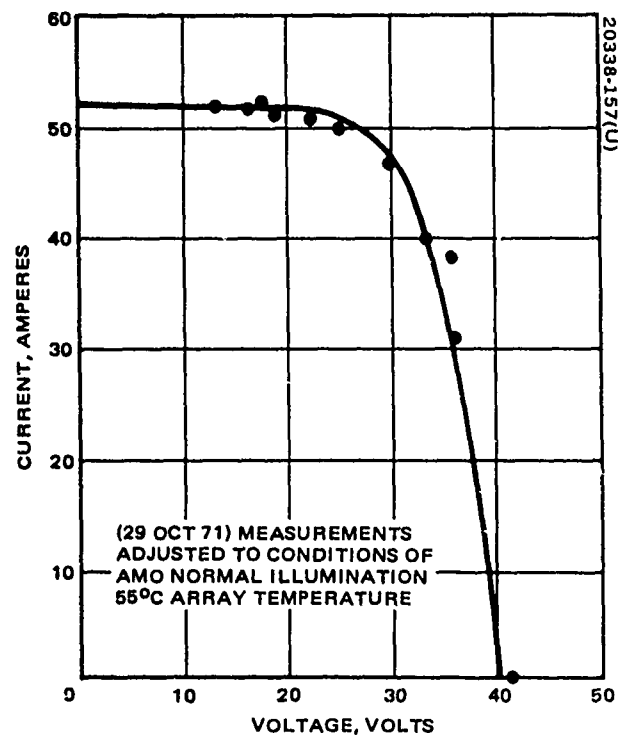


Figure A-4. Main Array Revolution 173 I-V Data

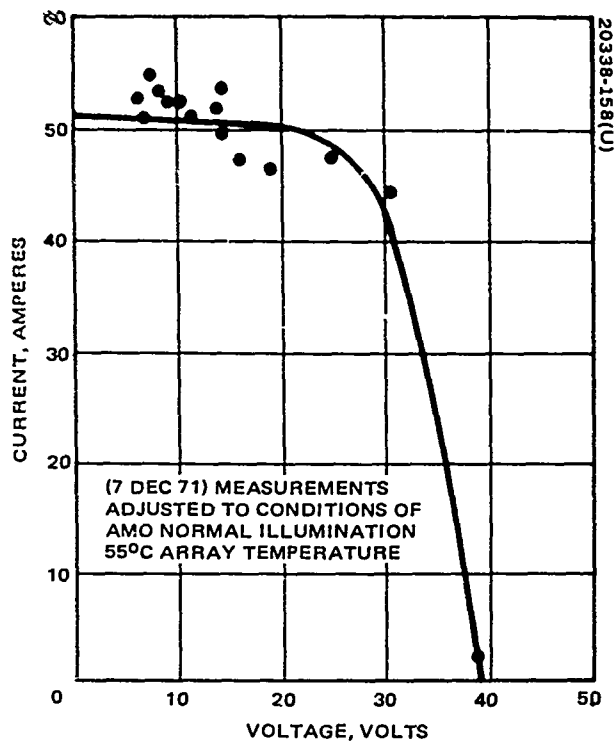


Figure A-5. Main Array Revolution 735 I-V Data

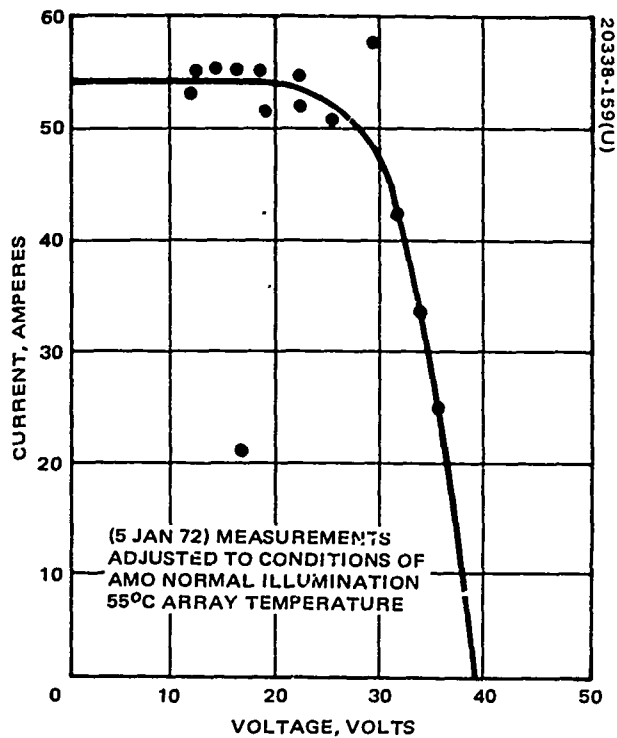


Figure A-6. Main Array Revolution 1147 I-V Data

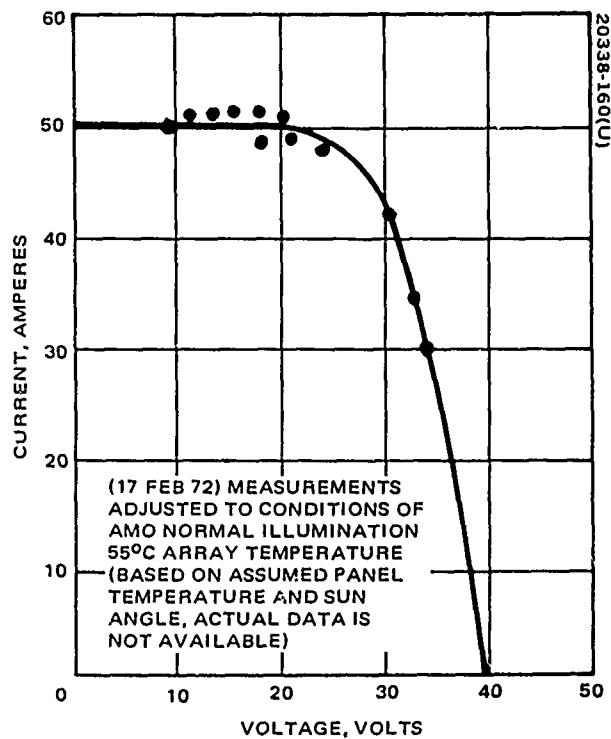


Figure A-7. Main Array Revolution 1762 I-V Data

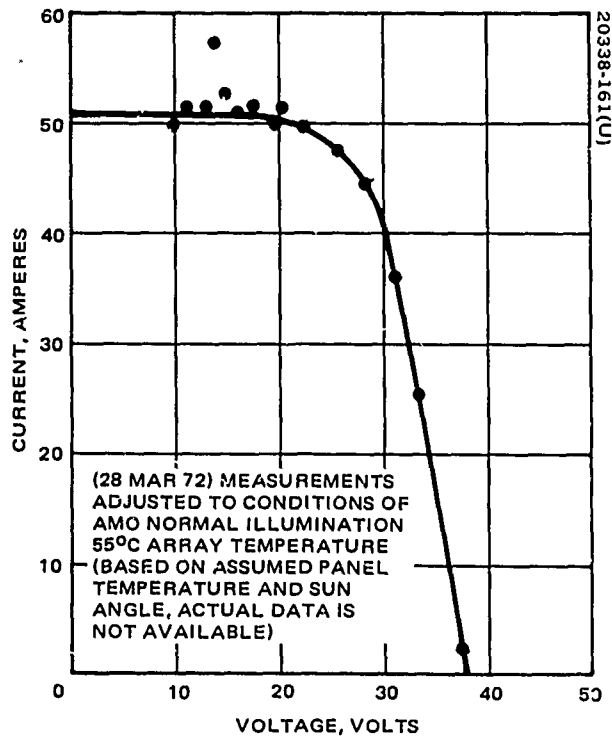


Figure A-8. Main Array Revolution 2365 I-V Data

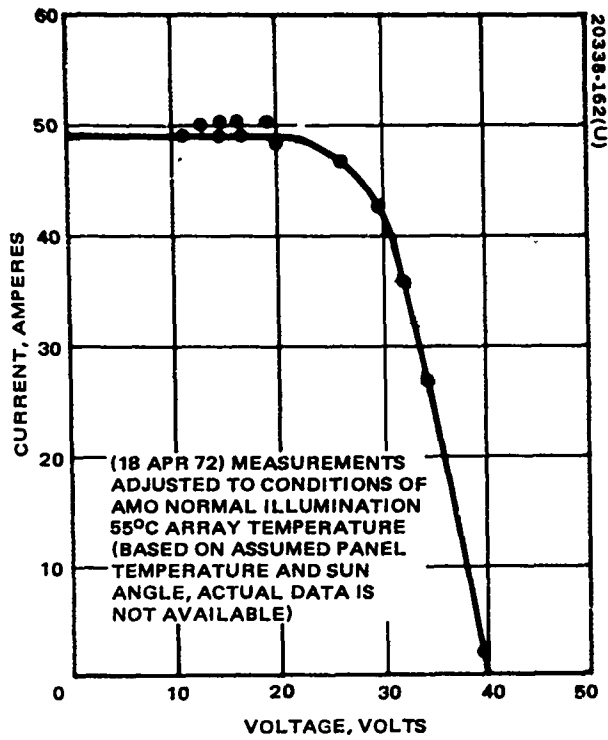


Figure A-9. Main Array Revolution 2639 I-V Data

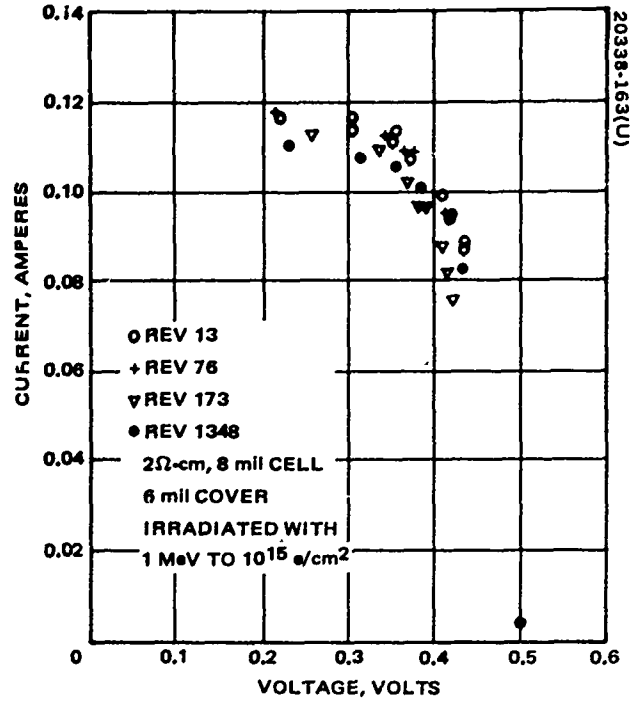


Figure A-10. Cell 0 I-V Data

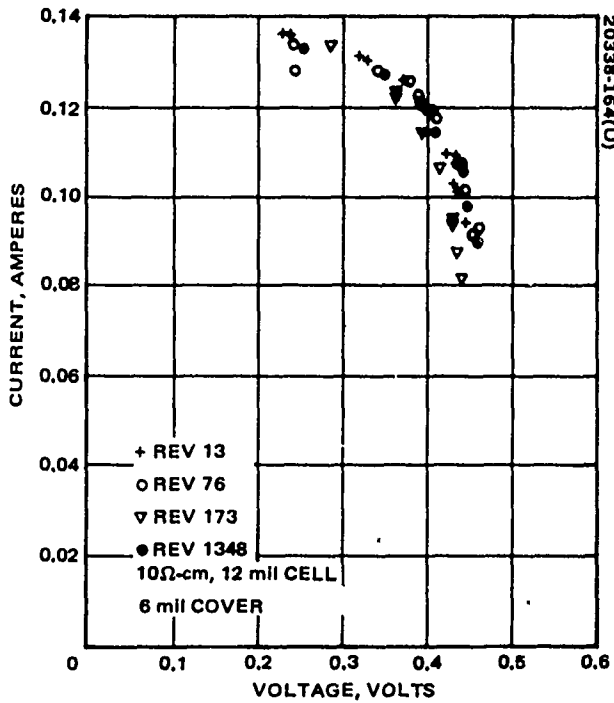


Figure A-11. Cell 1 I-V Data

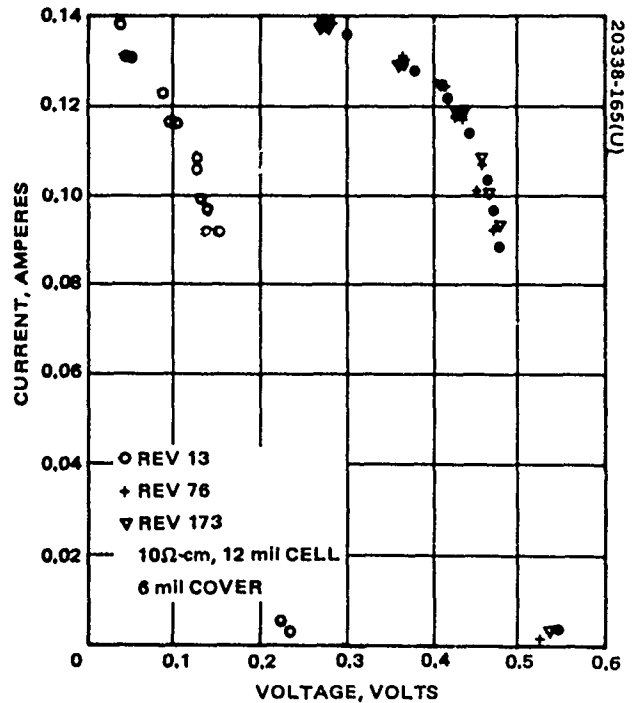


Figure A-12. Cell 3 I-V Data

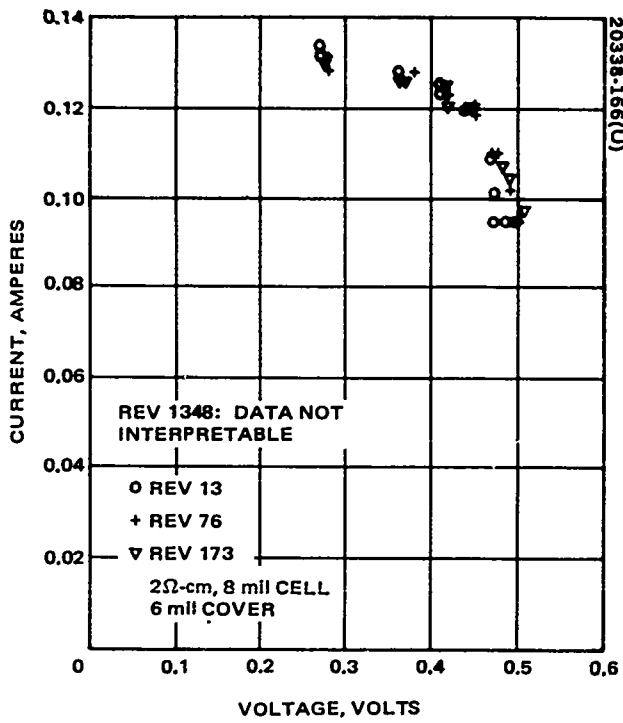


Figure A-13. Cell 4 I-V Data

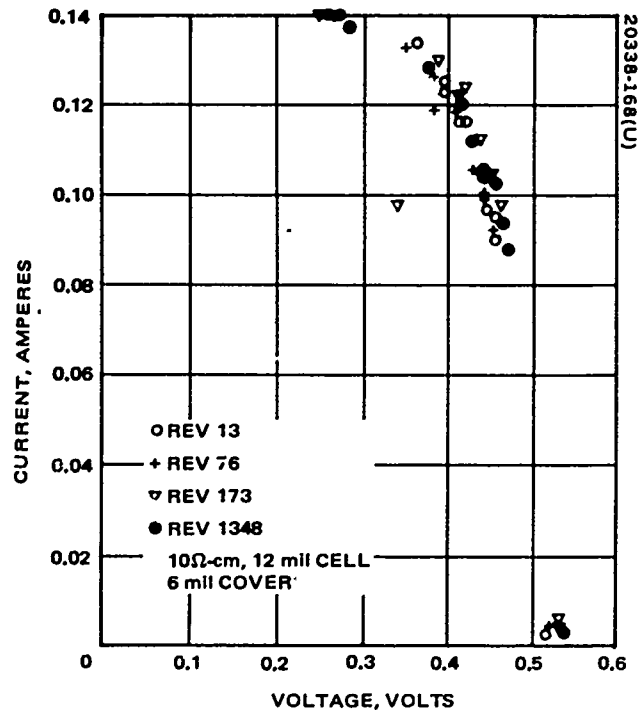


Figure A-15. Cell 8 I-V Data

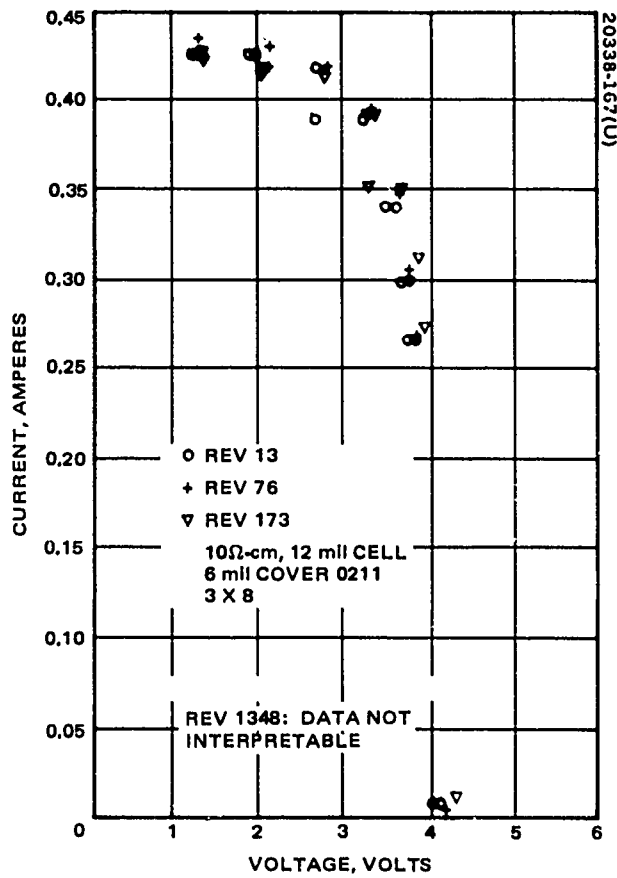


Figure A-14. Module 6 I-V Data



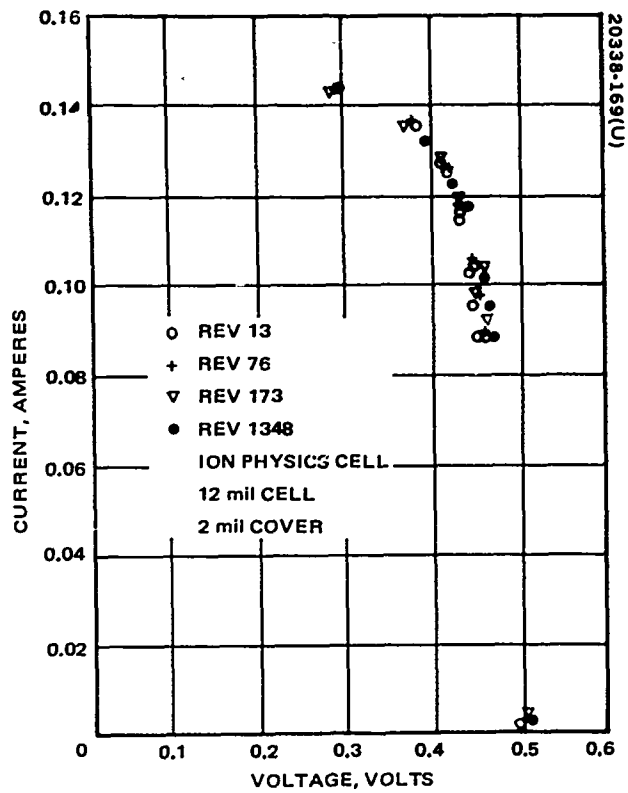


Figure A-16. Cell 9 I-V Data

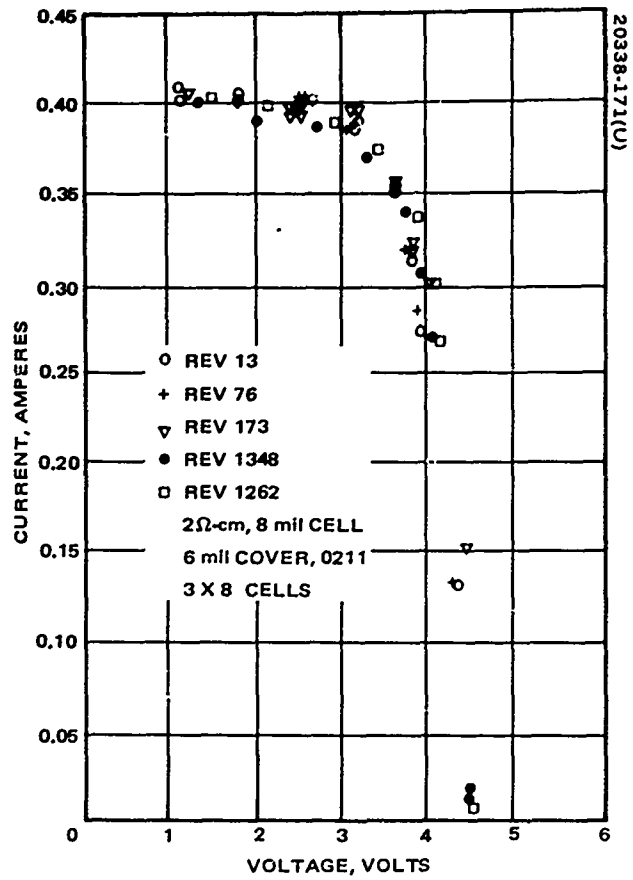


Figure A-18. Module 13 I-V Data

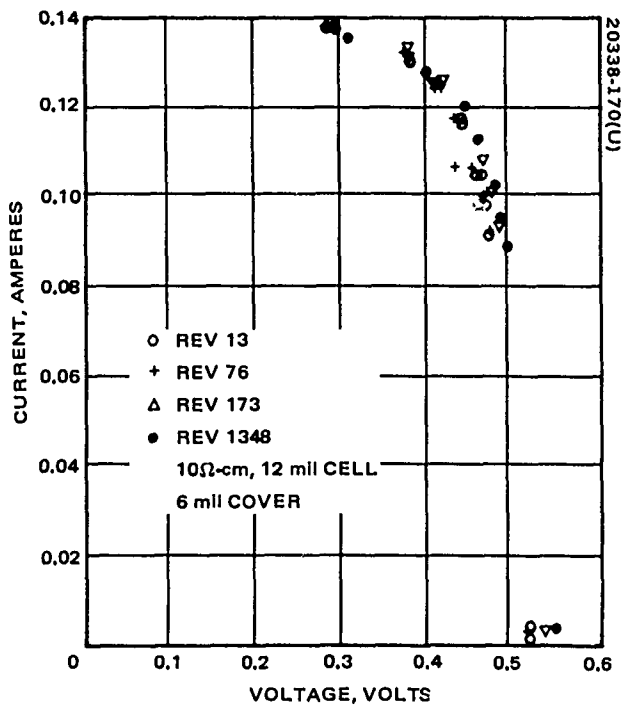


Figure A-17. Cell 10 I-V Data

APPENDIX B. DYNAMIC ANALYSIS DATA

"PRECEDING PAGE BLANK-NOT FILMED."

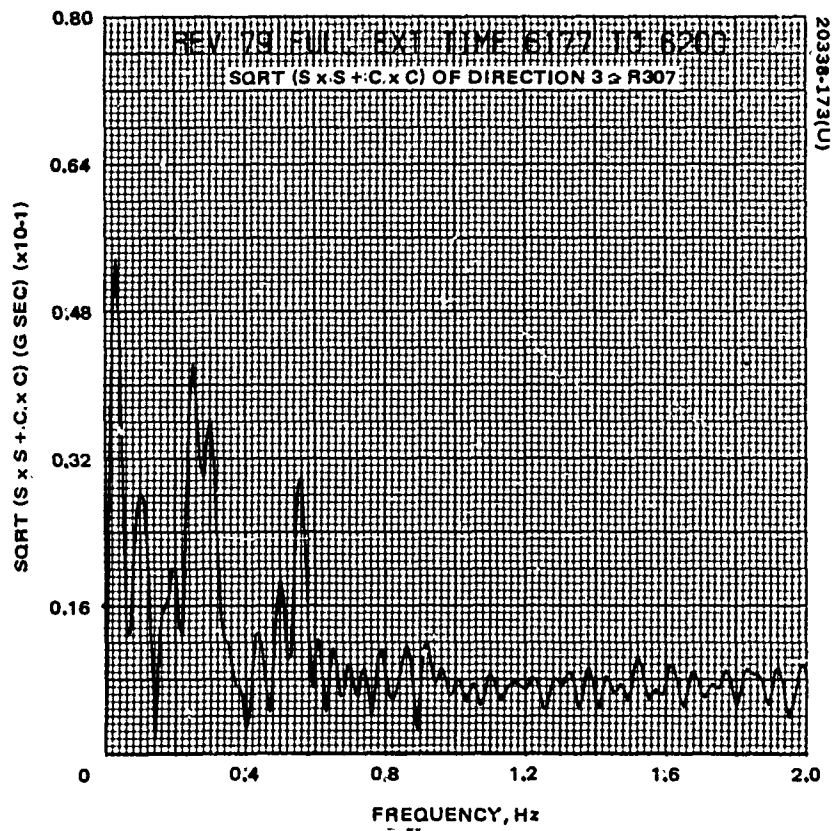
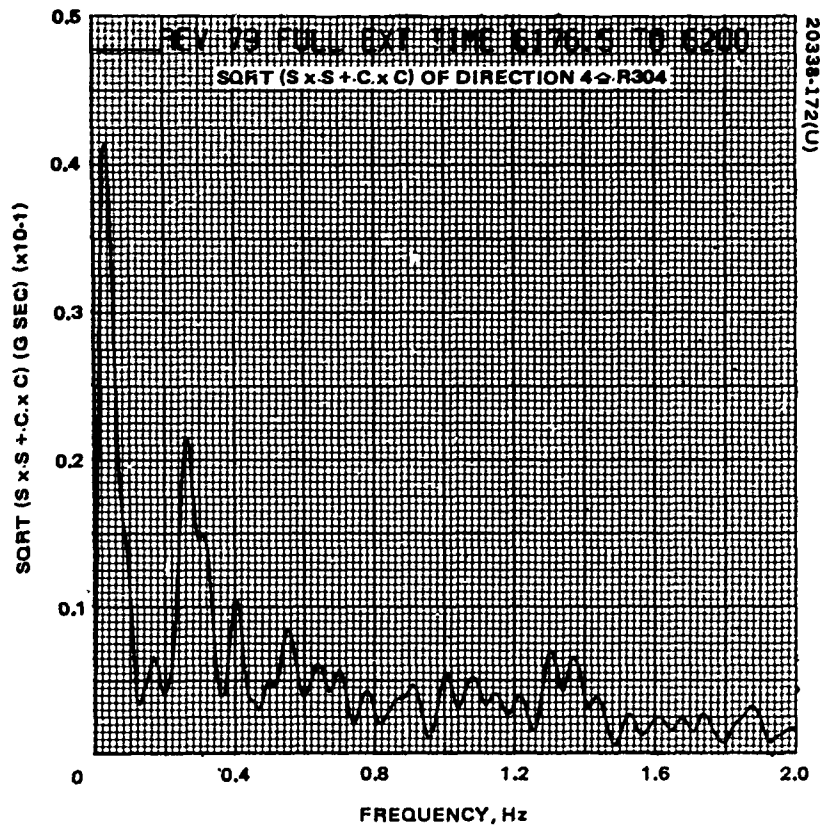


Figure B-1. Fourier Analysis Frequency Decomposition of Acceleration Time Histories

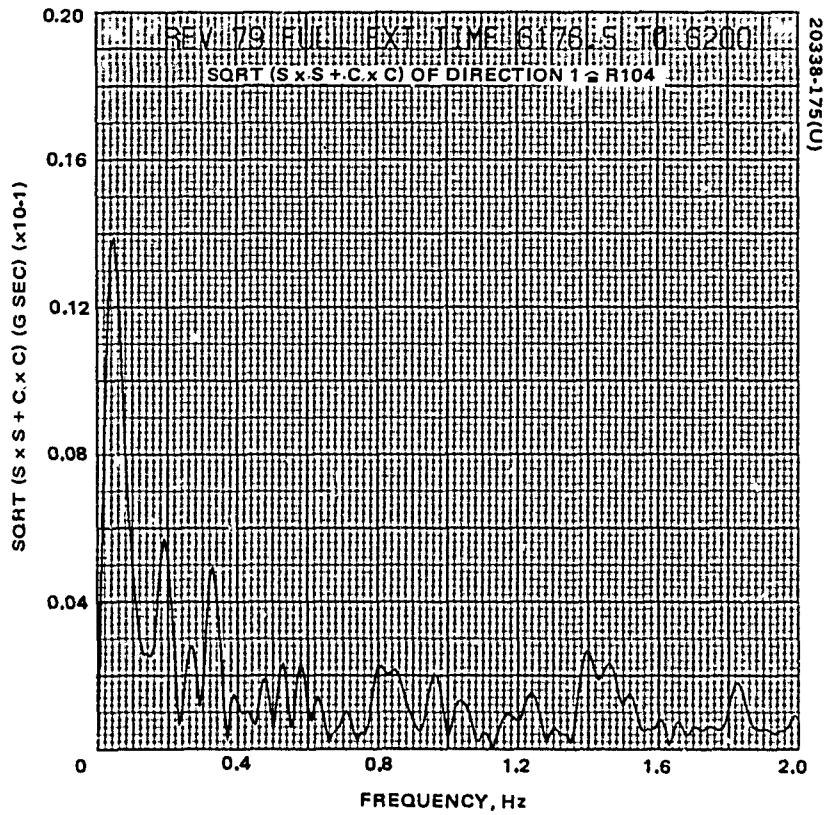
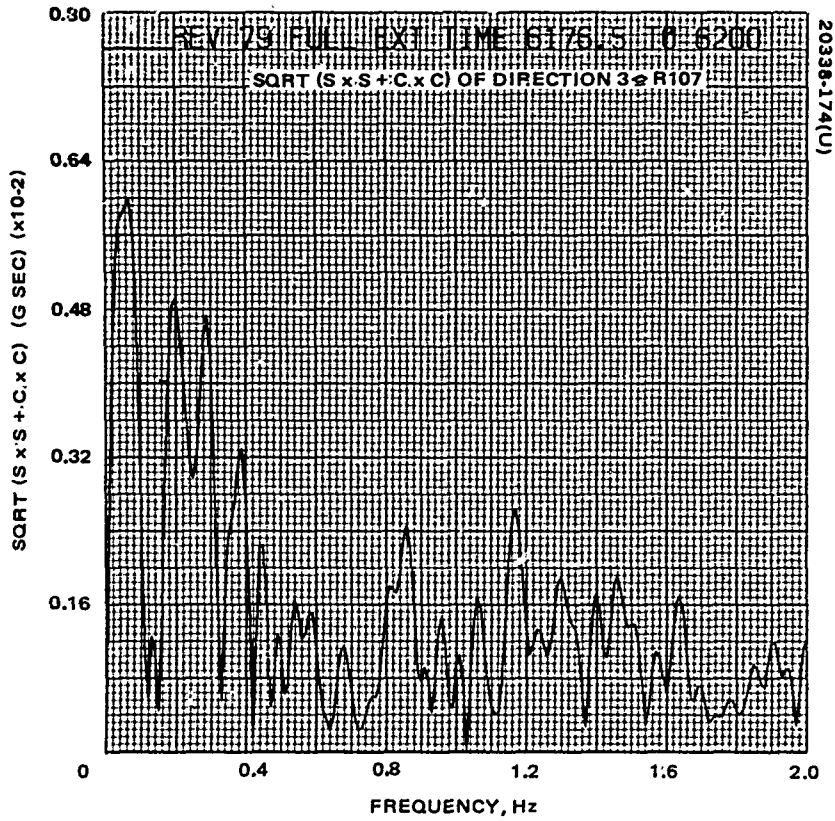


Figure B-1 (continued). Fourier Analysis Frequency Decomposition of Acceleration Time Histories

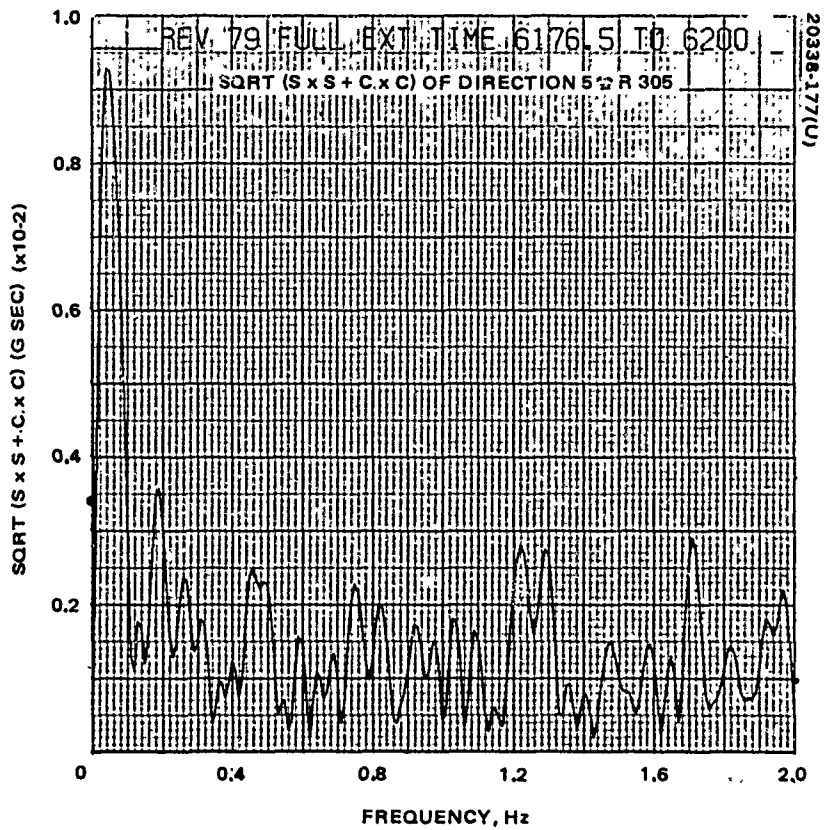
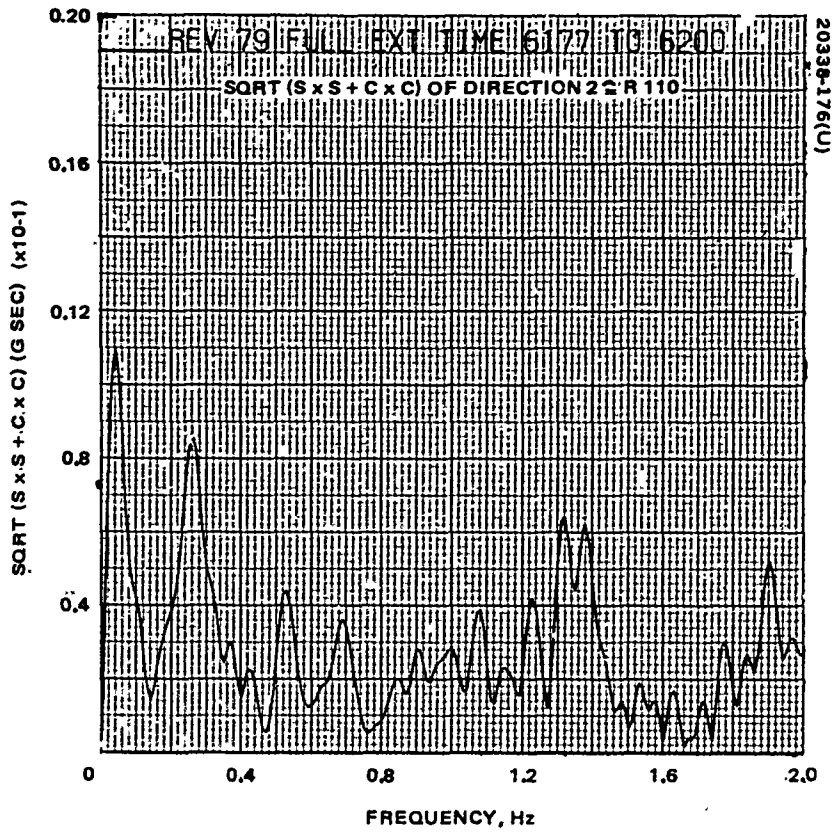


Figure B-1 (continued). Fourier Analysis Frequency Decomposition of Acceleration Time Histories

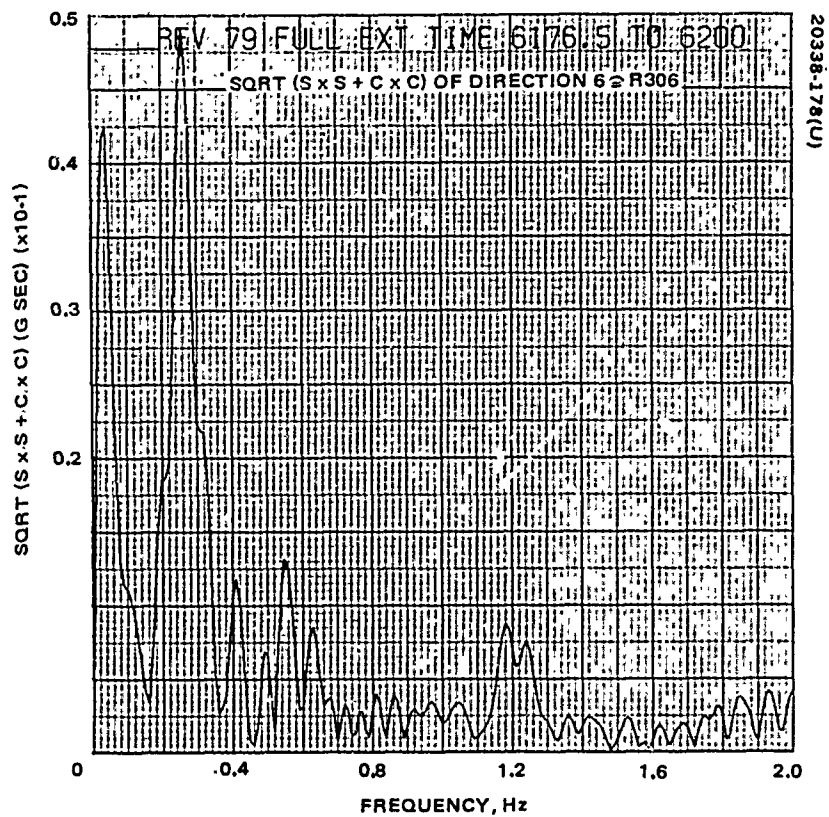
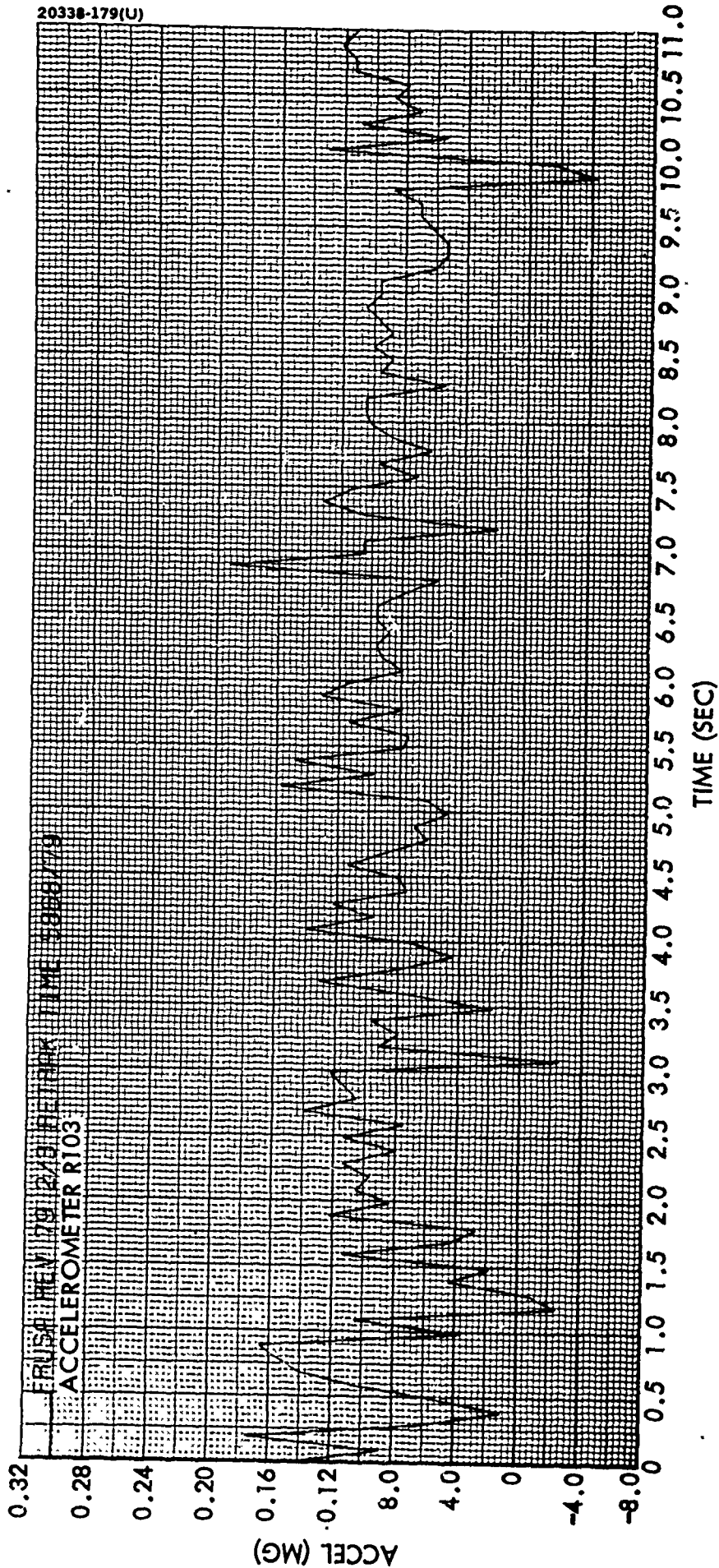
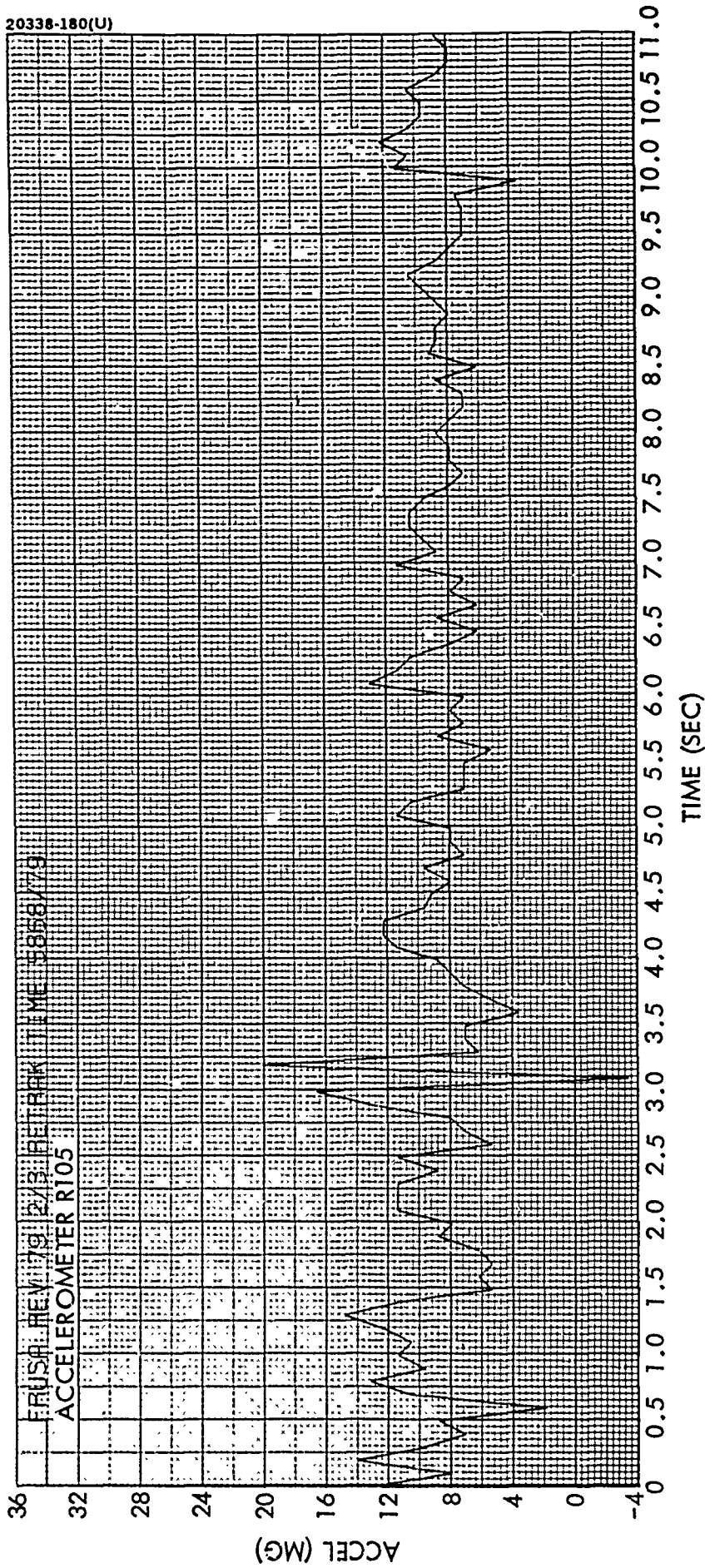


Figure B-1 (concluded). Fourier Analysis Frequency Decomposition of Acceleration Time Histories



a) Accelerometer R103

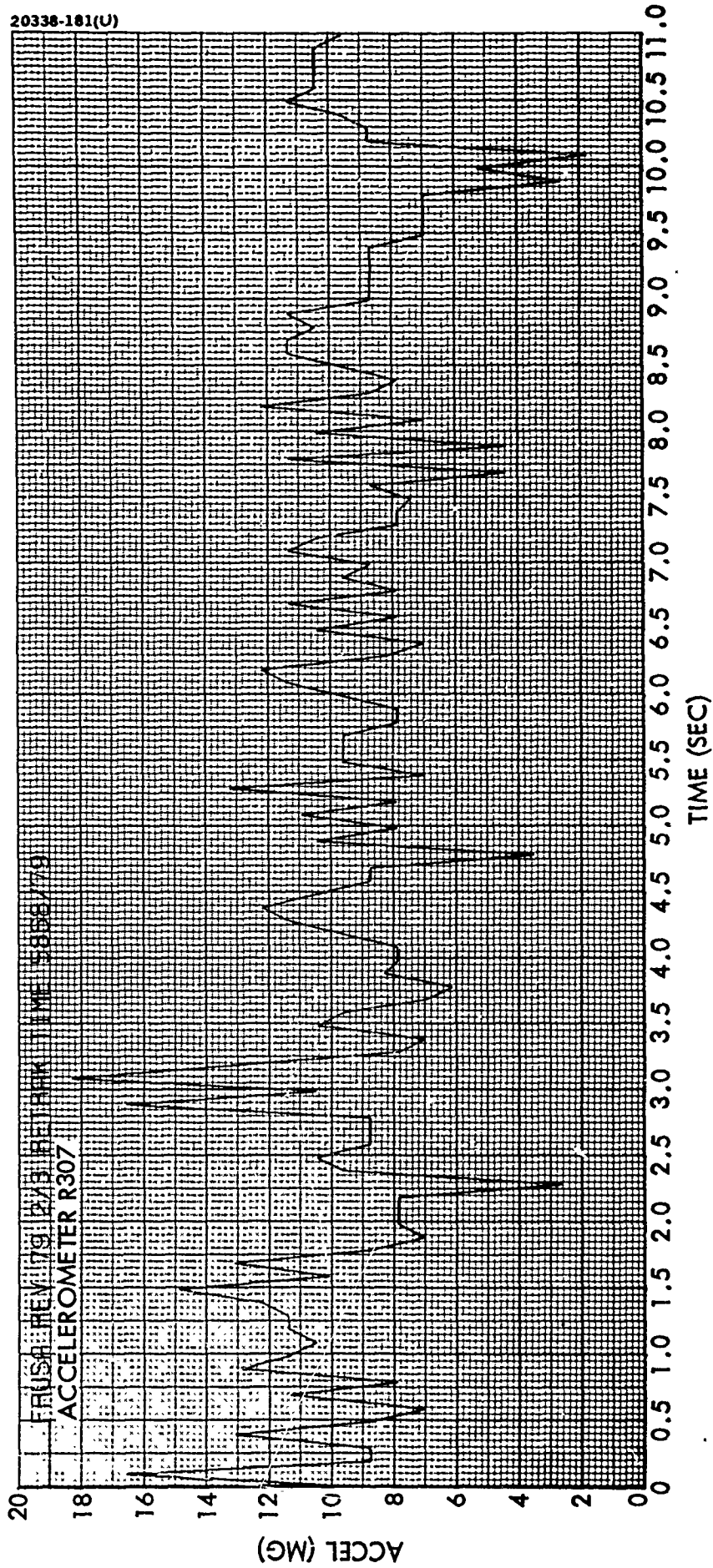
Figure B-2. Acceleration Time History, 2/3 Extended Array



b) Accelerometer R105

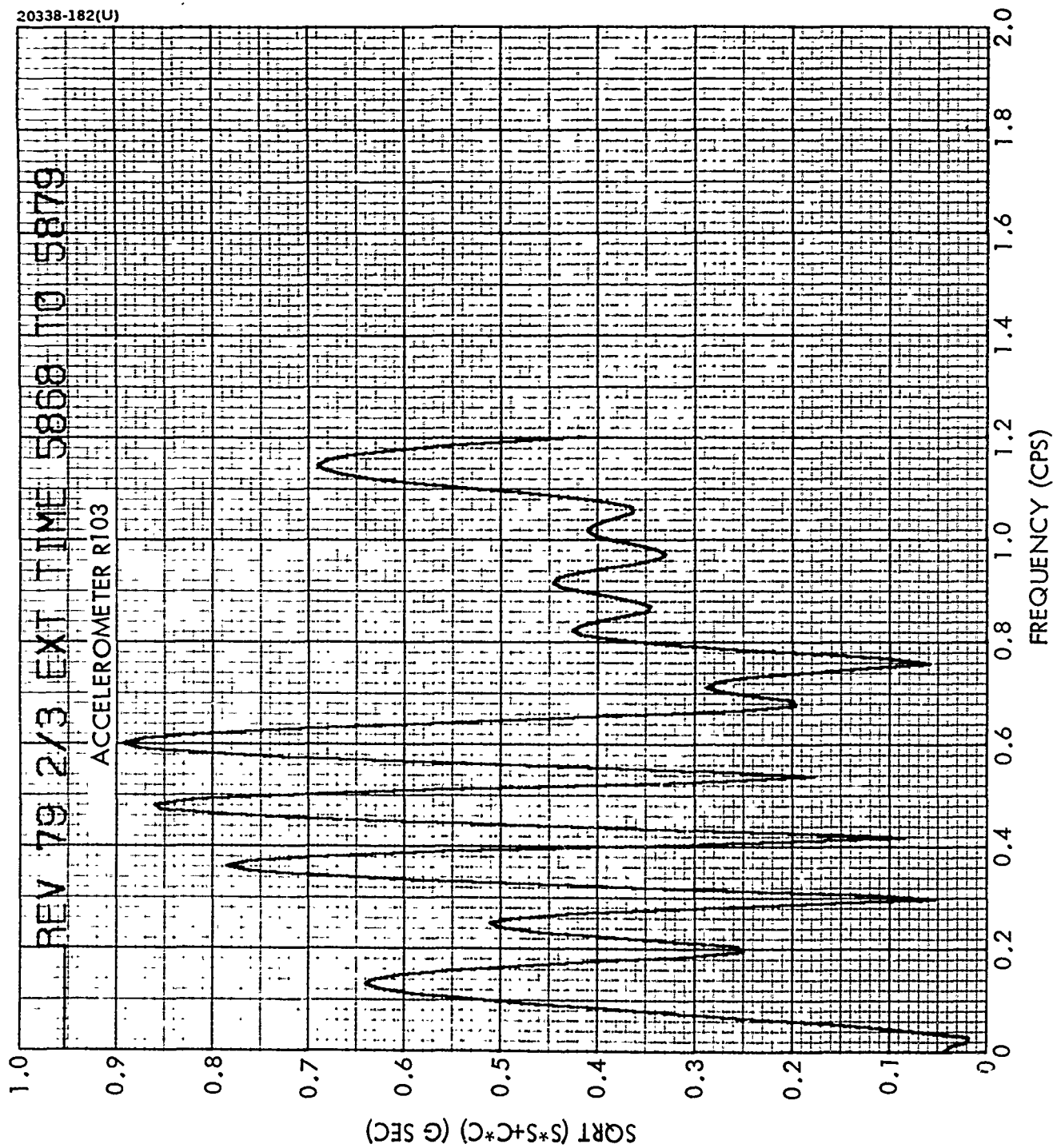
Figure B-2 (continued). Acceleration Time History, 2/3 Extended Array





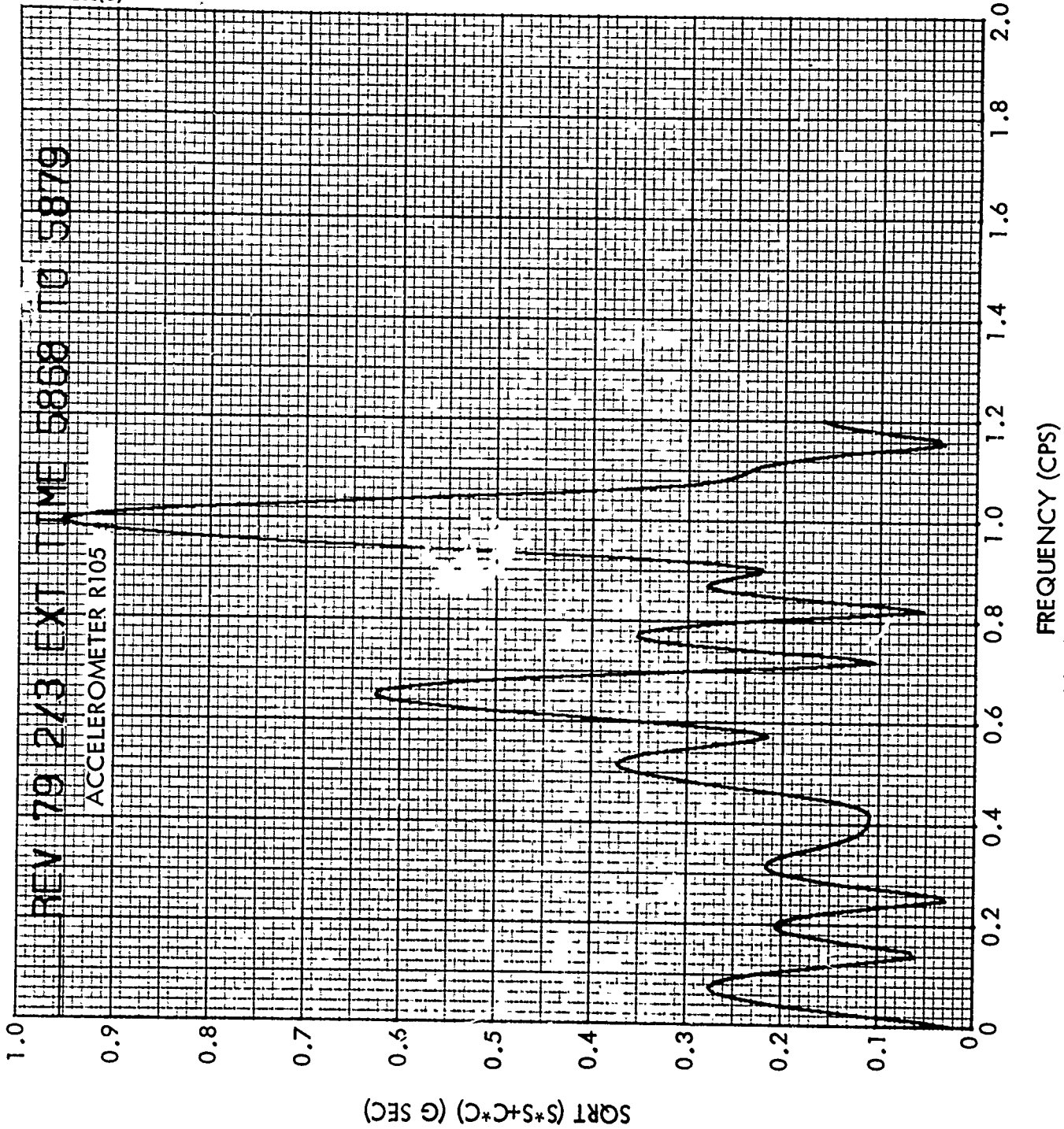
c) Accelerometer R307

Figure B-2 (concluded). Acceleration Time History, 2/3 Extended Array

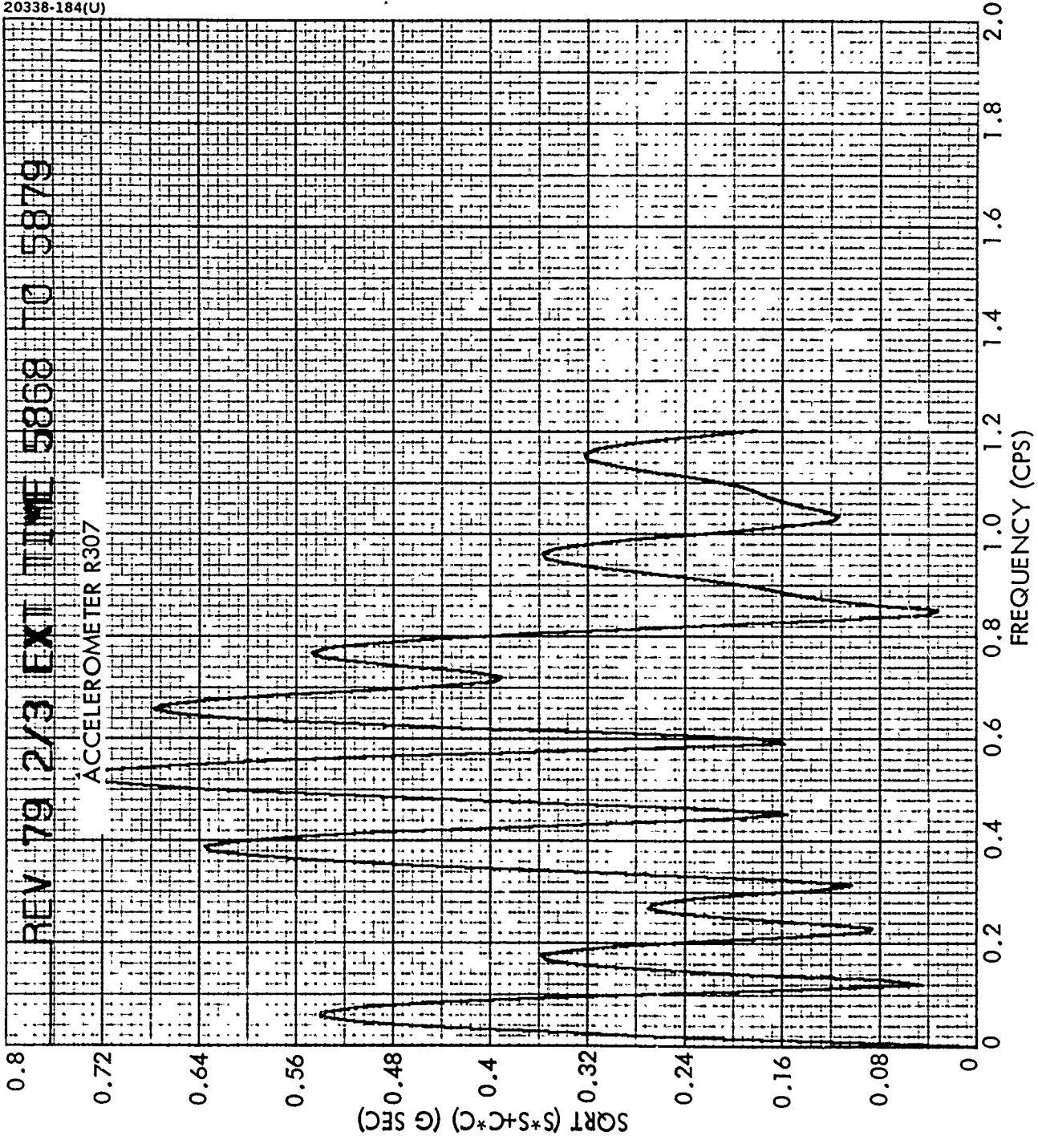


a) Accelerometer R103

Figure B-3. Fourier Analysis Frequency Decomposition of Acceleration Time History, 2/3 Extended Array

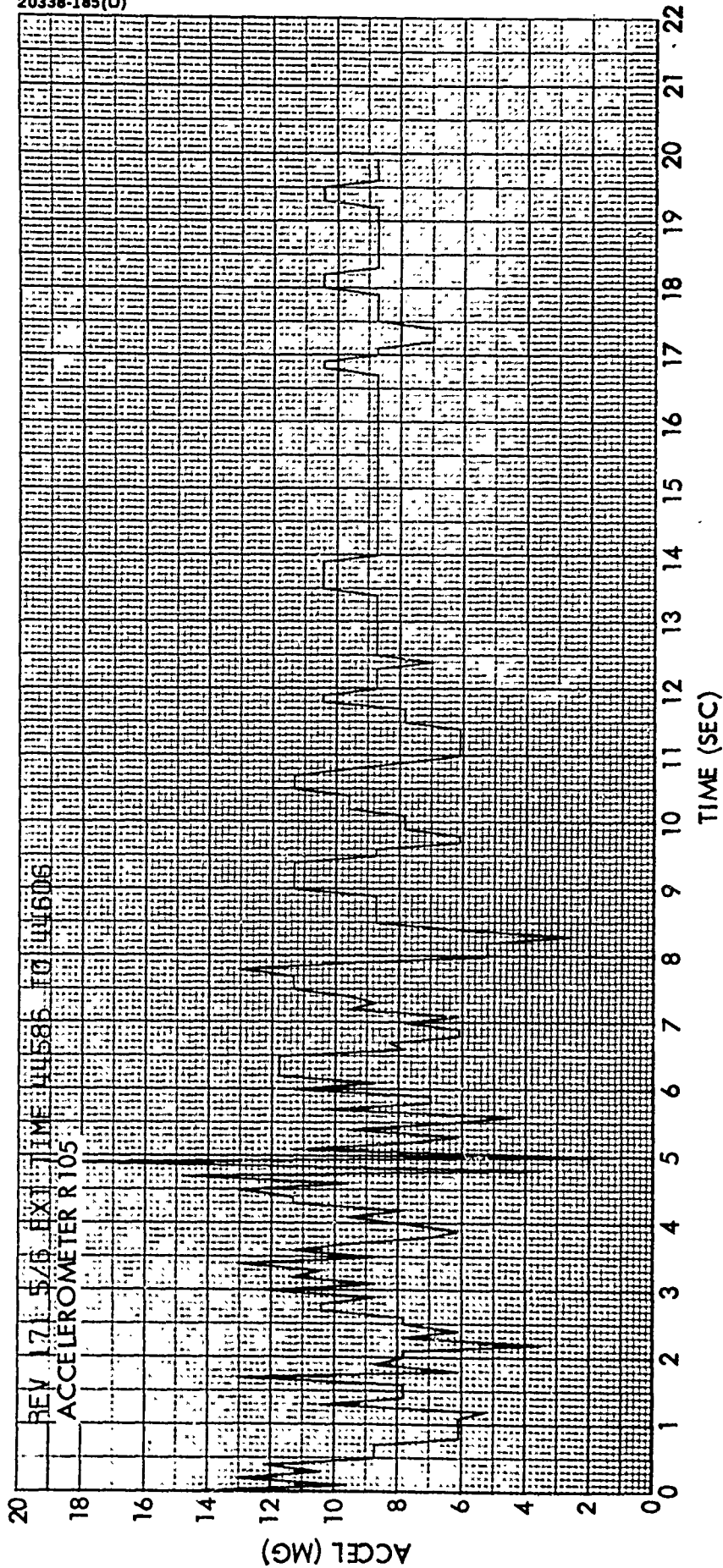


b) Accelerometer R105  
Figure B-3 (continued). Fourier Analysis Frequency Decomposition of Acceleration  
Time History, 2/3 Extended Array



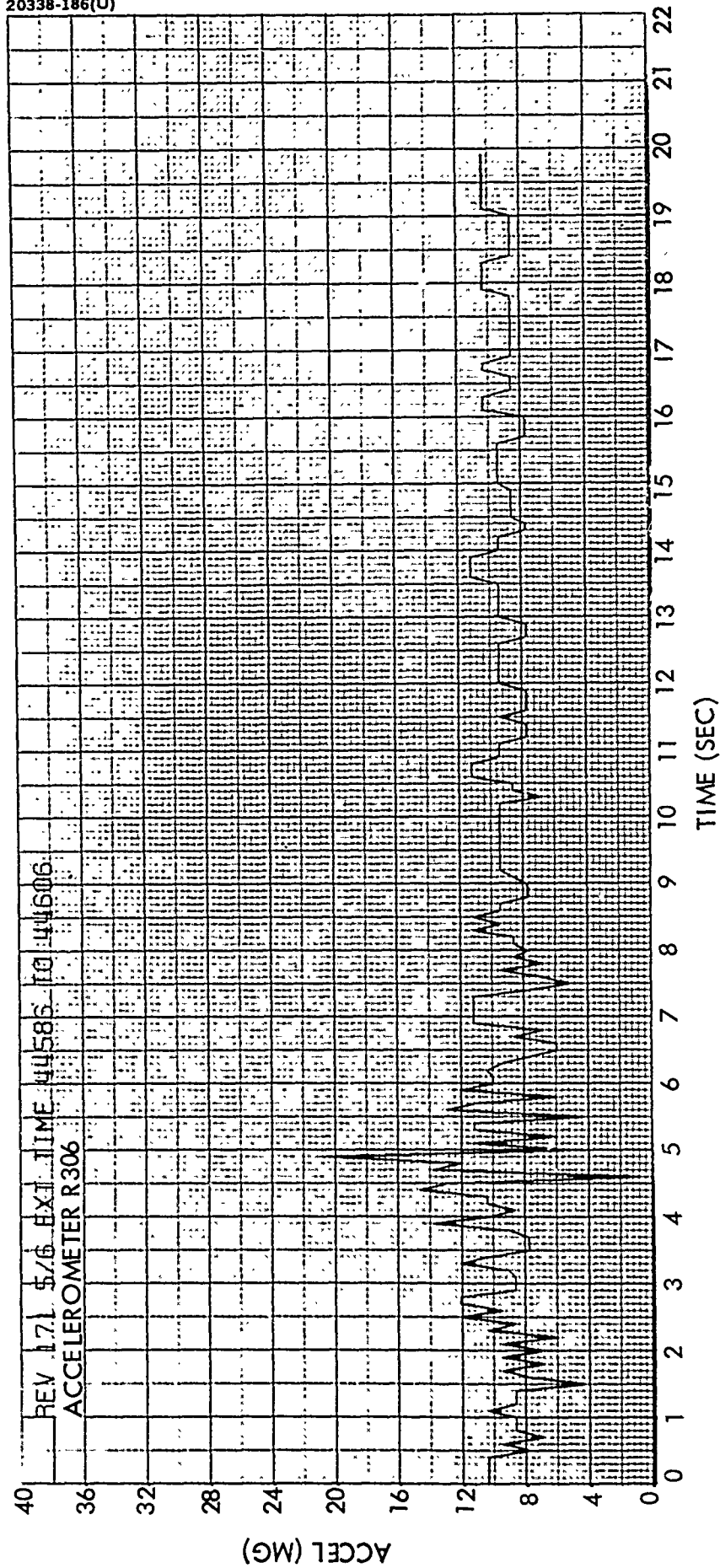
c) Accelerometer R307

Figure B-3 (concluded). Fourier Analysis Frequency Decomposition of Acceleration Time History, 2/3 Extended Array



a) Accelerometer R105

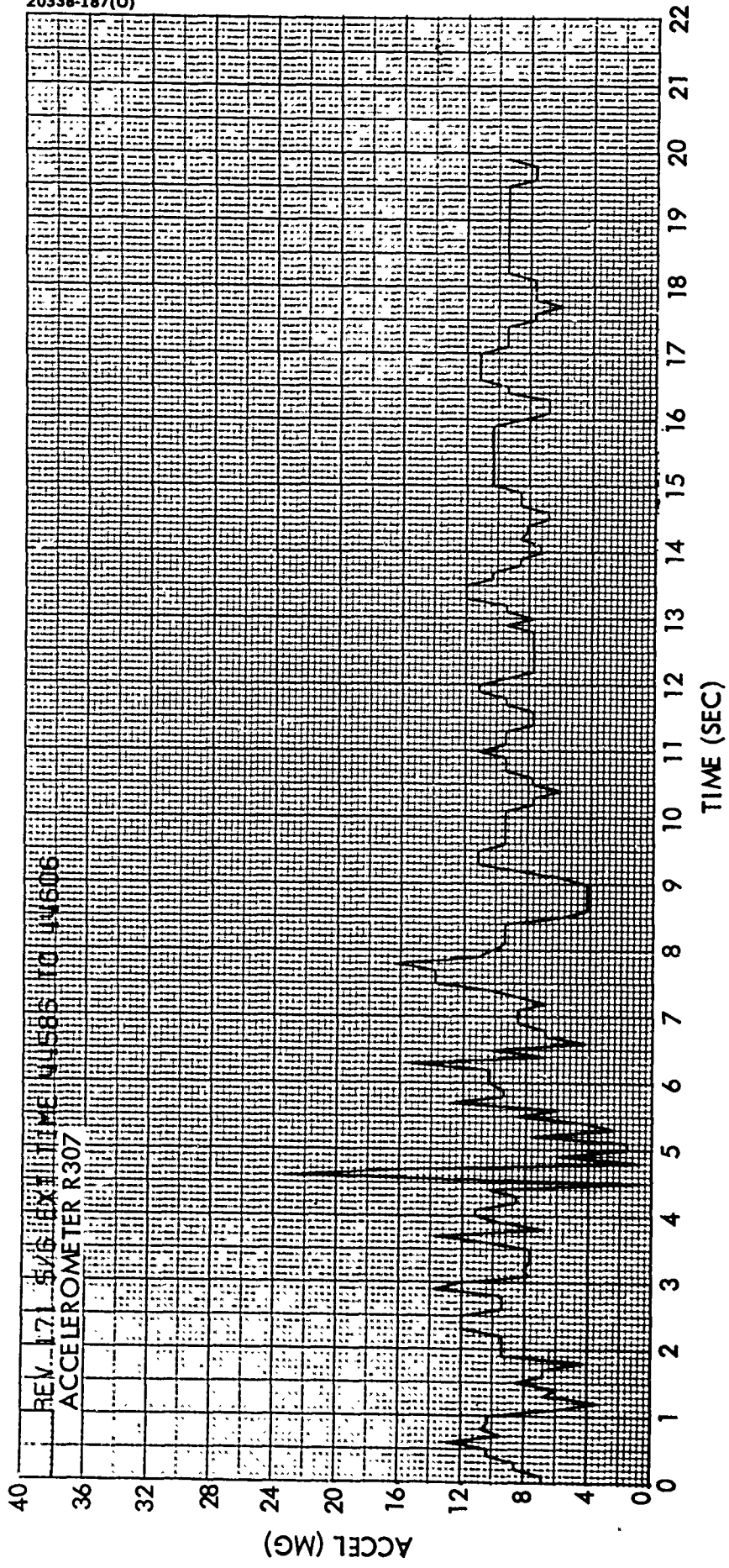
Figure B-4. Acceleration Time History, 5/6 Extended Array



b) Accelerometer R306

Figure B-4 (continued). Acceleration Time History. 5/6 Extended Array

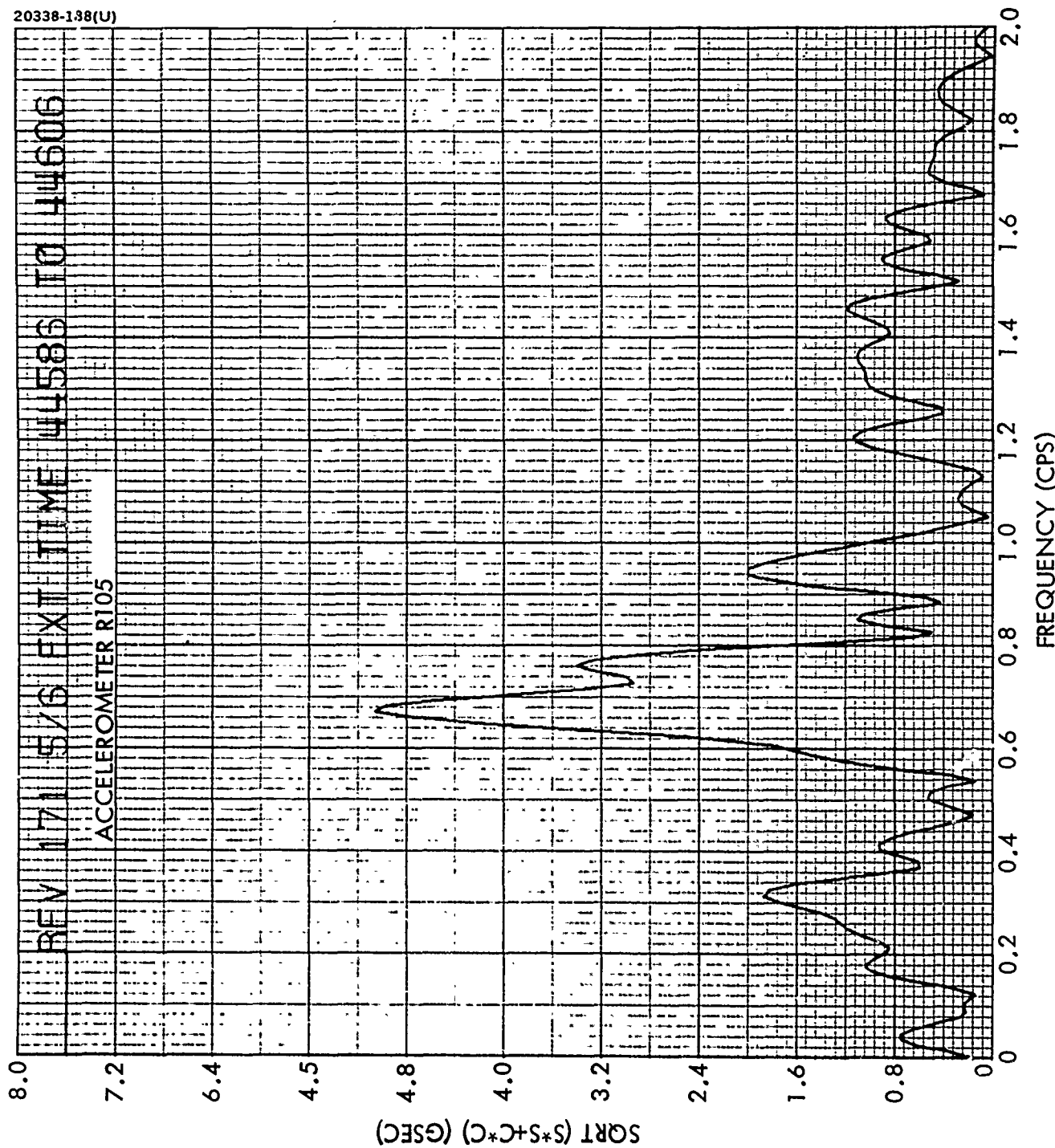




REV. 1.71 5/16 EXT. TIME 11585 TO 11606  
ACCELEROMETER R307

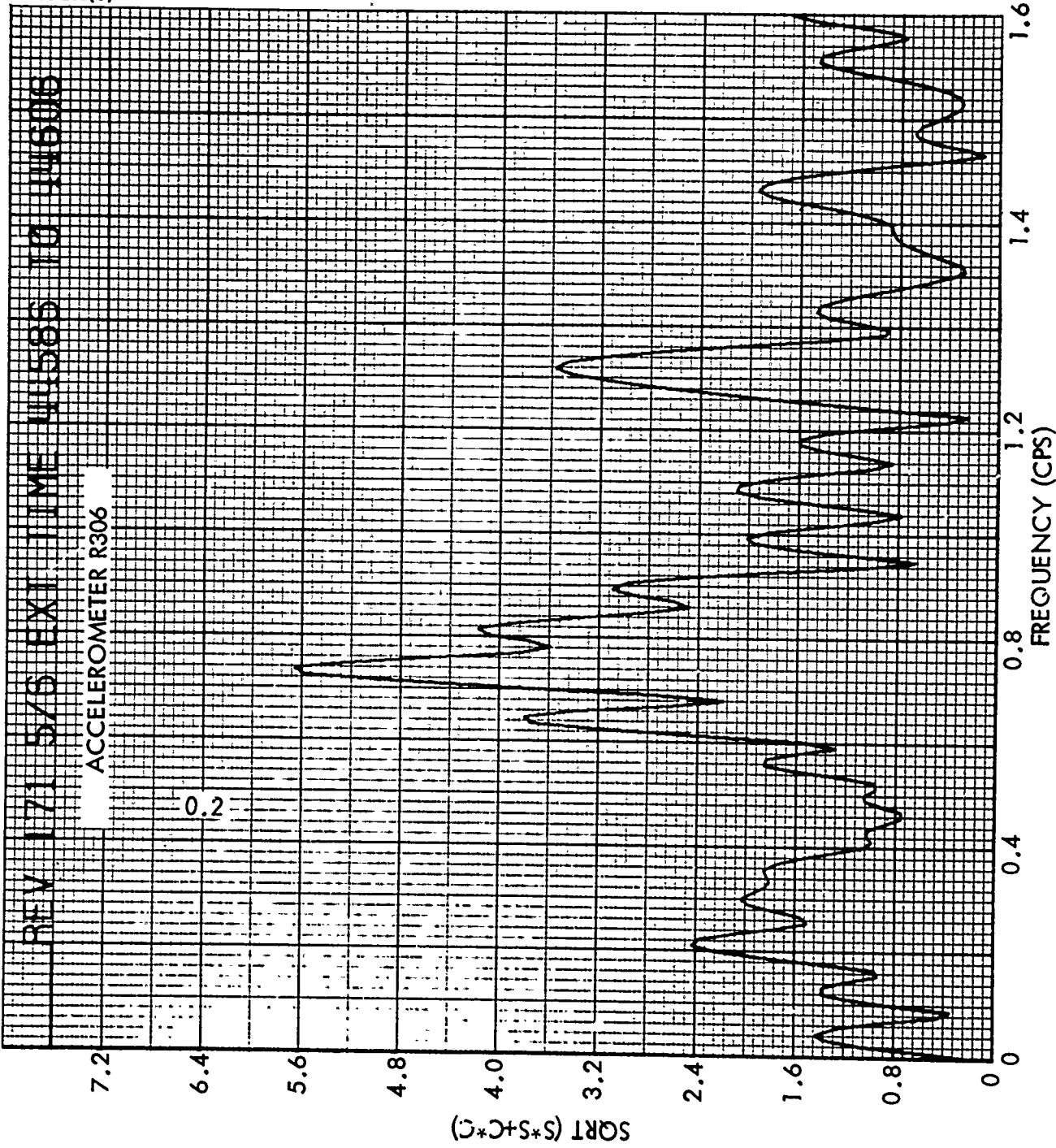
c) Accelerometer R307

Figure B-4(concluded). Acceleration Time History, 5/6 Extended Array



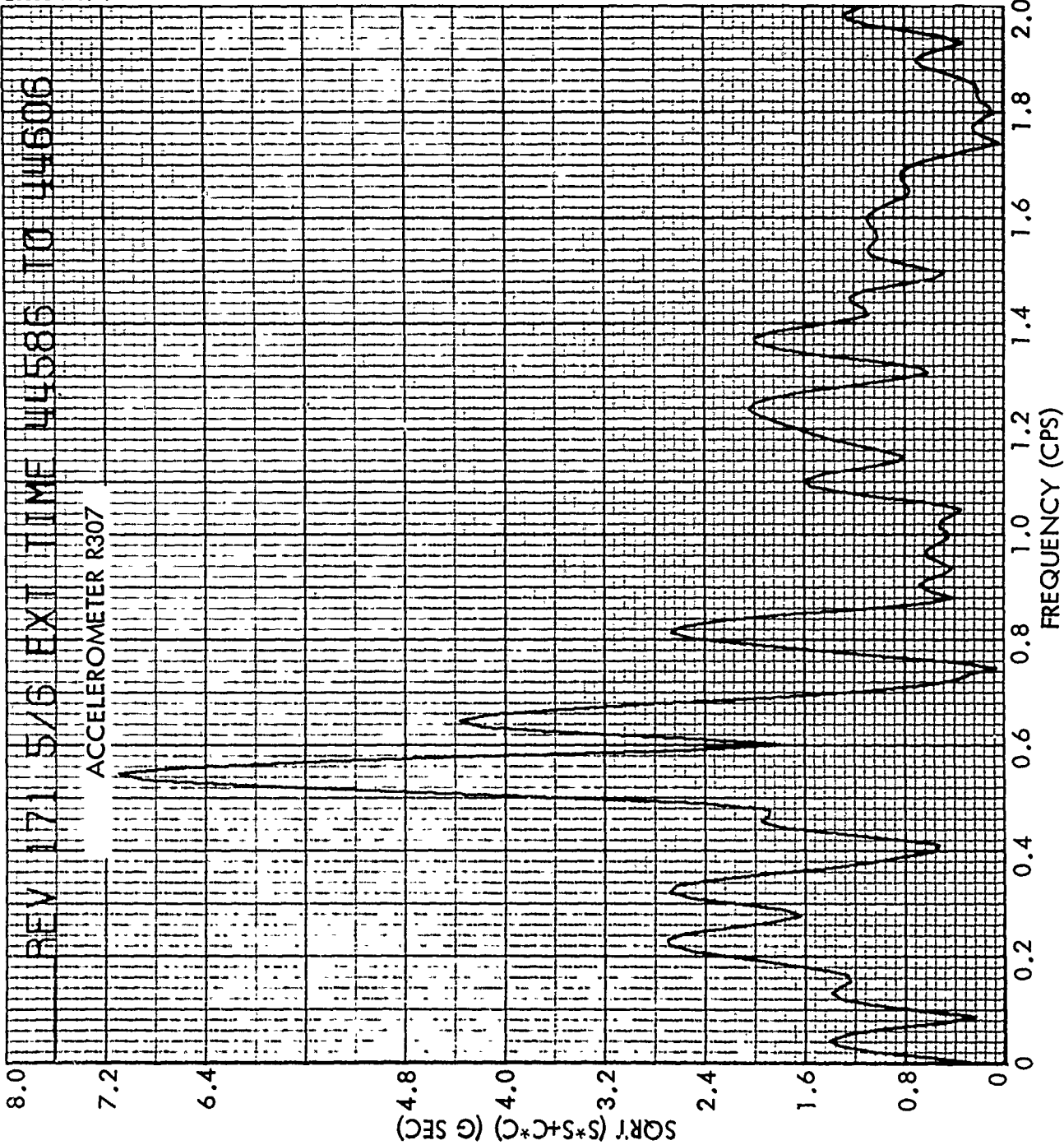
a) Accelerometer R105  
Figure B-5. Fourier Analysis Frequency Decomposition of Acceleration Time History, 5/6 Extended Array





b) Accelerometer R306

Figure B-5 (continued). Fourier Analysis Frequency Decomposition of Acceleration Time History, 5/6 Extended Array



c) Accelerometer R307  
Figure B-5 (concluded). Fourier Analysis Frequency Decomposition of Acceleration Time History, 5/6 Extended Array

APPENDIX C. 5 KW DESIGN DRAWINGS

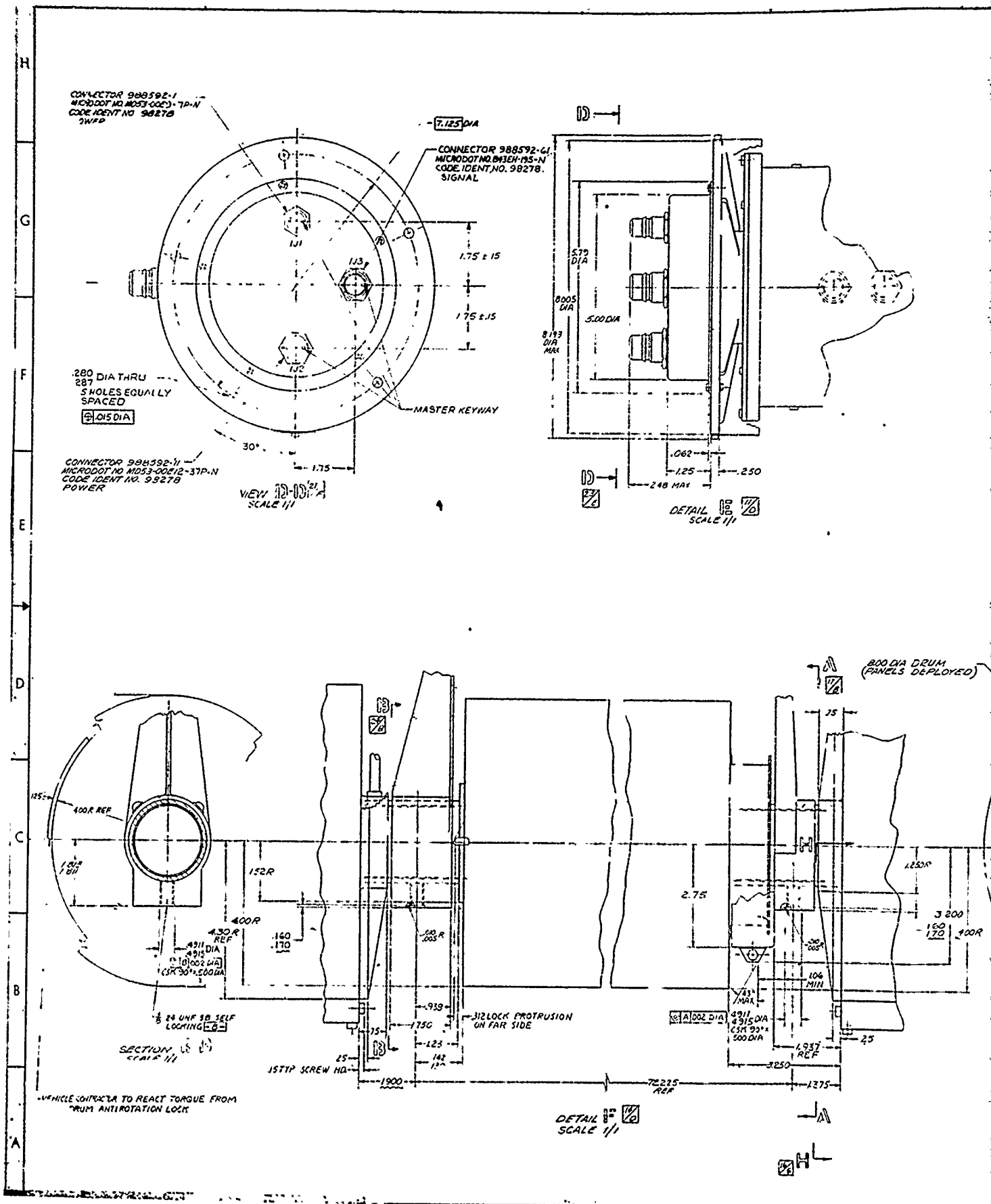
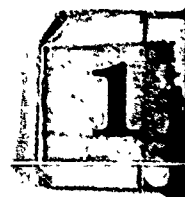
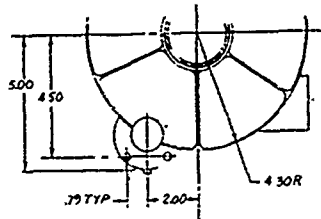


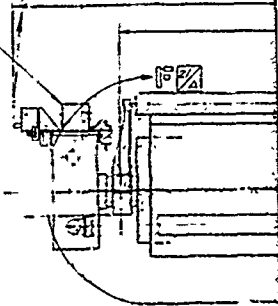
Figure C-1. Flexible Rolled-Up Solar Array (20338-221)





SECTION H-H  
SCALE 1/2  
(OPPOSITE END IS MIRROR IMAGE)

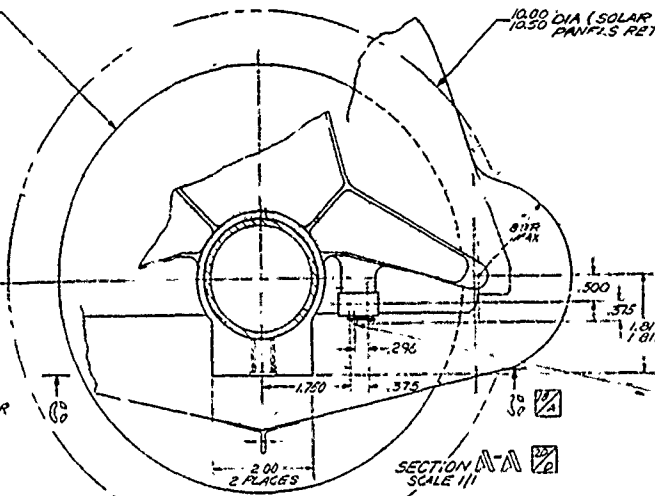
SOLAR SENSOR GROUP



SEPARATION PLANE

800 DIA DRUM  
(PANELS DEPLOYED)

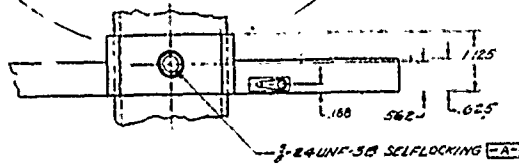
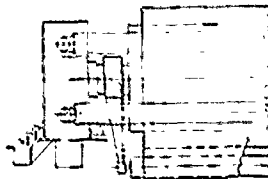
1000 DIA (SOLAR  
PANELS RETRACTED)



VEHICLE CONTRACTOR TO ACTUATE

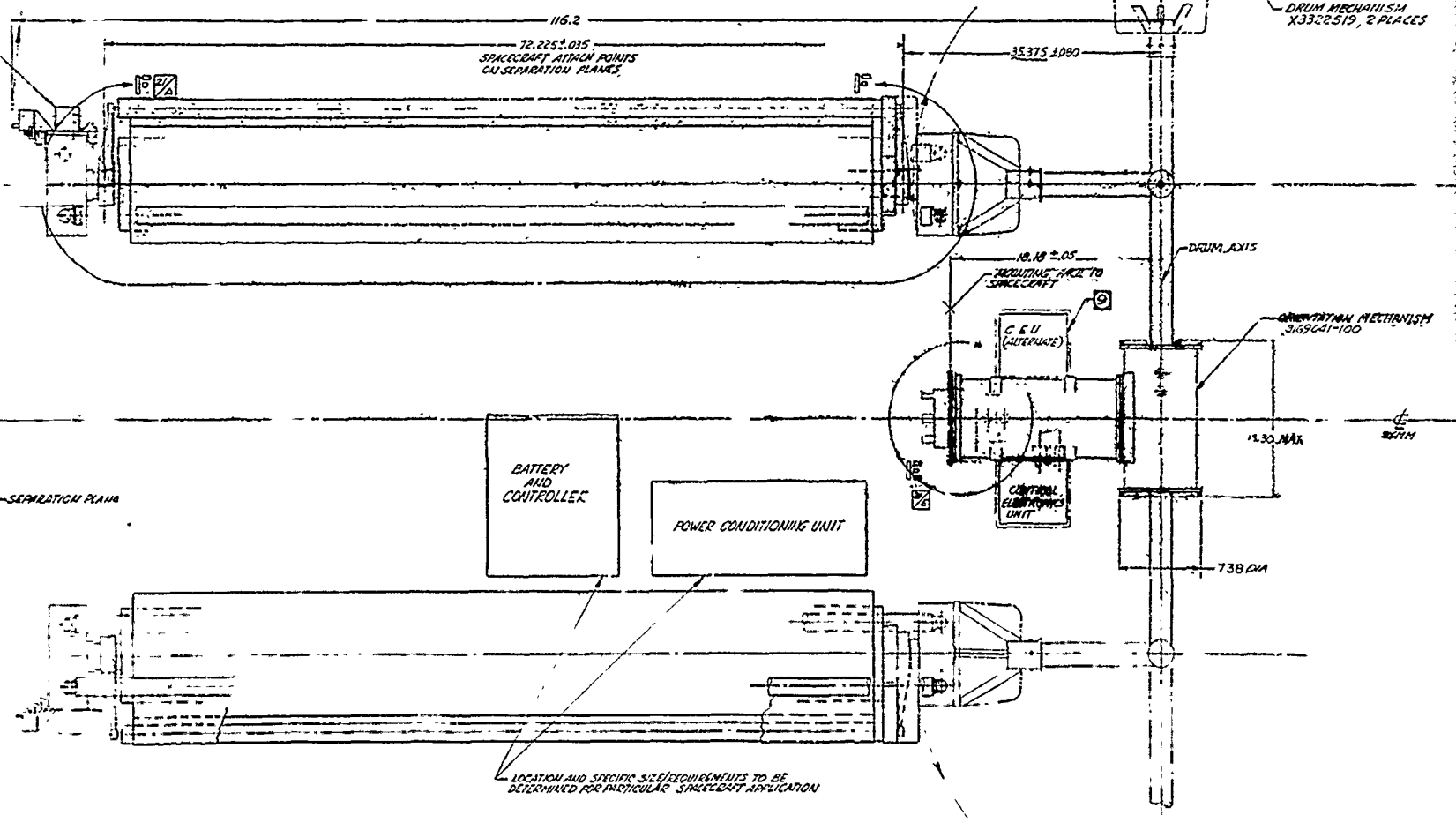
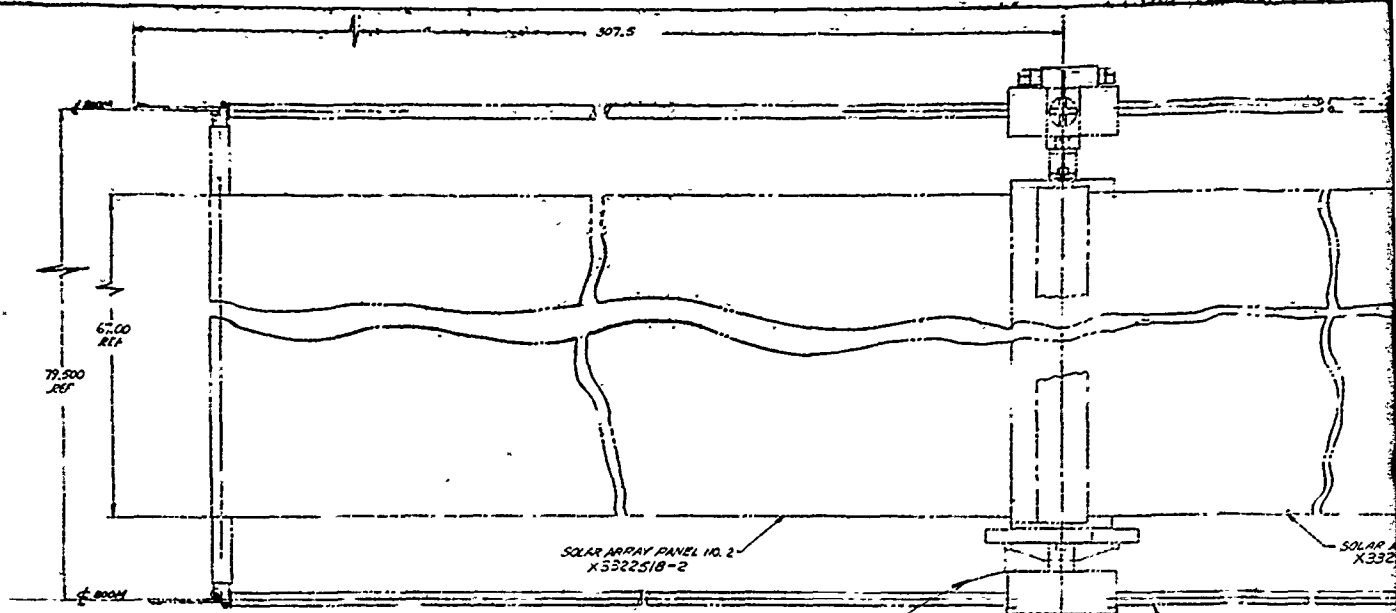
SECTION A-A  
SCALE 1/1

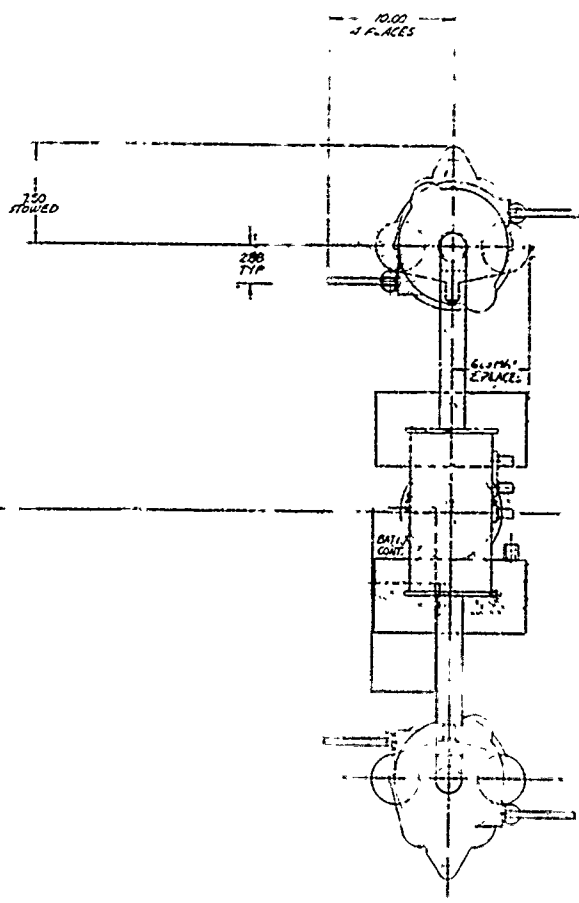
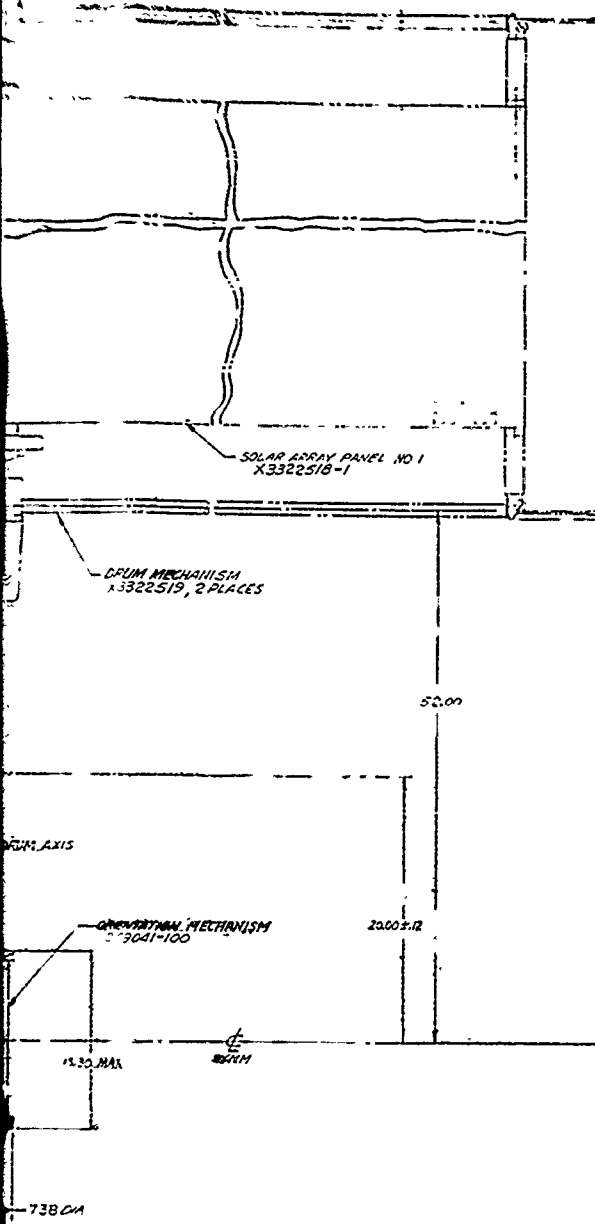
SEPARATION PLANE



VIEW C-C  
SCALE 1/1

REV	ISSUE NO	SECURITY CLASSIFICATION	NO	REV
	82577		X3322520	





- NOTES:
1. THIS DRAWING IS
  2. VENDOR ITEM
  3. PARTIAL REV. Dwg. PR. CHG.
  4. WEIGHT OF SYN. INDIVIDUAL UNIT & SUBSY.
  5. ESTIMATED TO BE AS SPEC.
  6. CENTERS OF GRAVITY SHOWN ON U.S.
  7. FOR BREAKDOWN

FOR INFORMATION  
 ALTERNATE C & ONE YEAR - OPT.

22577	X 3322520	
-------	-----------	--

G  
F  
E  
C

NOTES.

1. THIS DRAWING WILL SERVE AS INSTL CONTROL DWG
2. VENDOR ITEM - SEE SPEC CONTROL DWG (ALL 988XXX DWGS)
3. PARTIAL REF DES ARE SHOWN FOR COMPLETE AS PREFIX WITH UNIT NO OR SUBASSY
4. WEIGHT OF SYSTEM SHALL BE        LBS MAX  
INDIVIDUAL UNIT WEIGHTS SHALL BE AS SPECIFIED ON UNIT & SUBSYSTEM ICD'S.
5. ESTIMATED HEAT DISSIPATED WITHIN UNITS WILL BE AS SPECIFIED IN HAC SPECIFICATIONS.
6. CENTERS OF GRAVITY FOR INDIVIDUAL UNITS ARE SHOWN ON UNIT & SUBSYSTEM ICD'S
7. FOR BREAKDOWN OF CONTROL ITEMS (HOWN) SEE REFERENCE.

- ② FOR INFORMATION ON CONNECTORS SEE INDIVIDUAL UNIT ICD
- ② ALTERNATE C.E.U. REQUIRED FOR MISSIONS LONGER THAN ONE YEAR. OPTIONAL FOR SHORTER MISSIONS.

82577 X3322520

QTY REQD	PART OR IDENTIFYING NO.	NOMENCLATURE OR DESCRIPTION		ZONE	ITEM NO.
		LIST OF MATERIALS			
		HUGHES	HUGHES AIRCRAFT COMPANY CULVER CITY, CALIFORNIA		
		FLEXIBLE ROLLED UP SOLAR ARRAY 5KW			
		82577	X3322520		
		SCALE: 1" = 1'-0"			

82577 X3322520



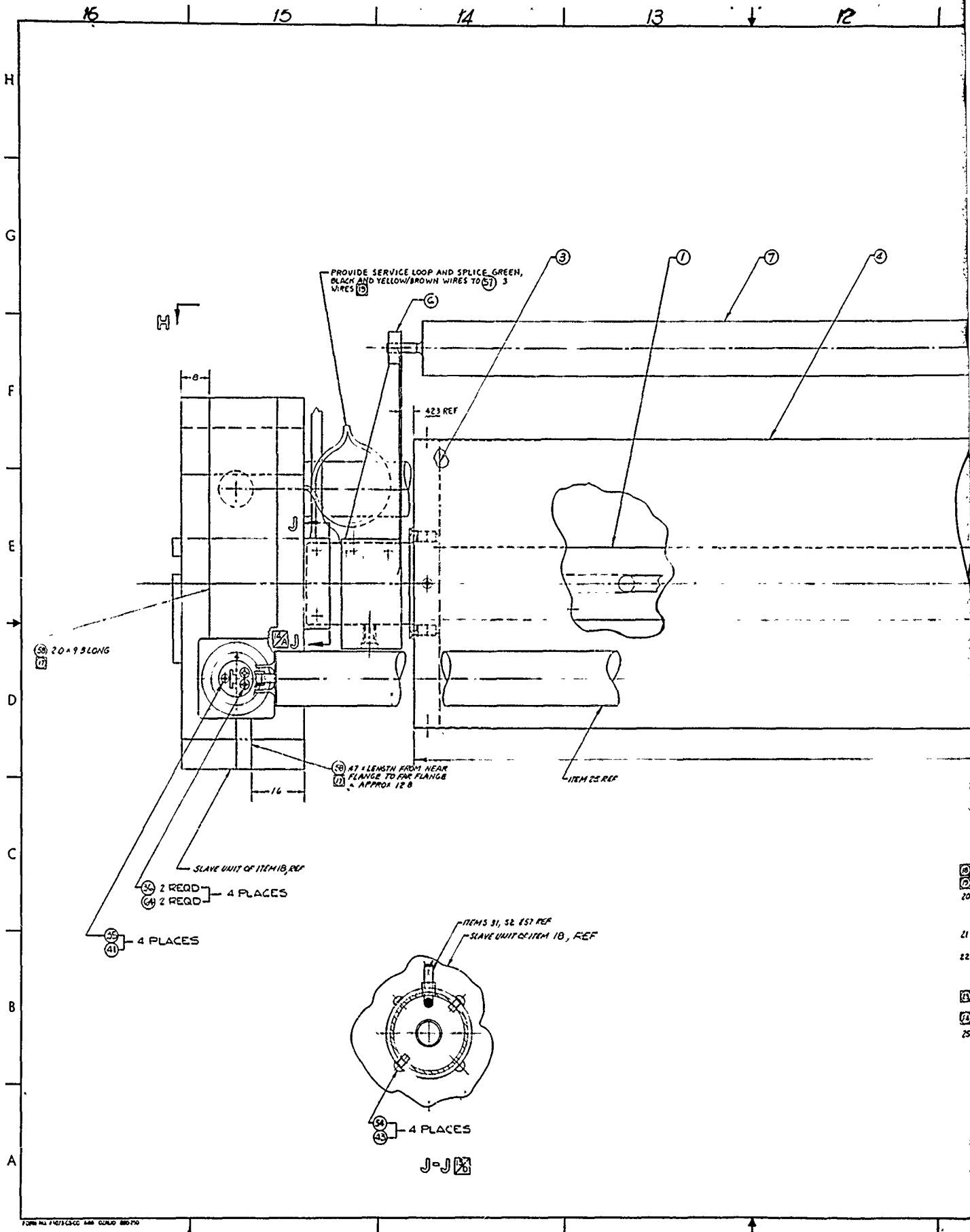
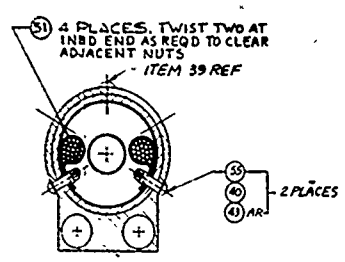


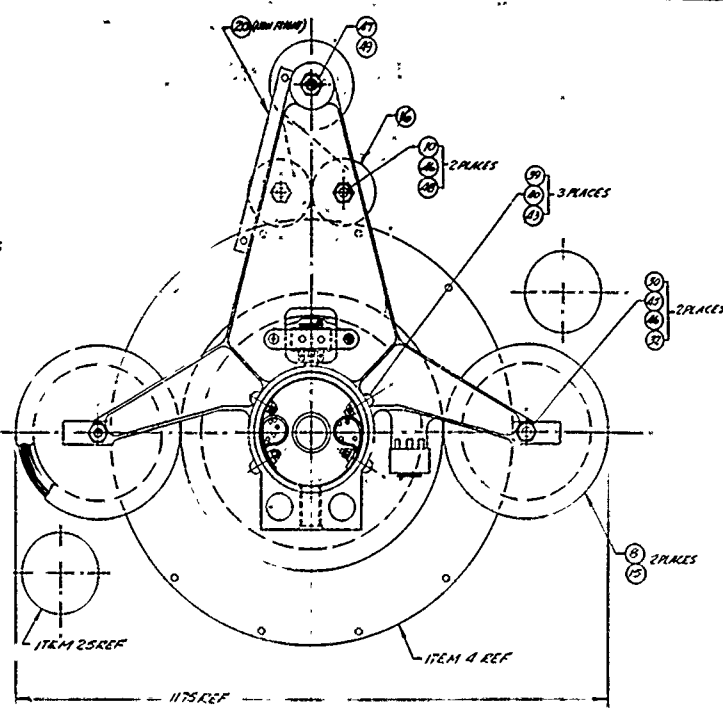
Figure C-2. Drum Mechanism (20338-222)



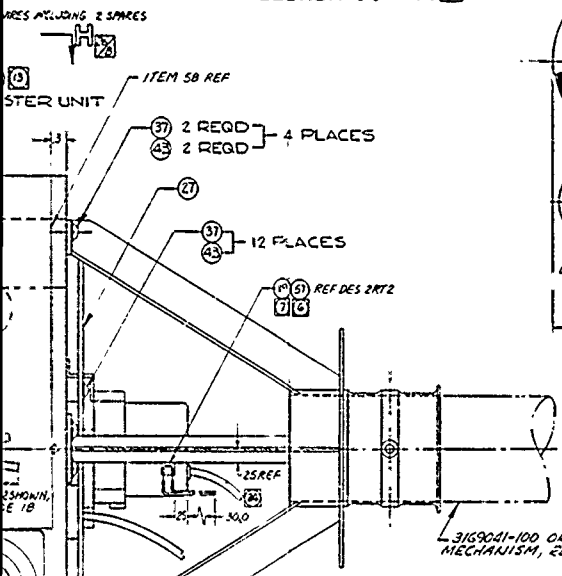




SECTION M - M



SECTION



NOTES - UNLESS OTHERWISE SPECIFIED

- 1 MAINTAIN HUMIDITY AT 60% OR LESS TO PROTECT BALL BEARINGS
- 2 PROTECT AND HANDLE THERMAL FINISHES PER HP 10-23
- 3 ASSEMBLE PER APPROPRIATE PARAGRAPHS OF FS 30932-009
- 4 FABRICATE WIRING HARNESSSES PER HP 14-2
- 5 SOLDER PER HP 11-47
- 6 SOLDER ITEM 57 TO ITEM 19 PER HP 11-48
- 7 BOND PER HP 16-33, CLIP OR 2. FORMAL TEST SPECIMENS ARE NOT REQD BUT CLEANLINESS OF WIRES AND OTHER FINISH SURFACES SHALL BE SUFFICIENT TO PROVIDE RELIABLE ADHESION.
- 8 TORQUE SCREWS AND/OR NUTS AS FOLLOWS:  
 NO 4 10 TO 30 IN-LBS  
 NO 6 100 TO 120 IN-LBS  
 NO 8 150 TO 200 IN-LBS  
 NO 10 200 TO 250 IN-LBS
- 9 SCREWS TO BE TIGHTENED TO ABOVE TORQUES ON NEXT ASSY, REF THEY MAY BE INSTALLED LOOSELY AT THIS ASSY
- 10 TORQUE ITEM 17 NUT, 20 TO 30 FT/LBS THEN BACK OFF  $0.5 \pm 0.2$  SAFETY WIRE TO PREVENT BOTH TIGHTENING AND LOOSENING
- 11 SCREW LENGTHS MAY BE VARIED ONE SIZE LONGER OR SHORTER AND MUST MEET THE MINIMUM PROTRUSION REQUIREMENTS OF MS 33588
- 12 SAFETY WIRE PER MS 33540 USING ITEM 59
- 13 ITEM 18 ACTUATOR UNIT CONSISTS OF A MASTER UNIT, SLAVE UNIT, TORQUE TUBE AND 125 DIA X .750 ROLLIN. SEE SOURCE CONTROL DWG OR VENDOR DWG 5842ES
- 14 KEEP WIRE BUNDLES FROM EACH ITEM 22 & EACH ITEM 21 SEPARATELY IDENTIFIABLE
- 15 FOR SCHEMATIC DIAGRAM SEE DWG 3169010-200
- 16 DETAIL IN 4X ACCORDS OF THE 1.5 KW FEUSA DESIGN.
- 17 BOND RECTANGULAR STRIPS OF ITEM 58 ALUMINIZED SIDE IN TO ITEM 19 PER HP 16-121 EXCLUDING PAR 3.2 AND 4.2. ADEQUATE PRECAUTIONS SHALL BE TAKEN TO PREVENT LIFTING OR OTHER DAMAGE TO THE GOLD PLATED SUBSTRATE IN THE AREAS NOT COVERED BY ITEM 58. AN ALTERNATE ADHESIVE IS PER HP 16-135, PAR 3.2.5 CURE TEMPERATURE SHALL NOT EXCEED 200°F. INTERRUPTS REQD TO CLEAR NAMEPLATES (NOTES CONTINUED IN ZONE II)

QTY	REV	PART OR IDENTIFYING NO.	NOMENCLATURE OR DESCRIPTION	ZONE	REF NO.
8	B	MS620 CCL	WASHER	14	64
2	-	3169075-1	COMPENSATOR, BOOM-FLIGHT	26	63
4	4	MS1210C4	NUT, SELF LOCKING	42	
12	12	MS3330-135	WASHER, LOCK	61	
16	16	AN960 C4	WASHER	60	
AK	AR	MS 20935C20	WIRE, SAFETY	7C	59
4	AR	MS 16-1329	200 THK, PLASTIC FILM, ALUMINIZED TERN	5A	50
AR	AR	MS 2-1610/1-24U	WIRE, INSULATED	-	57
4	4	MS1210C3A	SCREW, SELF-LOCKING	21A	56
4	4	MS1132 C-4	SCREW, PAN HD	69	55
8	8	MS1132C-2	SCREW, PAN HD	75	54
4	4	MS1102D4-5	SCREW, FLAT HD	6C	53
AR	AR	MS 3-1617/1-24U	WIRE SHIELDED	-	52
4	4	MS2320-R5	CLAMP	64	51
2	2	MS1102D2-3	SCREW, FLAT HEAD	33C	50
1	1	MS120-416L	WASHER, FLAT	30F	49
2	2	MS320C100	WASHER, FLAT	20F	48
1	1	MS1291C4	NUT, SELF LOCKING	20F	47
4	4	MS1291C3	NUT, SELF LOCKING	20F	46
2	2	MS130354 R183-C31	BLUSHING	9E	45
2	2	MS130354 R183-324	BLUSHING	7G	44
AR	AR	MS320C6	WASHER, FLAT	-	43
18	18	MS320 C6	WASHER, FLAT	4C	42
17	17	MS320C4	WASHER, FLAT	-	41

9	9	MS1291C3	NUT, SELF LOCKING		
5	5	MS1132C-4	SCREW, PAN HD		
18	18	MS1102D74L	PAN HD, SELF LOCKING		
20	20	MS1132C1	PAN HD		
8	8	MS1120C1	FILLISTER HD		
9	9	MS1102C4-5	PAN HD		
20	20	MS1102C4-7	SCREW, PAN HD		
4	4	MS320C2	WASHER, FLAT		
2	2	MS3113	CLIP, THERMAL COVER		
2	2	252520-1	CONTOUR CABLE,		
2	2	3163083	SPINDLE, NEGATOR SPOOL		
2	2	3163073	GUIDE, CABLE		
1	1	3163035-2	SPRING, WAVE		
1	1	3169076	PLATE, MTG - INB'D		
-	-	3169075	COMPENSATOR, BOOM-		
2	2	3169048	SPREADER BAR		
4	4	3169047	TENAC, BOOM END		
1	1	3169046	SUPPORT		
2	2	25252C2	CONTOUR CABLE, POWER		
1	1	3163019	LOCK PIN INSTL IN FLIGHT		
2	2	253377	SENSOR, TEMP		
1	1	252453	ACTUATOR EXTENDABLE BOOM		
1	1	3169036	NUT, JAM		
2	2	3169029	SPOOL, NEGATOR-CUSHION REEL		
2	2	3169028	SPOOL, NEGATOR-DRUM DRIVE		
2	2	3169027	COVER,		
1	1	3163017-3	GUIDE, CONTOUR CABLE		
1	1	3163017-2	GUIDE, CONTOUR CABLE		
1	1	3163017-1	GUIDE, CONTOUR CABLE		
2	2	3163023	SCREW, REDUCED DIA		
2	2	3169009	NEGATOR CUSHION REEL DRIVE		
2	2	3169008	NEGATOR DRUM DRIVE		
1	1	3169007	CUSHION REEL		
1	1	3169006-3	SUPPORT, CUSHION REEL, OUTBOARD		
1	1	3169005-3	SUPPORT, CUSHION REEL, INBOARD		
1	1	3169004	DRUM		
1	1	3169003	SUPPORT, OUTBOARD		
1	1	3169002	SUPPORT, INBOARD		
1	1	3169001	SPAR		

UNLESS OTHERWISE SPECIFIED DIMENSIONS ARE IN INCHES AND PER MILS (2) ANGLES .010 ± .03 ± .1 MP 30

FOR USAGE INFORMATION SEE UNDERGROUND DATA BOOKS

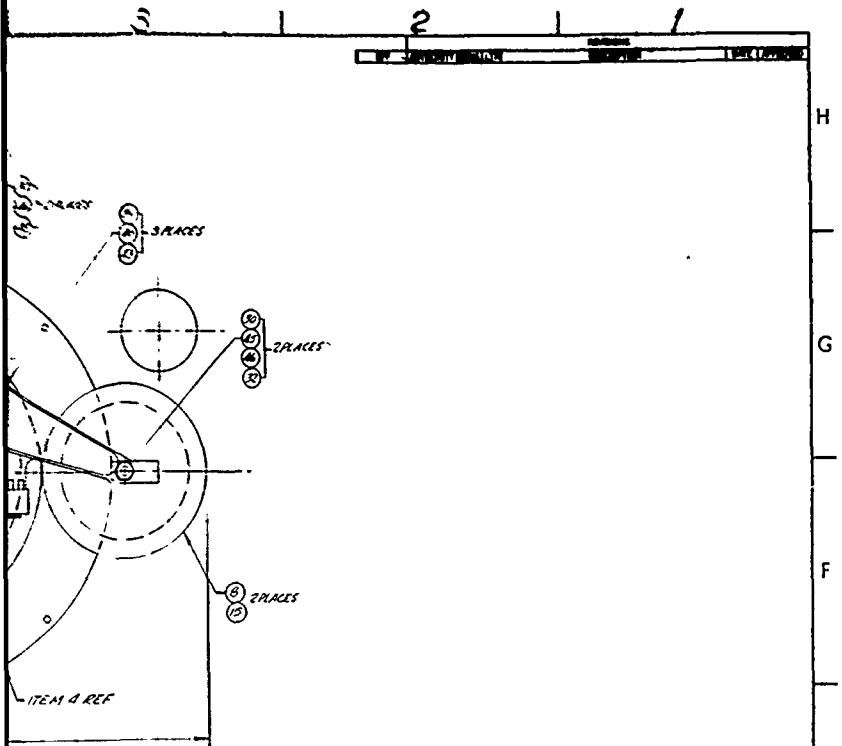
DATE: 11/81

SCALE: 1/1

DRUM MECHANISM

J 82577 X53225A





9	9	WAS1291G00	NUT, SELF LOCKING	5H	40
5	5	WAS1132C-4	SCREW, PAN HD	2E	59
18	18	WAS1000674L	PAN HD, SELF LOCKING	8C	38
20	20	WAS1132C1	PAN HD	4F	37
8	8	WAS1121C1	FILLISTER HD	KC	36
9	9	WAS10004-5	PAN HD	1S	35
20	20	WAS10004-7	SCREW, PAN HD	2E	34
4	4	WAS620C2	WASHER, FLAT	22H	33
2	2	3163113	CLIP THERMAL COVER	2E	32
2	2	252520-1	CONTOUR CABLE	2E	31
2	2	3163083	SPINDLE, NEGATOR SPOOL	2E	30
2	2	3163075	GUIDE, CABLE	2E	29
1	1	3163035-2	SPRING, WAVE	2E	28
1	1	3169076	PLATE, MTG - INB'D	2E	27
-	2	3169075	COMPENSATOR, BOOM	2E	26
2	2	3169048	SPREADER BAR	2E	25
4	4	3169047	TEGAS, BOOM END	2E	24
1	1	3169046	SUPPORT	2E	23
2	2	25252C2	CONTOUR CABLE, POWER	2E	22
1	1	3163019	LOCK PIN INSTL (NON FLIGHT)	2E	21
2	2	25252T	SENSOR, TEMP	2E	20
1	1	252453	ACTUATOR, EXTENDABLE BOOM	2E	19
1	1	3169036	NUT, JAM	2E	18
2	2	3169029	SPOOL, NEGATOR - CUSHION REEL	2E	17
2	2	3169028	SPOOL, NEGATOR - DRUM DRIVE	2E	16
2	2	3163027	COVER	2E	15
1	1	3163017-3	GUIDE, CONTOUR CABLE	2E	14
1	1	3163017-2	GUIDE, CONTOUR CABLE	2E	13
1	1	3163017-1	GUIDE, CONTOUR CABLE	2E	12
2	2	3163023	SCREW, REDUCED DIA	2E	11
2	2	3169009	NEGATOR, CUSHION CYL DRIVE	2E	10
2	2	3169008	NEGATOR, DRUM DRIVE	2E	9
1	1	3169007	CUSHION REEL	2E	8
1	1	3169006-3	SUPPORT, CUSHION REEL, OUTBOARD	2E	7
1	1	3169005-3	SUPPORT, CUSHION REEL, INBOARD	2E	6
1	1	3169004	DRUM	2E	5
1	1	3169003	SUPPORT, OUTBOARD	2E	4
1	1	3169002	SUPPORT, INBOARD	2E	3
1	1	3169001	SPAR	2E	2
1	1			2E	1

WASHER	16	64
COMPENSATOR, BOOM - FLIGHT	26	63
NUT, SELF LOCKING	61	62
WASHER, LOCK	61	61
WASHER	60	60
WIRE, SAFETY	7C	59
202 THK, PLASTIC RM ALUMINIZED TERM	5A	58
WIRE, INSULATED	-	57
SCREW, SELF-LOCKING	22W	56
SCREW, PAN HD	67	55
SCREW, PAN HD	12A	54
SCREW, FLAT HD	8C	53
WIRE SHIELDED	-	52
CLAMP	24H	51
SCREW, FLAT HEAD	23C	50
WASHER, FLAT	20F	49
WASHER, FLAT	20F	48
NUT, SELF LOCKING	20F	47
NUT, SELF LOCKING	20E	46
BUSHING	20E	45
BUSHING	20E	44
WASHER, FLAT	-	43
WASHER, FLAT	-	42
WASHER, FLAT	-	41

QTY		QTY	PART OR	NOMENCLATURE OR REFERENCE		ZONE	ITEM
REQD	ISSD	NO.	IDENTIFYING NO.	DESCRIPTION	REVISIONS		NO.
LIST OF MATERIALS							
HUGHES				HUGHES AIRCRAFT COMPANY CLAYTON CITY, CALIFORNIA			
DATE				DRAWN			
BY				DATE			
CHECKED				DATE			
APPROVED				DATE			
SCALE 1/1				SCALE 1/1			
J 82577				X5322519			

UNLESS OTHERWISE SPECIFIED  
DIMENSIONS ARE IN INCHES  
AND PER MILS (1000)  
XXX .XX X ANGLES  
# 010 # 03 # 1 # 2 # 30

FOR USAGE INFORMATION  
SEE DRAWING DATA SECTION

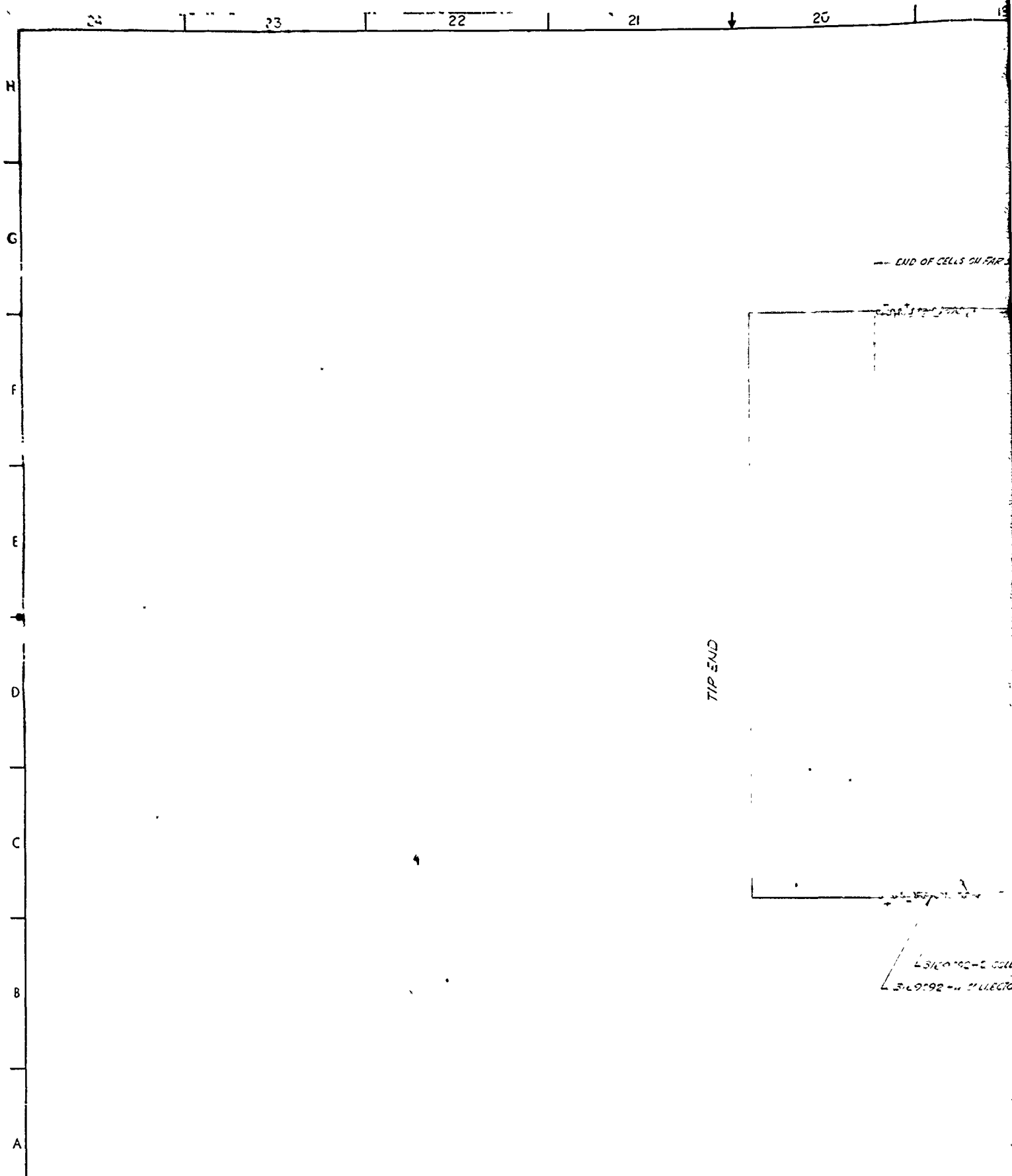
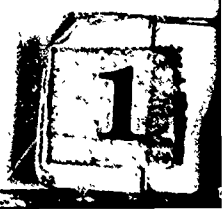


Figure C-3. Solar Panel Assembly (20338-223)

PRECEDING PAGE BLANK-NOT FILMED.



1.25  
77P  
1.25  
77P  
COND

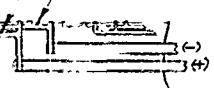
72

1.00  
1.00

END OF CELLS ON FAR SIDE

3169092-3 COLLECTOR BUS, 12 PLACES

3169092-1 COLLECTOR BUS 12 PLACES



(-)  
(+)

ROOT END

ROOT END

3169092-2 COLLECTOR BUS 2 PLACES

3169092-4 COLLECTOR BUS 12 PLACES

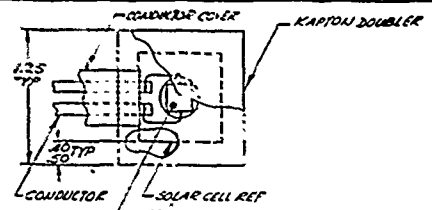
END OF CELLS ON THIS SIDE

VIEW OF PANEL FROM BACK SIDE  
(BUS INSULATOR (KAPTON) OMITTED)

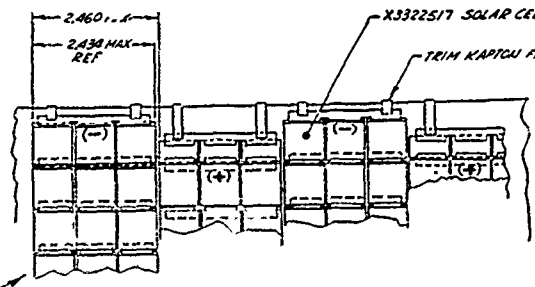
POWER BUS  
DRUM INTER  
TEMPERATURE SENS

SPN CODE CASE NO SECURITY CLASSIFICATION PART NO. 82577 X3322518

2



TEMPERATURE SENSOR INSTL  
 TYP 2 PLACES - 1 & -2  
 VIEWED FROM BACK SIDE



1.00  
 1.90 PRINTED AREA .30  
 .70

DETAIL

1 2 3 4 5 6 7

ROOT END

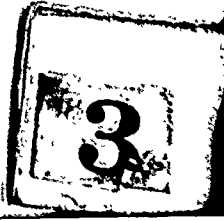
ROOT END

CELLS ON FAR SIDE

12.50 FOR -1  
 17.50 FOR -2

30L-58  
 123 CELLS \* 2.460 MAX P. TW

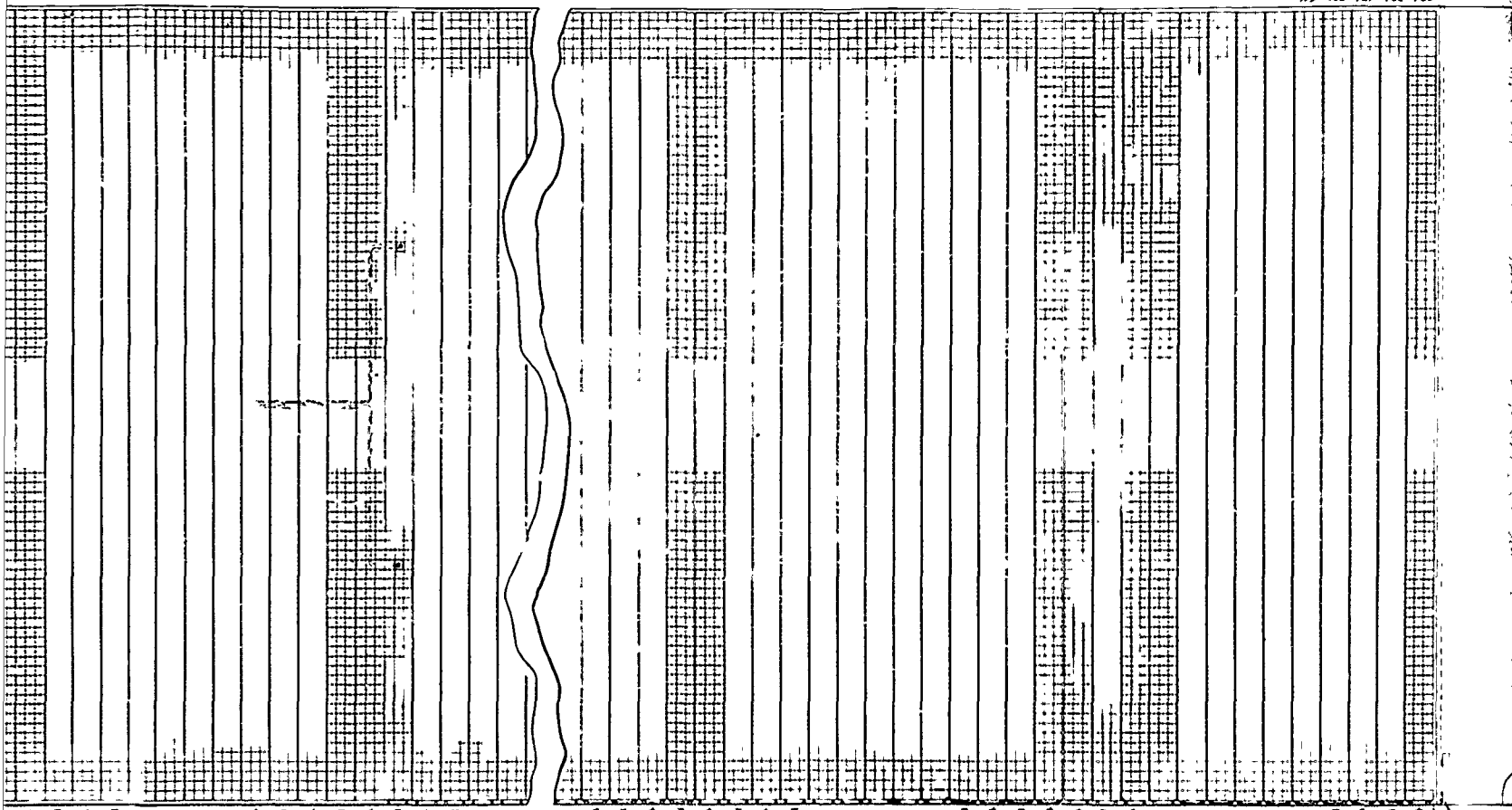
POWER BUSES (\* AND -)  
 DRUM INTERFACE  
 TEMPERATURE SENSOR LEADS (4)



9 8 7 6 5 4

NO. 4414 IN 4427  
NEW NO. 4414.2000

119 120 121 122 123



302.58  
12.5 - 12.5 @ 2.460 MAX PITCH

327.0 FOR -1  
332.0 FOR -2

- FAC  
- S. HA  
- NETA

100  
FOR -1

NOTES:

1. FABRICATE PER FS 30
2. PART NOT IN L/H ARE THOSE ON

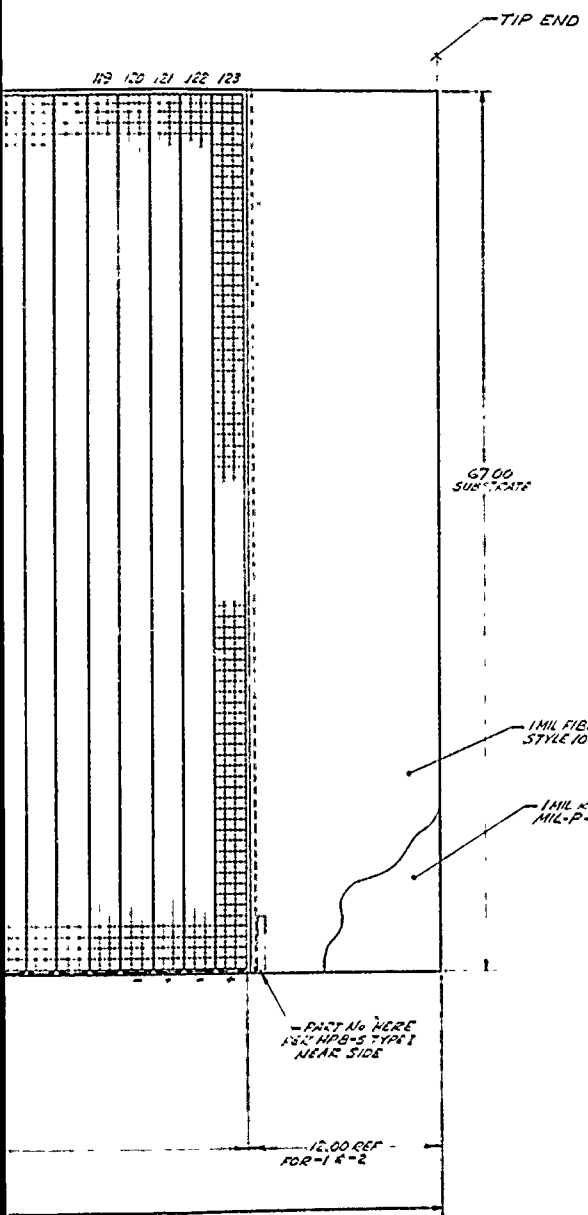
2577	X3322518	RV
------	----------	----

10 9 8 7 6 5 4





REV	AUTHORITY	DATE	DESCRIPTION	DATE APPROVED



QTY	PART OR PECO IDENTIFYING NO	NOMENCLATURE OR DESCRIPTION	REF QUANTITY	ZONE	ITEM NO
					37
					36
					35
					34
					33
					32
					31
					30
					29
					28
					27
					26
					25
					24
					23
					22
					21
					20
					19
					18
					17
					16
					15
					14
					13
					12
					11
					10
					9
					8
					7
					6
					5
					4
					3
					2
					1

- NOTES
- FABRICATE PER FS 30992-008 AS APPLICABLE
  - PART ALL IN 1/4" ARE THOSE OF THE AS KW FRUSA.

UNLESS OTHERWISE SPECIFIED DIMENSIONS ARE IN INCHES AND PER USAS Y14.5

FOR SCALE DATE

MATERIAL

FOR USAGE INFORMATION SEE ENGINEERING DATA RECORDS

NEXT ASSY USED ON APPLICATION

LIST OF MATERIALS

HUGHES AIRCRAFT COMPANY  
CLAYTON CITY, CALIFORNIA

SOLAR PANEL ASSY

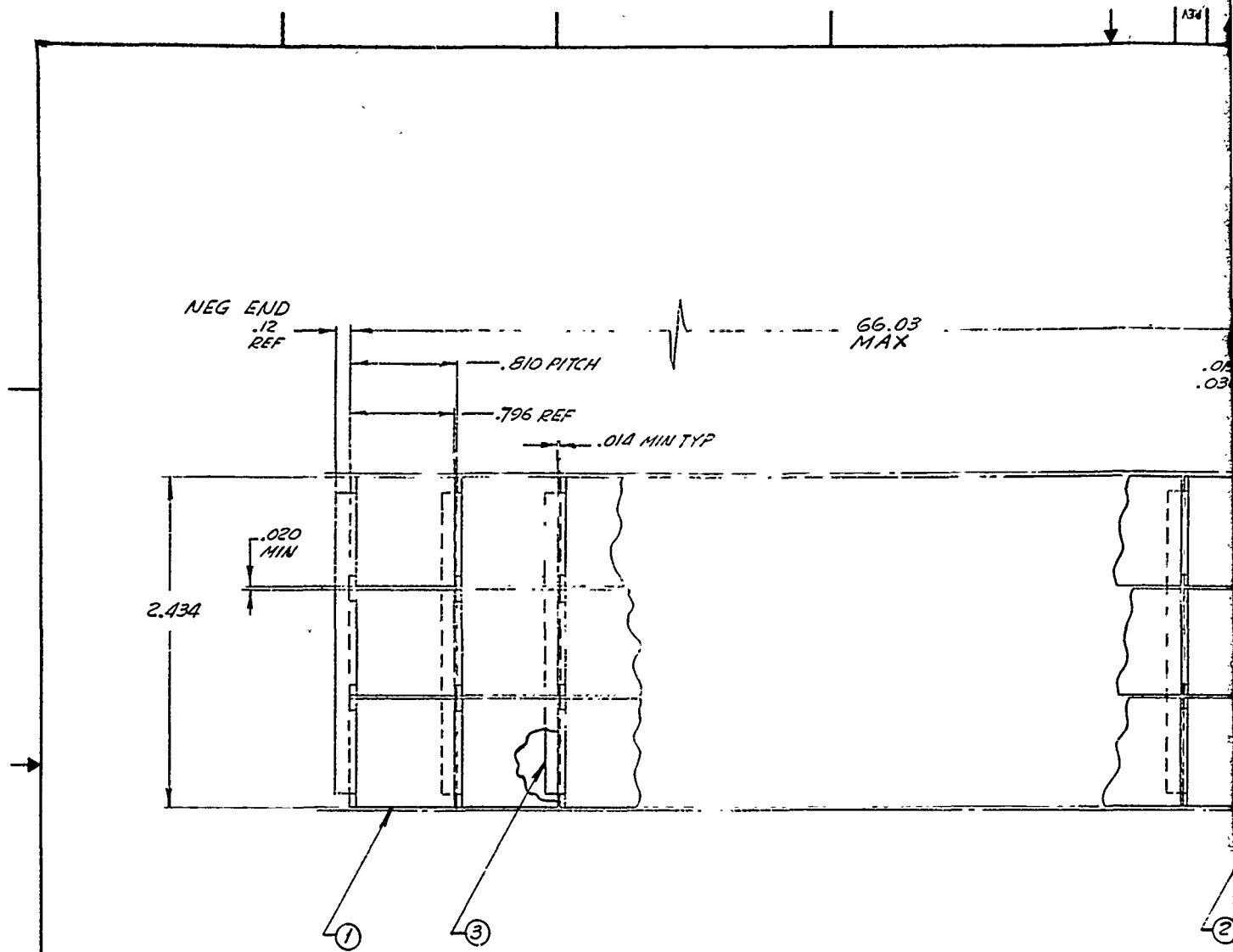
SIZE CODE DEPT NO  
J 82577 X3322518

SCALE 7/8" = 1" (NOTED) SHEET

H  
G  
F  
E  
D  
C  
B  
A

X3322500

X3322518



NOTES -

- ① VENDOR ITEM - SEE SOURCE CONTROL DWG.
- ② SOLAR CELL GROUP MUST LIE WITHIN CONFINES OF THIS ENVELOPE.
- 3. FABRICATE PER FAB SPEC (TBD)
- 4. ACCEPTANCE TESTING PER TS 30992-011.
- 5. IDENTIFY PER HP8-5, TYPE, WITH PART No., SERIAL No AND ELECTRICAL GRADE; SERIAL No's TO BE CONSECUTIVE, STARTING WITH No 1.

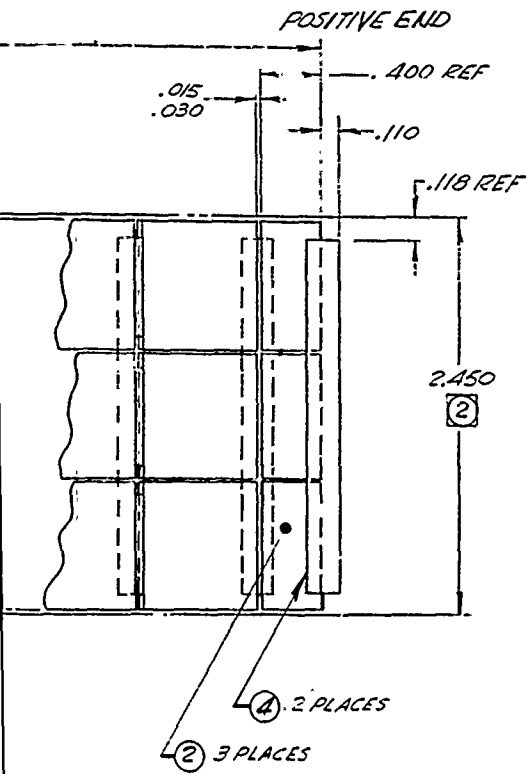
9/71 DIETRICH POST CLEARPRINT 1000H  
FORM NO. 11888-C3-CC 9-68

Figure C-4. Solar Cell Group, Triple Width (20338-224)



X3322517

REVISIONS			
EFF	AUTHORITY	ZONE	LTR



QTY REQD	CODE IDENT	PART NO. OR IDENTIFYING NO	NOMENCLATURE OR DESCRIPTION	ZONE	FIND NO.
					5
2		3205755-3	STRIP, POSITIVE END		4
81		3205754-3	STRIP, INTERCONNECTION		3
3		X3286385	SOLAR CELL, BLOCKING	1	2
283		253884	SOLAR CELL	1	1

UNLESS OTHERWISE SPECIFIED DIMENSIONS ARE IN INCHES AND PER ANS Y14.5		DR GAUTNER		DATE 9-1-57	<b>HUGHES</b> HUGHES AIRCRAFT COMPANY CULVER CITY, CALIFORNIA
XXX ± 0.10	XX ± 0.03	ANGLES ± 0° 30'	CHK		
MATERIAL		APPD		SIZE CODE IDENT NO	DRAWING NO.
NEXT ASSY		USED ON		D 82577	X3322517
APPLICATION				SCALE 3/16"	SHEET

REV X3322517

2

## APPENDIX D. ARRAY DYNAMICS ANALYSIS

In generating a set of general expressions for mass coupling coefficients associated with rigid body motions of the boom-panel combination for each of the normal modes of the combination, the following coordinate system is used: Index 1 denotes uniform lateral displacement of the entire combination; index 2 denotes motion corresponding to a root rotation about an axis perpendicular to the spanwise direction of the panel; and index 3 denotes the motion due to a normal mode. The coupling coefficients become then

$$\begin{aligned} \frac{1}{2}M(1, 3) = & (m_1 L) \left( A \left[ \frac{\sinh \alpha}{\alpha} - \frac{\sin \beta}{\beta} \right] + B \left[ \frac{1 - \cosh \alpha}{\alpha^2} + \frac{1 - \cos \beta}{\beta^2} \right] \right) \\ & + (m_2 L) \frac{1 - \cos \gamma}{\gamma} + M_3 \sin \gamma \end{aligned}$$

$$\begin{aligned} \frac{1}{2}M(2, 3) = & (m_1 L^2) \left( A \left[ \frac{\sinh \alpha}{\alpha} - \frac{\sin \beta}{\beta} + \frac{1 - \cosh \alpha}{\alpha^2} + \frac{1 - \cos \beta}{\beta^2} \right] \right. \\ & \left. + B \left[ \frac{\cosh \alpha}{\alpha^2} + \frac{\cos \beta}{\beta^2} - \frac{\sinh \alpha}{\alpha^3} - \frac{\sin \beta}{\beta^3} \right] \right) \\ & + (m_2 L^2) (\sin \gamma - \gamma \cos \gamma) / \gamma^2 + M_3 L \sin \gamma \end{aligned}$$

$$\begin{aligned} \frac{1}{2}M(3, 3) = & (m_1 L) \left( A^2 \left[ \frac{\sinh 2\alpha}{4\alpha} + \frac{\sin 2\beta}{4\beta} - \frac{\alpha \sinh \alpha \cos \beta + \beta \cosh \alpha \sin \beta}{p} + 1 \right] \right. \\ & \left. + B^2 \left[ \frac{\sinh 2\alpha}{4\alpha^3} + \frac{\sin 2\beta}{4\beta^3} + \frac{1}{p} \frac{\sinh \alpha \cos \beta}{\alpha} - \frac{\cosh \alpha \sin \beta}{\beta} - \frac{p}{p^2 - q^2} \right] \right. \\ & \left. + AB \left[ \frac{\sinh \alpha}{\alpha} - \frac{\sin \beta}{\beta} \right]^2 \right) \\ & + (m_2 L) \left[ 1 - \frac{\sin \gamma \cos \gamma}{\gamma} \right] / 2 + M_3 (\sin \gamma)^2 \end{aligned}$$

where

$$\alpha = \sqrt{p - q} \quad ; \quad \beta = \sqrt{p + q}$$

$$q = \frac{PL^2}{2EI} \cos\beta$$

$$p = \sqrt{q^2 + \omega^2 m_1 L^4 / EI}$$

$$\gamma = \omega L \sqrt{m_2 / P}$$

$EI = 59000 \text{ lb/in}^2$  = bending stiffness of a single boom

$L = 25.5 \text{ ft}$  = length of the boom

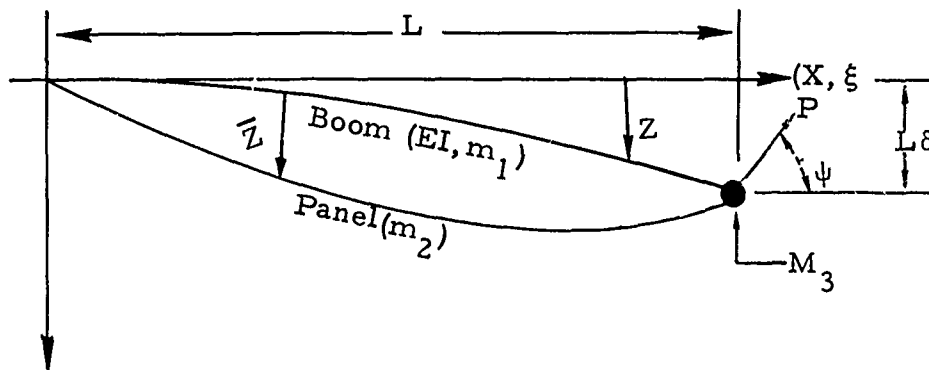
$m_1 = 0.087 \text{ lb/ft}$  = mass per unit length of the boom

$m_2 = 0.523 \text{ lb/ft}$  = mass per unit length of half of the panel

$P = 2 \text{ lb}$  = rigging load in the boom

$M_3 = 0.35 \text{ lb}$  = mass of half of the spreader bar

$\psi$  = slope of the panel at the unsupported end of the boom



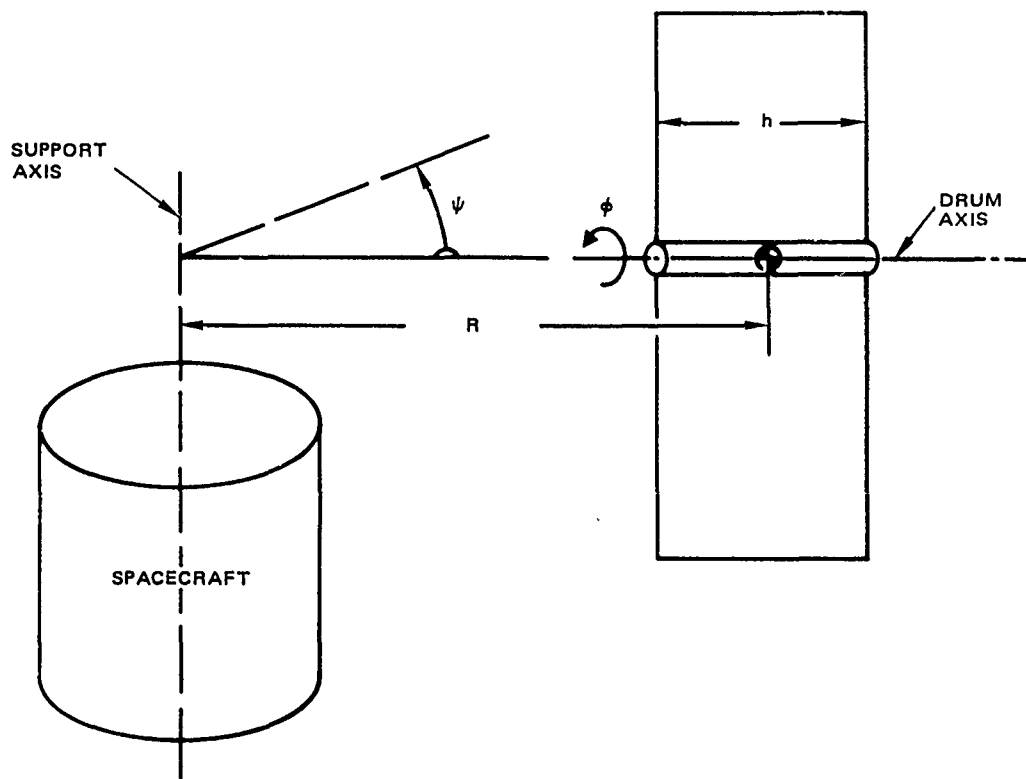
Transfer functions have been developed for space vehicle/array dynamic control studies. These transfer functions are summarized below for contributions from a two-panel assembly extended to both sides of the stowage drum. These contributions from the panels to equations of motion about the drum axis  $\phi$  and about the support axis  $\psi$  are as follows:

$$2 \left\{ M_b(2, 2) - \sum_i \frac{[M_{bi}(2, 3)]^2}{1 + (\omega_{bi}/s)^2} \right\} \ddot{\phi} = M_\phi ,$$

$$2 \left\{ R^2 M_b(1, 1) + \sin^2 \phi \left[ M_b(2, 2) - \sum_i \frac{[M_{bi}(2, 3)]^2}{1 + (\omega_{bi}/s)^2} \right] \right. \\ \left. + \cos^2 \phi \left[ M_t^*(1, 1) - \sum_i \frac{R^2 [M_{bi}(1, 3)]^2}{1 + (\omega_{bi}/s)^2} - \sum_i \frac{(h/2)^2 [M_{ti}(1, 3)]^2}{1 + (\omega_{ti}/s)^2} \right] \right\} \ddot{\psi} = M_\psi$$

The coordinates and angle assignment are illustrated in Figure D-1. Mass inertias connected with the drum mechanism, the orientation mechanism, and their structural tie are not included. Note, that in-plane bending and out-of-plane bending are identical in this analysis by virtue of modeling the panel as a string.

Values of  $M$  for  $i$  up to 3 are given in the following. Subscript ( $i$ ) refers to the order of the modes. The angle  $\phi$  is measured about the drum axis from a reference position when the plane of the panels contains the support axis.



20338-102(U)

Figure D-1. Relative Space Vehicle and Solar Array Position (Nomenclature)

### FISCA VIBRATION MODES

Panel: 25.6364 by 5.5 feet; 0.192 lb/ft<sup>2</sup>  
 Boom: 0.86 inch by 5 mils; 0.28 lb/in<sup>3</sup>; E = 30,000,000  
 Spreader bar: 0.715 pounds

#### BENDING MODE

Boom Euler load = 2.73617 pounds; boom load = 2 pounds

#### MODE ORDER 1

Frequency = 0.515482 R/S = 8.20415 E-2 Hz

#### Boom Modal Function

X/L	M, slugs	Z, feet	B.M., pounds
0	2.58816 E-3	0	23.5496
0.1	5.17632 E-3	1.79973 E-2	24.5313
0.2	5.17632 E-3	7.27533 E-2	24.6318
0.3	5.17632 E-3	0.164419	23.8496
0.4	5.17632 E-3	0.291823	22.2168
0.5	5.17632 E-3	0.452518	19.7974
0.6	5.17632 E-3	0.642882	16.6853
0.7	5.17632 E-3	0.85825	13.0003
0.8	5.17632 E-3	1.0931	8.88412
0.9	5.17632 E-3	1.34128	4.49457
1	2.58816 E-3	1.59619	1.16890 E-7

#### Panel Modal Function

X/L	M, slugs	Z, feet
0	2.10186 E-2	0
0.1	4.20373 E-2	0.204709
0.2	4.20373 E-2	0.40649
0.3	4.20373 E-2	0.602458
0.4	4.20373 E-2	0.78981
0.5	4.20373 E-2	0.965867
0.6	4.20373 E-2	1.12811
0.7	4.20373 E-2	1.27422
0.8	4.20373 E-2	1.40211
0.9	4.20373 E-2	1.50995
1	3.21211 E-2	1.59619



MODE ORDER 2

Frequency = 1.89339 R/S = 0.301342 Hz

Boom Modal Function

X/L	M, slugs	Z, feet	B.M., pounds
0	2.58816 E-3	0	-24.7626
0.1	5.17632 E-3	-1.85987 E-2	-24.5012
0.2	5.17632 E-3	-7.39124 E-2	-23.3711
0.3	5.17632 E-3	-0.164251	-21.4441
0.4	5.17632 E-3	-0.286735	-18.8411
0.5	5.17632 E-3	-0.437471	-15.7249
0.6	5.17632 E-3	-0.611802	-12.2934
0.7	5.17632 E-3	-0.804597	- 8.76892
0.8	5.17632 E-3	-1.01059	- 5.38762
0.9	5.17632 E-3	-1.22473	- 2.38813
1	2.58816 E-3	-1.44253	1.29365 E-8

Panel Modal Function

X/L	M, slugs	Z, feet
0	2.10186 E-2	0
0.1	4.20373 E-2	0.646037
0.2	4.20373 E-2	1.16927
0.3	4.20373 E-2	1.47026
0.4	4.20373 E-2	1.49177
0.5	4.20373 E-2	1.22972
0.6	4.20373 E-2	0.733933
0.7	4.20373 E-2	9.86349 E-2
0.8	4.20373 E-2	-0.555412
0.9	4.20373 E-2	-1.10389
1	3.21211 E-2	-1.44253

MODE ORDER 3

Frequency = 3.19551 R/S = 0.508582 Hz

Boom Modal Function

X/L	M, slugs	Z, feet	B.M., pounds
0	2.58816 E-3	0	31.1125
0.1	5.17632 E-3	2.27463 E-2	28.3144
0.2	5.17632 E-3	8.79248 E-2	24.5406
0.3	5.17632 E-3	0.189894	20.0319
0.4	5.17632 E-3	0.321919	15.1147
0.5	5.17632 E-3	0.476658	10.1789
0.6	5.17632 E-3	0.646746	5.65187
0.7	5.17632 E-3	0.825435	1.97123
0.8	5.17632 E-3	1.00725	- 0.4417
0.9	5.17632 E-3	1.1886	- 1.20589
1	2.58816 E-3	1.36839	- 1.30979 E-7

Panel Modal Function

X/L	M, slugs	Z, feet
0	2.10186 E-2	0
0.1	4.20373 E-2	1.02001
0.2	4.20373 E-2	1.50405
0.3	4.20373 E-2	1.19778
0.4	4.20373 E-2	0.262125
0.5	4.20373 E-2	-0.811262
0.6	4.20373 E-2	-1.45837
0.7	4.20373 E-2	-1.33916
0.8	4.20373 E-2	-0.516288
0.9	4.20373 E-2	0.577873
1	3.21211 E-2	1.36839

## FISCA VIBRATION MODES

Panel: 25.6364 by 5.5 feet;  $0.192 \text{ lb/ft}^2$   
Boom: 0.86 inch by 5 mils;  $0.28 \text{ lb/in}^3$ ;  $E = 30,000,000 \text{ psi}$   
Spreader bar: 0.715 pounds

### BENDING MODE

Boom Euler load = 2.73617 pounds; boom load = 2 pounds  
Tip deflection / boom span = 0

$M[1,1]$ , slugs = 0.966477 [or 31.1205 pounds]  
 $M[1,2]$ , slug-ft = 12.6731 [or 408.074 lb-ft]  
 $M[2,2]$ , slug-ft<sup>2</sup> = 221.459 [or 7130.99 lb-ft<sup>2</sup>]

### MODE ORDER 1

Frequency = 0.515482 R/S =  $8.20415 \text{ E-2 Hz}$

$M[1,3] = 0.859037$ ;  $M[2,3] = 14.7708$ ;  $M[3,3] = 1.0$

### MODE ORDER 2

Frequency = 1.89339 R/S = 0.301342 Hz

$M[1,3] = 0.293777$ ;  $M[2,3] = -1.15124$ ;  $M[3,3] = 1.0$

### MODE ORDER 3

Frequency = 3.19551 R/S = 0.508582 Hz

$M[1,3] = 0.185483$ ;  $M[2,3] = 0.507811$ ;  $M[3,3] = 1.0$

### TORSION MODE

Boom Euler load = 2.73617 pounds; boom load = 2 pounds  
Tip deflection/boom span = 0

$$\begin{array}{ll} M[1, 1], \text{ slugs} & = 0.415 \quad [\text{or } 13.364 \text{ pounds}] \\ M[1, 2], \text{ slug-ft} & = 5.4148 \quad [\text{or } 174.36 \text{ lb-ft}] \\ M[2, 2], \text{ slug-ft}^2 & = 94.167 \quad [\text{or } 3032.17 \text{ lb-ft}^2] \end{array}$$

#### MODE ORDER 1

Frequency = 0.0855 Hz

$$M[1, 3] = 0.547; \quad M[2, 3] = 9.544; \quad M[3, 3] = 1.0$$

#### MODE ORDER 2

Frequency = 0.3048 Hz

$$M[1, 3] = 0.0649; \quad M[2, 3] = -2.384; \quad M[3, 3] = 1.0$$

#### MODE ORDER 3

Frequency = 0.513 Hz

$$M[1, 3] = 0.1922; \quad M[2, 3] = 2.0495; \quad M[3, 3] = 1.0$$

R = see Figure 8-6

$$h/2 = 2.75 \text{ feet}$$

$$M_b(I, I) = 2(m_1 + m_2)L + 2M_3$$

$$M_b(2, 2) = \frac{2}{3}(m_1 + m_2)L^3 + 2M_3L^2$$

$$M_t^*(I, I) = \left(\frac{h}{2}\right)^2 * M_t(I, I)$$

NOTE: Subscripts b and t indicate bending and torsion, respectively.

DISTRIBUTION

Copies

Activities at WPAFB Ohio  
 20 AFAPL/POE-2  
 14 AFAPL/DOE/STINFO  
 1 AFAL/TSR  
 1 2750 ABWg/SSL  
 1 4950/PMNB/  
 1 ARL/LS/D. C. Reynolds  
 1 AFFDL/FEE/R. White  
 1 AFAL/AVVW/W. Kennedy  
 1 AFAL/AVNE/R. Conklin  
 1 AFML/LNE/W. Lehn  
 1 AFML/LTE/J. Whittebort  
 1 AFML/LTE/M. Bialer  
 1 FTD/TDP/Maj. J. Joyce

Other Air Force Activities  
 HQ USAF  
 Washington, D. C. 20330  
 1 SAMID  
 1 RDSE/Lt. Col. R. Wolfsberger  
 1 RDSC/Lt. Col. McCartney  
 HQ AFSC  
 Andrews AFB, Md. 20331  
 1 DLY/Lt. Col. R. Leiby  
 1 DLSP/Maj. T. Tomaskovic  
 1 DLSE/Capt. H. Bethel  
 Air University  
 Maxwell AFB, Alabama 36112  
 AFCL  
 L. G. Hanscom Field  
 Bedford, Mass. 01731  
 1 PHF/N. Yannoni  
 1 PHF/J. Silverman  
 1 PHF/P. Drevinsky  
 1 ESD/W. Sen  
 AFWL  
 Kirtland AFB, New Mexico 87117  
 1 SA/Capt. A. Willoughby  
 1 ET/Maj. J. E. Smith  
 1 DOPP/Lt. Col. Bowles  
 SAMSO  
 AF Unit Post Office  
 Los Angeles, California 90045  
 1 SYA/Col. E. P. Clark  
 1 SYE/Col. D. C. May  
 1 SYS/Lt. Col. J. A. Norly  
 1 XRC/Lt. Col. F. Stewart  
 1 SYAX/Maj. S. Gilbert  
 1 SYJ/Maj. W. Niles  
 1 CDPSY/Maj. Kaminsky  
 1 SYS/Capt. W. Mercer  
 1 SKR/Capt. W. Whitmeyer  
 1 SZ/Capt. Junger  
 1 SKE/Capt. Buchanan  
 1 XRYS/Capt. J. Hengle  
 1 NSSA-4/R. Silverman  
 OSD/DDR&E  
 Washington, D. C. 20330  
 1 Co. W. Henderson

Army  
 USAECOM  
 Ft. Monmouth, New Jersey 07703  
 1 AMSEL-TL-PE/E. Kittl  
 1 AMSEL-TL-PE/A. Herchakowski  
 U. S. Army Engineers  
 Research and Technology Division  
 Ft. Belvoir, Virginia 22060  
 1 Power Group/G. B. Manning  
 U. S. Army Research Office  
 Box CM, Duke Station  
 Durham, North Carolina  
 1 W. Jorgensen

Navy  
 Naval Research Laboratory  
 Washington, D. C. 20390  
 1 Code 6464/E. Brancato  
 1 Code 6465/R. Statler

Copies

Naval Air Systems Command  
 Propulsion Division  
 Washington, D. C. 20360  
 1 J. L. Byers  
 Naval Ordnance Test Station  
 China Lake, California 93555  
 1 Code 3519/M. Creusere

Other Department of Defense Activities  
 IDA  
 Science and Technology Division  
 400 Army-Navy Drive  
 Arlington, Virginia 22202  
 1 R. Hamilton  
 1 R. Briceland  
 Defense Nuclear Agency  
 Washington, D. C. 20305  
 1 RAEV  
 Defense Communications Agency  
 Systems Engineering Facility  
 Reston, Virginia 22070  
 1 C. S. Lorens  
 Defense Ceramic Information Center  
 Battelle Memorial Institute  
 Columbus, Ohio 43201  
 1 J. F. Lynch  
 Radiation Effects Information Center  
 Battelle Memorial Institute  
 Columbus, Ohio 43201  
 1 E. N. Wyler  
 1 R. Thatcher  
 Power Information Center  
 University City Science Institute  
 3401 Market Street  
 Philadelphia, Penn. 19104  
 1 J. J. Pierson  
 4 DDC Cameron Station  
 Alexandria, Va. 22314

NASA  
 NASA Headquarters  
 Washington, D. C. 20546  
 1 RPP/E. M. Cohn  
 1 MF/A. Liccarde  
 1 MF/M. Shaw  
 NASA - Houston MSC  
 Houston, Texas 77058  
 1 EP-5/J. L. Cioni  
 NASA - Ames Research Center  
 Moffett Field, California 94035  
 1 PES/R. Debs  
 1 N244/A. Wilbur  
 NASA - Lewis Research Center  
 Cleveland, Ohio 44135  
 1 D. Bernatowicz  
 1 H. Brandhorst  
 1 A. Forestieri  
 1 I. T. Myers  
 1 J. H. Lamneck  
 1 R. Lovell  
 1 T. Riley  
 1 B. L. Sater  
 1 Library  
 NASA - Marshall SFC  
 Huntsville, Alabama 35812  
 1 SE-ASTR-EN/J. Miller  
 1 PD-DO-EP/W. Brantley  
 NASA - Goddard SFC  
 Greenbelt, Maryland 20771  
 1 Code 760/W. Cherry  
 1 Code 481/K. Edinger  
 1 Code 633/M. Schack  
 NASA - Langley Research Center  
 Hampton, Virginia 23365  
 1 MS-188B/A. Heath  
 NASA - Jet Propulsion Laboratory  
 Pasadena, California 91103  
 1 P. Berman

DISTRIBUTION (Continued)

Copies

Copies

1 NASA - Jet Propulsion Laboratory (Cont)  
 1 L. Runkle  
 1 R. Yasui

Other Government Agencies

1 National Science Foundation  
 Research Applications Division  
 Washington, D. C. 20550  
 J. C. Denton

1 Environmental Protection Agency  
 Ann Arbor, Michigan 48105  
 G. Thur

1 Department of Interior  
 Office of the Secretary  
 Washington, D. C. 20240  
 F. F. Parry

1 Department of Transportation  
 Applied Technology Division  
 Washington, D. C. 20591  
 Capt. J. R. Iversen

Non-Government Agencies

1 Aerospace Corporation  
 P. O. Box 95085  
 Los Angeles, California 90045

1 L. Aukerman  
 1 E. Bersinger  
 1 E. Bobach  
 1 S. Bower  
 1 C. Crickmay  
 1 R. Cooper  
 1 A. Digiacomo  
 1 L. Gibson  
 1 G. Goldfarb  
 1 S. Grove/Library  
 1 H. Killian  
 1 J. Krisilas  
 1 B. Krishan  
 1 D. Haxton  
 1 T. Lee  
 1 D. Pecka  
 1 H. Samson  
 1 P. Schall  
 1 D. Scrooc  
 1 J. Statsinger  
 1 A. Straubinger  
 1 B. Wald  
 1 D. Willens

1 The Boeing Company  
 Aerospace Group  
 P. O. Box 3999  
 Seattle, Washington 98124  
 1 R. Browne  
 1 E. Horne  
 1 H. Oman  
 1 S. Springate  
 1 Library

1 Brown University  
 Department of Engineering  
 Providence, Rhode Island 02912  
 J. Loferski

1 COMSAT  
 2100 L Street, NW  
 Washington, D. C. 20037  
 D. Curtin

1 Centralab  
 4501 Arden Drive  
 El Monte, California 91734  
 1 P. Iles  
 1 K. Ling

1 Clevite Corporation  
 540 East 105 Street  
 Cleveland, Ohio 44138  
 D. Parkinson

1 EOS, Inc.  
 300 Halstead  
 Pasadena, California 91107

1 W. Menetrey  
 1 D. Stewart

1 Fairchild Hiller Corporation  
 Germantown, Maryland 20767  
 1 D. Haskell  
 1 W. King

1 Heliotek  
 12500 Gladstone  
 Sylmar, California 91324  
 1 E. Ralph  
 1 P. Payne

1 Hughes Aircraft Company  
 Aerospace Division  
 El Segundo, California 90245  
 1 E. Felkel  
 1 E. Smith  
 1 E. Stofel  
 1 G. Wolff

1 Ion Physics Corporation  
 South Bedford Street  
 Burlington, Mass. 01803  
 F. Bartels

1 John Hopkins University  
 Applied Physics Laboratory  
 Silver Springs, Maryland 20910  
 1 R. Fischell  
 1 L. V. Reuger  
 1 W. Ray  
 1 R. Sullivan

1 General Electric Company  
 Valley Forge Space Center  
 P. O. Box 8555  
 Philadelphia, Penn. 19101  
 1 W. Beecraft  
 1 F. Blake  
 1 K. Hanson  
 1 J. Peden  
 1 D. Ulrich

1 Lockheed Missiles and Space Company  
 P. O. Box 504  
 Sunnyvale, California 94088  
 1 L. Chidester  
 1 D. Hennessee  
 1 R. Lynn  
 1 K. Ray  
 1 G. Turner

1 McDonnell-Douglas Corporation  
 Santa Monica, California 90706  
 1 W. Murray  
 1 R. Waters

1 McDonnell-Douglas Corporation  
 Huntington Beach, California 92647  
 A. D. Tonelli

1 McDonnell-Douglas Corporation  
 P. O. Box 516  
 St. Louis, Missouri 63166  
 J. Wolter

1 Gulf-General Atomics, Inc.  
 P. O. Box 608  
 San Diego, California 92112  
 J. A. Naber

1 MIT Lincoln Laboratories  
 Lexington, Mass. 02173  
 1 J. Farnsworth  
 1 A. Stanley

1 MIT  
 Department of Electrical Engineering  
 Cambridge, Mass. 02193  
 M. Dresselhaus

DISTRIBUTION (Continued)

Copies

Philco-Ford Corporation  
WDL  
Palo Alto, California 94303  
1 D. Briggs  
1 H. Pollard  
1 D. Reynard  
RCA  
Astro-Electronics Division  
Princeton, New Jersey 08540  
1 H. Bilskey  
1 G. Brucker  
1 T. Faith  
1 H. Schwartzberg  
1 T. Wylie  
Ryan Aeronautical Company  
San Diego, California 92122  
1 W.M. Cattrell  
Spectrolab  
12500 Gladstone  
1 Sylmar, California 91324  
TRW Systems Group  
1 Space Park  
Redondo Beach, California  
1 J. Carter  
1 G. Downing  
1 W. Luft  
1 H. Riess

Copies

Westinghouse Electric Corporation  
R&D Center, Churchill Burrough  
Pittsburg, Penn. 15235  
1  
Westinghouse Electric Corporation  
Semiconductor Division  
Youngwood, Penn. 01803  
1 K.H. Sun  
1 J. Johnson  
University of Delaware  
Physics Department  
Newark, Delaware 19711  
1 K.W. Boer  
University of Pennsylvania  
113 Towne Bldg.  
Philadelphia, Penn. 19104  
1 Martin Wolf

**DOCUMENT CONTROL DATA - R & D**

*Security classification of title, body of abstract and indexing annotation must be entered when the overall report is classified*

1. ORIGINATING ACTIVITY (Corporate author) Hughes Aircraft Company Space and Communications Group El Segundo, California		2a. REPORT SECURITY CLASSIFICATION Unclassified	
		2b. GROUP Not applicable	
3. REPORT TITLE  Flexible Rolled-Up Solar Array Final Report			
4. DESCRIPTIVE NOTES (Type of report and inclusive dates) Final Technical Report, 1 July 1968 through 31 May 1972			
5. AUTHOR(S) (First name, middle initial, last name) Edward O. Felkel George Wolff			
6. REPORT DATE 30 June 1972	7a. TOTAL NO. OF PAGES 307	7b. NO. OF REFS None	
8a. CONTRACT OR GRANT NO. F33615-68-C-1676	9a. ORIGINATOR'S REPORT NUMBER(S) 72(41)-11244/B3532		
b. PROJECT NO. 682J			
c.	9b. OTHER REPORT NO(S) (Any other numbers that may be assigned this report) SCG 20338R		
d.			
10. DISTRIBUTION STATEMENT Distribution limited to U.S. Government Agencies only: test and evaluation: June 1972. Other requests for this document must be referred to the Air Force Aero Propulsion Laboratory (POE-2, Wright-Patterson Air Force Base, Ohio 45433)			
11. SUPPLEMENTARY NOTES Not applicable		12. SPONSORING MILITARY ACTIVITY Air Force Aero Propulsion Laboratory POE-2 Wright-Patterson AFB, Ohio 45433	
13. ABSTRACT This report summarizes the design, development, qualification, and flight test of a 1.5-kw flexible rolled-up solar array power system. This system was launched on a thrust augmented Thor/Agema vehicle system into a 400 nm polar orbit on 17 October 1971, has successfully completed a 6 month flight test, and continues to provide spacecraft power.  The criteria, design tradeoffs, and analyses that led to the configuration of the 5.5-by 32-foot solar array, the two-axis sun acquisition and tracking orientation mechanism, and the associated power electronics and instrumentation units are described. The results of development, qualification, and flight test are presented, as well as recommendations for design improvements or developments for future similar applications. The recommendations include principal parameters and performance data such as array aspect ratios, weight, and natural frequency for systems ranging from 0.5 to 20 kw.  The flight data illustrate the compatibility of the flexible solar array concept with flight systems. Power output has been excellent with no evidence of mechanical damage from boost, deployment, or operational environments. Peak power degradation has been reflective of the normal reaction of solar cells to the space environment. Spacecraft and array dynamic interactions have been minimal and vehicle integration has proven straightforward and effective.  In conclusion, the report illustrates the viability of the 1.5-kw flexible array design as a flight power system in its own right and also as a module of power systems to the 20-kw level.			



KEY WORDS	LINK A		LINK B		LINK C	
	ROLE	WT	ROLE	WT	ROLE	WT
Solar array						
Satellite power supply						
Flexible panel						
Extension and retraction						
Multi-kilowatt						
Sun tracking						
Orientation mechanism						
Attitude control						
Dynamic stability						
Solar cell design, flight test, qualification						
Thorad/Agna						
Rolled-up						
Dynamic models						
Radiation degradation						
Spacecraft reactions						
Deployment mechanisms						
1.5 kw						
Telemetry						
Acceleration						
Temperatures						
Slip rings						
Booms						
Sun sensors						